Ship noise localization study

ECHO Program study summary

The Vancouver Fraser Port Authority-led Enhancing Cetacean Habitat and Observation (ECHO) Program manages the analysis of underwater acoustic data acquired by Transport Canada's Boundary Pass Underwater Listening Station (ULS) in southern British Columbia. The ULS consists of two hydrophone arrays, each equipped with four hydrophones, which collect data on underwater noise from vessels, marine life, and other sources. This hydrophone array configuration can be used to localize – or determine the specific location of – underwater sounds near the station.

What questions was the study trying to answer?

The study was seeking to answer the following key questions:

- What is the best methodology to localize noise from passing ships captured by the ULS?
- Can this methodology be used to identify different noise sources along the length of a ship hull?

Who conducted the project?

JASCO Applied Sciences (Canada) Ltd. conducted the study. JASCO are retained by Transport Canada to deploy and operate the Boundary Pass ULS, and by the port authority to analyze the ULS data.

What methods were used?

Underwater noise from a vessel can be generated by several sources, most notably the propeller and main engine. Other onboard equipment such as generators and pumps produce noise and vibrations which can transmit through the hull into the water. Water flow past the bow and along the hull, or turbulence at the wake, may also generate underwater noise.

To potentially identify these different noise sources through localization or noise mapping along the ship hull, this study was conducted in two parts: Part 1 included developing and evaluating methods for localization and ship noise mapping, while Part 2 involved applying the best-performing methods to a sub-set of vessels (44 ships) measured at the ULS.

Signal processing methods referred to as "beamforming" and "high-resolution direction of arrival algorithms" were applied to determine the directions of received sounds at the hydrophone arrays of the ULS as ships passed by.

The Boundary Pass ULS consists of two 4-element tetrahedral hydrophone arrays, with hydrophones separated by 1.65 m, positioned 301 m from each other, in line with and mid-way between the in-bound and out-bound shipping lanes. The ULS collected data 24-hours a day, at sampling rate of 512,000 samples per second (10 Hz to 256 kHz recording bandwidth) with 24-bit resolution.

Computational methods were used to calculate the location and amplitude of noise sources based on the arrival of sounds at the hydrophone elements of the ULS. Beamforming and angle of arrival methods were performed using all 8-elements of the two compact hydrophone arrays as a single larger, but sparse array, and using the compact arrays individually to determine the best methods for localization.

What were the key findings?

Part 1 - Localization methods

- While evaluating several methods of beamforming and localization, it was determined that the optimal methods varied by sound frequency.
- Low frequency sounds (below ~300 Hz) were best localized using all eight hydrophones of the two compact arrays as one large sparse array, processed by a standard wideband beamformer.
- The time synchronization accuracy of 1 ms between the two compact hydrophone arrays was the limiting factor for 300 Hz maximum frequency for this method.
- Above ~300Hz, the single four-element hydrophone arrays could be used individually; however, their direction of arrival angle resolution was limited.
- Two additional more advanced “angle of arrival” methods, MUSIC and Capon, were investigated for use at higher frequencies (generally 1 kHz to 10 kHz), both of which showed better resolution.
- Localization was less effective in intermediate frequencies between ~150 Hz to 1 kHz because the compact array hydrophone separations are small relative to the sound wavelengths.

Part 2 – Ship noise localization

- All methods were effective at localizing the loudest noise source to within ~10-15 metres for ships 300 metres or more from the arrays, for frequencies up to 150 Hz.
- A louder (higher amplitude) noise source can mask other, quieter noise sources nearby. If these quieter noise sources dominant in specific frequencies, however, the secondary source can be localized.
- Generally, Part 2 results indicated all frequency components originate from small areas of ships within about 20 m of their stern.
- In half of the measurements from Part 2, two dominant noise sources at the stern of the ships, approximately 10-15 m apart could be identified. These are likely the propeller and the engine.
- The localization methods could not detect other noise sources along the length of the hull, indicating other noise sources are likely masked by louder engine and propeller noise.

Conclusions and next steps

The geometry and hydrophone placement of the Boundary Pass ULS was effective for localizing noise sources using both arrays combined for low frequencies below ~150 Hz, and at higher frequencies above 1 kHz using an individual array. Localization at intermediate frequencies was less effective. Localization effectiveness between 150 Hz and 1 kHz could be improved by increasing the dimensions of each of the compact arrays and by improving their synchronization accuracy.

Most of the vessel noise originates from an area within about 20 metres at the stern of the vessel. In approximately half of the vessels selected for in-depth localization, two separate noise sources at the stern of the vessel could be identified, separated by ~10 metres, likely the propeller and the engine.

The findings of the localization study support previous hypotheses that the majority of underwater noise generated by ships underway is caused by the engine and the propeller, and that these components should be the target of vessel noise reduction efforts.

Localization of Ship Noise Feasibility and Application Study

Using the Boundary Pass Underwater Listening Station Compact Acoustic Arrays

Submitted to:

Krista Trounce
Vancouver Fraser Port Authority
Contract: B-313-2020

Authors:

Ildar R. Urazghildiiev
David E. Hannay

JASCO Applied Sciences (Canada) Ltd
Suite 2305-4464 Markham Street.
Victoria, B.C., Canada, V8Z 7X8
Tel: +1-250-483-3300
Fax: +1-250-483-3301
www.jasco.com

29 October 2021

P001583
Document 02380
Version 1.0 Final

Suggested citation:

Urazghildiiev, I.R. and D.E. Hannay. 2021. *Localization of Ship Noise Feasibility and Application Study: Using the Boundary Pass Underwater Listening Station Compact Acoustic Arrays*. JASCO Document 02380, Version 1.0 Final. Technical report by JASCO Applied Sciences for Vancouver Fraser Port Authority.

Disclaimer:

The results presented herein are relevant within the specific context described in this report. They could be misinterpreted if not considered in the light of all the information contained in this report. Accordingly, if information from this report is used in documents released to the public or to regulatory bodies, such documents must clearly cite the original report, which shall be made readily available to the recipients in integral and unedited form.

Contents

Figures

Tables

Executive Summary

The Vancouver Fraser Port Authority's Enhancing Cetacean Habitat Observation (ECHO) Program supports studies aimed at evaluating noise emissions of shipping activities in the southern Salish Sea. The ECHO Program is collaborating with Transport Canada and JASCO Applied Sciences (Canada) Ltd. to operate an advanced underwater listening station (ULS) in Boundary Pass between the in-bound and out-bound shipping lanes leading to and from the Port of Vancouver. Since June 10, 2020, the ULS has been performing real-time measurements of underwater noise emissions of most passing ships, capturing on average 17 ship passes per day. This system is also tracking ambient noise levels and performing real-time detections of marine mammals 24 hours per day. The ULS is comprised of two compact hydrophone arrays of four hydrophones each as shown in the photograph of Figure 1 below. The arrays can localize sound sources, and the present study has applied that ability to identify where on the passing ships that radiated underwater noise originates. The project has produced noise maps showing spatial distribution of noise emissions intensity along the length and breadth of ship hulls. This report describes the results of a two-part study, involving an initial task of developing and evaluating methods for processing the ULS data to generate high resolution noise maps of ships. The second task applied the best-performing methods from part 1 to 44 ship pass measurements obtained from the ULS in June 2021.

It is presently understood that underwater noise produced by large commercial ships originates from several sources on those ships. The ship's propellers and engines, generally positioned near the stern of the ship, are believed to be responsible for most of the underwater sound radiated by ships travelling at normal operating speeds, although that may not always be true for all vessel categories and at all sound frequencies. Large machinery including the main engines, transmissions, drivetrain, generators, pumps, thrusters, winches, and other equipment also generate vibrations and noise. Water flow past the bow and along the entire area of submerged hull can become turbulent and may produce flow-induced noise either directly or by inducing vibration on parts of the hull. Similarly, turbulence and air bubbles trapped in the wake might be responsible for some noise. The relative intensities of sound energy from these sources are poorly understood, largely because it is very difficult to simultaneously measure and localize the underwater noises while the ships are underway. The Boundary Pass ULS has localizing capabilities that can resolve the spatial distribution of some noises emitted from different locations along ship hulls as they transit past. Specifically, signal processing methods referred to as "beamforming" and "angle of arrival" localization algorithms can be applied to determine the direction of received sounds reaching the ULS's arrays produced by ships passing nearby.

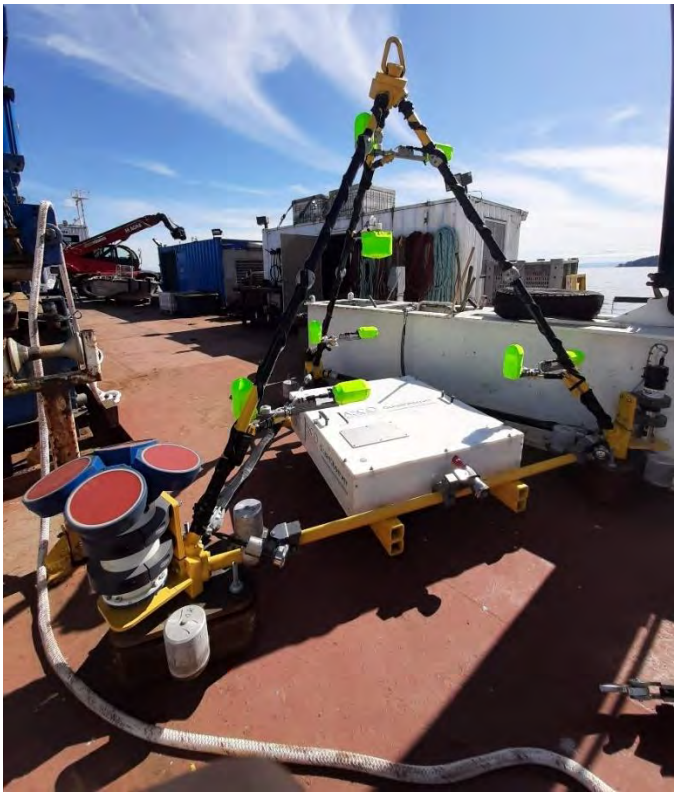

Figure 1. (right) Photograph of one of the two identical ULS hydrophone frames. The hydrophones are inside the green protective shields.

Several methods of beamforming and noise localization were investigated in part 1 of this study, and it was found that the the optimal methods varied by sound frequency. For lower frequency sounds, up to a few hundred hertz, the best performance for localization accuracy was achieved using a standard wideband beamformer (e.g., Haykin 1985), applied to a composite array of 8 hydrophones comprised of all hydrophones on both compact array frames. This approach made use of (and required) the accurate time synchronization (within 1 ms) implemented between the ULS's compact arrays implemented using a custom NTP server. This beamforming can measure the noise intensity of sounds generated by sources anywhere in a 3-dimensional volume surrounding the compact arrays, albeit with several limitations. The sound intensity from a source at any location in this volume is estimated by "steering" the beamformer to that location. Beam steering is the process of changing the listening direction of the main lobe of a beamformer's beam pattern by introducing time delays or phase changes to the signals of the hydrophones of the array. When measuring noise emissions from a ship, the problem is slightly easier because the sound sources are constrained to the ship's hull (and possibly its wake), which can be approximated by a limited planar area close to the sea surface. Noise maps of the hull can be made by steering the beamformer to scan across an area around the ship and record the intensity at each location in the scan. This process is repeated many times as the ship moves past the arrays of the ULS – a processing step found necessary to improve the mapping resolution.

The signals received at the two compact arrays when treated as a single synchronized system were found to lose coherence at higher sound frequencies. Coherence loss occurs due to inhomogeneities in the water along the sound propagation paths that lead to small differences, on the scale of milliseconds, in the times these signals arrive at the hydrophones. The time error caused by the array synchronization difference would be systematic, leading to a uniform localization position shift, and not likely responsible for the type of coherence issues observed. Small time differences are less important for low frequency sounds, but they become a greater fraction of the acoustic wave period as sound frequency increases. As a result, the combined composite array became ineffective above a few hundred hertz. We found that good performance at frequencies above 1 kHz (1000 hertz) could still be obtained, but the approach had to be modified to beamform with the individual compact arrays rather than grouping them into a composite array. The beams of the individual arrays can be steered to listen in each specified direction, but they have limited ability to determine distance. This is less a problem here because the distance of a beam aimed at a ship can be determined by the beam intersection with the sea surface. The beam crossing point is scanned across the area of the hull and the acoustic intensity received at each point is recorded. A full scan of the ship's hull is performed multiple times as the ship passes overhead of the arrays and the results of the multiple scans can be viewed separately or summed to improve the noise map resolution.

A limitation of standard beamforming with small arrays of just a few hydrophones is that the main beamformer lobe width (beamwidth) becomes large, thus limiting the ability to accurately resolve the directions to and locations of sound sources. We investigated two more advanced "angle of arrival" (AOA) estimation algorithms, the MUSIC algorithm and the Capon algorithm (Haykin 1985, Johnson and Dudgeon 1993, Van Trees 2002). Both algorithms can detect the presence of two point sources separated by a half the beamwidth of the standard beamformer. These methods were found to provide a marked improvement in the resolution of the noise maps obtained for sound frequencies above 1 kHz.

All methods implemented here were found to be effective at localizing the loudest noise sources (presumably the ship propellers and engines) to within about 10–15 m for sounds from vessels over 300 m away at frequencies from 5 Hz to 150 Hz. This ability is quite remarkable, but there are important limitations. One limitation of these methods is that they can "leak" energy from the directions of loud sources (e.g., the ship's propellers) to nearby directions that may contain other sound sources (e.g., engines) that may produce lower amplitude sounds. The presence of the louder source can mask other nearby but weaker sources. This problem is partly mitigated by applying these methods in the frequency domain; they can still resolve secondary sources if the weaker source is dominant in at least some frequency bands. Interestingly, the results generally showed all spectral (frequency) components originated from small areas of ships within about 20 m of their sterns. In about half of the measurements there were two dominant sound sources identified, separated by 10–15 m. These separated sources are likely the engines and propellers, since those are commonly mounted 10–15 meters apart (e.g., Figure 2). The "snapshot" views used for beamforming and for AOA methods, were calculated with 1 second time

windows and even smaller snapshot times might be warranted; at 15 knots a ship would have moved approximately 7.5 m during a snapshot time window and this may have reduced the ability to resolve finer scale spatial scales. Nevertheless, the approach was still able to resolve at least two sources separated by about 10 m if they dominated in at least some frequency bands. This finding suggests that nearly all noise from these large commercial ships originated from a limited area close to the propellers and engines. It has very important implications for sound mitigation in ships, because those mitigations may only be needed for the screws and over a small area of the hull.

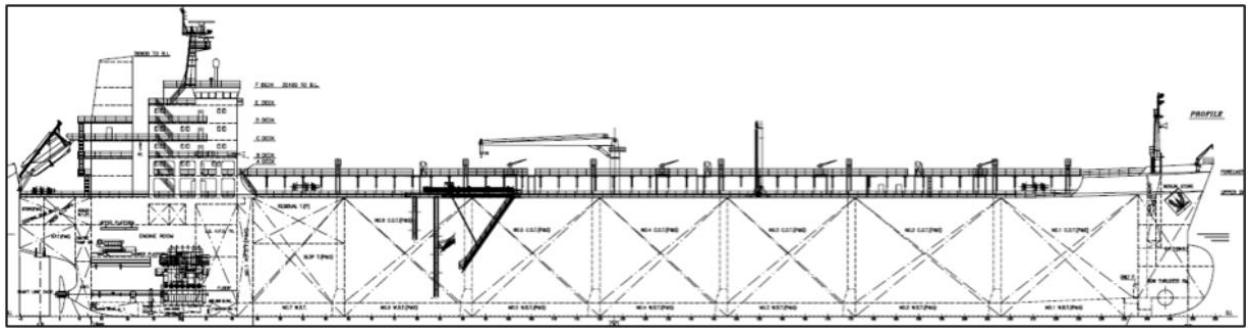

Figure 2. Diagram of a tanker's mechanical geometry to illustrate typical engine placement relative to the ship's propeller.

Some key findings of this project are:

1. The ULS hydrophone geometry of two compact tetrahedral arrays separated by ~300 m was most effective for noise localization at frequencies below 150 Hz. This was achieved by combining the two compact arrays into a single large but sparse array.
2. Above 150 Hz, loss of acoustic signal coherence between the compact arrays led to reduced performance of the combined array beamforming. The coherence loss is attributed to small differences in the signal arrival times at the compact arrays due to ocean inhomogeneities. This does not affect lower sound frequencies with larger periods.
3. At frequencies of 1 kHz to 10 kHz, standard beamforming and the Capon and MUSIC angle of arrival methods provided good localizing ability (to within ~40 m) when applied to the individual compact arrays. This method was not effective below 1000 Hz due to large beamwidths of the individual compact arrays.
4. At low frequencies, less than 150 Hz, beamforming on the combined array would normally lead to poor performance due to a beamforming limitation known as "grating lobes", which causes ambiguity in determining the directions of received sounds. However, the study found that grating lobes could be substantially supressed by averaging results from processing multiple 1-second intervals (snapshots) during each ship pass. The grating lobes move between snapshots, but the primary beam lobe remains in the direction of interest. Therefore, averaging the snapshots significantly enhanced the beamformer primary signal relative to the grating lobes.
5. A further limitation of the localizing methods tested was that a single loud source could mask nearby sources that were quieter. However, the quieter sources could still be resolved well if they were physically separated by a few tens of meters or if they were dominant in at least some frequency bands. In many cases it was clear there were two sources with different dominant frequencies.
6. Very good localizing effectiveness was found for frequencies below 150 Hz, allowing source localization to within 10–15 m along the hulls of ships passing at approximately 200–350 m horizontal distance. The localization abilities from 150 Hz to 1000 Hz were generally reduced by coherence loss as discussed above. Localizing abilities for sound frequencies from 1 kHz to 10 kHz were again good, allowing a spatial resolution of approximately 40 m in that frequency range.

7. The results of applying these localization methods to Boundary Pass ULS data indicate that nearly all noise from these ships originates from a relatively small area of perhaps dimension 20 m close to the stern – likely mainly from their propellers and engines. We did not detect other systematic noise sources near ship bows or in their wakes where turbulence might be found. These sound sources may still be present, but their amplitudes will be much lower than the engine and propeller noise and they are therefore masked.
8. It was hypothesized that engine noise might be localized 10–20 m in front of the propellers, due to their relative forward physical positioning. Two dominant noise sources, typically separated by 10–20 m, were identified near the stern in approximately half the ship passes examined. Often, but not always, the forward source, likely the engine, dominated at the lowest frequencies (less than 20 Hz). The same forward source may produce noise also at higher frequencies, but those would not be visible in the noise maps due to masking by the stronger aft source.
9. The localizing resolution above 1 kHz was not sufficient to identify sources spaced closely (within about 40 m). The results of applying the MUSIC and CAPON methods provided noise source spatial resolution of about 20–50 m, and these results also showed that nearly all noise at higher frequencies originated from near the ship sterns. These results did not discern more than one source on each ship, but again weak sources even near the bows of ships could be masked by the stronger sources near the stern.

1. Introduction

1.1. Background

The Vancouver Fraser Port Authority (VFPA) has supported several initiatives since 2015 that investigate underwater noise emissions of commercial ships, with an end goal of understanding and managing shipping effects on marine wildlife. This has in large part been driven by concern about the effects of anthropogenic noise on the critically endangered Southern Resident Killer Whale (SRKW) population. The major shipping lanes leading to the Port of Vancouver pass through critical habitat for SRKW and these ships, together with the BC Ferries fleet, are the dominant underwater noise producers in that habitat.

In collaboration with several stakeholders, including government, first nations and industry, VFPA through its Enhancing Cetacean Habitat Observation (ECHO) Program continues to support projects that directly measure underwater noise produced by ships visiting the Port of Vancouver. In a collaboration with Ocean Networks Canada and JASCO Applied Sciences, VFPA supported the installation and operation of a cabled underwater listening station (ULS) in Strait of Georgia in September 2015. That station operated into April 2018, collecting several thousand high quality ship noise measurements, and producing the first version of the ECHO ship noise database. In 2018 VFPA commissioned a follow-up study by JASCO and Ocean Networks Canada to explore alternate locations along the major shipping lanes for a new ULS (ONC and JASCO, 2017). That study identified a site in Boundary Pass, south of Saturna Island, as being optimal due to its relatively deep water and because the shipping lanes narrow there, allowing measurements of vessels passing in both directions to be made from a single recording location between the lanes. The ECHO program started a new ship measurement program at that location in summer 2018 using autonomous recorders deployed on the seabed. Working with Transport Canada, VFPA recommended continuation and expansion of that project, and in fall 2018 Transport Canada announced support under their Whales Initiative for a semi-permanent cabled ULS in Boundary Pass. Transport Canada let a contract to JASCO to build a dual hydrophone array based ULS system. The project included support for continuing the ECHO autonomous recorder measurements until the cabled system could be developed and deployed. The Boundary Pass ULS was finally deployed in May 2020 and commissioned June 10, 2020. VFPA has supported the analysis of data from the Boundary Pass autonomous recorders and ULS to obtain radiated noise measurements from ships. These measurements have been added to the ECHO Program ship noise database, which now stores more than 20,000 vessel pass measurements, making it the largest such database in the world.

1.2. General Features of the Boundary Pass ULS

The Boundary Pass Underwater Listening Station is unique due to its use of dual synchronized hydrophone arrays. Water depth at the ULS site is 191 m, which meets ANSI S12.64 (2009) and ISO 17208 standards for ship underwater radiated noise (URN) measurements for ships up to about 130 m in length. The ULS's arrays each consist of 4 operating hydrophones positioned in symmetric tetrahedrons (triangular pyramids) with adjacent hydrophones separated by 1.65 m. The two arrays are deployed on the seabed, separated by 300.5 m approximately parallel to the shipping lanes, so that the closest point of approach (CPA) distance for passing ships is similar at both arrays. A map of the deployment of the arrays relative to ship traffic density is provided in Figure 3, and an illustration of the array geometry relative to a typical passing ship is provided in Figure 4. The array data on all hydrophone channels are digitized with sample rate 512 kHz using 24-bit samples. The raw data were decimated by a factor of 10 prior to further analysis for the 1–10 kHz frequency band, and by a factor of 100 for the analyses below 1 kHz. An automated URN measurement system captures navigation and ship metadata as ships sail past the ULS. That processing system makes use of a cepstral-based techniques to accurately identify CPA times for each compact array, but no further directional analysis using multiple hydrophones is normally performed.

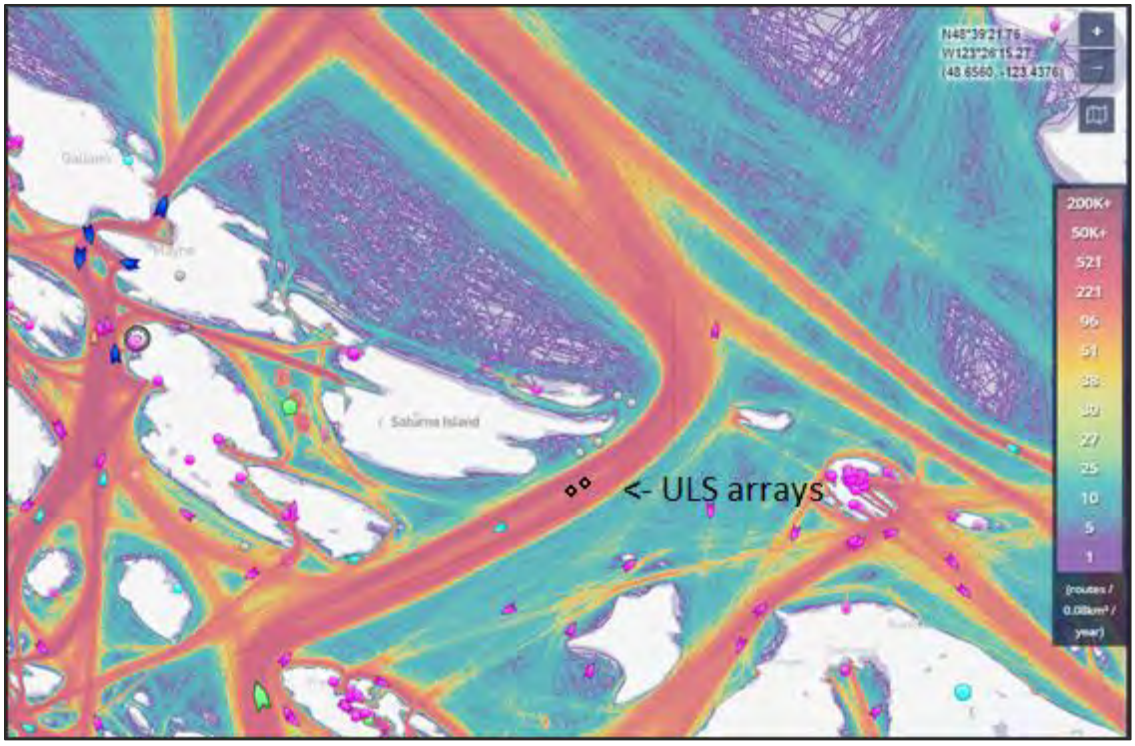

Figure 3. Boundary Pass ULS compact array deployment locations , represented by two black dots, and ship traffic density from Marine Traffic (www.marinetraffic.com). Units of colour are routes per 0.8 km^2 per year.

Figure 4. Illustration of the geometry of the two compact arrays of the Boundary Pass Underwater Listening Station relative to the nominal commercial vessel lane direction, indicated by the ship orientation. Water depth is 191 m at the station and the arrays are separated by 300.5 m.

1.3. Overview of Ship Noise Localization Approaches

The Boundary Pass ULS's dual synchronized arrays were originally intended for localizing the calls of marine mammals to understand their spatial distributions relative to the shipping lanes, and potentially to track animals in real-time near passing ships. It was recognized that the dual array noise localizing abilities could be applied to sounds produced also by ships, and that capability has been exploited in the present study.

In the first part of this study, we evaluated several approaches for estimating the spatial distribution of noise on different parts of a passing ship's hull. We found that different localization methods were optimal in different frequency bands. At lower frequencies (approximately 5–150 Hz) we found that standard beamforming, using both ULS arrays treated as one larger coherent array, provided the best results. This method required averaging many 1-second time snapshots, making use of the forward motions of ships to supress grating lobes in the beam patterns of this sparse array. At higher frequencies (~150–250 Hz) signal coherence becomes lost between the individual ULS arrays and the approach of combining the arrays, that was suitable for lower frequencies, was no longer effective. At these higher frequencies it was still possible to perform beamforming using the four hydrophones on each individual array, but the relatively large beamwidths (e.g., 51.7 degrees at 1000 Hz) provided marginal resolution for noise mapping along ship hulls. In part 1 of this study, we also evaluated two Angle of Arrival (AOA) techniques (Capon and MUSIC) that improve angular resolution of noise sources to within approximately half the standard beamformer beamwidths. These methods produced much better results for frequencies above 1 kHz. The mathematical representations of the beamformer and AOA estimation methods and the array geometry approaches are described in Section 2. These methods were automated and applied to Boundary Pass ULS data for ships passing within 350 m horizontal distance of at least one of the arrays in real-time starting June 1, 2021. The real-time application required less manual work than applying it to the existing recorded data, even though existing data were available back to June 10, 2020. Those previous data are still available and could be used to extend the analysis presented here. On June 17 one of the arrays malfunctioned and the angular resolving capability of the system, at least at low frequencies, was substantially reduced. Nevertheless, in the 17-day period with the automated system working and both arrays operating there were 44 separate ship pass measurements processed by the noise mapping system. Of these, 42 ships made a single pass and two ships passed twice. Noise maps for all of 44 of these ship passes are provided in Appendix A. Results for one ship of each of several vessel categories (vehicle carrier, container ship, bulk carrier, tanker) are also provided in Section 3. The results of mapping for all ships are reviewed and commented on in Table 2 of Section 3. A general discussion of the features of ship noise distributions and a discussion of possible hydrophone array geometry changes that could improve the noise mapping effectiveness is provided in Section 4.

2. Methods

2.1. Approximate Source Positions

The first step of the noise mapping analysis defines a two-dimensional horizontal frame of reference, surrounding a ship's hull, for mapping the distribution of noise sources on the ship. This frame of reference moves with the ship and provides the coordinate system on which its noise maps are produced. An initial estimate of the frame of reference was obtained using ship positions obtained from Automatic Information System (AIS) records sent via VHF transmissions from the ships and received at a receiving station on Saturna Island. The AIS tracks were initially corrected for timing errors, AIS position off-track errors that appear to be randomly distributed, and systematic offsets that were identified with an approximate acoustic ship tracking algorithm. The acoustic tracking approach in this initial step was a broadband time-difference-of-arrival (TDOA) algorithm that is accurate when the ships are close to the arrays. An example of received AIS positions and corrected ship positions for a pass of the bulk carrier are shown in Figure 5. The corrected positions are still approximate at this stage, but they facilitate using smaller search zones for the higher resolution localization analyses methods applied afterwards, making the application more efficient.

Approximate ship positions were defined for a series of consecutive 1.0 second data "snapshots" as each ship passed the ULS, so the time of the start of each snapshot relative to the previous one is $t_{i+1} - t_i = 1.0\ s$. Each snapshot corresponds with the approximate position of the loudest source on the ship (likely the ship's propeller) at the time of the snapshot. A total of K such ship positions, $\boldsymbol{r}(t_1), \ldots, \boldsymbol{r}(t_K)$, were defined for the multiple snapshots over the duration of each ship's pass. The initial snapshot position was set as the closest point of approach (CPA) of the ship to the first array minus half of the ship length, $\boldsymbol{r}(t_1) = \boldsymbol{r}_{CPA1} - 0.5 l_{ship}\boldsymbol{e}$, where the ship length was determined from the Marine Traffic™ ship database. Likewise, the final position was set as close as possible to the ship's CPA to the second array plus half of the ship length, $\boldsymbol{r}(t_K) = \boldsymbol{r}_{CPA2} + 0.5 l_{ship}\boldsymbol{e}$, where $\boldsymbol{e}$ is the unit distance vector in the direction of the ship's course. An example of the approximate corrected ship positions for snapshots of one ship pass are represented by the blue dots in Figure 7 in Section 2.4.

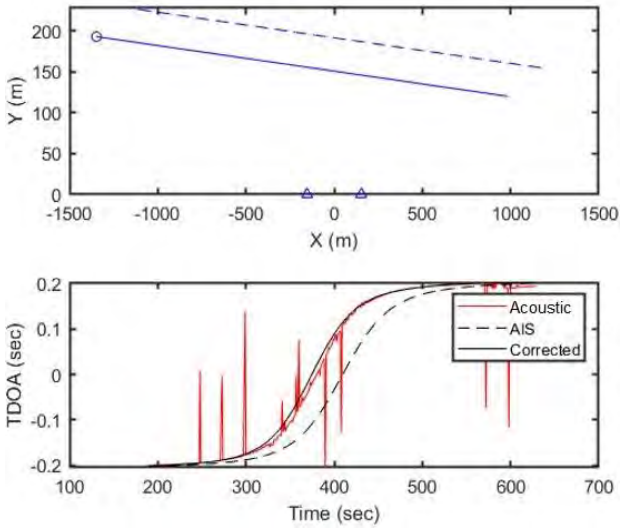

Figure 5. Top: Automatic identification system (AIS) locations (dashed line) and corrected track (solid line) for a Bulk Carrier during a northeast transit. Bottom: the acoustic track from TDOA using both arrays (red); AIS-based TDOA (black dashed line); and corrected track TDOA (solid black line).

2.2. Ship Measurements Selected

Acoustic data from 44 passes of 42 ships (2 ships passed twice) were analyzed for this study. Only large ship categories: Bulk Carrier, Container Ship, Tanker, and Vehicle Carrier were analyzed. Cruise Ships would normally be available for this analysis, but those sailings were curtailed during the study period due to COVID-19 pandemic restrictions. The set of ship passes is listed in Table 1, with ship names and pass times omitted as the ECHO Program treats that information confidentially.

Table 1. List of ship pass measurements selected for analysis. Asterisks on the vessel type indicate the two cases (one Bulk Carrier and one Containership) where the same ships performed two separate passes.

Pass Identifier	Ship type	Length (m)	Breadth (m)	Draught (m)	Closest point of approach (m)	Ground speed (kn)
1	*Bulk Carrier*	292	45	17.3	244	10.3
2	*Container*	210	30	9.1	240	17.1
3	*Container*	349	46	12.6	201	20.4
4	*Bulk Carrier**	190	32	6.9	192	12.9
5	*Bulk Carrier*	229	32	9.2	260	11.8
6	*Bulk Carrier*	235	38	14.6	273	13.1
7	*Container*	363	45	13.1	214	17.2
8	*Bulk Carrier*	228	35	8.9	261	13
9	*Bulk Carrier*	200	31	12.4	1216	14.2
10	*Bulk Carrier**	190	32	13.1	192	13.6
11	*Container*	332	48	12.8	281	19.1
12	*Bulk Carrier*	199	32	12.4	266	14.2
13	*Bulk Carrier*	292	45	16.7	210	13.4
14	*Bulk Carrier*	225	32	7.6	207	13.9
15	*Container*	294	32	11.5	278	18.9
16	*Container*	280	40	13.5	212	17.1
17	*Bulk Carrier*	229	32	7.6	222	14.2
18	*Container*	210	30	8.7	234	20.5
19	*Container*	264	32	10.8	692	21.9
20	*Bulk Carrier*	200	32	7.1	281	11.7
21	*Bulk Carrier*	228	36	7.3	270	10.9
22	*Container***	260	32	11.4	230	14.6
23	*Bulk Carrier*	225	32	14.4	202	12.7
24	*Bulk Carrier*	183	31	10.2	268	12.4
25	*Container***	260	32	9.9	206	18
26	*Bulk Carrier*	229	32	7.0	240	14.8
27	*Bulk Carrier*	199	30	7.8	235	14.2
28	*Container*	224	33	8.5	272	21.1
29	*Bulk Carrier*	199	32	12.7	207	13.7

30	*Container*	304	40	12.3	230	19.1
31	*Bulk Carrier*	229	38	7.8	192	14.2
32	*Bulk Carrier*	229	38	8.1	197	12.6
33	*Vehicle Carrier*	199	32	8.2	209	17.2
34	*Bulk Carrier*	225	33	13.5	244	13.2
35	*Container*	277	40	14.1	193	18.2
36	*Tanker*	277	48	9.6	277	12.9
37	*Bulk Carrier*	182	32	11.3	203	12.7
38	*Bulk Carrier*	180	30	9.5	293	14.9
39	*Bulk Carrier*	180	28	6.6	218	12.6
40	*Bulk Carrier*	171	27	8.9	237	13.6
41	*Bulk Carrier*	185	30	7.4	198	14.3
42	*Bulk Carrier*	292	45	11.8	209	14.1
43	*Container*	347	43	9.5	260	16.9
44	*Bulk Carrier*	225	32	8.0	221	12.9
45	*Container*	209	30	10.3	269	18.5

2.3. Array Geometries

This study analyzed data from all 8 hydrophones of the two 4-element compact arrays of the Boundary Pass ULS. Each compact array has four hydrophones oriented in a symmetrical tetrahedron with hydrophone transducers all separated by 1.65 m (photograph of an array is provided in Figure 1). The arrays are deployed on steel frames that are weighted and rest on the seabed. This geometry leads to the lower 3 hydrophones lying on the vertices of an equilateral triangle in a horizontal plane, 1.2 m above the seafloor, with the fourth (top) hydrophone centred above the lower three, approximately 2.4 m above the seafloor. The two arrays are deployed 300.5 m apart, between and parallel to the inbound and outbound shipping lanes in Boundary Pass, as shown in the map of Figure 3. An illustration of the geometry including a ship passing overhead is provided in Figure 4.

In Part 1 of this study, three hydrophone geometry combinations were examined:

- A single combined array of 8 hydrophones. This approach is possible because the two compact arrays are time synchronized to within 1 ms.
- Two independent arrays of 4 hydrophones each.
- A virtual array of many hydrophones that makes use of ships' movement past the fixed stationary hydrophones.

The examination of these configurations found that the combined array and virtual array analysis provided nearly identical results for the low-(5–150 Hz) and mid-(100–1000 Hz) frequency bands defined here. These approaches however were not useful above 300 Hz due to loss of signal coherence between the two compact arrays. The final geometries implemented for analyzing a larger number of ship passes were as follows:

1. Localization of low- (5–150 Hz) and mid-frequency (100–1000 Hz) noise sources was performed by beamforming using all 8 hydrophones of the combined array.
2. Localization of high-frequency (1000–10000 Hz) noise sources was performed by beamforming and AOA estimation separately on both compact arrays.

2.4. Processing Low and Mid-frequencies – Combined array

Noise maps of low- and mid-frequency noise sources were produced using standard coherent beamforming of all hydrophones of both arrays treated as a single larger array of 8 hydrophones. The spatial spectrum computed using a wideband beamformer (BF) for the position $\boldsymbol{r}$, time t, and frequency f, is:

$$S_{BFC}(\boldsymbol{r}, f, t) = \|\boldsymbol{a}_C^H(\boldsymbol{r}, f)\boldsymbol{P}_C(f, t)\|^2 , f \in B,\ \boldsymbol{r} \in U_C(t), t \in U_t. \quad (1)$$

where B is the set of low- and mid-frequencies; $\boldsymbol{a}_C(\boldsymbol{r}, f)$ is the 8-dimensional steering vector of the combined array; $\boldsymbol{P}_C(f, t)$ is the covariance vector of ship noise on the normalized spectral outputs of 8 channels of the combined array; $U_C(t)$ is the search area of the combined array at time t; U_t is the observation interval; and symbol "H" denotes Hermitian transpose. Figure 6 shows an illustration of the positions of a ship at 4 time samples, $t \in \{t_1, \ldots, t_4\}$ to illustrate the approach for the combined array. Solid lines originating from the combined array center represent the directions (actually the focus points $\boldsymbol{r}$) of the set of beams specified by the steering vectors $\boldsymbol{a}_C(\boldsymbol{r}, f)$ used to compute the BF spectra (1).

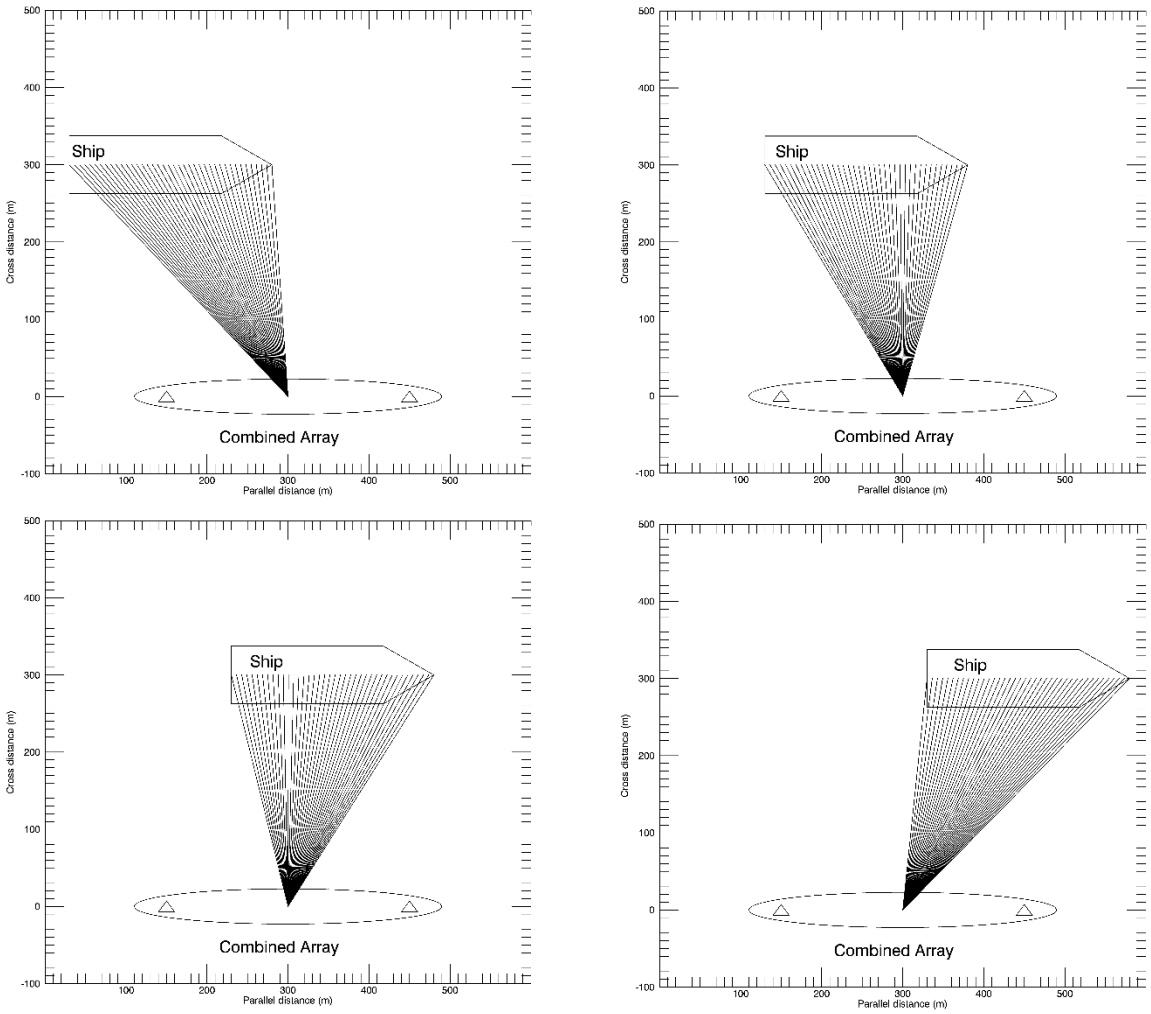

Figure 6 Illustration of the positions of a ship, with directions of beams computed by the BF (1) from the combined array approach at four times during a ship pass. For brevity, these diagrams show only the set of beams along the ship's centre, but several rows of these beams were implemented to map a 100 m wide swath along the ship path. The individual compact array locations are indicated by the triangles.

The BF output (1) was computed at multiple times (or snapshots), $t \in U_t = \{t_1, \ldots, t_K\}$, corresponding to K different ship positions. The time difference between consequent snapshots was $t_{i+1} - t_i = 1.0\ s$. Figure 7 shows the AIS-based coordinates locations (black x's) and estimated positions of a ship's dominant noise source (solid black line). Each BF output in the 1 s snapshots was estimated by applying the BF (1) to 20 rectangular time widows of 0.1 s each, with 0.05 s overlap, and averaging the responses. BF responses in the frequency domain therefore had a resolution of approximately 10 Hz.

The ship (dominant source) positions at times t_i, $\boldsymbol{r}(t_i), i = 1 \ldots K$, were used to reference the BF output (1), and are represented by blue dots in Figure 7. Red dot shows the ship position at closest point of approach (CPA) to the combined array center, $r_{CPA} = r(t_{CPA})$, which is equidistant between the compact arrays A and B. For each time sample, the position $\boldsymbol{r}(t_i)$ was chosen as the center of the localization search area. The search area, $U_C(t_i)$, was specified as a rectangle oriented along the ship's course vector. The boundaries or the rectangle in the longitudinal direction (the length dimension of the search area) were $[\boldsymbol{r}(t_i) - 100\ m, \boldsymbol{r}(t_i) + l_{ship}\boldsymbol{e} + 150\ m]$, where l_{ship} is the ship length and $\boldsymbol{e}$ is the unit distance vector in the direction of the ship's course The boundaries in transverse direction were $\boldsymbol{r}(t_i) \pm 50\ m$ so the width of the search area is therefore 100 m. The search area corresponding to the time t_{CPA}, $U_C(t_{CPA})$ is shown in Figure 7 by the blue dashed line.

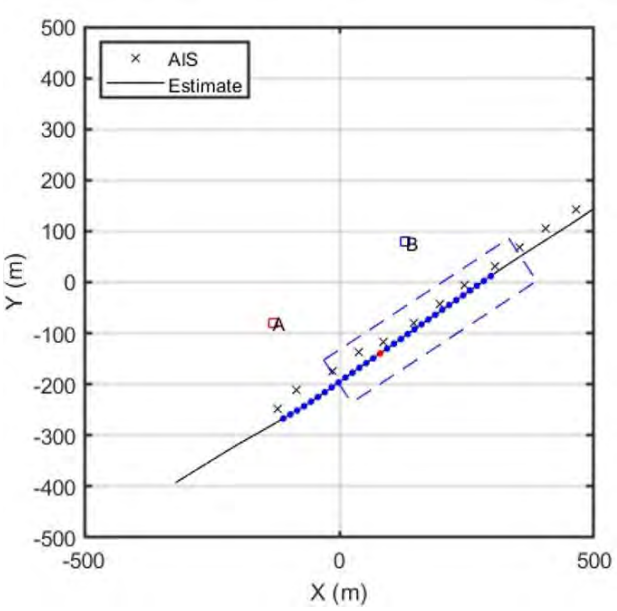

Figure 7. Automatic identification system (AIS) locations (black x's) and corrected track (solid black line) for a Bulk Carrier during its northeast transit. Blue dots display the ship snapshot positions, $\boldsymbol{r}(t_1), \ldots, \boldsymbol{r}(t_K)$ determined by the beamformer in 1 second time steps. The red dot indicates the snapshot closest to the midpoint of Arrays A and B, and this is approximately the position of the ship's propeller relative to the localization search area, represented by the dashed blue outlined rectangle. This area is 100 m wide and equal to the ship length plus 250 m (from 100 m behind to 150 m in front). The ship search areas at other times (and other ship positions) are automatically translated to this reference area that can be considered as moving with the ship. All noise maps are therefore referenced to this zone.

The 3D noise maps in the spatio-frequency domain were calculated by summing the beamformer outputs (1) over all K time snapshots associated with the ship:

$$P_{BFC}(\boldsymbol{r}, f) = \sum_t \; S_{BFC}(\boldsymbol{r}, f, t). \tag{2}$$

The 2D noise maps in the spatial domain were computed by summing the noise maps (2) over all frequencies:

$$G_{BFC}(\boldsymbol{r}) = \sum_{f \in B} P_{BFC}(\boldsymbol{r}, f). \tag{3}$$

The 2D vector $\boldsymbol{r}$ can be represented in a new ship-based coordinate system with the origin specified by the ship position at CPA point, $\boldsymbol{r}_{CPA} = \boldsymbol{r}(t_{CPA})$, (see red dot in Figure 7), and with the axes placed in longitudinal and transverse directions relative to the ship's hull, such that, $\boldsymbol{r} = \left[R_{long}, R_{transverse}\right]^T$. Then 3D noise maps (2) can be represented in the ship-based coordinate system as $P_{BFC}\left(R_{long}, R_{transverse}, f\right)$. The map can also be converted into another 2D noise map representing the distribution of noise sources in only the ship's longitudinal direction and frequency,

$$P_{BFC}\left(R_{long}, f\right) = \max_{R_{transverse}} P_{BFC}\left(R_{long}, R_{transverse}, f\right). \tag{4}$$

Correspondingly, the 2D noise map $G_{BFC}(\boldsymbol{r})$ (3) can be transformed into a 1D noise map representing sum of noise intensities over all frequencies along the longitudinal position on the ship,

$$B_{BFC}\left(R_{long}\right) = \max_{R_{transverse}} G_{BFC}\left(R_{long}, R_{transverse}\right). \tag{5}$$

The noise maps (4) and (5) are referenced to the loudest source on the ship, such that the point $R_{long} = 0$ likely corresponds to the ship's propeller.

Figure 8 (top panels) presents a theoretical 2D noise map $P_{BFC}\left(R_{long}, f\right)$ (4) in the spatio-frequency domain computed for a modelled single source with uniform frequency spectrum below 1 kHz at location (0,0). The results are shown in two frequency ranges: 6 to 150 Hz and 100 to 1000 Hz. Figure 8 (middle panels) show the noise maps in the spatial domain only (3), $G_{BFC}\left(R_{long}, R_{transverse}\right)$. The bottom panels of Figure 8 show 1D noise maps (5) indicating intensity versus position ahead of the ship's dominant source (longitudinal direction, R_{long}). Figure 9 shows the same plots for the case of two modelled sources, with equal intensity, separated by 50 m. Figure 10 shows the BF response when the intensity of the second source is 3 dB lower than that of the first source. Figure 11 presents the BF response for the case of three modelled sources with coordinates [0; 0], [0, 50] and [0, 150] m. The intensity of the second and third sources are 3 dB lower than that of the first source.

The theoretical results presented in Figures 8 to 11 demonstrate that the developed BF-based technique implemented on the 8-channel combined array should be able to accurately resolve the locations of several point sources. The spatial resolution, i.e., the ability to localize point sources, depends on their spectral properties (relative amplitudes and frequency content). The theoretical spatial resolution for wide-band sources generally increases as frequency increases. However, the ability to resolve secondary sources is reduced when there is a dominant source present nearby with greater intensity, by more than approximately 2 dB, in the same frequency bands. Secondary sources can be missed altogether if their intensity is much below that of the dominant source at all frequencies.

The frequency domain results (top panels of Figures 8 to 11) show a strong response at the correct longitudinal position but also include grating lobe patterns. The positions of the grating lobes vary with frequency and are largely averaged out in the wide-band results (middle panels). The grating lobes can also be suppressed by averaging the BF output computed for several ship view angles (snapshots); see Figures 8 to 11, middle and bottom panels. At frequencies above a few hundred hertz, the signal is theoretically localized with high resolution, but this result depends on coherence of the signal between the two arrays. Coherence was found to be lost above 300 Hz on the compact arrays with 300.5 m separation.

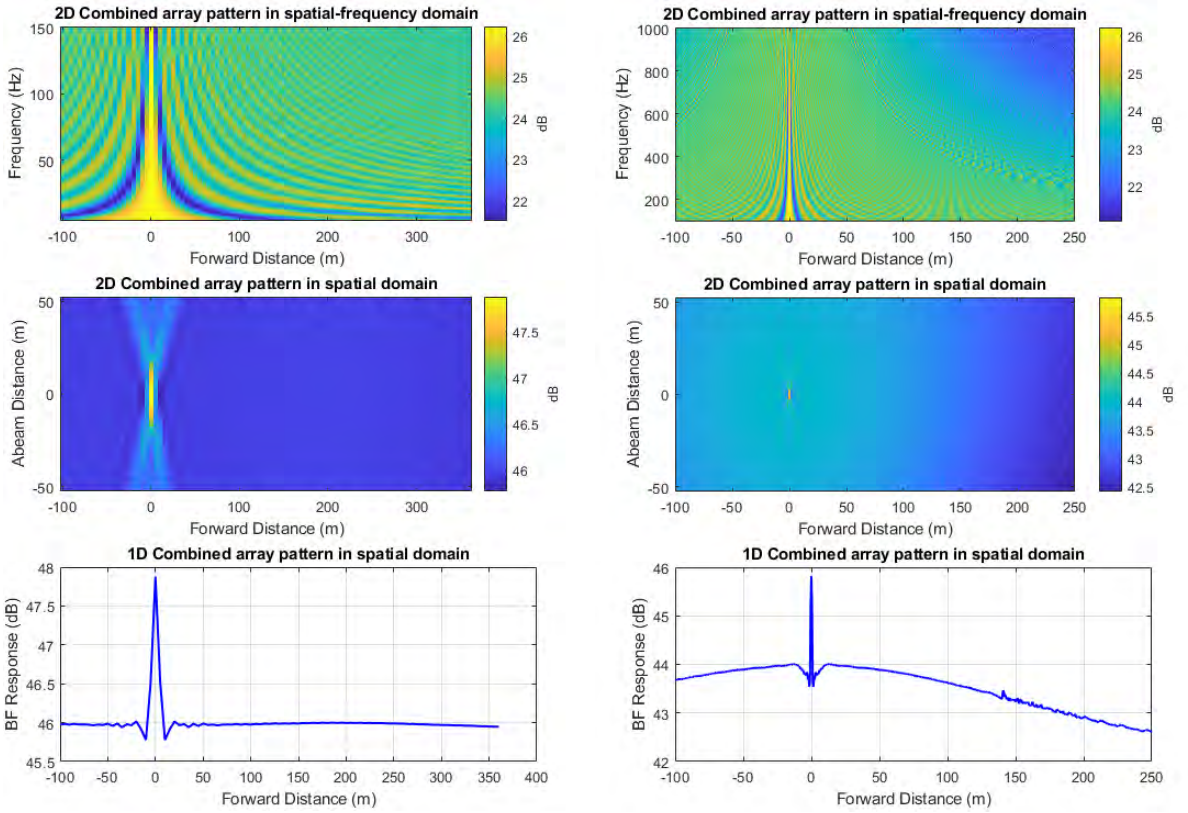

Figure 8. Theoretical beamformer response for the combined array to a single modelled source over the frequency ranges 6 to150 Hz (left) and 100 to1000 Hz (right). The intensity scale in the upper plots is unreferenced decibels.

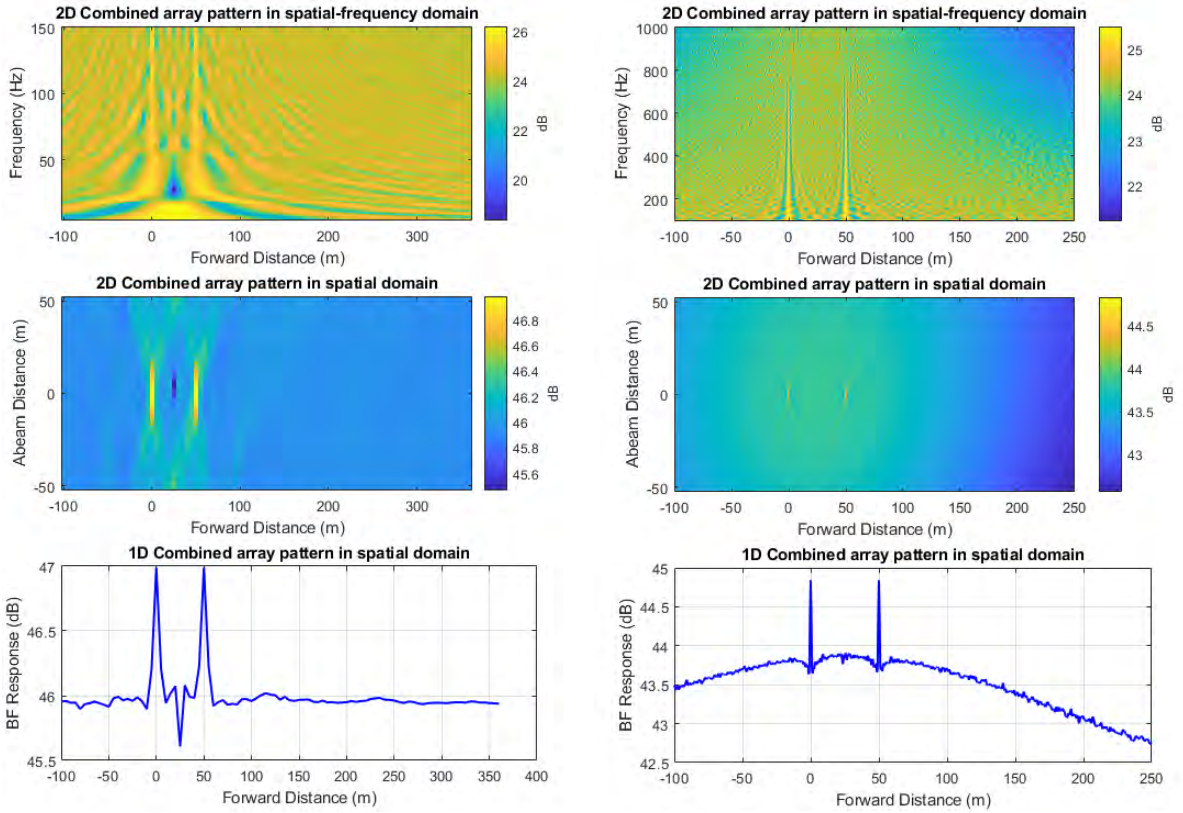

Figure 9. Theoretical response of the combined array beamformer for two modelled sources with the same intensity separated by 50 m over the frequency ranges 6 to150 Hz (left) and 100 to1000 Hz (right). The intensity scale in the upper plots is unreferenced decibels.

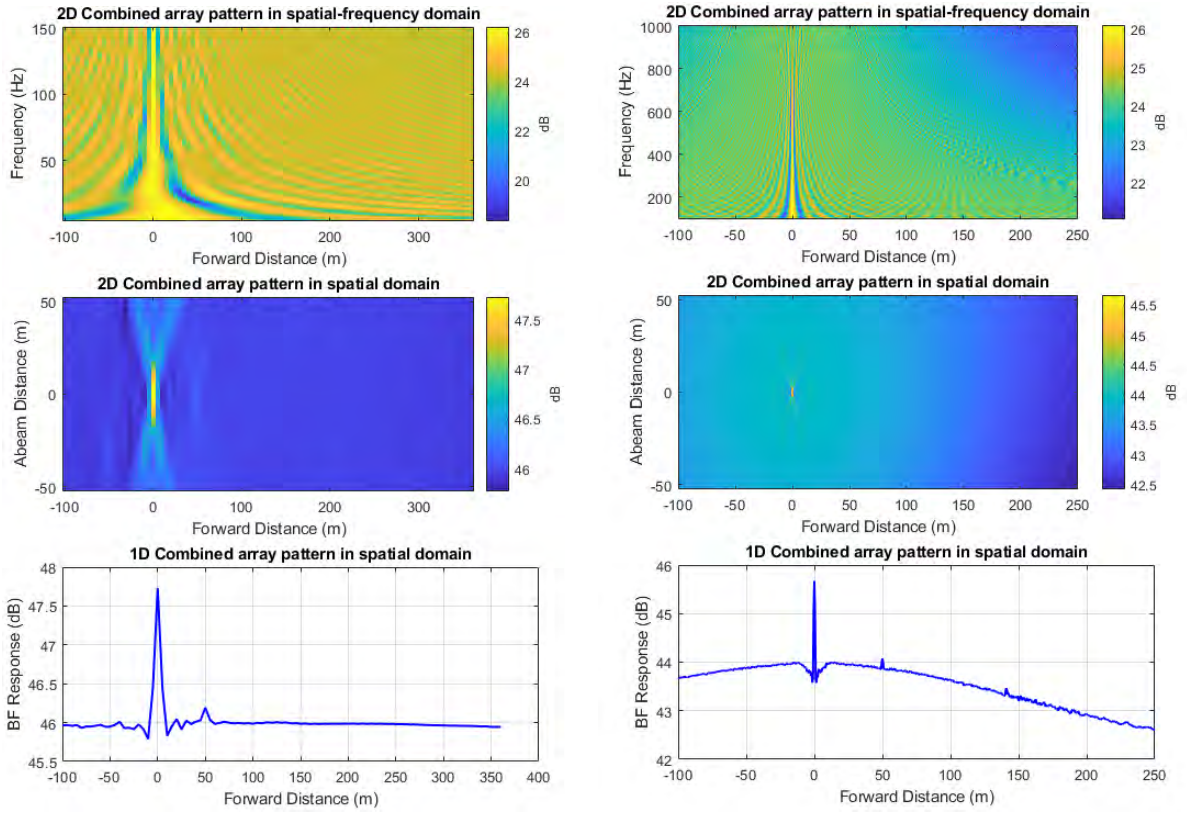

Figure 10. Theoretical response of combined array beamformer response for two modelled sources, with different intensities, separated by 50 m over the frequency ranges 6 to150 Hz (left) and 100 to1000 Hz (right). The intensity of the forward source is 3 dB lower than that of the aft source.

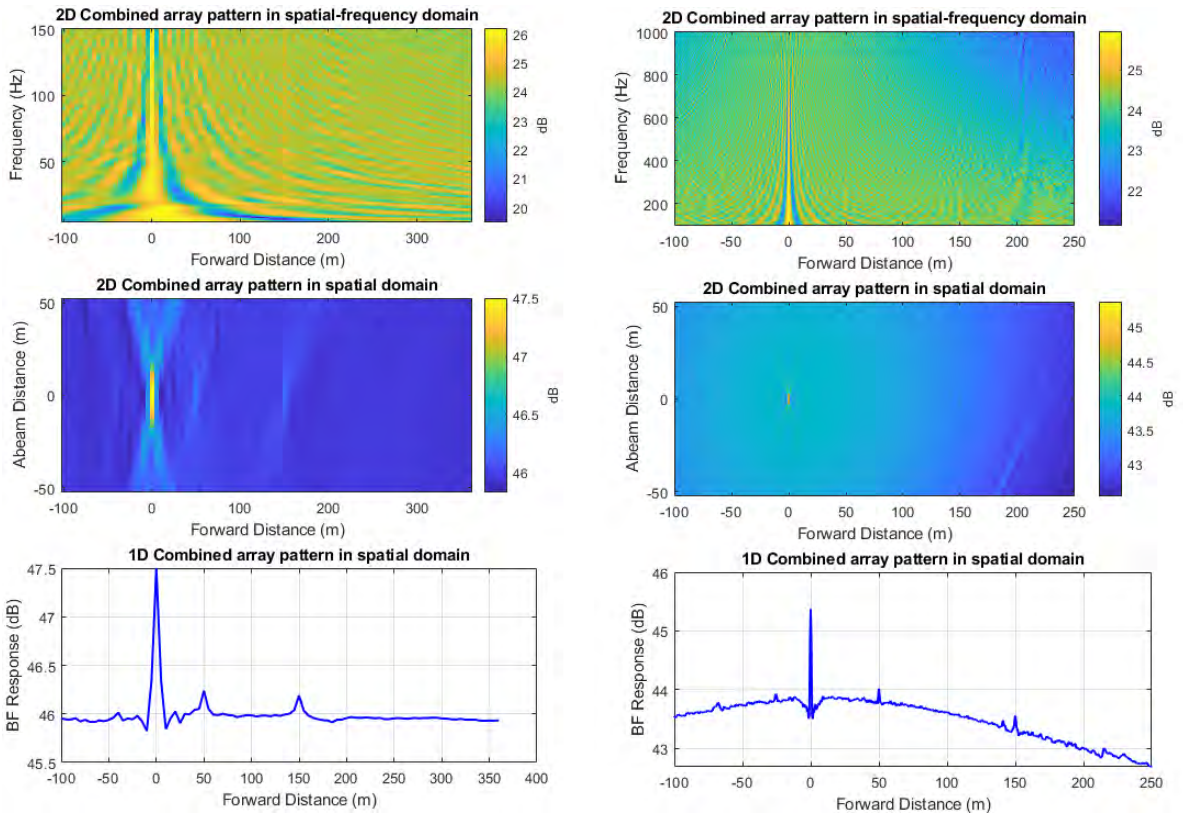

Figure 11. Theoretical response of the combined array beamformer for three modelled sources with different intensities over the frequency ranges 6 to150 Hz (left) and 100 to1000 Hz (right). Source coordinates are [0; 0], [0, 50] and [0, 150] m. The intensities of the middle and forward sources are 3 dB lower than the intensity of the aft source.

An example of the BF output with real ship data, $P_{BFC}(R_{long}, f)$, $G_{BFC}(R_{long}, R_{transverse})$, and $B_{BFC}(R_{long})$ is presented in Figure 12. Differential Doppler shifts were computed with the expected radial speeds of the ship relative to the individual hydrophones and these were accounted for in the MF band by the beamformer. The radial speed is the component of a ship's velocity in the direction of the hydrophone relative to the ship. The effect of Doppler shift on the low frequency band was negligible. The low frequency response at less than 150 Hz is similar to that of the modelled source (Figure 8) but higher frequency response for localization resolution is much poorer. This is likely due to reduced signal coherence at higher frequencies. Nevertheless, the approach has some localizing power over the full 100 Hz – 1000 Hz band but it would not be sufficient to resolve multiple sources separated by less than about 50–100 m.

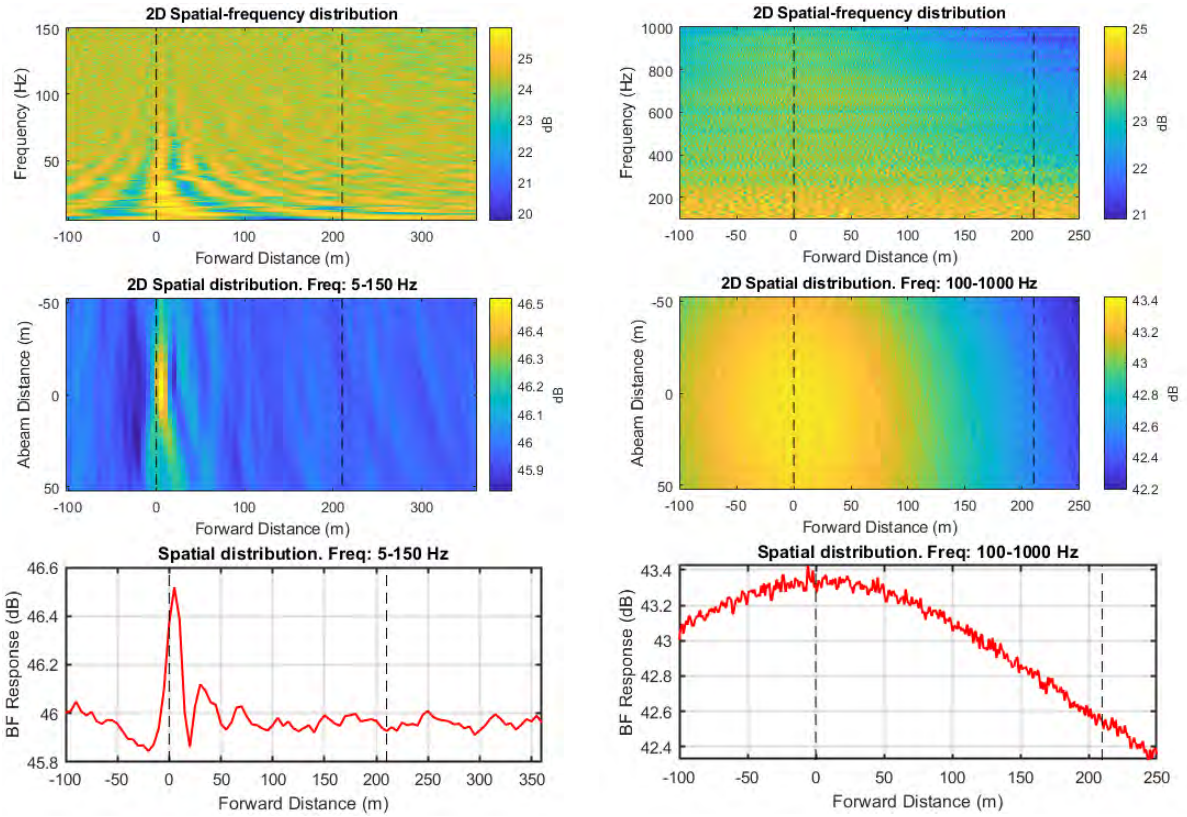

Figure 12. Noise maps: 2D maps in spatial-frequency domain (top); 2D maps in spatial domain (middle); and 1D map relative forward distance (bottom) for data from a real ship pass. Frequency range is 5 to150 Hz (left) and 100 to1000 Hz (right). The vertical dashed lines represent the positions of the stern and bow of the ship.

Figure 12 shows the noise maps for a real ship pass. This result suggests the presence of a single dominant source (propeller) located near the stern of the ship. The result demonstrates the quite good ability of the combined array approach to localize a noise source on the ship at low frequencies (5–150 Hz) and the reduced resolution at higher frequencies (100–1000 Hz). Other point sources are not clearly visible on the noise maps because they are either not present or their levels are lower than those of the dominant source and they are masked by that source. The real ship noise maps of Figure 12 are similar for the 5–150 Hz frequency band to corresponding theoretical results in Figure 10. However, the 100–1000 Hz real ship results are clearly inferior to the corresponding theoretical result. This is attributed to loss of signal coherence between the two arrays at higher frequencies as discussed previously.

2.5. Processing High-Frequencies – Individual Arrays

Localization of HF (1–10 kHz) noise sources was not possible using the combined array because the ship noise received by hydrophones of the two arrays had lost coherence at frequencies above approximately 250 Hz. Instead, HF band noise maps were calculated by beamforming the 4 hydrophones of each compact array independently. To improve angular resolution, we implemented two angle-of-arrival (AOA) estimation techniques in addition to the standard wideband beamformer (Haykin 1985, Johnson and Dudgeon 1993, Van Trees 2002, Urazghildiiev et al. 2021). As in the case of combined array, the spatial spectrum computed using the wideband BF for the position $\boldsymbol{r}$, time t, and frequency f, is

$$S_{BFA}(\boldsymbol{r}, f, t) = \|\boldsymbol{a}_A^H(\boldsymbol{r}, f)\boldsymbol{P}_A(f, t)\|^2, f \in B, \ \boldsymbol{r} \in U_A(t), t \in U_t. \quad (6)$$

Here B is the set of high frequencies; $\boldsymbol{a}_A(\boldsymbol{r}, f)$ is the 4-dimensional steering vector of the single array; $\boldsymbol{P}_A(f, t)$ is the covariance vector of ship noise on the outputs of 4 channels of the array; U_t is the observation time interval; and $U_A(t)$ is the search area of the individual array at time t.

Figure 13 shows an illustration of the positions of a ship at 4 time samples, $t \in \{t_1, \ldots, t_4\}$. Solid lines originating from the individual array centers show the directions of beams specified by the steering vectors $\boldsymbol{a}_A(\boldsymbol{r}, f)$ used to compute the BF spectra (6).

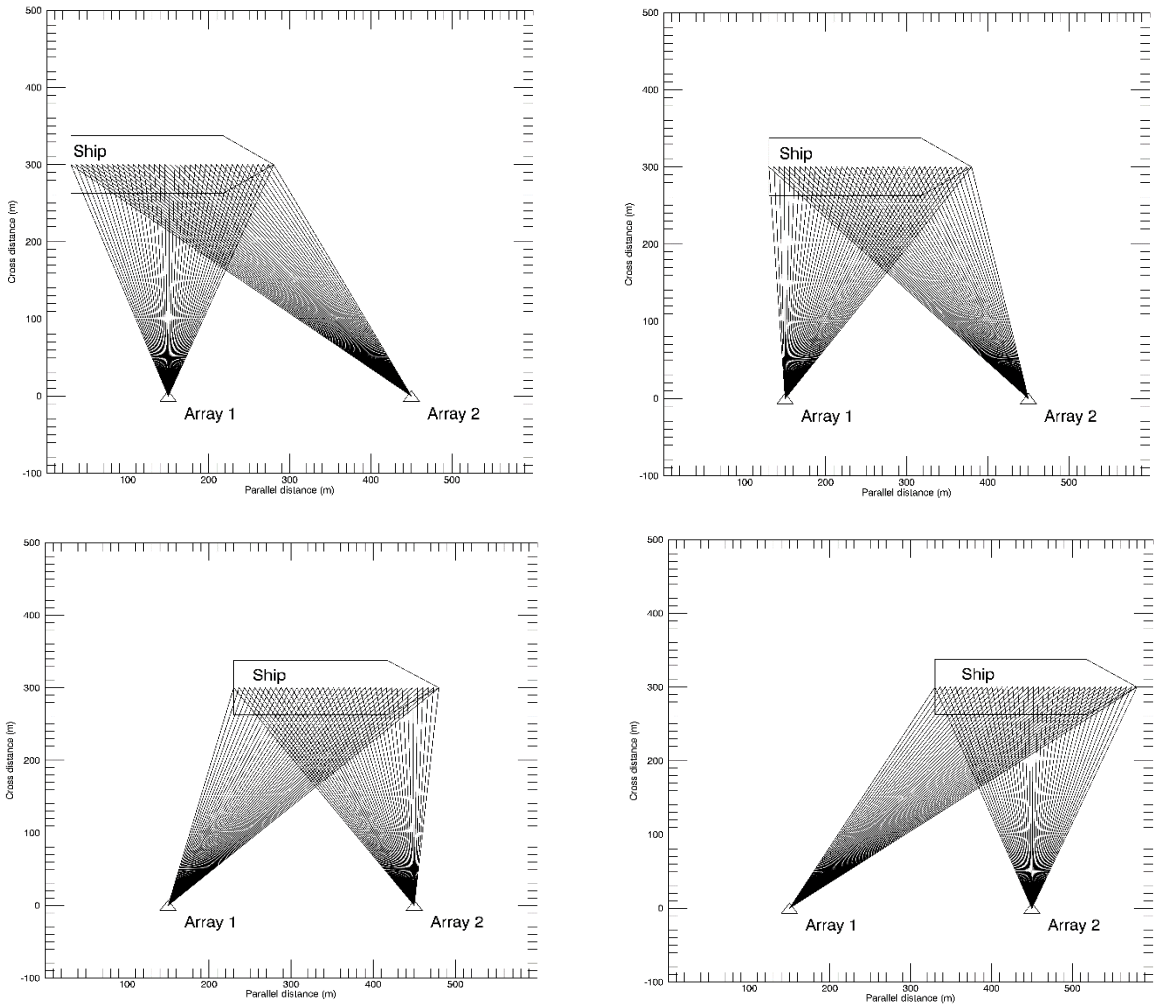

Figure 13. Illustration of the positions of individual beams (represented by single black lines) used to compute the BF spectra (6) at different time samples, t Multiple beams originate from each of the two arrays for each time sample.

The BF spectrum (6) was computed for the same K time samples, $t \in U_t = \{t_1, \ldots, t_K\}$, as the BF spectrum (1) of the combined array. The time difference between consecutive snapshots was $t_{i+1} - t_i = 1.0\ s$. For each time sample, the position $\boldsymbol{r}(t_i)$ was chosen as the center of the search area. Because individual compact arrays are small relative to array-to-ship distances, the accurate measurement of array-to-source distances using each array independently was not possible. Therefore, for individual arrays, the noise localization processing neglected the dimension perpendicular to the ship track. The search area the search area, $U_A(t_i)$, was specified as a line oriented along the ship's course vector, such that $S_{BFA}(\boldsymbol{r}, f, t) = S_{BFA}(R_{long}, f, t)$. The boundaries of the line in the longitudinal direction (the length of the search area) were $[\boldsymbol{r}(t_i) - 100\ m, \boldsymbol{r}(t_i) + l_{ship}\boldsymbol{e} + 150\ m]$, where l_{ship} is the ship length and $\boldsymbol{e}$ is the unit distance vector in the direction of the ship's course.

The choice of the search area for an individual array is illustrated in Figure 14. The left panel of this figure shows the position of the array, AIS-based coordinates of the ship (black "x"), and corrected positions of the stern (black dots). Blue dots show the positions of the stern over the observation interval, $\boldsymbol{r}(t_i), t_i \in U_t$. The position of the propeller at the beginning of the observation interval, $\boldsymbol{r}(t_1)$, is shown by blue "Δ". Red dots show the positions of the bow, $\boldsymbol{r}(t_i) + l_{ship}\boldsymbol{e}, t_i \in U_t$. The position of the bow at the beginning of the observation interval, $\boldsymbol{r}(t_1) + l_{ship}\boldsymbol{e}$, is shown by red "Δ". The centres of the search area $U_A(t_i)$ correspond the the ship's stern positions, $\boldsymbol{r}(t_i)$, and are shown by blue dots. Black symbols "○" show the boundaries of the of the search area. The right panel shows the azimuths of the stern (blue) and bow (red). Black lines indicate the boundaries of the search area in azimuth and time domain, respectively.

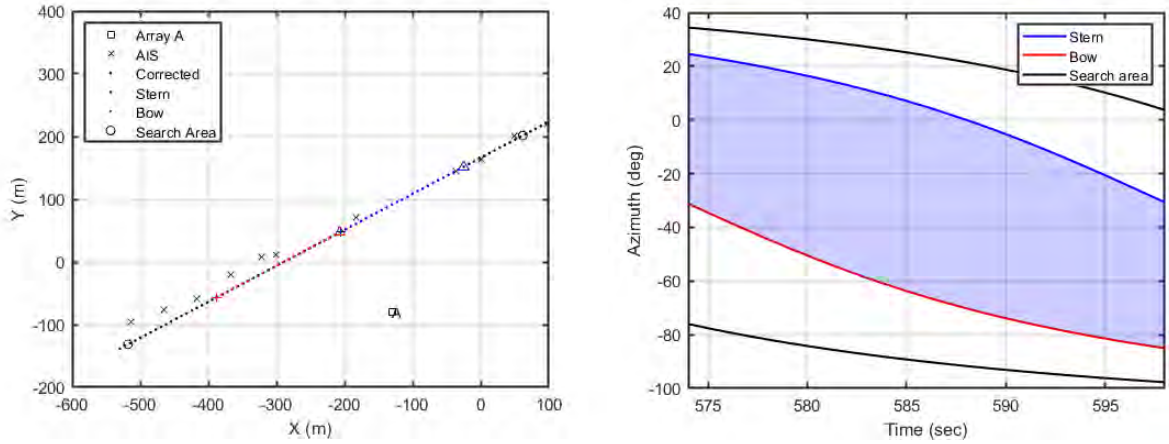

Figure 14. Left: AIS locations (black x's) and corrected track (black dots) for a Bulk Carrier during its northeast transit. Blue dots display the ship's stern positions, $\boldsymbol{r}(t_1), \ldots, \boldsymbol{r}(t_K)$, over the observation interval. Red dots show the bow positions for the same time snapshots. Right: azimuths of the stern (blue) and bow (red). Black lines show the boundaries of the search area in azimuth and in time.

Optimal performance for beamforming occurs when the hydrophone spacing is approximately half of one acoustic wavelength, but good performance is usually obtained for approximately a frequency decade centred at that frequency. Beamforming at frequencies with wavelengths smaller than twice the hydrophone spacing leads to the existence of “grating lobes” which admit sound energy from angles different than the steering direction, and therefore can lead to ambiguous sound source localizations; the grating lobes of the beamformer beam pattern point in directions different than the main lobe steering direction, so it is not possible to know if the sound source is located in the main lobe direction or in the directions of one or more of the grating lobes. The half wavelength frequency of the ULS’s compact arrays is 440 Hz, so within the frequency range from 1000 to 10000 Hz the arrays patterns contain multiple grating lobes (see Figure 15). As in the case of combined arrays, the grating lobes were suppressed by averaging the BF spectra (6) in time, as the ship moves past the arrays, and through frequency. This averaging enhances the main BF beam because the main beam at the steering angle remains constant while the grating lobes change position with frequency and beam steering angle. Figure 15 shows the enhancing effect of averaging over frequency.

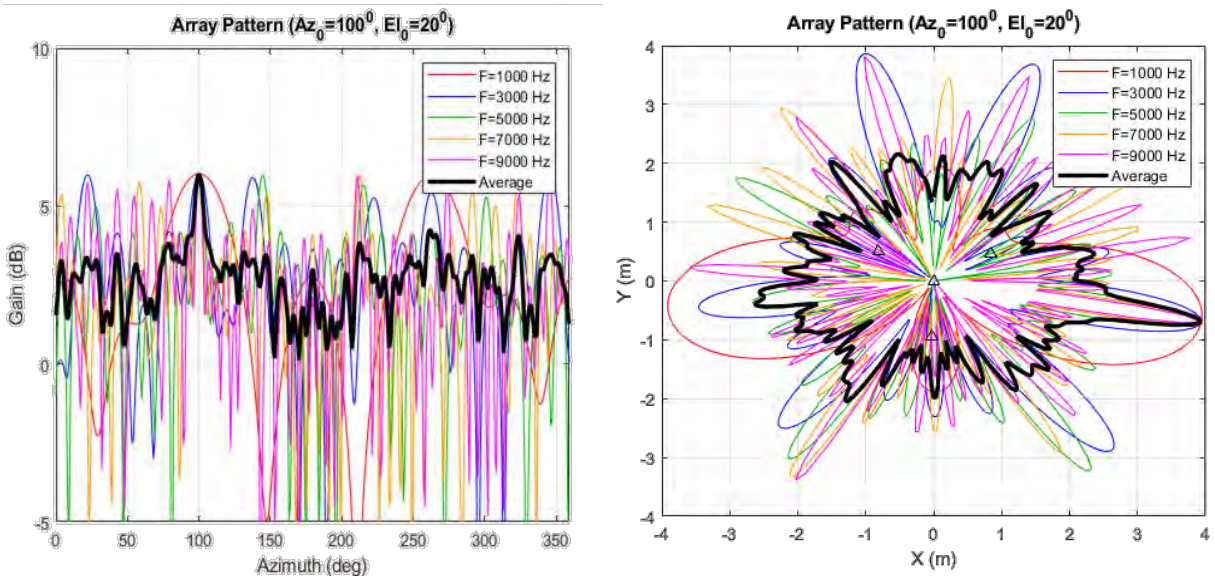

Figure 15. Horizontal beam patterns (theoretical) for the individual ULS compact arrays in rectangular coordinates (left) and in polar coordinates (right) for several frequencies between 1000 and 10000 Hz. The beam steering angle here is 100° in azimuth and for an elevation angle of 20°.

Figures 16 and 39 present the theoretical individual array beamformer response for a single modelled source over the frequency range 1 kHz to10 kHz. Figure 18 shows the BF response for two modelled sources separated by 100 m. Its left panel shows the case of sources with equal intensities, and right panels shows the response of the second source intensity set 10 dB lower than that of the first source.

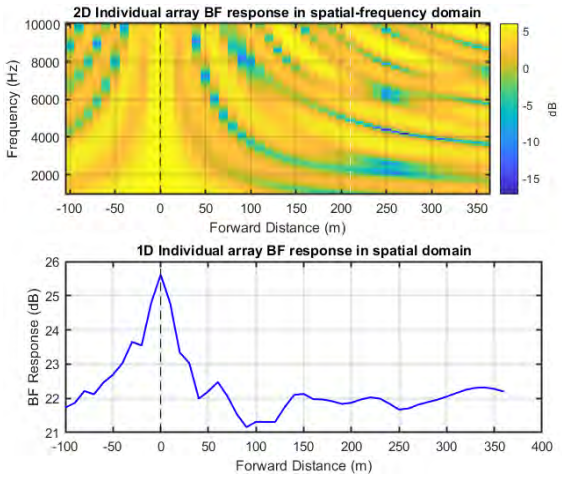

Figure 16. Theoretical beamformer response for a single compact array to a single modelled source over the frequency ranges 1 to10 kHz. The intensity scale in the upper plots are unreferenced decibels.

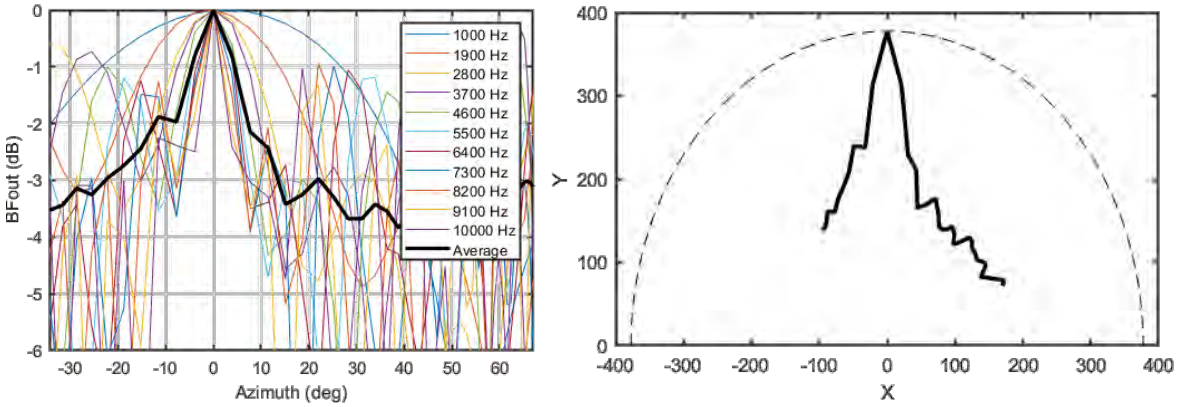

Figure 17. Left panel: theoretical BF response versus azimuth angle of individual compact arrays at several frequencies between 1 kHz and 10 kHz, with average. Right panel: polar plot of average of BF response 1 to 10 kHz vs azimuth.

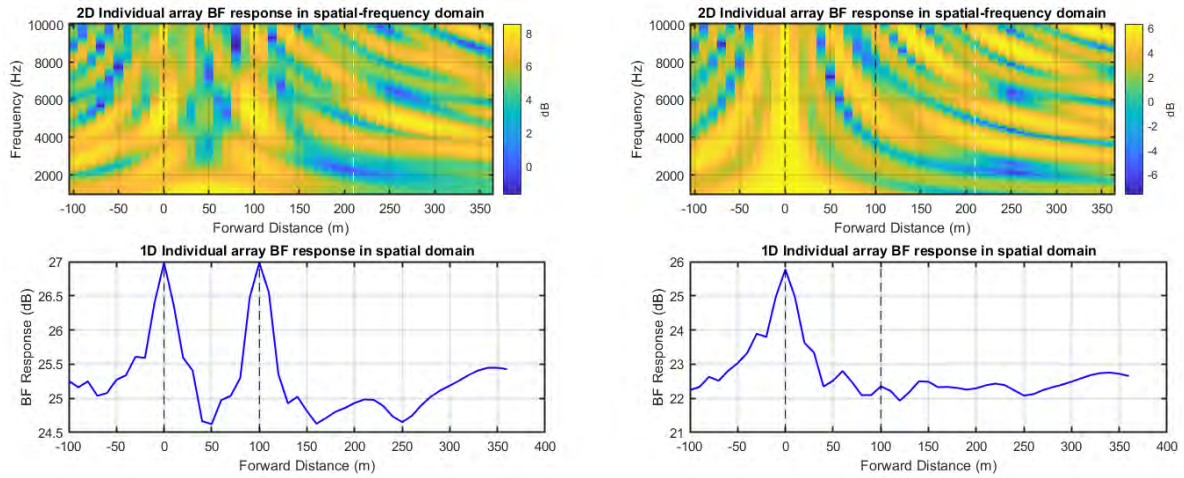

Figure 18. Theoretical individual array beamformer response for two modelled sources separated by 100 m over the frequency ranges 1000 to10000 Hz. Left: source intensities are equal. Right: the intensity of the second source is 10 dB lower than the intensity of the first source.

These results demonstrate that the BF technique implemented on the single array can accurately resolve two or more point sources of similar intensity. However, as in the case of combined arrays, the presence of a single dominant source (such as the propeller) reduces the ability to resolve other nearby sources at the same frequencies.

The frequency domain results (Figure 16, top panel) show a strong response at the correct position of the point source but also include grating lobes that can reduce the resolution of other nearby sources. The grating lobes were suppressed by averaging the BF output computed for several ship view angles (snapshots) or averaging over frequency (Figure 16, bottom panel).

Similarly to (2), the 2D noise map in spatio-frequency domain representing distribution of noise sources along the position relative to ship (longitudinal direction) and frequency was computed as

$$P_{BFA}(R_{long}, f) = \sum_t S_{BFA}(R_{long}, f, t). \quad (7)$$

In addition to (7), we also computed the noise map in time domain by summing the spectrum (6) over multiple frequencies for each time sample, t:

$$Q_{BFA}(R_{long}, t) = \sum_{f \in B'} S_{BFA}(R_{long}, f, t), \quad (8)$$

where $B' \subseteq B$ is a sub-set of frequencies within the HF band B.The noise map (8) shows the spatial distribution of noise sources producing sounds within sub-set of frequencies, B', relative to the position of the dominat source, $\boldsymbol{r}(t)$, measured at different ship positions relative to arrays.

Noise map examples provided by the BF estimator with real ship pass signals are shown in Figure 19. Top panels show the spatial distribution $P_{BFA}(R_{long}, f)$ (7) over forward distance (relative to the ship's stern), and versus sound frequency. The distribution was computed by averaging BF spectra at each frequency over the time interval between the two time instances when bow and engine of the ship were at CPA to arrays A and B. The dashed horizontal lines show the positions of the stern (red) and bow (white) of the ship. The bottom panels show the spatial distribution $Q_{BFA}(R_{long}, t)$ (8) over forward distance in time domain. For each time frame, the spatial distribution was computed as average BF output within the frequency range $B' = \{1000, 3000\}$ Hz. In this plot, the white vertical dashed line indicates the CPA time of bow, and red vertical line displays the CPA time of engine.

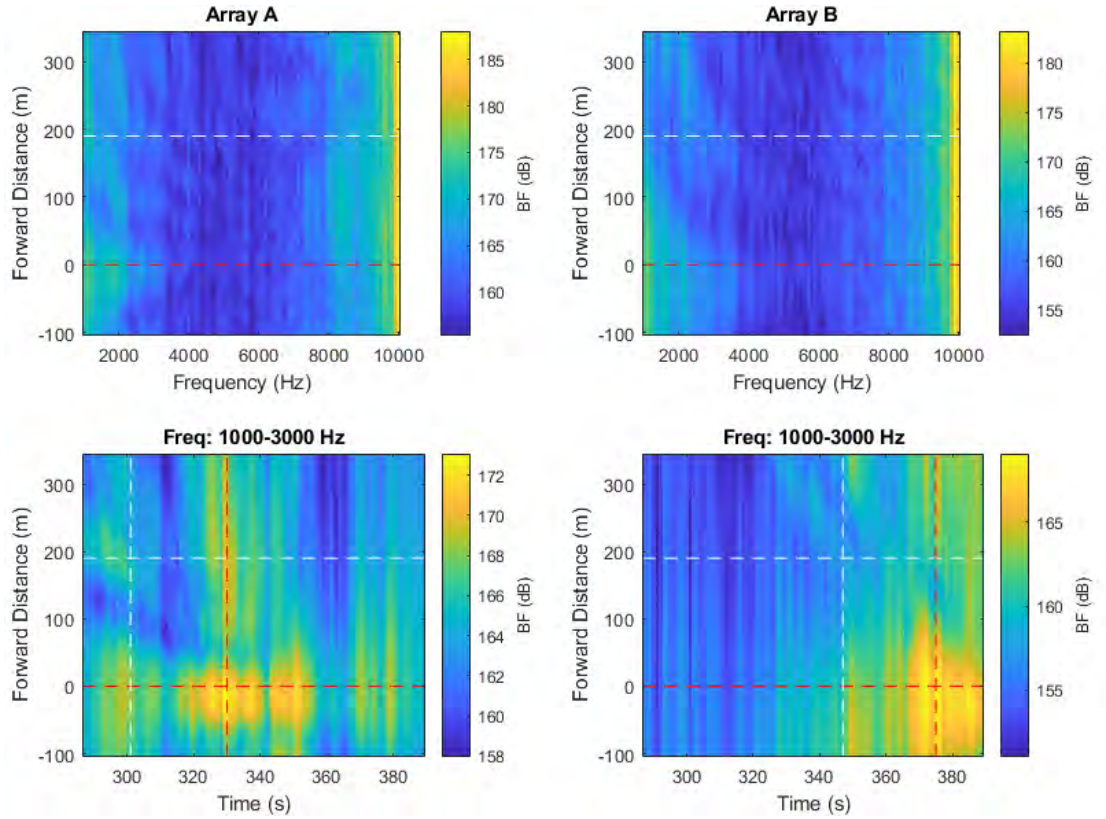

Figure 19. Noise maps provided by the beamformer using real ship data. Top panels: Spatial distributions of noise sources over forward distance and frequency. Bottom panels: Spatial distributions of noise sources over forward distance and time.

Because the BF spectrum, $S_{BF}(\boldsymbol{r},f,t)$, is proportional to the energy of the received acoustic signal in angular and frequency domain, the BF provides the highest accuracy of localization of spatially distributed sources. The disadvantage of the BF is that its angular resolution is limited by the beamwidth of the arrays. Over the frequency range from 1000 Hz to 10000 Hz, the beamwidth of the ULS arrays decreases from 51.2 to 5.2 degrees. The beamwidth at 1000 Hz is quite wide and likely not sufficiently narrow to resolve different sound sources on ships. Therefore, in addition to the BF, we also applied two other AOA estimation methods that yield better angular resolution of point sound sources. These methods are based on the Capon and MUSIC algorithms, respectively, (Haykin 1985, Johnson and Dudgeon 1993, Van Trees 2002). The spatial distributions provided by the Capon and MUSIC algorithms are:

$$S_C(\boldsymbol{r},f,t) = \boldsymbol{a}_A^H(\boldsymbol{r},f,t)\boldsymbol{P}_A(f,t)^{-1}\boldsymbol{a}_A(\boldsymbol{r},f,t)(\boldsymbol{r},f,t), f \in B,\ \ \boldsymbol{r} \in U_A(t). \quad (9)$$

$$S_{MUSIC}(\boldsymbol{r},f,t) = \boldsymbol{a}_A^H(\boldsymbol{r},f,t)[\boldsymbol{I}-\boldsymbol{\Pi}]\boldsymbol{a}_A(\boldsymbol{r},f,t), \quad (10)$$

where $\boldsymbol{\Pi}$ is the projection matrix into signal subspace obtained from eigen-vectors of the covariance matrix; and $\boldsymbol{I}$ is the identity matrix. In Equations (9) to (10), the temporal dependence of vector $\boldsymbol{r}$ and matrix $\boldsymbol{\Pi}$ are omitted for brevity.

The angular resolution of the Capon and MUSIC estimators are approximately twice that of the standard BF (i.e., the admitting angular range is about half the BF beamwidth). An important property of the Capon estimator is that the maxima of its inverse spectrum $S_C(\boldsymbol{r},f,t)^{-1}$ is proportional to the intensities of the detected sources. This property can be useful to understand the relative strengths of point sources detected. The signal maxima of the inverse MUSIC spectrum $S_{MUSIC}(\boldsymbol{r},f,t)^{-1}$ are proportional to the Euclidean distance between the search vector, $\boldsymbol{a}_A(f,\boldsymbol{r},t)$, and the signal subspace specified by the projection matrix, $\boldsymbol{\Pi}$. This distance is independent of the source intensity, so it is not representative of the relative source strength. In general, both algorithms provide comparable angular resolution and were both

applied to detect and estimate relative positions of point sources on the ship passes monitored. Noise maps $P_{BFA}(R_{long}, f)$ (7) and $Q_{BFA}(R_{long}, t)$ (8), computed using the Capon (9) and MUSIC (10) algorithms, are shown respectively in Figure 20 and Figure 21. The decibel scales of these figures are not absolute, so they cannot be used to determine the absolute acoustic signal power of the sounds identified.

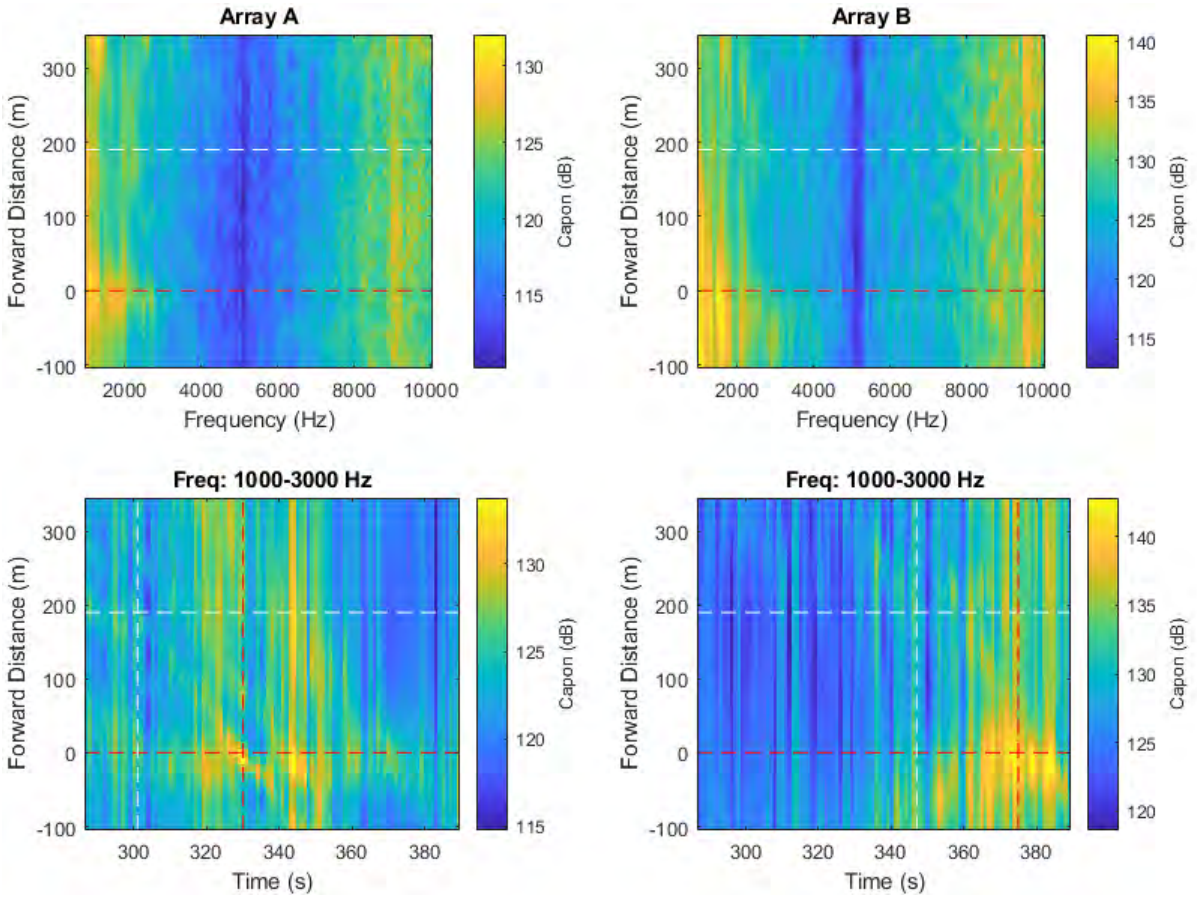

Figure 20. Noise maps provided by the Capon algorithm. Top panels: Spatial distributions of noise sources over forward distance and frequency. Bottom panels: Spatial distributions of noise sources over forward distance and time. Horizontal dashed lines represent the stern and bow positions. Vertical dashed lines represent the times associated with the CPA's of the bow and stern passing the individual arrays. The response colour decibel scale is relative so does not represent absolute signal intensity.

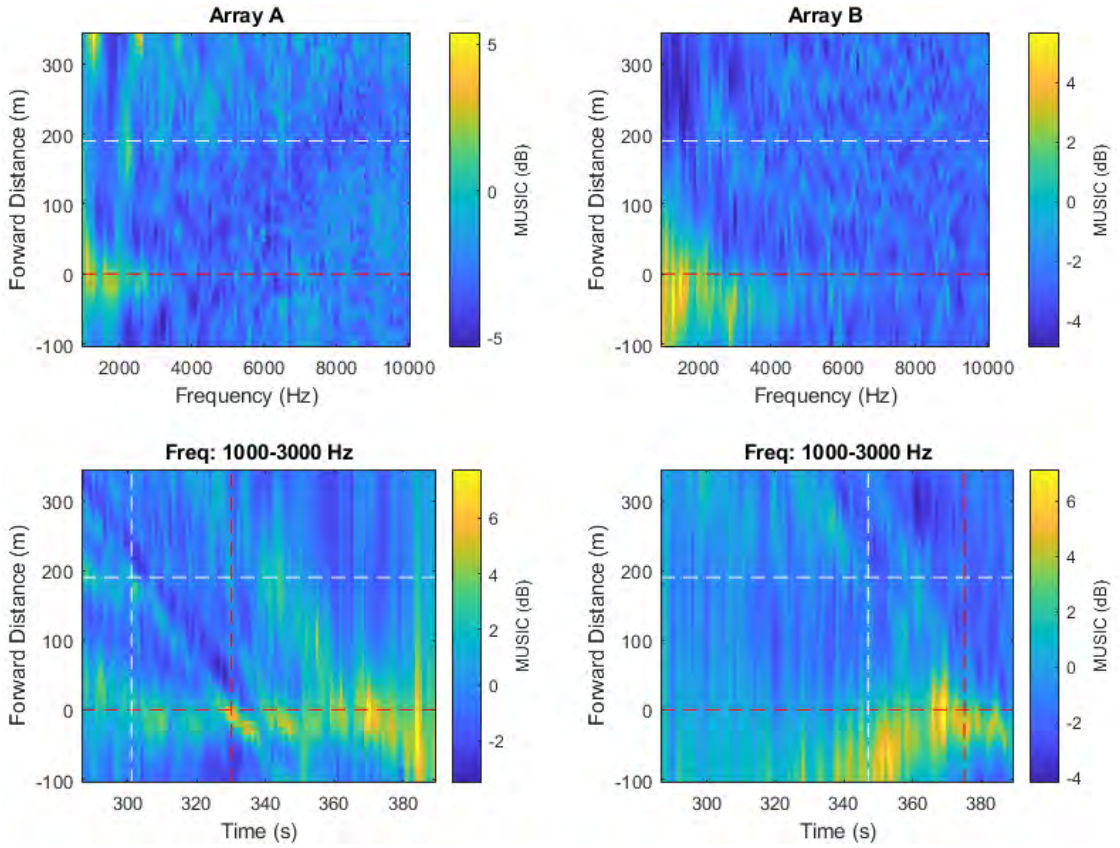

Figure 21. Noise maps provided by the MUSIC algorithm. Top panels: Spatial distributions of noise sources over forward distance and frequency. Bottom panels: Spatial distributions of noise sources over forward distance and time. Horizontal dashed lines represent the stern and bow positions. Vertical dashed lines represent the times associated with the CPA's of the bow and stern passing the individual arrays. The response colour decibel scale is relative so does not represent absolute signal intensity.

The real ship noise maps presented in Figures 19 to 21 appear to show a single dominant source (likely the propeller) near the stern of the ship at all frequencies. The performance of Array A is slightly better than Array B in the 1–10 kHz band for the BF, Capon and MUSIC approaches. That is attributed to one of the four hydrophones on Array B malfunctioning, The malfunctioning hydrophone did not appreciably affect the lower frequency results.

2.6. Averaging Noise Maps using Multiple Passes

Because the resulting noise maps are referenced to the loudest source on the ship, likely the ship's propeller, the maps from multiple passes can potentially be averaged to emphasize real noise sources that will remain in the same relative position on each pass. Random noises such as from waves against the hull or from unstable turbulence would not be common to multiple passes and will be suppressed.

This approach of averaging was not extensively tested in Phase II study because only two of the ships passed twice. The trajectories of the first of these ships (passes #4 and #10) are shown in Figure 22 and their LF noise maps are shown in Figure 23. Two LF maps computed for two passes of the second ship (passes #22 and #25) are shown in Figure 24. These plots show the presence of two sources generated noise at different frequencies and separated by 25–50 m. Averaging of noise maps might be performed in the future using a greater number of ship pass results. Averaging could improve resolution of the maps by enhancing the localization response of consistent sound sources and suppressing features such as side lobes and grating lobes.

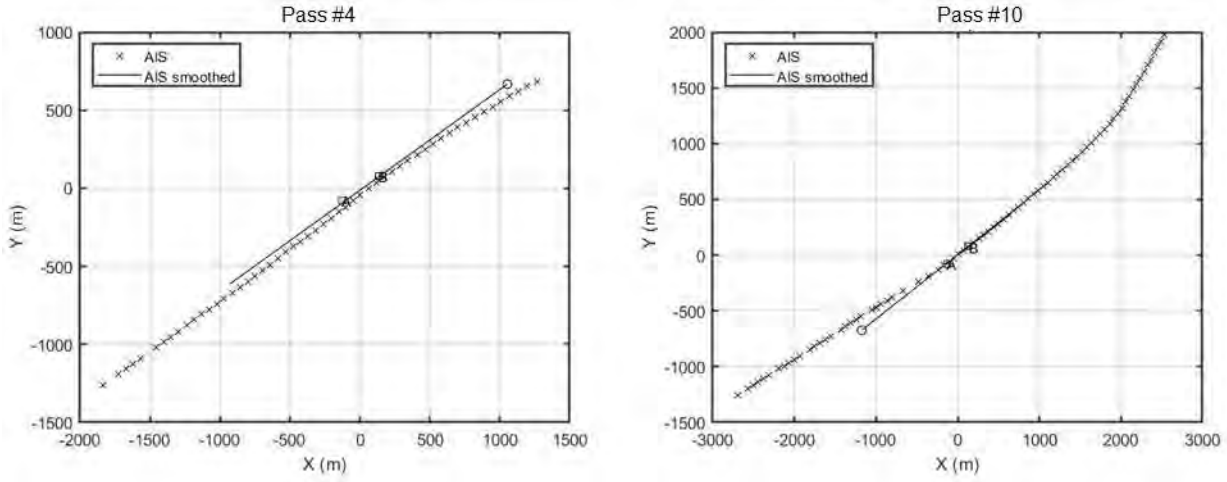

Figure 22. Trajectories of two passes (#4 – inbound travelling northeast, and #10 outbound travelling southwest) of the first of the two ships that passed the ULS twice. The vessel draught was 6.9 m and speed 12.9 kn inbound, and draught 13.1 m and speed 13.6 kn outbound.

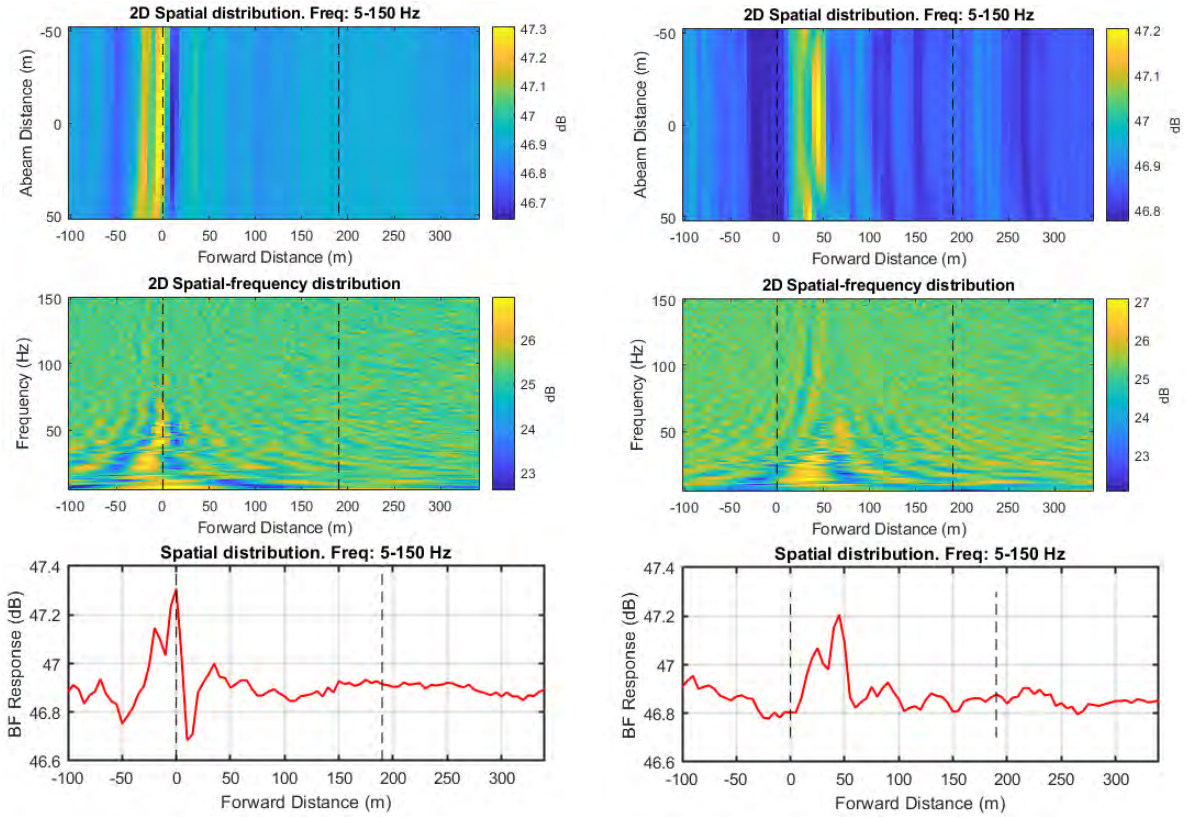

Figure 23. Low-frequency noise maps obtained for two passes: #4 inbound (left) and #10 outbound (right) of the first ship that passed the ULS twice.

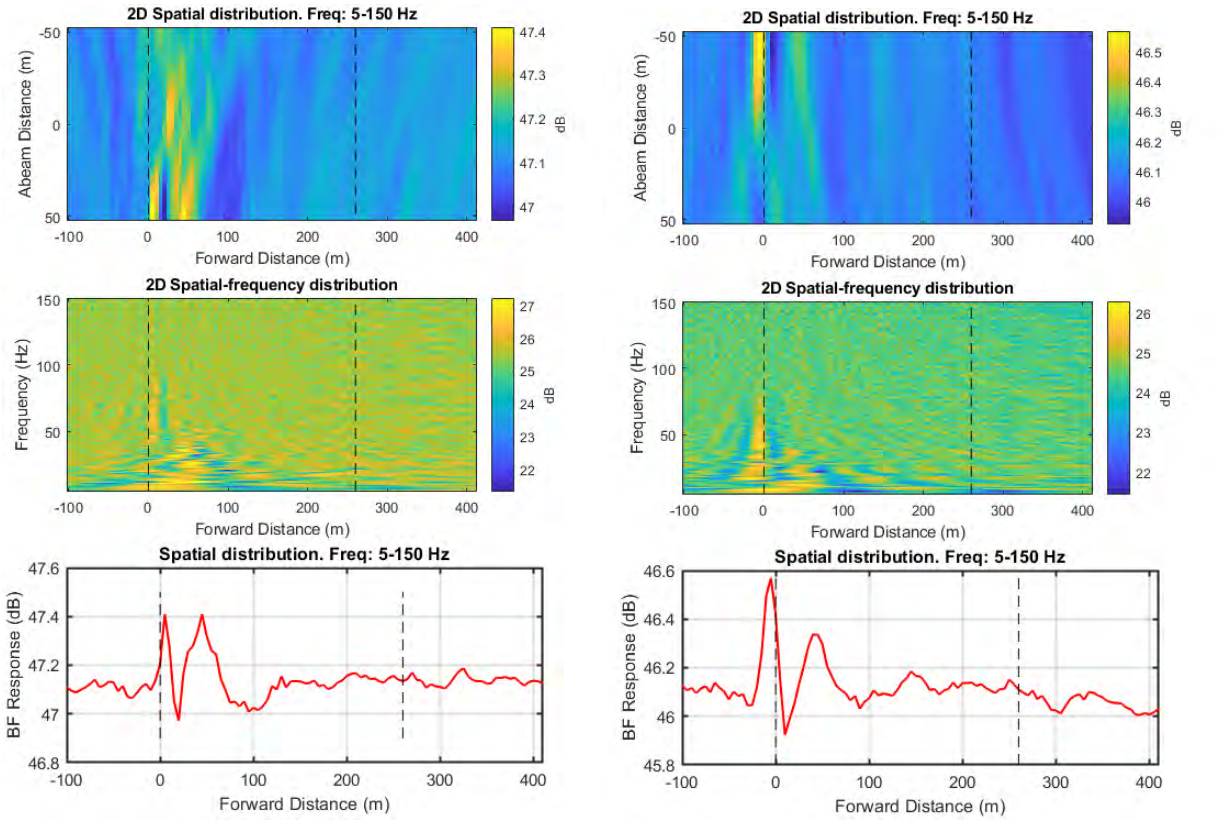

Figure 24. Low-frequency noise maps obtained for two passes: #22 (left) and #24 (right) of the second ship that passed the ULS twice.

2.7. Automatic Processing for Evaluating Noise Maps

The algorithms described above were implemented in a software system that was set up to automatically process data from the Boundary Pass ULS in real time. Data processing consisted of the following steps:

1. Initialization (extracting the information about the ship; computing smoothed and interpolated coordinates of the ship based AIS track).
2. Estimating received levels (RL) and average power spectrum density (PSD) of ship noise on the top hydrophones of both compact arrays.
3. Estimating TDOA for all channels of both arrays and frequency domain correlations using discrete Fourier transform (DFT) spectra using all channels of both arrays.
4. Correction of the AIS-based coordinates and finding the trajectory of the dominant noise source using the TDOA measurements.
5. Estimating the distribution of low-frequency (5–150 Hz) and mid-frequency (100–1000 Hz) noise sources using the wideband beamforming (BF) algorithm implemented on the combined array of 8 hydrophones.
6. Estimating the distribution of high-frequency (1000–10000 Hz) noise sources using wideband high-resolution Capon and MUSIC algorithms implemented separately on arrays A and B.
7. Generating graphic plots of the combined array BF responses in spatial and spatial-frequency domains and BF output along forward distance of the ship, as described in Sections 2.4 and 2.5.

3. Results

3.1. Review of Noise Maps from All Ships

The methods described in Section 2 were applied to all 44 ship passes (see Table 1). Noise maps were calculated for all passes, and these are provided in Appendix A. A sample of noise maps for five ships, one from each ship category, is also provided in Section 3.2. In Table 2 we provide a review of the noise map results for all ships, including discussions of the sources localized and describing their respective frequency distributions.

Table 2. Summary of noise localization results for the 44 ship passes analyzed. Details about the passes, including the corresponding ship lengths, CPA, and speed over ground are provided in Table 1.

Pass Identifier	Ship type	Results
1	Bulk Carrier	LF: high localization accuracy of main source from 5–20 Hz and 50–120 Hz. A second source may be present and dominant from 25–50 Hz that is aft of the first source by about 10 m. MF: marginal localization, mainly with response of the BF to the small apertures of the closely spaced hydrophones in each of the compact arrays (those hydrophones are still part of the combined sparse array). This creates a broad peak with limited resolving power. There is also a weak coherent response from the sparse aperture at about -30 m forward distance that matches the LF localization position. HF: high localization accuracy of one dominant source provided by Capon and MUSIC.
2	Container	LF: very high localization accuracy; single dominant source 20–150 Hz, with possible second source below 10 Hz that is slightly forward, by up to 30 m, but this second source could be a grating lobe artefact. MF: good localization accuracy HF: high localization accuracy single source BF, Capon and MUSIC. These localizations show the source aft of the location provided by the LF beamforming.
3	Container	LF: high localization accuracy of dominant source 10–100 Hz; possible second source below 10 Hz, ~60 m forward of the dominant source. MF: moderate localization accuracy HF: low localization accuracy all algorithms
4	Bulk Carrier*	LF: high localization accuracy; possible secondary source at 30–50 Hz, 10–15 m aft of dominant source. This is very similar to the result of Pass #1. MF: moderate localization accuracy HF: high localization accuracy all algorithms.
5	Bulk Carrier	LF: very high localization accuracy of a dominant source 20 -300 Hz; possible secondary source below 20 Hz, 10–15 m forward of dominant source. This measurement has a significantly higher coherence frequency than most others. MF: Very high localization accuracy – due to coherence up to 300 Hz. The single dominant source above 100 Hz appears at the same location as the dominant low frequency source, and localized to within approximately 10 m. HF: high localization accuracy of one dominant source provided by all algorithms.
6	Bulk Carrier	LF: very high localization accuracy; there appears to be two sources with similar amplitude, approximately 20 m apart, that partially overlap in frequency. The forward source is 10–130 Hz while the aft is 50–130 Hz. MF: moderate to low localization accuracy HF: medium localization accuracy of one dominant source provided by BF; accurate localization by Capon and MUSIC algorithms.

7	Container	LF: good localization accuracy but only up to about 70 Hz, with apparent loss of coherence above that frequency. Single dominant source at least at these lower frequencies. MF: moderate accuracy. HF: moderate localization accuracy of one dominant source provided by the BF; low localization accuracy by Capon and moderate by MUSIC
8	Bulk Carrier	LF: high localization accuracy; appears to be single dominant source 10–150 Hz, but perhaps a second source about 10 m aft, with sound energy dominant between 20–40 Hz. MF: good localization accuracy HF: high localization accuracy of the dominant source provided by all algorithms.
9	Bulk Carrier*	LF: Somewhat unusual case with a dominant localized source (50 – 150 Hz) and a lower frequency (10–30 Hz) source about 15 m aft. The frequency range 30–50 Hz has no dominant main lobe peak, although the grating lobe pattern is consistent with higher frequency lobes through that frequency range. MF: good coherence up to 200 Hz and very good localization. HF: medium localization accuracy of the dominant source provided by all algorithms.
10	Container	LF: high localization accuracy; possible secondary source 10–15 m forward of dominant source, but only below about 20 Hz. MF: good coherence up to 200 Hz and good localization. HF: low to medium localization accuracy of the dominant source provided by all algorithms. Interestingly, best localization appears to occur after the stern passed the arrays, but the reason for that has no been investigated.
11	Container	LF: good localization accuracy of a single source 10–100 Hz MF: moderate accuracy HF: Very high localization accuracy of one dominant source provided by all algorithms.
12	Bulk Carrier	LF: two noise sources present: aft source dominates 5–45 Hz, while forward source, about 20 m forward, dominates 50–100 Hz. MF: low to moderate accuracy HF: high localization accuracy of one dominant source provided by all algorithms.
13	Bulk Carrier	LF: high localization accuracy of a dominant source 30–120 Hz with possible second source 5–30 Hz forward by 15 m MF: moderate accuracy HF: high localization accuracy of the dominant source provided by all algorithms.
14	Bulk Carrier	LF: very high localization accuracy of a single source 5–150 Hz. MF: high localization accuracy of one source as the signal is coherent up to approximately 200 Hz. HF: high localization accuracy of one dominant source provided by all algorithms.
15	Container	LF: modelerate localization accuracy of one source 30–130 Hz; second source forward by approximately 50 m, 5–15 Hz. MF: low localization accuracy. HF: high localization accuracy of one dominant source provided by all algorithms.
16	Container	LF: high localization accuracy of a dominant source 10–80 Hz, and a second source aft by about 50 m, 20–30 Hz. The spectral shapes of signals measured on the two arrays differed and may have been affected by another vessel that passed 450 seconds earlier. MF: low localization accuracy – BF output is maximum before vessel pass. HF: low localization accuracy by BF, Capon and MUSIC algorithms.
17	Bulk Carrier	LF: very high localization accuracy of one source 5–150 Hz, and a second source perhaps 5 m forward 40–55 Hz. MF: Signal was coherent to almost 400 Hz, resulting in the highest resolution detection of all pass measurements, to within 5 m. The position of this source is slightly aft (5 m) of the first LF source HF: moderate localization accuracy of one dominant source provided by all algorithms.

18	Container	LF: high localization accuracy of one source 40–100 Hz. A second source may be present slightly forward between 5–40 Hz but this could be an artefact caused by a grating lobe pattern. MF: moderate localization accuracy. HF: moderate localization accuracy of one dominant source provided by all algorithms.
19	Container	LF: moderate localization accuracy of one source 5–80 Hz. The presence of another vessel is observed in the spectrogram and that may have caused interference. MF: moderate localization accuracy. HF: low localization accuracy by all algorithms.
20	Bulk Carrier	LF: very high localization accuracy of one source 10–150 Hz. MF: moderate localization accuracy. HF: moderate accuracy of BF but low accuracy by Capon and MUSIC algorithms.
21	Bulk Carrier	LF: moderate localization accuracy of probably one source 5–150 Hz. The grating lobe pattern is non-uniform 40–80 Hz, leading to uncertainty in identifying secondary sources. MF: high localization accuracy. HF: very high localization accuracy of one dominant source provided by all algorithms.
22	Container**	LF: low localization accuracy due to a non-uniform grating lobe pattern that has some ambiguity as to which lobe represents the main beam and which are grating lobes. This resulted in 3 peaks in the noise map, at 0 m (50–150 Hz), 20 m (50–100 Hz) and 45 m (20–40 Hz) from the stern. MF: high localization accuracy, with the peak corresponding with the 45 m peak of the LF results HF: low localization accuracy provided by all algorithms.
23	Bulk Carrier	LF: high localization accuracy of one source 20–150 Hz and possible second source aft of first at 10–25 Hz. There is also a possible third source 10 m forward of first source at 5–10 Hz. MF: good localization accuracy with peak response corresponding with the first source of LF analysis. HF: low localization accuracy by all algorithms.
24	Bulk Carrier	LF: very high localization accuracy of one source 5–40 Hz and 80–140 Hz. A second source is identified 10 m aft 45–80 Hz. MF: low localization accuracy – perhaps due to the presence of another vessel present nearby during the measurement. HF: moderate localization accuracy of one dominant source provided by Capon and MUSIC algorithms.
25	Container**	LF: moderate localization accuracy of one source 20–100 Hz. Possible second source 5–30 Hz at 40 m forward of first source. MF: moderate localization accuracy slightly forward of first source of LF result. HF: low localization accuracy of the dominant source provided by all algorithms.
26	Bulk Carrier	LF: low localization accuracy of a source at 5–60 Hz. The grating lobe pattern is not as uniform as in other measurements, making resolution of other possible sources difficult. There may be a second source approximately 10 m forward of the first source in a narrow band of frequencies near 10 Hz. MF: low localization accuracy. The BF response is quite flat, with only a 0.1 dB variation. This makes localizing sources difficult, but there is a maximum in the response at about 100 m forward of the first LF source, produced mainly by sounds 800–1000 Hz. HF: moderate localization accuracy with BF, showing one source at 100 m forward of the first LF source and matching the location of the MF localization. Capon and MUSIC did not localize a source.
27	Bulk Carrier	LF: very high localization accuracy of a source 20–120 Hz. A possible second source 10–40 m forward of the first source may be present 5–15 Hz but this could be a grating lobe artefact. MF: high localization accuracy with position matching that of the first LF source. HF: very high localization accuracy of one dominant source provided by all algorithms.

28	Container	LF: very high localization accuracy with behaviour similar to that of Pass 27, with a first source 20–150 Hz and second source 5–10 Hz approximately 15 m forward. Again, this second source could be a grating lobe artefact. MF: high localization accuracy of one source with position matching that of the first LF source. This localization due to energy from 300–1000 Hz. HF: high localization accuracy of one dominant source provided by all algorithms.
29	Bulk Carrier	LF: very high localization accuracy to within 5 m of one source 20–140 Hz. Possible localization of second source below 10 Hz approximately 20 m forward, but this could be a grating lobe artefact. MF: very high localization accuracy of one source matching the position of the first LF source. This is dominated by sound energy 600–1000 Hz. HF: high localization accuracy of one dominant source provided by all algorithms.
30	Container	LF: very high localization accuracy of one source 15–150 Hz. Likely localization of second source 5–15 Hz about 20–40 m forward of first source. MF: high localization accuracy of one source matching position of first LF source. HF: very high localization accuracy of one dominant source provided by all algorithms.
31	Bulk Carrier	LF: high localization accuracy of one source 20–120 Hz. Possible second source 10–40 m forward but could be grating lobe artefact. MF: One source localized 100–200 Hz matching position of first LF source. Second broadband source localized at 200–1000 Hz with highest BF response about 20 m forward of first source. HF: low localization accuracy provided by all algorithms.
32	Bulk Carrier	LF: moderate localization accuracy of one source at 25–130 Hz, but with two other maxima approximately 20 m aft and 20 m forward. The grating lobe pattern is unusual and the two secondary sources may be artefacts of that pattern. MF: low localization accuracy, with the maximum BF response approximately 40 m aft of the first LF source. HF: low localization accuracy provided by all algorithms.
33	Vehicle Carrier	LF: high localization accuracy of one source 20–120 Hz. Possible second source dominant in narrow frequency band near 10 Hz at about 20 m forward of first source. MF: moderate localization of broadband 200–1000 Hz sound energy matching position of first LF source. HF: high localization accuracy of one dominant source provided by all algorithms, with MUSIC providing best result.
34	Bulk Carrier	LF: very high localization accuracy of just one source 13–150 Hz, with second source 5 Hz and 10 Hz at about 15 m forward of first source. MF: high localization of broadband noise 300–1000 Hz centred approximately at position of first LF source. HF: high localization accuracy of one dominant source provided by all algorithms.
35	Container	LF: moderate localization accuracy of one source 20–70 Hz. Grating lobe pattern loses coherence above 70 Hz. No second source observed here. MF: moderate localization accuracy of sound with maximum BF response approximately 20 m forward of LF source position, but this is not well localized. HF: moderate localization accuracy provided by all algorithms.
36	Tanker	LF: very high localization accuracy of one source 5–10 Hz and 20–120 Hz, with second possible source near 10–15 Hz at 15–20 m forward of first source. MF: moderate localization accuracy with BF response maximum near or slightly in front of first LF source. HF: high localization accuracy provided by all algorithms.
37	Bulk Carrier	LF: high localization accuracy of one source 15–70 Hz. The centre beam lobe appears to decay above 70 Hz even though the grating lobe pattern remains stable to over 100 Hz. MF: high localization accuracy of energy 200–1000 Hz with maximum BF response at position of LF source. HF: high localization accuracy provided by all algorithms. MUSIC performed better than Capon.

38	Bulk Carrier	LF: very high localization accuracy of one source 15–140 Hz. Some variation in position of the main lobe below 40 Hz but it is not abrupt. No clear secondary source maximum. MF: moderate localization accuracy with BF response maximum matching position of LF source localization. HF: high localization accuracy provided by all algorithms.
39	Bulk Carrier	LF: very high localization accuracy (within 5 m) for one source 15–150 Hz. A second source may be dominant at 10 Hz about 15 m forward of first source. This measurement has high coherence, extending to over 200 Hz. MF: very high localization of coherent sound up to 200 Hz, providing a localization centred at about 5 m aft of the first LF localization. HF: high localization accuracy of the dominant source provided by all algorithms.
40	Bulk Carrier	LF: very high localization accuracy of one source 20–75 Hz. At 10–15 Hz and 75–120 Hz a second source may be approximately 5 m forward of the first source MF: very high localization accuracy (within 5 m) of coherent sound energy 100–200 Hz at position of first LF source. Broadband 200–1000 Hz energy localized possibly slightly forward of this location. HF: very high localization accuracy of one dominant source provided by all algorithms.
41	Bulk Carrier	LF: very high localization accuracy of one source 55–150 Hz. A second source 10–50 Hz localized approximately 5 m aft of first source. A possible narrowband third source at 10 Hz localized 20 m forward of first source. MF: very high localization of coherent energy 100–350 Hz matching first LF source and MF broadband BF response maximum. This demonstrates the agreement of directions obtained by the sparse and close-spaced elements of the combined array. HF: low localization accuracy by all algorithms.
42	Bulk Carrier	LF: high localization accuracy of one source 20–60 Hz. Main lobe coherence seems lost above 60 Hz. Possible second source 5–15 Hz about 15 m forward of first source. MF: No coherent localization but broadband maximum of 200–1000 Hz energy occurs approximately 15 m forward of first LF source. HF: low to moderate localization accuracy provided by all algorithms.
43	Container	LF: low localization accuracy as it seems the system may have incorrectly chosen the reference frame. MF: It appears the BF maximum occurs beyond the aft end of the reference frame, as the response decreases moving forward in the frame. HF: all algorithms tracked the source near the aft end of the reference frame, consistent with the frame being positioned too far forward in space.
44	Bulk Carrier	LF: very high localization accuracy of one source 15–150 Hz. No secondary sources are detected. MF: very high localization of coherent energy 100–300 Hz matching LF source position. Interestingly, the maximum MF response, other than the coherent peak, occurs forward of the peak by about 20 m. HF: very high localization accuracy of one source by all algorithms.

In the following sections we provide samples of the spectra and noise maps for one ship of each ship category (Bulk Carrier, Container Ship, Vehicle Carrier, and Tanker). The results for all 44 ship passes are provided in Appendix A.

3.2. Example Results for Each Vessel Category

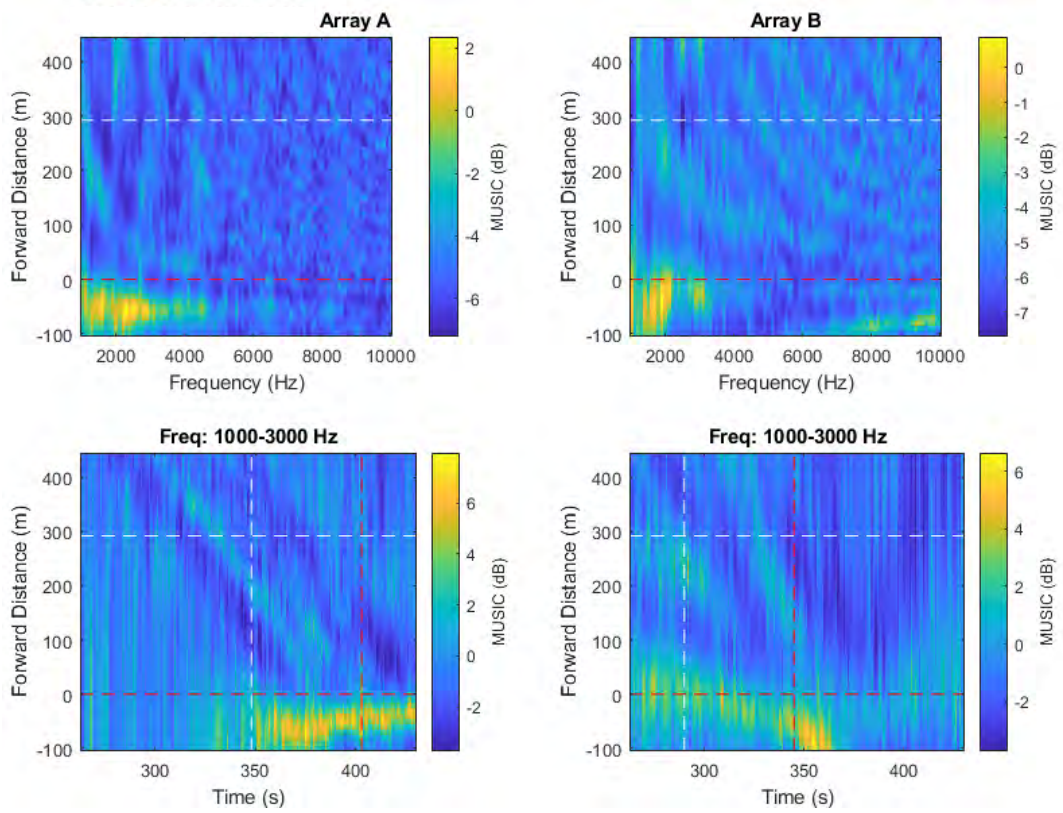

Figure 25. High-frequency noise maps (7), (8), obtained using the spatial spectra provided by the MUSIC algorithm implemented using individual arrays.

3.2.1. Container Ship (Pass #2)

3.2.1.1. Ship Noise Spectra

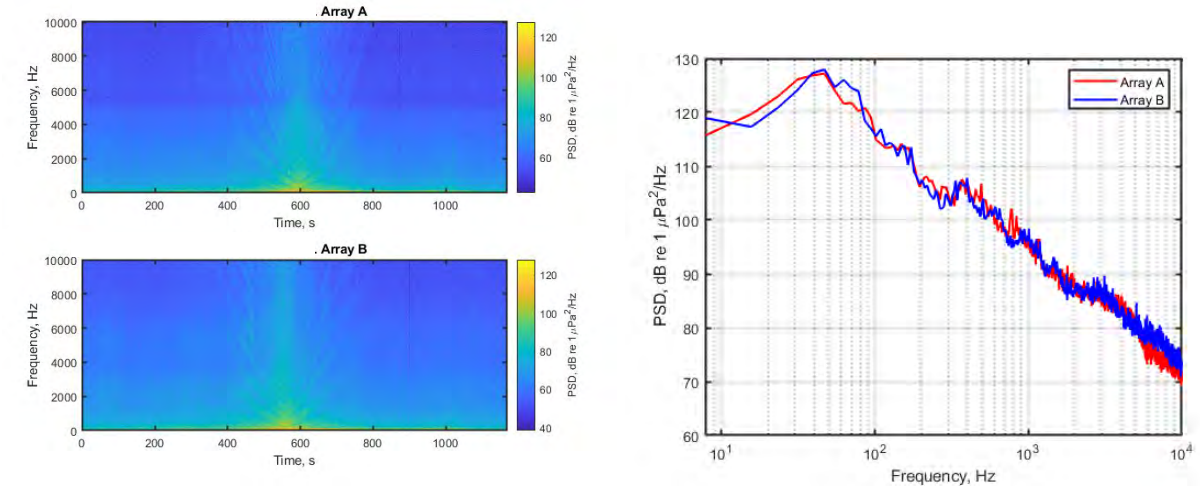

Figure 26. Spectrograms (left) and PSD (right) of ship noise from Pass #2 on top hydrophones of Arrays A and B.

3.2.1.2. Low- and Mid-frequency Noise Maps

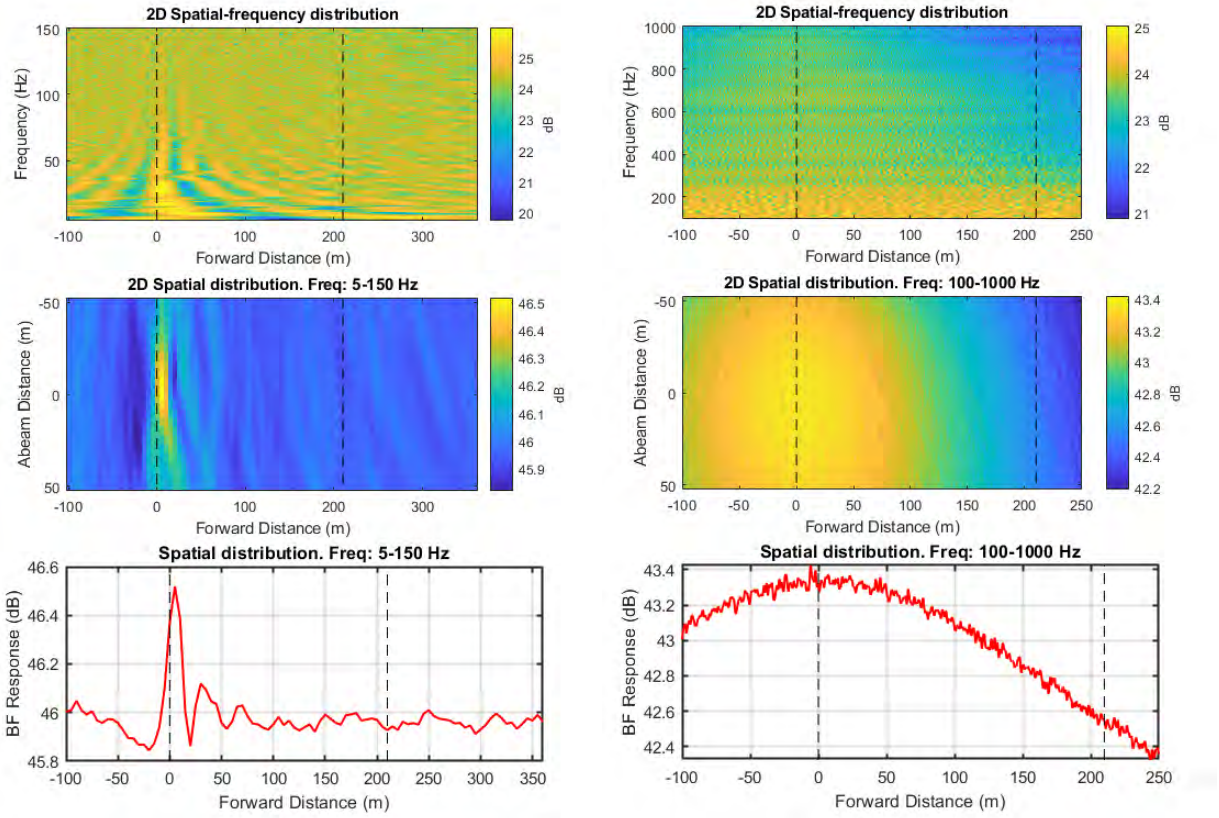

Figure 27. Noise maps from beamforming vessel pass #2 with combined array: left column panels show results for the frequency band 5–150 Hz while right column panels show the frequency band 100–1000 Hz.

3.2.1.3. High-frequency Noise Maps

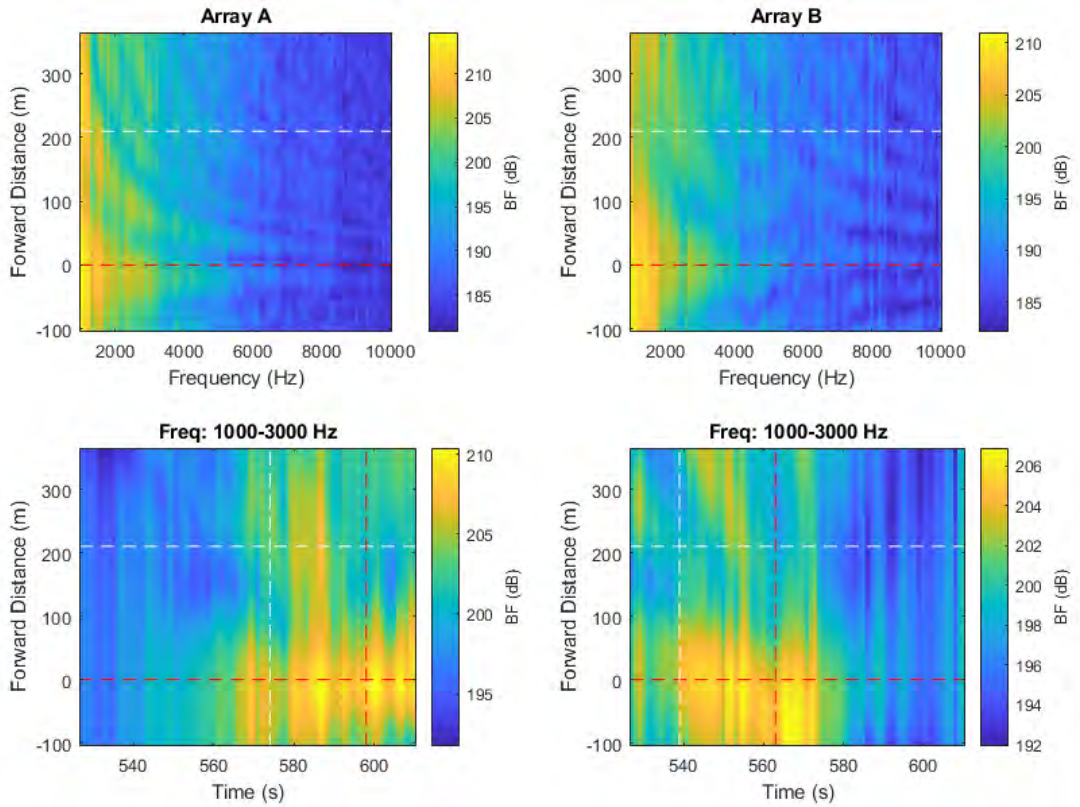

Figure 28. High-frequency (1–10 kHz) noise maps from beamforming ship pass #2 on individual arrays. Horizontal dashed lines indicate the stern and bow positions of the ship. Vertical dashed lines represent the CPA times of the bow and stern at each array. Left panels are from Frame A, right panels are from Frame B.

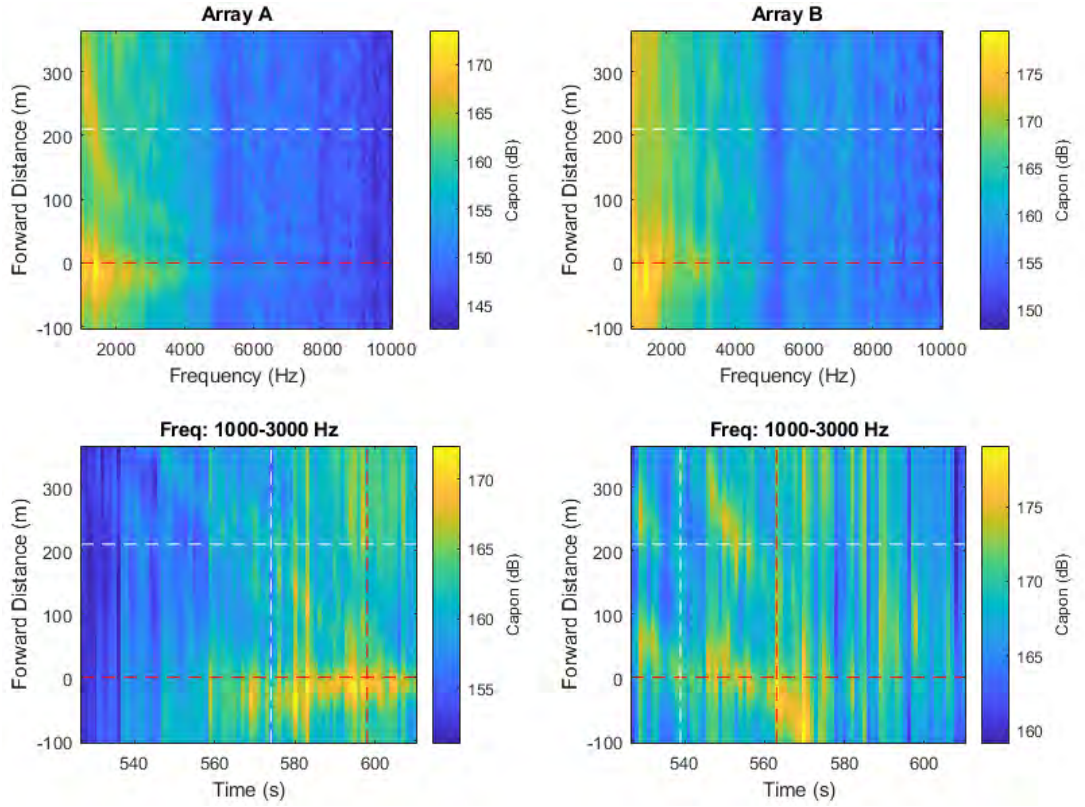

Figure 29. High-frequency noise maps (7), (8), obtained using the spatial spectra provided by the Capon algorithm implemented using individual arrays.

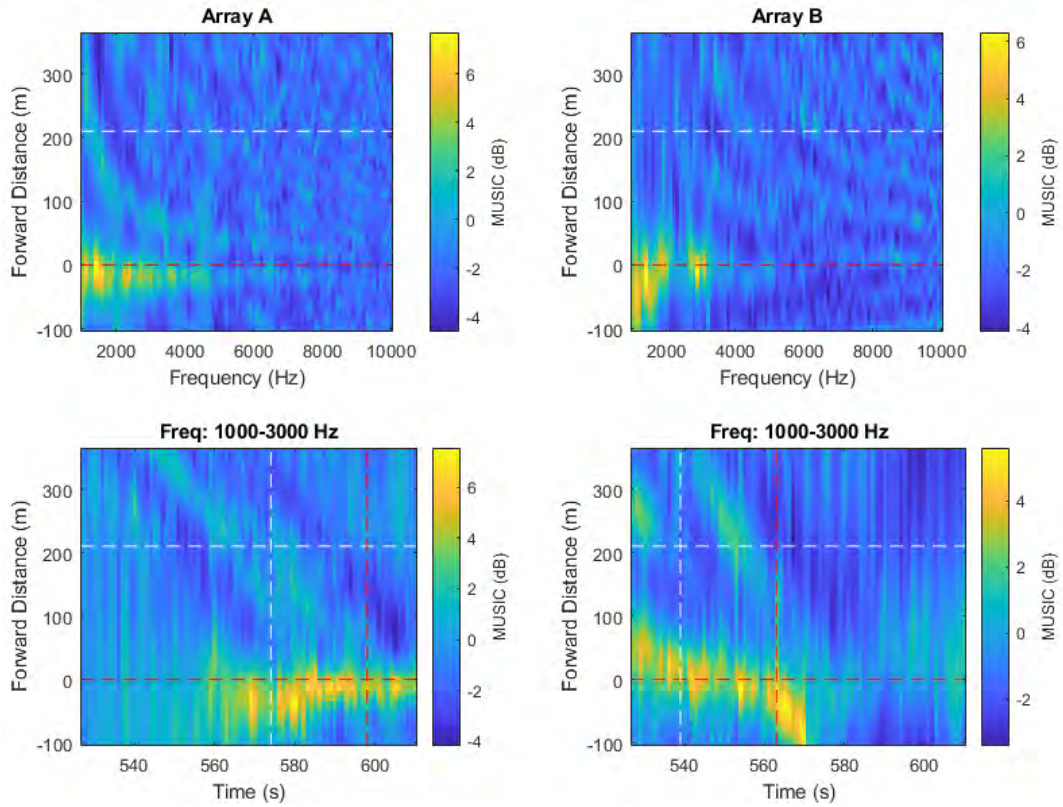

Figure 30. High-frequency noise maps (7), (8), obtained using the spatial spectra provided by the MUSIC algorithm implemented using individual arrays.

3.2.2. Bulk Carrier (Pass #27)

3.2.2.1. Ship Noise Spectra

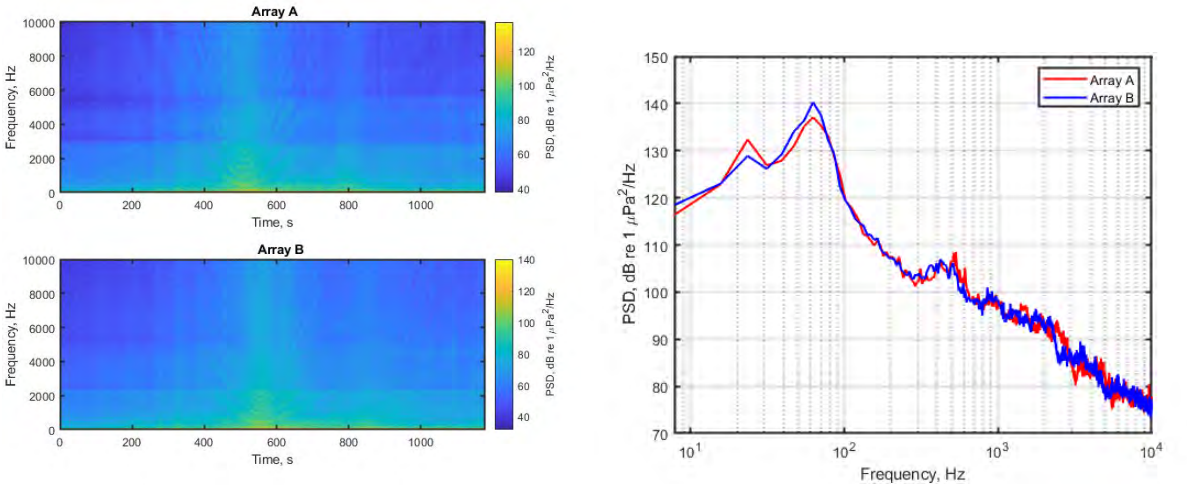

Figure 31. Spectrograms (left) and PSD (right) of ship noise from Pass #27 on top hydrophones of Arrays A and B.

3.2.2.2. Low- and Mid-frequency Noise Maps

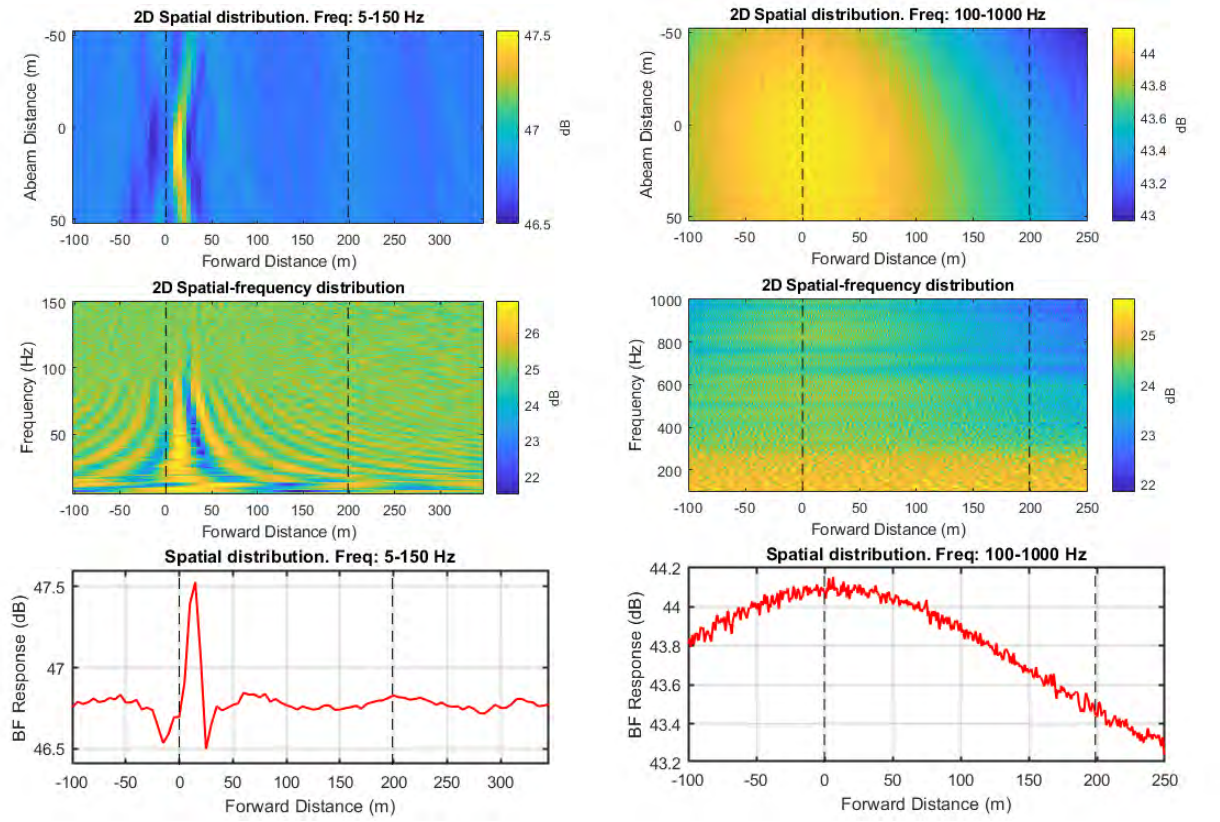

Figure 32. Noise maps from beamforming vessel pass #27 with combined array: left column panels show results for the frequency band 5–150 Hz while right column panels show the frequency band 100–1000 Hz.

3.2.2.3. High-frequency Noise Maps

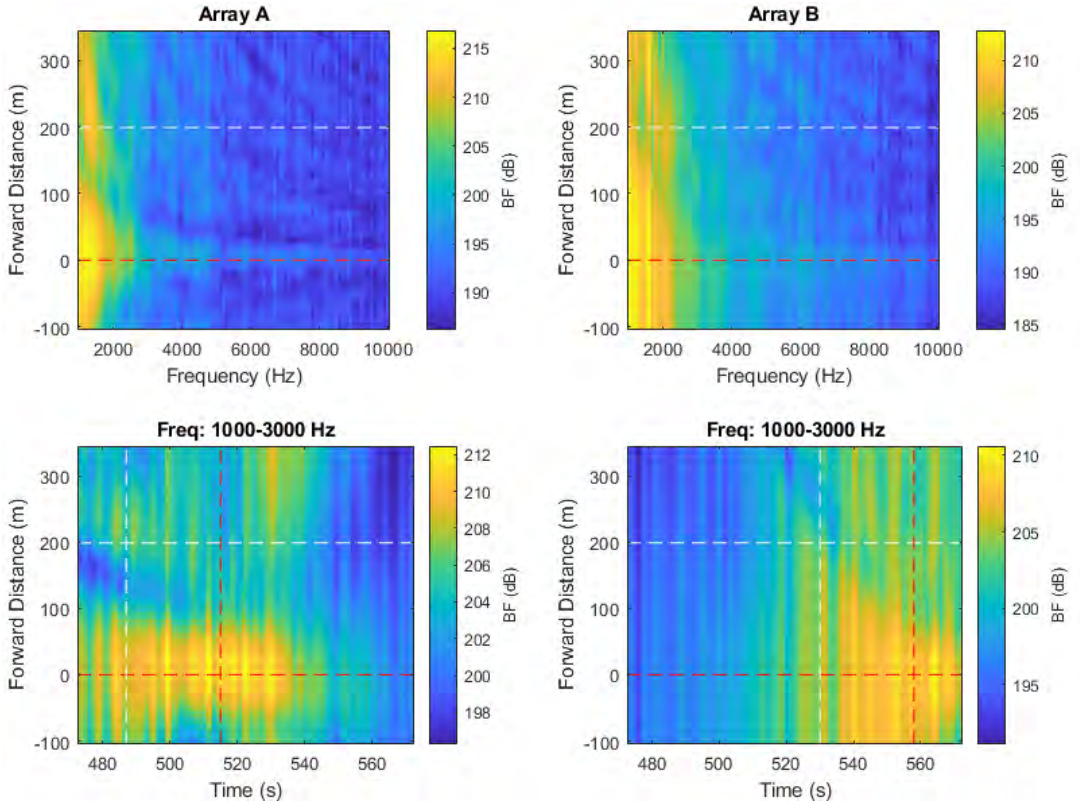

Figure 33. High-frequency (1–10 kHz) noise maps from beamforming ship pass #27 on individual arrays. Horizontal dashed lines indicate the stern and bow positions of the ship. Vertical dashed lines represent the CPA times of the bow and stern at each array. Left panels are from Frame A, right panels are from Frame B.

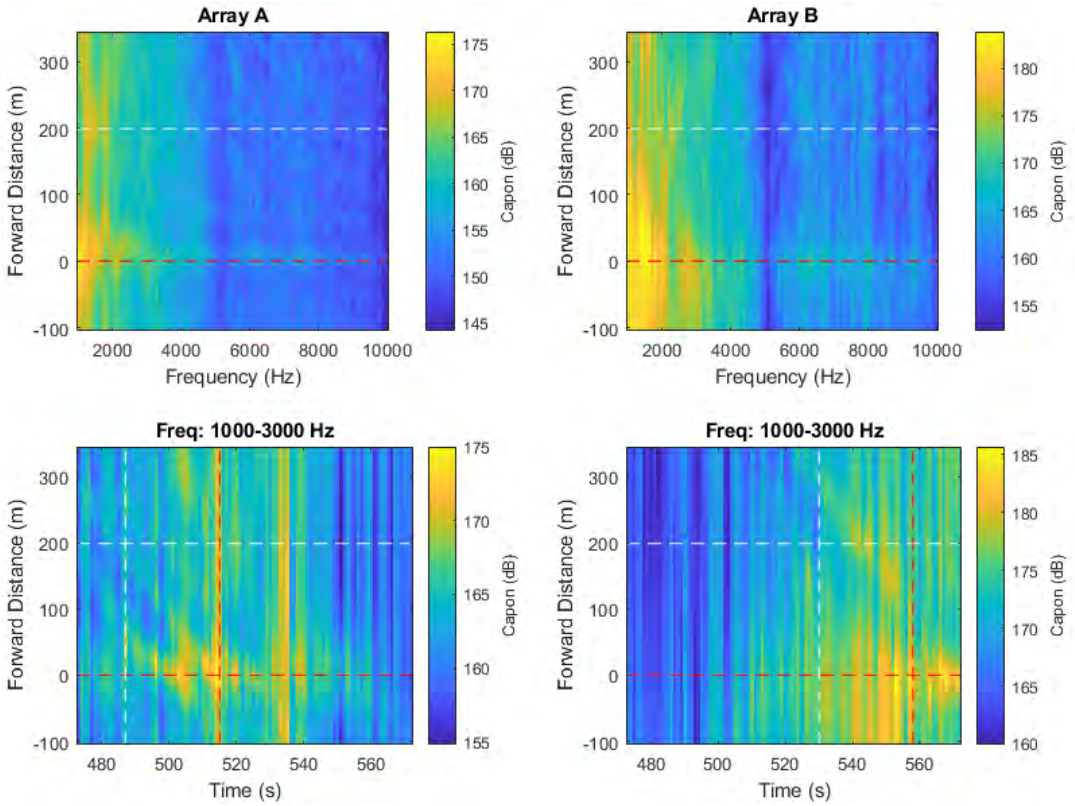

Figure 34. High-frequency noise maps (7), (8), obtained using the spatial spectra provided by the Capon algorithm implemented using individual arrays.

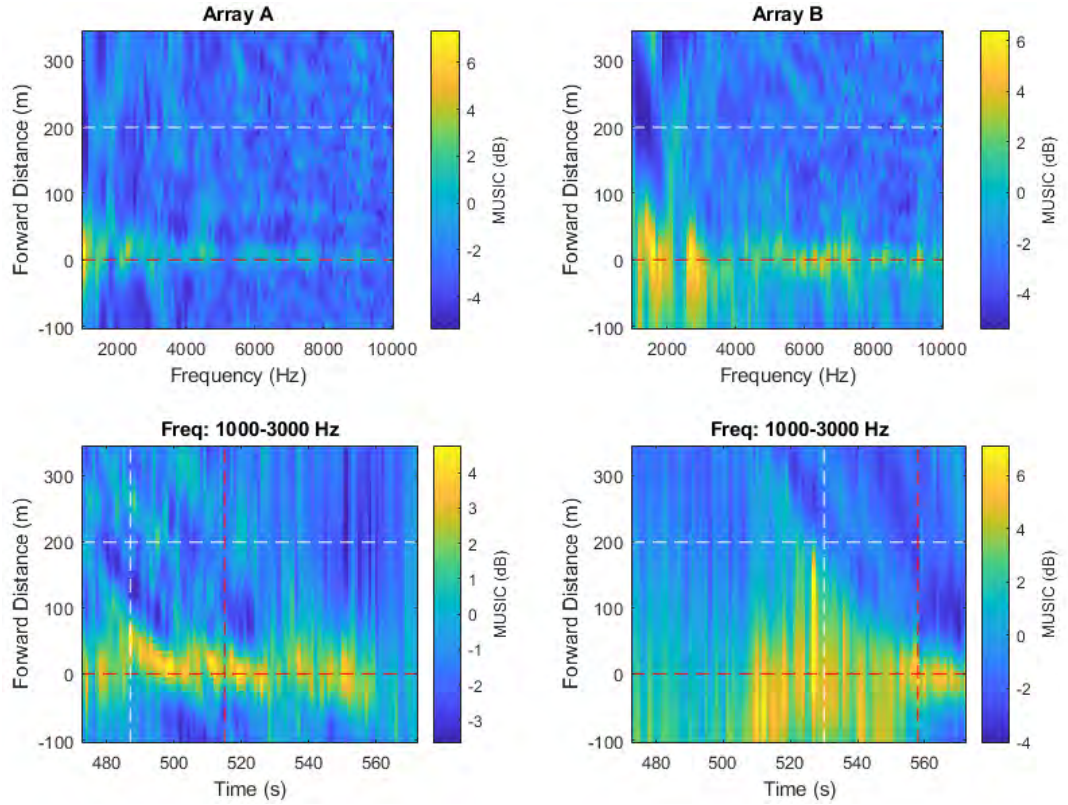

Figure 35 High-frequency noise maps (7), (8), obtained using the spatial spectra provided by the MUSIC algorithm implemented using individual arrays.

3.2.3. Vehicle Carrier (Pass #33)

3.2.3.1. Ship Noise Spectra

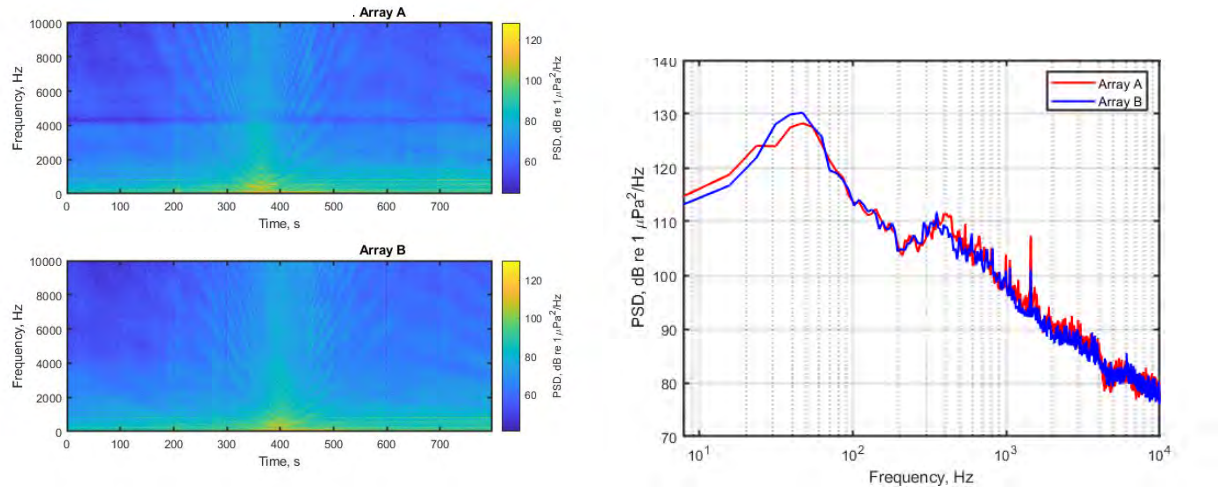

Figure 36. Spectrograms (left) and PSD (right) of ship noise from Pass #33 on top hydrophones of Arrays A and B.

3.2.3.2. Low- and Mid-frequency Noise Maps

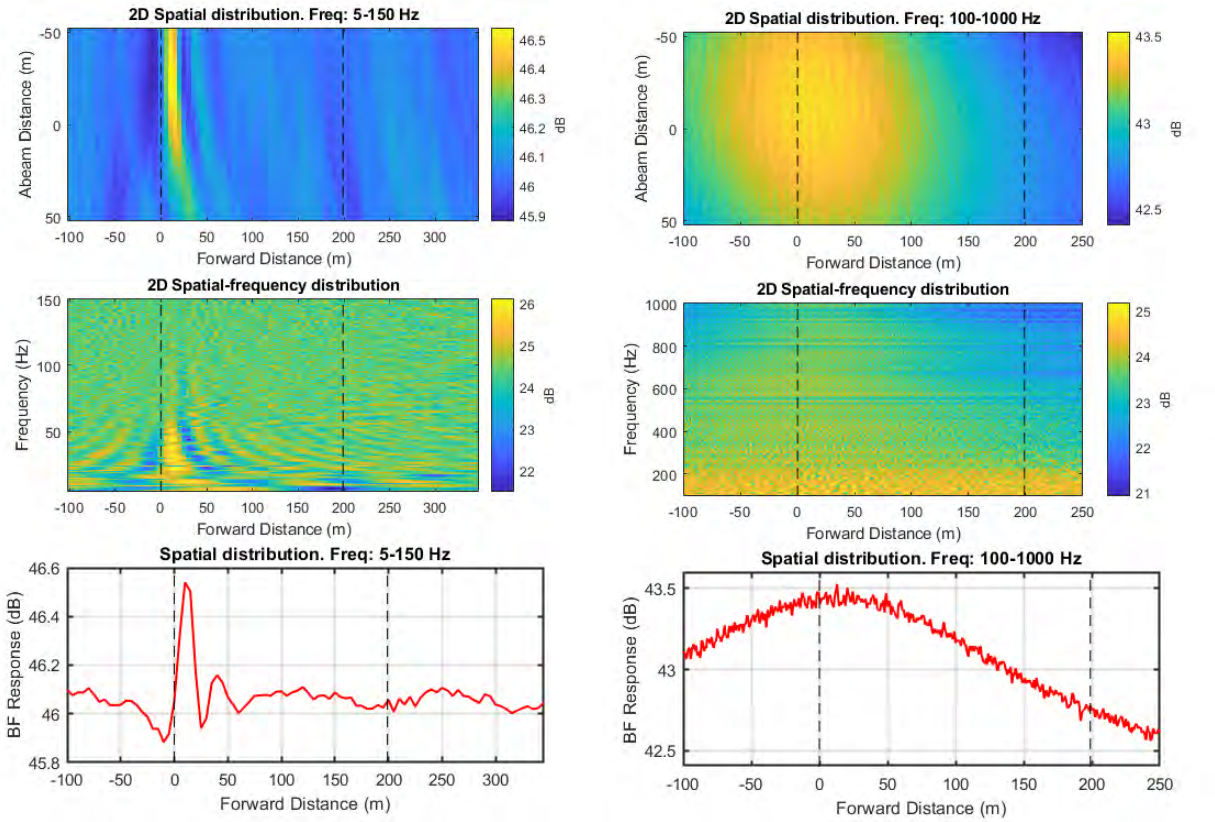

Figure 37. Noise maps from beamforming vessel pass #33 with combined array: left column panels show results for the frequency band 5–150 Hz while right column panels show the frequency band 100–1000 Hz.

3.2.3.3. High-frequency Noise Maps

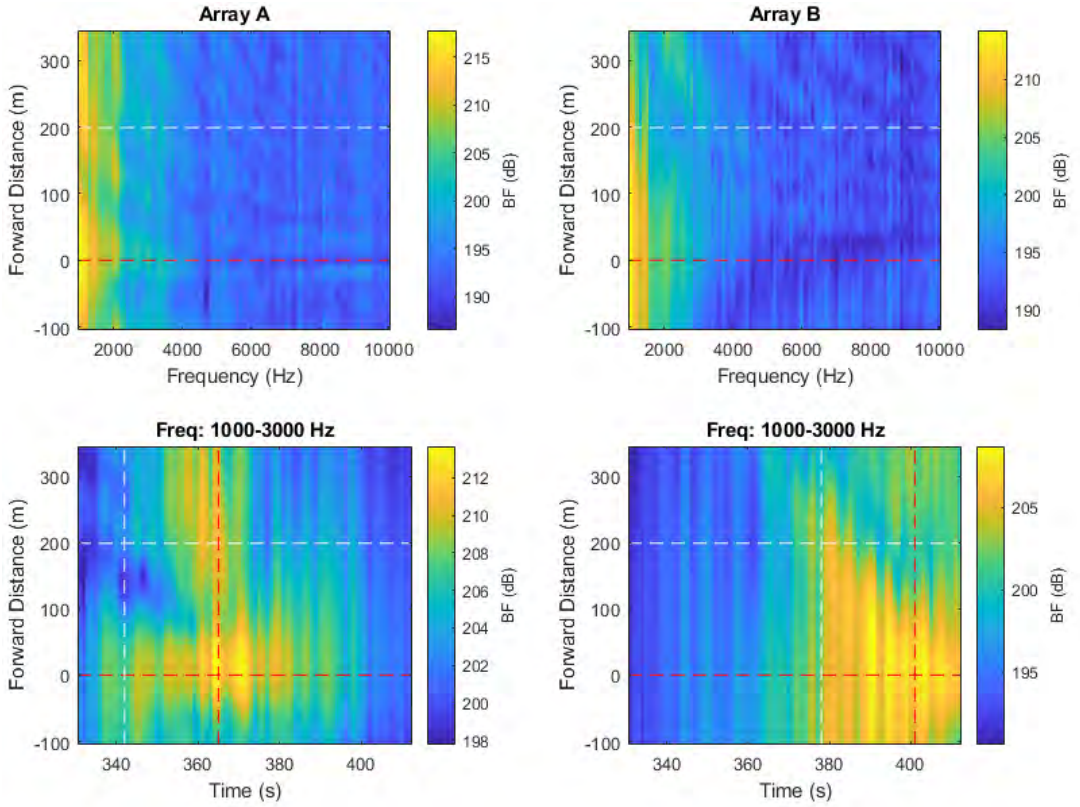

Figure 38. High-frequency (1–10 kHz) noise maps from beamforming ship pass #33 on individual arrays. Horizontal dashed lines indicate the stern and bow positions of the ship. Vertical dashed lines represent the CPA times of the bow and stern at each array. Left panels are from Frame A, right panels are from Frame B.

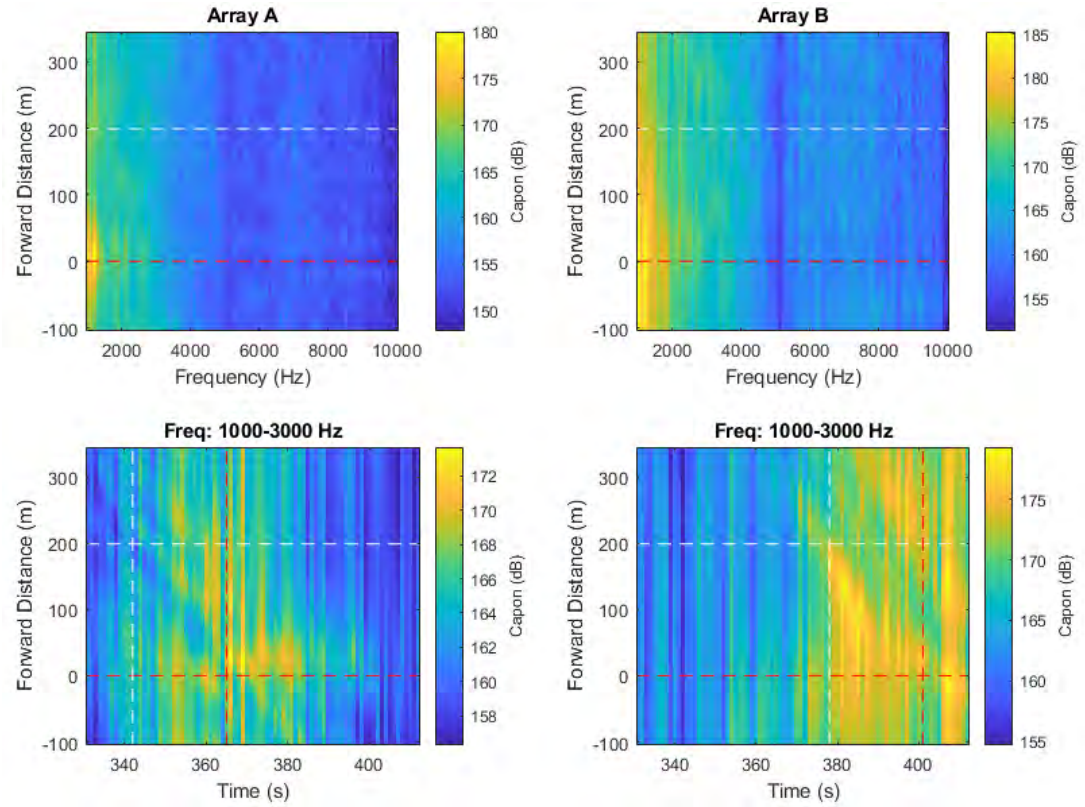

Figure 39. High-frequency noise maps (7), (8), obtained using the spatial spectra provided by the Capon algorithm implemented using individual arrays.

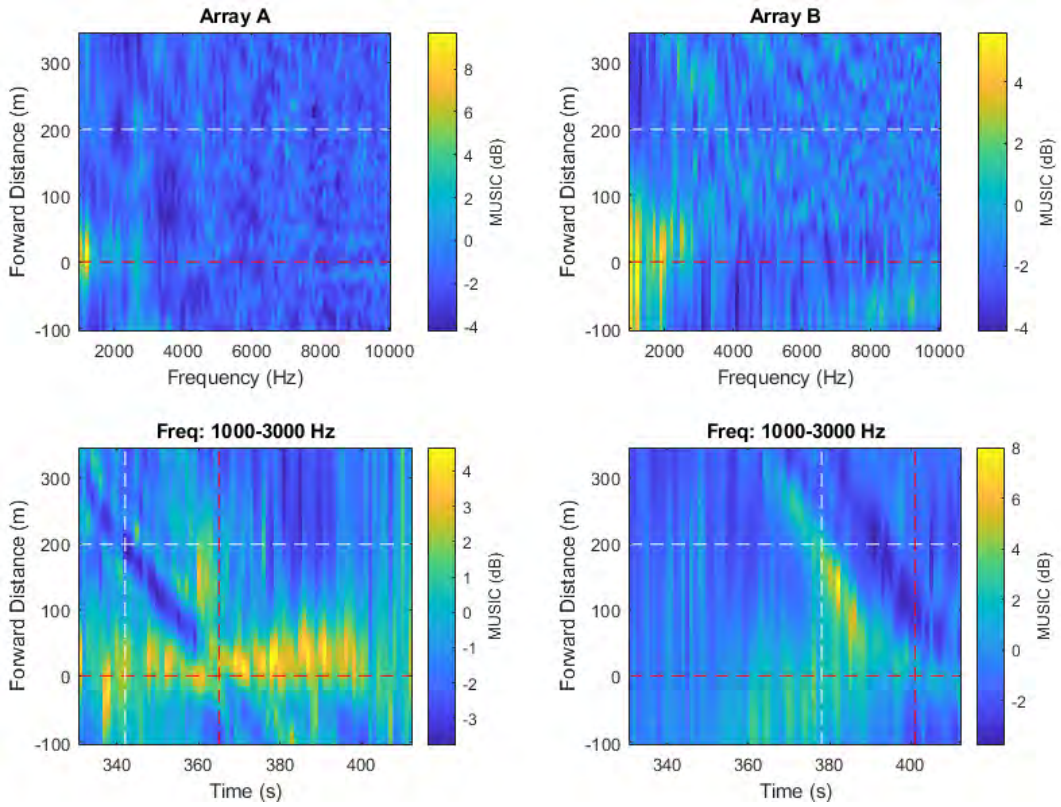

Figure 40. High-frequency noise maps (7), (8), obtained using the spatial spectra provided by the MUSIC algorithm implemented using individual arrays.

3.2.4. Tanker (Pass #36)

3.2.4.1. Ship Noise Spectra

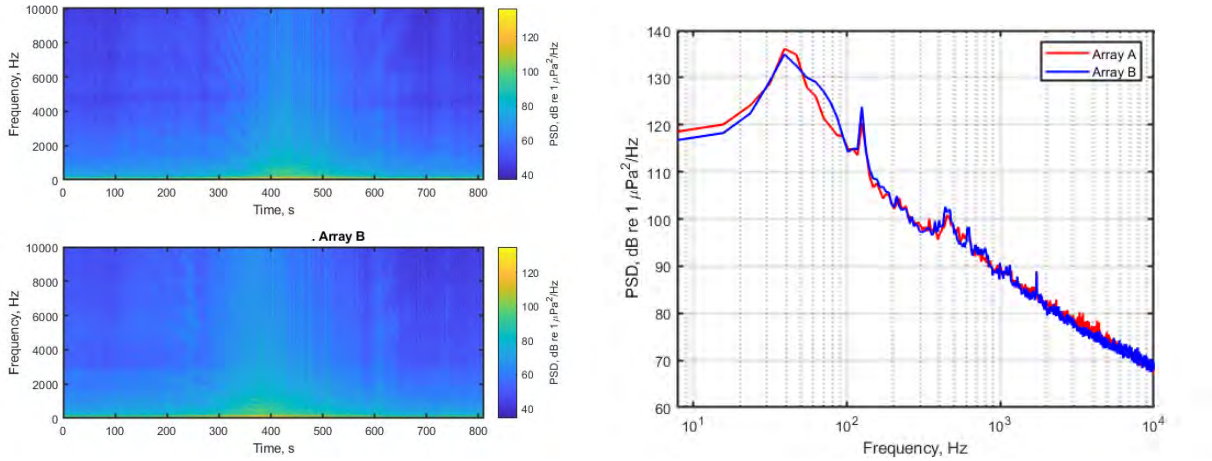

Figure 41 Spectrograms (left) and PSD (right) of ship noise from Pass #36 on top hydrophones of Arrays A and B.

3.2.4.2. Low- and Mid-frequency Noise Maps

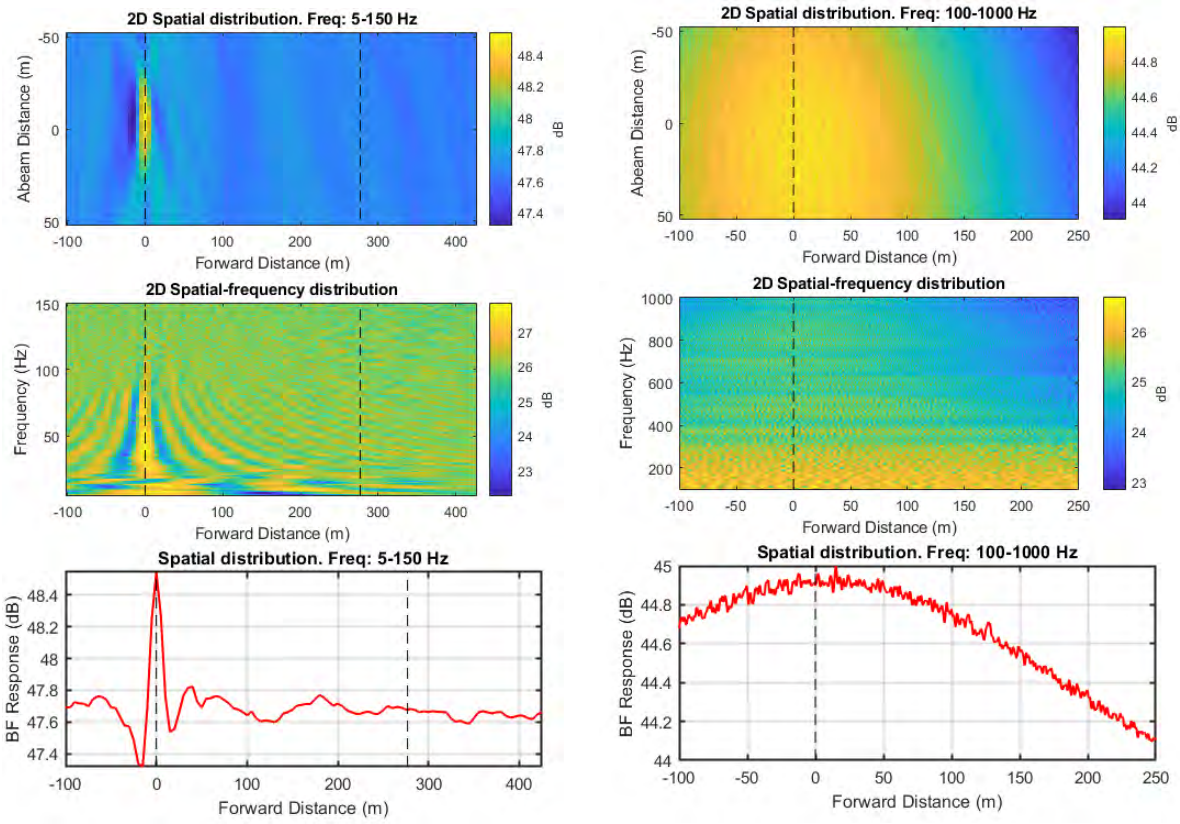

Figure 42. Noise maps from beamforming ship pass #36 with combined array: left column panels show results for the frequency band 5–150 Hz while right column panels show the frequency band 100–1000 Hz.

3.2.4.3. High-frequency Noise Maps

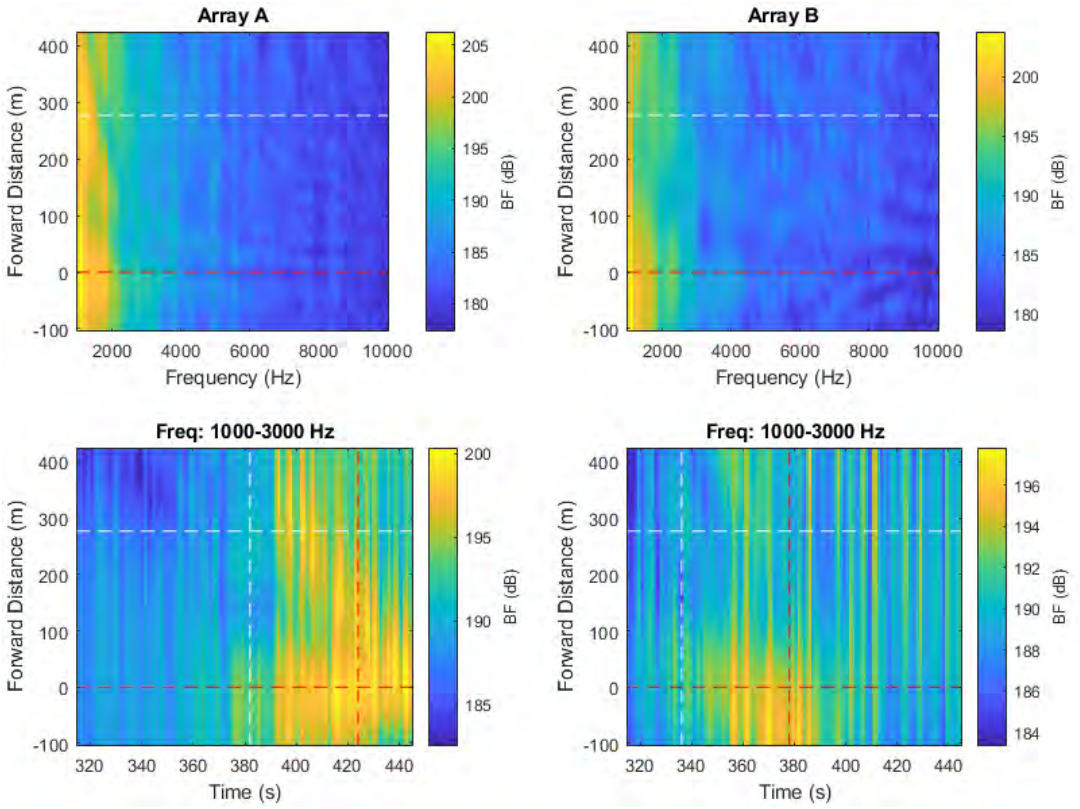

Figure 43. High-frequency (1–10 kHz) noise maps from beamforming ship pass #36 on individual arrays. Horizontal dashed lines indicate the stern and bow positions of the ship. Vertical dashed lines represent the CPA times of the bow and stern at each array. Left panels are from Frame A, right panels are from Frame B.

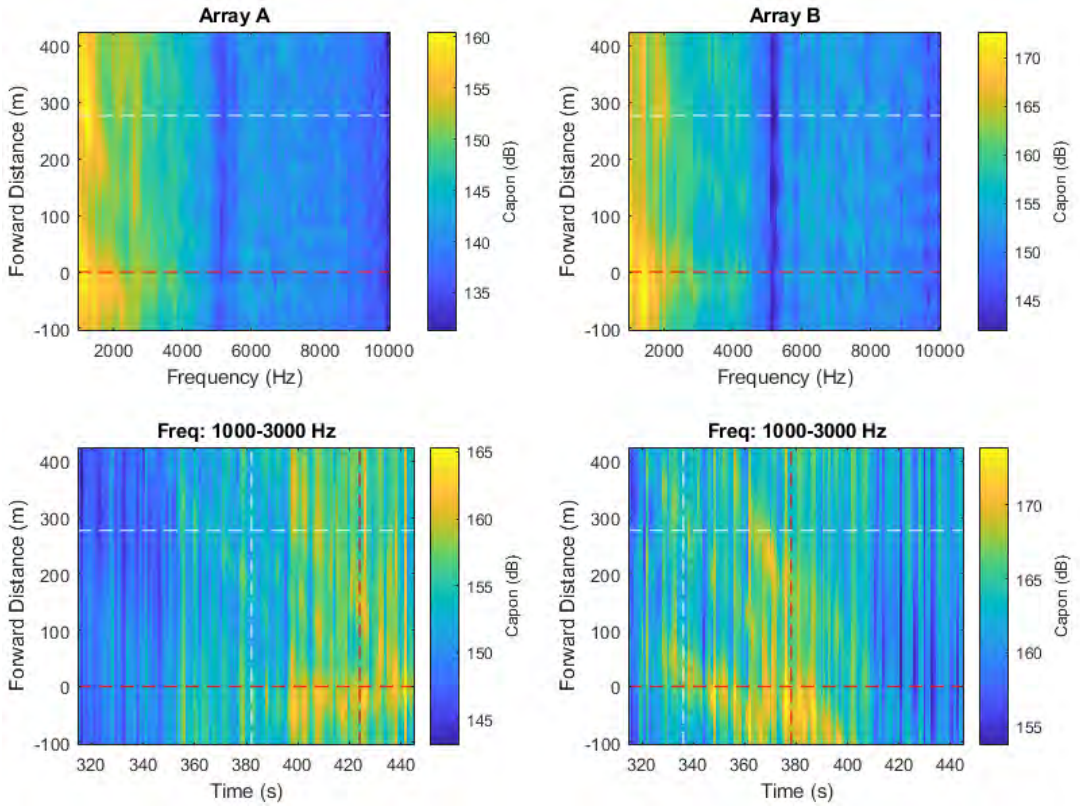

Figure 44. High-frequency noise maps (7), (8), obtained using the spatial spectra provided by the Capon algorithm implemented using individual arrays.

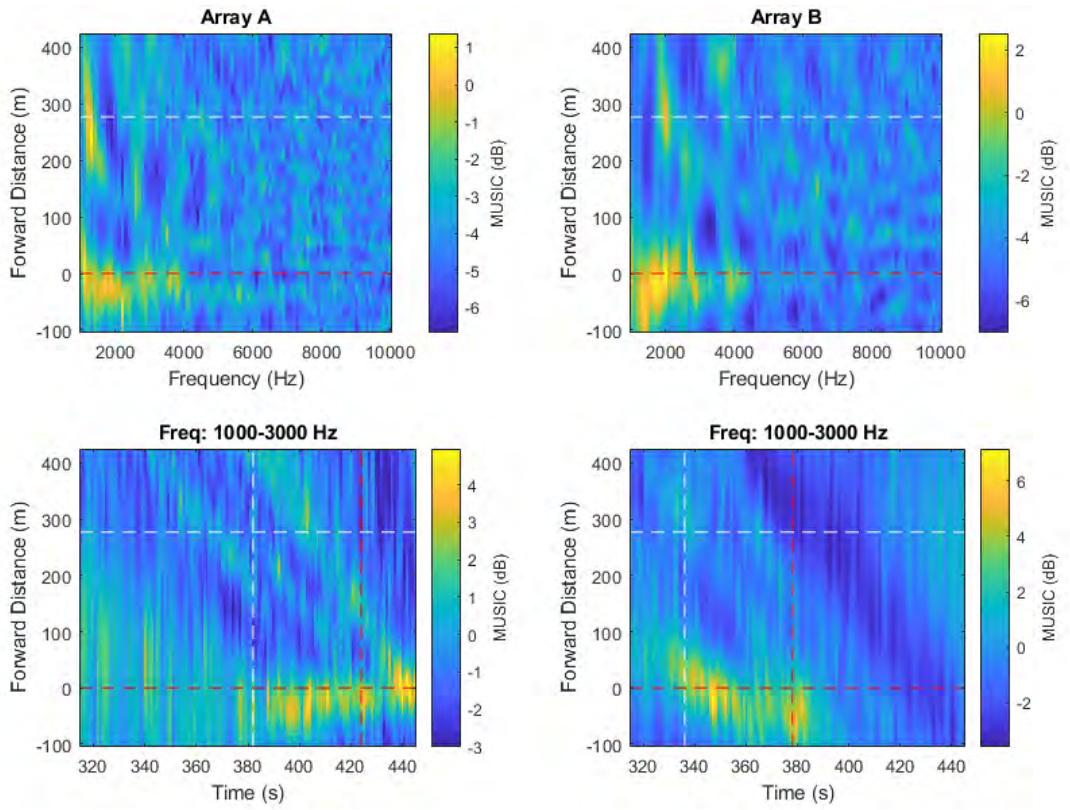

Figure 45. High-frequency noise maps (7), (8), obtained using the spatial spectra provided by the MUSIC algorithm implemented using individual arrays.

4. Summary

4.1. Review of Localizing Methods

This study tested methods for localizing noise from ships to marine acoustic data collected on two compact tetrahedral arrays of the Boundary Pass ULS. The development and testing phase of the project investigated performance of three localizing algorithms: a beamformer (BF) and two high resolution direction of arrival approaches (Capon and MUSIC algorithms).

An early finding was that standard BF, applied to the individual compact arrays over limited time windows, produced poor angular resolution of sound sources for acoustic frequencies less than approximately 1000 Hz. The individual array beamforming produced better but still marginal resolution above 1000 Hz when averaged over many 1-second data time windows. Substantial improvement in angular resolution above 1000 Hz was obtained with the Capon and MUSIC algorithms applied to the individual compact array data. These algorithms could localize sounds to within a few tens of meters even when analyzing short time windows. All three approaches, BF, Capon and MUSIC, were applied to the larger dataset of 44 ship passes in the second part of the study and discussed in Section 4.2.

The two compact arrays were time synchronized to within 1 ms and it was found that all 8 hydrophones of both compact arrays could be combined into a single larger array for beamforming lower frequency signals below 1000 Hz. Two frequency bands were defined: low frequency (LF) from 5 Hz to 150 Hz, and mid-frequency (MF) from 100 Hz to 1000 Hz. The BF was first applied to single 1-second time snapshots in both bands, with marginal localization abilities noted. This marginal performance was attributed to the beamforming issue of “grating lobes” that occurs when hydrophones are spaced at more than approximately half an acoustic wavelength. With a 300 m spacing of the compact arrays, the limiting

frequency for grating lobes is less than 3 Hz, so grating lobes are present throughout the entire LF and MF bands. However, the grating lobe problem was substantially overcome by averaging the BF results of multiple time windows. Ship movements between different time windows lead to a shifting of the grating lobes while the primary beam remains focussed in the steered direction to a specific location on the ship's hull. Thus, the averaging suppresses the grating lobes relative to the primary beam, resulting in unambiguous listening directions that can be accurately focussed on positions on the ship's hull. This approach provided noise source resolution to within approximately 10–15 m on hulls for sound frequencies in the LF band. While a theoretical assessment found this approach could also yield very good performance at higher frequencies (e.g., see right panels of Figures 8 to 11), we found its results started to degrade above 150–300 Hz. The degradation is attributed to loss of coherence of signals between the two arrays, attributed to effect of random ocean sound speed fluctuations that cause small differential time differences in the arrival times of ship noise signals between the arrays that are separated by 300.5 m. The small time differences are less important for lower frequency sounds, which have larger time periods, and that is why better performance is achieved in the LF band.

4.2. Results

4.2.1. Noise Map Formats Produced

The following methods were applied to data from 44 ship passes in Boundary Pass, with CPA distances less than 350 m:

1. Standard beamformer applied to the data of all 8 hydrophones of both arrays, treated as a single combined array, for two frequency bands: 5 Hz to 150 Hz and 100 Hz to 1000 Hz. The results were computed in many 1-second time intervals, and these were averaged to produce noise maps in three formats:
    a. BF response versus abeam and forward distances
    b. BF response versus forward distance and sound frequency
    c. BF response versus forward distance
2. Standard beamformer applied to individual compact array data for the frequency band 1 kHz to 10 kHz. Noise maps are produced separately for both arrays in the following formats:
    a. BF response versus frequency and forward distance
    b. BF response versus time and forward distance
3. Capon and MUSIC angle of arrival algorithms applied to individual compact array data for the frequency band 1 kHz to 10 kHz. Noise maps are produced separately for both arrays and both methods in the following formats:
    a. BF response versus frequency and forward distance
    b. BF response versus time and forward distance

4.2.2. Discussion of Approaches and Ship Noise Distributions

The noise maps for all 44 ship passes are provided in Appendix A. A detailed review of the results for each ship pass are provided in Table 2. Some of the key findings of the method development work and results of applying these methods to real Boundary Pass ULS ship data are listed below.

1. The ULS hydrophone geometry of two compact tetrahedral arrays separated by ~300 m was most effective for noise localization at frequencies below 150 Hz. This was achieved by combining the two compact arrays into a single large but sparse array.
2. Above 150 Hz, loss of acoustic signal coherence between the compact arrays led to reduced performance of the combined array beamforming. The coherence loss is attributed to small differences in the signal arrival times at the compact arrays due to ocean inhomogeneities. This does not affect lower frequencies with larger periods.
3. At frequencies of 1 kHz to 10 kHz, standard beamforming and the Capon and MUSIC angle of arrival methods provided good localizing ability (to within ~40 m) when applied to the individual compact arrays. This method was not effective below 1000 Hz due to large beamwidths of the individual compact arrays.
4. At low frequencies, less than 150 Hz, beamforming on the combined array would normally lead to poor performance due to a beamforming limitation known as “grating lobes”, which causes ambiguity in determining the directions of received sounds. However, the study found that grating lobes could be substantially supressed by averaging results from processing multiple 1-second intervals (snapshots) during each ship pass. The grating lobes move between snapshots, but the primary beam lobe remains in the direction of interest. Therefore, averaging the snapshots significantly enhanced the beamformer primary signal relative to the grating lobes.
5. A further limitation of the localizing methods tested was that a single loud source could mask nearby sources that were quieter. However, the quieter sources could still be resolved well if they were physically separated by a few tens of meters or if they were dominant in at least some frequency bands. In many cases it was clear there were two sources with different dominant frequencies.
6. Very good localizing effectiveness was found for frequencies below 150 Hz, allowing source localization to within 10–15 m along the hulls of ships passing at approximately 200–350 m horizontal distance. The localization abilities from 150 Hz to 1000 Hz were generally reduced by coherence loss as discussed above, although a few measurements showed coherence at frequencies over 300 Hz. Those cases (e.g. Pass 17) produced very accurate localizations to within 5 m for sounds at frequencies 150–300 Hz. Localizing abilities for sound frequencies from 1 kHz to 10 kHz were again good, allowing a spatial resolution of approximately 40 m in that frequency range.
7. The results of applying these localization methods to Boundary Pass ULS data indicate that nearly all noise from these ships originates from a relatively small area of perhaps dimension 20 m close to the stern – likely mainly from their propellers and engines. We did not detect other systematic noise sources near ship bows or in their wakes where turbulence might be found. These sound sources may still be present, but their amplitudes will be much lower than the engine and propeller noise and they are therefore masked. This finding has important implications for noise mitigations, which could be effective if applied only over small areas of ships near the propellers and engine. This finding also suggests that measurement systems designed to characterize ship noise may not need to be placed as far from large ships as current measurement standards require; the current ISO and ANSI measurement standards require the minimum measurement distance to be at least one ship length, which may be excessive for very large ships.

8. It was hypothesized that engine noise might be localized 10–20 m in front of the propellers, due to their relative forward physical positioning. Two dominant noise sources, typically separated by 10–20 m, were identified near the stern in approximately half the ship passes examined. Often, but not always, the forward source, expected to be the engine, dominated in narrow bands below 20 Hz. The same forward source may produce noise also at higher frequencies, but those would not be visible in the noise maps due to masking by the stronger aft source (likely the propeller). This was an interesting finding, because there are known low frequency sounds produced by propellers, such as the blade rate fundamental often below 10 Hz and its harmonics that would be expected to mask the engine noise at the same frequencies. The dominance (in some vessels) of engine noise also at these low frequencies was not expected. An alternate explanation is that low frequency propeller noise interacts with the hull, leading to a resonant emission or reflection from the hull a few meters in front of the propeller at the same frequencies, but that is speculative.
9. The localizing resolution above 1 kHz was not sufficient to identify sources spaced closely (within about 30 m in most cases). The results of applying the MUSIC and CAPON methods provided noise source spatial resolution of about 20–40 m, and these results also showed that nearly all noise at higher frequencies originated from near the ship sterns. These results did not discern more than one source on each ship, but again weak sources even near the bows of ships could be masked by the stronger sources near the stern.

The tests of different hydrophone combination approaches found that the combined hydrophone array provided much better performance than the individual arrays. This is not surprising since the individual array processing discards time difference information between the hydrophones of the two synchronized arrays. For example, if a sound is measured simultaneously on the compact arrays, then we know the source is located equidistant from both arrays. This extra information leads to much narrower beamwidths, providing much improved spatial resolution of noise source distributions. It, however, leads to the issue of grating lobe ambiguity, that would be difficult to overcome with a non-moving noise source. However, as discussed in this report, the grating lobes can be suppressed by averaging multiple views of vessels, from different angles, as they sail past the ULS hydrophone arrays .

While a systematic analysis of noise localization performance versus ship speed and CPA distance has not been completed, this might be performed when more data are acquired. One of the two compact arrays of the Boundary Pass ULS is temporarily offline but will be serviced in October 2021 (just weeks from completion of this report). It is intended that the automated localization system developed for this study will be restarted when the second array is back online, and a very large number of measurements (perhaps thousands) should soon be available.

Finally, a limitation of the system performance was noted in the mid-frequency band, from about 200 Hz to 1 kHz. This was due to coherence loss between the two compact arrays starting at 150–250 Hz. That could be overcome by shortening the compact array separation or by adding hydrophones between them. Since signal coherence with 300 m array separation is good to approximately 150 Hz, it is hypothesized that reducing the separation by a factor of about 6 (to 50 m separation) would provide adequate coherence to approximately 1000 Hz. In fact, a single hydrophone cabled 50 m off each of the arrays could provide substantial improvement for this type of localization analysis. This would be a fairly easy modification for future deployments of these systems.

The most important finding of this study was that most of the noise radiated from vessels originates from a small area near their sterns. The important noise sources are likely the propellers and engines. We did not identify noise sources at other locations on vessels, however those sources could have been masked by the louder sources near the stern. Nevertheless, this finding suggests that noise mitigations could be focussed on the engines and propellers for effective reduction of overall noise emissions of these vessels. The physical size of the mitigation technologies could smaller and likely less expensive than would be the case if larger areas of the hull needed quieting.

Literature Cited

Haykin, S. 1985. *Array signal processing*. Prentice-Hall, Inc., Englewood Cliffs, NJ. 493 p.

Johnson, D.H. and D.E. Dudgeon. 1993. *Array Signal Processing: Concepts and Techniques*. Prentice Hall, Englewood Cliffs, NJ, USA. 533 p.

Urazghildiiev, I.R., B. Martin, and D.E. Hannay. 2021. The Accuracy of Bearing Estimates of Wideband Signals Produced by Marine Animals. *IEEE Journal of Oceanic Engineering* 46(3): 1057-1067. https://doi.org/10.1109/JOE.2020.3040703.

Van Trees, H.L. 2002. *Optimum array processing: Part IV of detection, estimation, and modulation theory*. John Wiley & Sons, New York.

Appendix A. Noise Maps

A.1. Pass #1 (Type: Bulker. Length: 292 m. Speed: 10.3 kn)

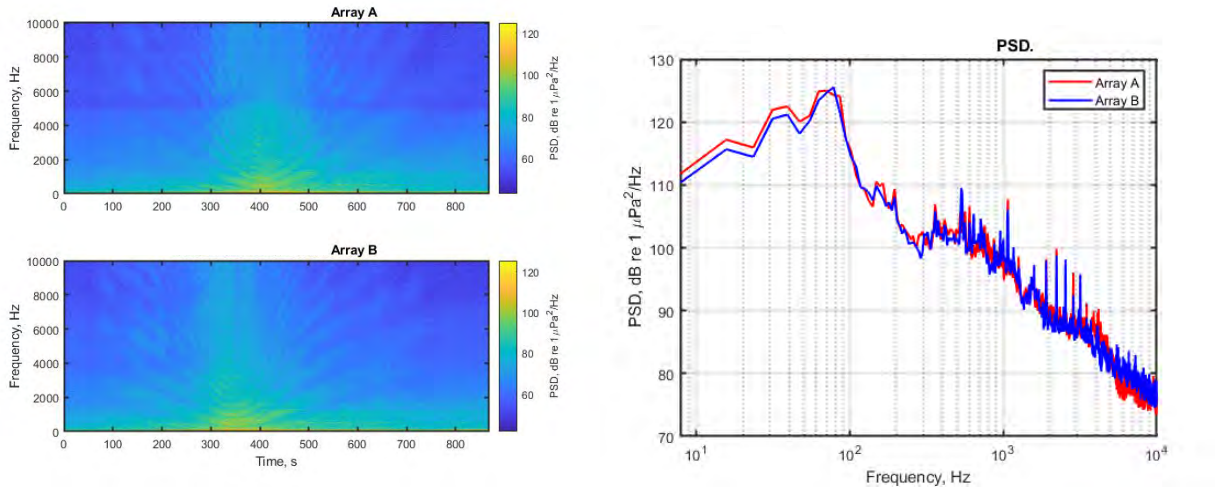

Figure 46 Spectrograms (left) and PSD (right) of ship noise observed on outputs of Arrays A and B.

A.1.1. Low- and mid-frequency noise maps

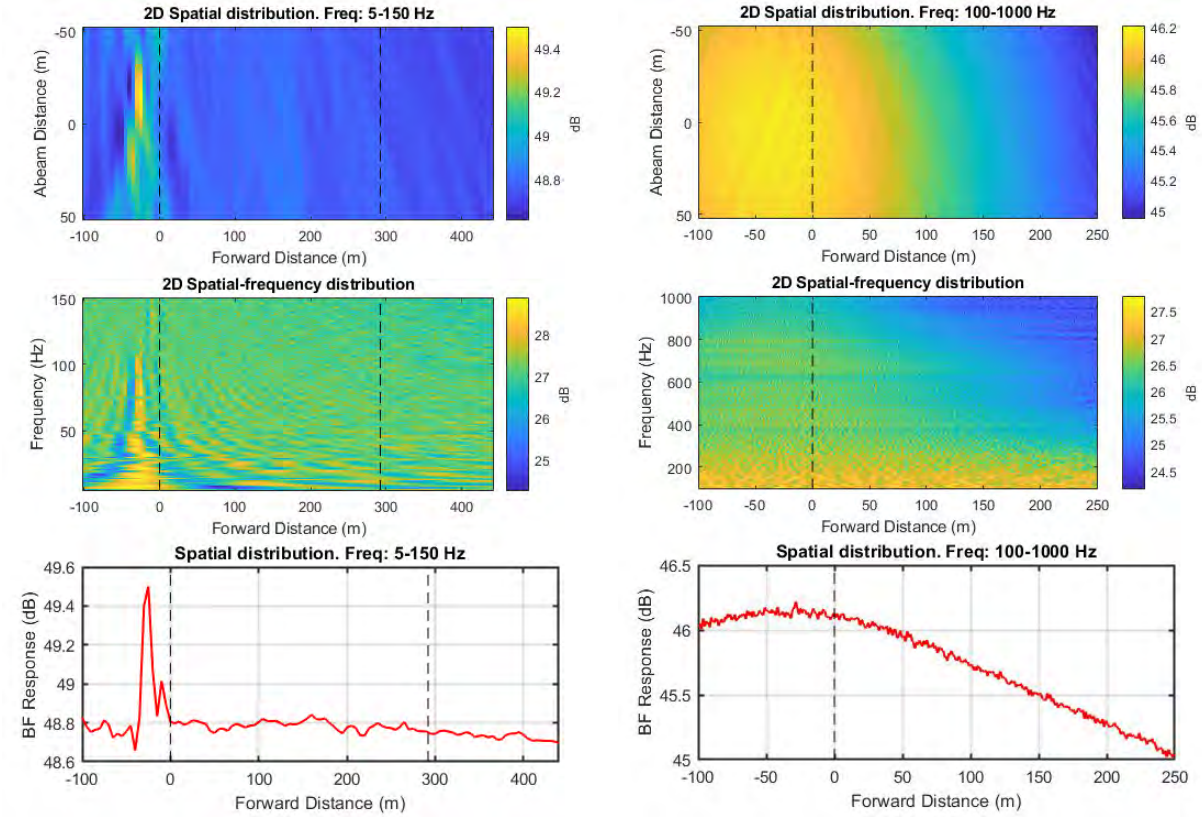

Figure 47 Noise maps from standard beamforming using combined array for Vessel Pass #1: 2D maps in spatial domain for two frequency ranges (top); 2D maps in vessel forward distance and frequency domain for two frequency ranges (middle); and graph of BF response versus forward distance for two frequency ranges (bottom). Frequency ranges are 5 to150 Hz (left) and 100 to 1000 Hz (right).

A.1.2. High-frequency noise maps

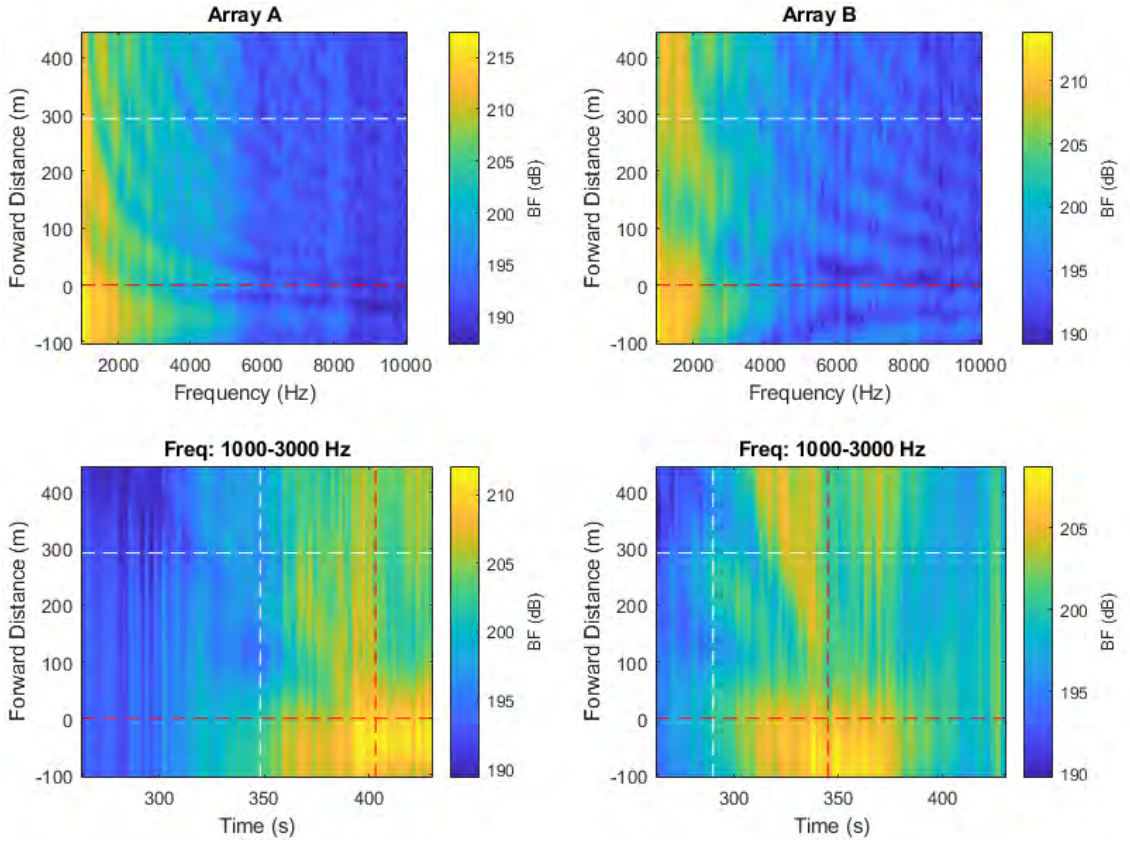

Figure 48 High-frequency noise maps from beamforming with individual arrays. Top maps show the BF response versus forward distance along vessel, measured approximately from the stern, versus frequency. Bottom maps show BF response versus forward distance and snapshot time. Horizontal dashed lines indicate the stern and bow positions of the vessel. Vertical dashed lines represent the CPA times of the bow and stern at each array.

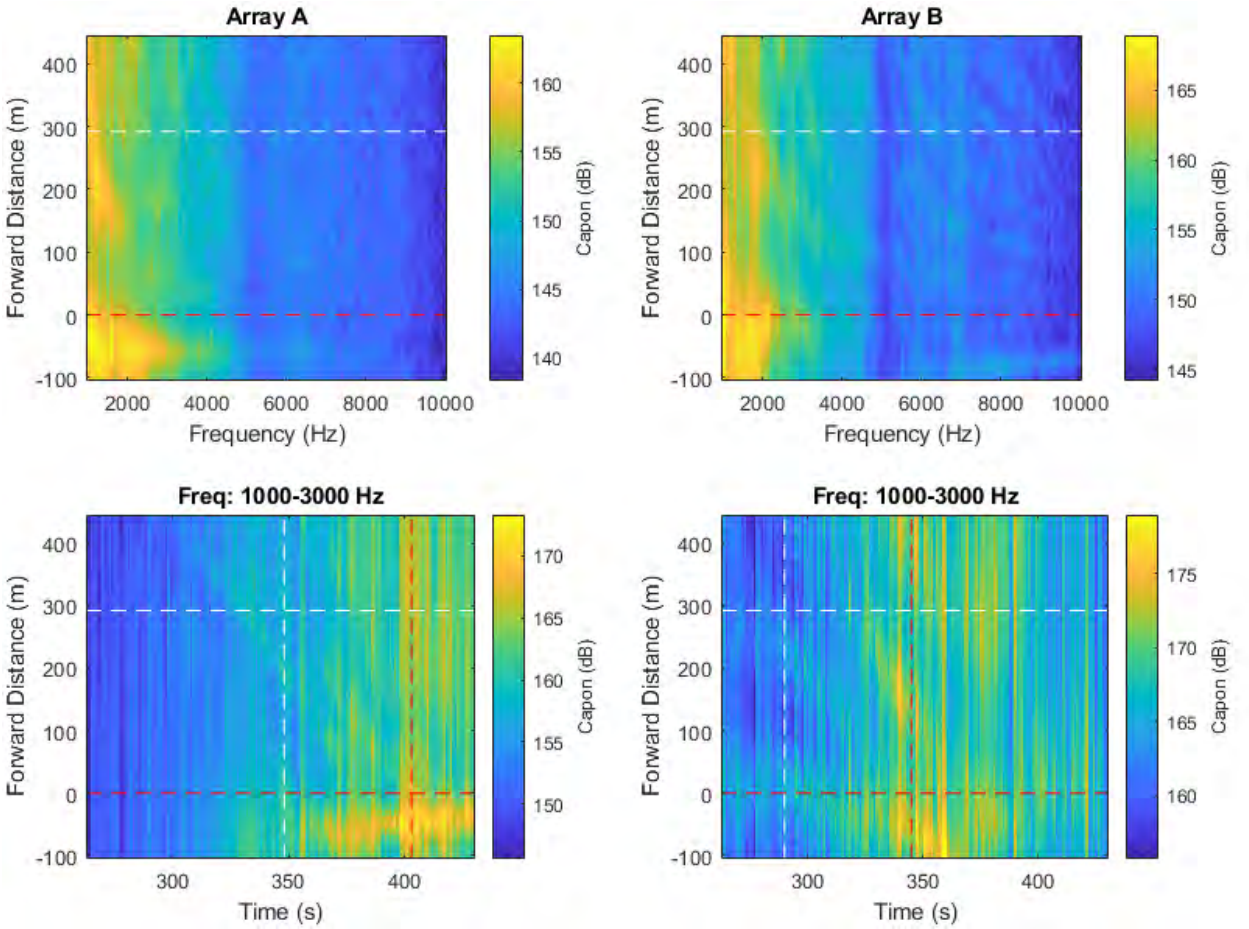

Figure 49 High-frequency noise maps obtained using the spatial spectra provided by the Capon algorithm implemented using individual arrays.

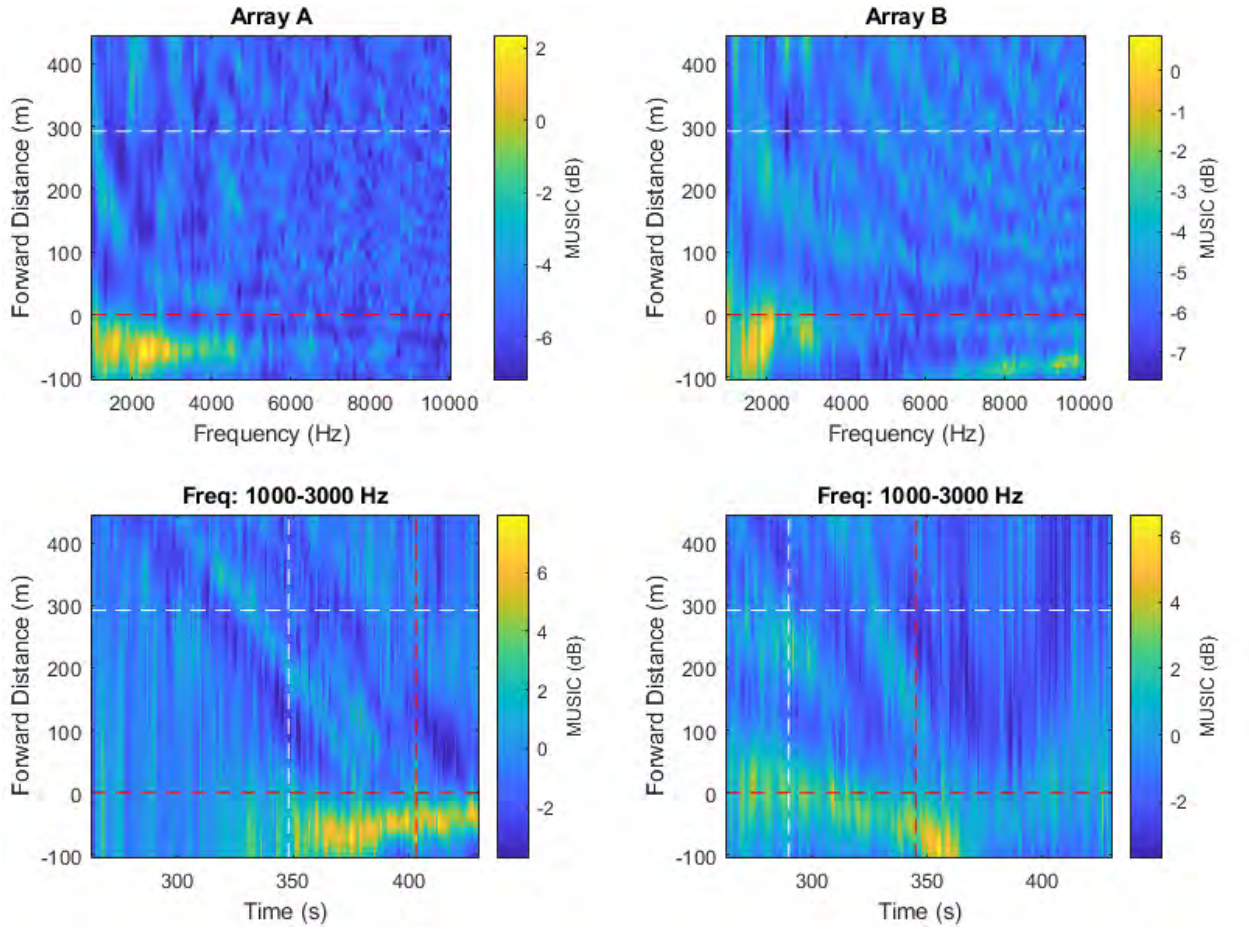

Figure 50 High-frequency noise maps obtained using the spatial spectra provided by the MUSIC algorithm implemented using individual arrays.

A.2. Pass #2 (Type: Container. Length: 210 m. Speed: 17.1 kn)

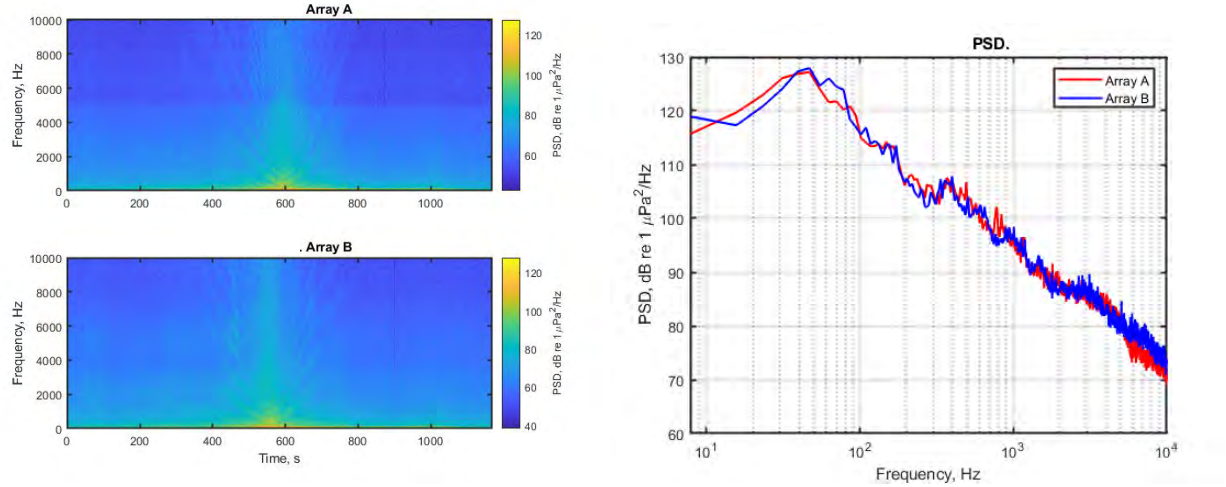

Figure 51 Spectrograms (left) and PSD (right) of ship noise observed on outputs of Arrays A and B.

A.2.1. Low- and mid-frequency noise maps

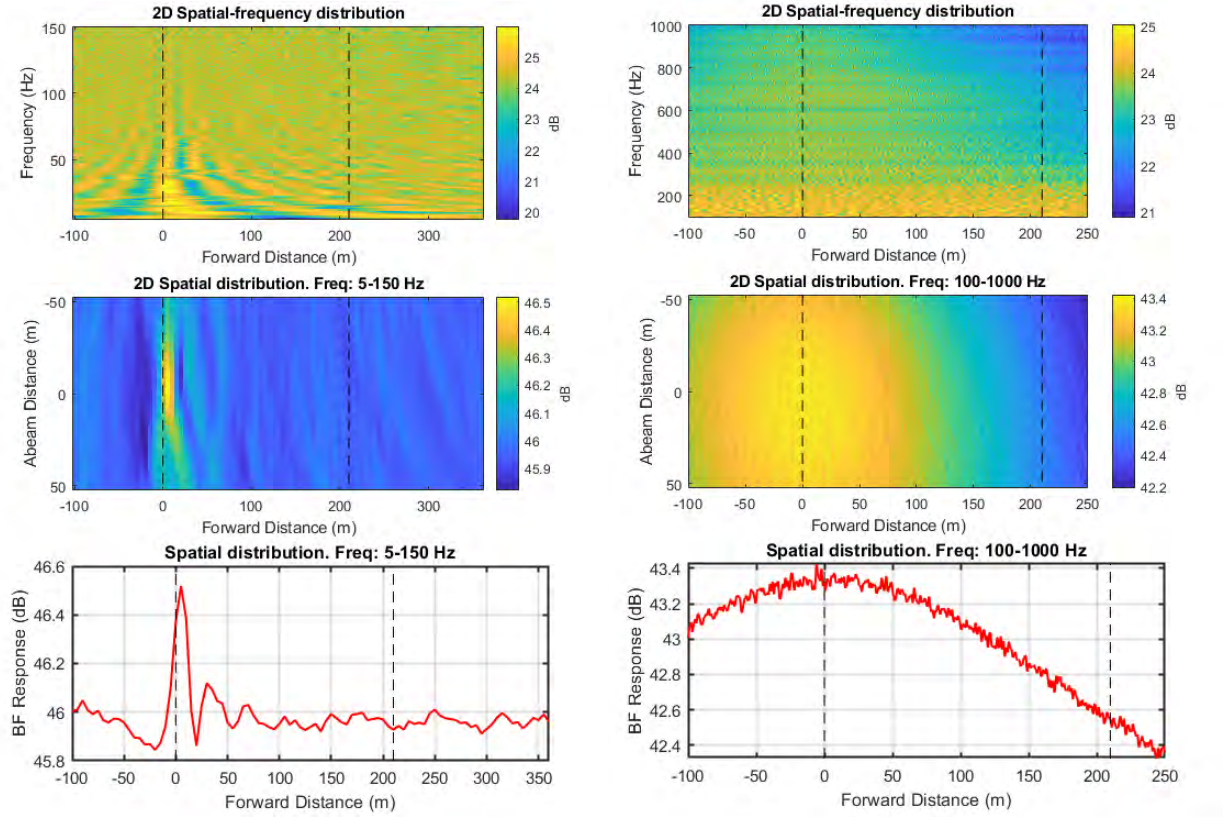

Figure 52 Noise maps from standard beamforming using combined array for Vessel Pass #2: 2D maps in spatial domain for two frequency ranges (top); 2D maps in vessel forward distance and frequency domain for two frequency ranges (middle); and graph of BF response versus forward distance for two frequency ranges (bottom). Frequency ranges are 5 to150 Hz (left) and 100 to1000 Hz (right)

A.2.2. High-frequency noise maps

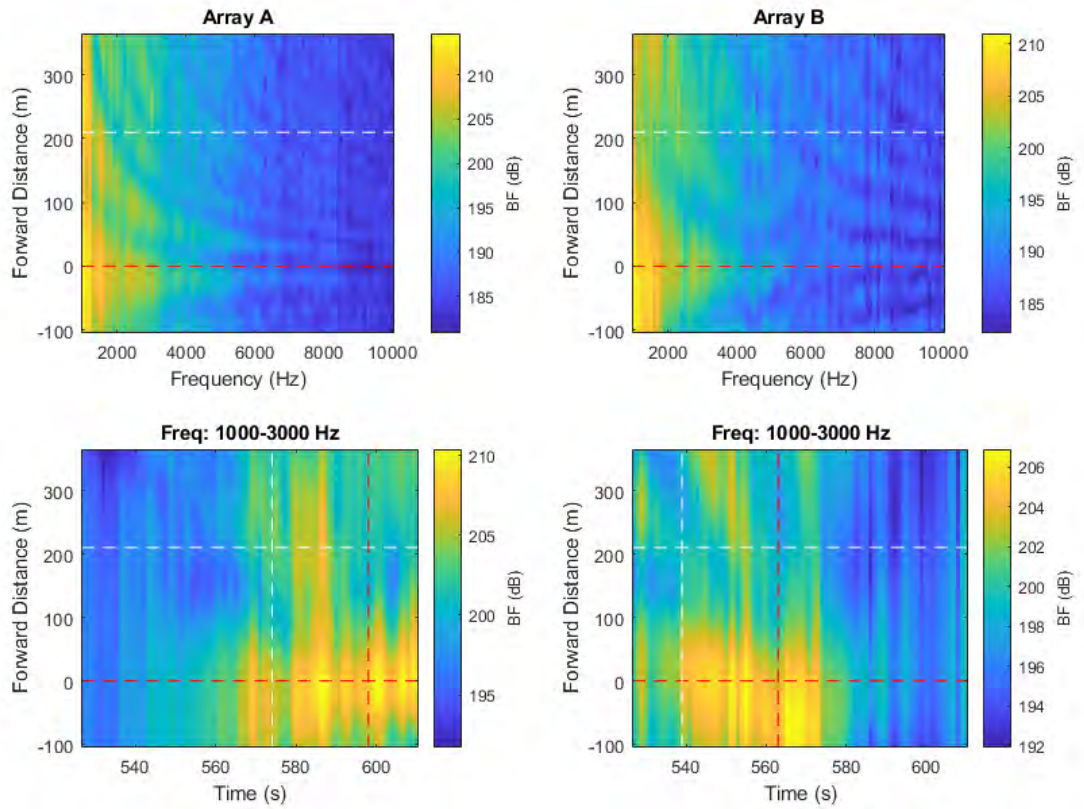

Figure 53 High-frequency noise maps from beamforming with individual arrays. Top maps show the BF response versus forward distance along vessel, measured approximately from the stern, versus frequency. Bottom maps show BF response versus forward distance and snapshot time. Horizontal dashed lines indicate the stern and bow positions of the vessel. Vertical dashed lines represent the CPA times of the bow and stern at each array.

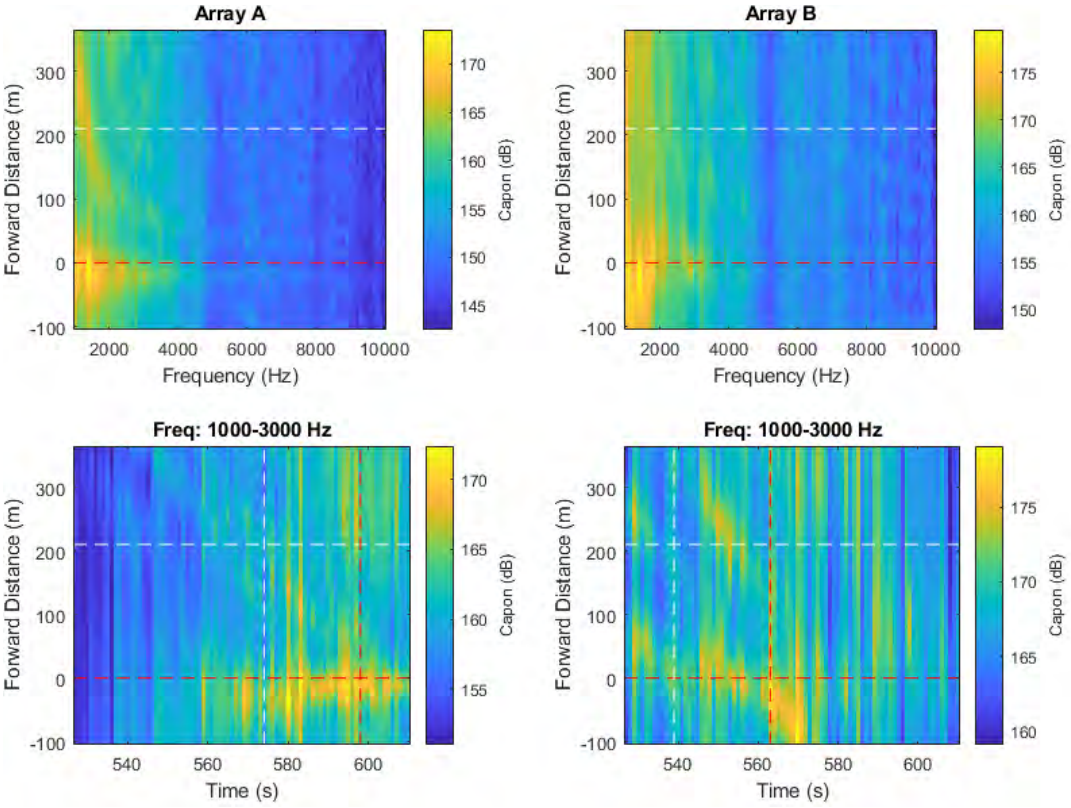

Figure 54 High-frequency noise maps obtained using the spatial spectrums provided by the Capon algorithm implemented using individual arrays.

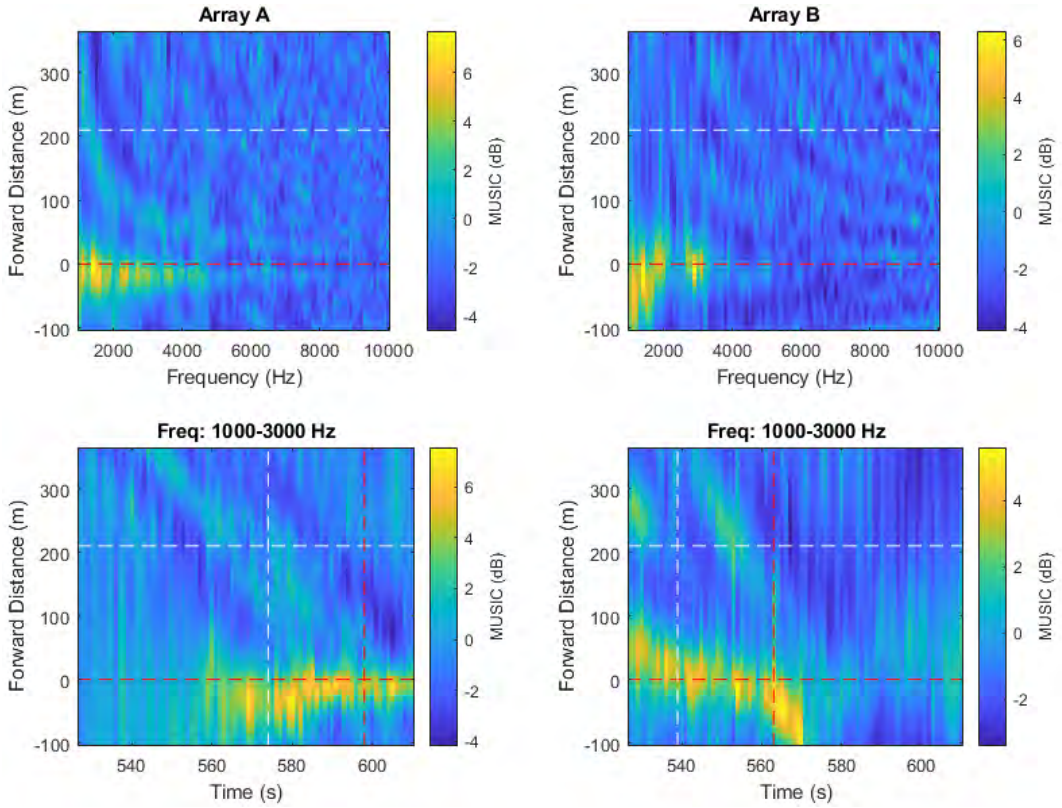

Figure 55 High-frequency noise maps obtained using the spatial spectrums provided by the MUSIC algorithm implemented using individual arrays.

A.3. Pass #3 (Type: Container. Length: 349 m. Speed: 20.4 kn)

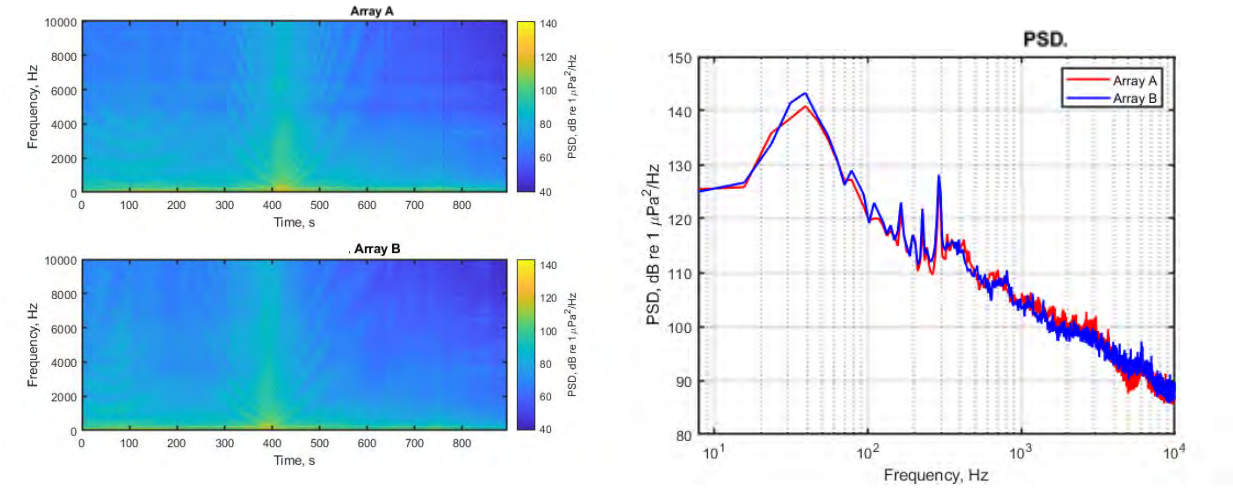

Figure 56 Spectrograms (left) and PSD (right) of ship noise observed on outputs of Arrays A and B.

A.3.1. Low- and mid-frequency noise maps

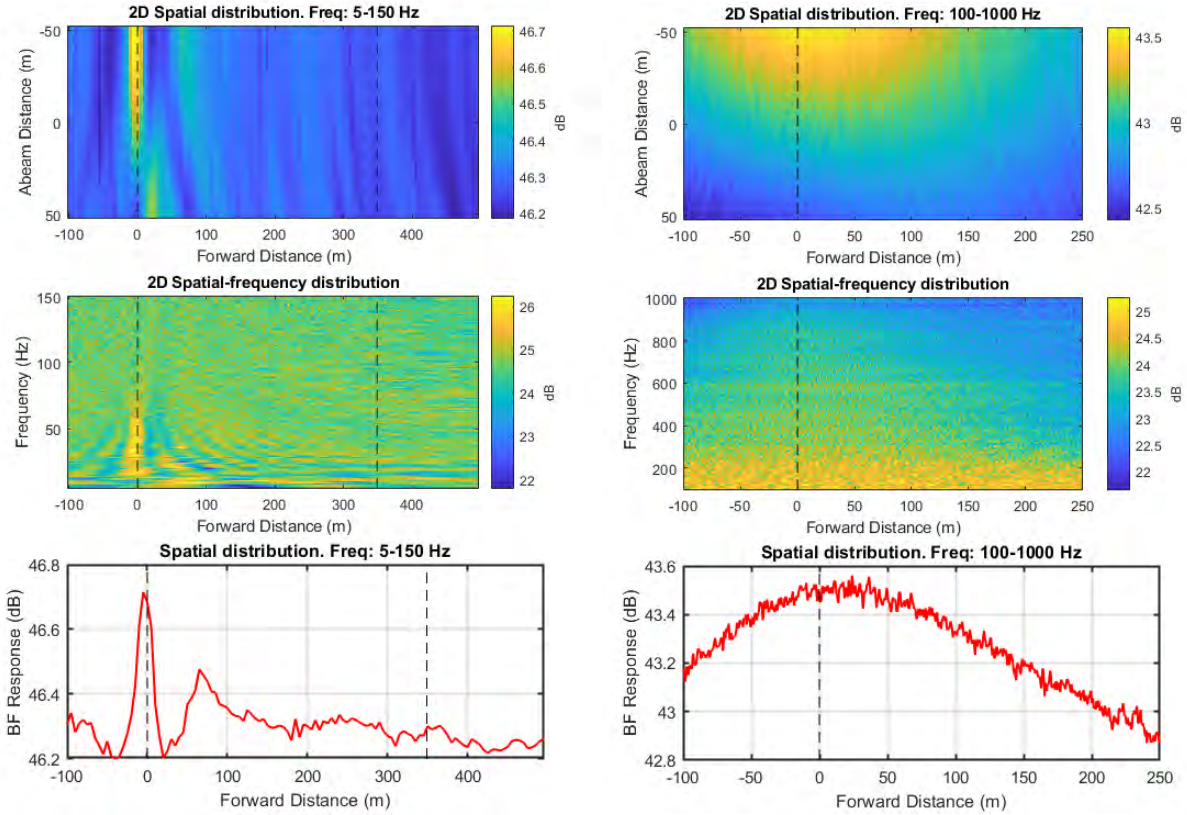

Figure 57 Noise maps from standard beamforming using combined array for Vessel Pass #3: 2D maps in spatial domain for two frequency ranges (top); 2D maps in vessel forward distance and frequency domain for two frequency ranges (middle); and graph of BF response versus forward distance for two frequency ranges bottom). Frequency ranges are 5 to150 Hz (left) and 100 to1000 Hz (right).

A.3.2. High-frequency noise maps

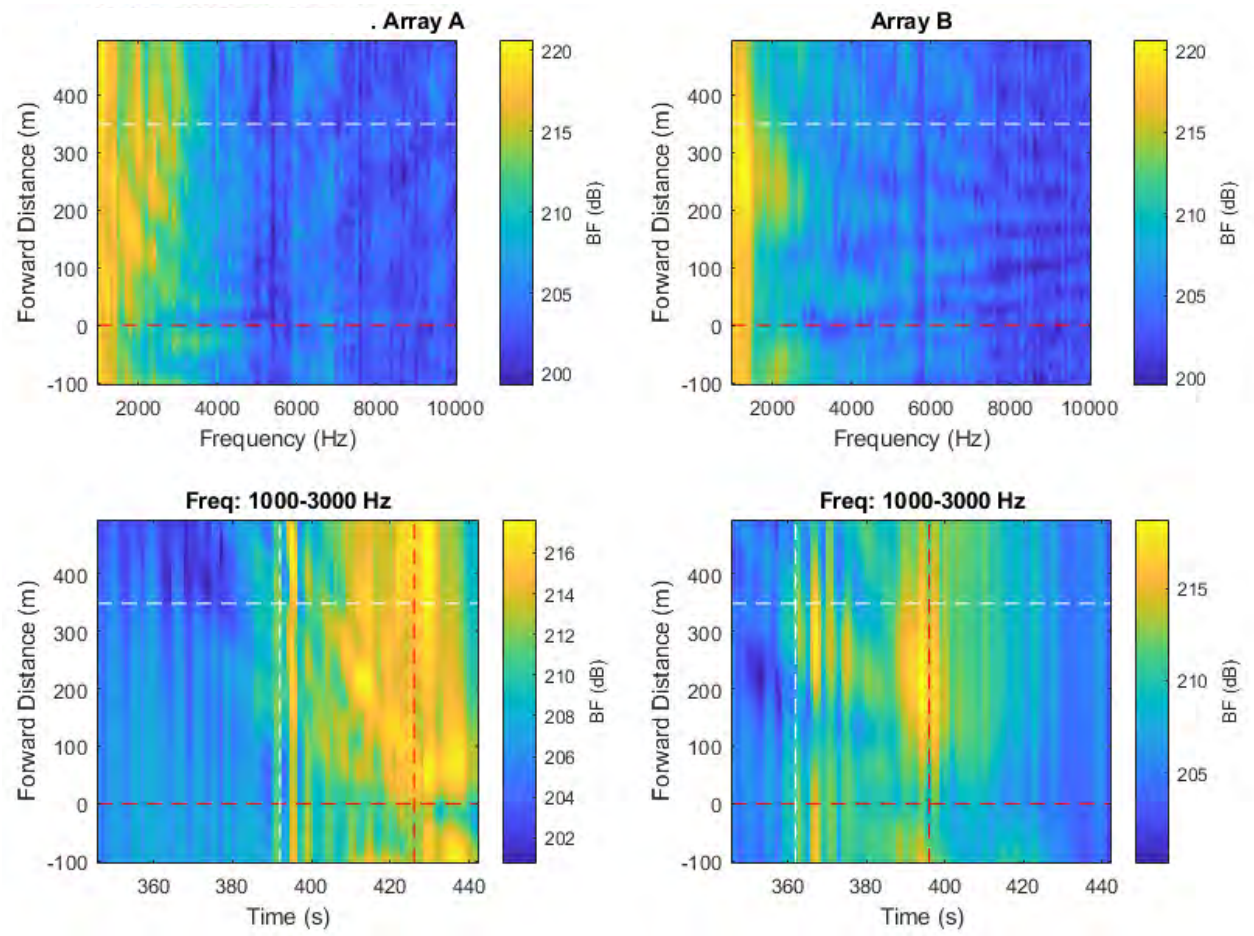

Figure 58 High-frequency noise maps from beamforming with individual arrays. Top maps show the BF response versus forward distance along vessel, measured approximately from the stern, versus frequency. Bottom maps show BF response versus forward distance and snapshot time. Horizontal dashed lines indicate the stern and bow positions of the vessel. Vertical dashed lines represent the CPA times of the bow and stern at each array.

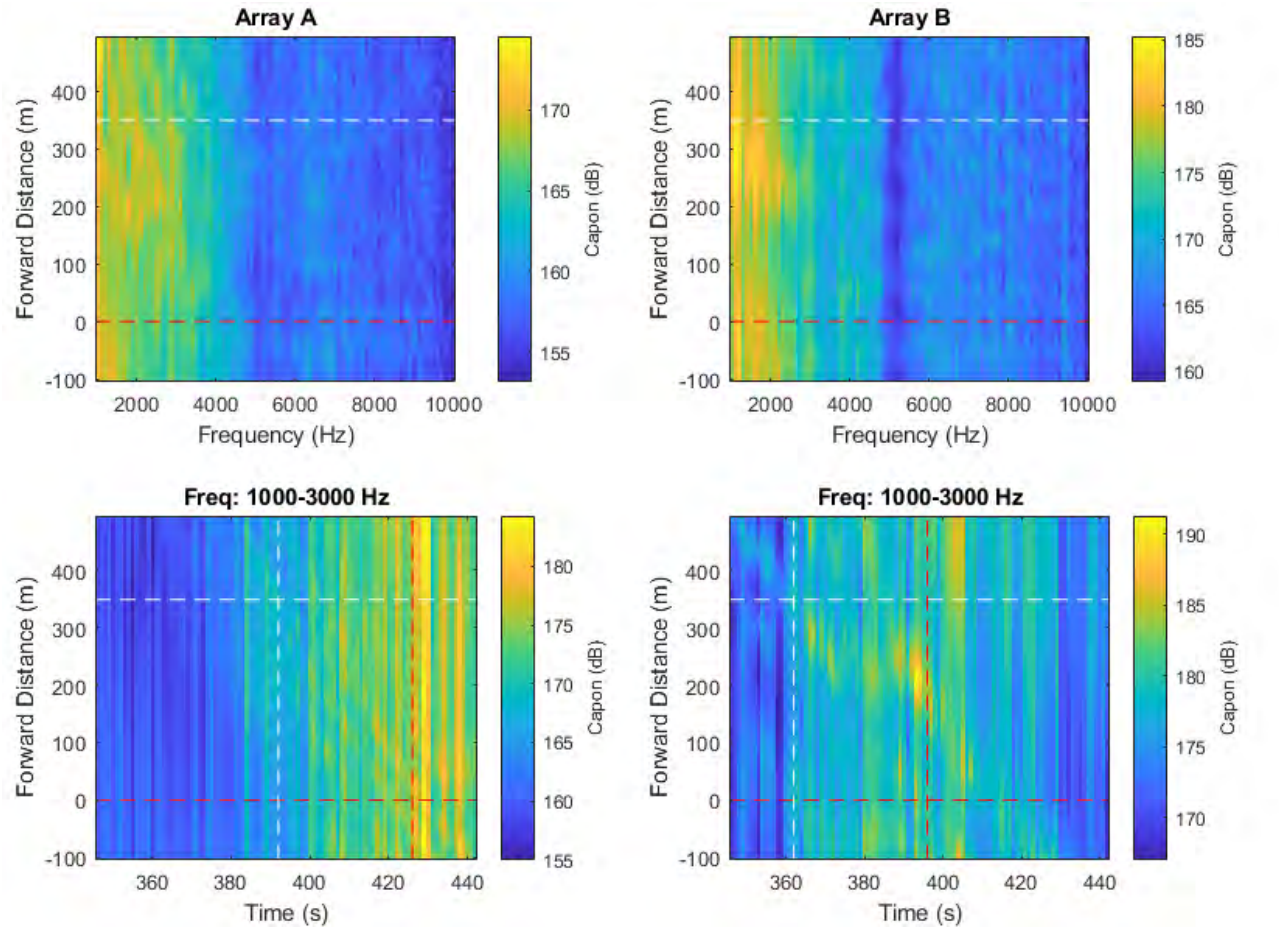

Figure 59 High-frequency noise maps obtained using the spatial spectra provided by the Capon algorithm implemented using individual arrays.

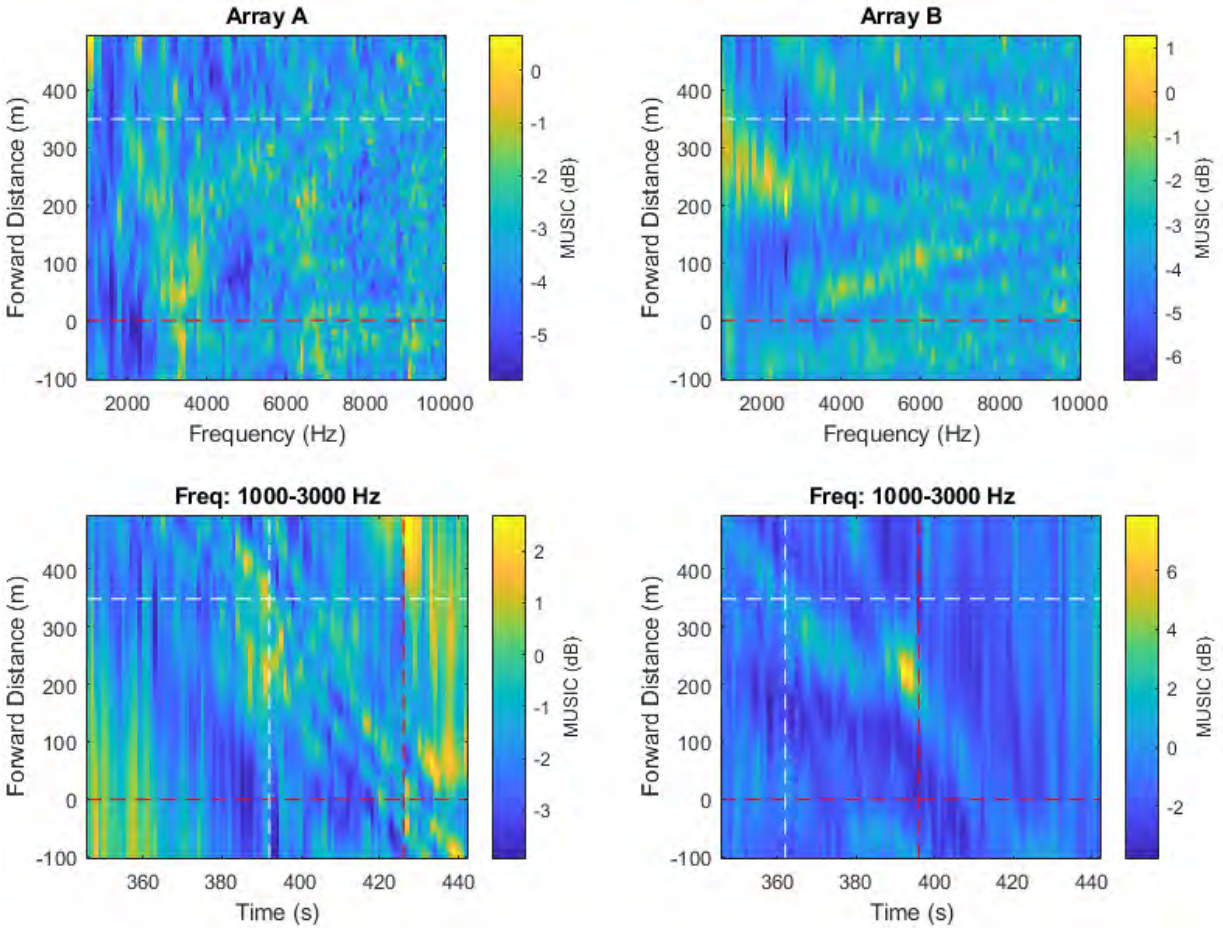

Figure 60 High-frequency noise maps obtained using the spatial spectra provided by the MUSIC algorithm implemented using individual arrays.

A.4. Pass #4 (Type: Bulker. Length: 190 m. Speed: 12.9 kn)

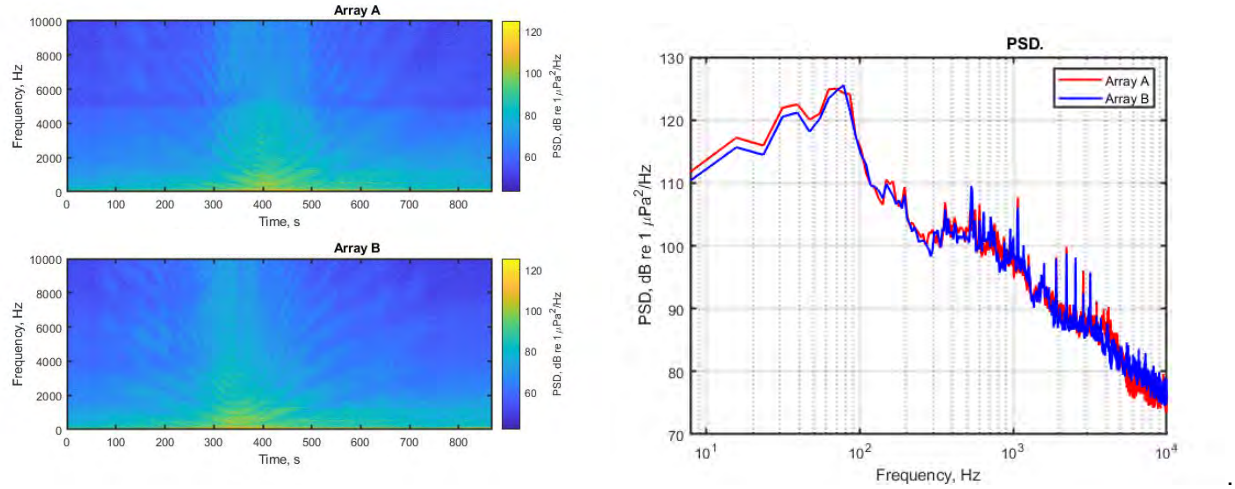

Figure 61 Spectrograms (left) and PSD (right) of ship noise observed on outputs of Arrays A and B.

A.4.1. Low- and mid-frequency noise maps

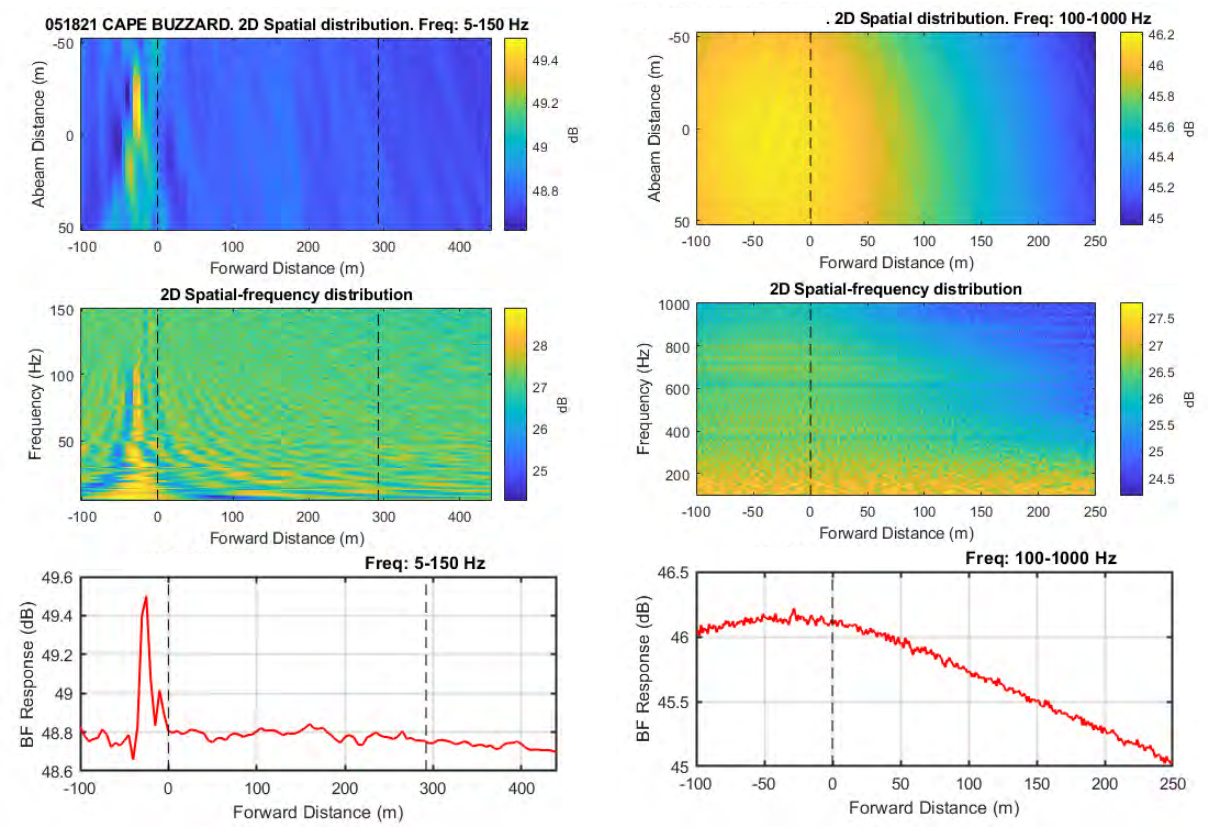

Figure 62 Noise maps from standard beamforming using combined array for Vessel Pass X: 2D maps in spatial domain for two frequency ranges (top); 2D maps in vessel forward distance and frequency domain for two frequency ranges (middle); and graph of BF response versus forward distance for two frequency ranges bottom). Frequency ranges are 5 to150 Hz (left) and 100 to1000 Hz (right).

A.4.2. High-frequency noise maps

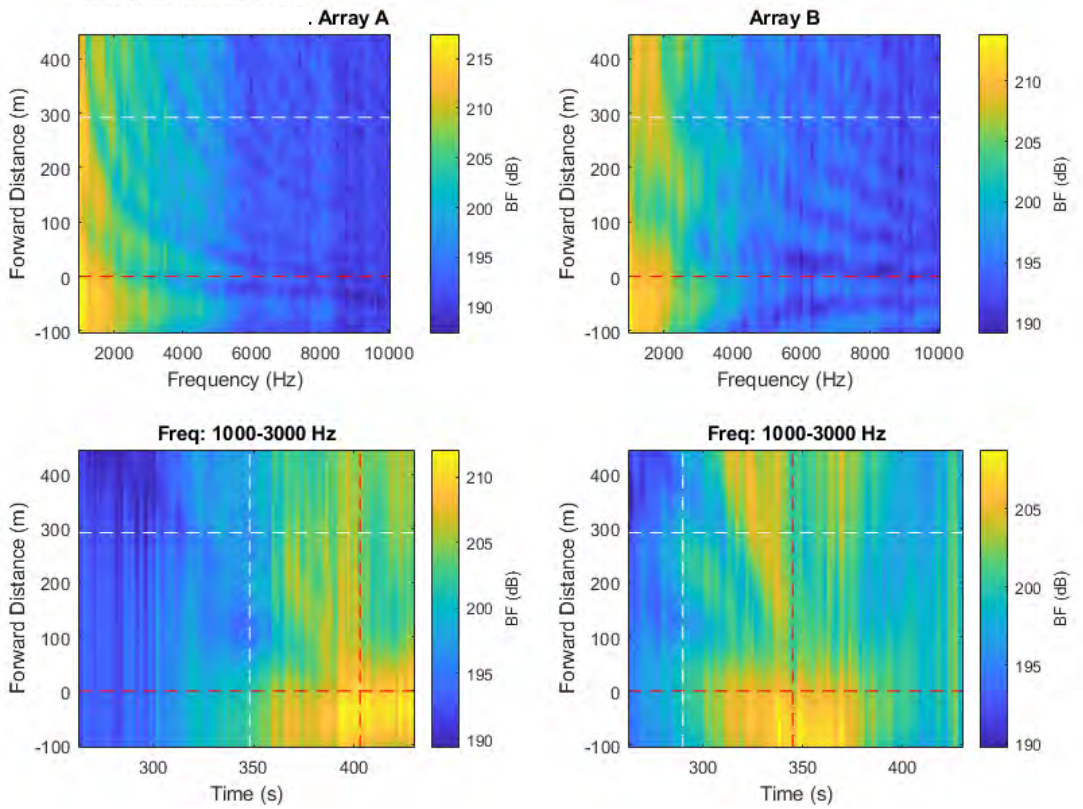

Figure 63 High-frequency noise maps from beamforming with individual arrays. Top maps show the BF response versus forward distance along vessel, measured approximately from the stern, versus frequency. Bottom maps show BF response versus forward distance and snapshot time. Horizontal dashed lines indicate the stern and bow positions of the vessel. Vertical dashed lines represent the CPA times of the bow and stern at each array.

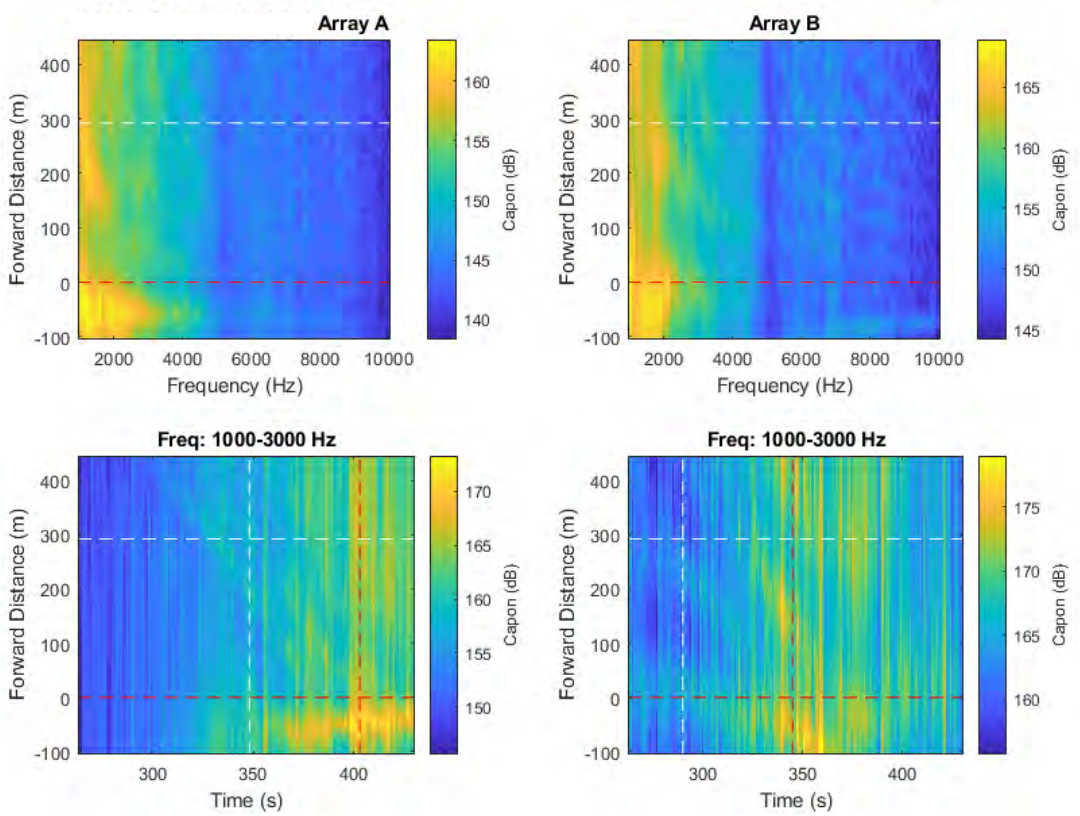

Figure 64 High-frequency noise maps obtained using the spatial spectrums provided by the Capon algorithm implemented using individual arrays.

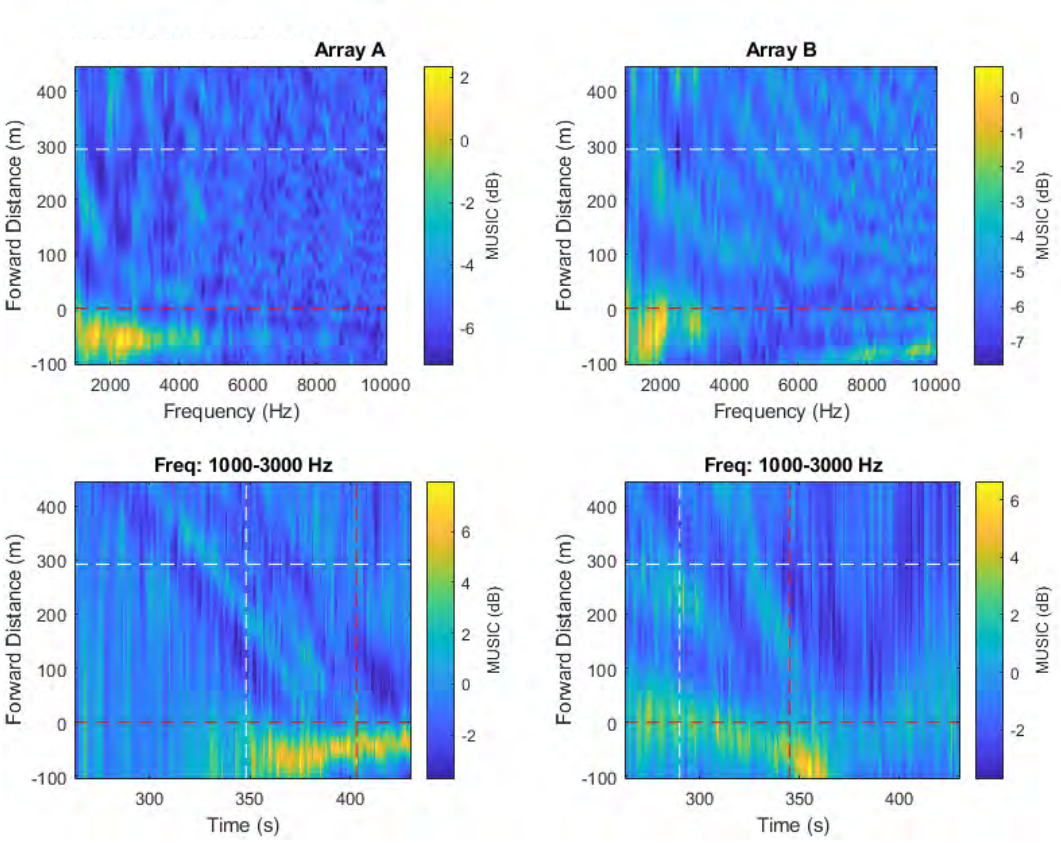

Figure 65 High-frequency noise maps obtained using the spatial spectrums provided by the MUSIC algorithm implemented using individual arrays.

A.5. Pass #5 (Type: Bulker. Length: 229 m. Speed: 11.8 kn)

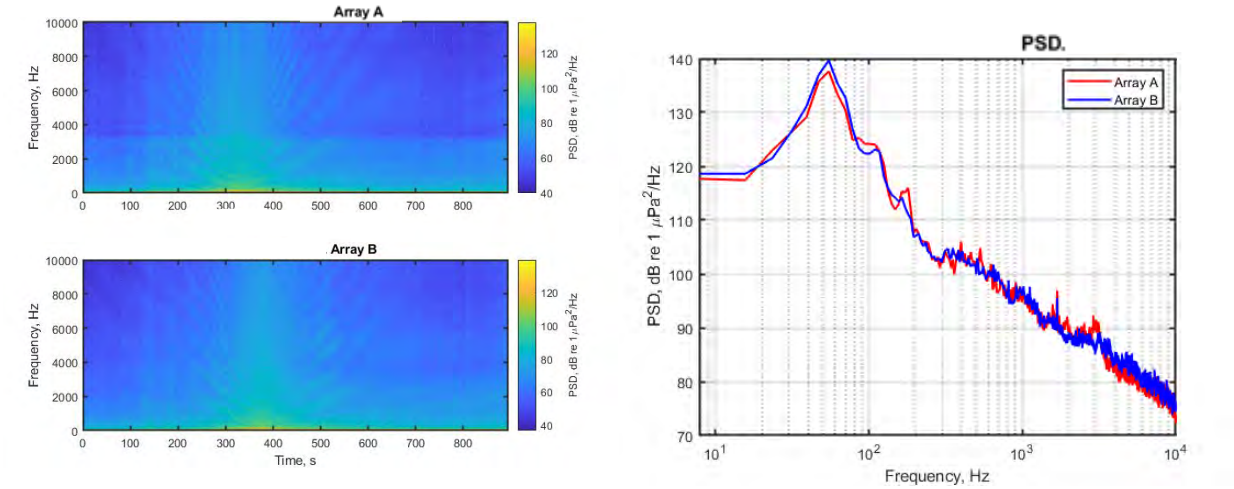

Figure 66 Spectrograms (left) and PSD (right) of ship noise observed on outputs of Arrays A and B.

A.5.1. Low- and mid-frequency noise maps

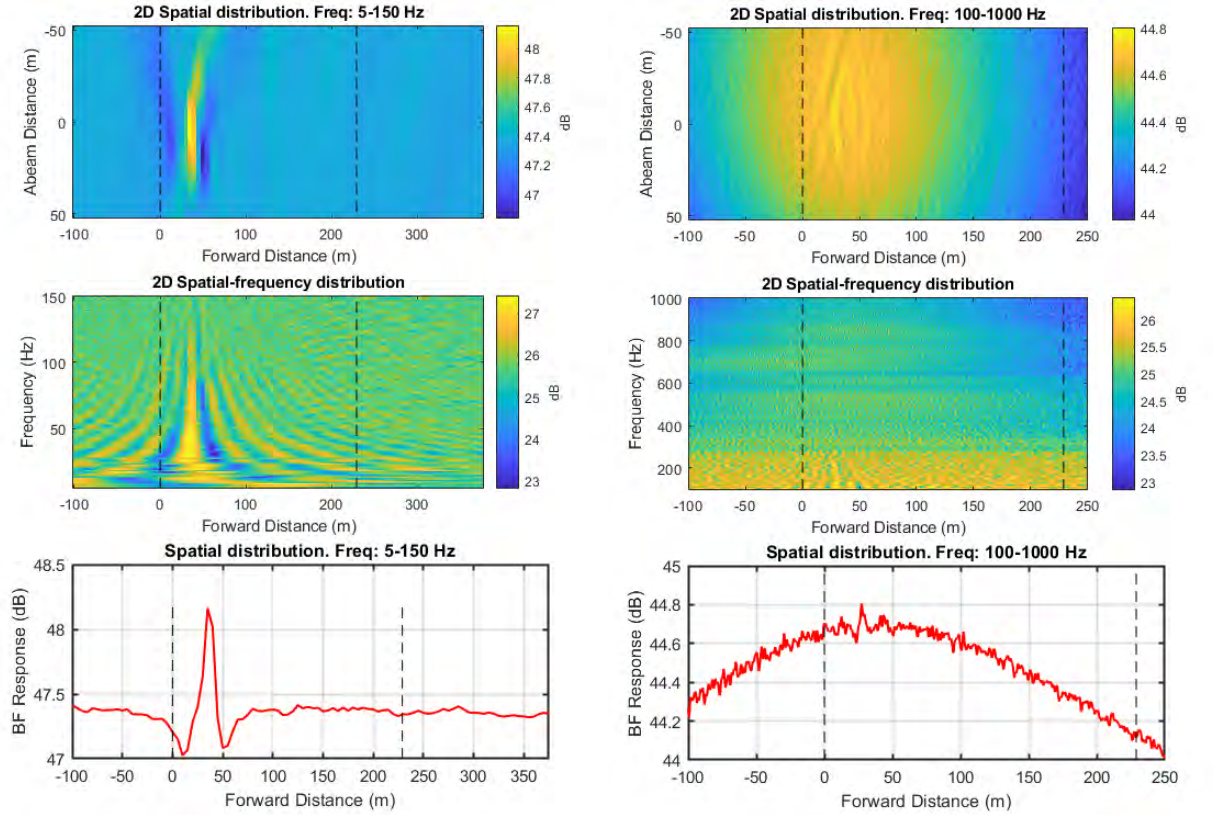

Figure 67 Noise maps from standard beamforming using combined array for Vessel Pass #5: 2D maps in spatial domain for two frequency ranges (top); 2D maps in vessel forward distance and frequency domain for two frequency ranges (middle); and graph of BF response versus forward distance for two frequency ranges bottom). Frequency ranges are 5 to150 Hz (left) and 100 to1000 Hz (right).

A.5.2. High-frequency noise maps

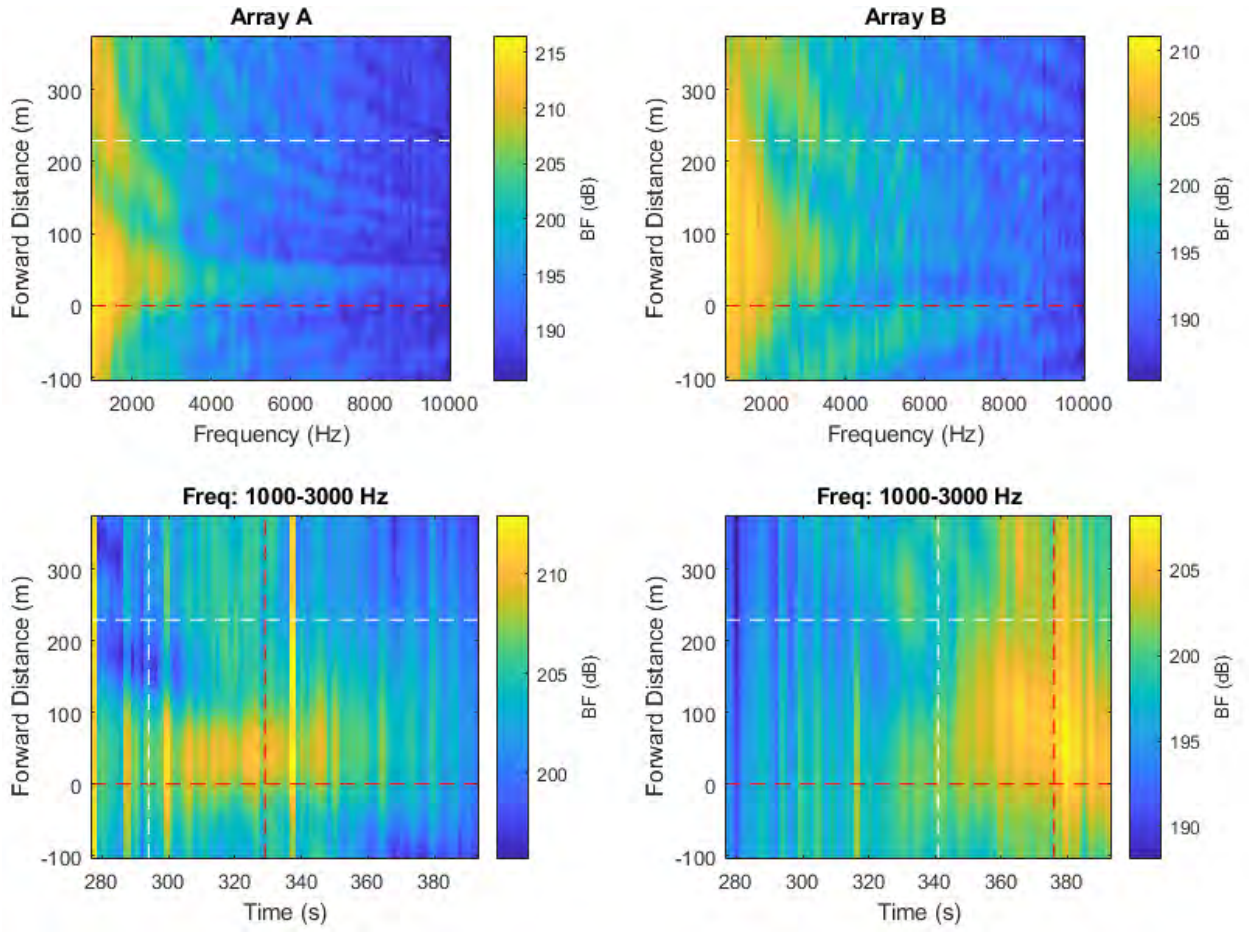

Figure 68 High-frequency noise maps from beamforming with individual arrays. Top maps show the BF response versus forward distance along vessel, measured approximately from the stern, versus frequency. Bottom maps show BF response versus forward distance and snapshot time. Horizontal dashed lines indicate the stern and bow positions of the vessel. Vertical dashed lines represent the CPA times of the bow and stern at each array.

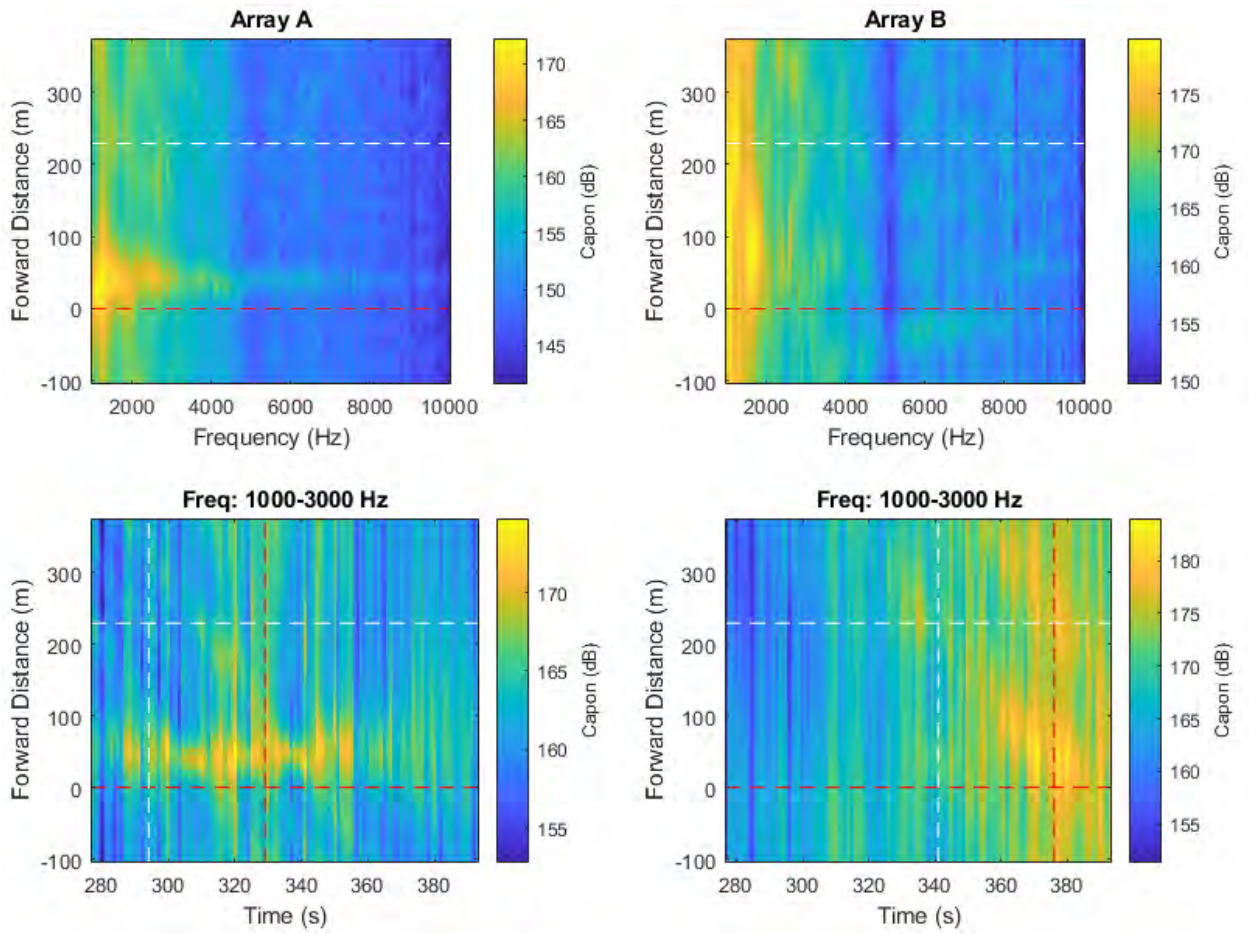

Figure 69 High-frequency noise maps obtained using the spatial spectra provided by the Capon algorithm implemented using individual arrays.

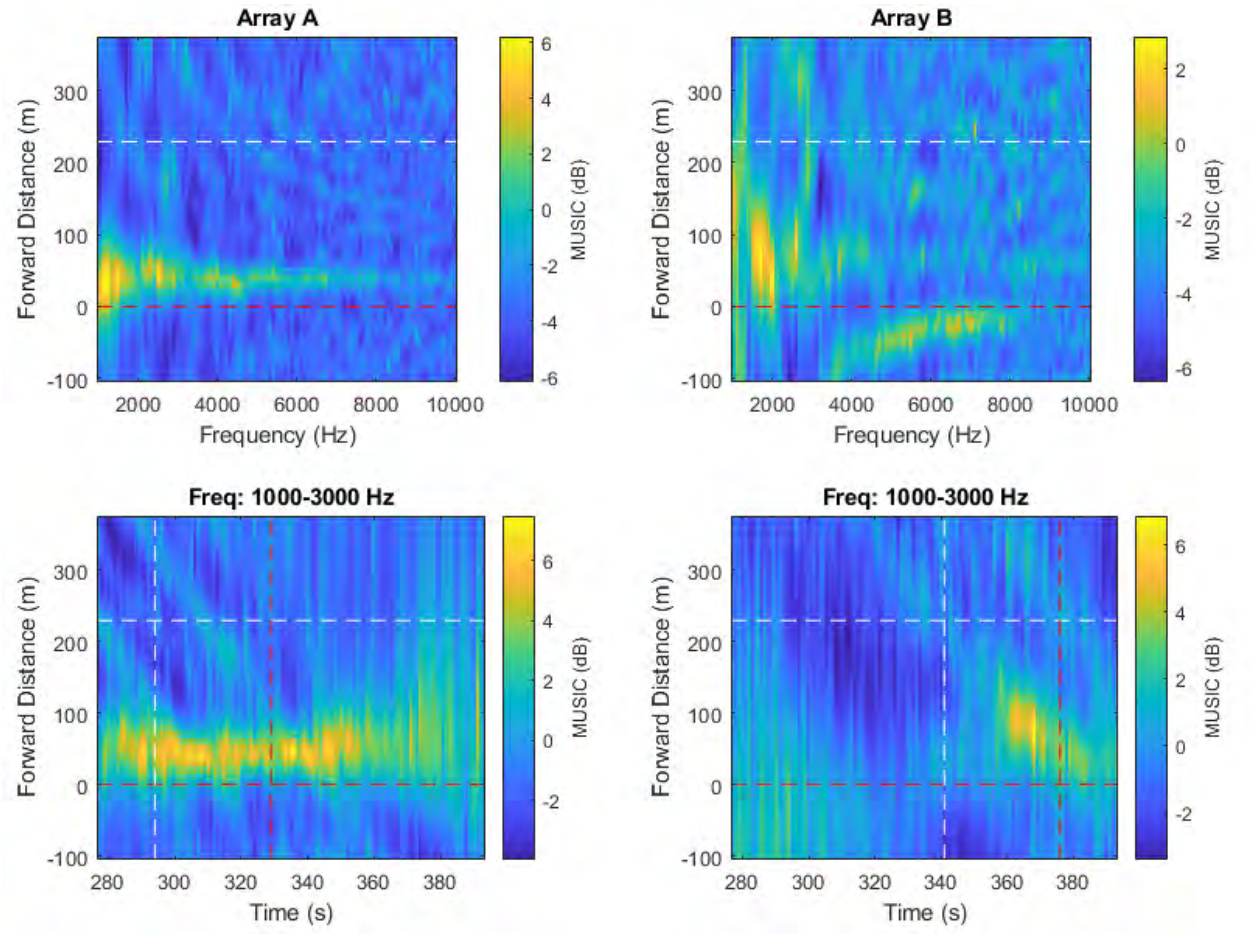

Figure 70 High-frequency noise maps obtained using the spatial spectra provided by the MUSIC algorithm implemented using individual arrays.

A.6. Pass #6 (Type: Bulker. Length: 235 m. Speed: 13.1 kn)

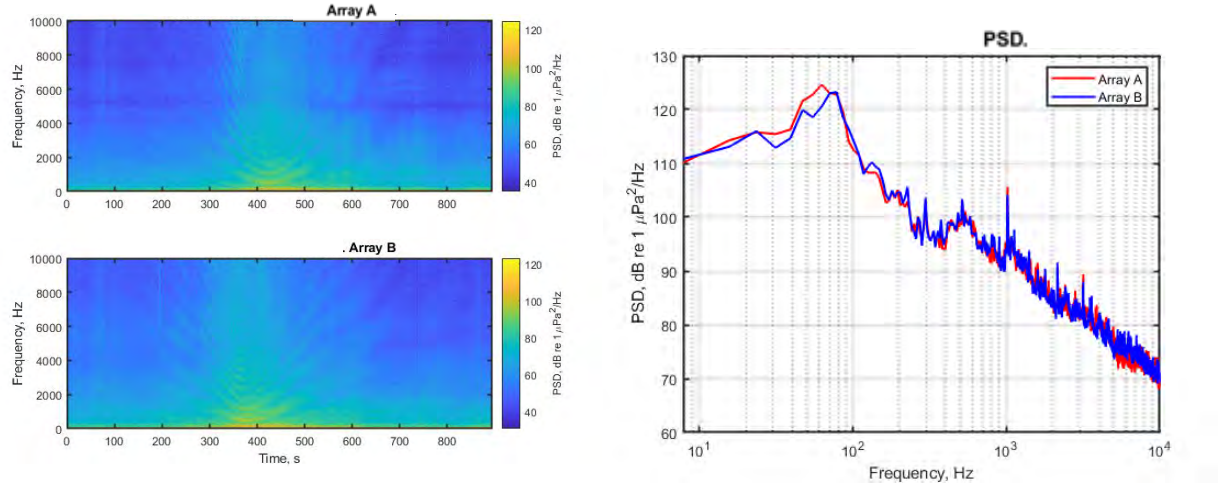

Figure 71 Spectrograms (left) and PSD (right) of ship noise observed on outputs of Arrays A and B.

A.6.1. Low- and mid-frequency noise maps

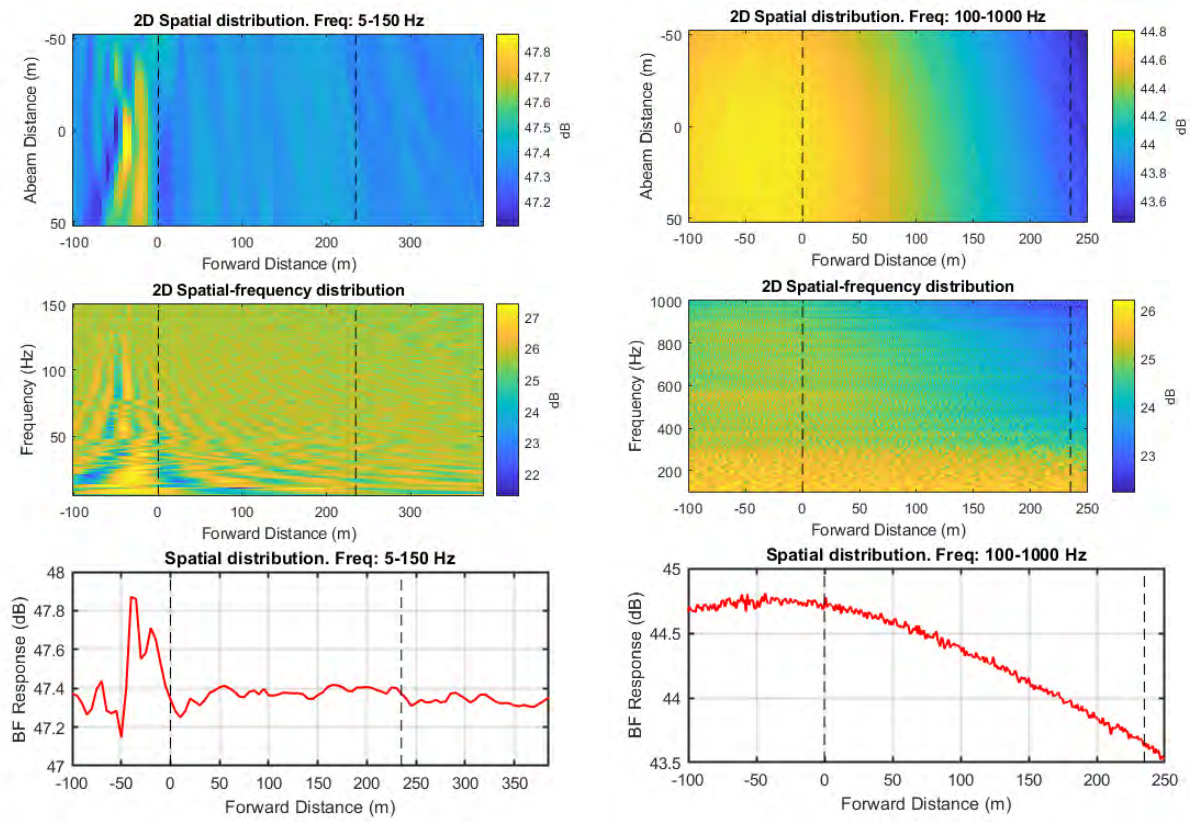

Figure 72 Noise maps from standard beamforming using combined array for Vessel Pass #6: 2D maps in spatial domain for two frequency ranges (top); 2D maps in vessel forward distance and frequency domain for two frequency ranges (middle); and graph of BF response versus forward distance for two frequency ranges bottom). Frequency ranges are 5 to150 Hz (left) and 100 to1000 Hz (right).

A.6.2. High-frequency noise maps

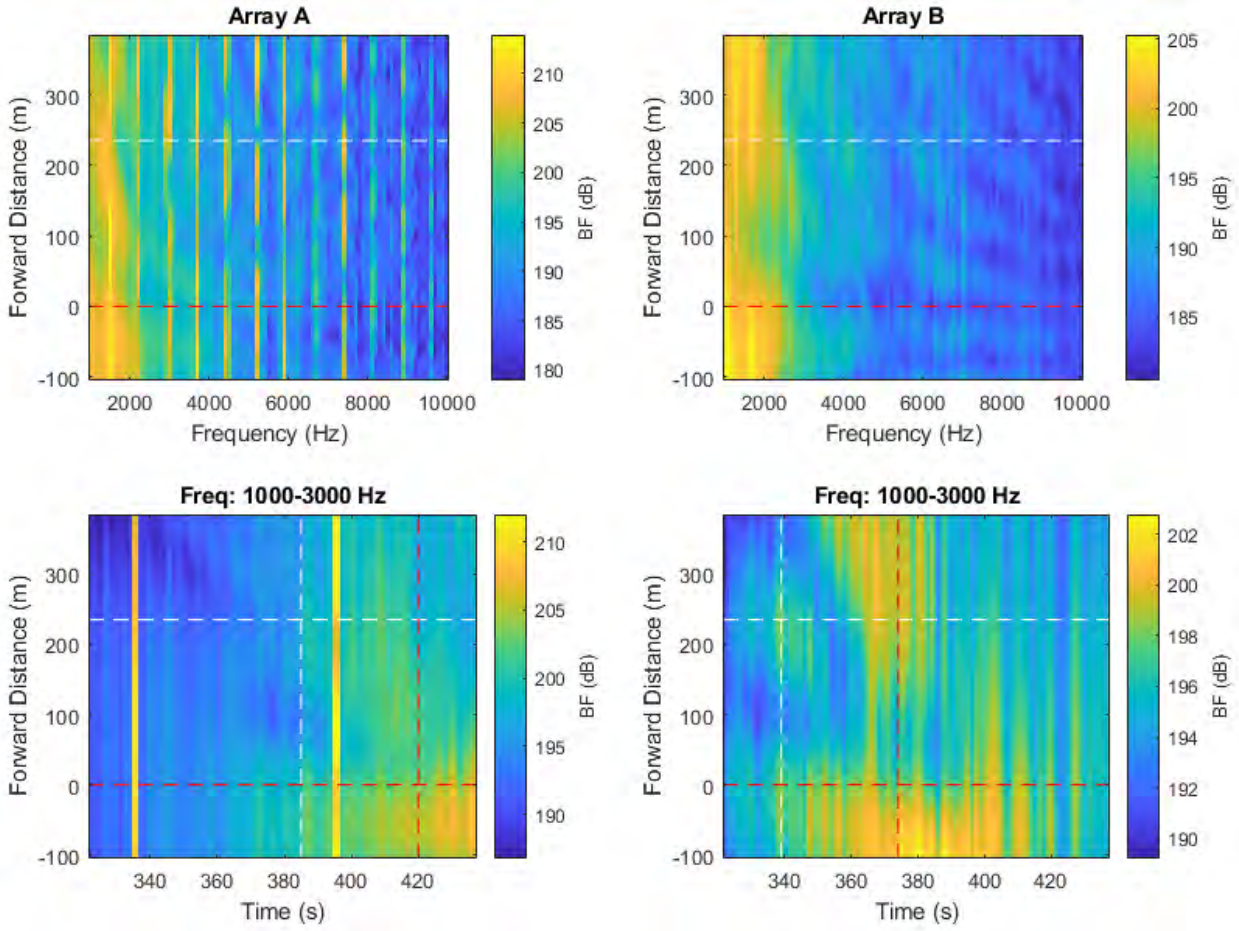

Figure 73 High-frequency noise maps from beamforming with individual arrays. Top maps show the BF response versus forward distance along vessel, measured approximately from the stern, versus frequency. Bottom maps show BF response versus forward distance and snapshot time. Horizontal dashed lines indicate the stern and bow positions of the vessel. Vertical dashed lines represent the CPA times of the bow and stern at each array.

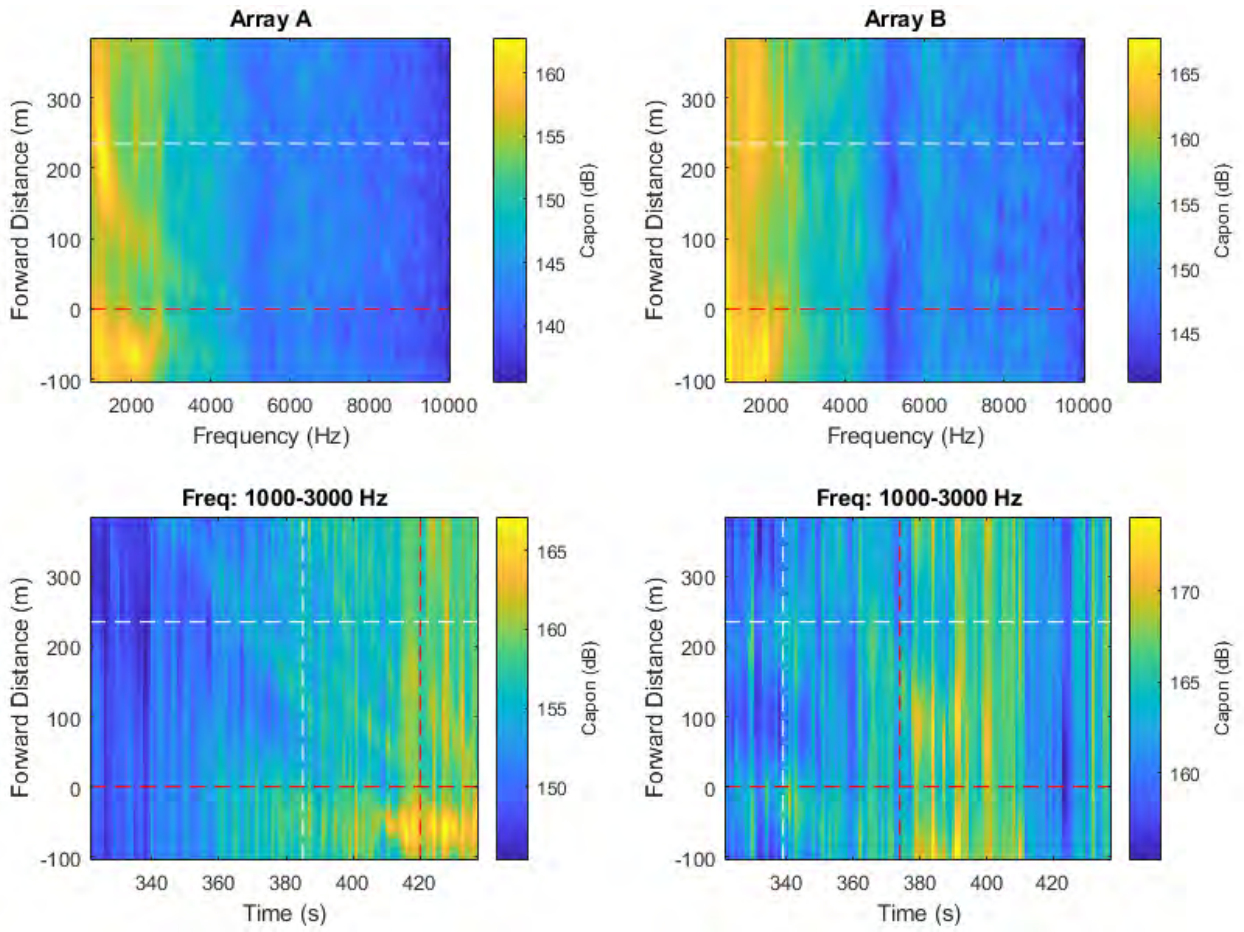

Figure 74 High-frequency noise maps obtained using the spatial spectra provided by the Capon algorithm implemented using individual arrays.

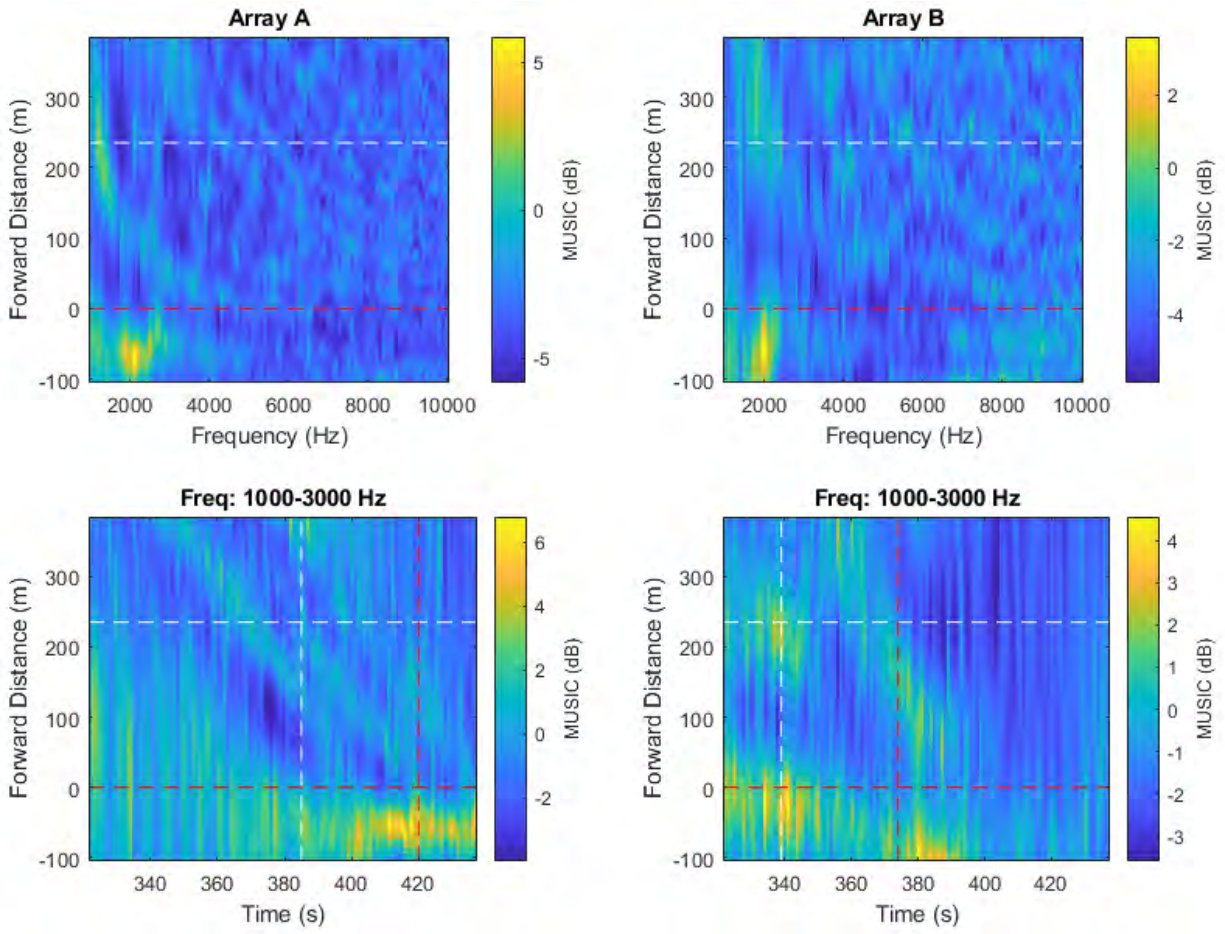

Figure 75 High-frequency noise maps obtained using the spatial spectra provided by the MUSIC algorithm implemented using individual arrays.

A.7. Pass #7 (Type: Container. Length: 363 m. Speed: 17.2 kn)

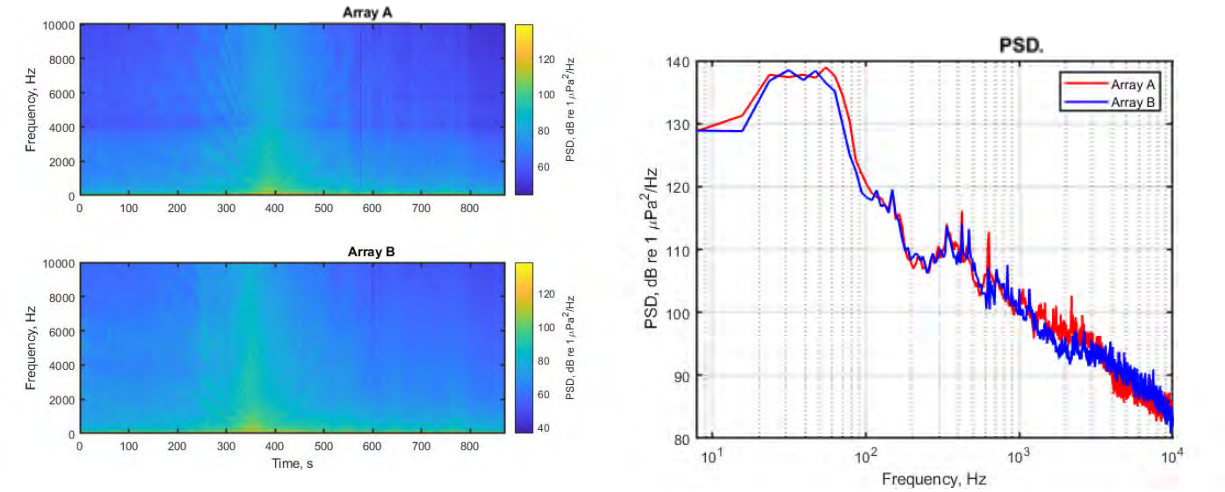

Figure 76 Spectrograms (left) and PSD (right) of ship noise observed on outputs of Arrays A and B.

A.7.1. Low- and mid-frequency noise maps

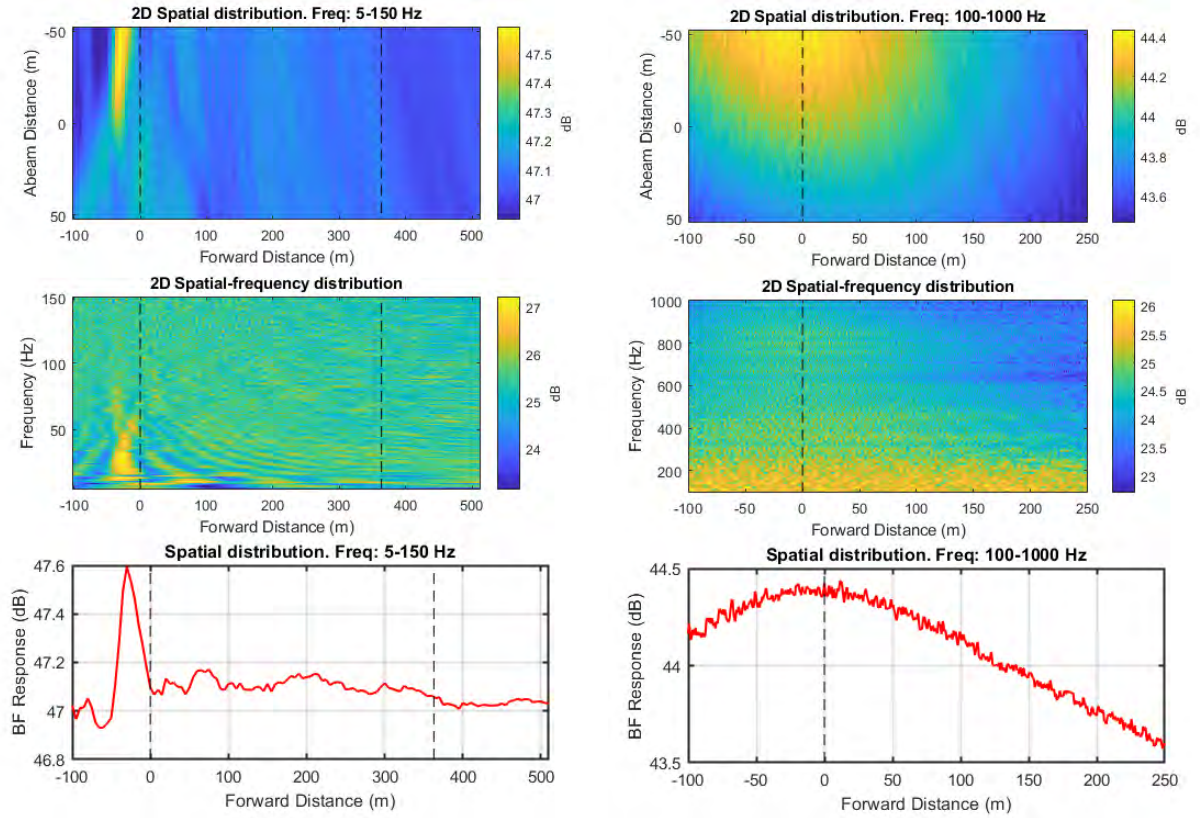

Figure 77 Noise maps from standard beamforming using combined array for Vessel Pass #7: 2D maps in spatial domain for two frequency ranges (top); 2D maps in vessel forward distance and frequency domain for two frequency ranges (middle); and graph of BF response versus forward distance for two frequency ranges bottom). Frequency ranges are 5 to150 Hz (left) and 100 to1000 Hz (right).

A.7.2. High-frequency noise maps

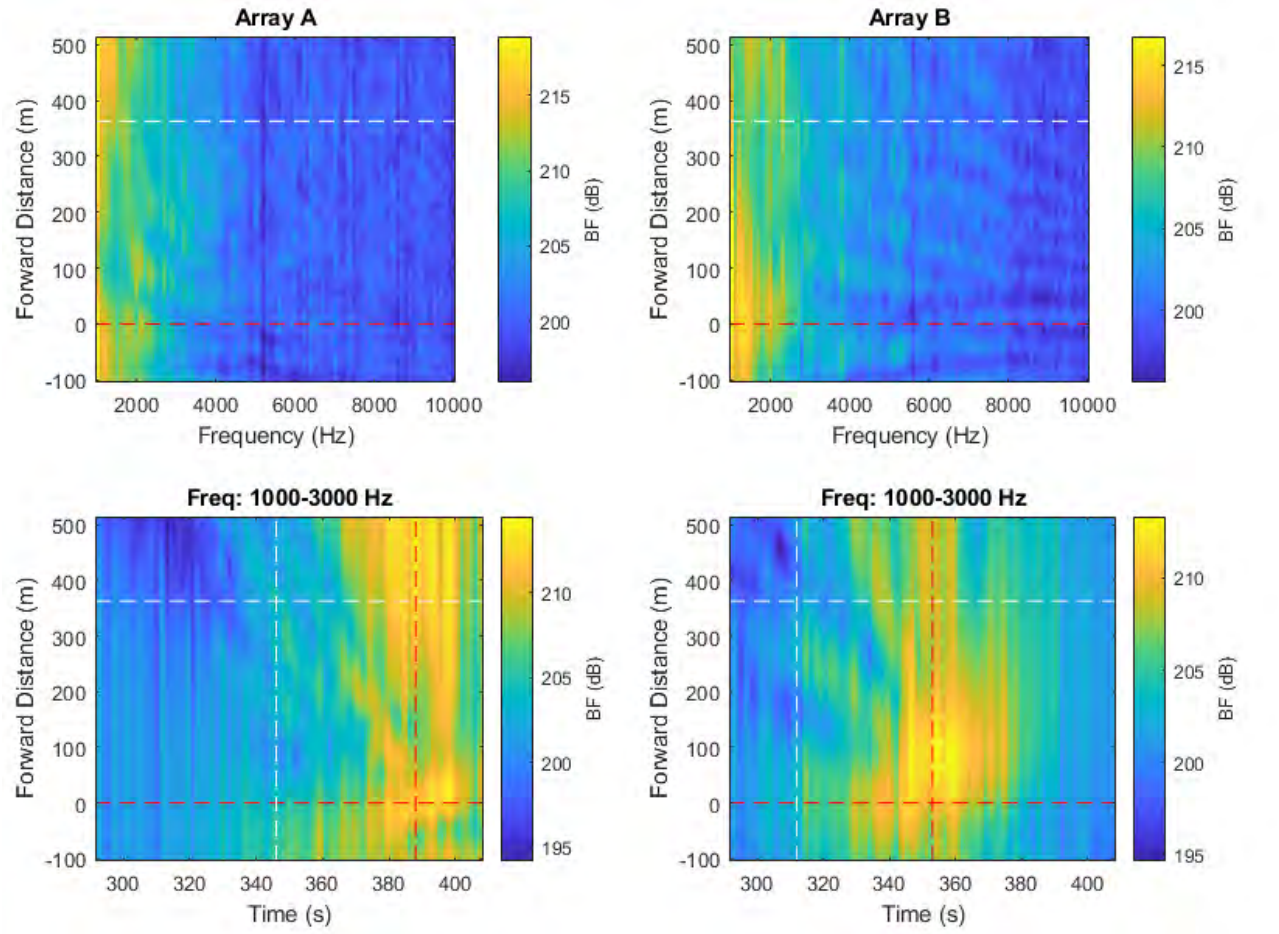

Figure 78 High-frequency noise maps from beamforming with individual arrays. Top maps show the BF response versus forward distance along vessel, measured approximately from the stern, versus frequency. Bottom maps show BF response versus forward distance and snapshot time. Horizontal dashed lines indicate the stern and bow positions of the vessel. Vertical dashed lines represent the CPA times of the bow and stern at each array.

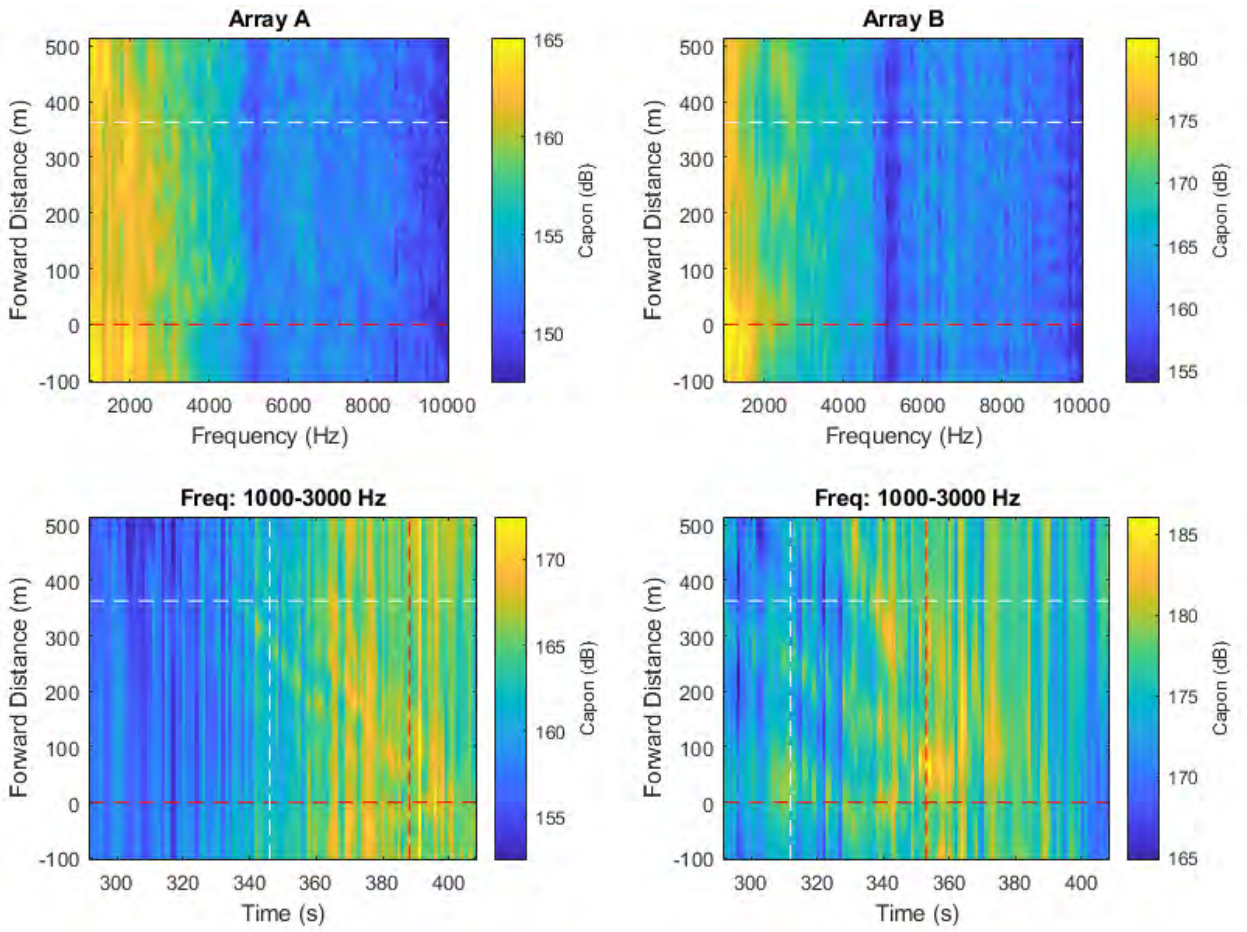

Figure 79 High-frequency noise maps obtained using the spatial spectra provided by the Capon algorithm implemented using individual arrays.

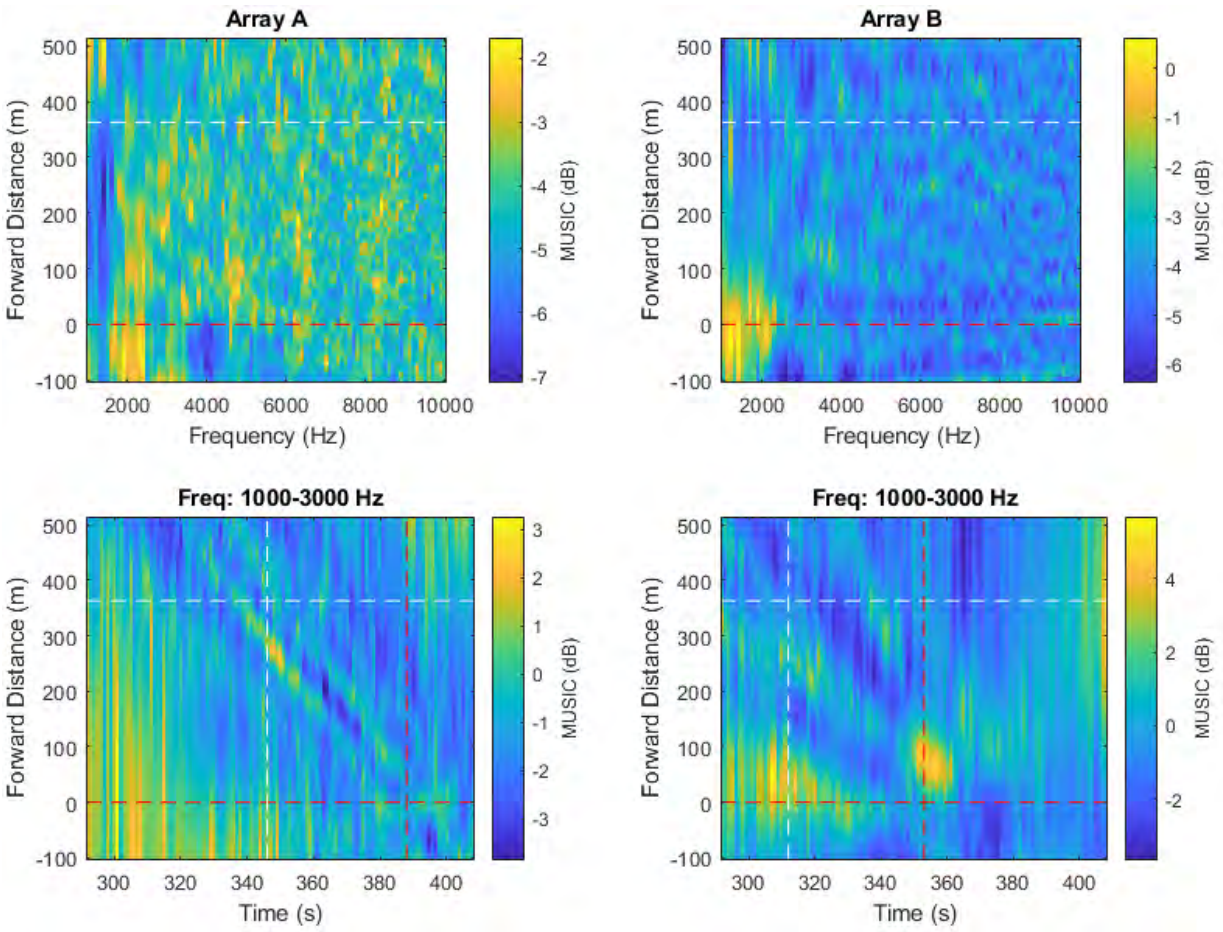

Figure 80 High-frequency noise maps obtained using the spatial spectra provided by the MUSIC algorithm implemented using individual arrays.

A.8. Pass #8 (Type: Bulker. Length: 228 m. Speed: 13.0 kn)

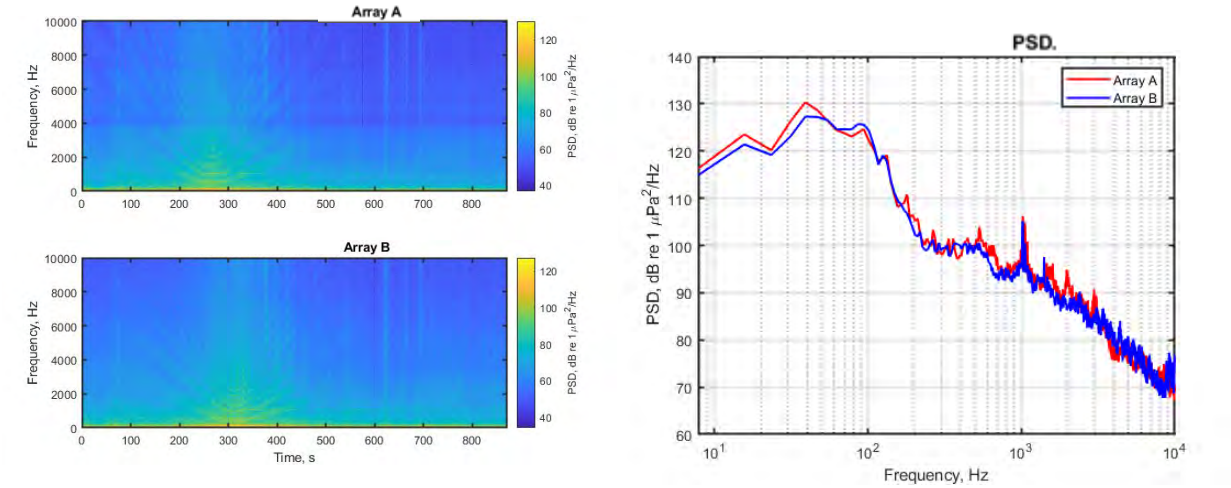

Figure 81 Spectrograms (left) and PSD (right) of ship noise observed on outputs of Arrays A and B.

A.8.1. Low- and mid-frequency noise maps

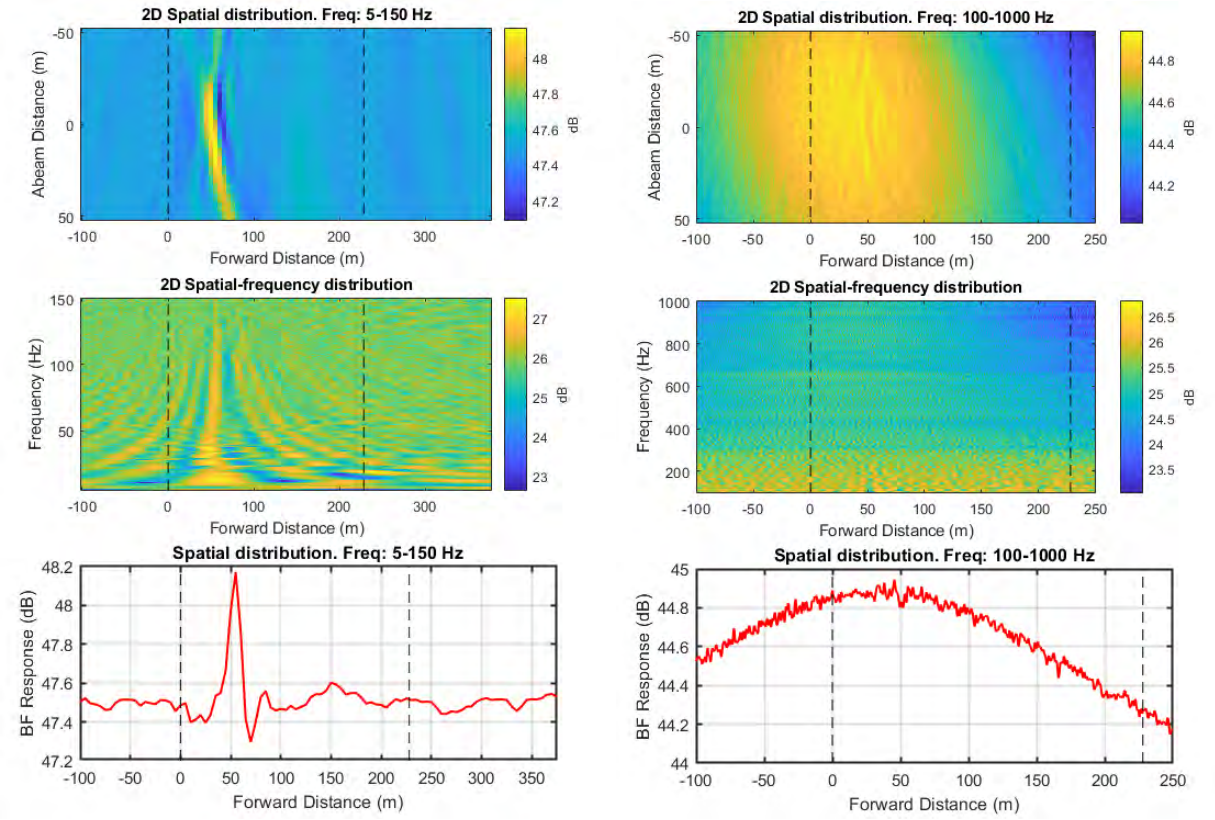

Figure 82 Noise maps from standard beamforming using combined array for Vessel Pass #8: 2D maps in spatial domain for two frequency ranges (top); 2D maps in vessel forward distance and frequency domain for two frequency ranges (middle); and graph of BF response versus forward distance for two frequency ranges bottom). Frequency ranges are 5 to150 Hz (left) and 100 to1000 Hz (right).

A.8.2. High-frequency noise maps

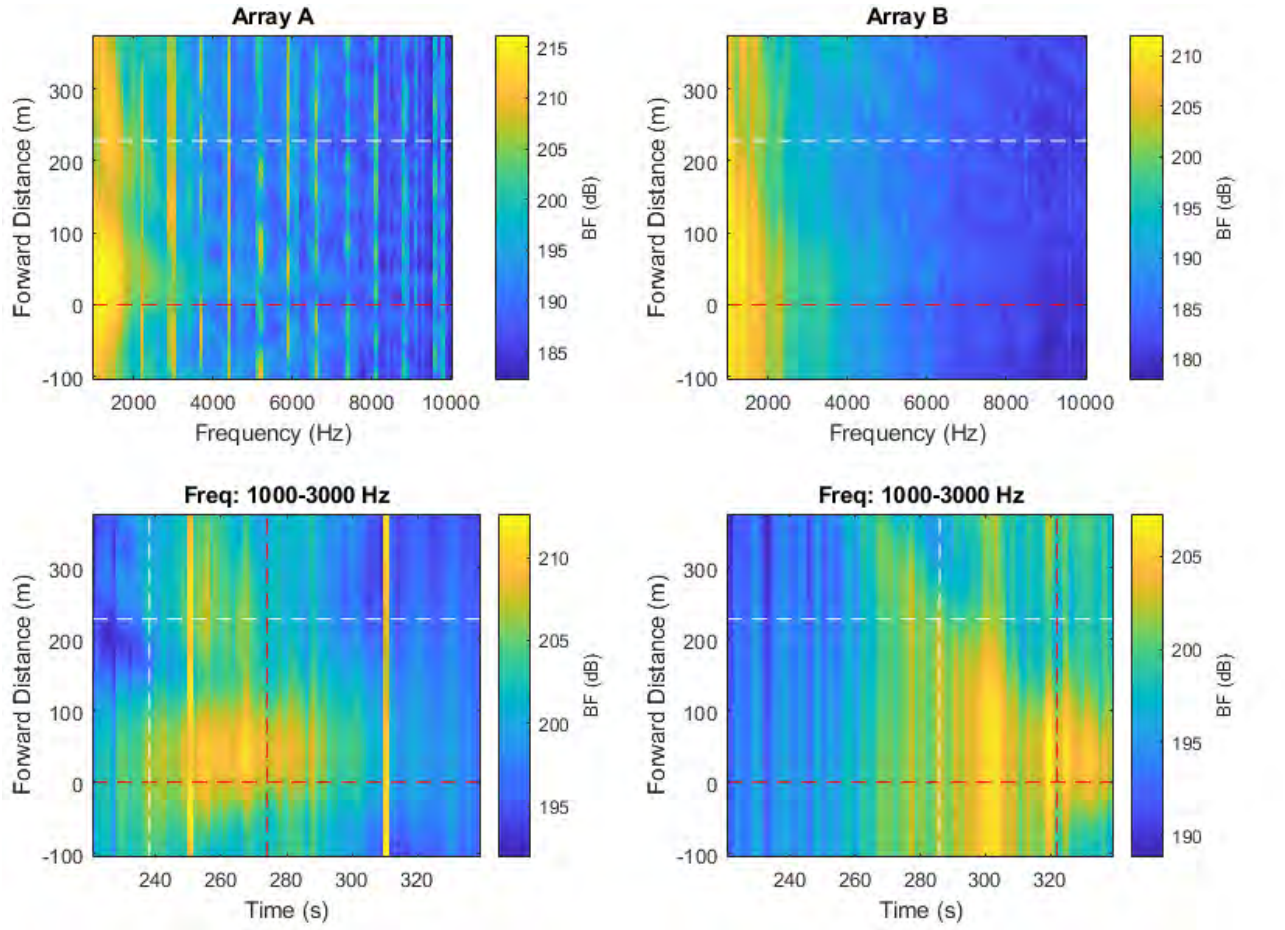

Figure 83 High-frequency noise maps from beamforming with individual arrays. Top maps show the BF response versus forward distance along vessel, measured approximately from the stern, versus frequency. Bottom maps show BF response versus forward distance and snapshot time. Horizontal dashed lines indicate the stern and bow positions of the vessel. Vertical dashed lines represent the CPA times of the bow and stern at each array.

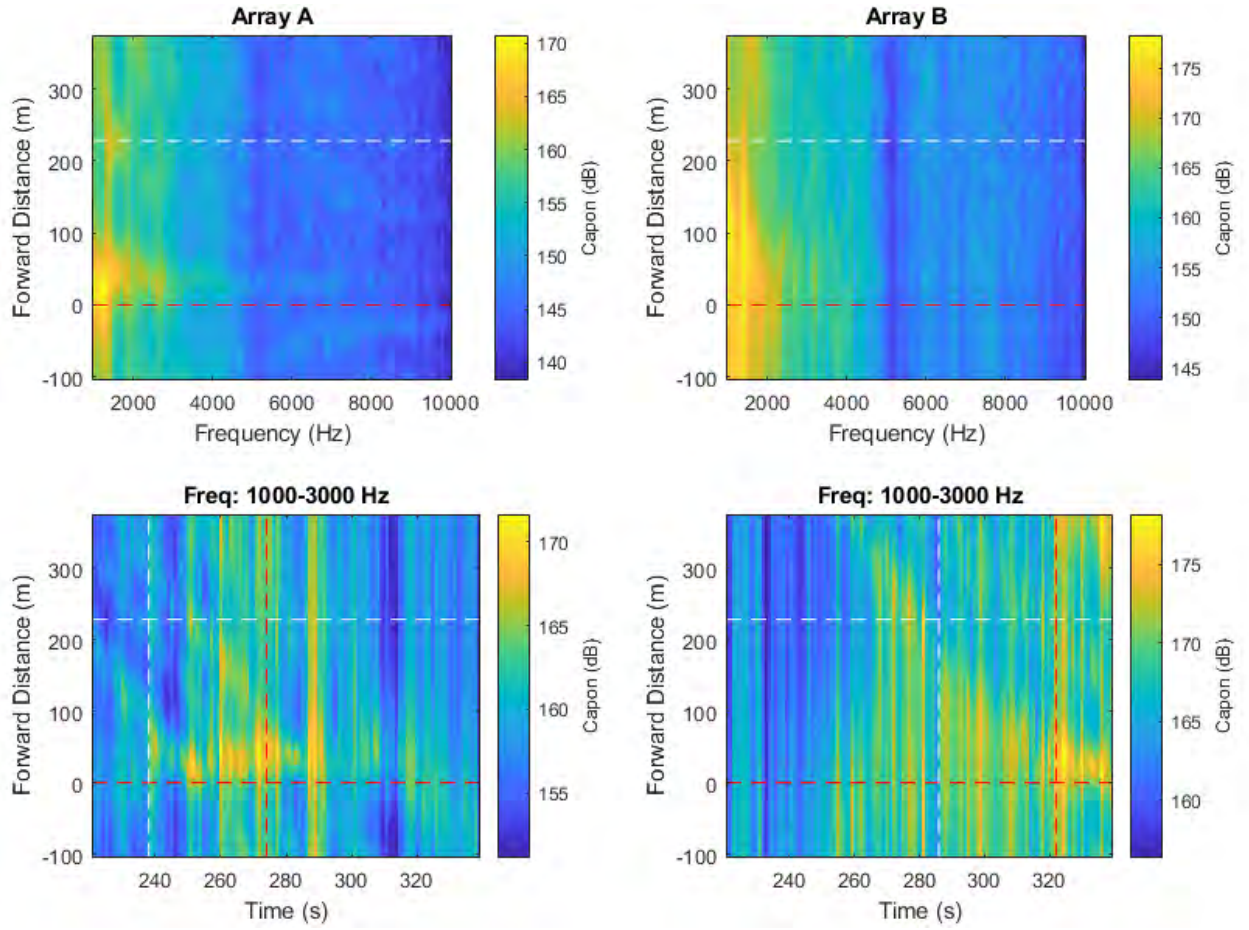

Figure 84 High-frequency noise maps obtained using the spatial spectra provided by the Capon algorithm implemented using individual arrays.

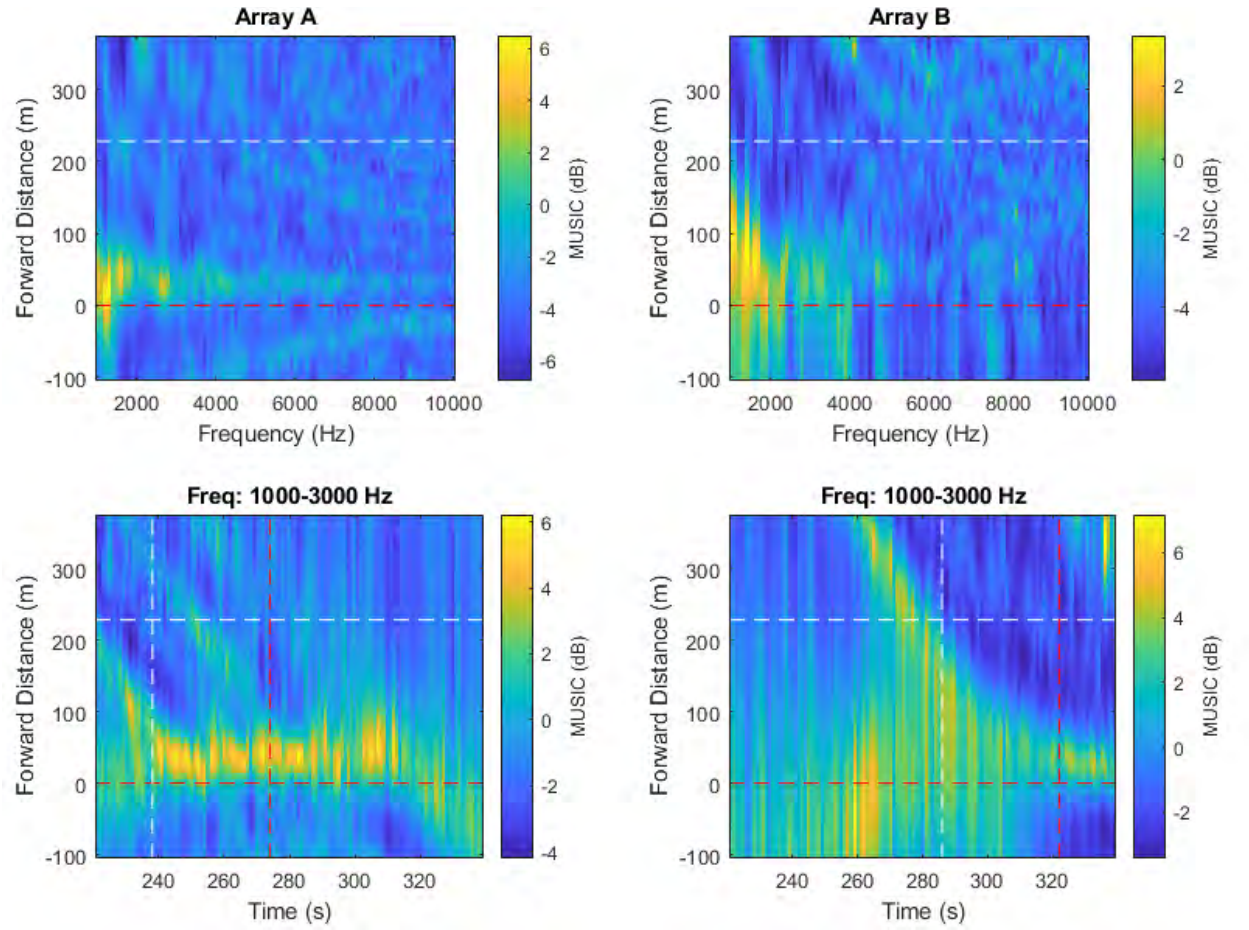

Figure 85 High-frequency noise maps obtained using the spatial spectra provided by the MUSIC algorithm implemented using individual arrays.

A.9. Pass #9 (Type: Bulker. Length: 190 m. Speed: 13.6 kn)

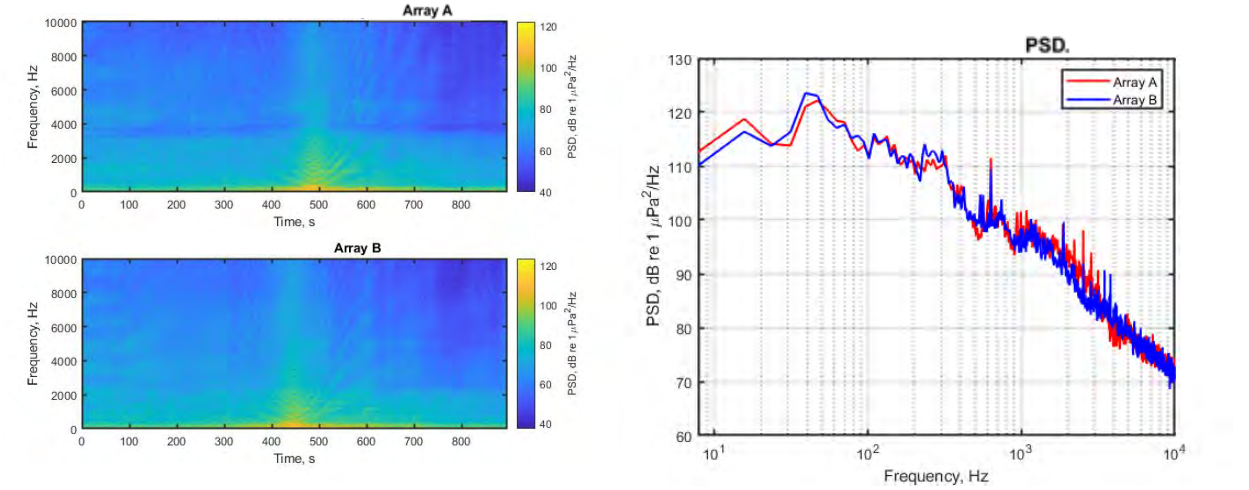

Figure 86 Spectrograms (left) and PSD (right) of ship noise observed on outputs of Arrays A and B.

A.9.1. Low- and mid-frequency noise maps

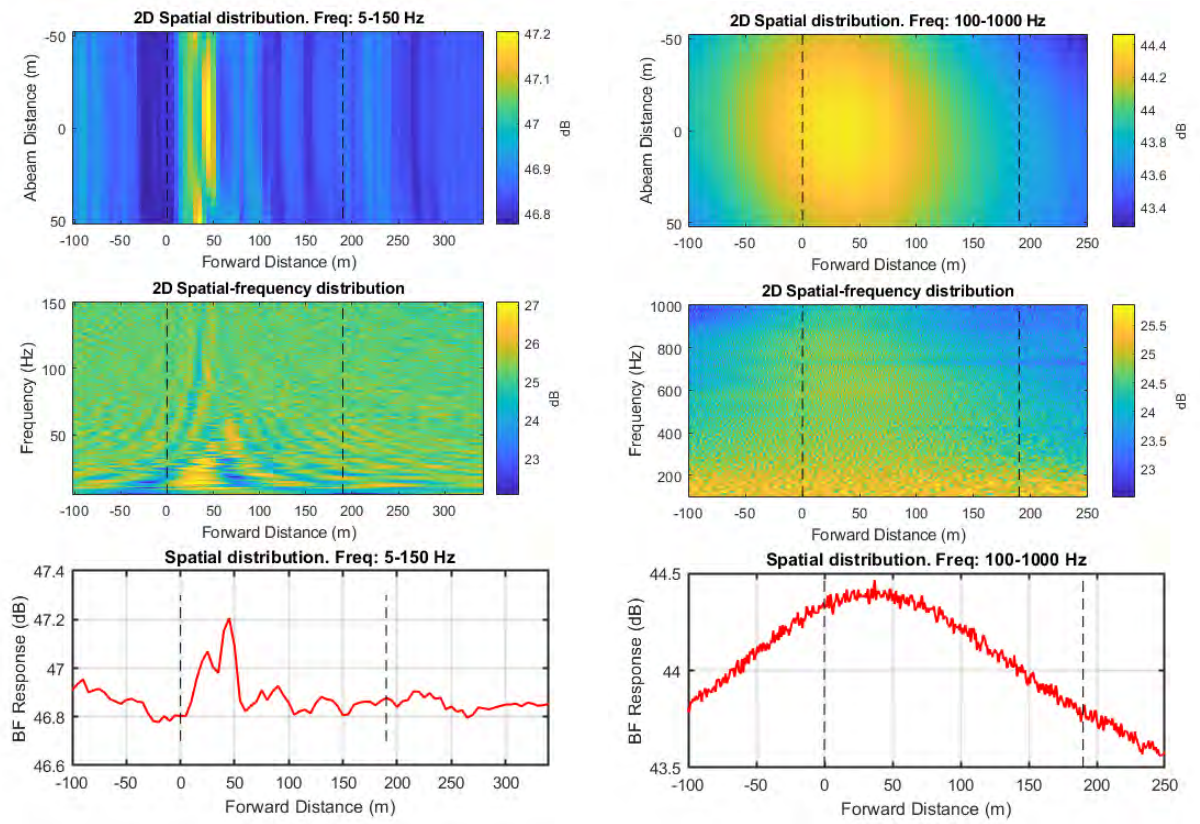

Figure 87 Noise maps from standard beamforming using combined array for Vessel Pass #9: 2D maps in spatial domain for two frequency ranges (top); 2D maps in vessel forward distance and frequency domain for two frequency ranges (middle); and graph of BF response versus forward distance for two frequency ranges (bottom). Frequency ranges are 5 to150 Hz (left) and 100 to1000 Hz (right).

A.9.2. High-frequency noise maps

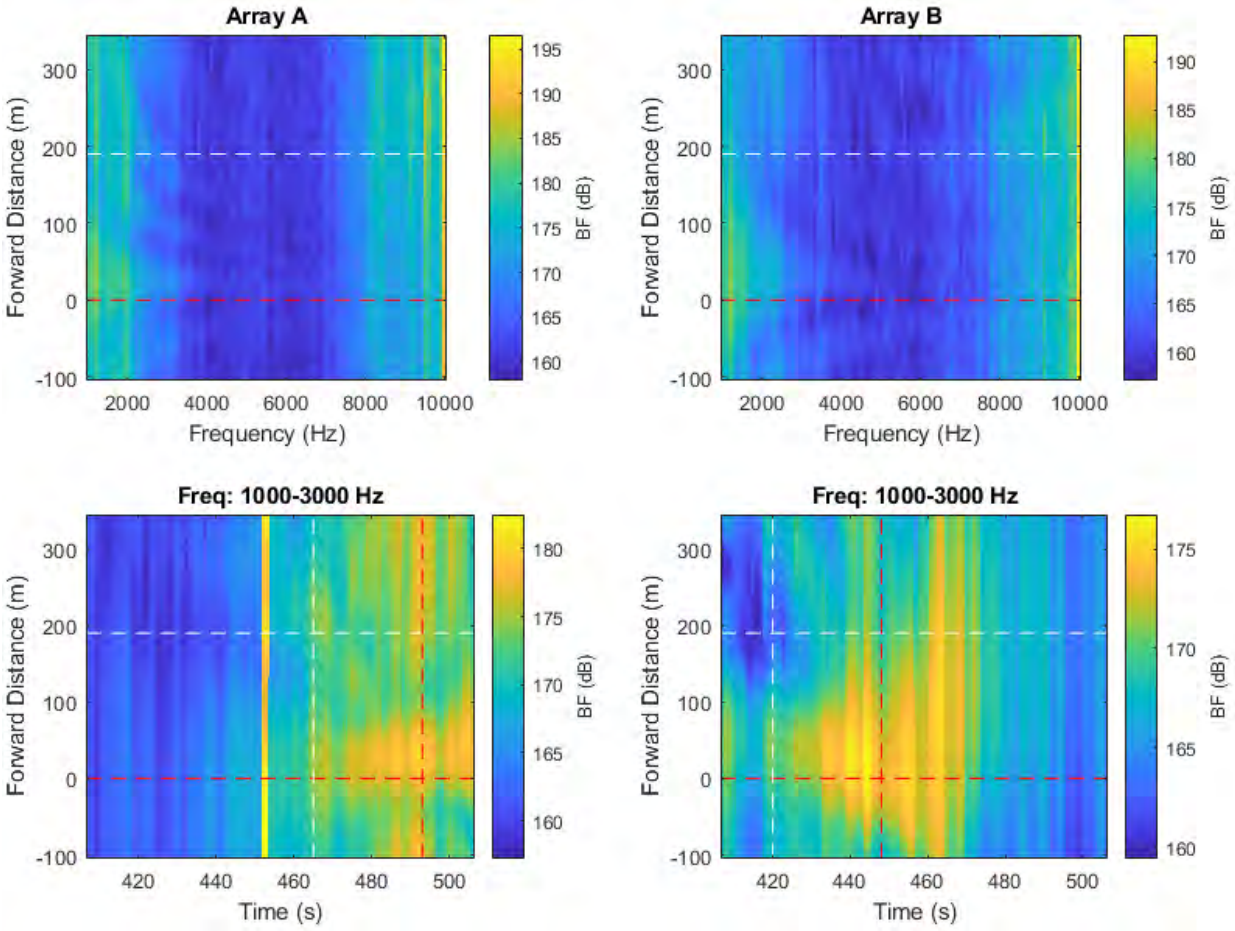

Figure 88 High-frequency noise maps from beamforming with individual arrays. Top maps show the BF response versus forward distance along vessel, measured approximately from the stern, versus frequency. Bottom maps show BF response versus forward distance and snapshot time. Horizontal dashed lines indicate the stern and bow positions of the vessel. Vertical dashed lines represent the CPA times of the bow and stern at each array.

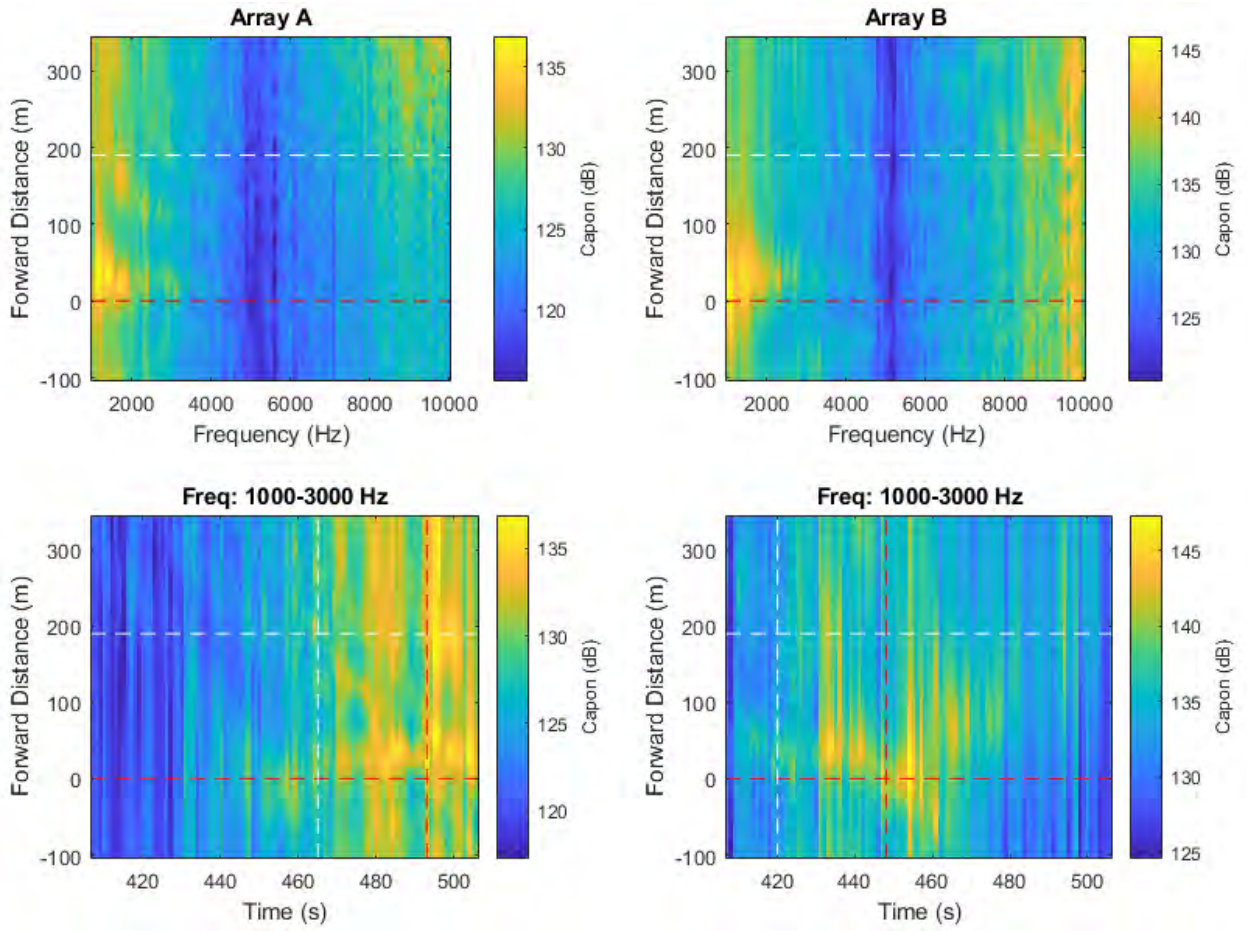

Figure 89 High-frequency noise maps obtained using the spatial spectra provided by the Capon algorithm implemented using individual arrays.

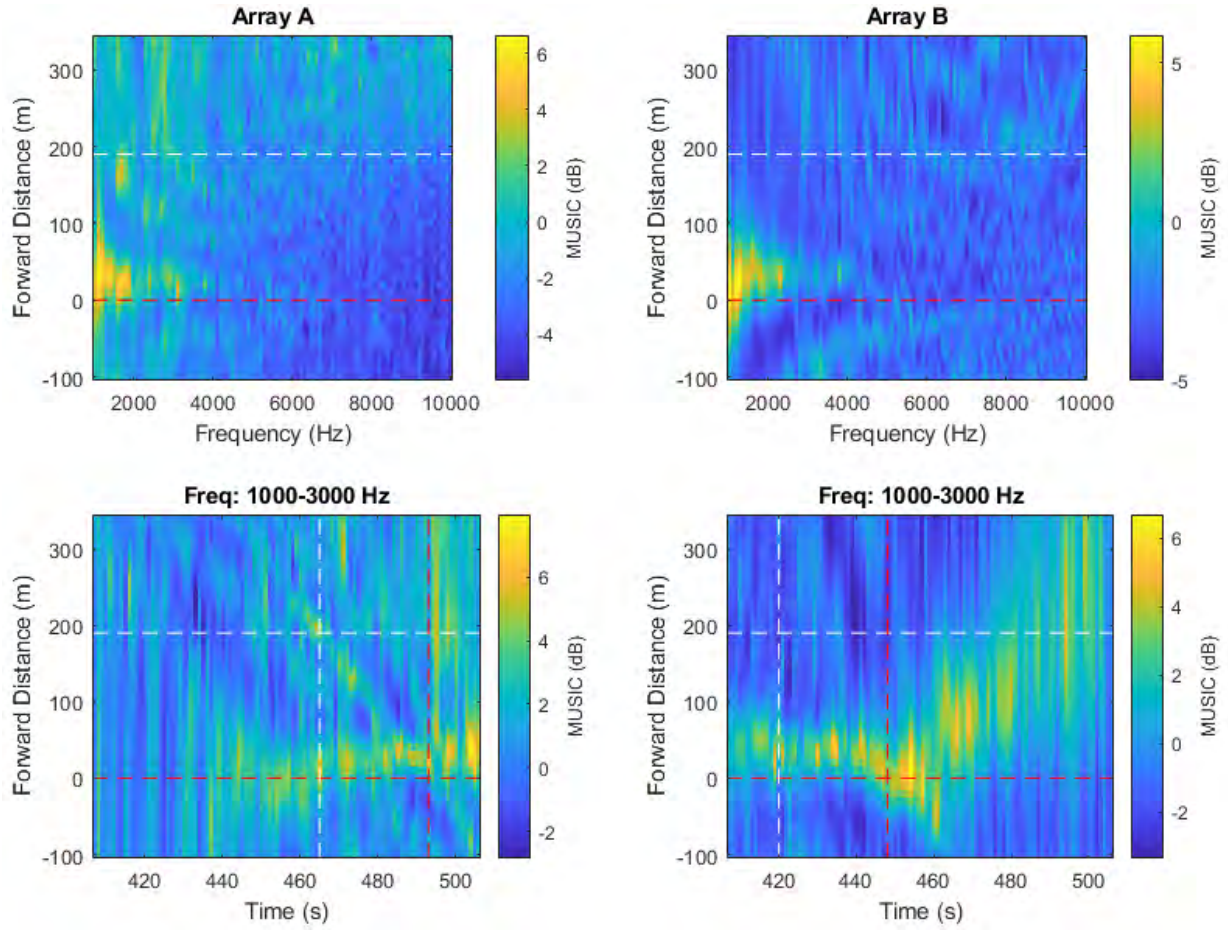

Figure 90 High-frequency noise maps obtained using the spatial spectra provided by the MUSIC algorithm implemented using individual arrays.

A.10. Pass #10 (Type: Container. Length: 209 m. Speed: 18.5 kn)

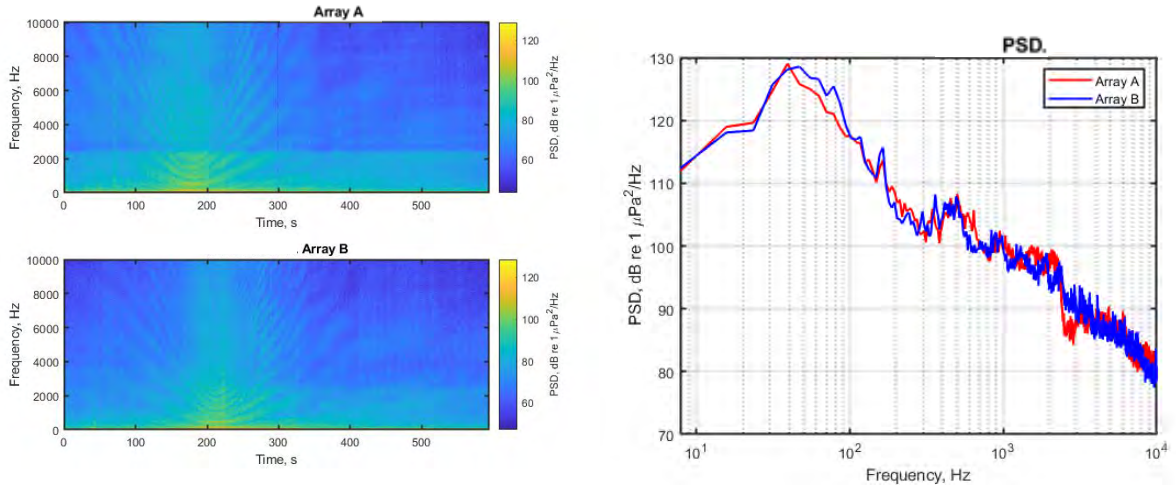

Figure 91 Spectrograms (left) and PSD (right) of ship noise observed on outputs of Arrays A and B.

A.10.1. Low- and mid-frequency noise maps

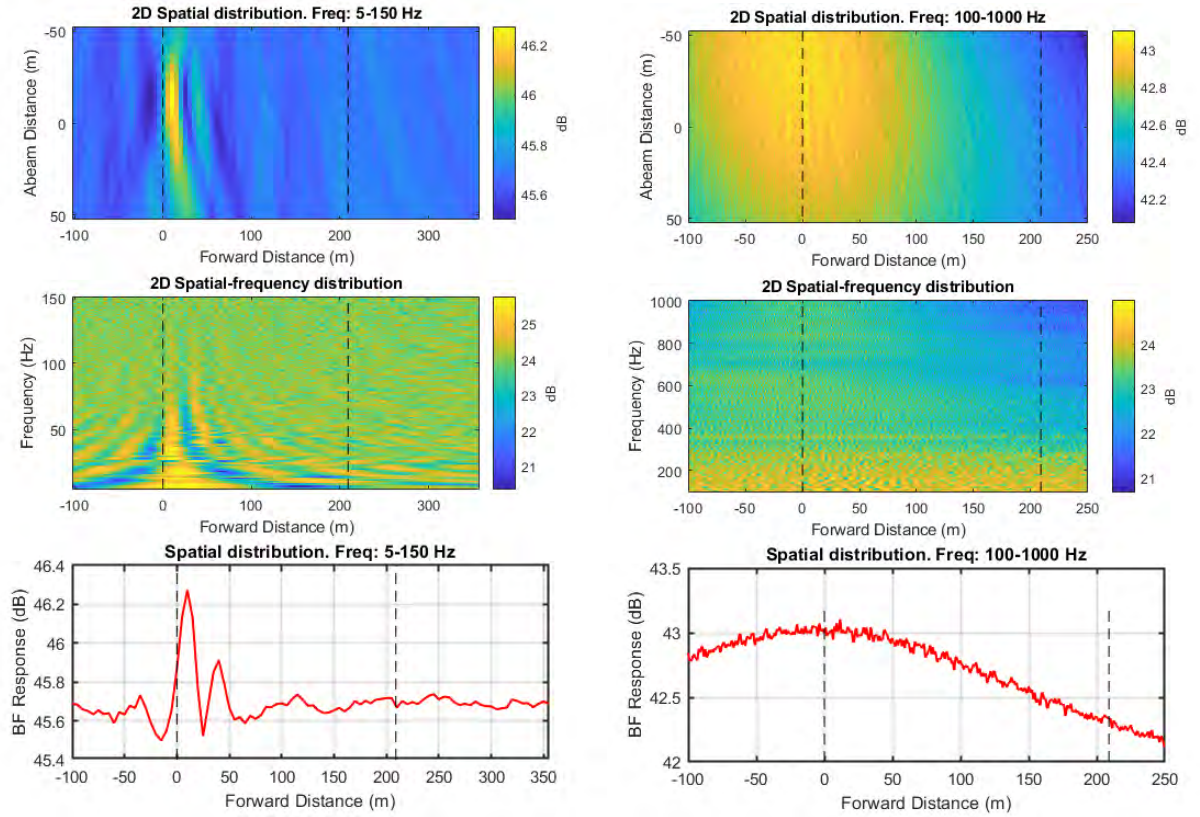

Figure 92 Noise maps from standard beamforming using combined array for Vessel Pass #45: 2D maps in spatial domain for two frequency ranges (top); 2D maps in vessel forward distance and frequency domain for two frequency ranges (middle); and graph of BF response versus forward distance for two frequency ranges bottom). Frequency ranges are 5 to150 Hz (left) and 100 to1000 Hz (right).

A.10.2. High-frequency noise maps

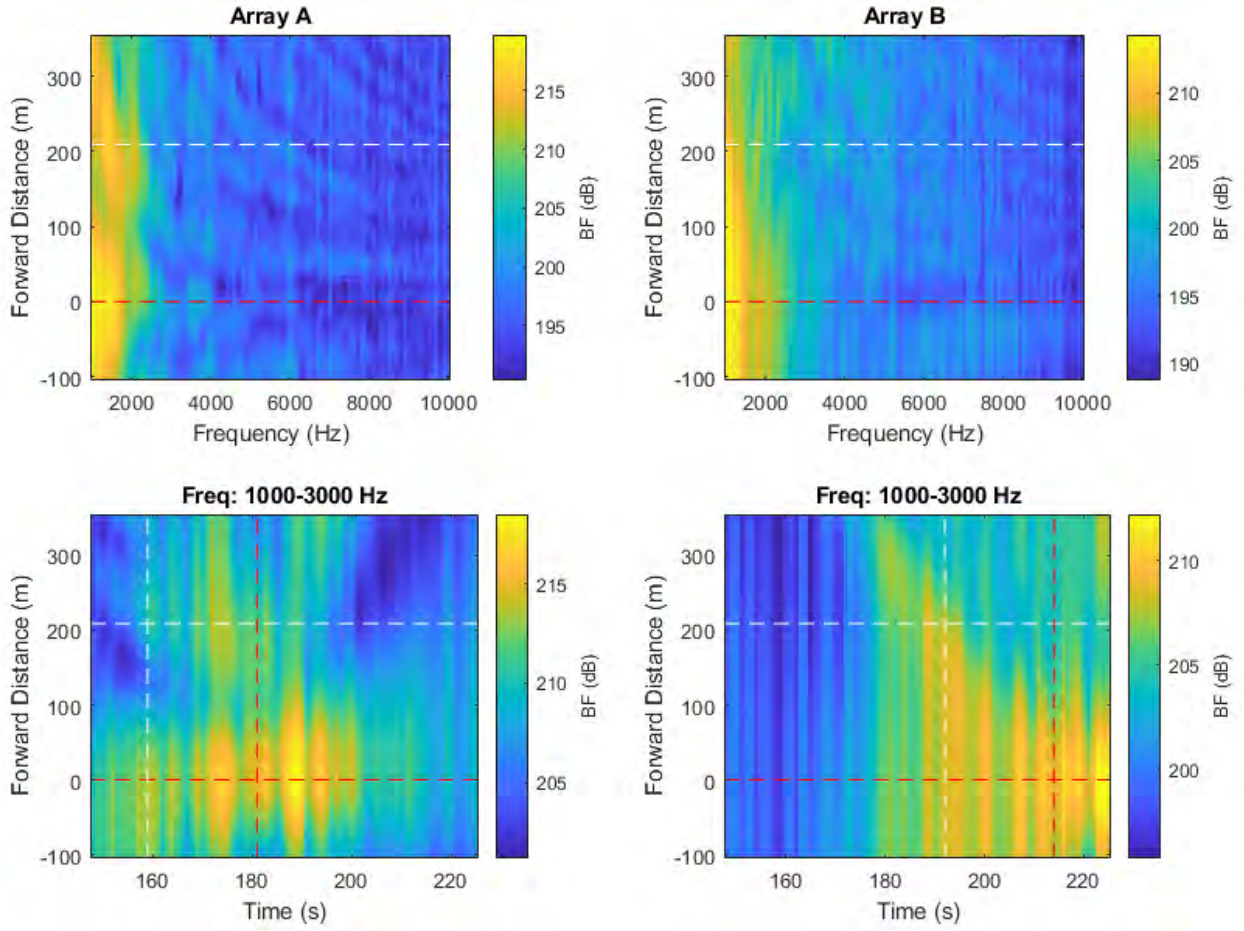

Figure 93 High-frequency noise maps from beamforming with individual arrays. Top maps show the BF response versus forward distance along vessel, measured approximately from the stern, versus frequency. Bottom maps show BF response versus forward distance and snapshot time. Horizontal dashed lines indicate the stern and bow positions of the vessel. Vertical dashed lines represent the CPA times of the bow and stern at each array.

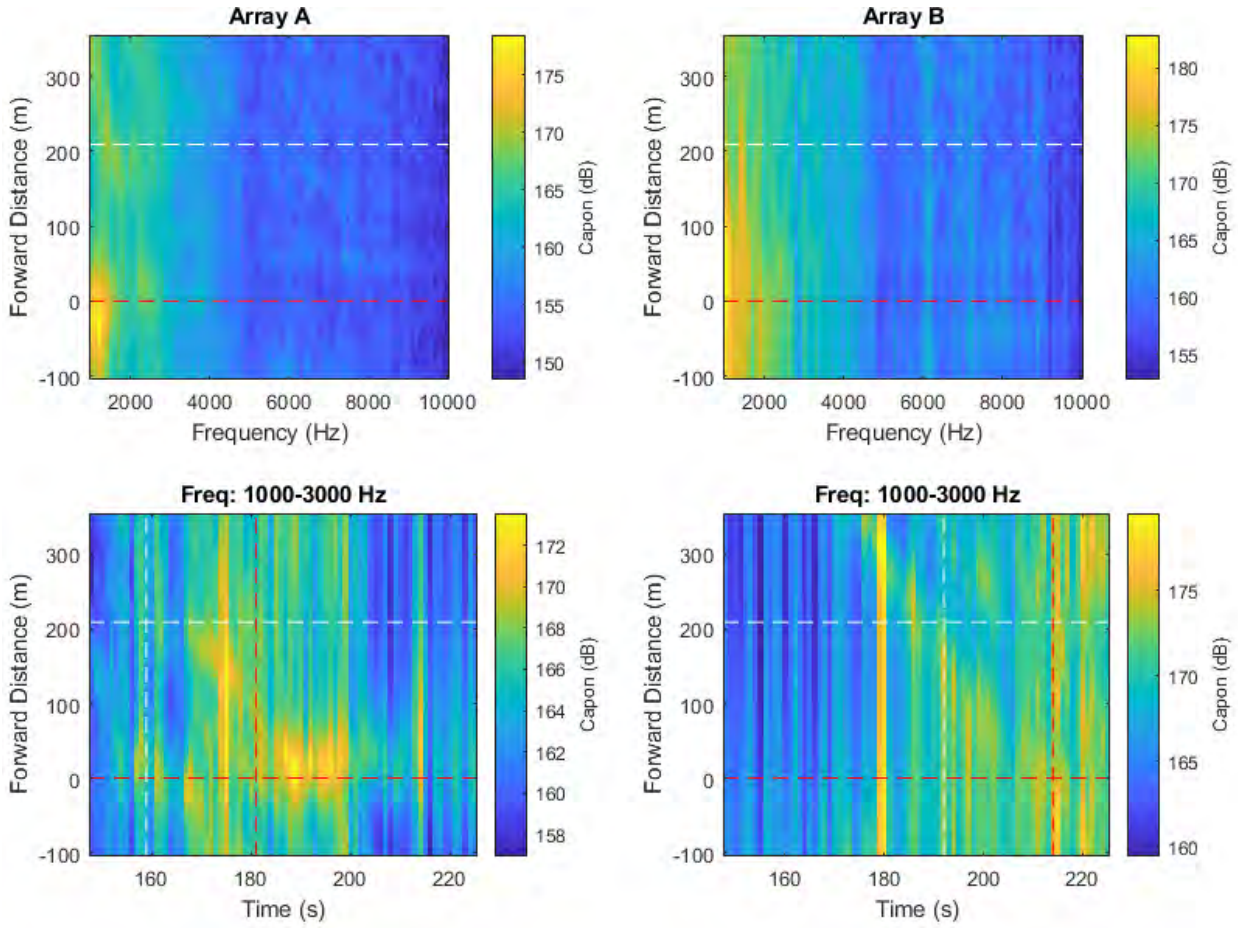

Figure 94 High-frequency noise maps obtained using the spatial spectra provided by the Capon algorithm implemented using individual arrays.

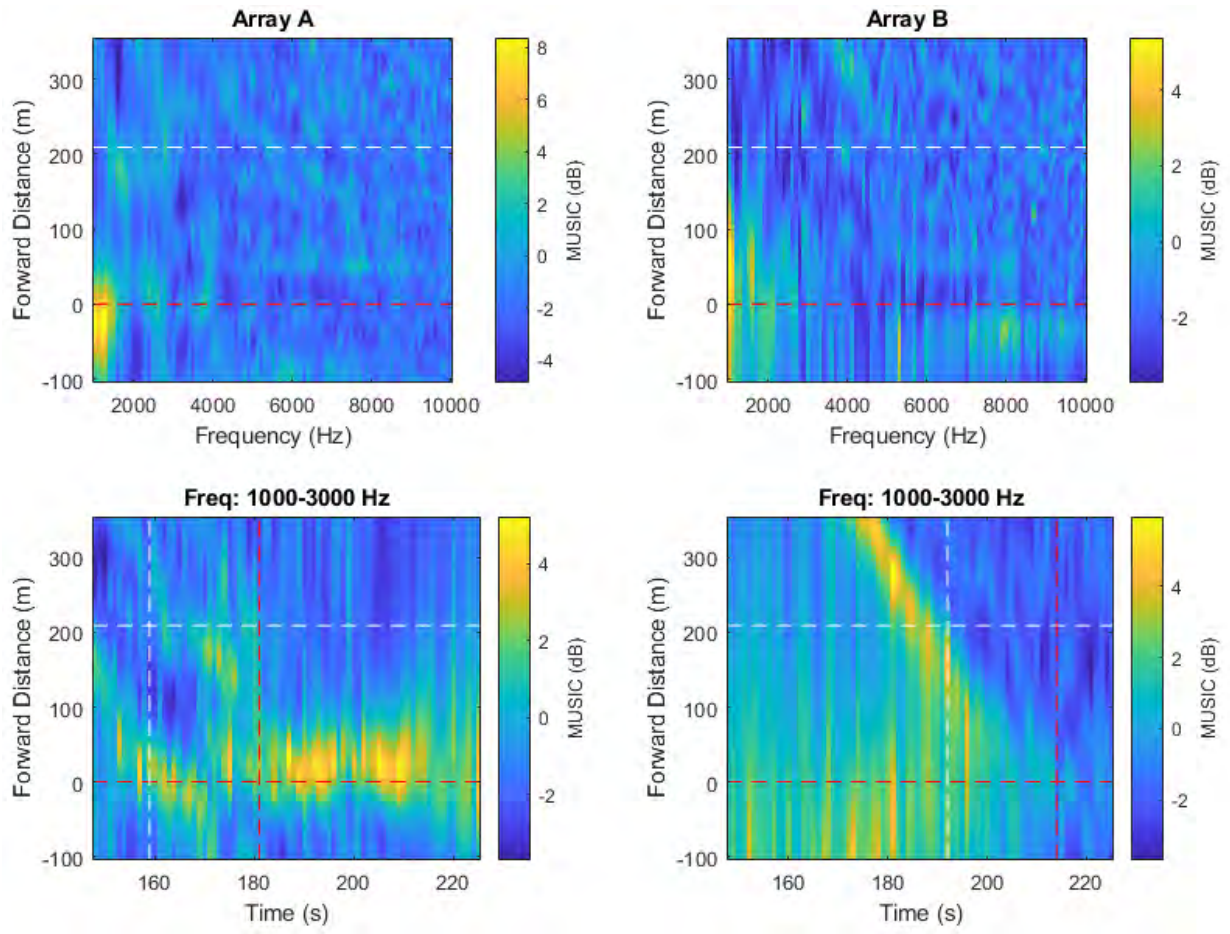

Figure 95 High-frequency noise maps obtained using the spatial spectra provided by the MUSIC algorithm implemented using individual arrays.

A.11. Pass #11 (Type: Container. Length: 332 m. Speed: 19.1 kn)

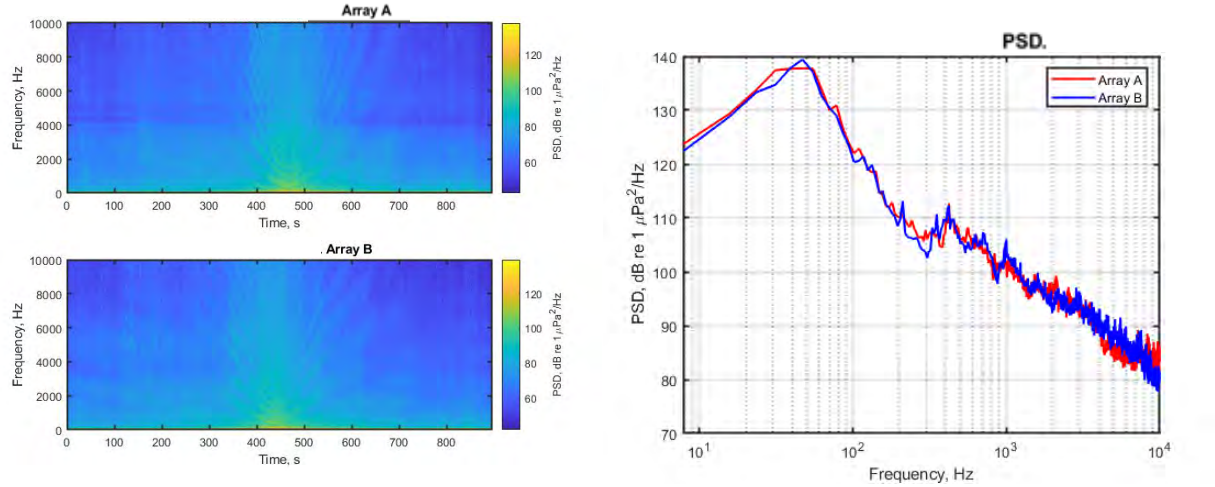

Figure 96 Spectrograms (left) and PSD (right) of ship noise observed on outputs of Arrays A and B.

A.11.1. Low- and mid-frequency noise maps

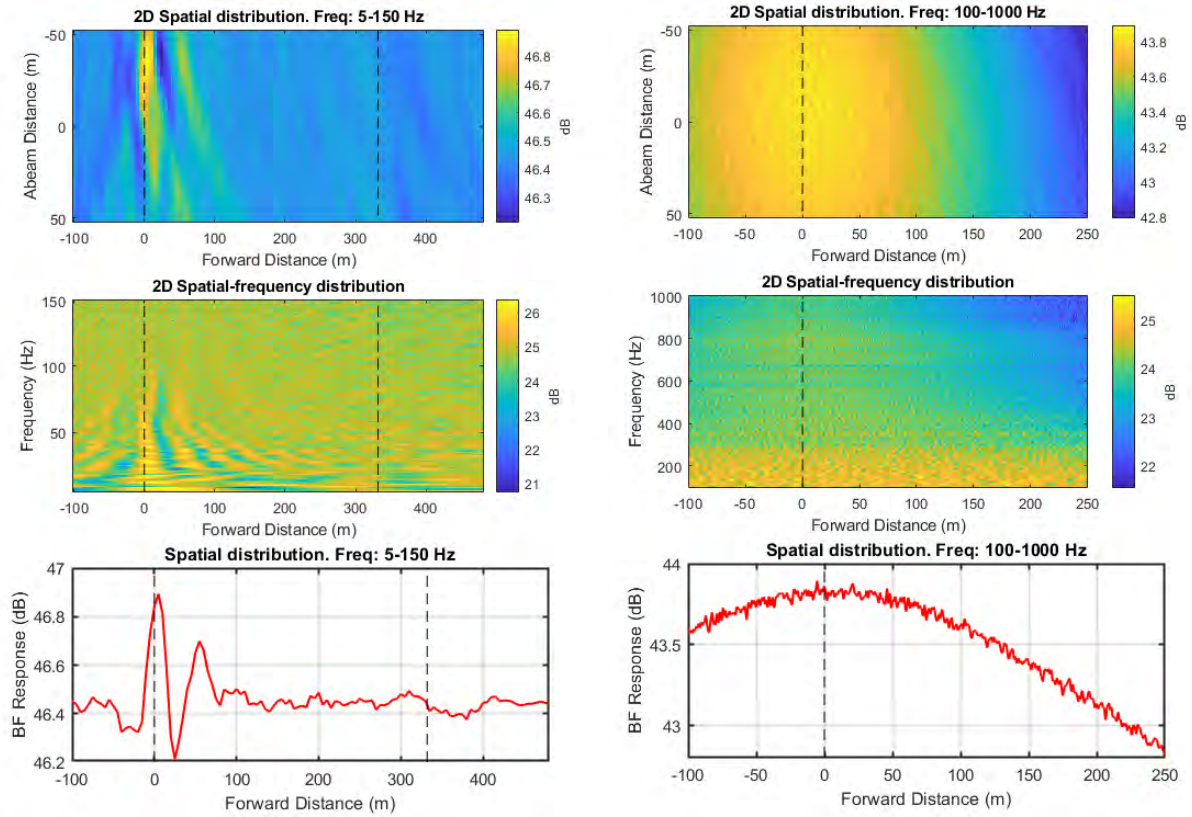

Figure 97 Noise maps from standard beamforming using combined array for Vessel Pass #11: 2D maps in spatial domain for two frequency ranges (top); 2D maps in vessel forward distance and frequency domain for two frequency ranges (middle); and graph of BF response versus forward distance for two frequency ranges bottom). Frequency ranges are 5 to150 Hz (left) and 100 to1000 Hz (right).

A.11.2. High-frequency noise maps

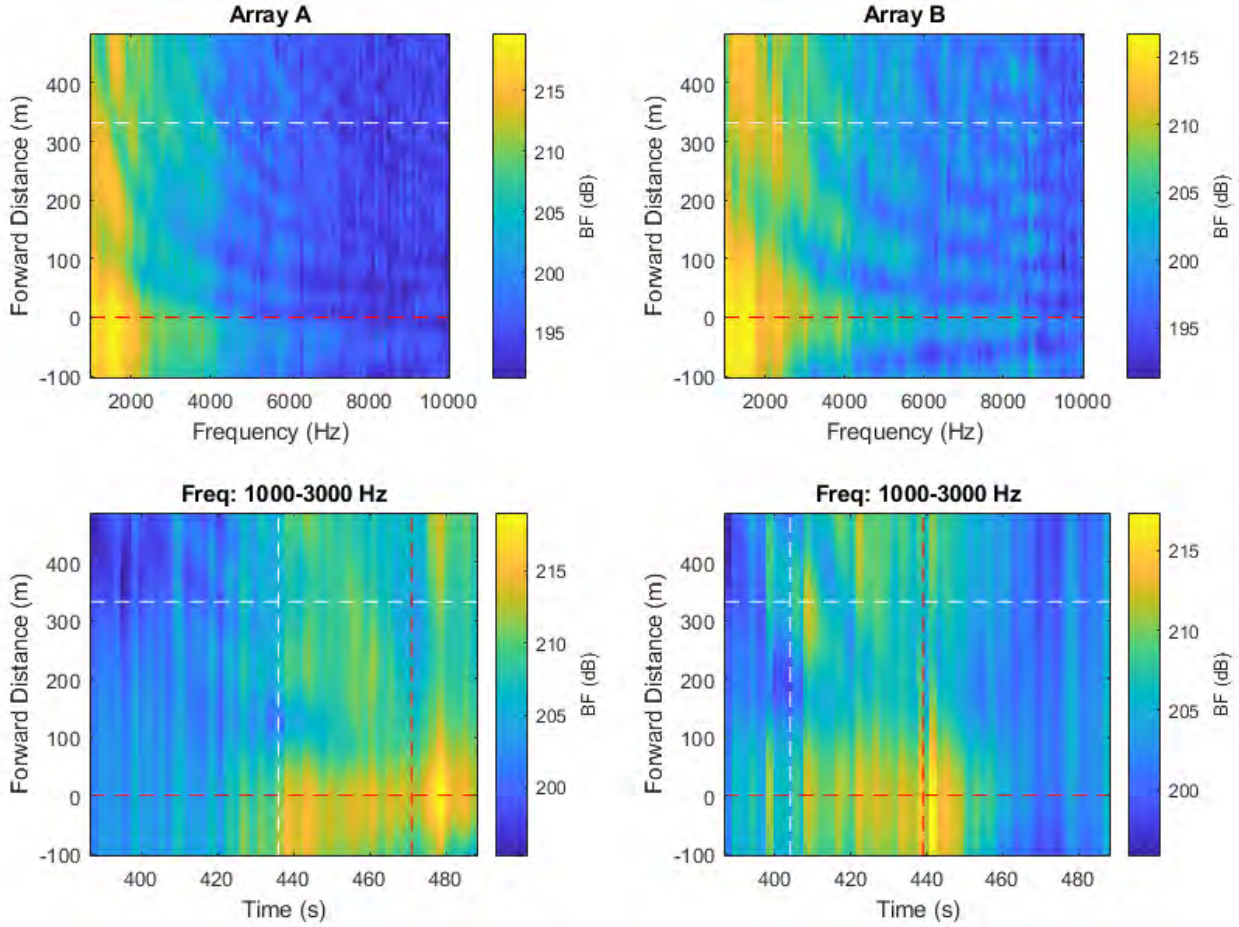

Figure 98 High-frequency noise maps from beamforming with individual arrays. Top maps show the BF response versus forward distance along vessel, measured approximately from the stern, versus frequency. Bottom maps show BF response versus forward distance and snapshot time. Horizontal dashed lines indicate the stern and bow positions of the vessel. Vertical dashed lines represent the CPA times of the bow and stern at each array.

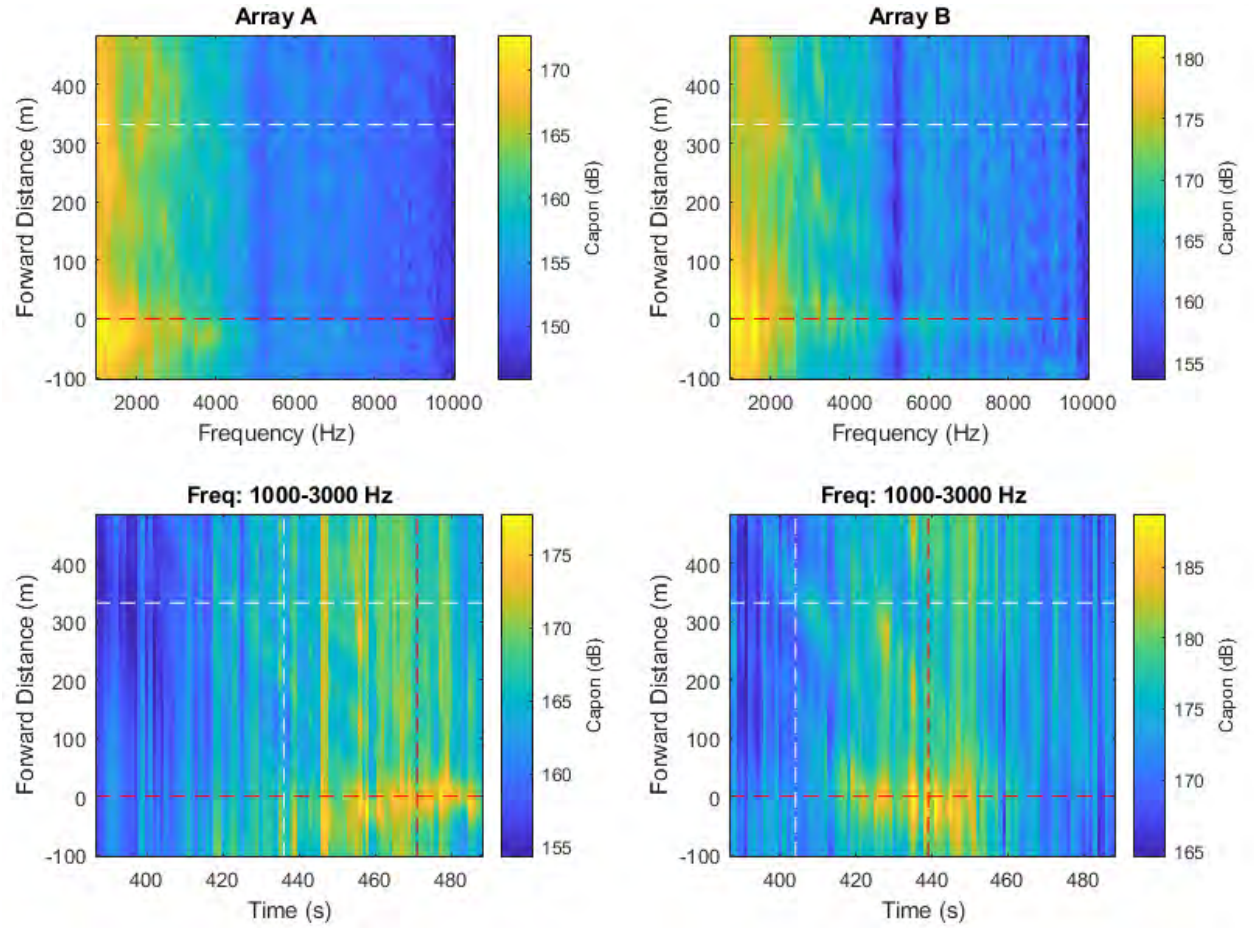

Figure 99 High-frequency noise maps obtained using the spatial spectra provided by the Capon algorithm implemented using individual arrays.

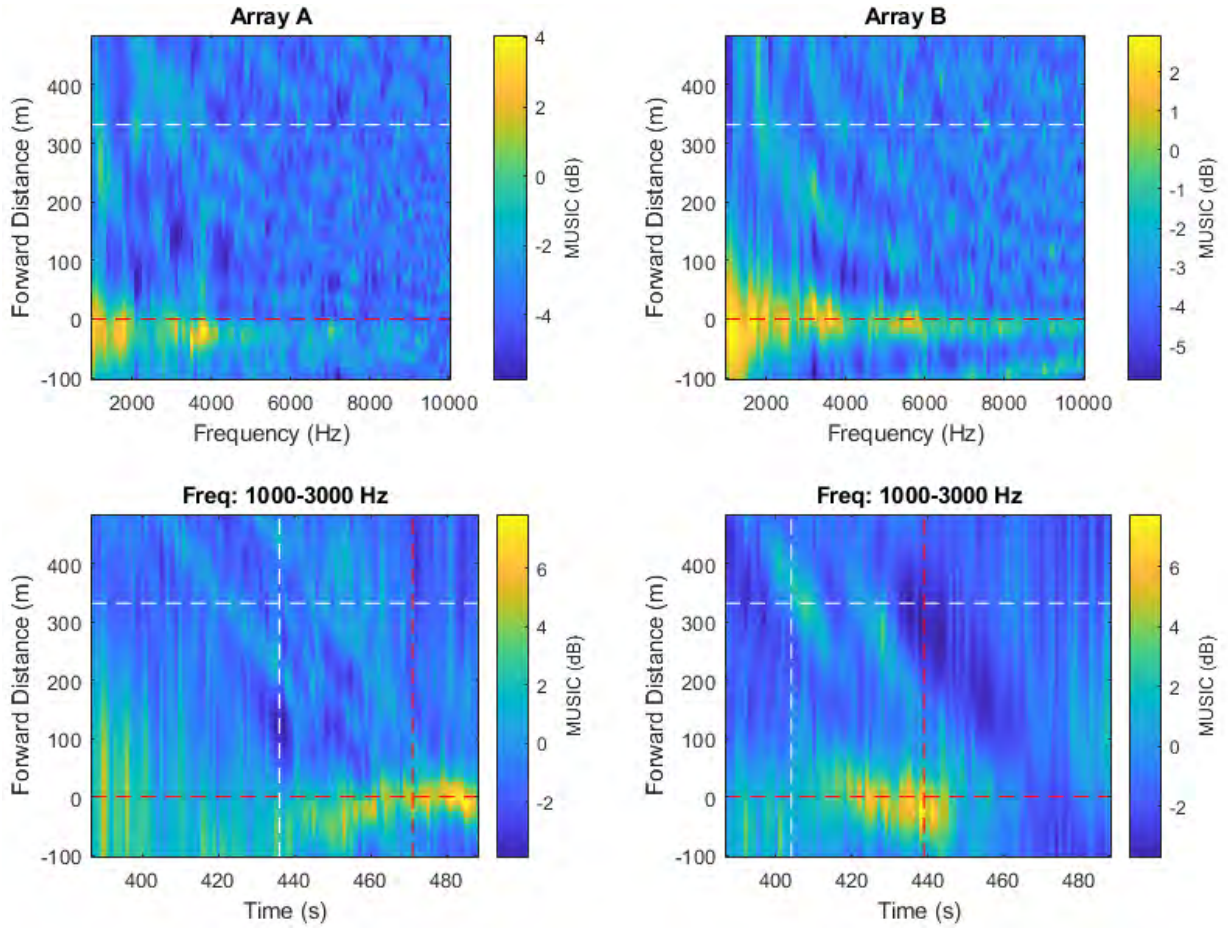

Figure 100 High-frequency noise maps obtained using the spatial spectra provided by the MUSIC algorithm implemented using individual arrays.

A.12. Pass #12 (Type: Bulker. Length: 199 m. Speed: 14.2 kn)

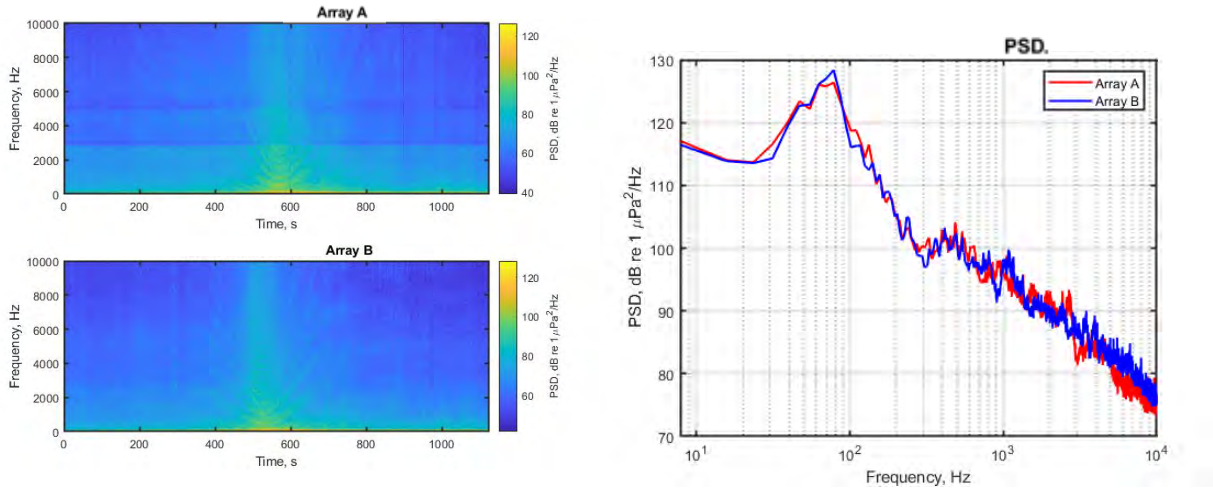

Figure 101 Spectrograms (left) and PSD (right) of ship noise observed on outputs of Arrays A and B.

A.12.1. Low- and mid-frequency noise maps

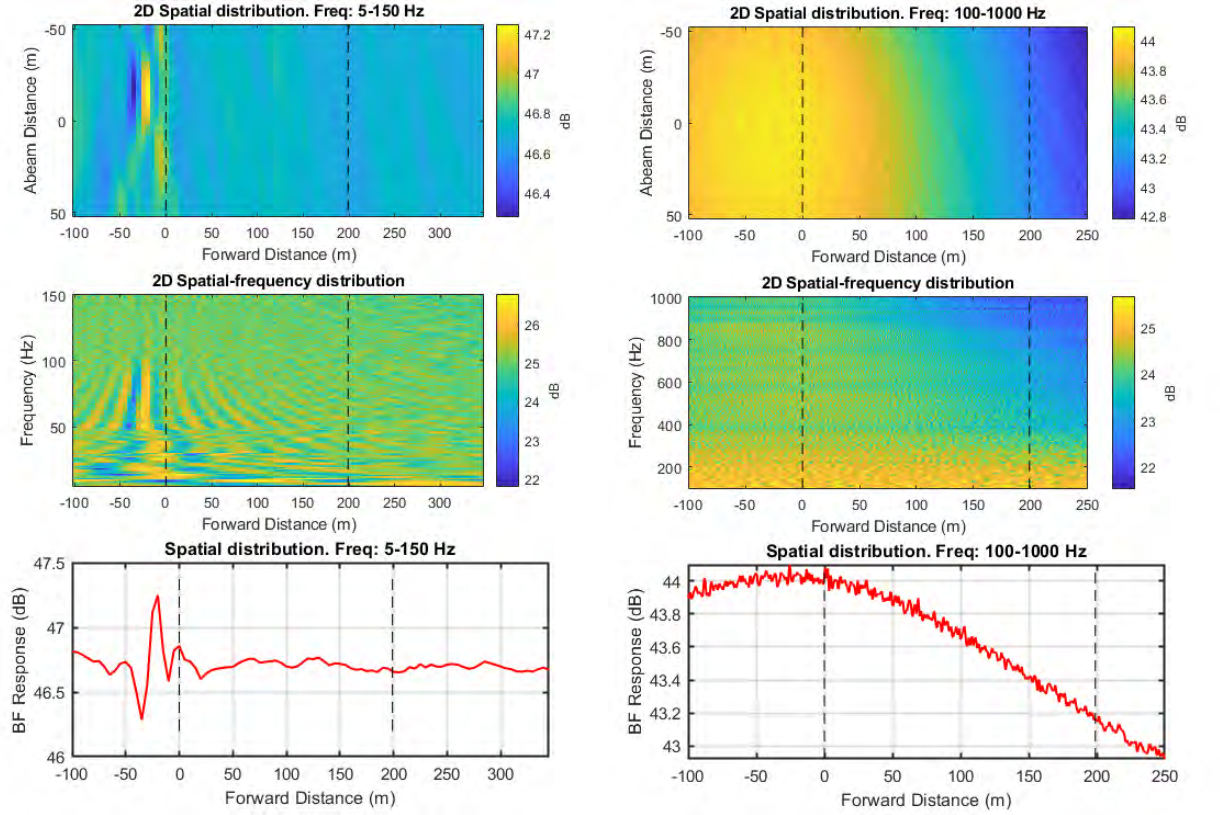

Figure 102 Noise maps from standard beamforming using combined array for Vessel Pass #12: 2D maps in spatial domain for two frequency ranges (top); 2D maps in vessel forward distance and frequency domain for two frequency ranges (middle); and graph of BF response versus forward distance for two frequency ranges bottom). Frequency ranges are 5 to150 Hz (left) and 100 to1000 Hz (right).

A.12.2. High-frequency noise maps

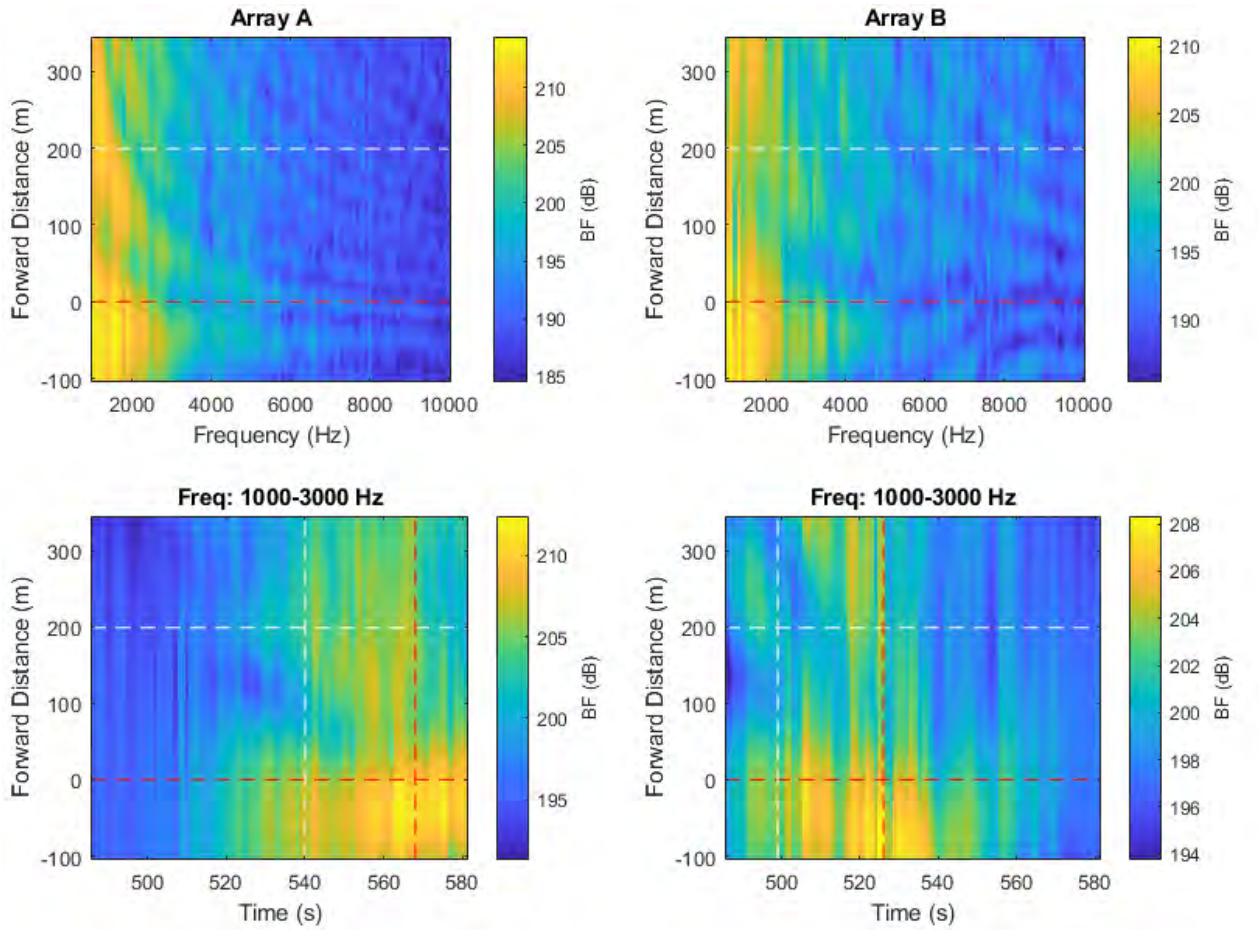

Figure 103 High-frequency noise maps from beamforming with individual arrays. Top maps show the BF response versus forward distance along vessel, measured approximately from the stern, versus frequency. Bottom maps show BF response versus forward distance and snapshot time. Horizontal dashed lines indicate the stern and bow positions of the vessel. Vertical dashed lines represent the CPA times of the bow and stern at each array.

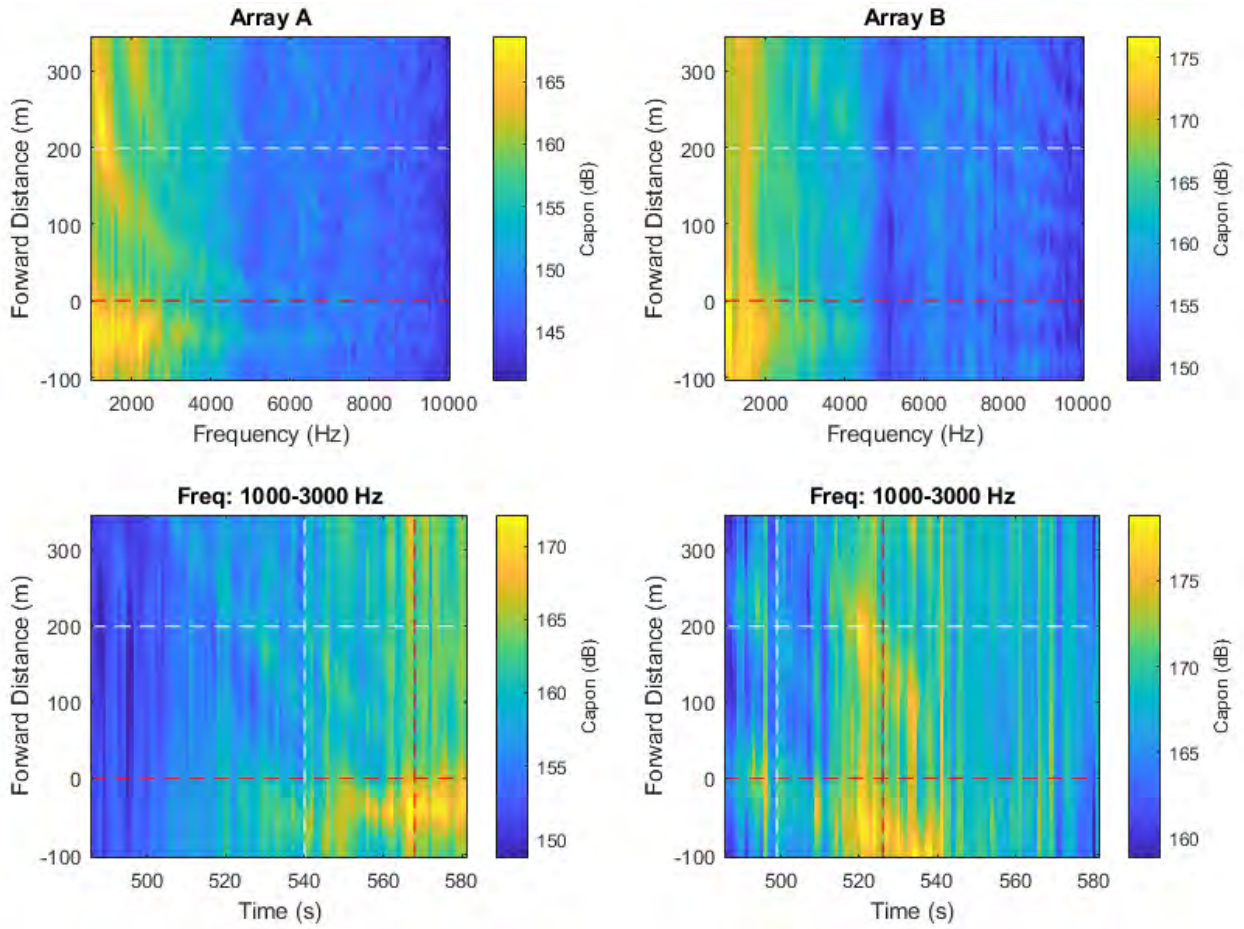

Figure 104 High-frequency noise maps obtained using the spatial spectra provided by the Capon algorithm implemented using individual arrays.

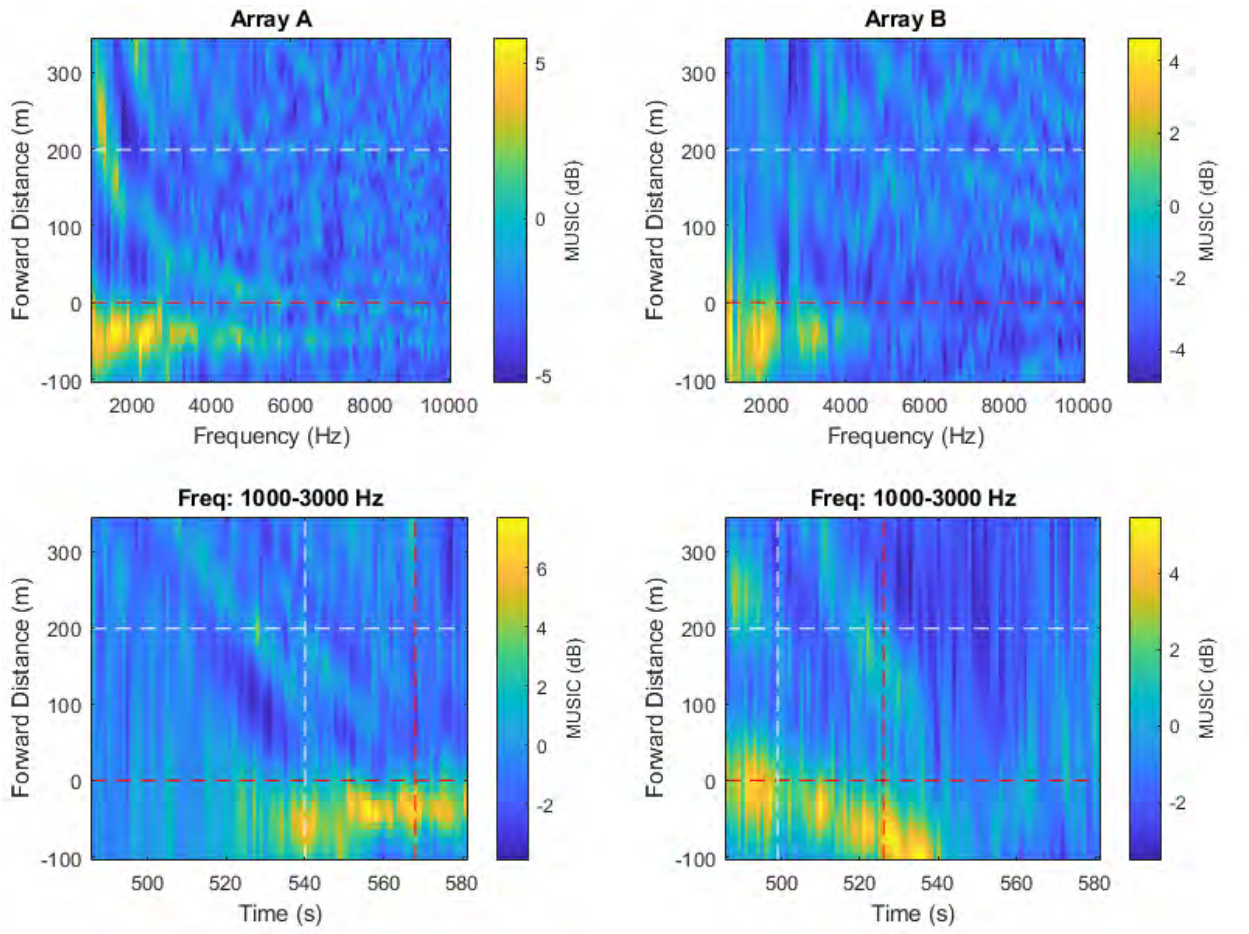

Figure 105 High-frequency noise maps obtained using the spatial spectra provided by the MUSIC algorithm implemented using individual arrays.

A.13. Pass #13 (Type: Bulker. Length: 292 m. Speed: 13.4 kn)

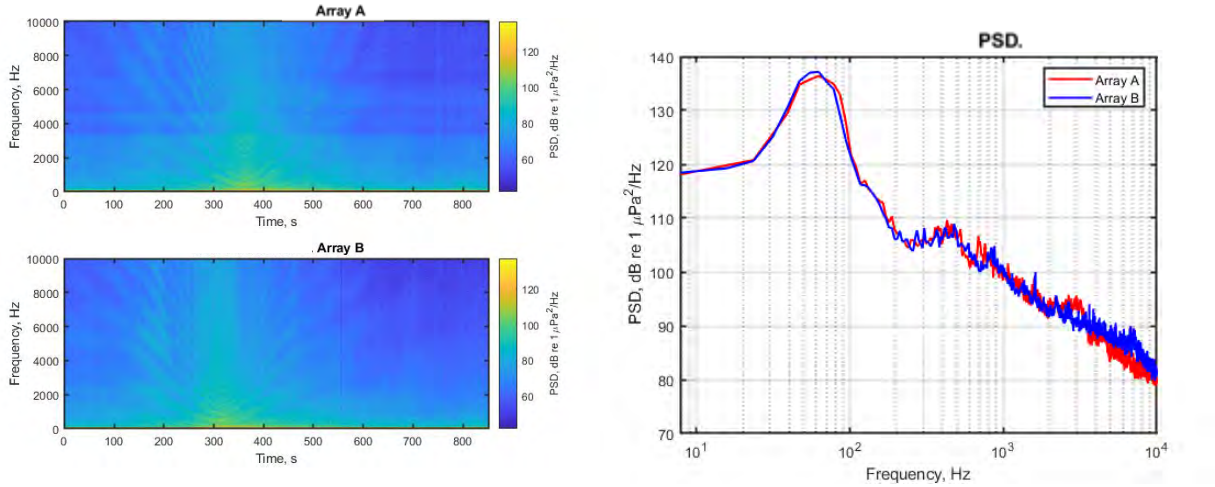

Figure 106 Spectrograms (left) and PSD (right) of ship noise observed on outputs of Arrays A and B.

A.13.1. Low- and mid-frequency noise maps

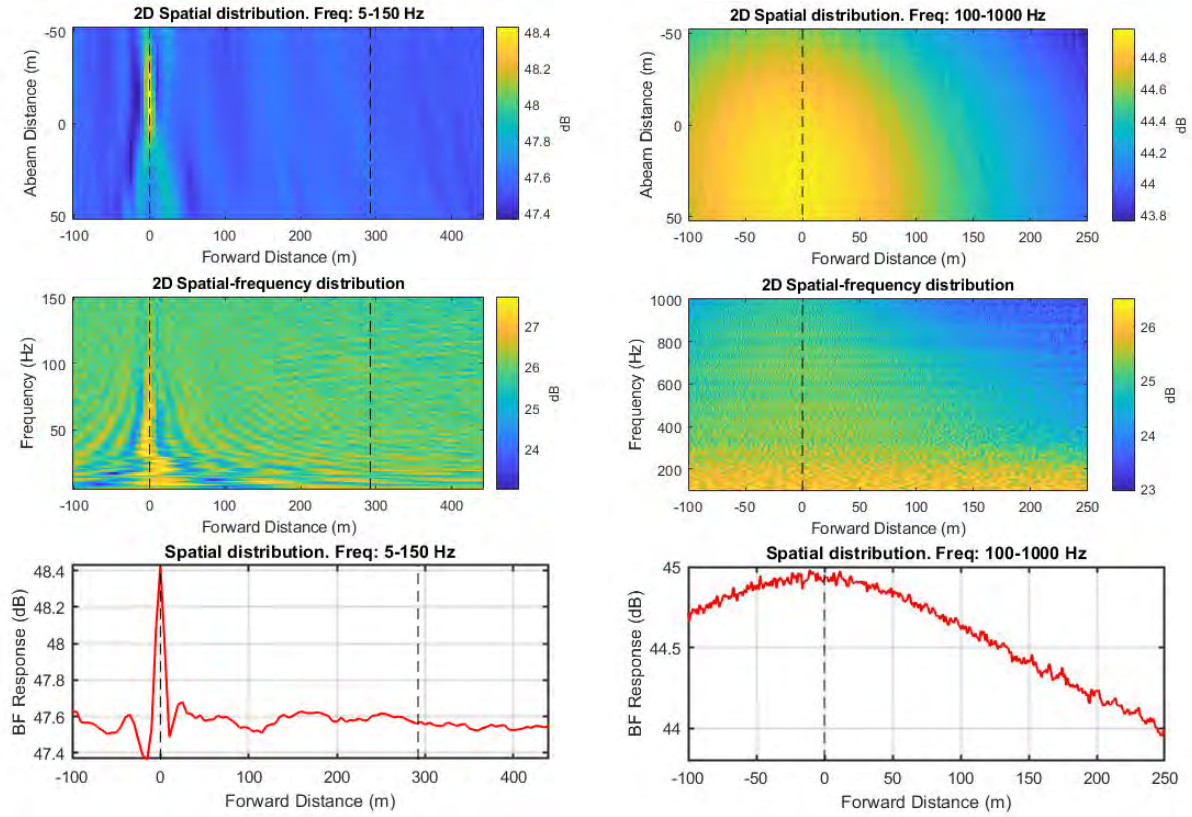

Figure 107 Noise maps from standard beamforming using combined array for Vessel Pass #13: 2D maps in spatial domain for two frequency ranges (top); 2D maps in vessel forward distance and frequency domain for two frequency ranges (middle); and graph of BF response versus forward distance for two frequency ranges bottom). Frequency ranges are 5 to150 Hz (left) and 100 to1000 Hz (right).

A.13.2. High-frequency noise maps

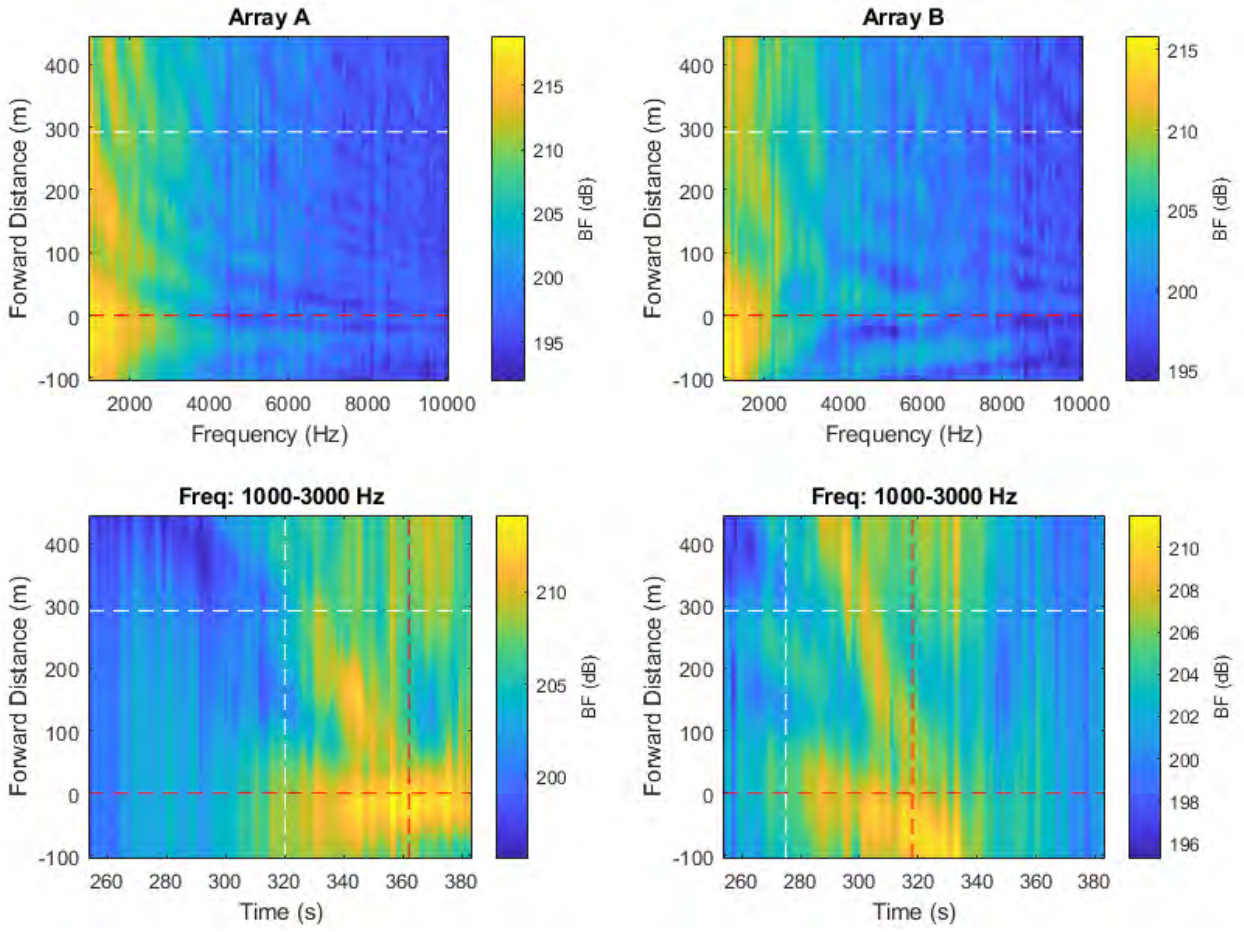

Figure 108 High-frequency noise maps from beamforming with individual arrays. Top maps show the BF response versus forward distance along vessel, measured approximately from the stern, versus frequency. Bottom maps show BF response versus forward distance and snapshot time. Horizontal dashed lines indicate the stern and bow positions of the vessel. Vertical dashed lines represent the CPA times of the bow and stern at each array.

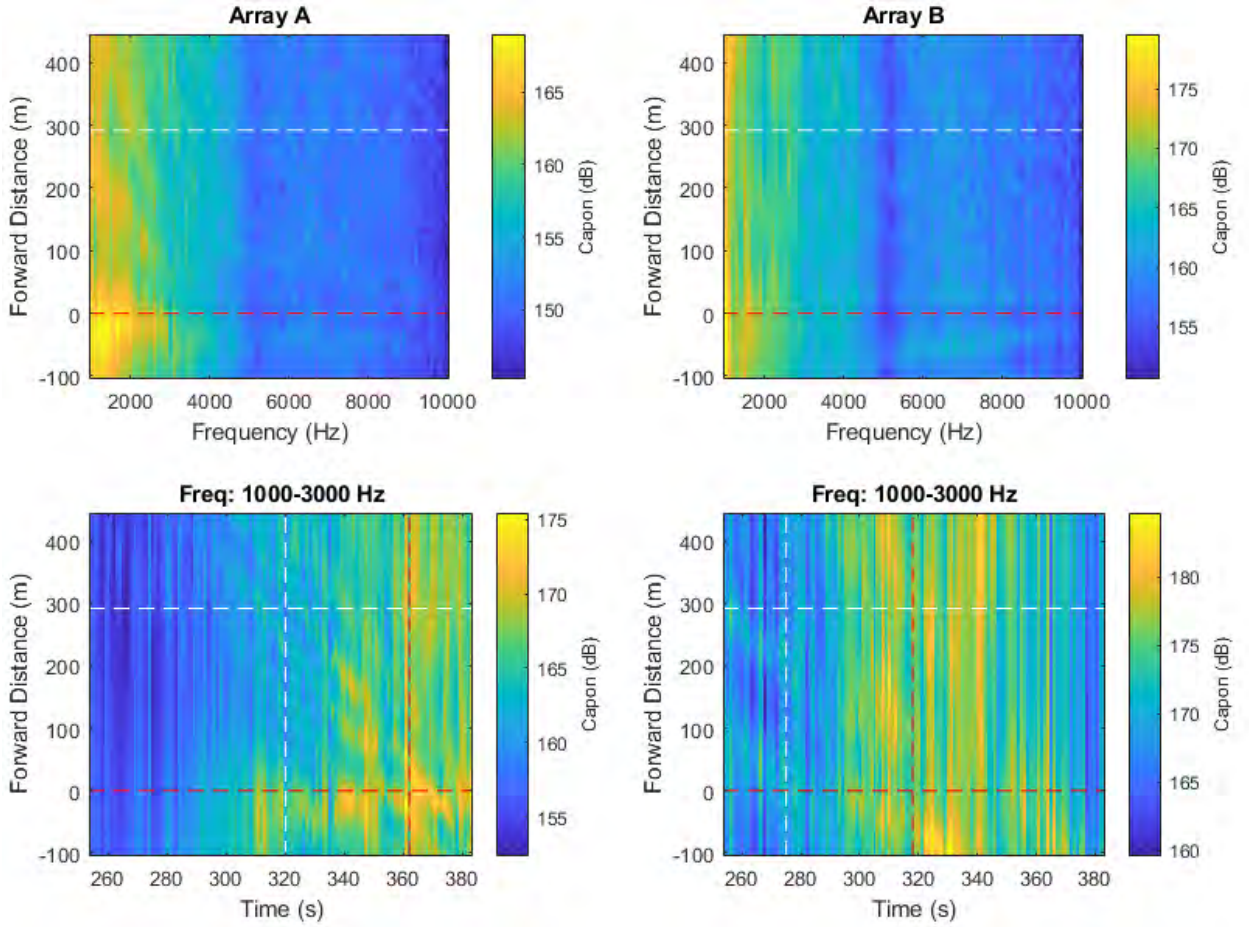

Figure 109 High-frequency noise maps obtained using the spatial spectra provided by the Capon algorithm implemented using individual arrays.

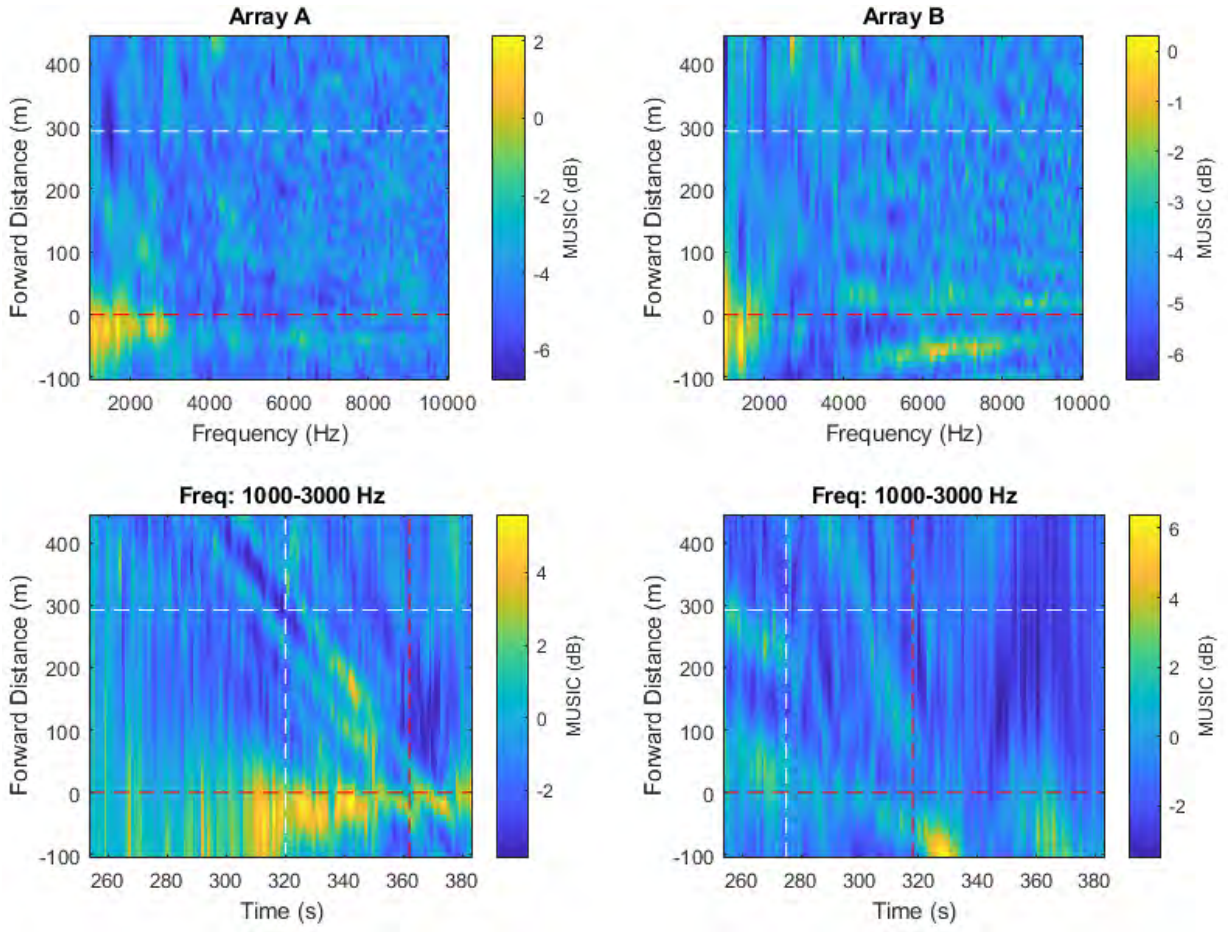

Figure 110 High-frequency noise maps obtained using the spatial spectra provided by the MUSIC algorithm implemented using individual arrays.

A.14. Pass #14 (Type: Bulker. Length: 225 m. Speed: 13.9 kn)

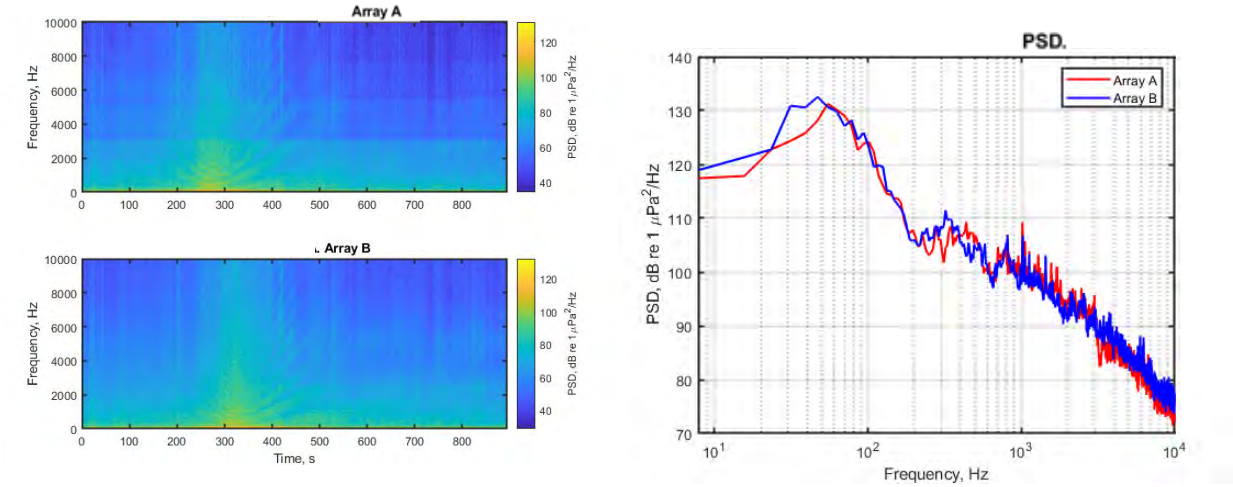

Figure 111 Spectrograms (left) and PSD (right) of ship noise observed on outputs of Arrays A and B.

A.14.1. Low- and mid-frequency noise maps

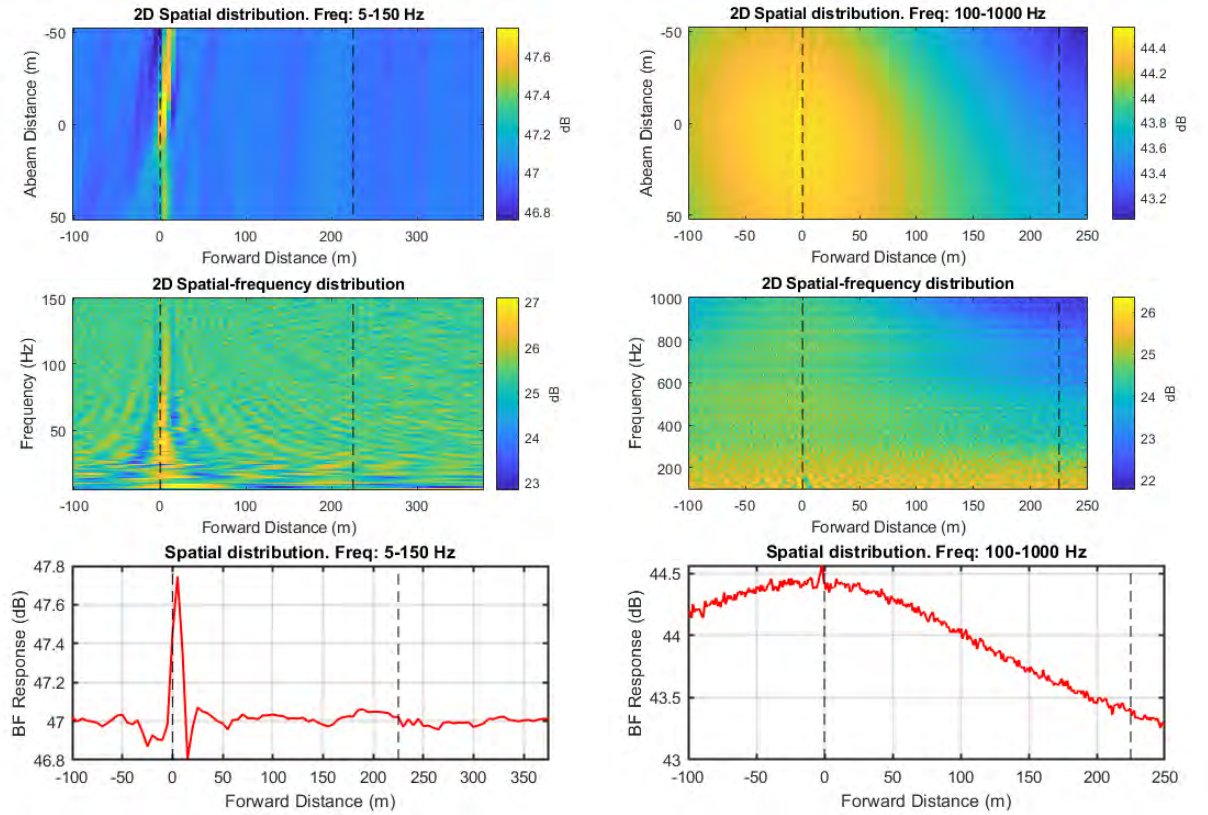

Figure 112 Noise maps from standard beamforming using combined array for Vessel Pass #14: 2D maps in spatial domain for two frequency ranges (top); 2D maps in vessel forward distance and frequency domain for two frequency ranges (middle); and graph of BF response versus forward distance for two frequency ranges bottom). Frequency ranges are 5 to150 Hz (left) and 100 to1000 Hz (right).

A.14.2. High-frequency noise maps

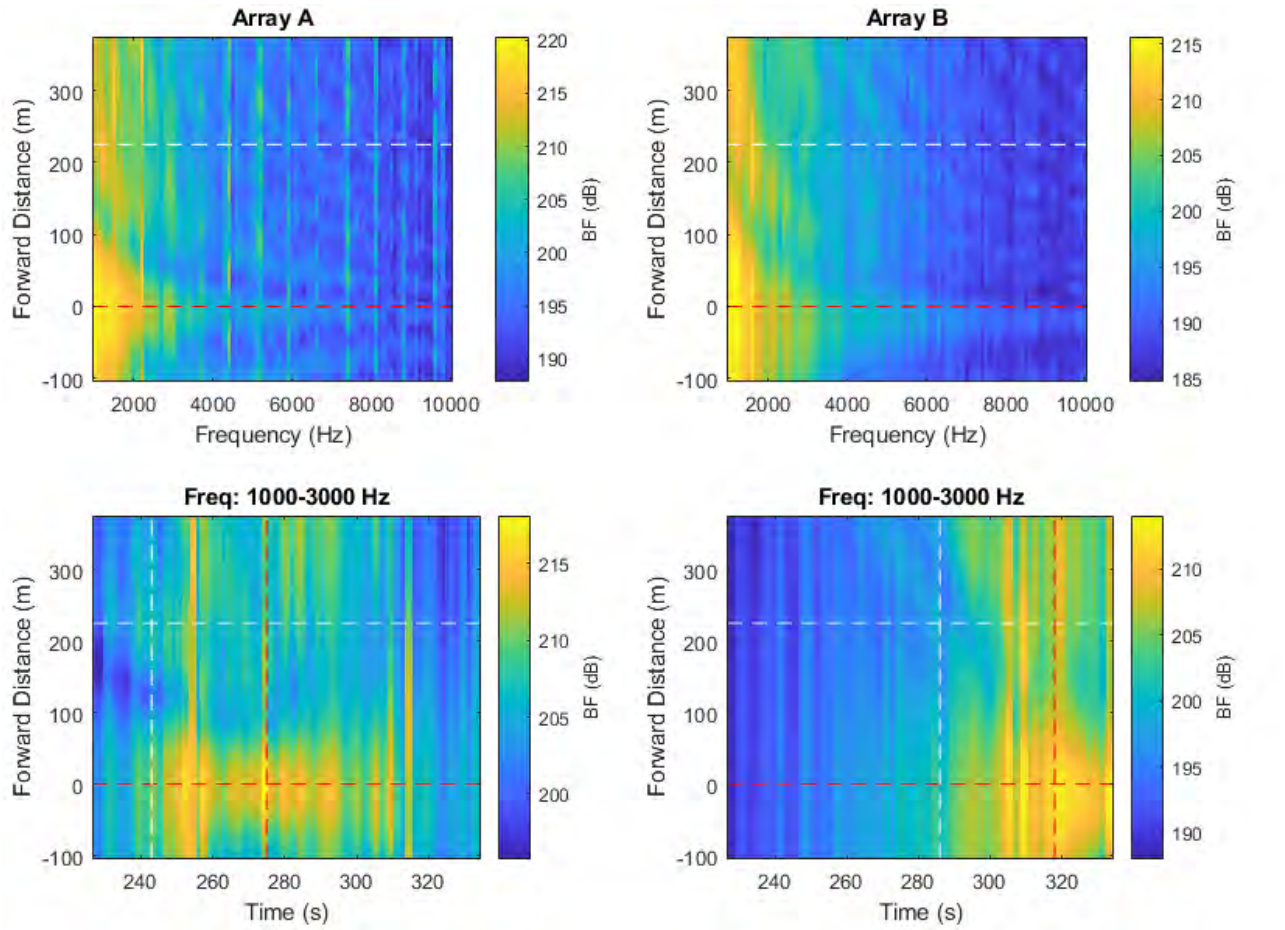

Figure 113 High-frequency noise maps from beamforming with individual arrays. Top maps show the BF response versus forward distance along vessel, measured approximately from the stern, versus frequency. Bottom maps show BF response versus forward distance and snapshot time. Horizontal dashed lines indicate the stern and bow positions of the vessel. Vertical dashed lines represent the CPA times of the bow and stern at each array.

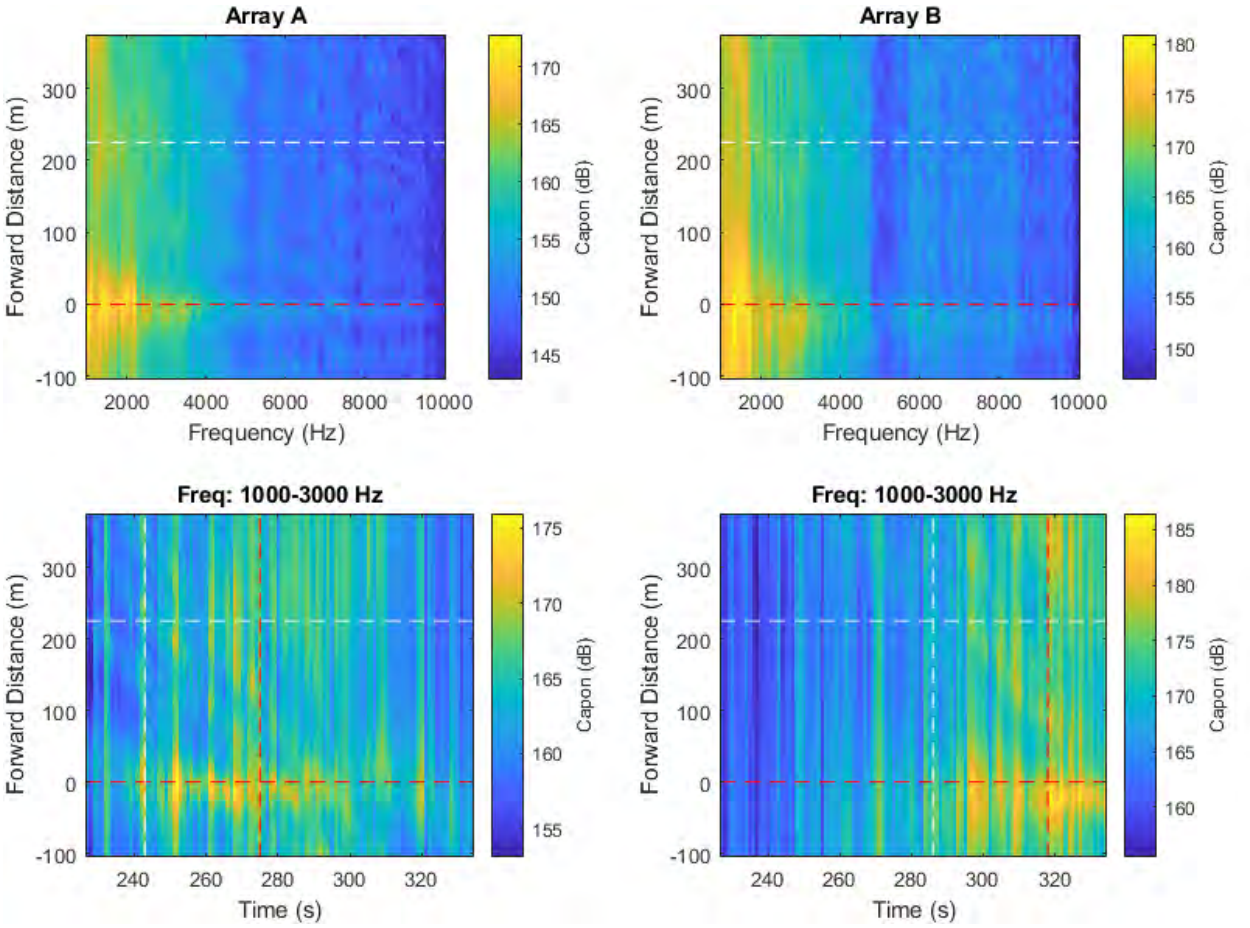

Figure 114 High-frequency noise maps obtained using the spatial spectra provided by the Capon algorithm implemented using individual arrays.

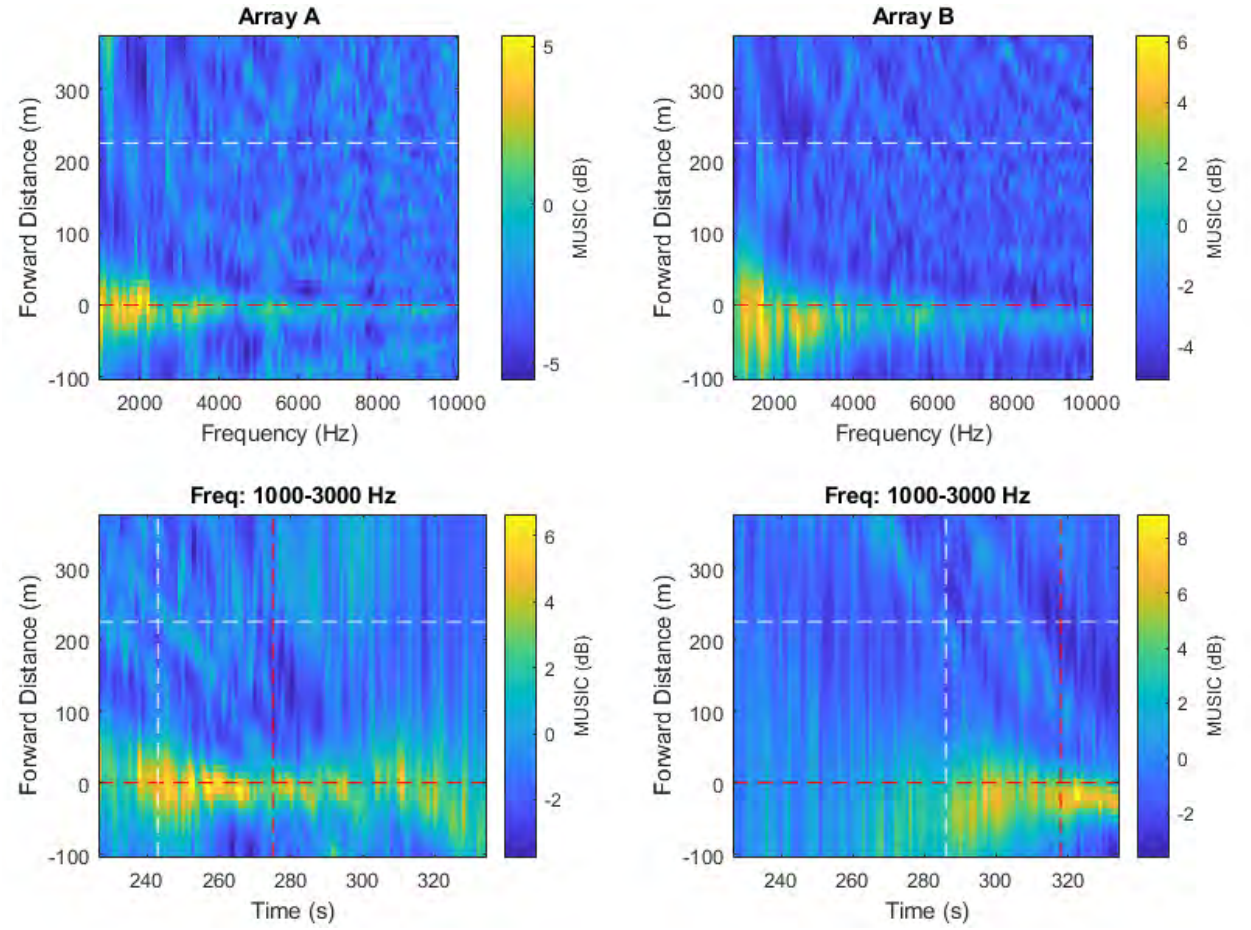

Figure 115 High-frequency noise maps obtained using the spatial spectra provided by the MUSIC algorithm implemented using individual arrays.

A.15. Pass #15 (Type: Container. Length: 294 m. Speed: 18.9 kn)

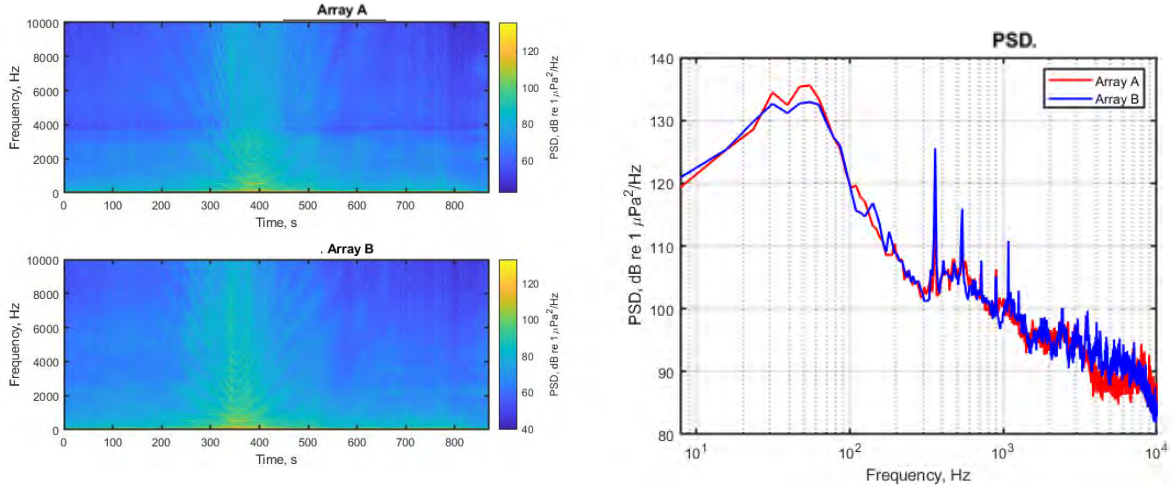

Figure 116 Spectrograms (left) and PSD (right) of ship noise observed on outputs of Arrays A and B.

A.15.1. Low- and mid-frequency noise maps

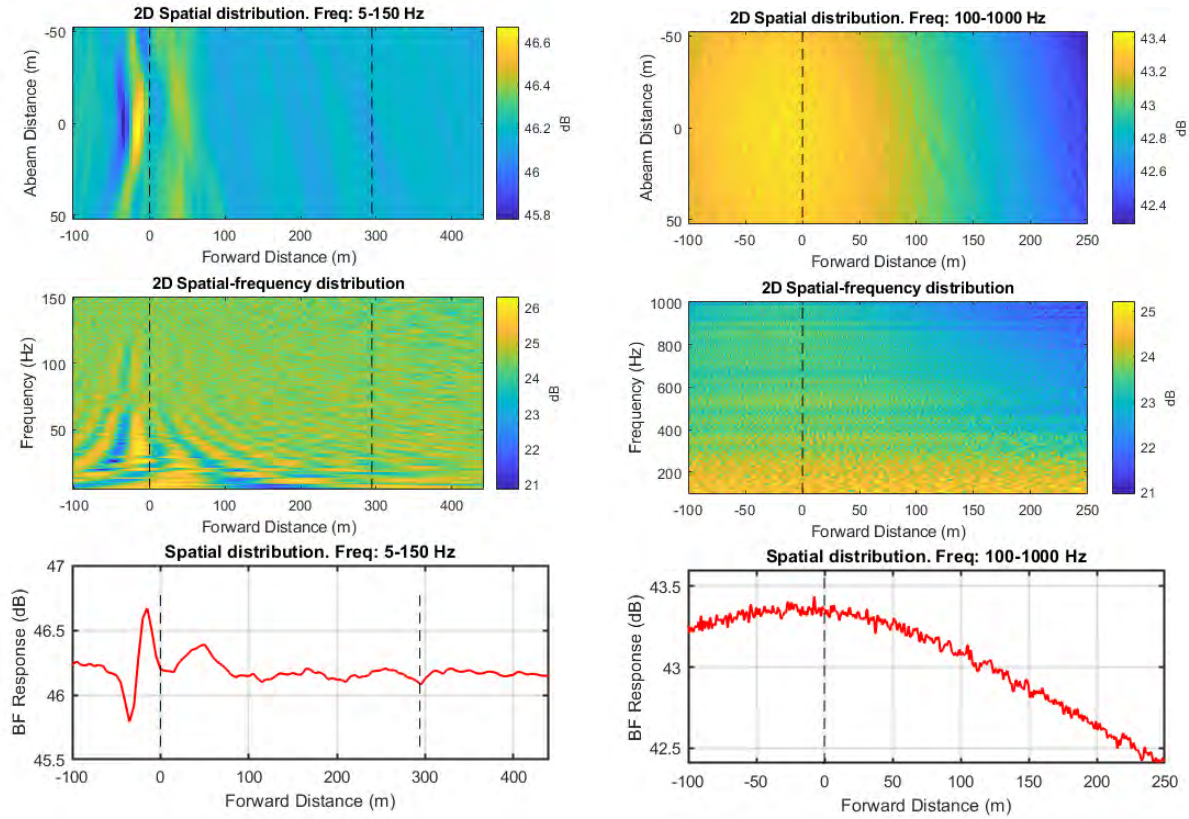

Figure 117 Noise maps from standard beamforming using combined array for Vessel Pass #15: 2D maps in spatial domain for two frequency ranges (top); 2D maps in vessel forward distance and frequency domain for two frequency ranges (middle); and graph of BF response versus forward distance for two frequency ranges bottom). Frequency ranges are 5 to150 Hz (left) and 100 to1000 Hz (right).

A.15.2. High-frequency noise maps

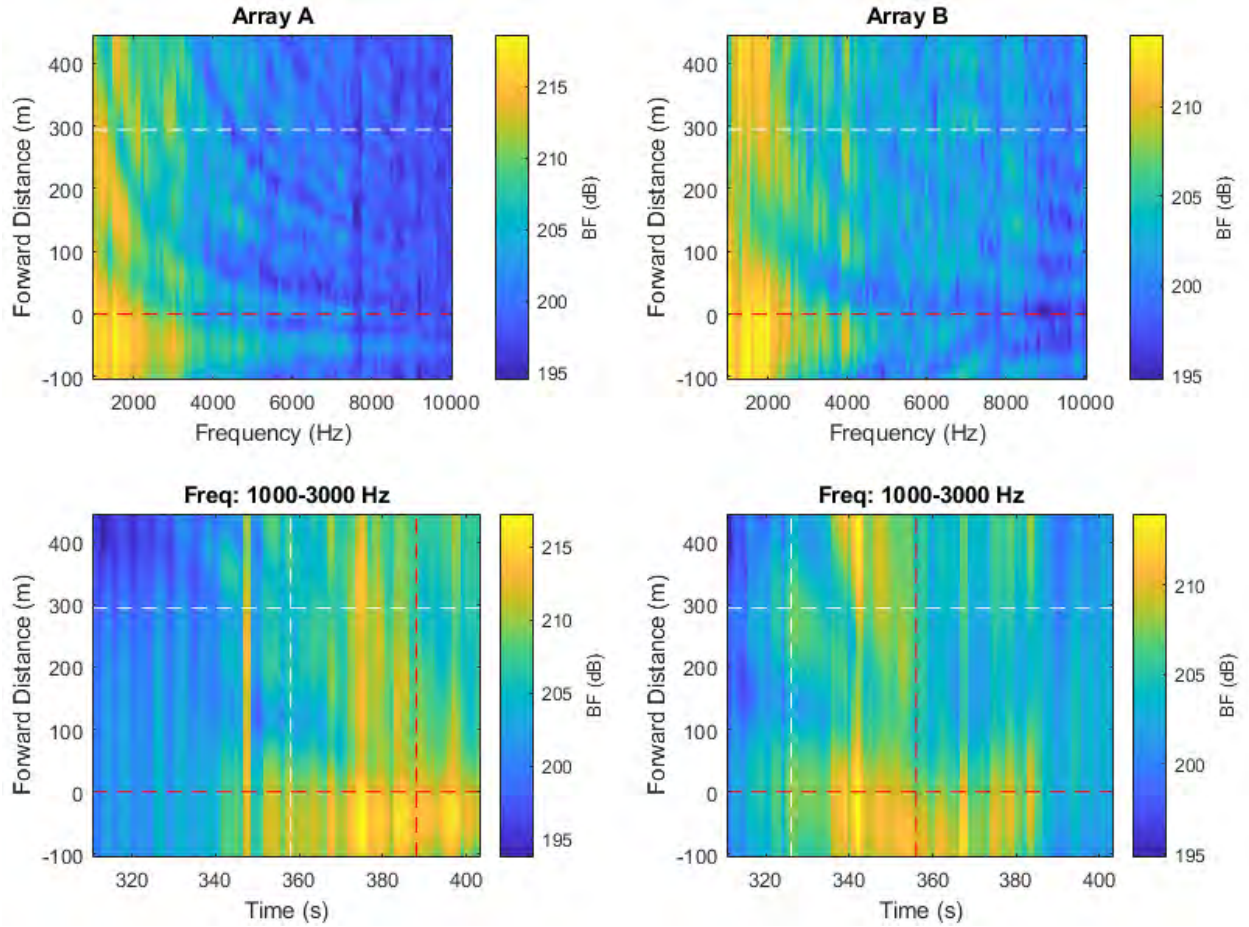

Figure 118 High-frequency noise maps from beamforming with individual arrays. Top maps show the BF response versus forward distance along vessel, measured approximately from the stern, versus frequency. Bottom maps show BF response versus forward distance and snapshot time. Horizontal dashed lines indicate the stern and bow positions of the vessel. Vertical dashed lines represent the CPA times of the bow and stern at each array.

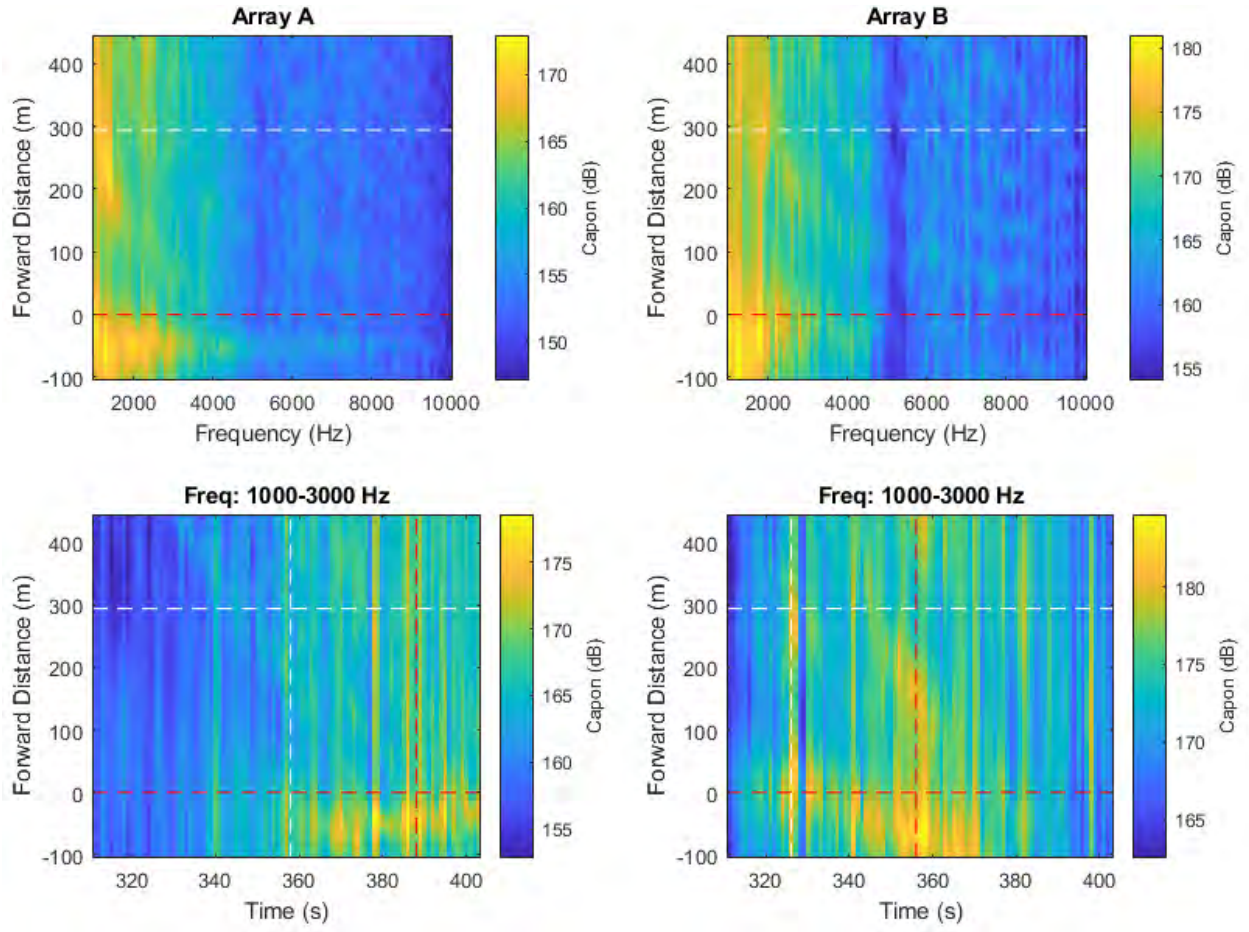

Figure 119 High-frequency noise maps obtained using the spatial spectra provided by the Capon algorithm implemented using individual arrays.

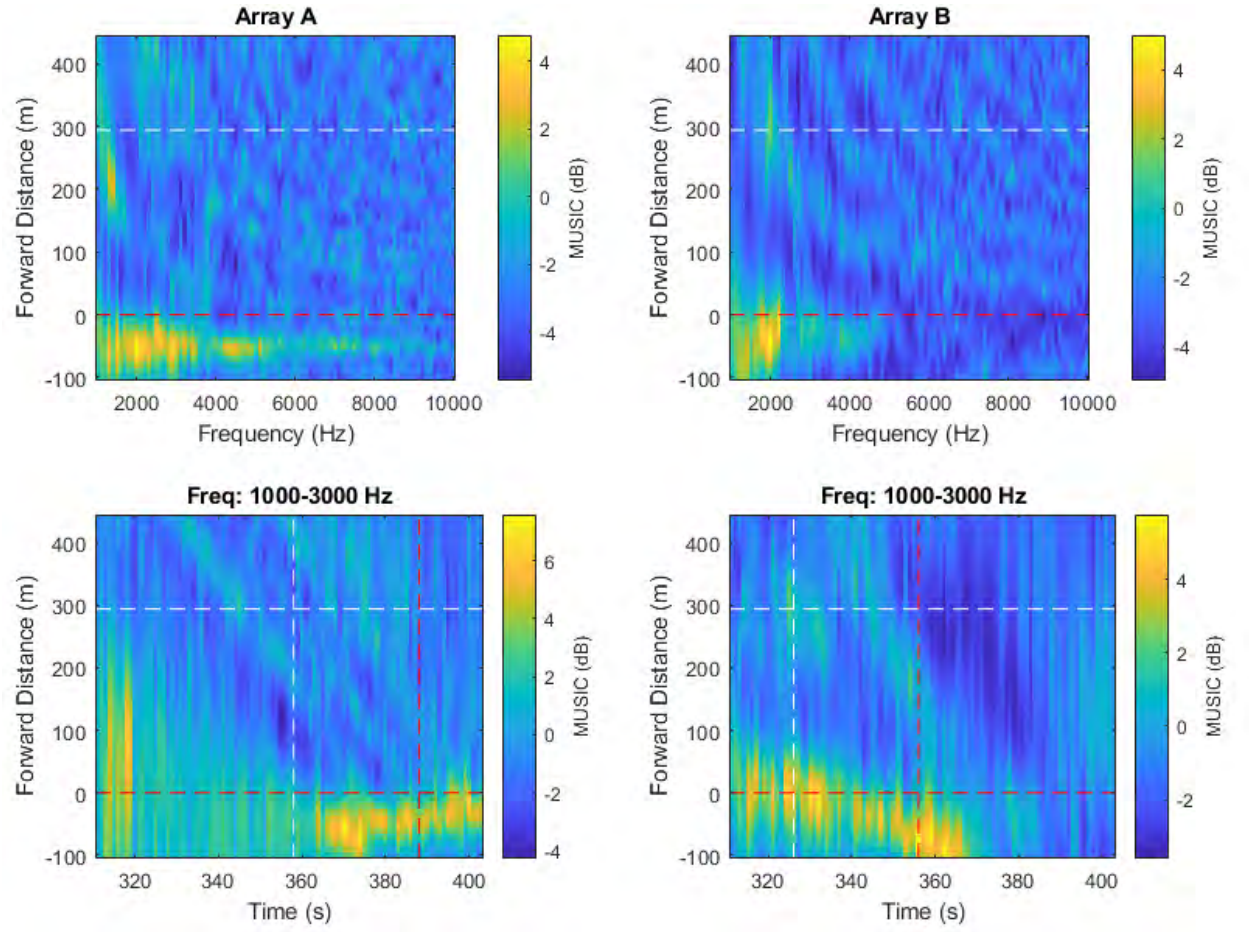

Figure 120 High-frequency noise maps obtained using the spatial spectra provided by the MUSIC algorithm implemented using individual arrays.

A.16. Pass #16 (Type: Container. Length: 280 m. Speed: 17.1 kn)

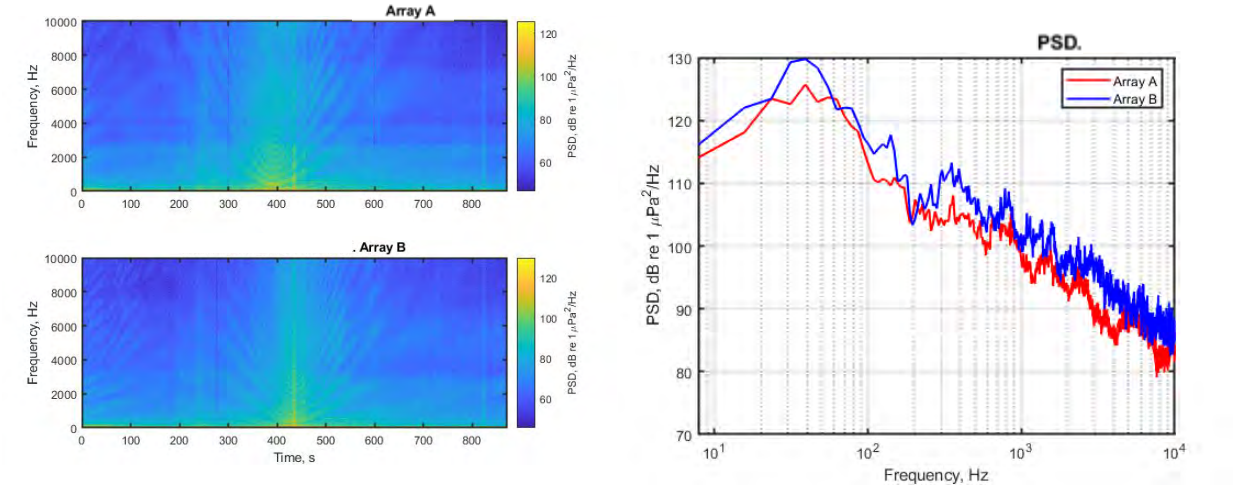

Figure 121 Spectrograms (left) and PSD (right) of ship noise observed on outputs of Arrays A and B.

A.16.1. Low- and mid-frequency noise maps

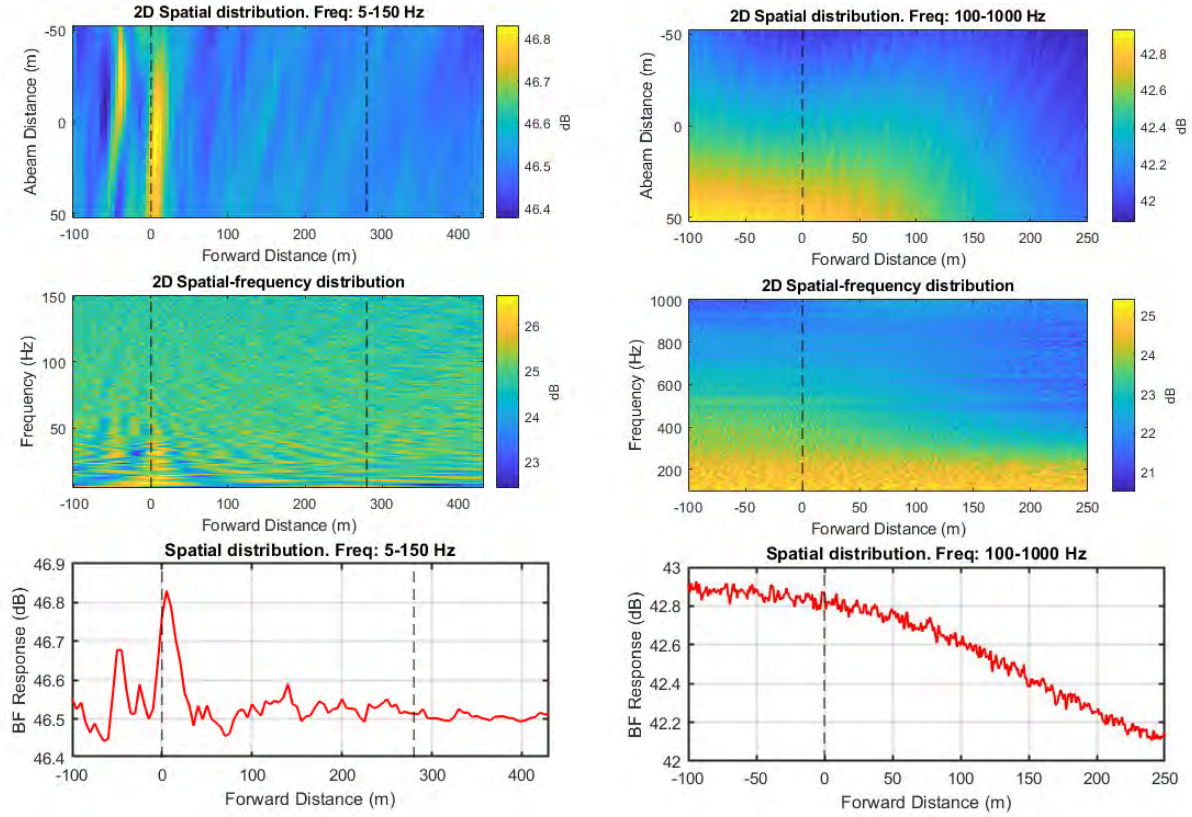

Figure 122 Noise maps from standard beamforming using combined array for Vessel Pass #16: 2D maps in spatial domain for two frequency ranges (top); 2D maps in vessel forward distance and frequency domain for two frequency ranges (middle); and graph of BF response versus forward distance for two frequency ranges (bottom). Frequency ranges are 5 to150 Hz (left) and 100 to1000 Hz (right).

A.16.2. High-frequency noise maps

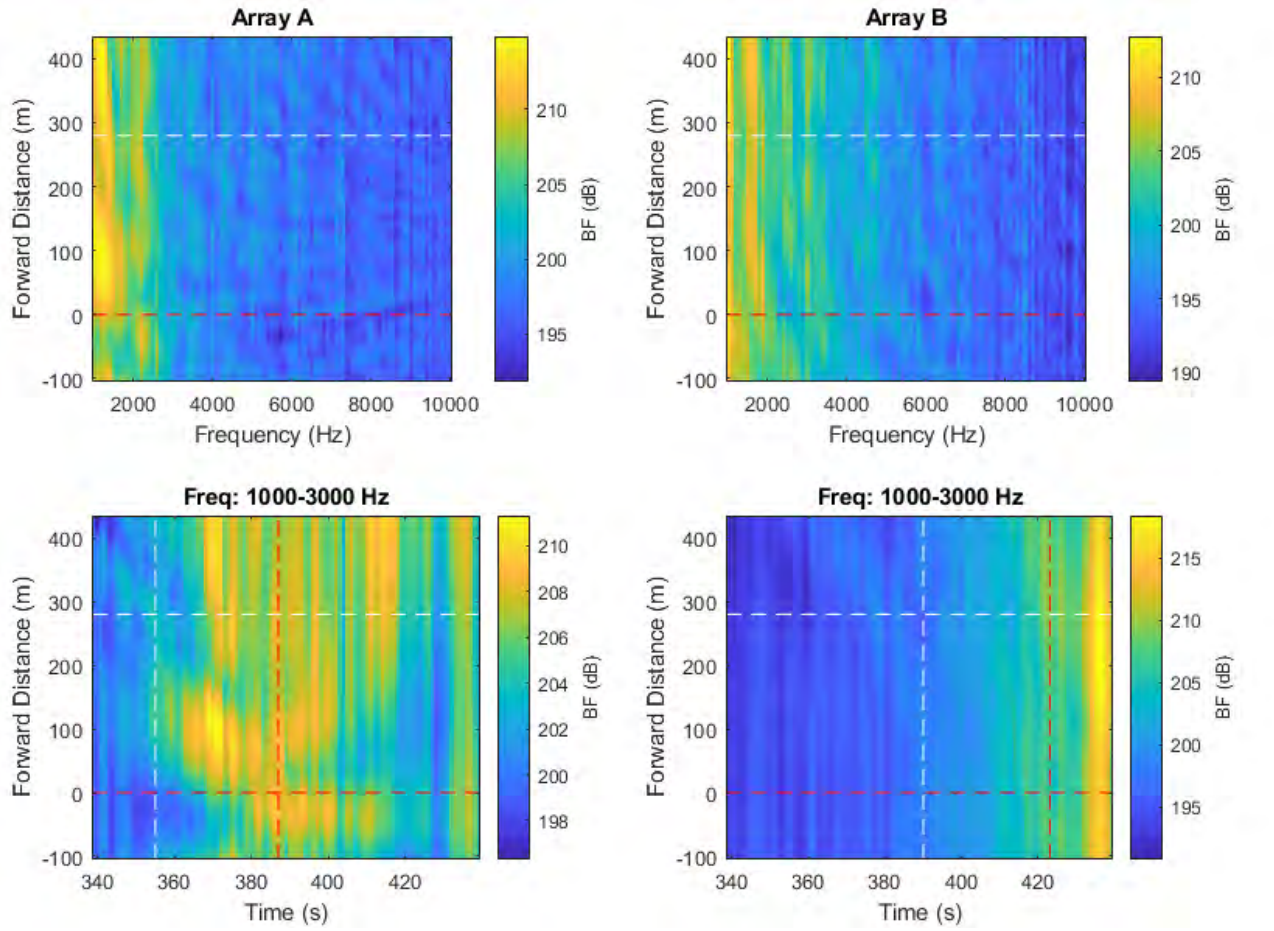

Figure 123 High-frequency noise maps from beamforming with individual arrays. Top maps show the BF response versus forward distance along vessel, measured approximately from the stern, versus frequency. Bottom maps show BF response versus forward distance and snapshot time. Horizontal dashed lines indicate the stern and bow positions of the vessel. Vertical dashed lines represent the CPA times of the bow and stern at each array.

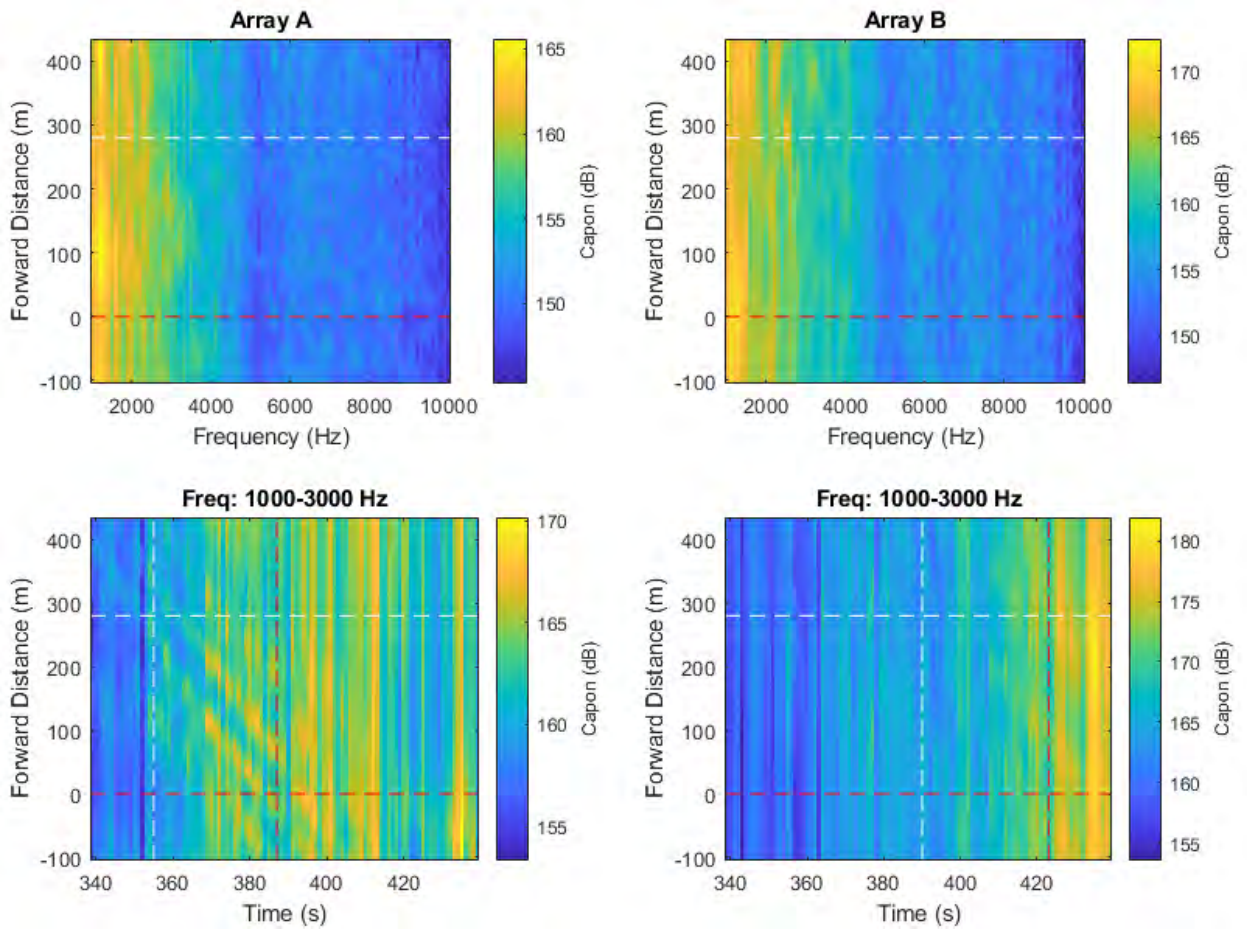

Figure 124 High-frequency noise maps obtained using the spatial spectra provided by the Capon algorithm implemented using individual arrays.

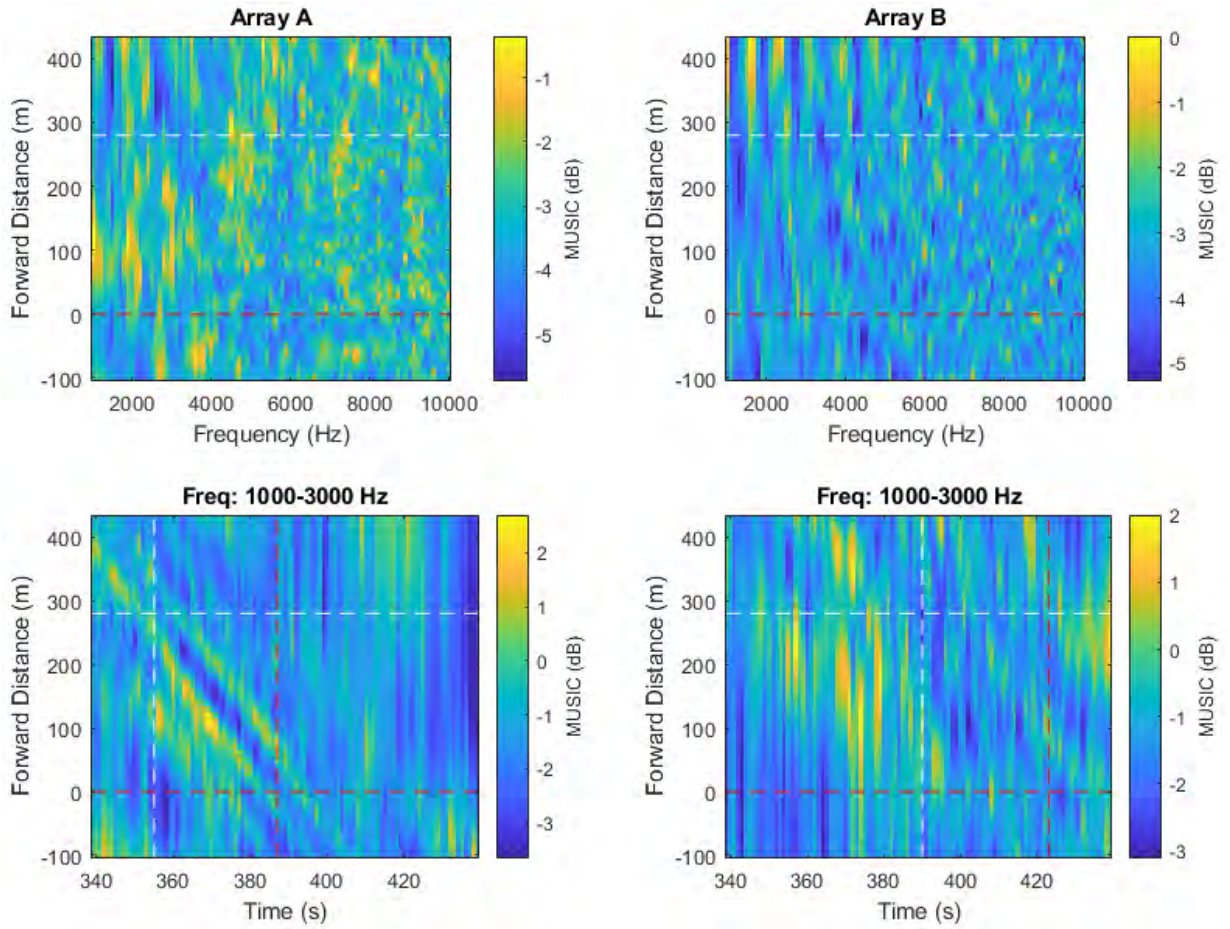

Figure 125 High-frequency noise maps obtained using the spatial spectra provided by the MUSIC algorithm implemented using individual arrays.

A.17. Pass #17 (Type: Bulker. Length: 229 m. Speed: 14.2 kn)

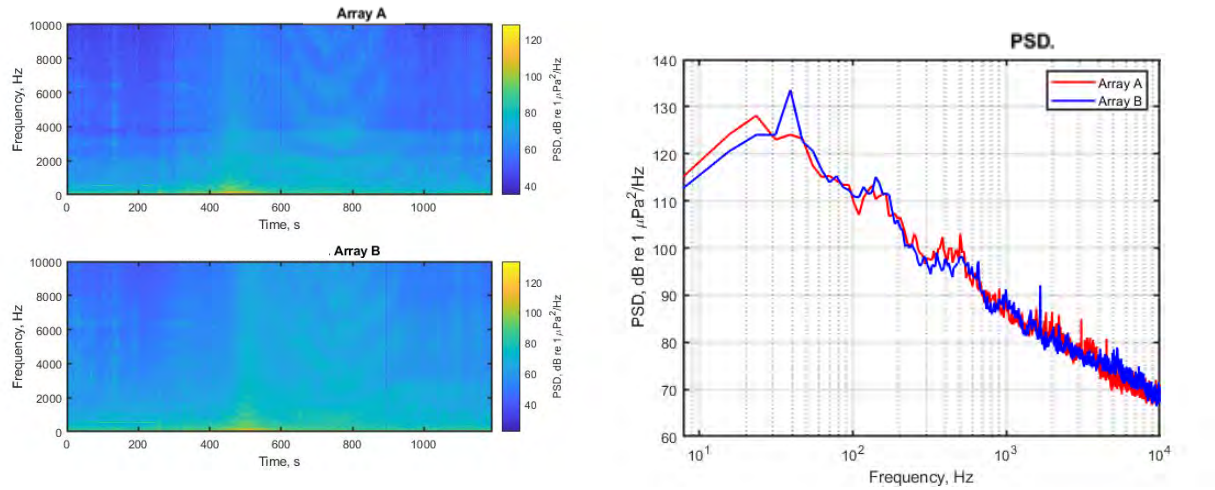

Figure 126 Spectrograms (left) and PSD (right) of ship noise observed on outputs of Arrays A and B.

A.17.1. Low- and mid-frequency noise maps

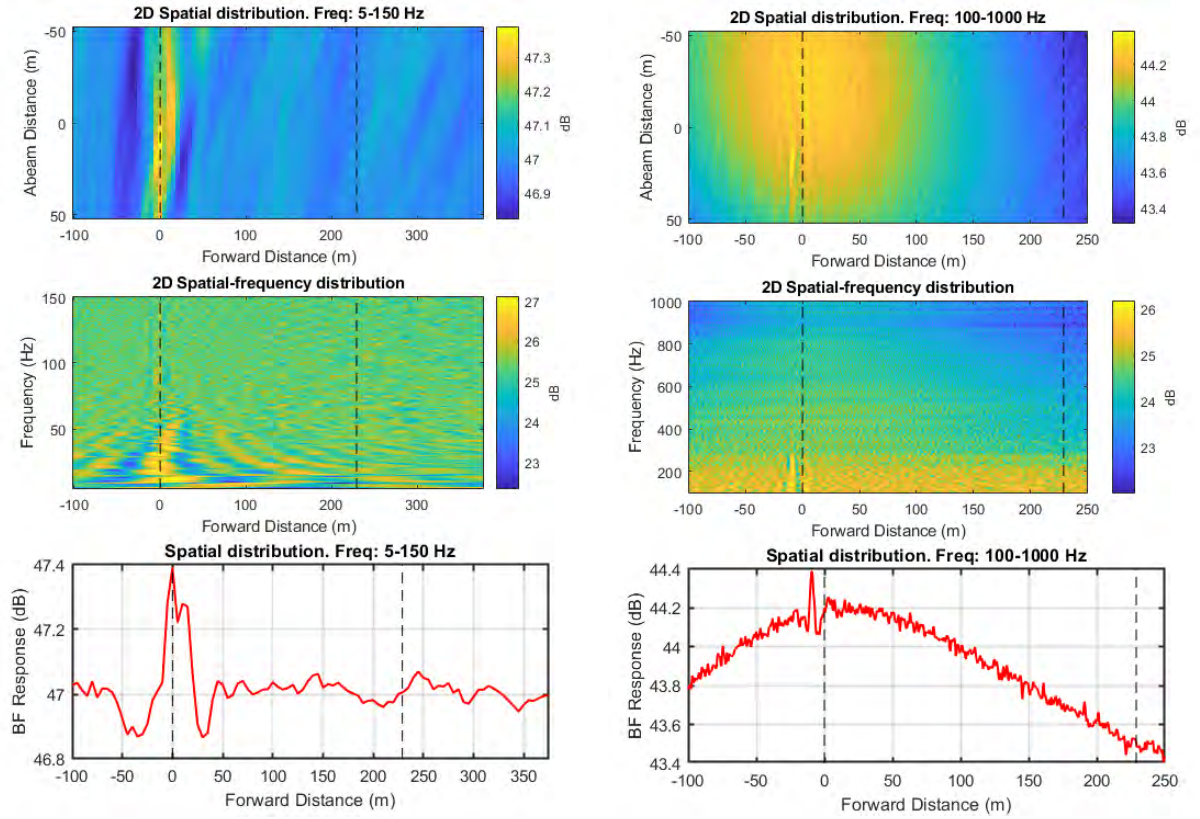

Figure 127 Noise maps from standard beamforming using combined array for Vessel Pass #17: 2D maps in spatial domain for two frequency ranges (top); 2D maps in vessel forward distance and frequency domain for two frequency ranges (middle); and graph of BF response versus forward distance for two frequency ranges bottom). Frequency ranges are 5 to150 Hz (left) and 100 to1000 Hz (right).

A.17.2. High-frequency noise maps

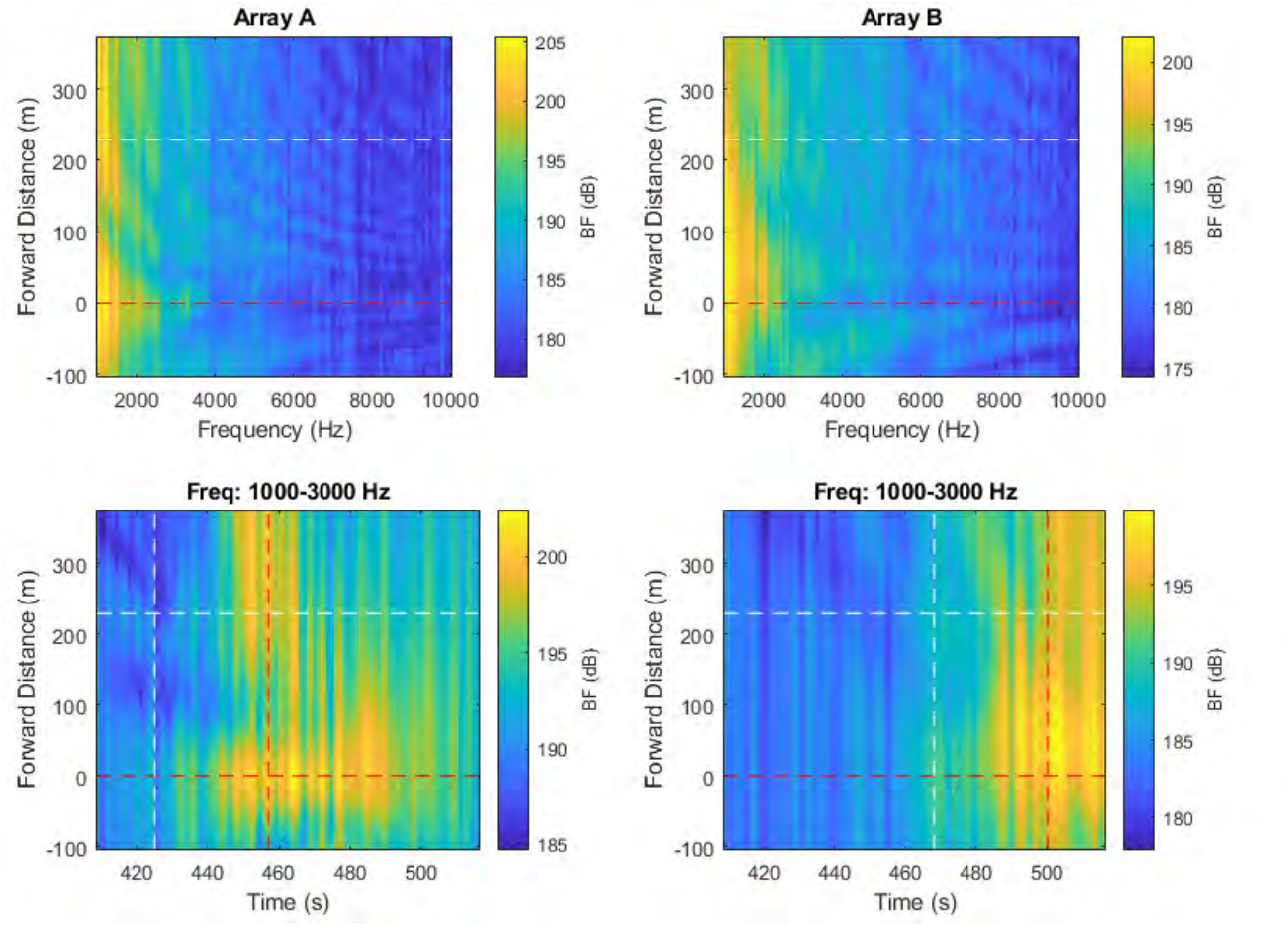

Figure 128 High-frequency noise maps from beamforming with individual arrays. Top maps show the BF response versus forward distance along vessel, measured approximately from the stern, versus frequency. Bottom maps show BF response versus forward distance and snapshot time. Horizontal dashed lines indicate the stern and bow positions of the vessel. Vertical dashed lines represent the CPA times of the bow and stern at each array.

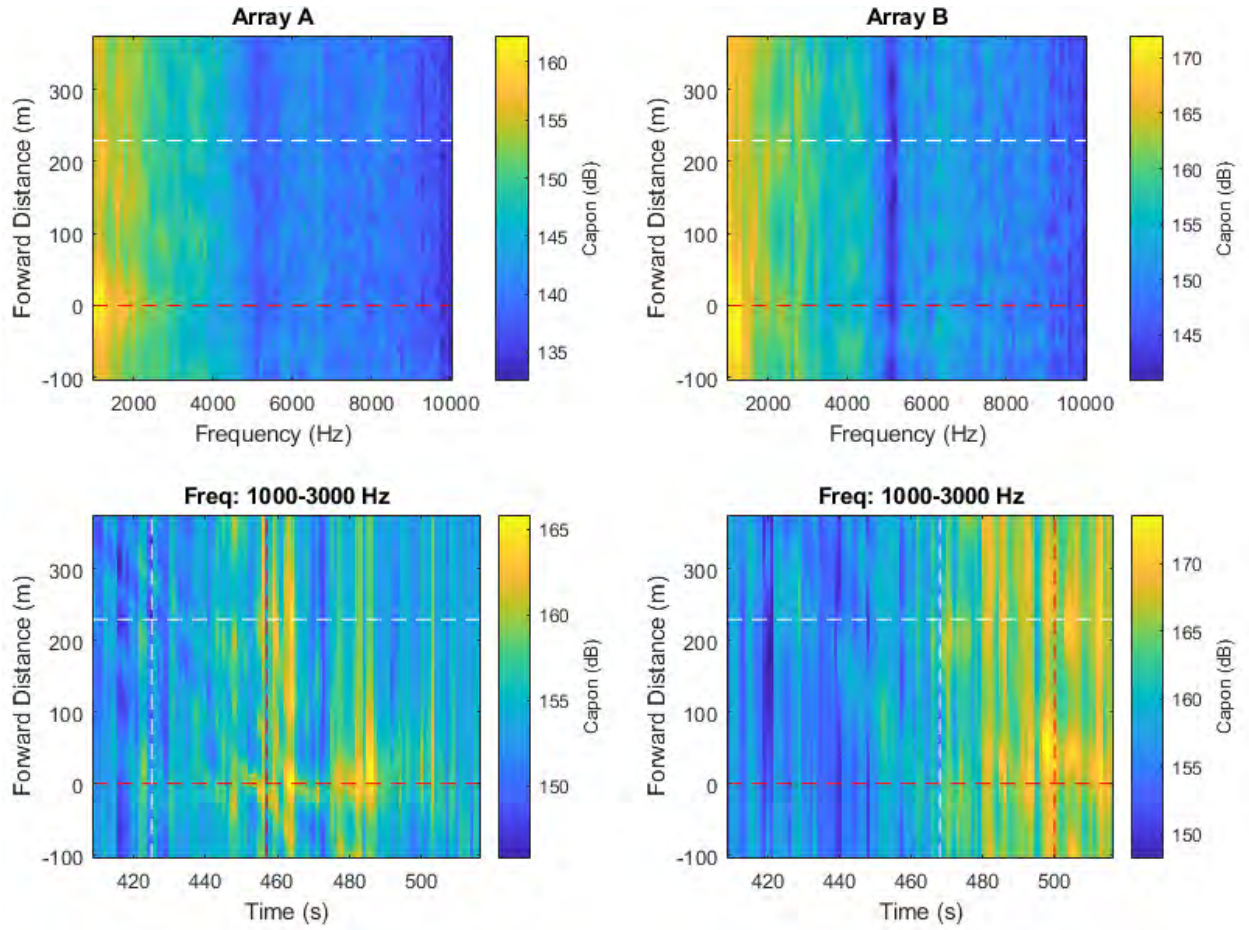

Figure 129 High-frequency noise maps obtained using the spatial spectra provided by the Capon algorithm implemented using individual arrays.

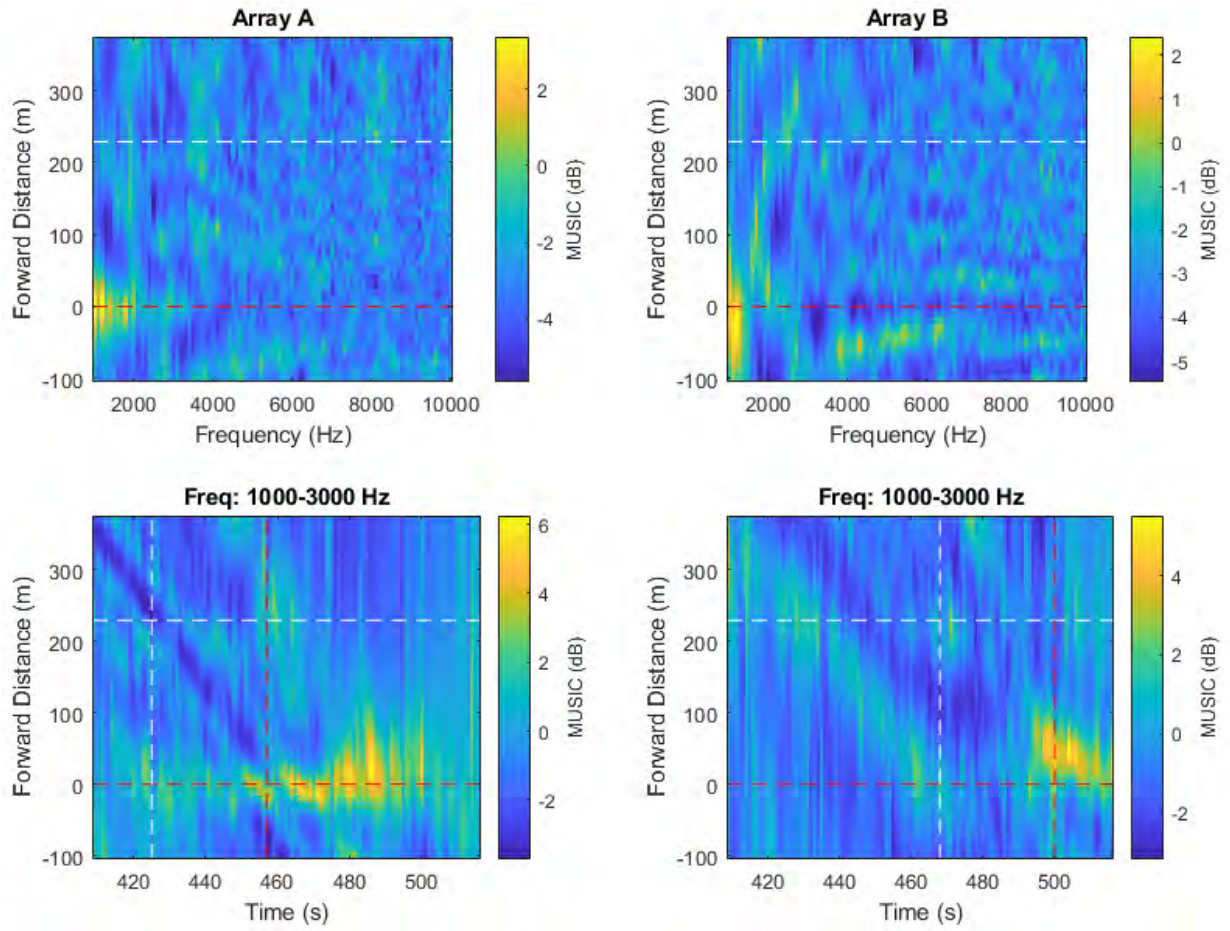

Figure 130 High-frequency noise maps obtained using the spatial spectra provided by the MUSIC algorithm implemented using individual arrays.

A.18. Pass #18 (Type: Container. Length: 210 m. Speed: 20.5 kn)

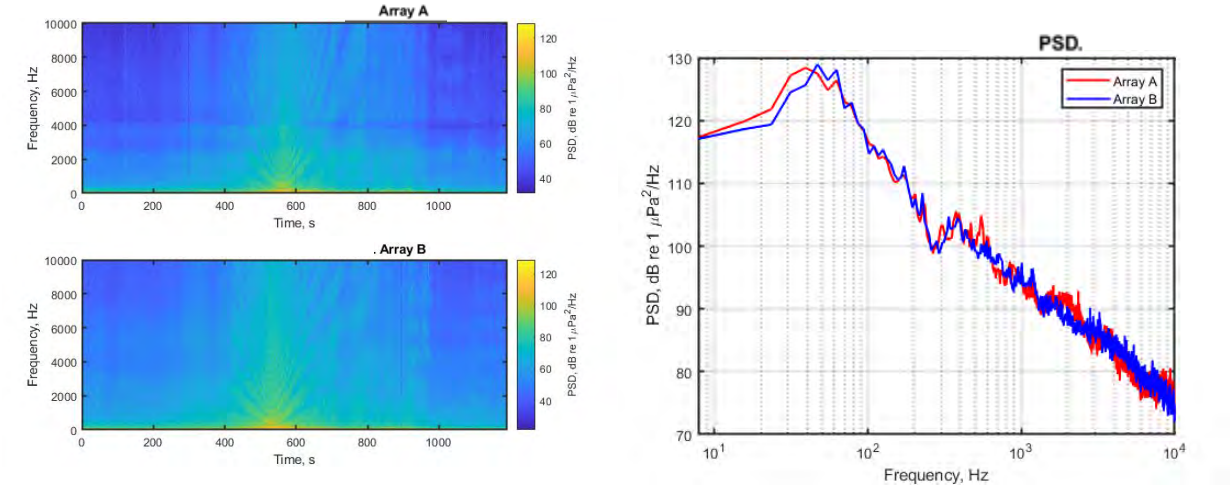

Figure 131 Spectrograms (left) and PSD (right) of ship noise observed on outputs of Arrays A and B.

A.18.1. Low- and mid-frequency noise maps

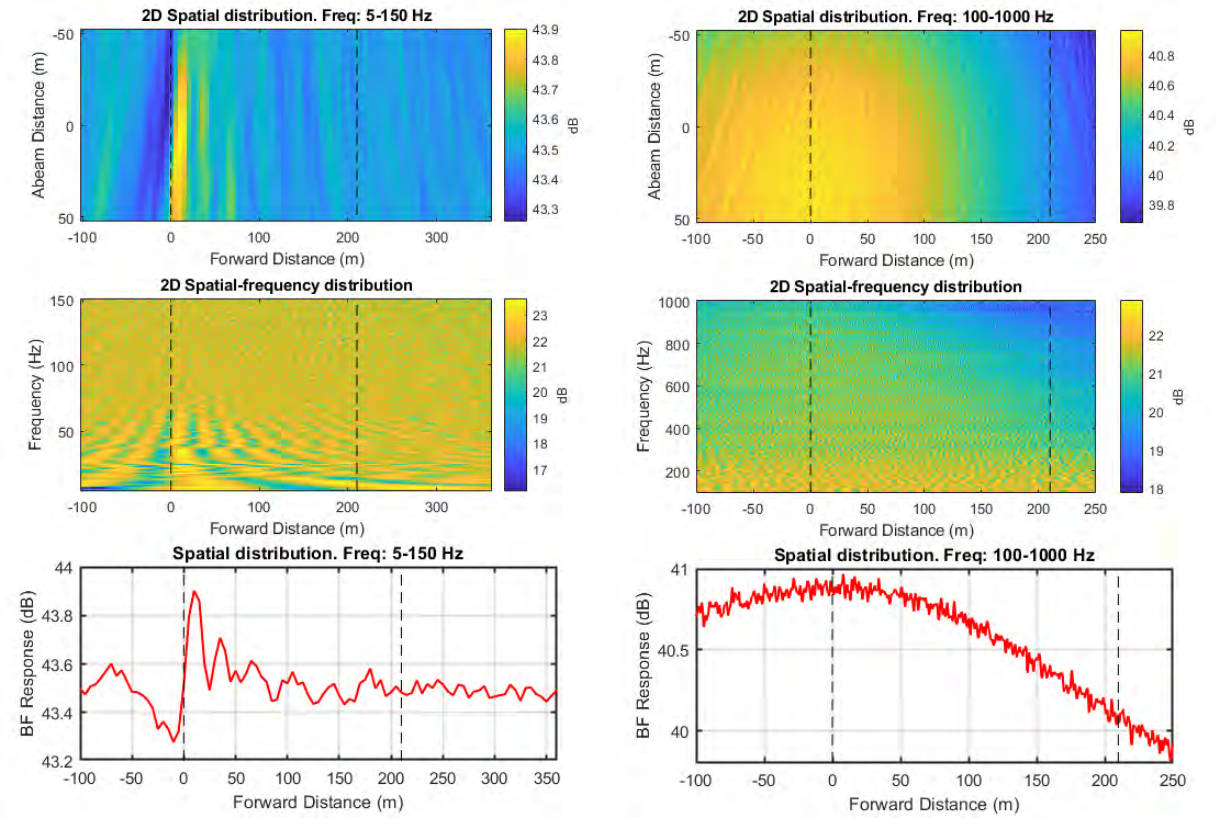

Figure 132 Noise maps from standard beamforming using combined array for Vessel Pass #18: 2D maps in spatial domain for two frequency ranges (top); 2D maps in vessel forward distance and frequency domain for two frequency ranges (middle); and graph of BF response versus forward distance for two frequency ranges bottom). Frequency ranges are 5 to150 Hz (left) and 100 to1000 Hz (right).

A.18.2. High-frequency noise maps

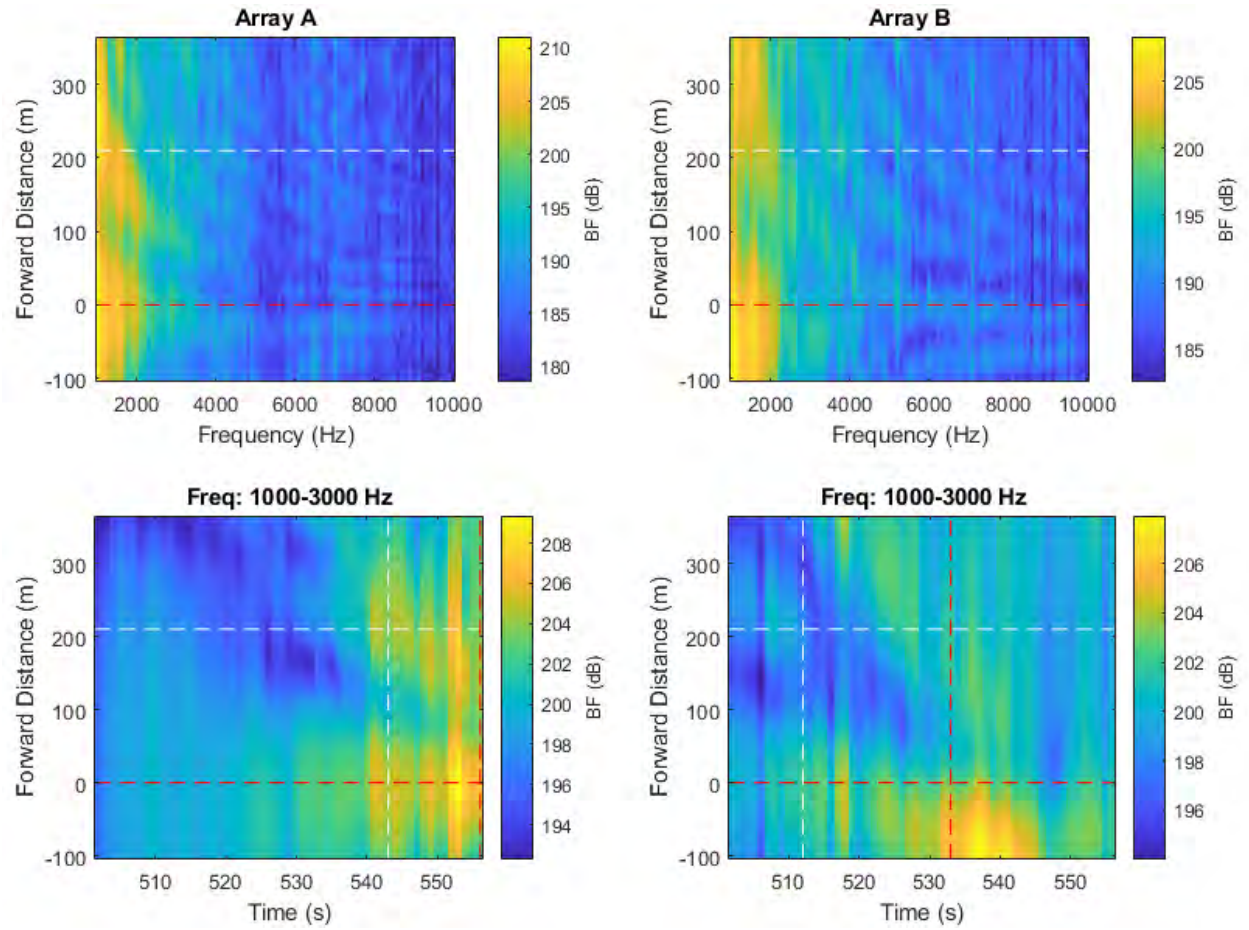

Figure 133 High-frequency noise maps from beamforming with individual arrays. Top maps show the BF response versus forward distance along vessel, measured approximately from the stern, versus frequency. Bottom maps show BF response versus forward distance and snapshot time. Horizontal dashed lines indicate the stern and bow positions of the vessel. Vertical dashed lines represent the CPA times of the bow and stern at each array.

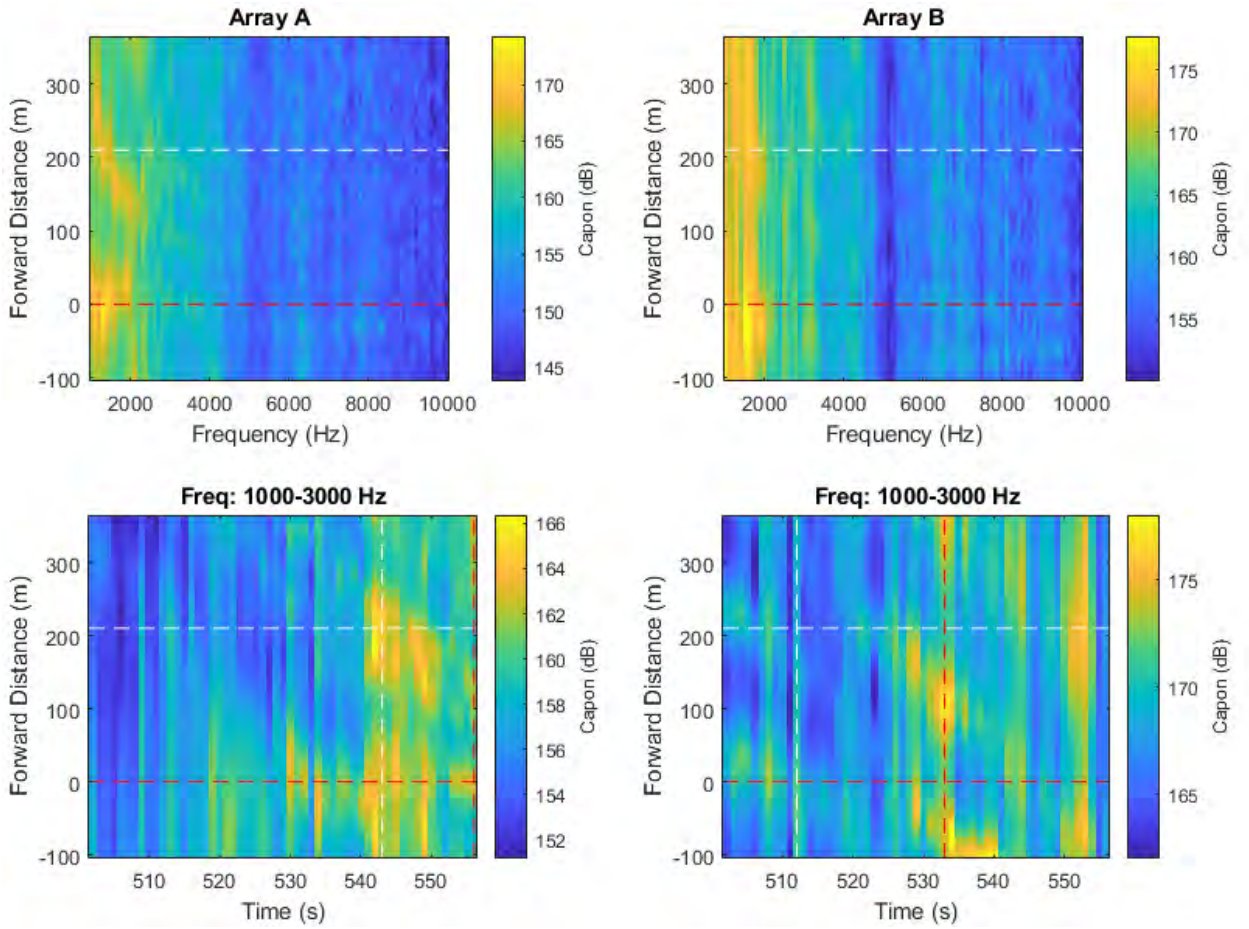

Figure 134 High-frequency noise maps obtained using the spatial spectra provided by the Capon algorithm implemented using individual arrays.

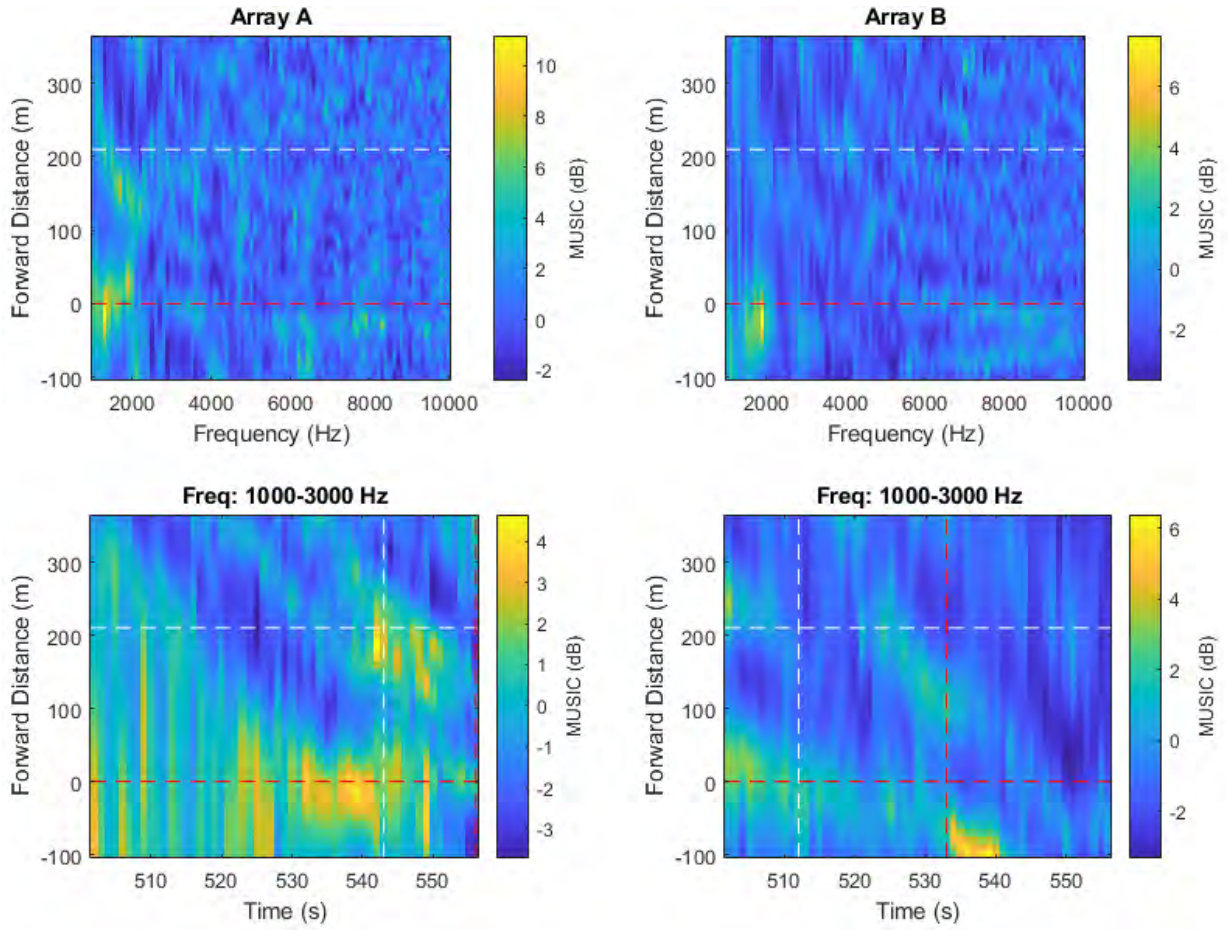

Figure 135 High-frequency noise maps obtained using the spatial spectra provided by the MUSIC algorithm implemented using individual arrays.

A.19. Pass #19 (Type: Container. Length: 264 m. Speed: 21.9 kn)

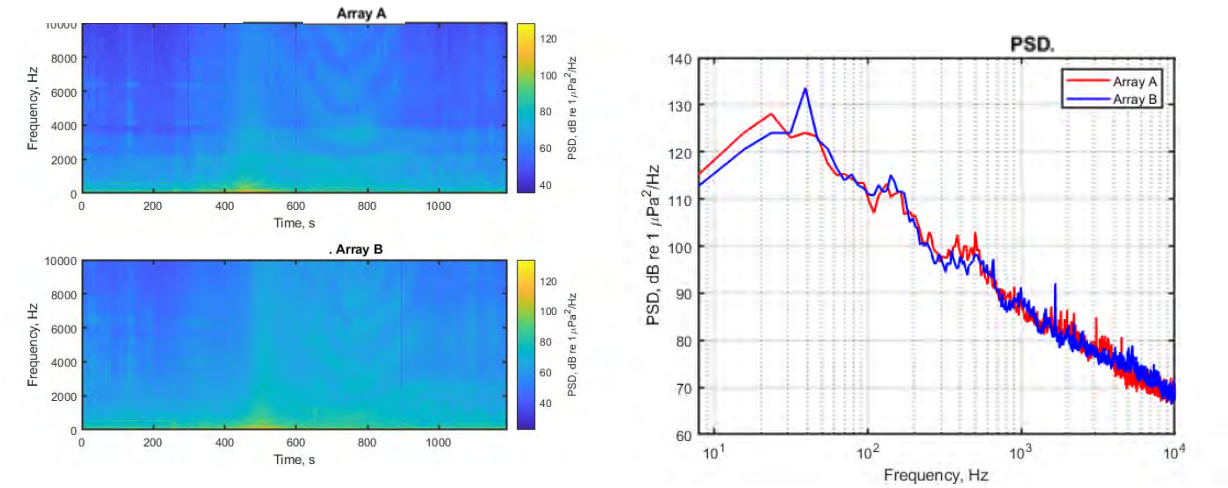

Figure 136 Spectrograms (left) and PSD (right) of ship noise observed on outputs of Arrays A and B.

A.19.1. Low- and mid-frequency noise maps

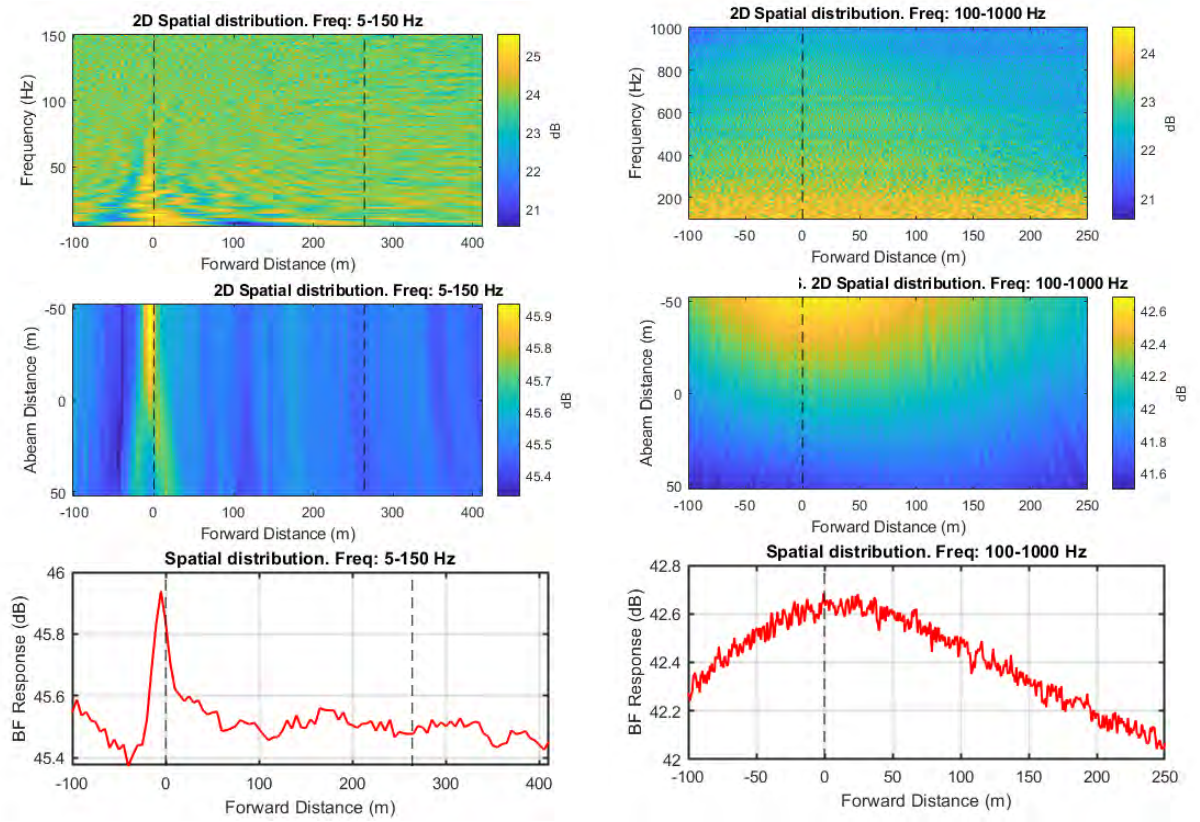

Figure 137 Noise maps from standard beamforming using combined array for Vessel Pass #19: 2D maps in spatial domain for two frequency ranges (top); 2D maps in vessel forward distance and frequency domain for two frequency ranges (middle); and graph of BF response versus forward distance for two frequency ranges bottom). Frequency ranges are 5 to150 Hz (left) and 100 to1000 Hz (right).

A.19.2. High-frequency noise maps

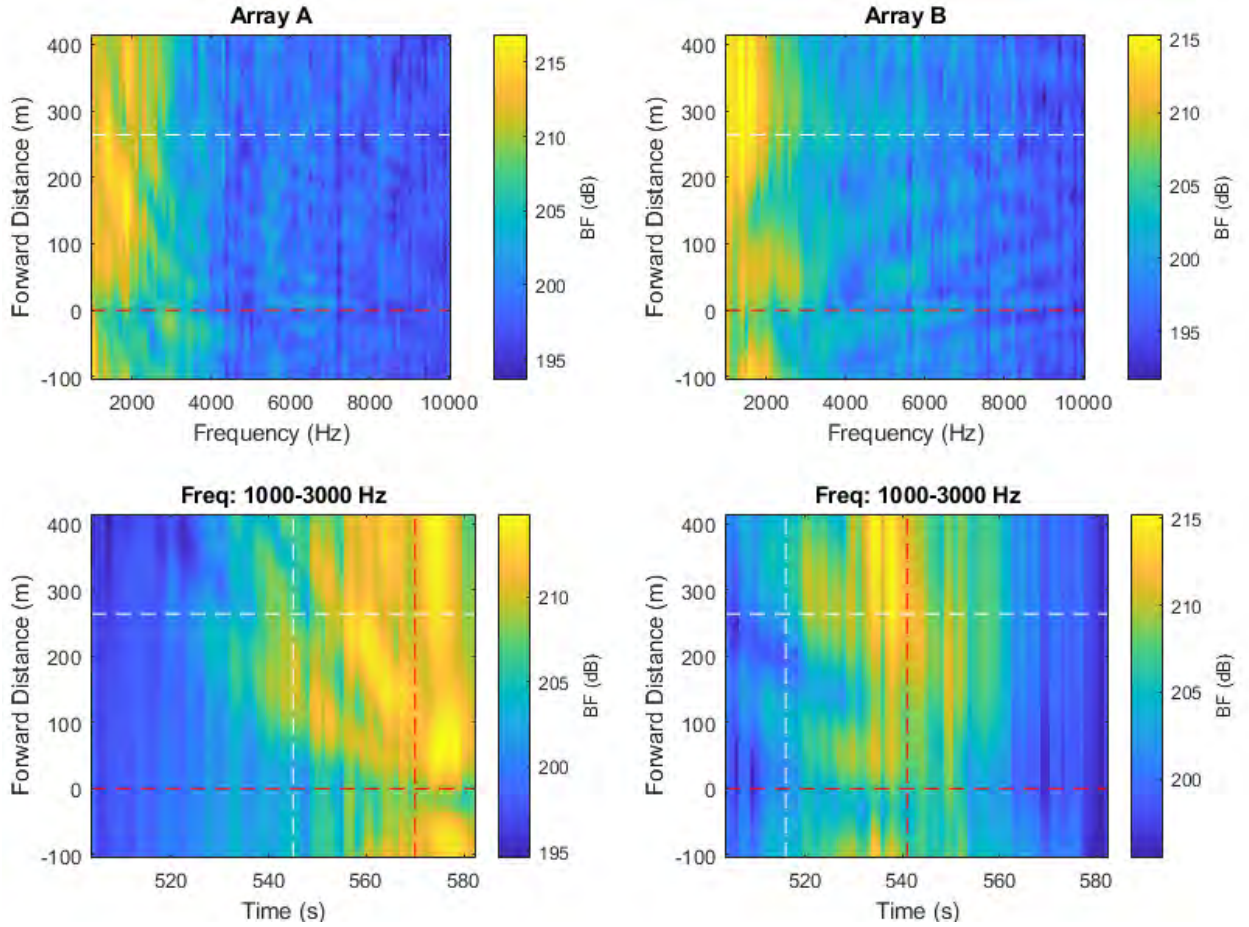

Figure 138 High-frequency noise maps from beamforming with individual arrays. Top maps show the BF response versus forward distance along vessel, measured approximately from the stern, versus frequency. Bottom maps show BF response versus forward distance and snapshot time. Horizontal dashed lines indicate the stern and bow positions of the vessel. Vertical dashed lines represent the CPA times of the bow and stern at each array.

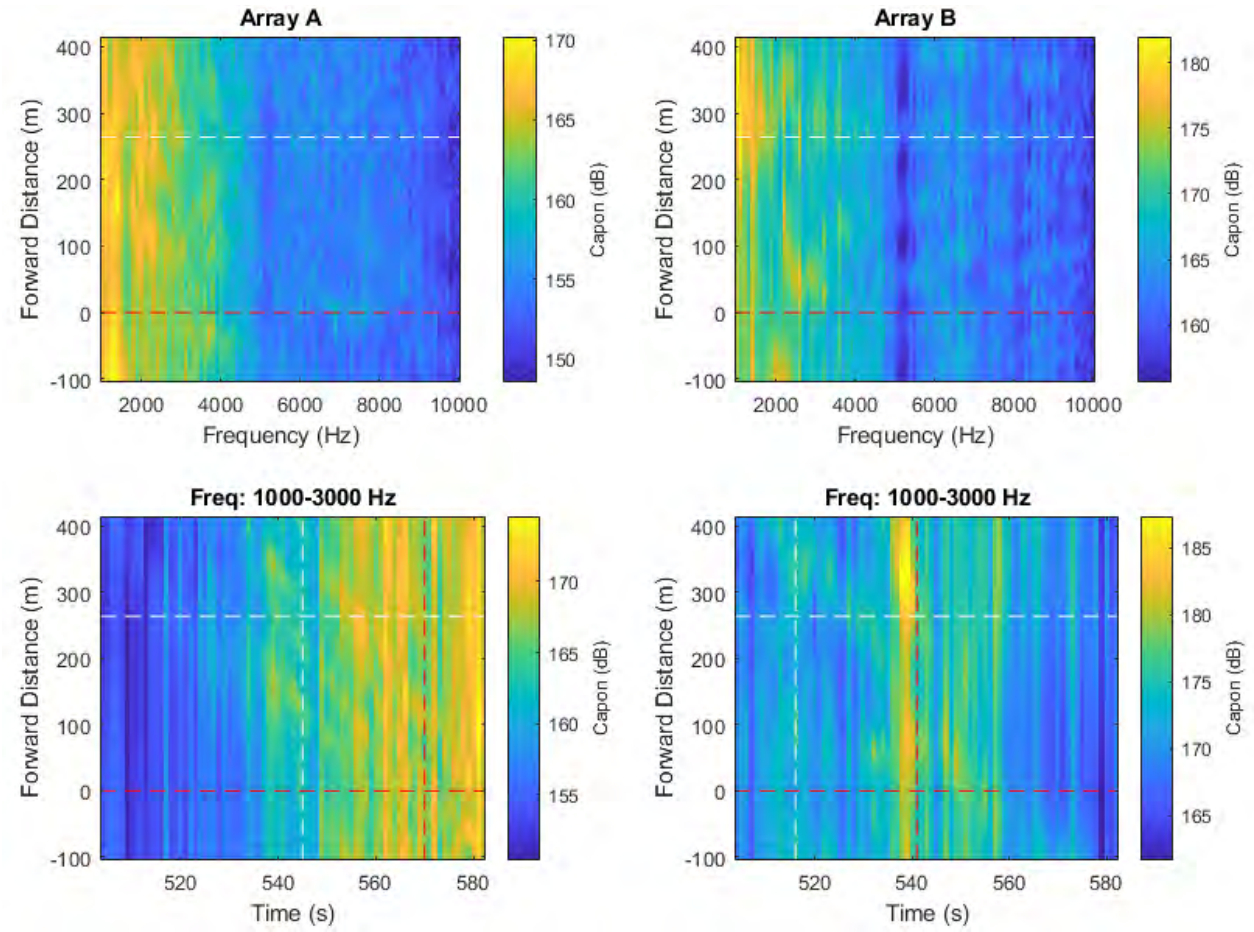

Figure 139 High-frequency noise maps obtained using the spatial spectra provided by the Capon algorithm implemented using individual arrays.

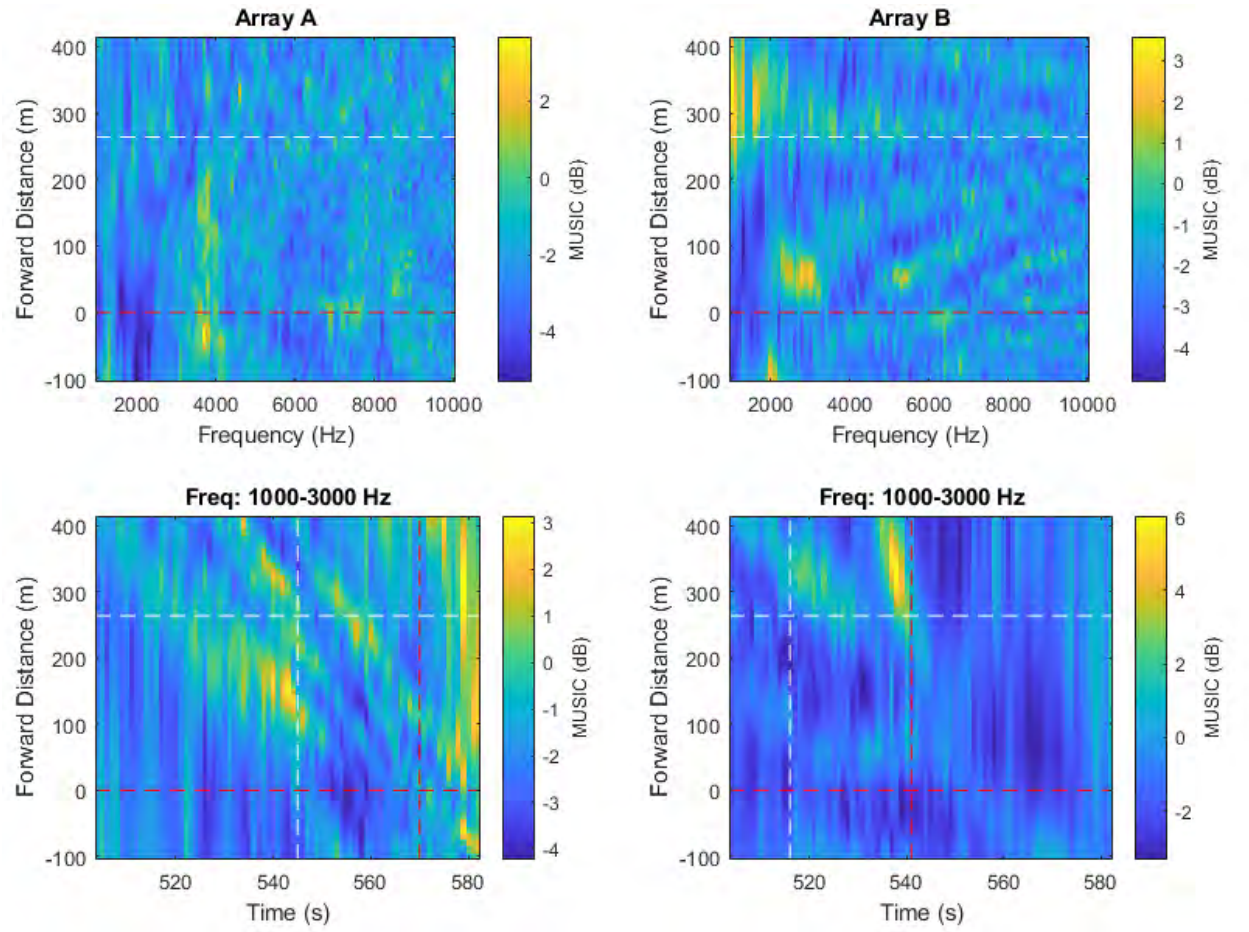

Figure 140 High-frequency noise maps obtained using the spatial spectra provided by the MUSIC algorithm implemented using individual arrays.

A.20. Pass #20 (Type: Bulker. Length: 200 m. Speed: 11.7 kn)

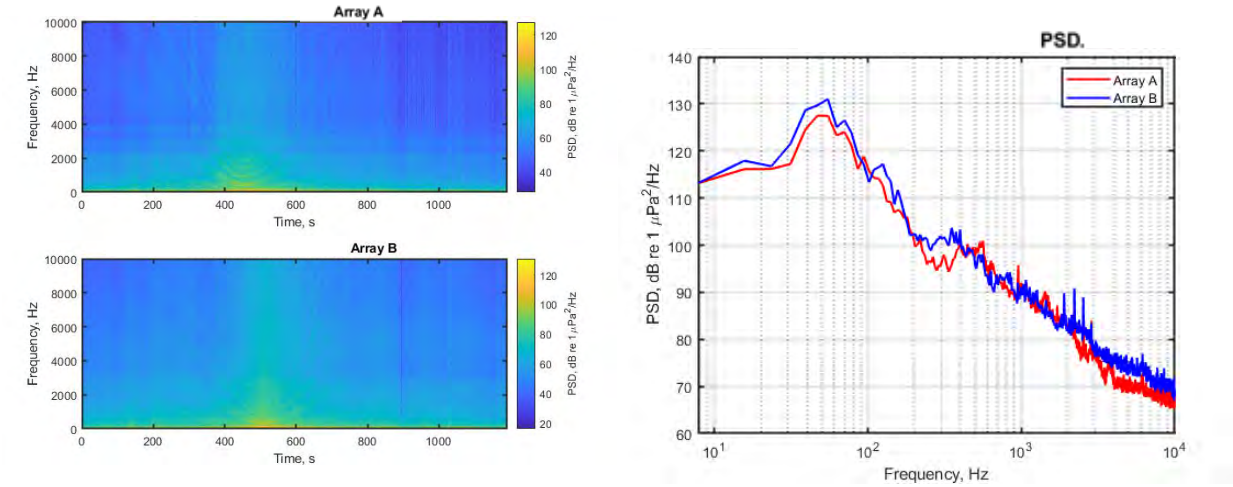

Figure 141 Spectrograms (left) and PSD (right) of ship noise observed on outputs of Arrays A and B.

A.20.1. Low- and mid-frequency noise maps

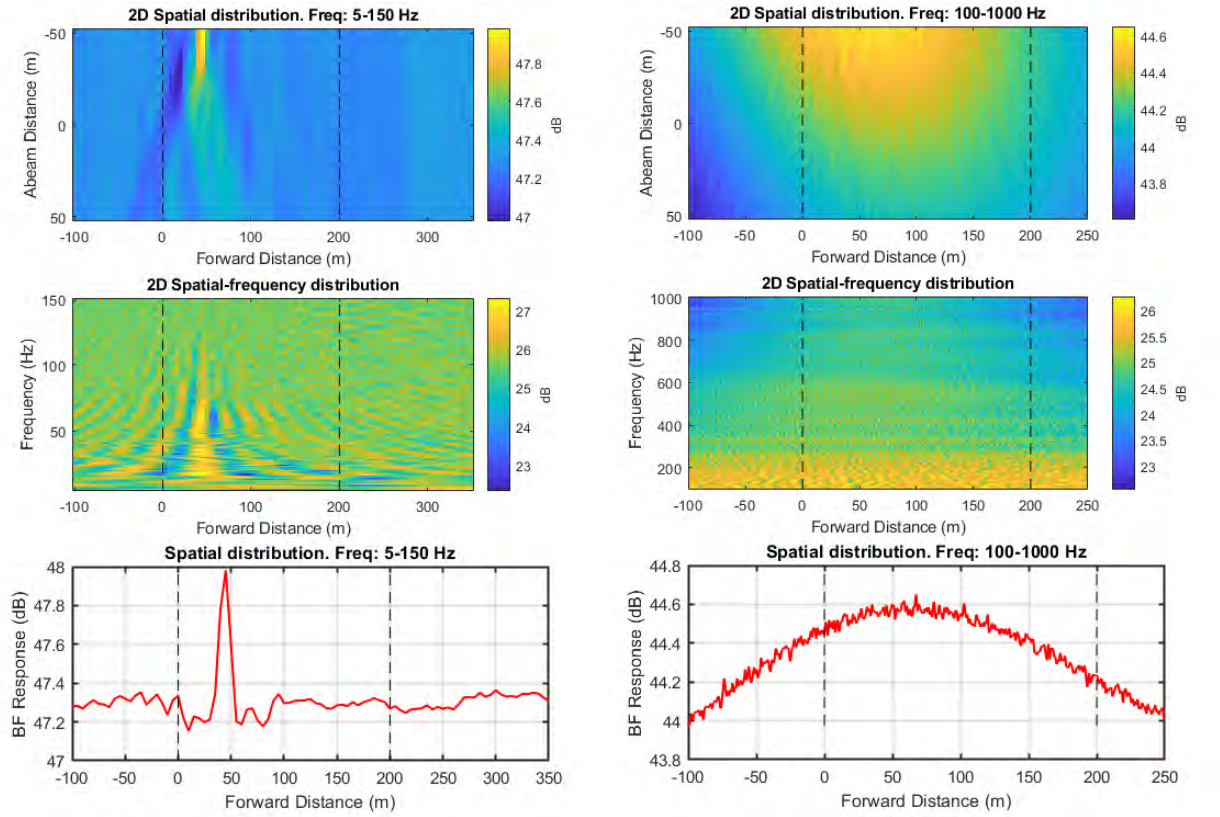

Figure 142 Noise maps from standard beamforming using combined array for Vessel Pass #20: 2D maps in spatial domain for two frequency ranges (top); 2D maps in vessel forward distance and frequency domain for two frequency ranges (middle); and graph of BF response versus forward distance for two frequency ranges bottom). Frequency ranges are 5 to150 Hz (left) and 100 to1000 Hz (right).

A.20.2. High-frequency noise maps

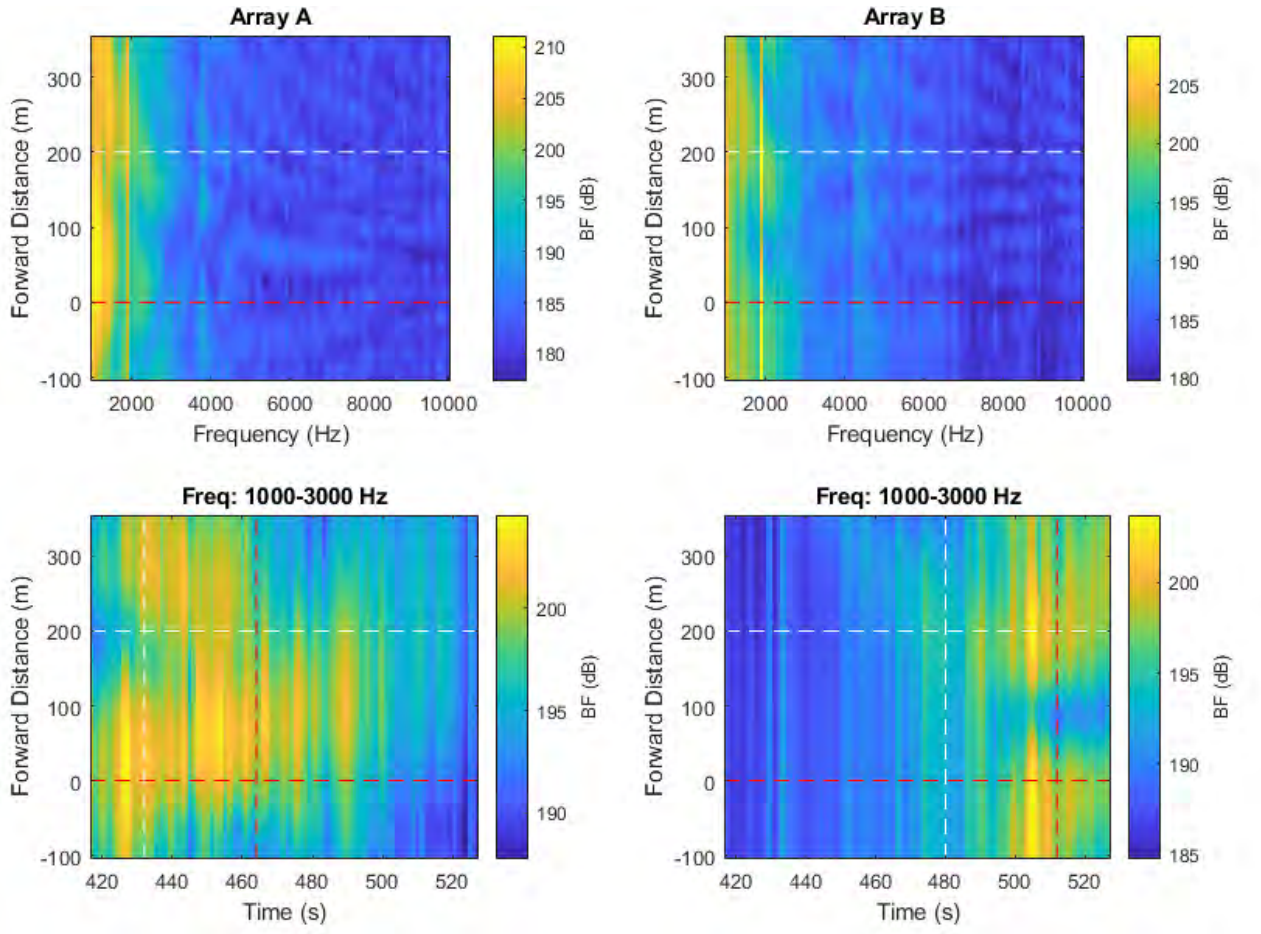

Figure 143 High-frequency noise maps from beamforming with individual arrays. Top maps show the BF response versus forward distance along vessel, measured approximately from the stern, versus frequency. Bottom maps show BF response versus forward distance and snapshot time. Horizontal dashed lines indicate the stern and bow positions of the vessel. Vertical dashed lines represent the CPA times of the bow and stern at each array.

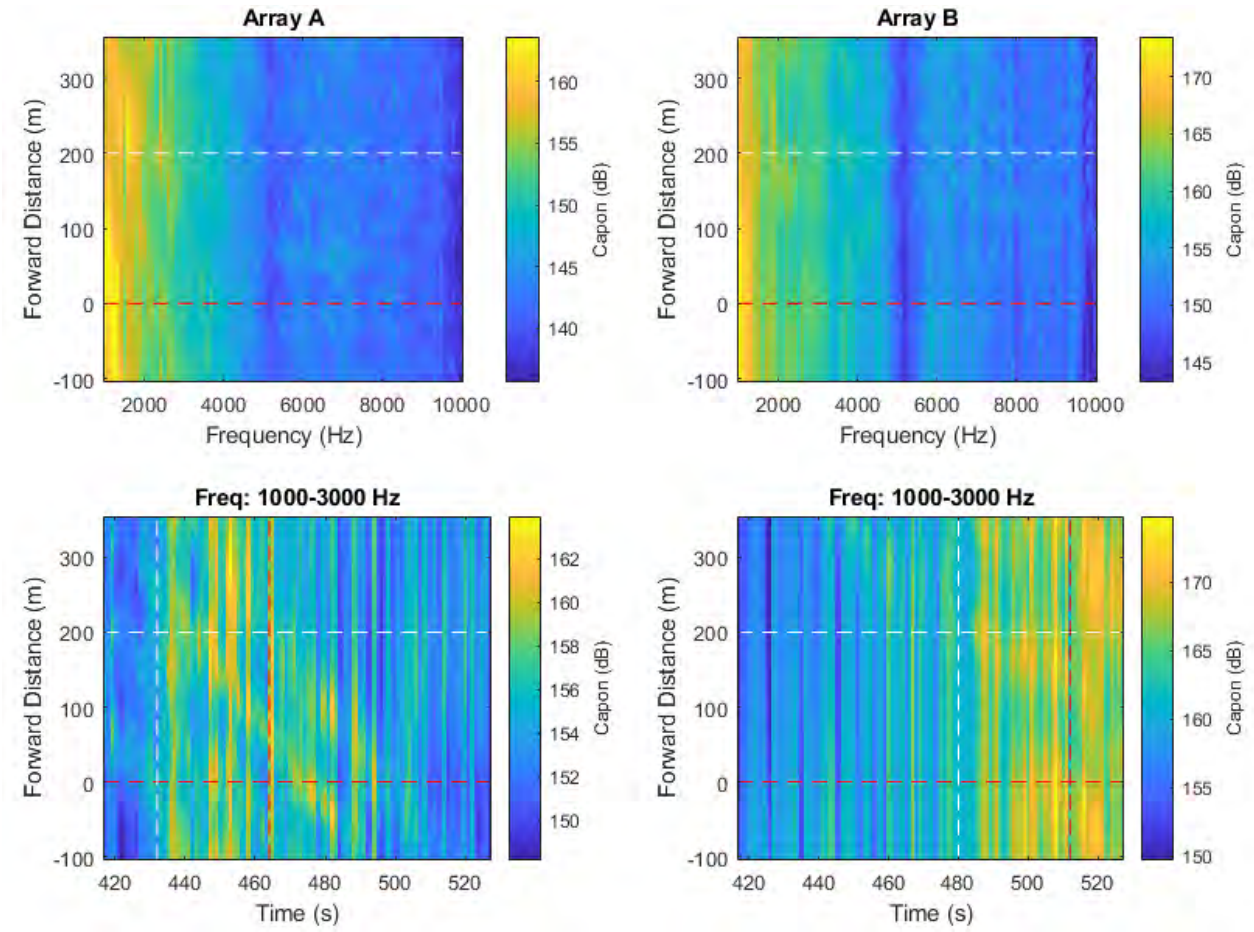

Figure 144 High-frequency noise maps obtained using the spatial spectra provided by the Capon algorithm implemented using individual arrays.

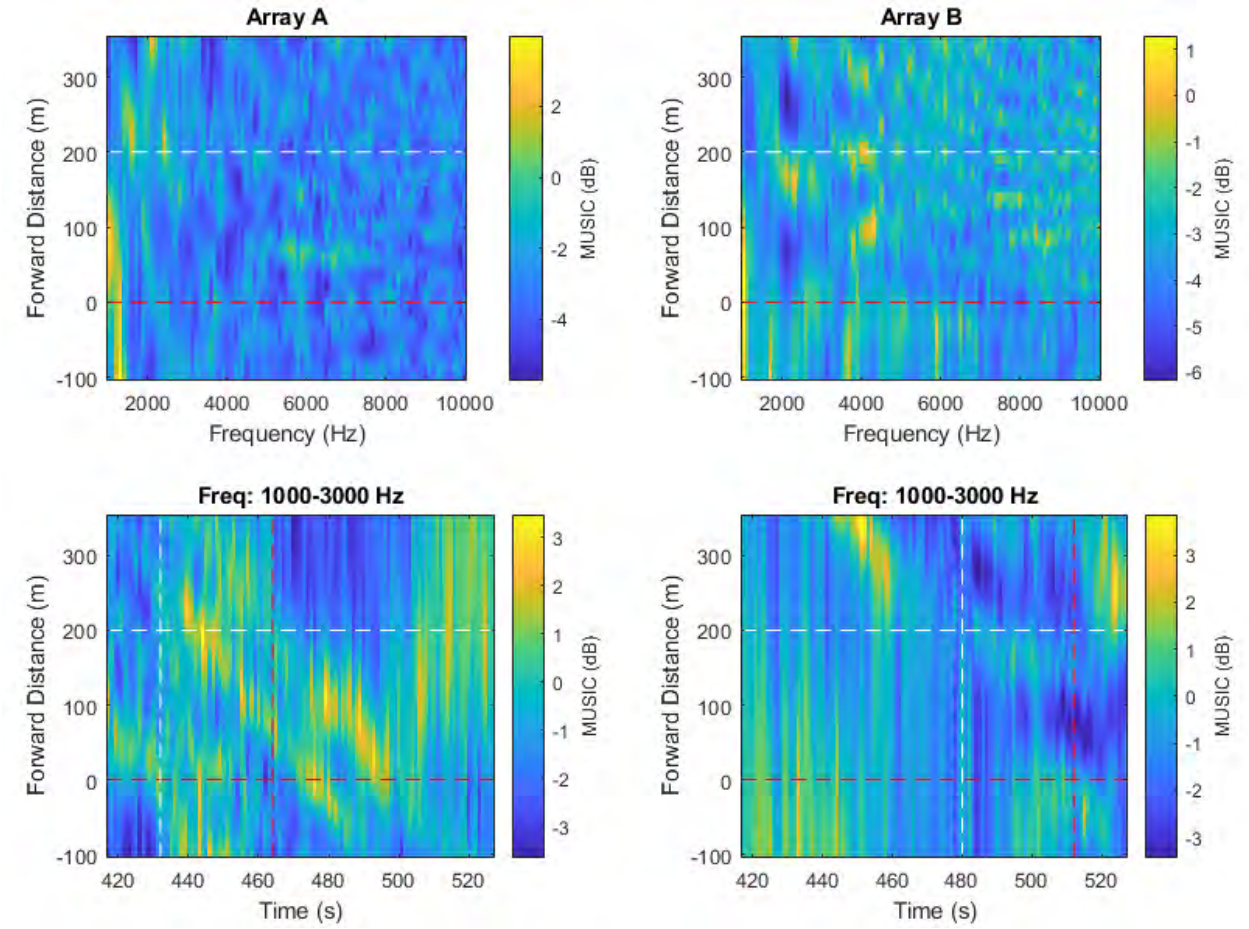

Figure 145 High-frequency noise maps obtained using the spatial spectra provided by the MUSIC algorithm implemented using individual arrays.

A.21. Pass #21 (Type: Bulker. Length: 228 m. Speed: 10.9 kn)

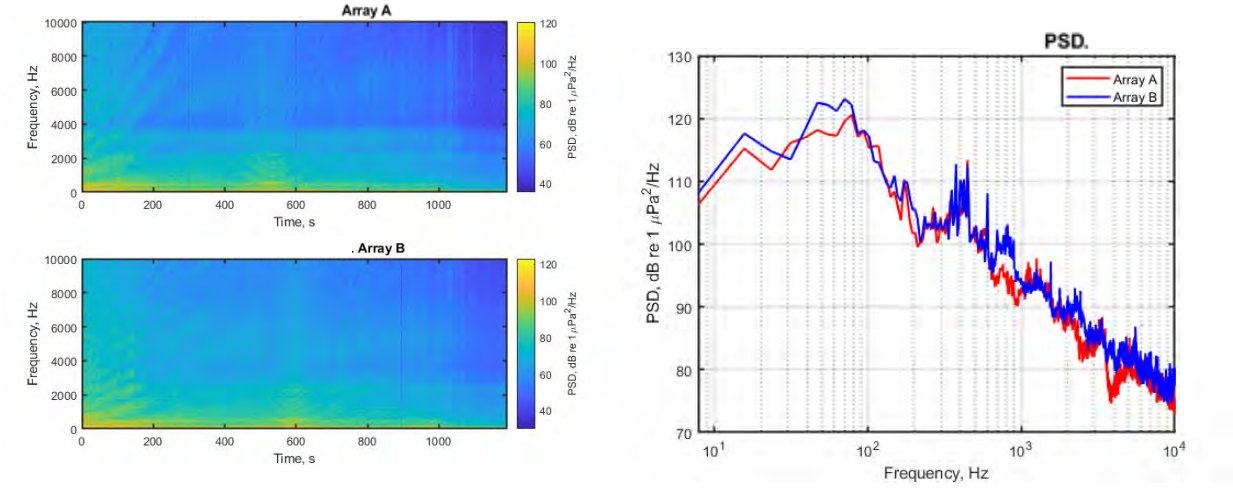

Figure 146 Spectrograms (left) and PSD (right) of ship noise observed on outputs of Arrays A and B.

A.21.1. Low- and mid-frequency noise maps

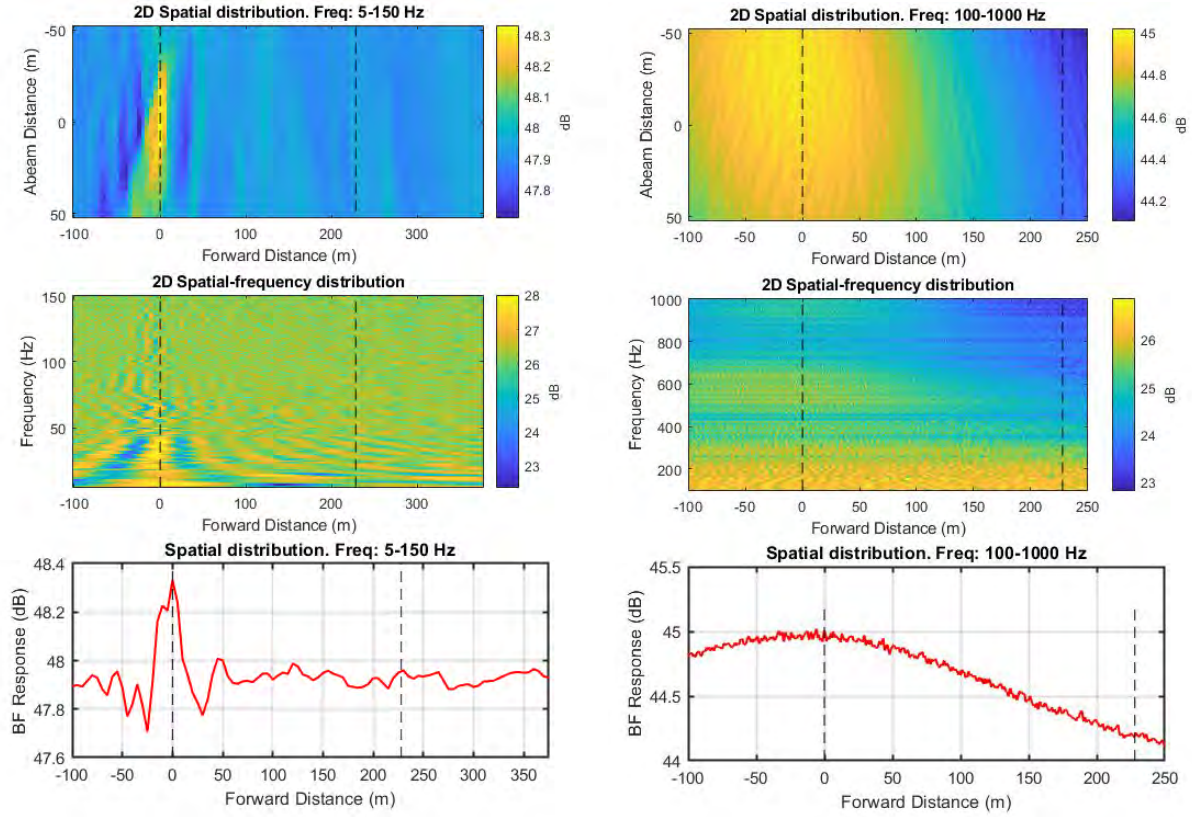

Figure 147 Noise maps from standard beamforming using combined array for Vessel Pass #21: 2D maps in spatial domain for two frequency ranges (top); 2D maps in vessel forward distance and frequency domain for two frequency ranges (middle); and graph of BF response versus forward distance for two frequency ranges bottom). Frequency ranges are 5 to150 Hz (left) and 100 to1000 Hz (right).

A.21.2. High-frequency noise maps

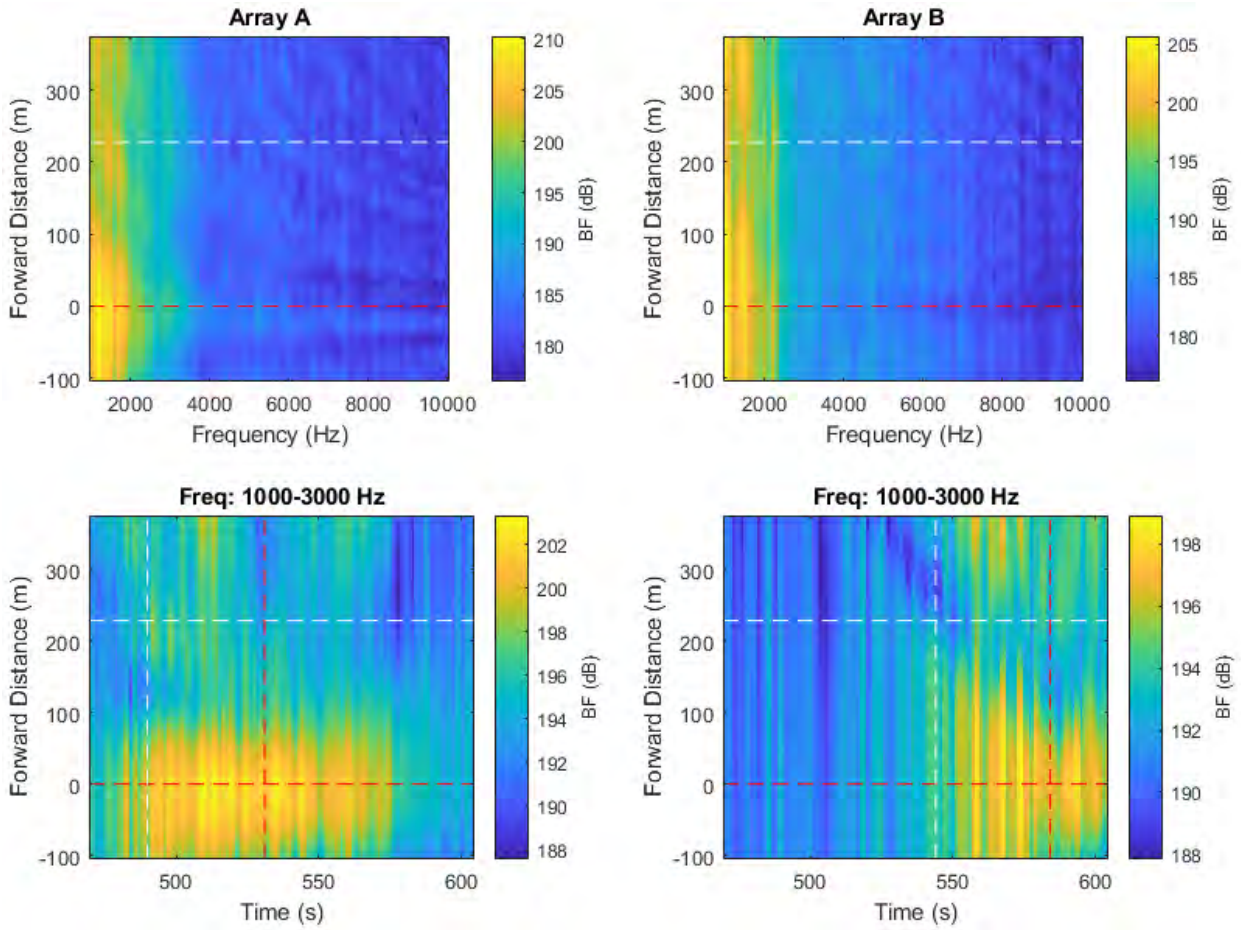

Figure 148 High-frequency noise maps from beamforming with individual arrays. Top maps show the BF response versus forward distance along vessel, measured approximately from the stern, versus frequency. Bottom maps show BF response versus forward distance and snapshot time. Horizontal dashed lines indicate the stern and bow positions of the vessel. Vertical dashed lines represent the CPA times of the bow and stern at each array.

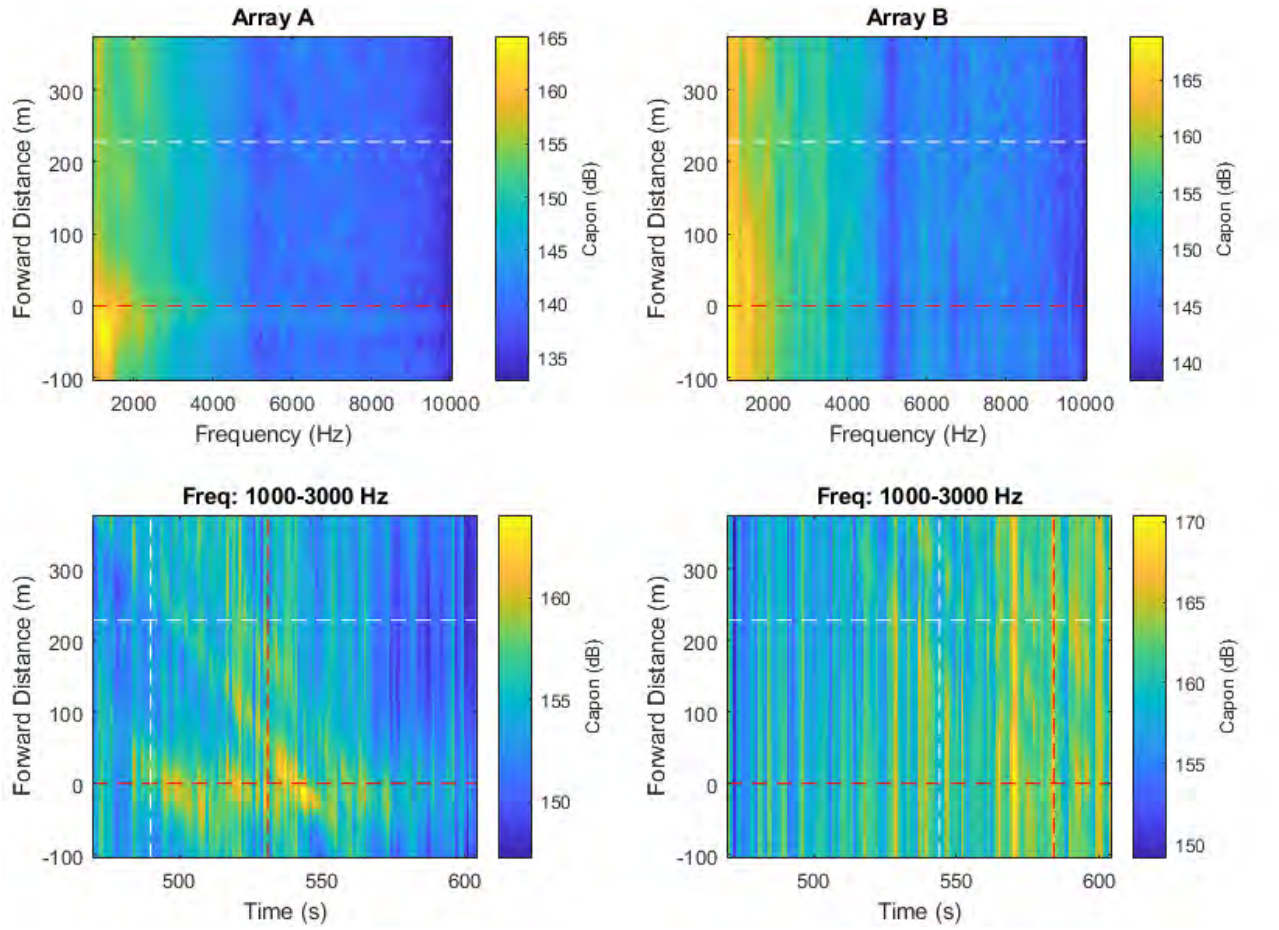

Figure 149 High-frequency noise maps obtained using the spatial spectra provided by the Capon algorithm implemented using individual arrays.

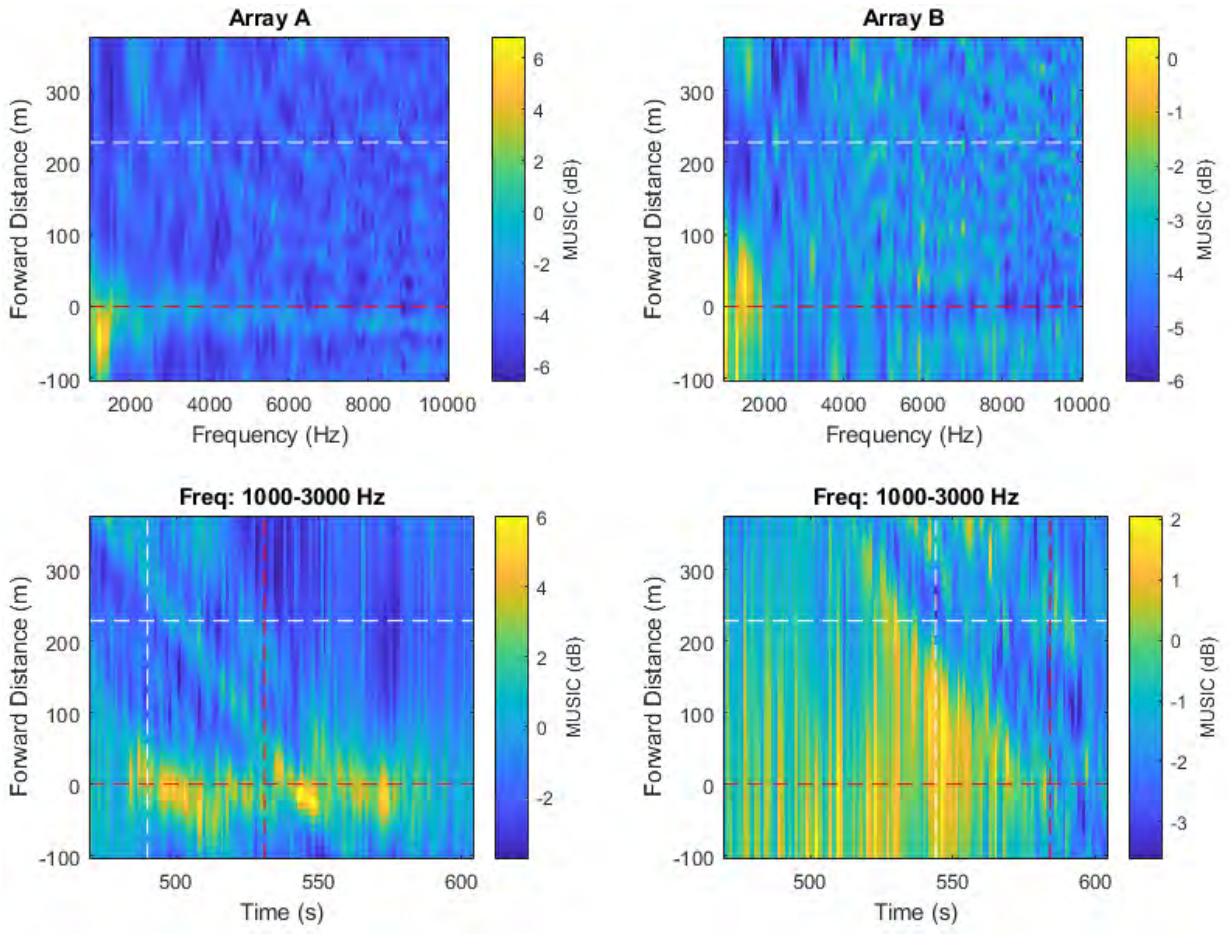

Figure 150 High-frequency noise maps obtained using the spatial spectra provided by the MUSIC algorithm implemented using individual arrays.

A.22. Pass #22 (Type: Bulker. Length: 260 m. Speed: 14.6 kn)

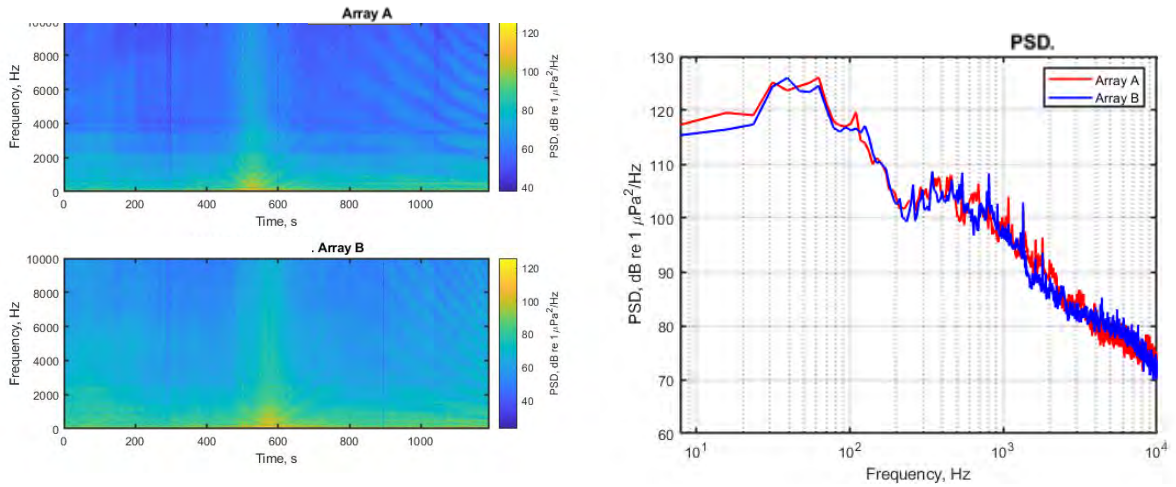

Figure 151 Spectrograms (left) and PSD (right) of ship noise observed on outputs of Arrays A and B.

A.22.1. Low- and mid-frequency noise maps

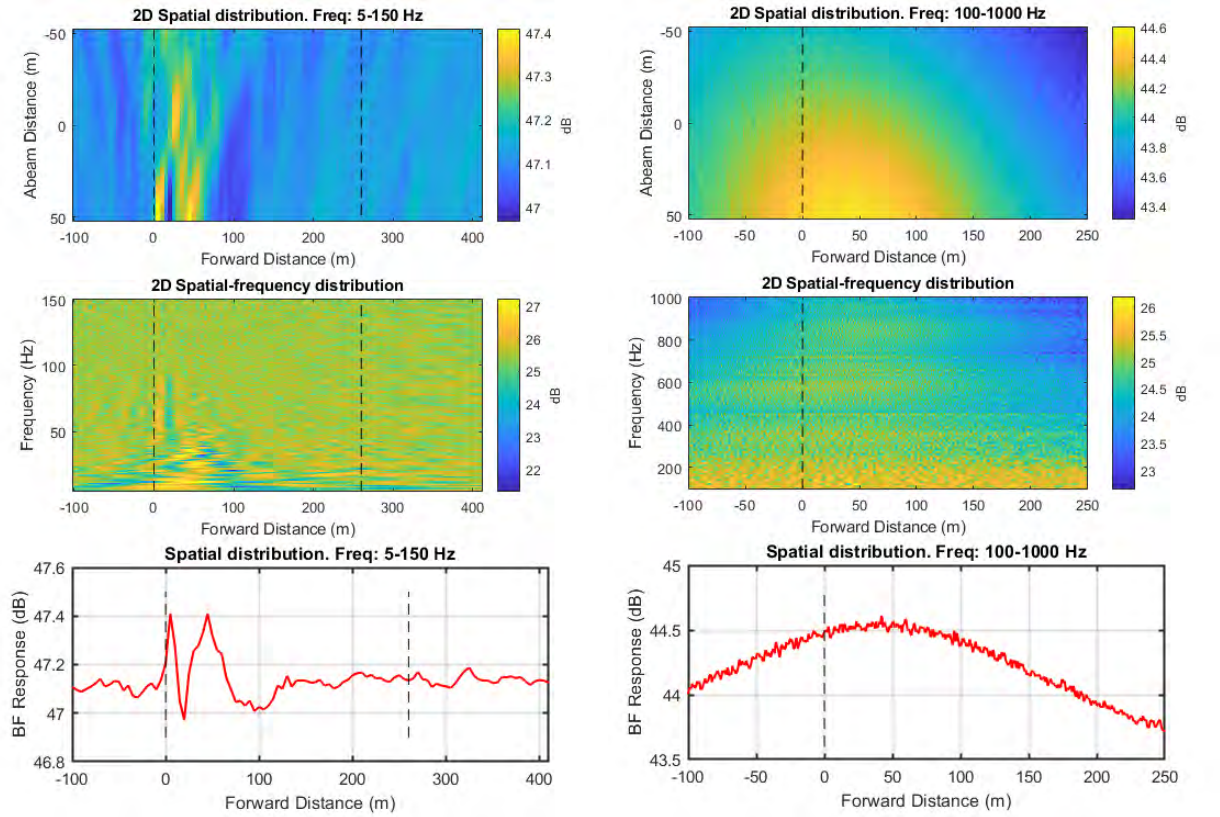

Figure 152 Noise maps from standard beamforming using combined array for Vessel Pass #22: 2D maps in spatial domain for two frequency ranges (top); 2D maps in vessel forward distance and frequency domain for two frequency ranges (middle); and graph of BF response versus forward distance for two frequency ranges bottom). Frequency ranges are 5 to150 Hz (left) and 100 to1000 Hz (right).

A.22.2. High-frequency noise maps

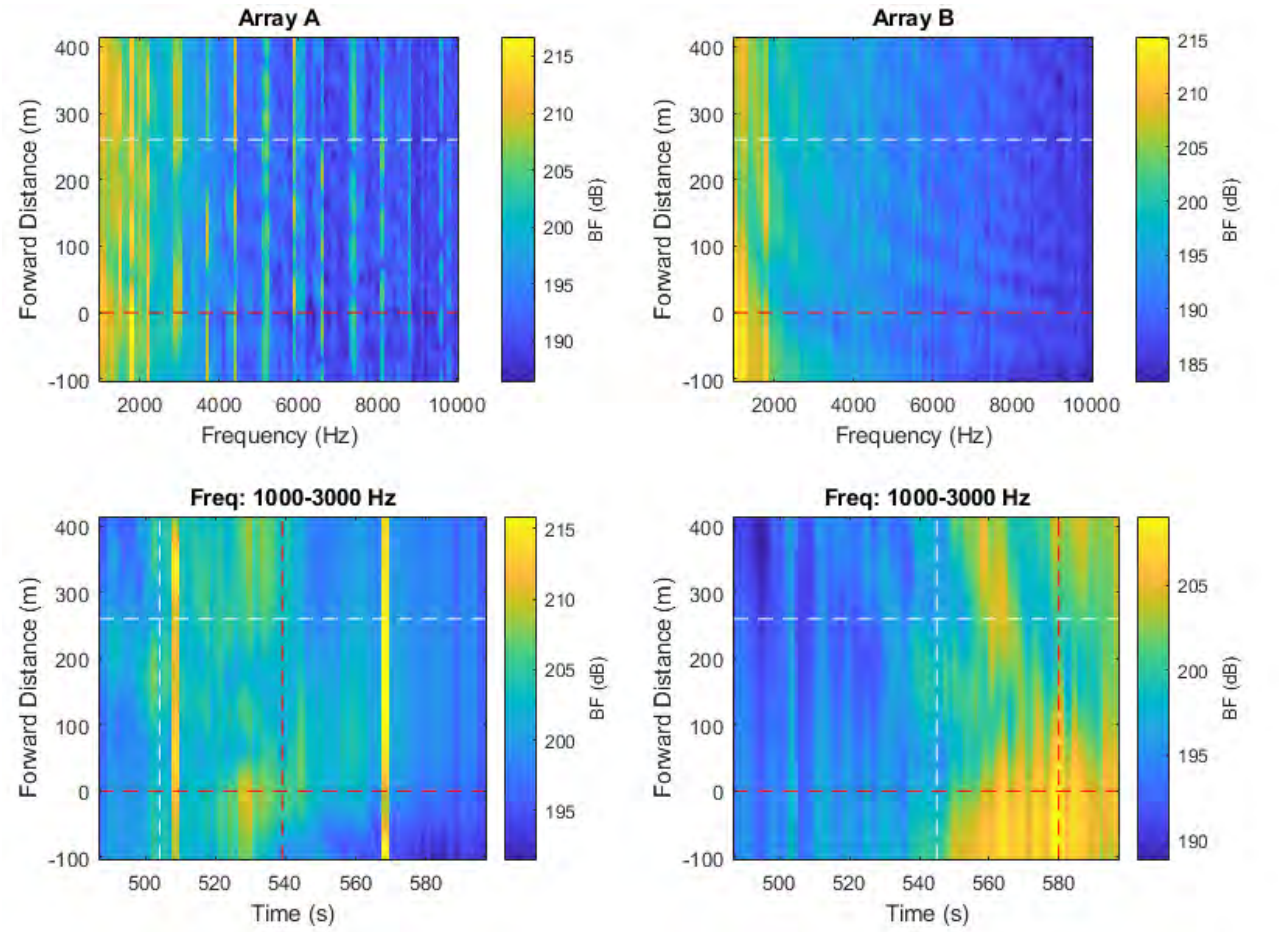

Figure 153 High-frequency noise maps from beamforming with individual arrays. Top maps show the BF response versus forward distance along vessel, measured approximately from the stern, versus frequency. Bottom maps show BF response versus forward distance and snapshot time. Horizontal dashed lines indicate the stern and bow positions of the vessel. Vertical dashed lines represent the CPA times of the bow and stern at each array.

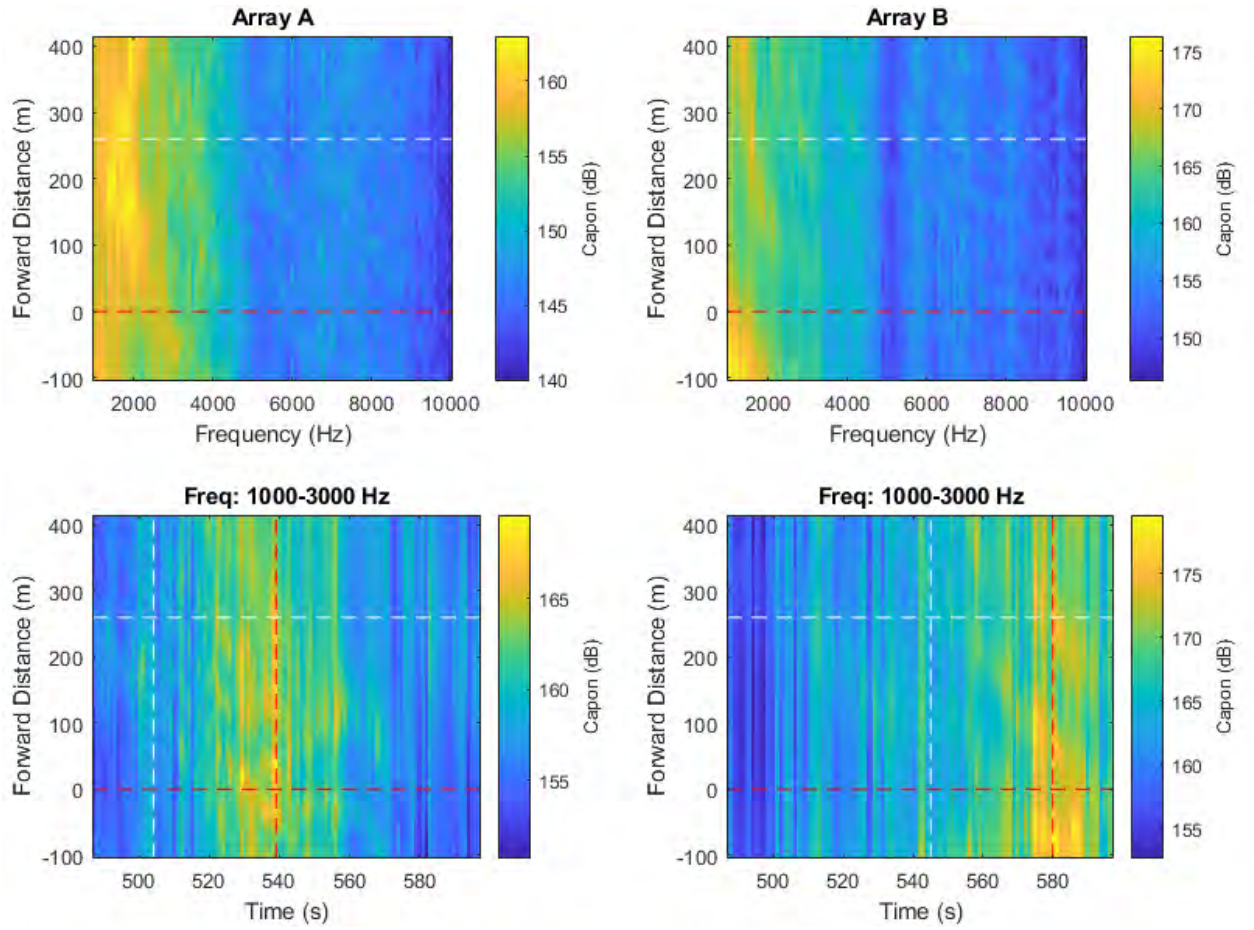

Figure 154 High-frequency noise maps obtained using the spatial spectra provided by the Capon algorithm implemented using individual arrays.

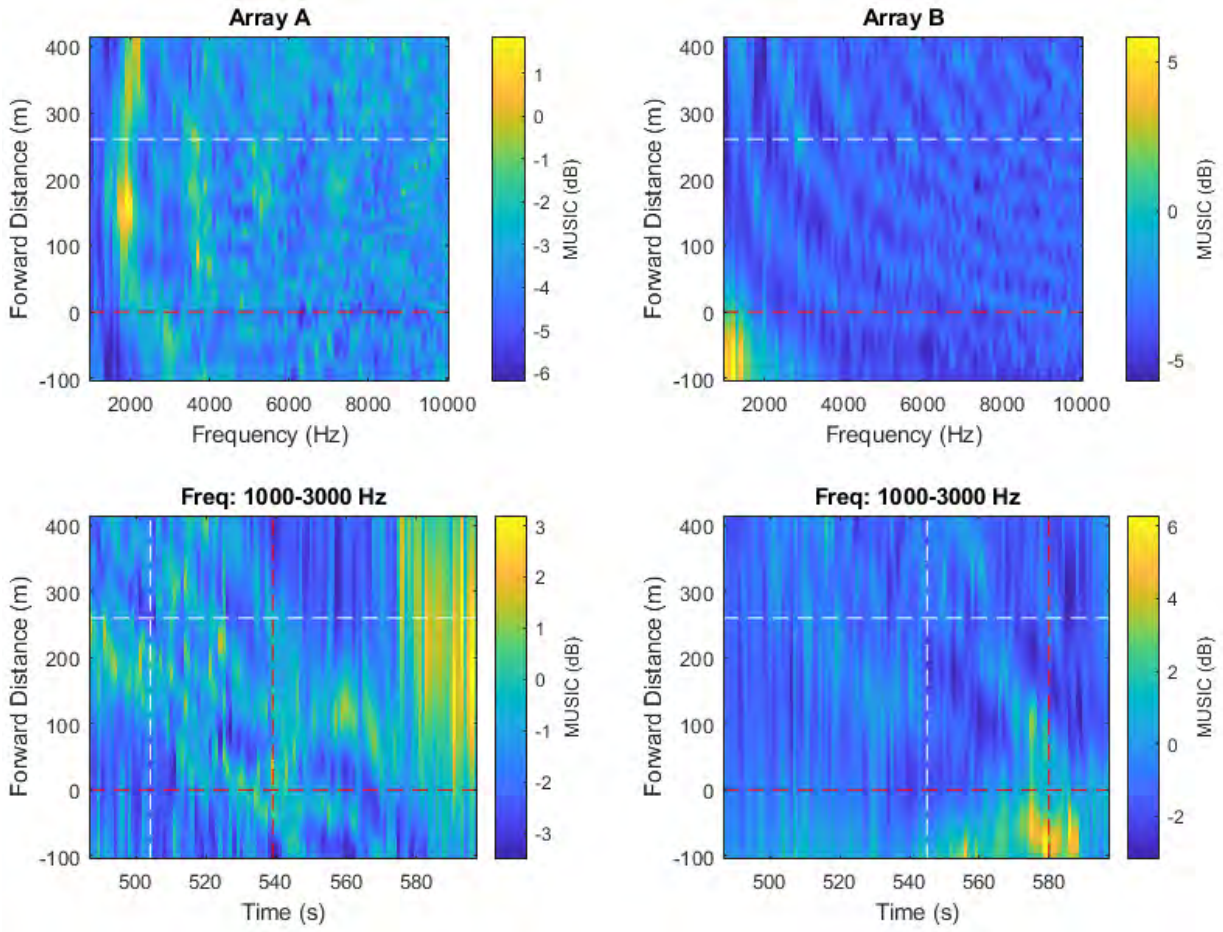

Figure 155 High-frequency noise maps obtained using the spatial spectra provided by the MUSIC algorithm implemented using individual arrays.

A.23. Pass #23 (Type: Bulker. Length: 225 m. Speed: 12.7 kn)

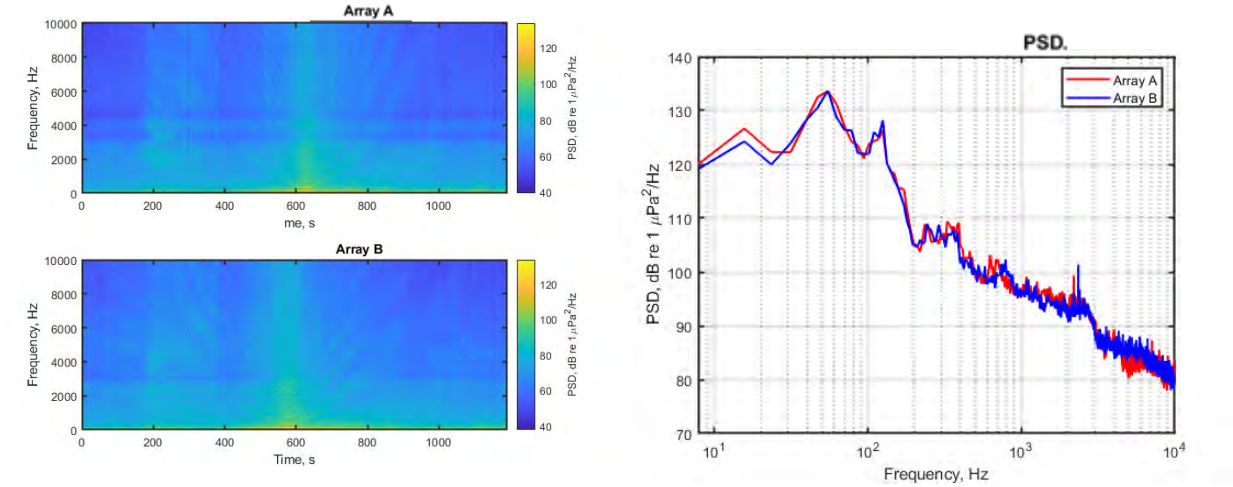

Figure 156 Spectrograms (left) and PSD (right) of ship noise observed on outputs of Arrays A and B.

A.23.1. Low- and mid-frequency noise maps

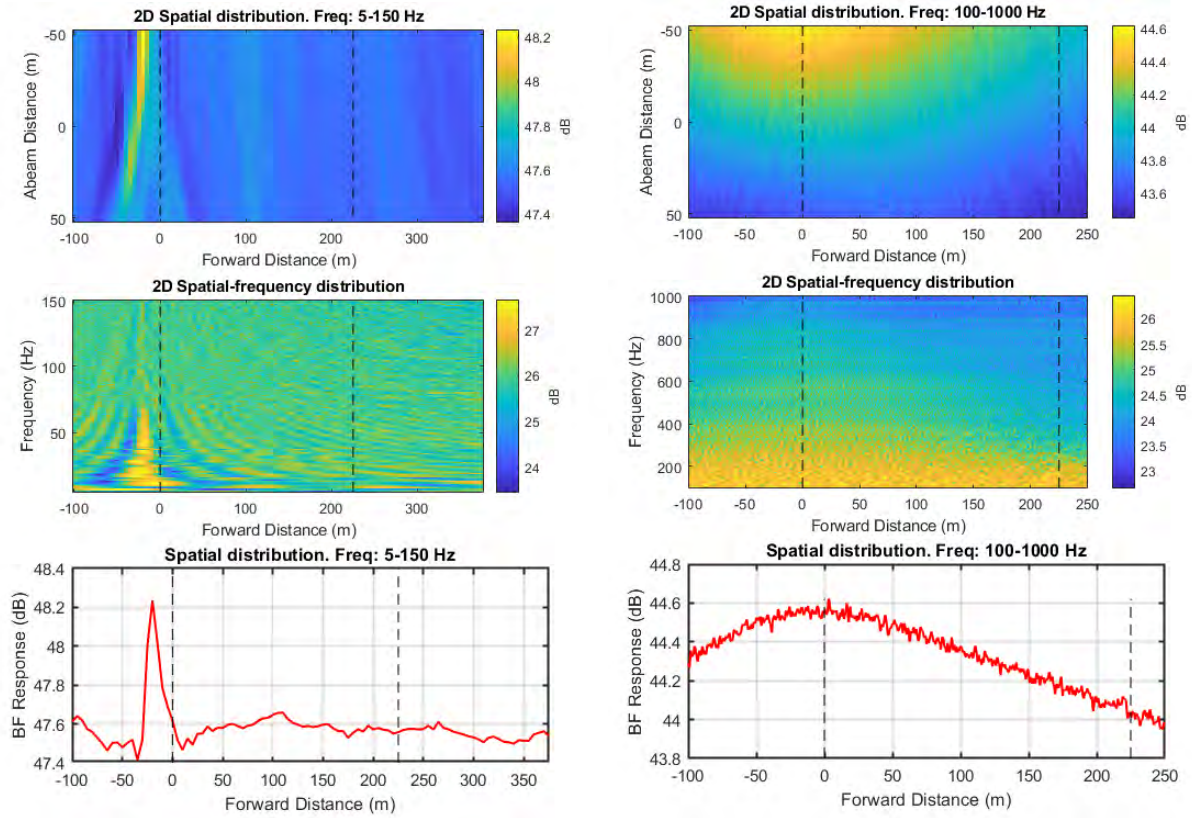

Figure 157 Noise maps from standard beamforming using combined array for Vessel Pass #23: 2D maps in spatial domain for two frequency ranges (top); 2D maps in vessel forward distance and frequency domain for two frequency ranges (middle); and graph of BF response versus forward distance for two frequency ranges bottom). Frequency ranges are 5 to150 Hz (left) and 100 to1000 Hz (right).

A.23.2. High-frequency noise maps

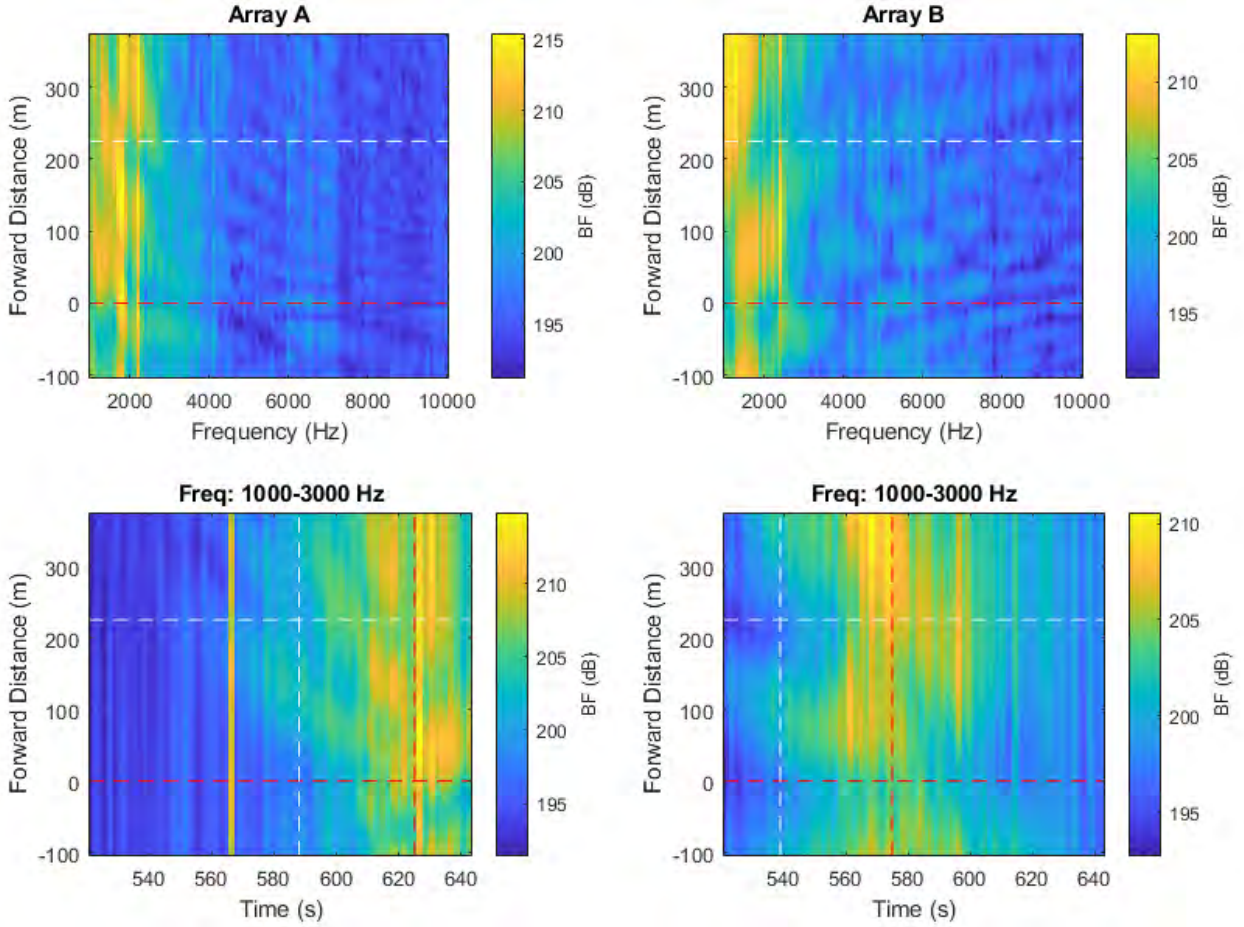

Figure 158 High-frequency noise maps from beamforming with individual arrays. Top maps show the BF response versus forward distance along vessel, measured approximately from the stern, versus frequency. Bottom maps show BF response versus forward distance and snapshot time. Horizontal dashed lines indicate the stern and bow positions of the vessel. Vertical dashed lines represent the CPA times of the bow and stern at each array.

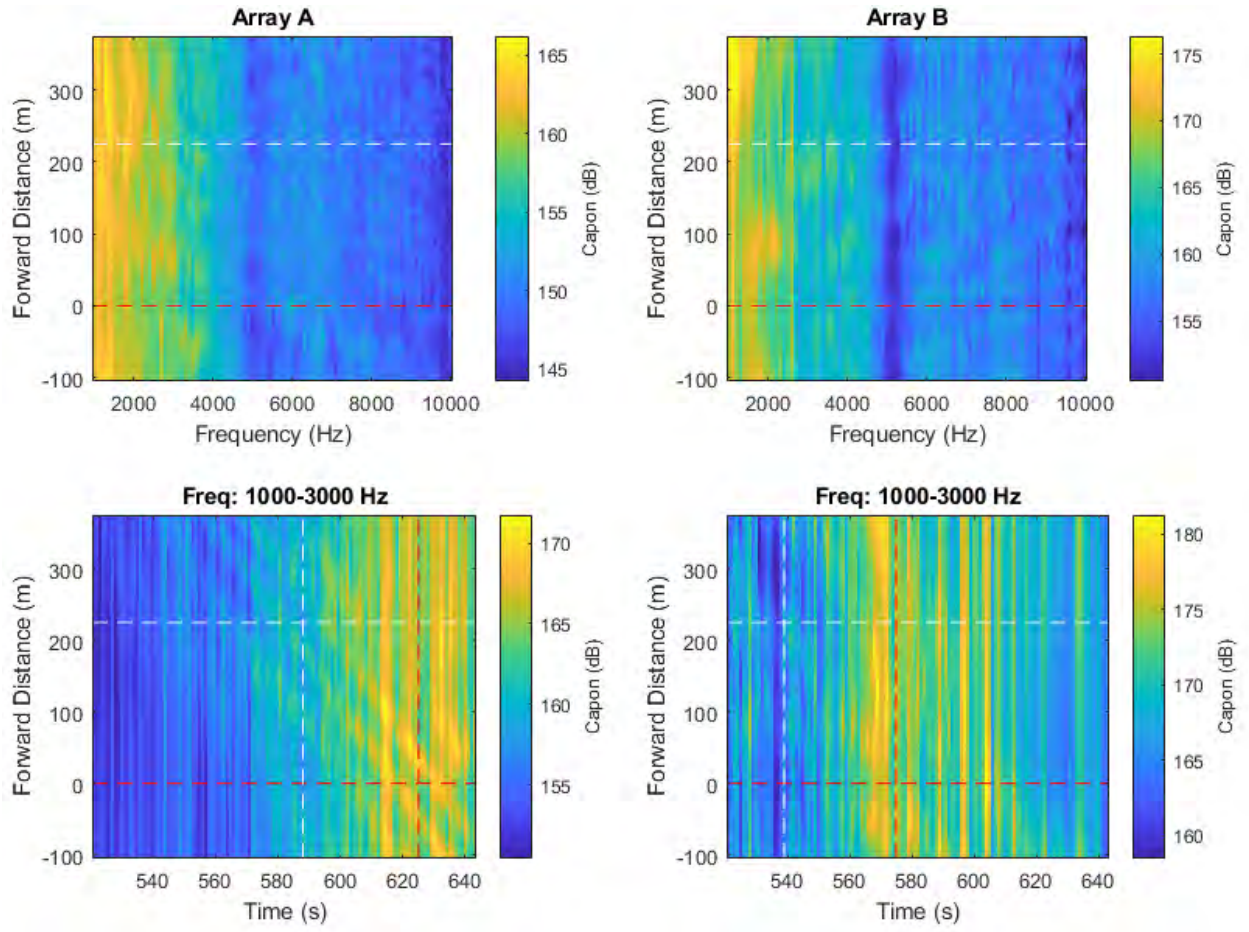

Figure 159 High-frequency noise maps obtained using the spatial spectra provided by the Capon algorithm implemented using individual arrays.

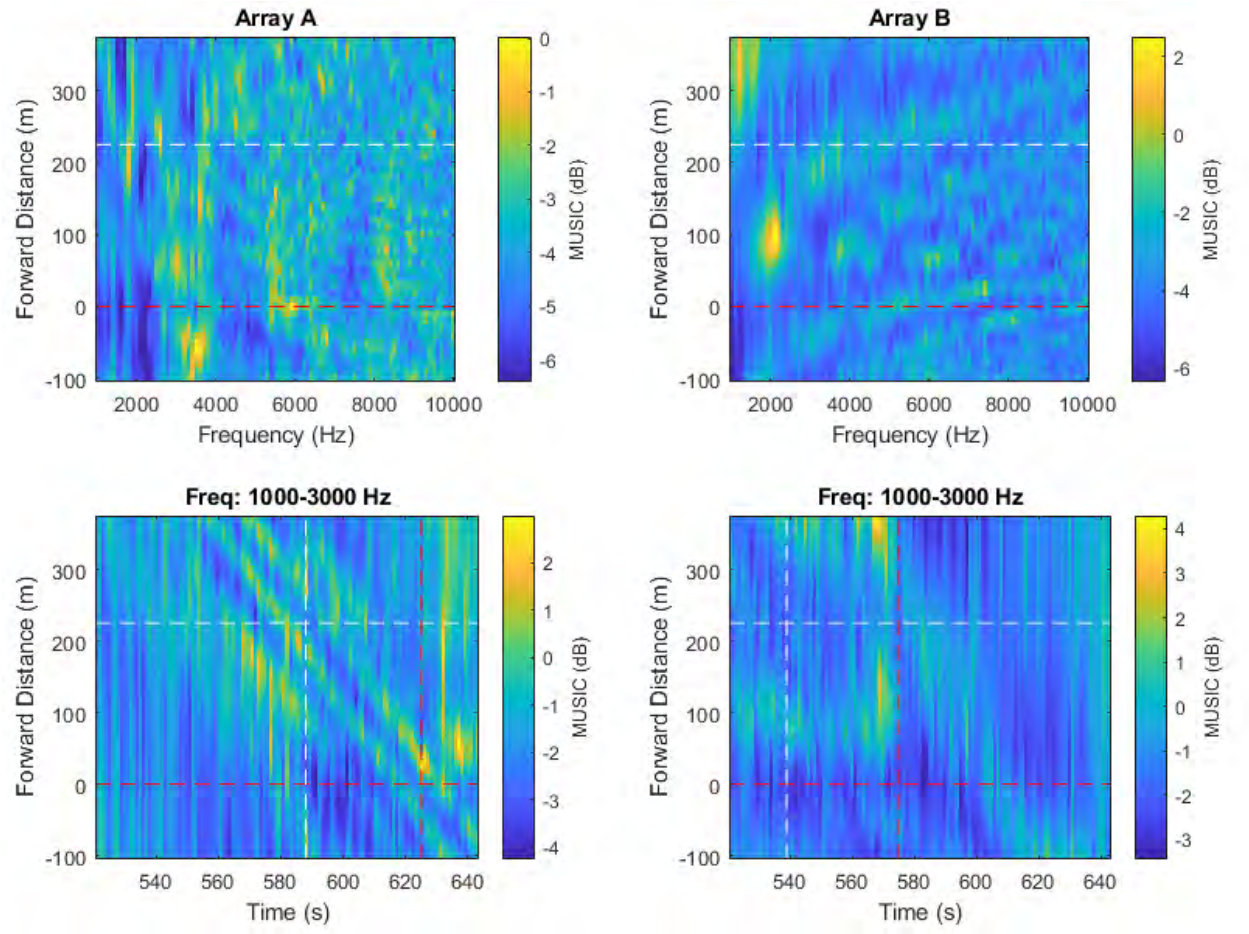

Figure 160 High-frequency noise maps obtained using the spatial spectra provided by the MUSIC algorithm implemented using individual arrays.

A.24. Pass #24 (Type: Cargo. Length: 183 m. Speed: 12.4 kn)

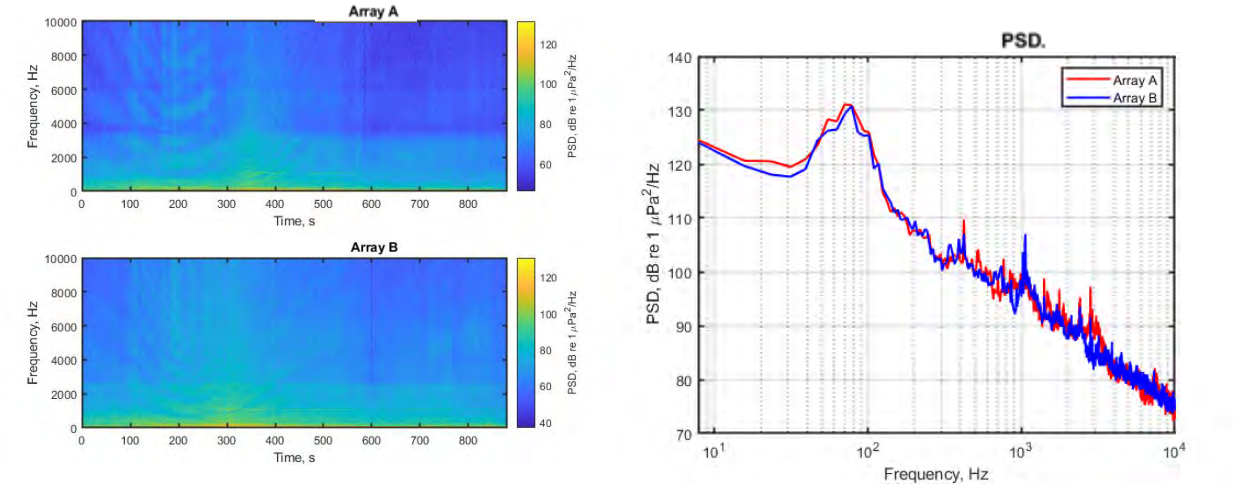

Figure 161 Spectrograms (left) and PSD (right) of ship noise observed on outputs of Arrays A and B.

A.24.1. Low- and mid-frequency noise maps

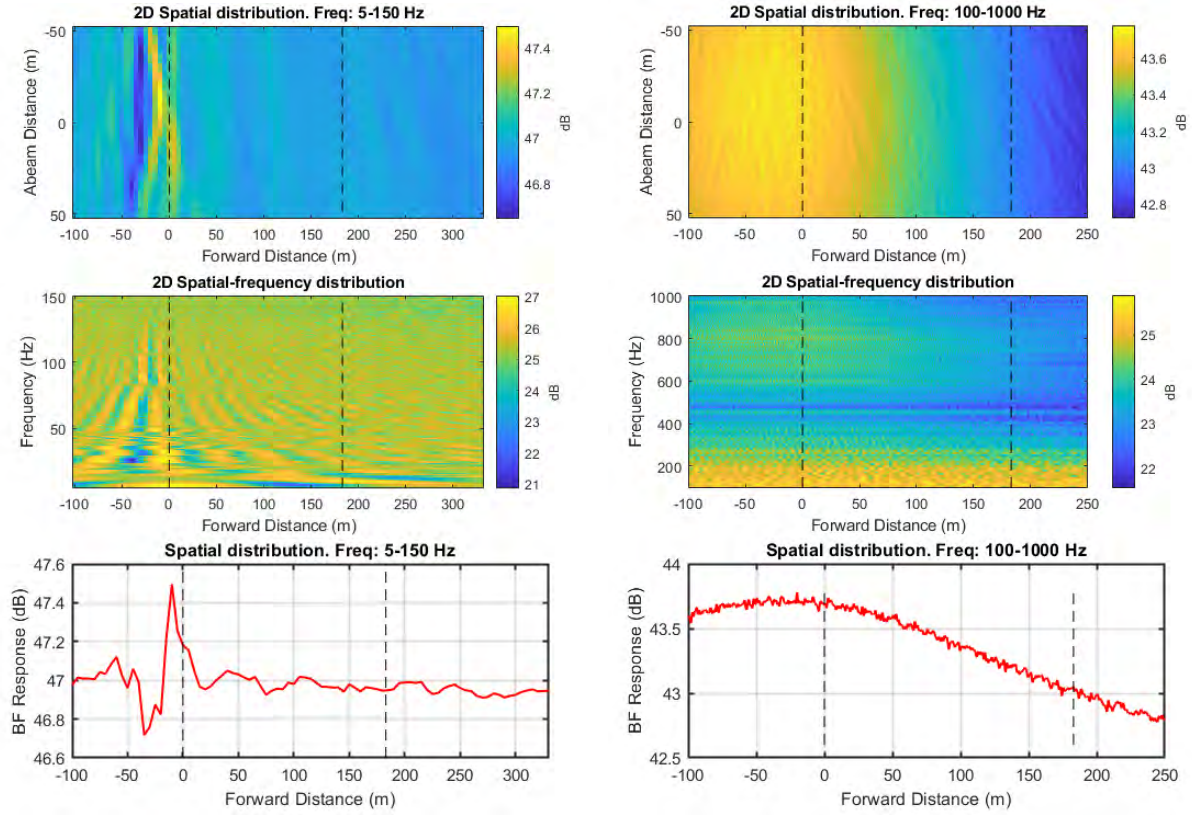

Figure 162 Noise maps from standard beamforming using combined array for Vessel Pass #24: 2D maps in spatial domain for two frequency ranges (top); 2D maps in vessel forward distance and frequency domain for two frequency ranges (middle); and graph of BF response versus forward distance for two frequency ranges bottom). Frequency ranges are 5 to150 Hz (left) and 100 to1000 Hz (right).

A.24.2. High-frequency noise maps

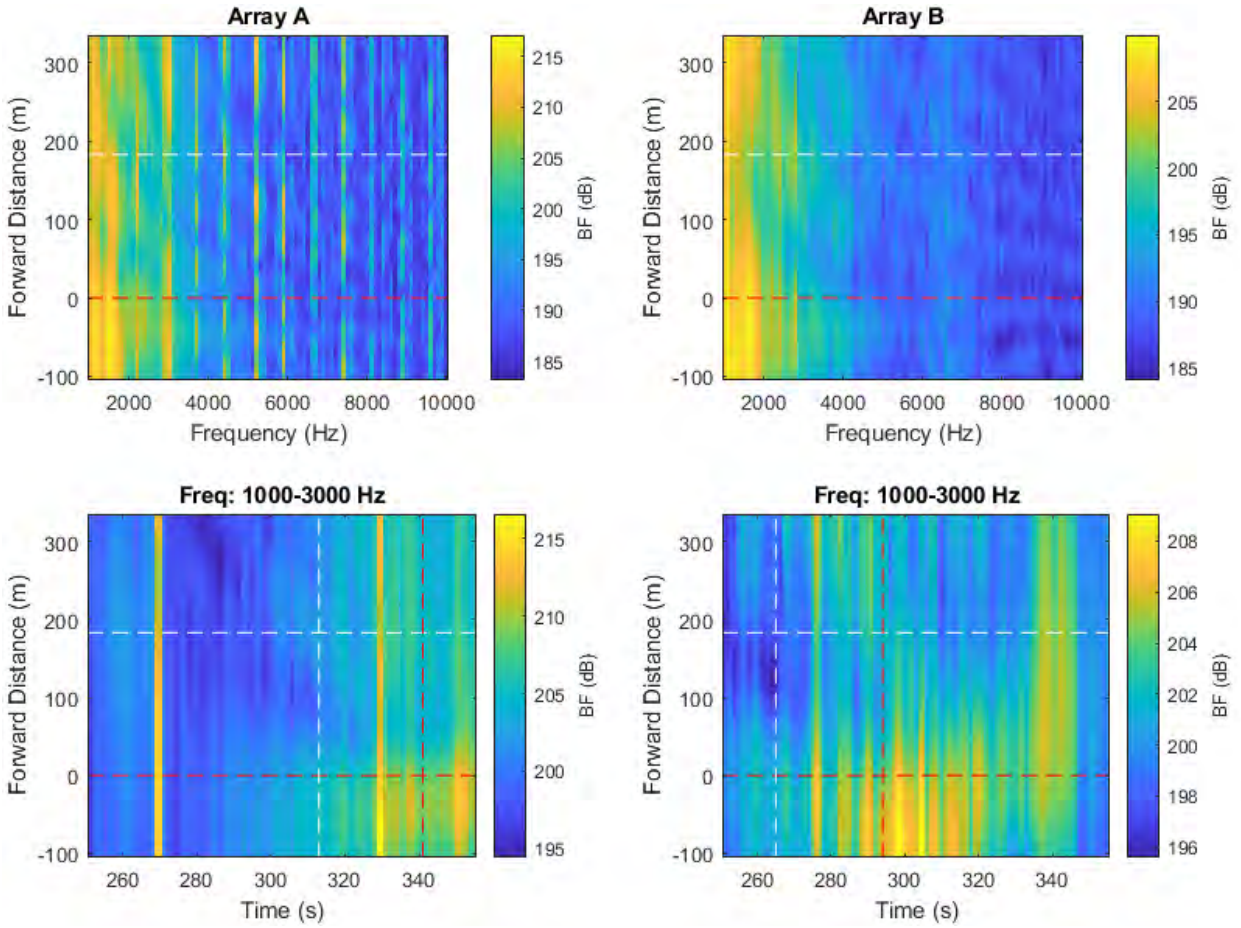

Figure 163 High-frequency noise maps from beamforming with individual arrays. Top maps show the BF response versus forward distance along vessel, measured approximately from the stern, versus frequency. Bottom maps show BF response versus forward distance and snapshot time. Horizontal dashed lines indicate the stern and bow positions of the vessel. Vertical dashed lines represent the CPA times of the bow and stern at each array.

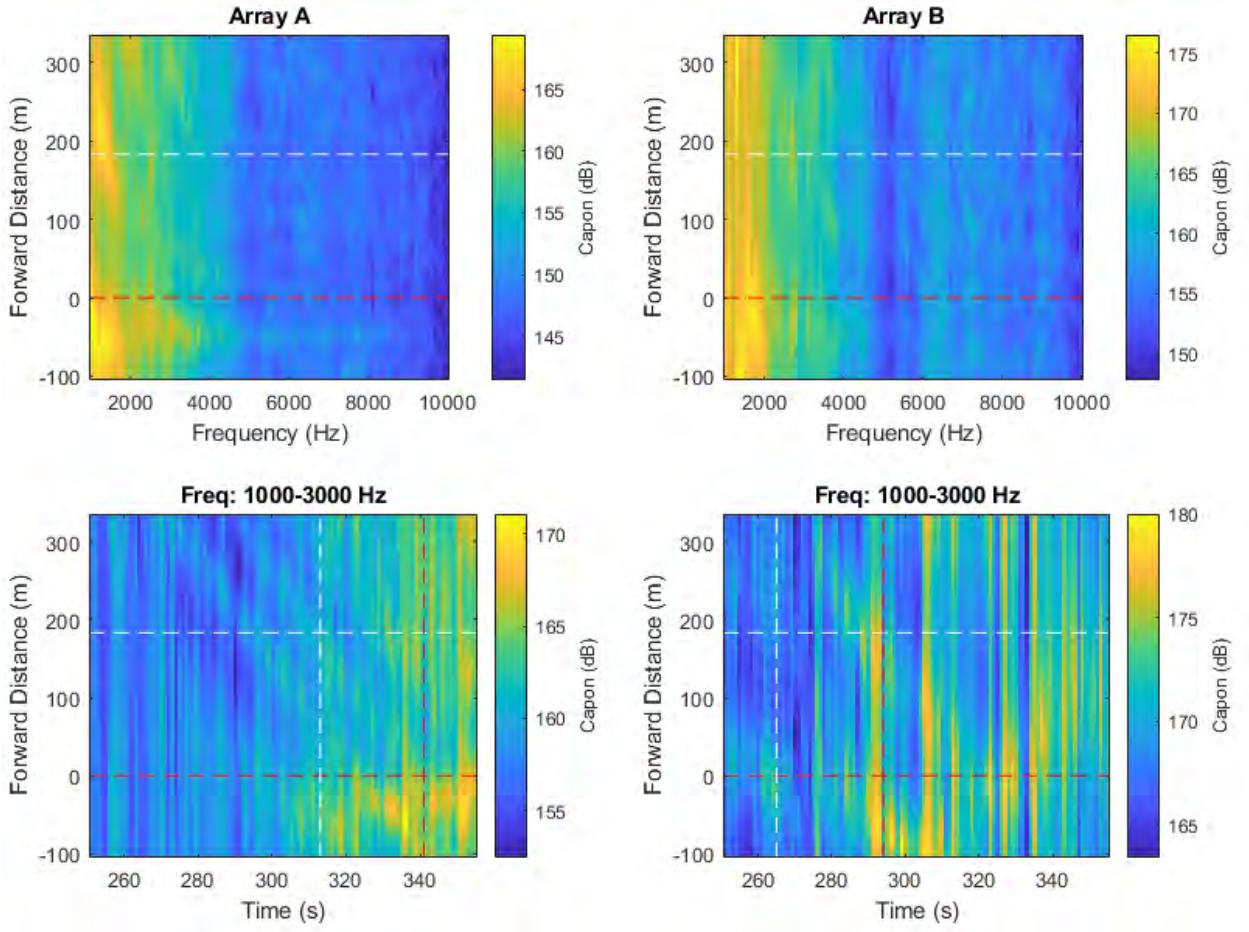

Figure 164 High-frequency noise maps obtained using the spatial spectra provided by the Capon algorithm implemented using individual arrays.

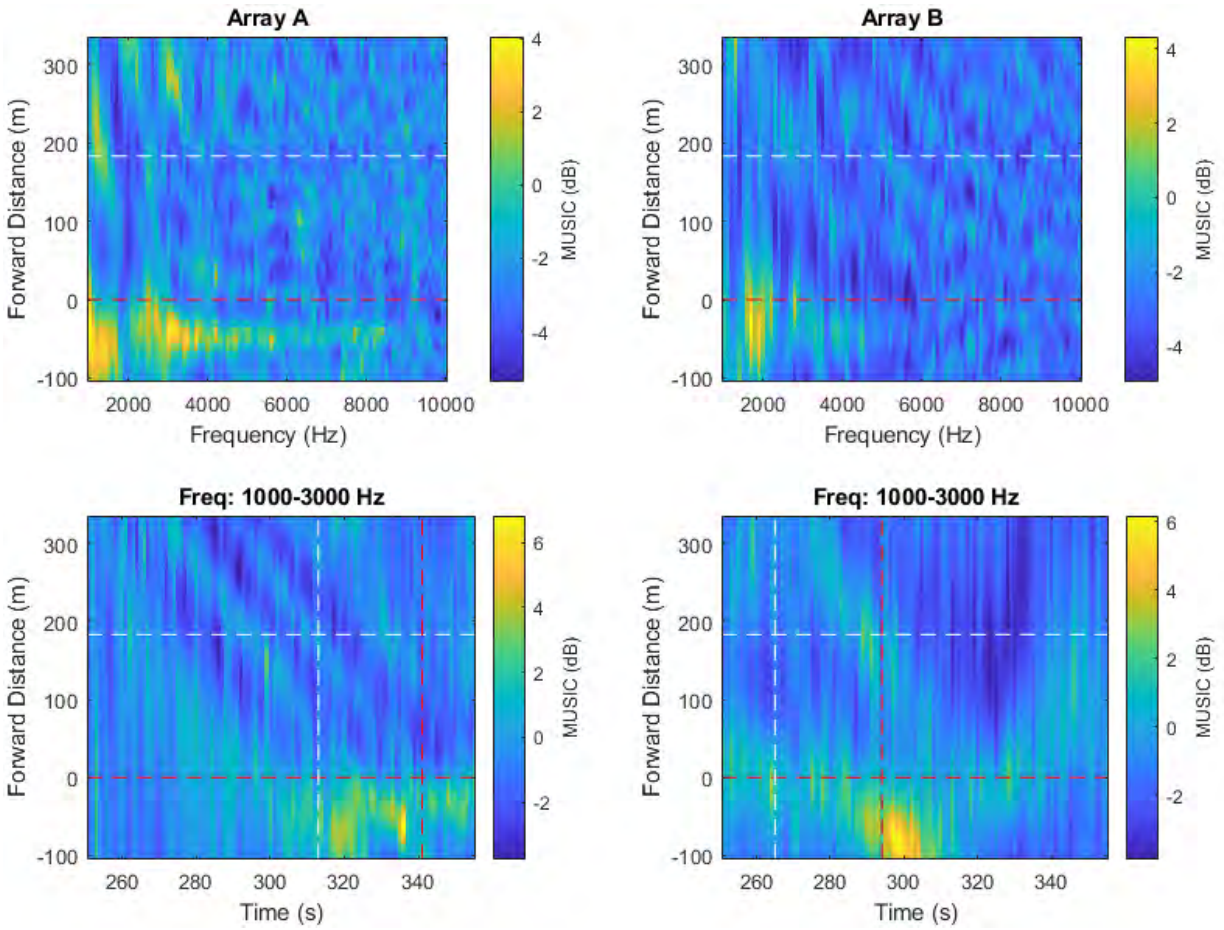

Figure 165 High-frequency noise maps obtained using the spatial spectra provided by the MUSIC algorithm implemented using individual arrays.

A.25. Pass #25 (Type: Bulker. Length: 260 m. Speed: 18.0 kn)

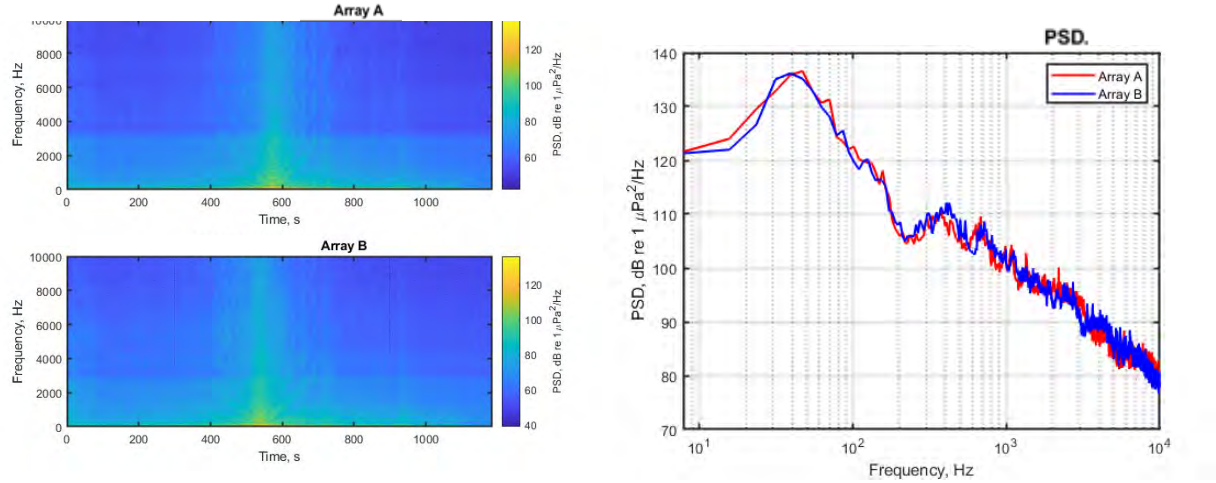

Figure 166 Spectrograms (left) and PSD (right) of ship noise observed on outputs of Arrays A and B.

A.25.1. Low- and mid-frequency noise maps

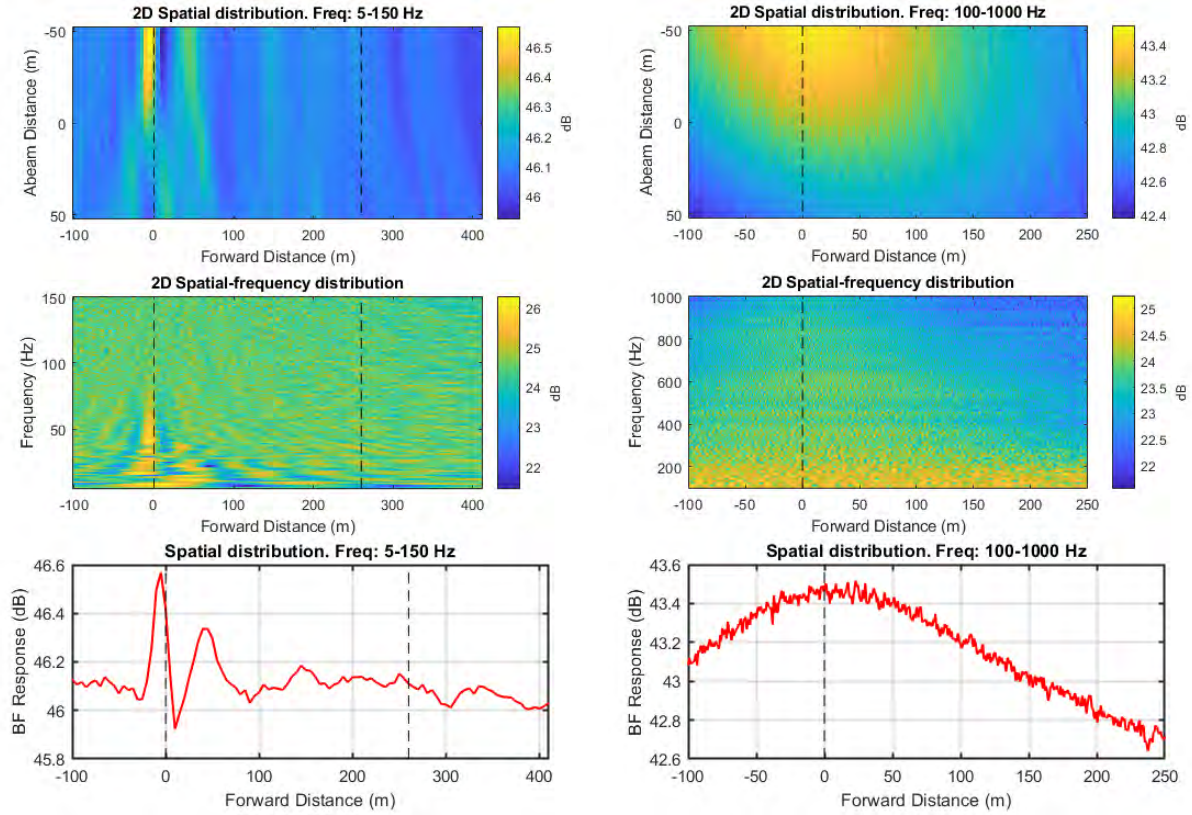

Figure 167 Noise maps from standard beamforming using combined array for Vessel Pass #25: 2D maps in spatial domain for two frequency ranges (top); 2D maps in vessel forward distance and frequency domain for two frequency ranges (middle); and graph of BF response versus forward distance for two frequency ranges bottom). Frequency ranges are 5 to150 Hz (left) and 100 to1000 Hz (right).

A.25.2. High-frequency noise maps

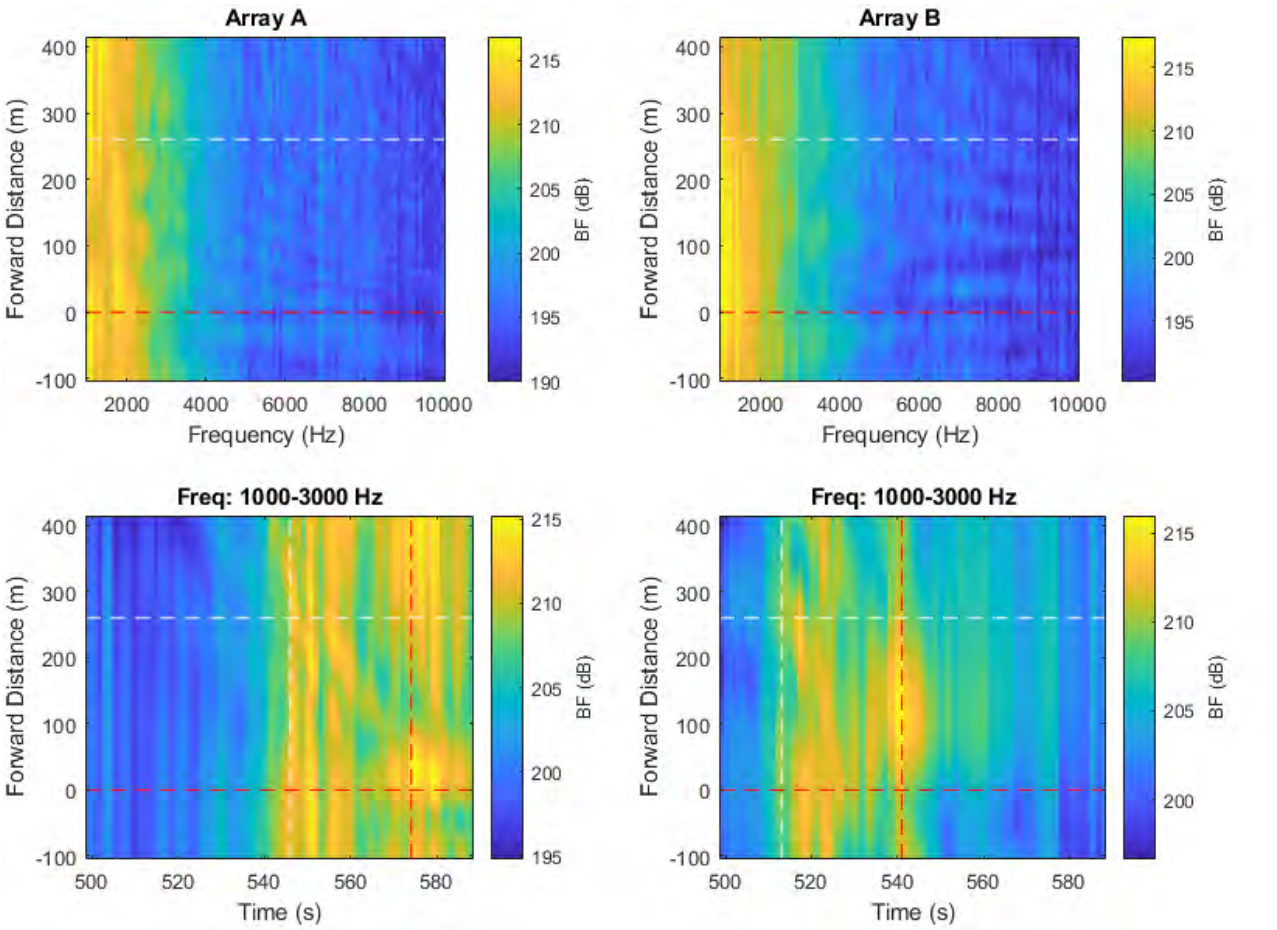

Figure 168 High-frequency noise maps from beamforming with individual arrays. Top maps show the BF response versus forward distance along vessel, measured approximately from the stern, versus frequency. Bottom maps show BF response versus forward distance and snapshot time. Horizontal dashed lines indicate the stern and bow positions of the vessel. Vertical dashed lines represent the CPA times of the bow and stern at each array.

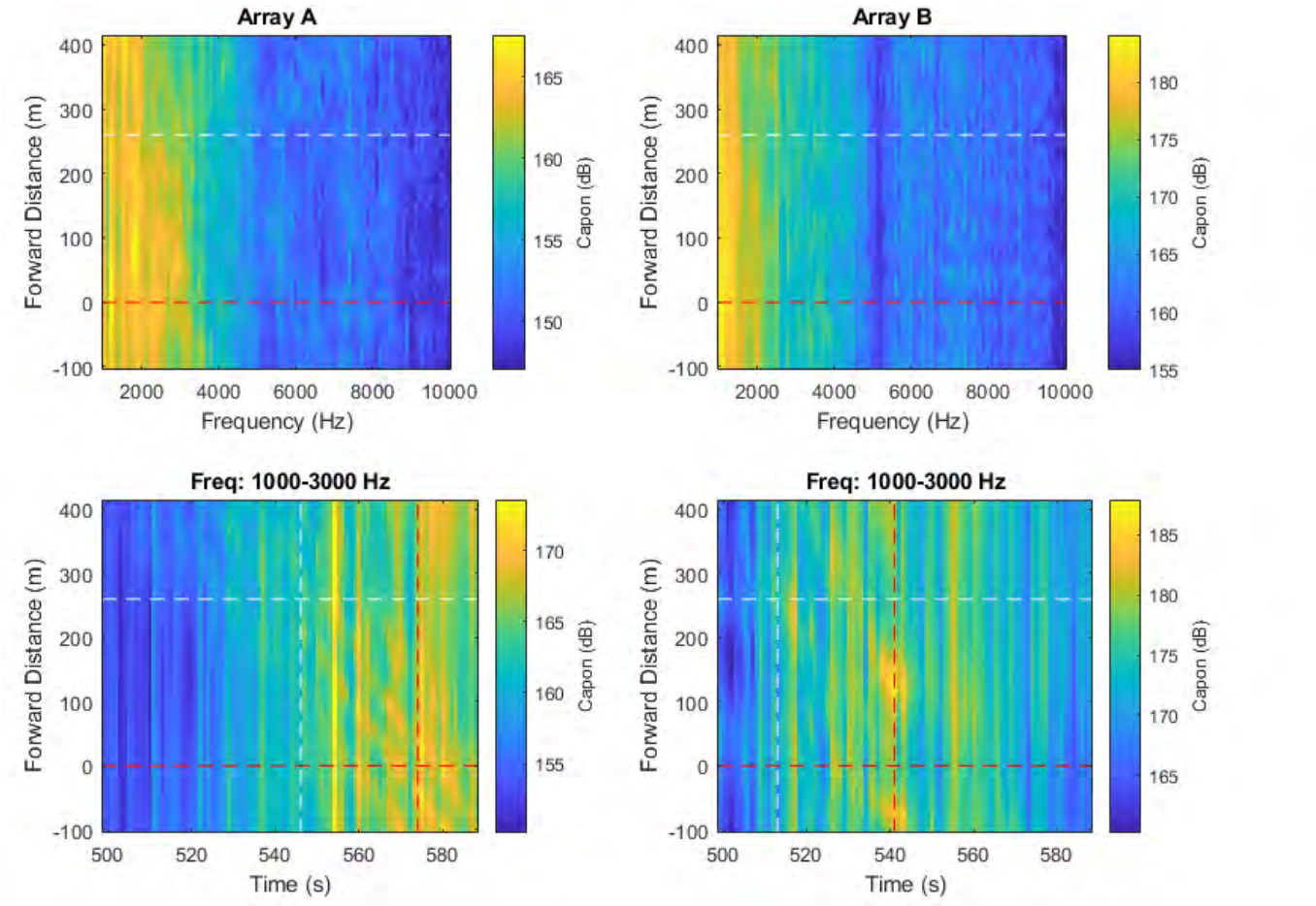

Figure 169 High-frequency noise maps obtained using the spatial spectra provided by the Capon algorithm implemented using individual arrays.

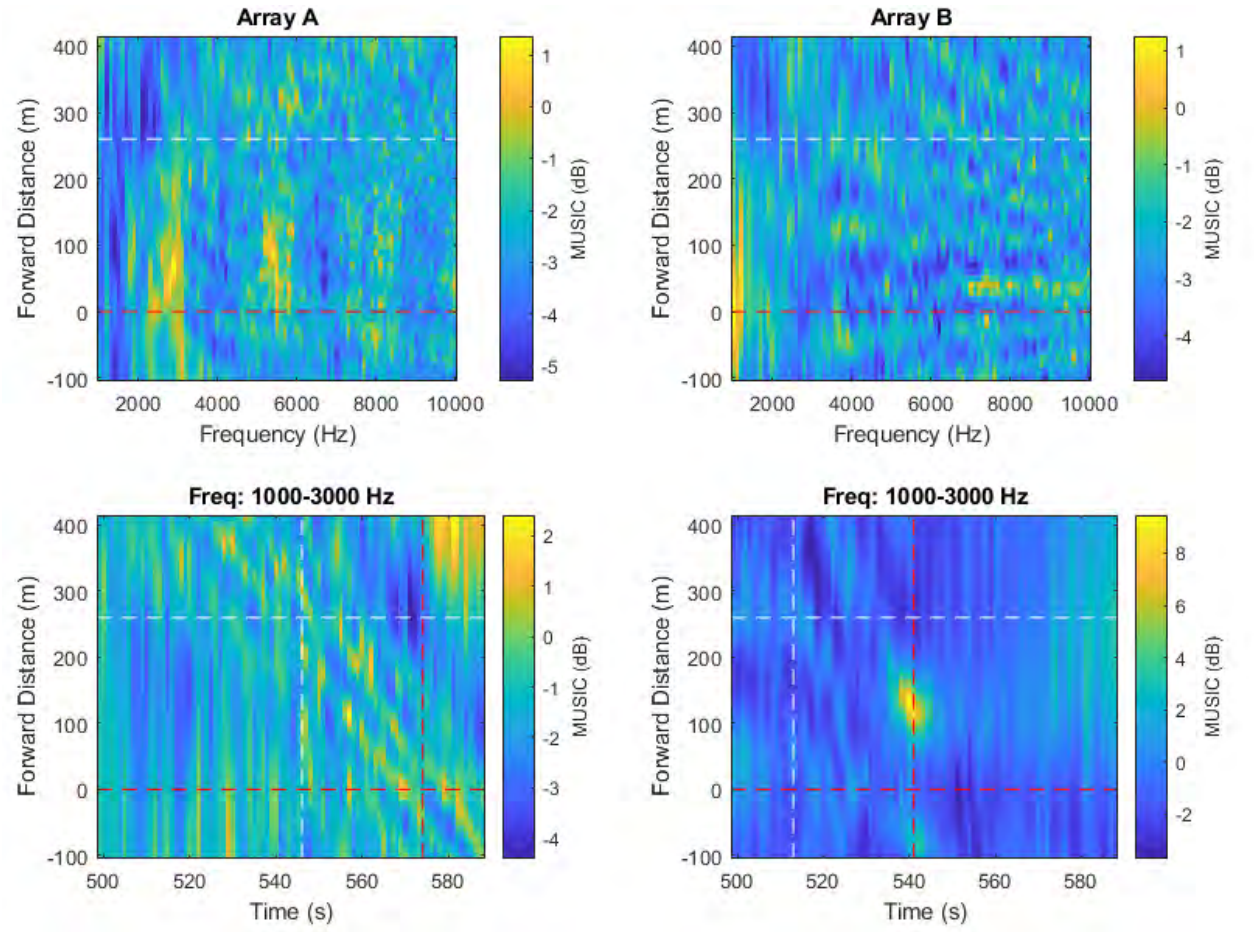

Figure 170 High-frequency noise maps obtained using the spatial spectra provided by the MUSIC algorithm implemented using individual arrays.

A.26. Pass #26 (Type: Bulker. Length: 229 m. Speed: 14.8 kn)

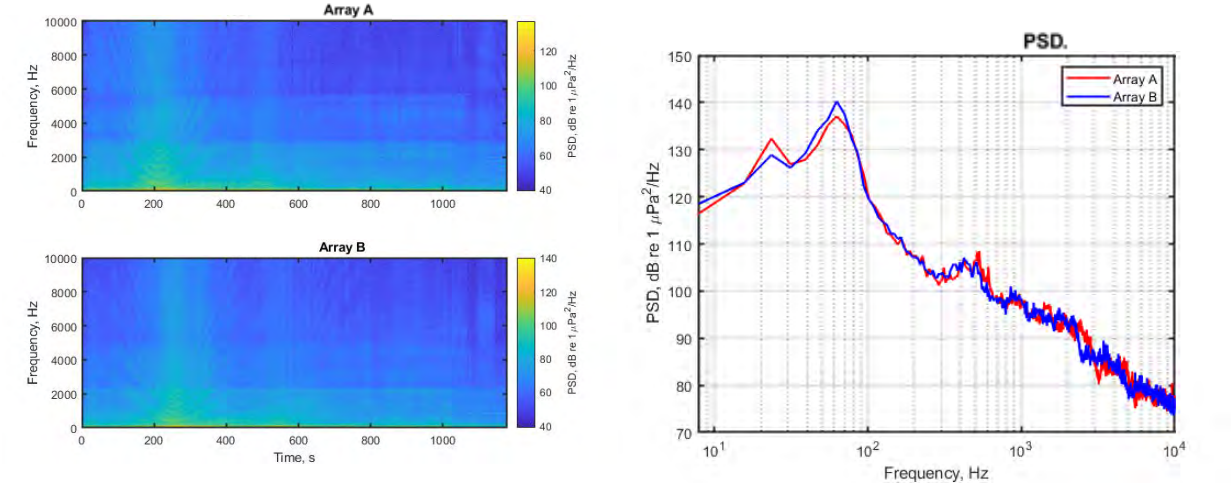

Figure 171 Spectrograms (left) and PSD (right) of ship noise observed on outputs of Arrays A and B.

A.26.1. Low- and mid-frequency noise maps

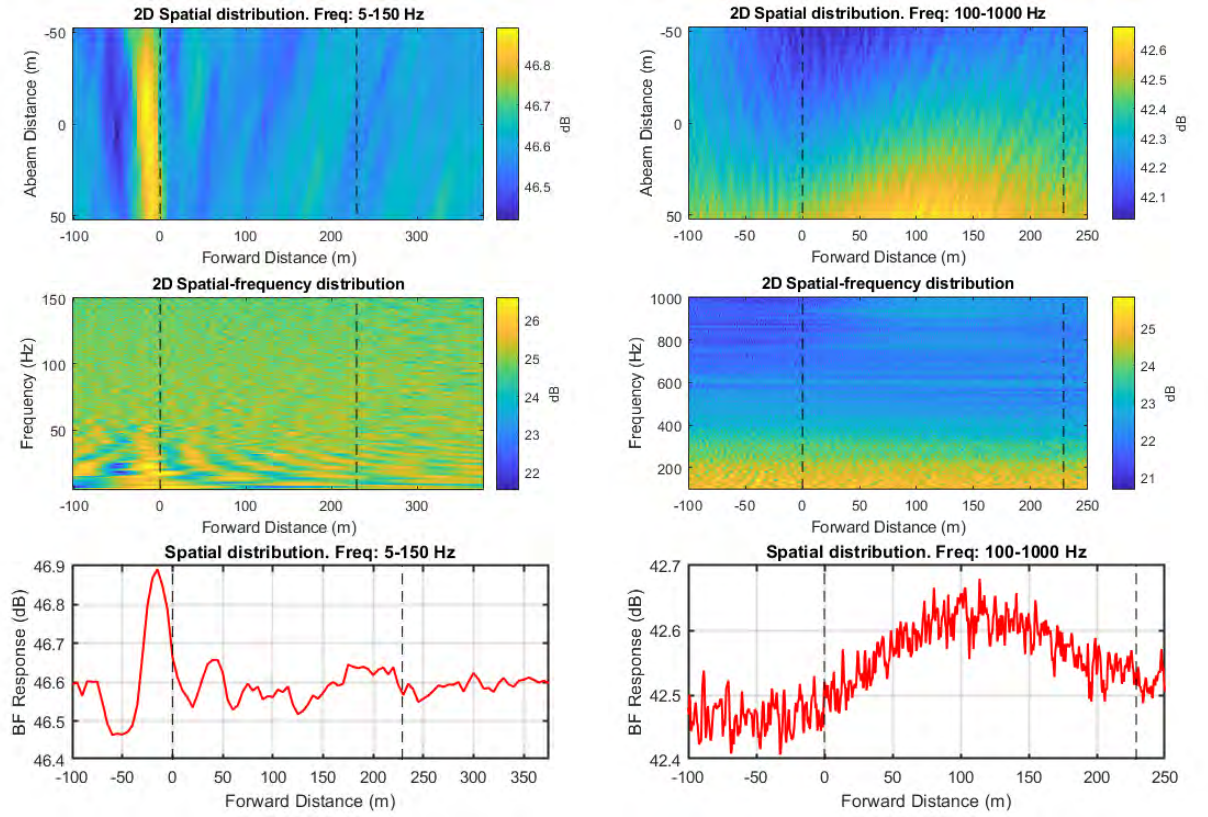

Figure 172 Noise maps from standard beamforming using combined array for Vessel Pass #26: 2D maps in spatial domain for two frequency ranges (top); 2D maps in vessel forward distance and frequency domain for two frequency ranges (middle); and graph of BF response versus forward distance for two frequency ranges (bottom). Frequency ranges are 5 to150 Hz (left) and 100 to1000 Hz (right).

A.26.2. High-frequency noise maps

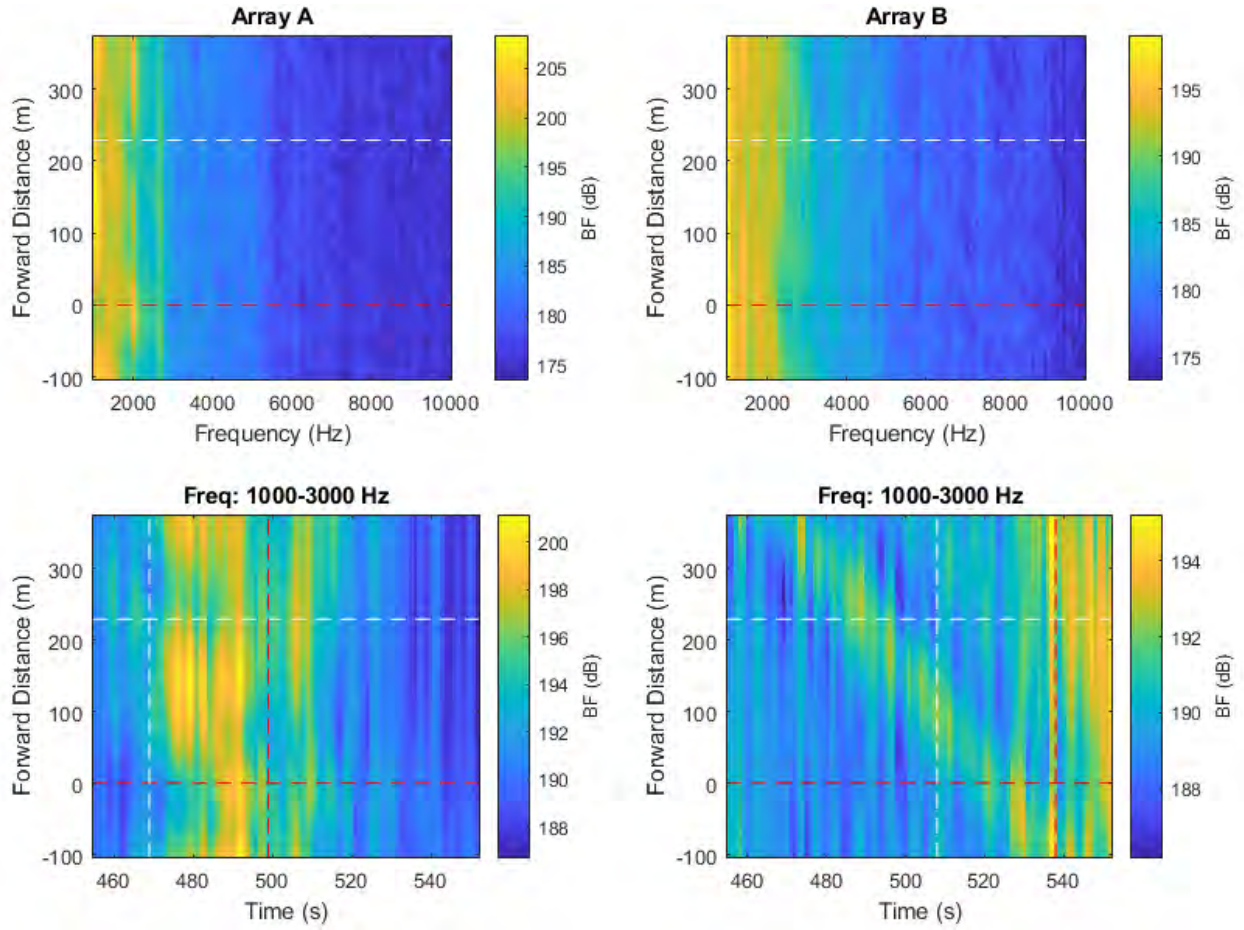

Figure 173 High-frequency noise maps from beamforming with individual arrays. Top maps show the BF response versus forward distance along vessel, measured approximately from the stern, versus frequency. Bottom maps show BF response versus forward distance and snapshot time. Horizontal dashed lines indicate the stern and bow positions of the vessel. Vertical dashed lines represent the CPA times of the bow and stern at each array.

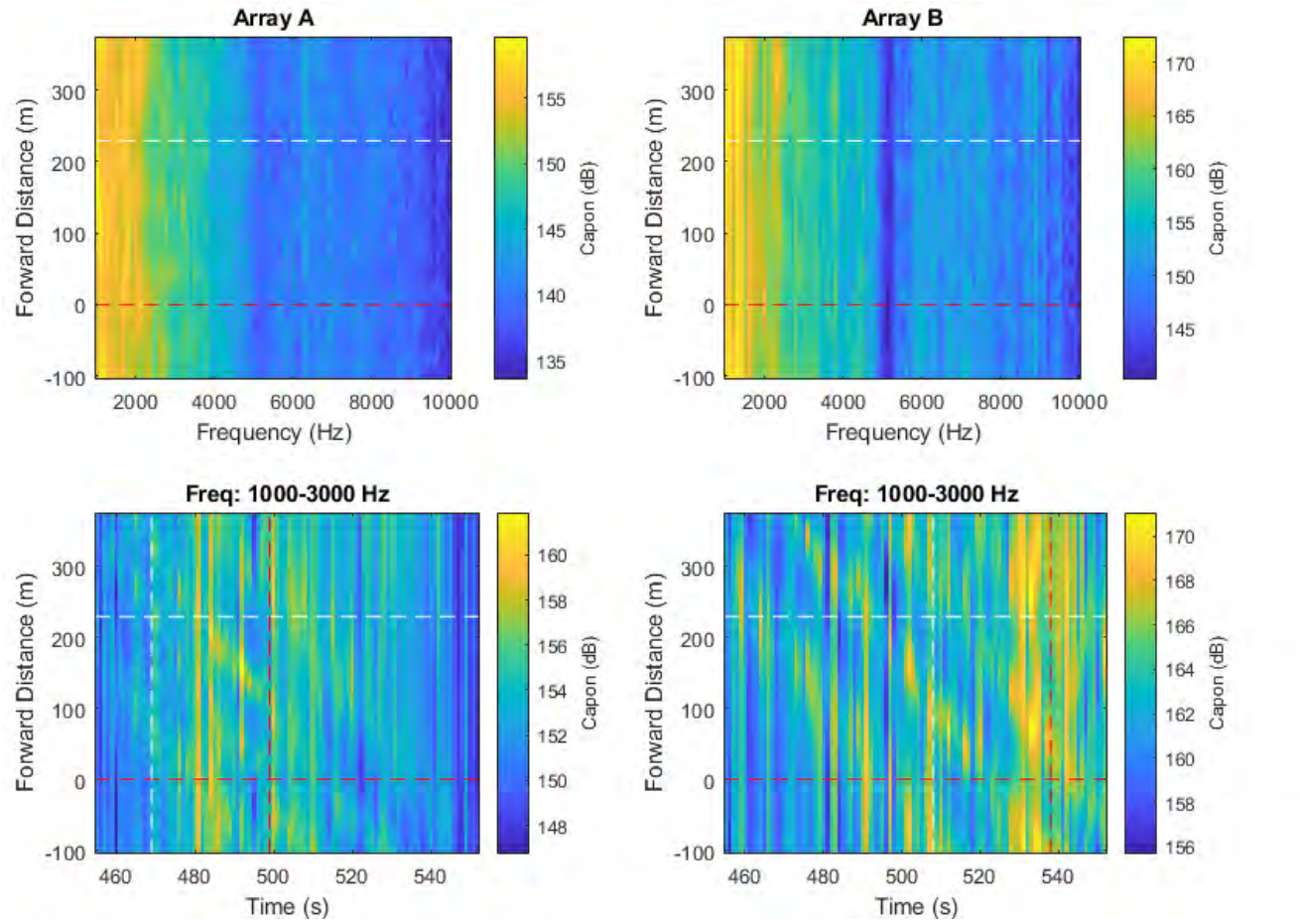

Figure 174 High-frequency noise maps obtained using the spatial spectra provided by the Capon algorithm implemented using individual arrays.

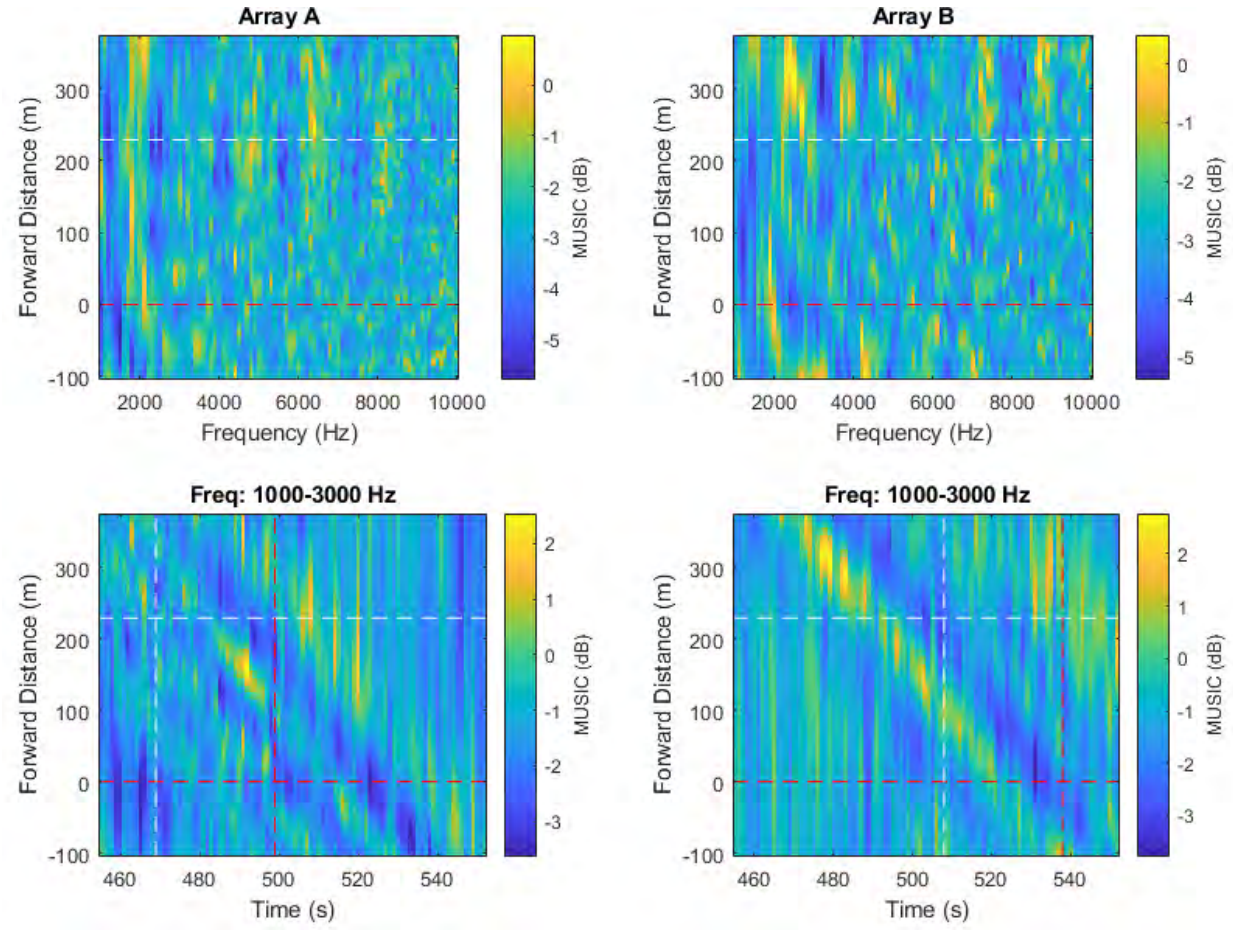

Figure 175 High-frequency noise maps obtained using the spatial spectra provided by the MUSIC algorithm implemented using individual arrays.

A.27. Pass #27 (Type: Cargo. Length: 183 m. Speed: 12.4 kn)

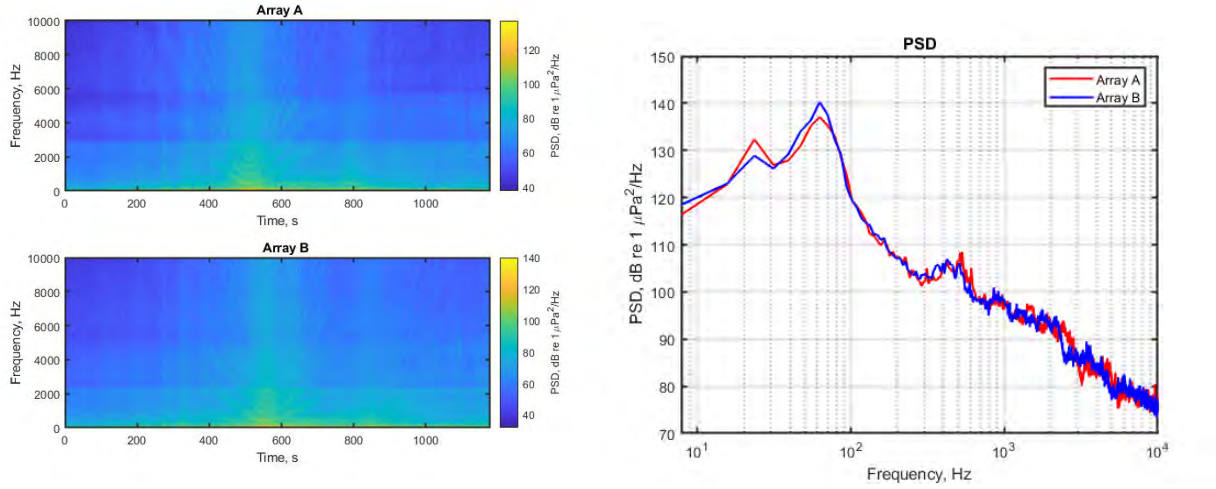

Figure 176 Spectrograms (left) and PSD (right) of ship noise observed on outputs of Arrays A and B.

A.27.1. Low- and mid-frequency noise maps

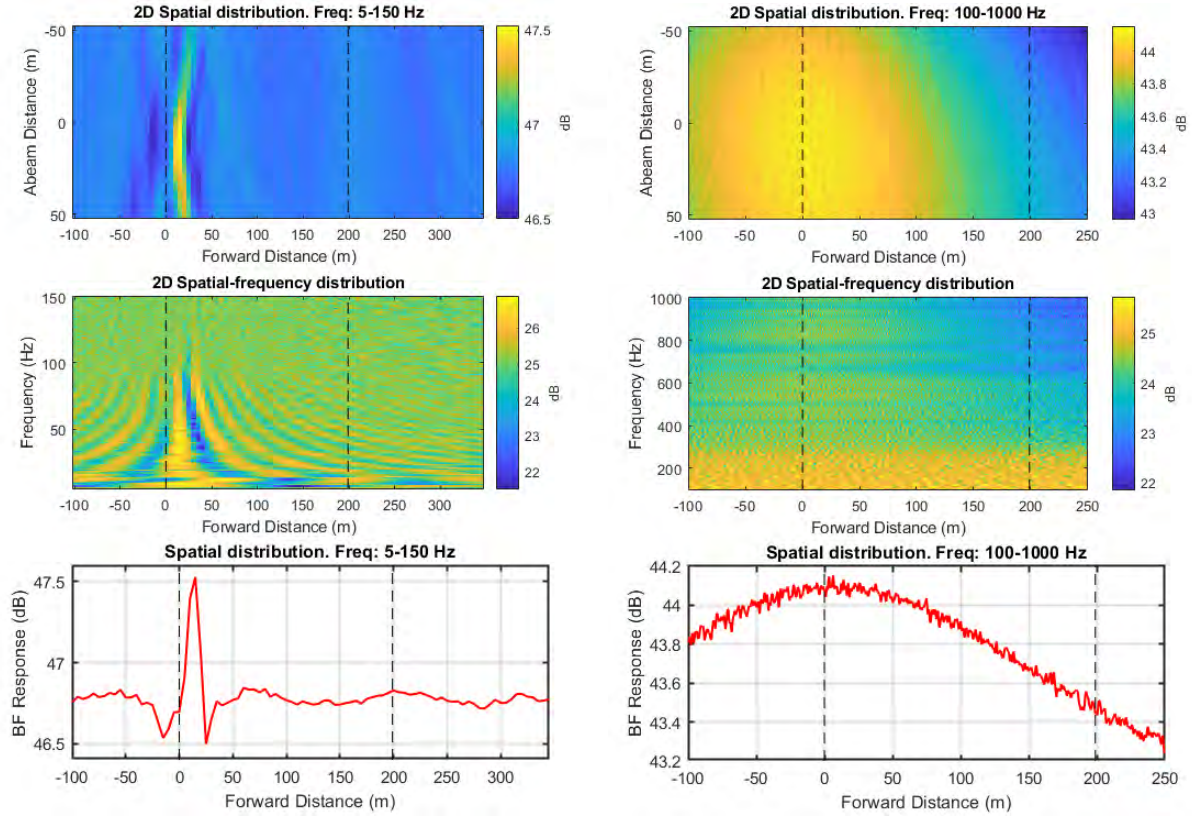

Figure 177 Noise maps from standard beamforming using combined array for Vessel Pass #27: 2D maps in spatial domain for two frequency ranges (top); 2D maps in vessel forward distance and frequency domain for two frequency ranges (middle); and graph of BF response versus forward distance for two frequency ranges (bottom). Frequency ranges are 5 to150 Hz (left) and 100 to1000 Hz (right).

A.27.2. High-frequency noise maps

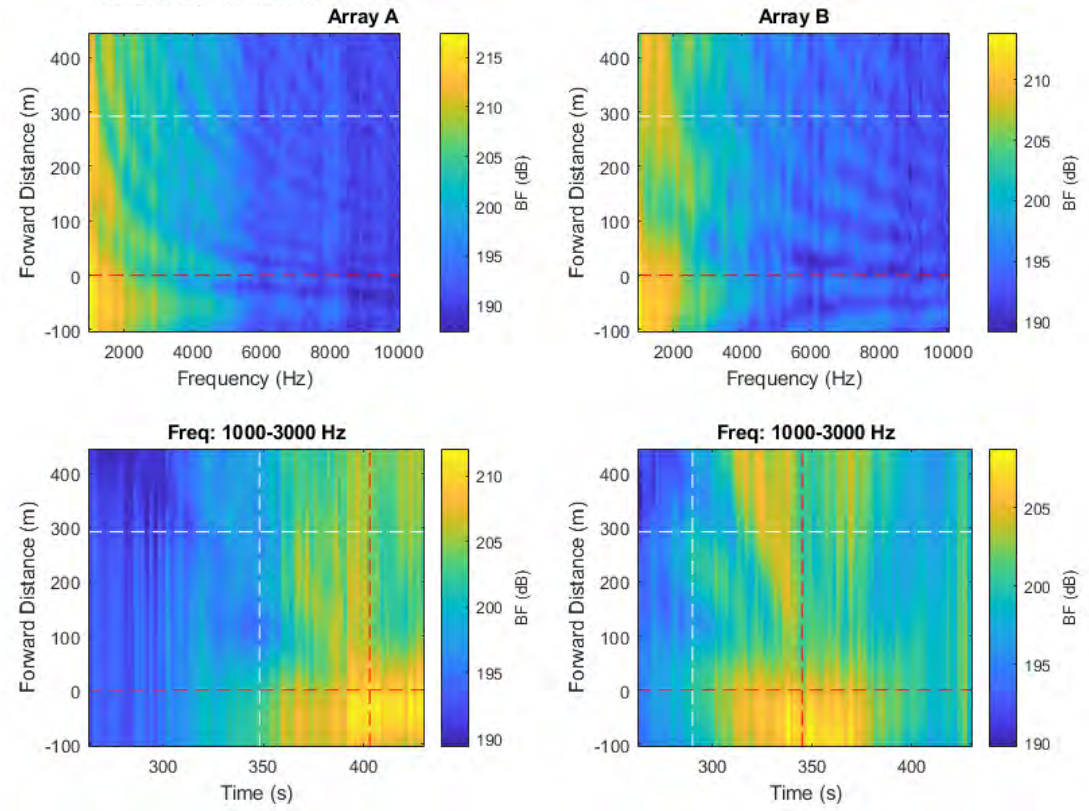

Figure 178 High-frequency noise maps from beamforming with individual arrays. Top maps show the BF response versus forward distance along vessel, measured approximately from the stern, versus frequency. Bottom maps show BF response versus forward distance and snapshot time. Horizontal dashed lines indicate the stern and bow positions of the vessel. Vertical dashed lines represent the CPA times of the bow and stern at each array.

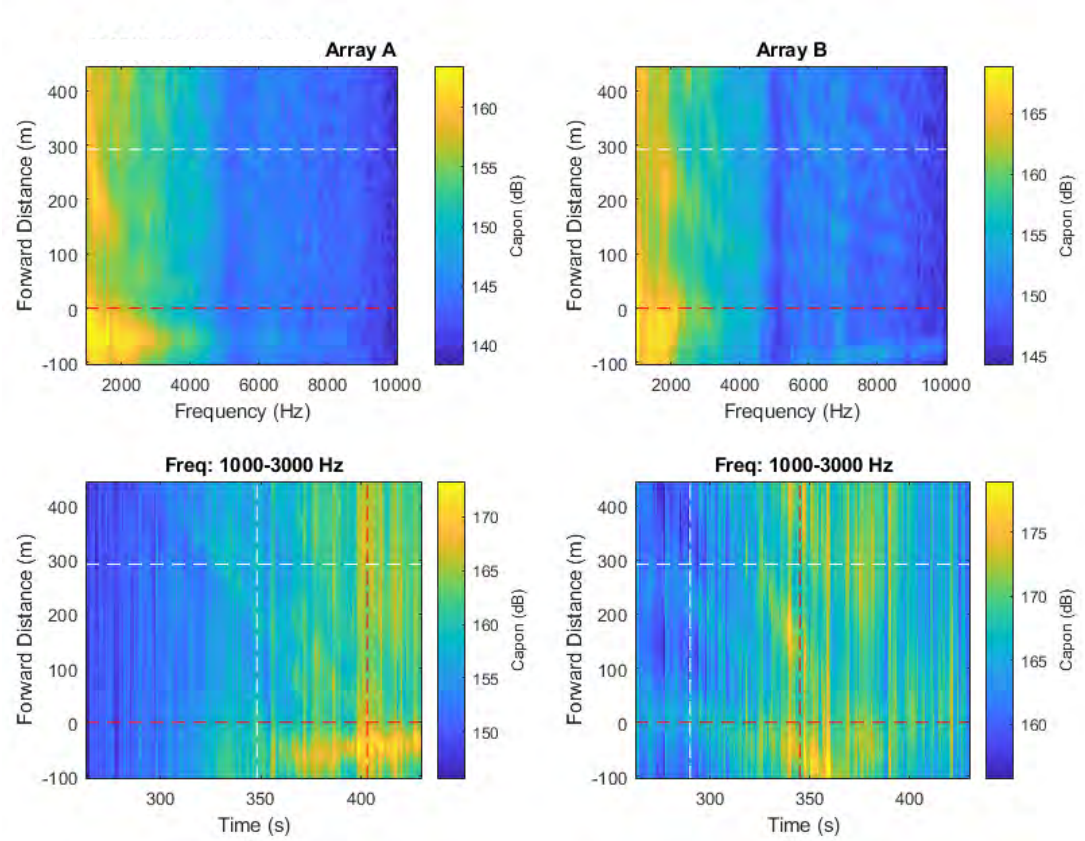

Figure 179 High-frequency noise maps obtained using the spatial spectra provided by the Capon algorithm implemented using individual arrays.

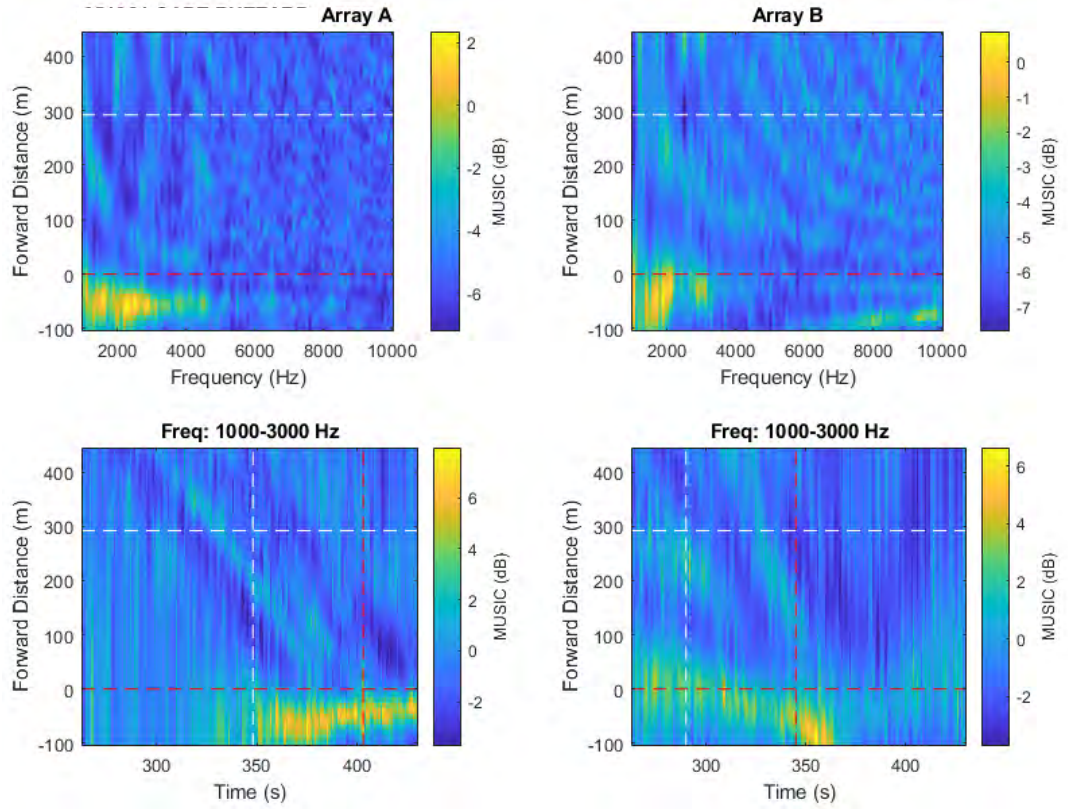

Figure 180 High-frequency noise maps obtained using the spatial spectra provided by the MUSIC algorithm implemented using individual arrays.

A.28. Pass #28 (Type: Container. Length: 224 m. Speed: 21.1 kn)

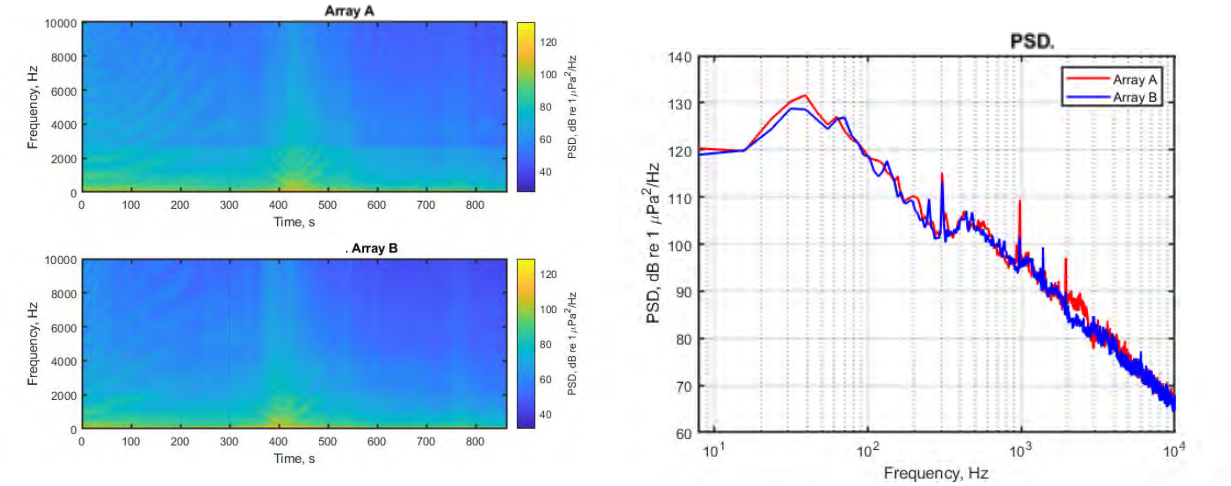

Figure 181 Spectrograms (left) and PSD (right) of ship noise observed on outputs of Arrays A and B.

A.28.1. Low- and mid-frequency noise maps

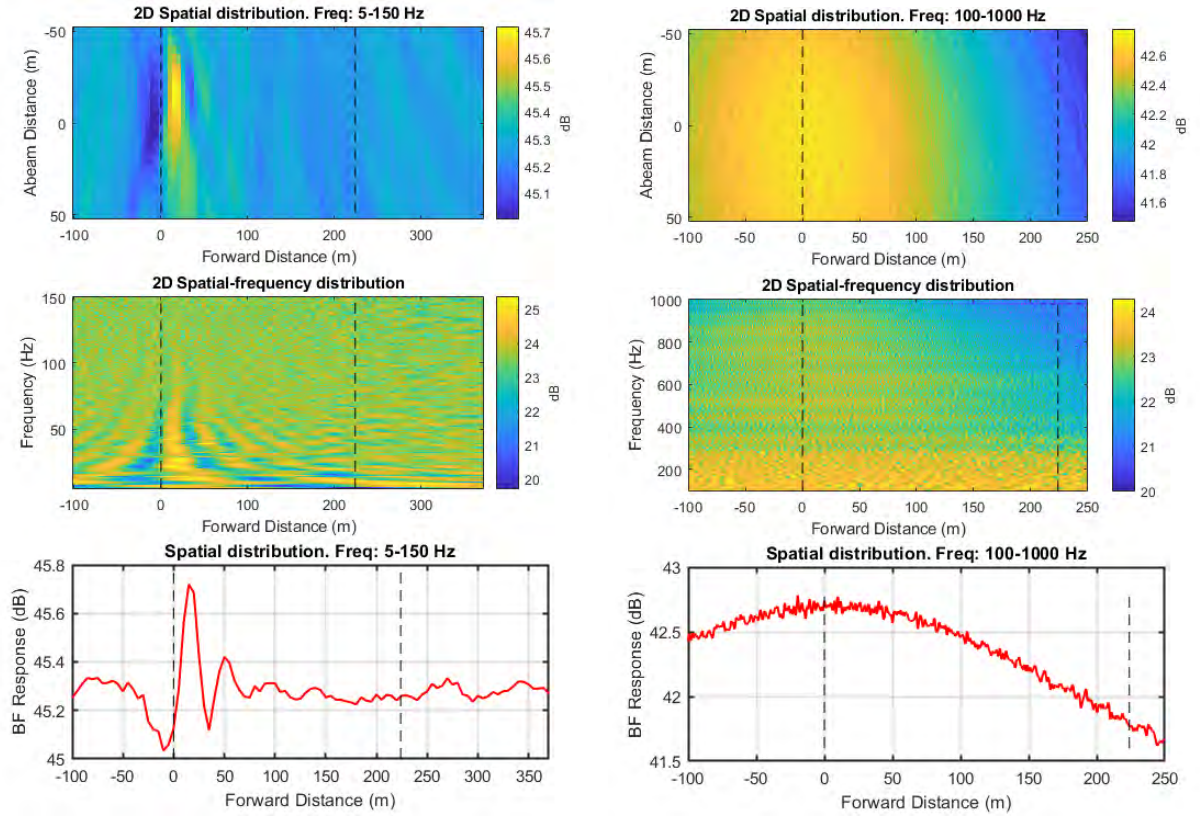

Figure 182 Noise maps from standard beamforming using combined array for Vessel Pass #28: 2D maps in spatial domain for two frequency ranges (top); 2D maps in vessel forward distance and frequency domain for two frequency ranges (middle); and graph of BF response versus forward distance for two frequency ranges (bottom). Frequency ranges are 5 to150 Hz (left) and 100 to1000 Hz (right).

A.28.2. High-frequency noise maps

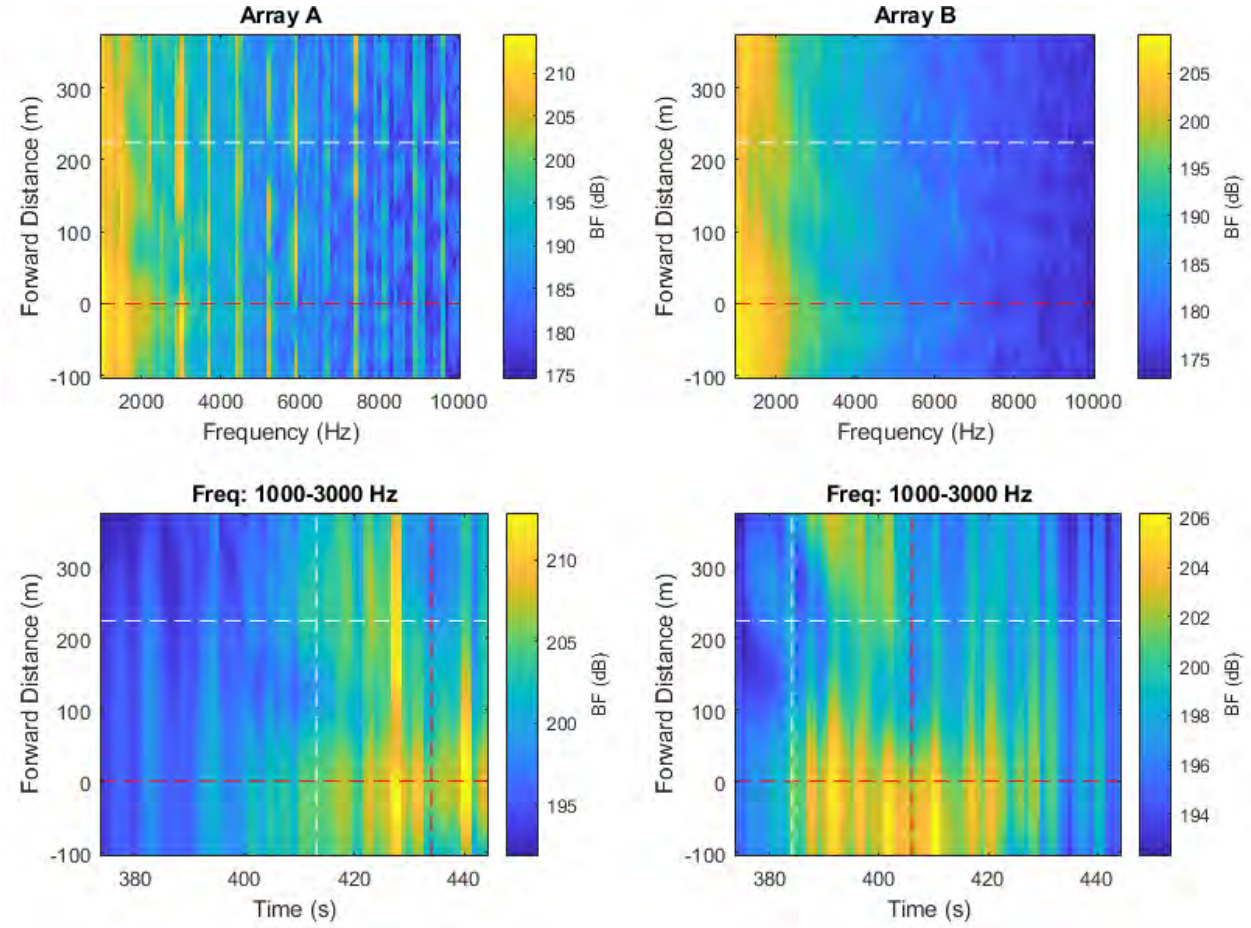

Figure 183 High-frequency noise maps from beamforming with individual arrays. Top maps show the BF response versus forward distance along vessel, measured approximately from the stern, versus frequency. Bottom maps show BF response versus forward distance and snapshot time. Horizontal dashed lines indicate the stern and bow positions of the vessel. Vertical dashed lines represent the CPA times of the bow and stern at each array.

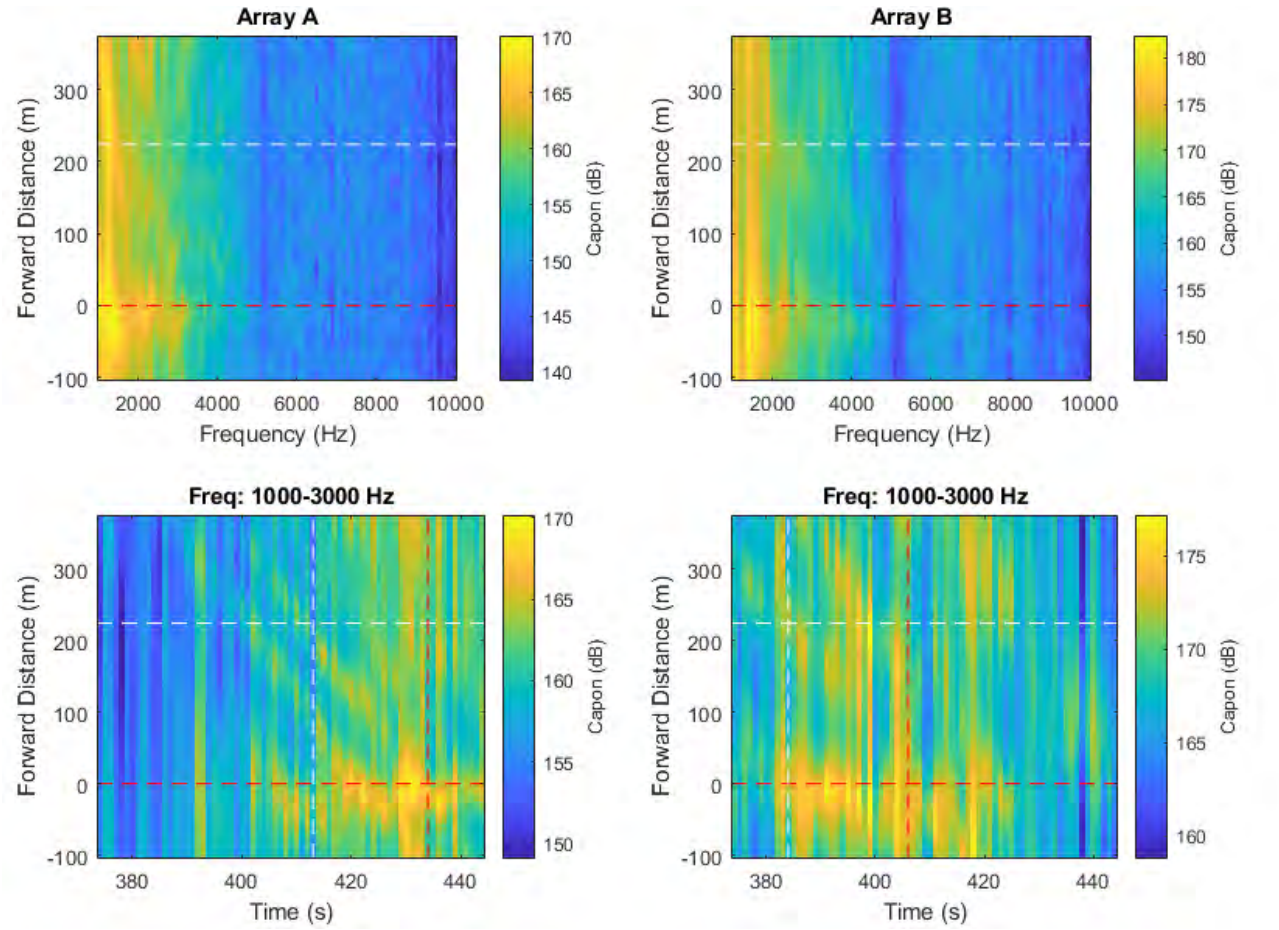

Figure 184 High-frequency noise maps obtained using the spatial spectra provided by the Capon algorithm implemented using individual arrays.

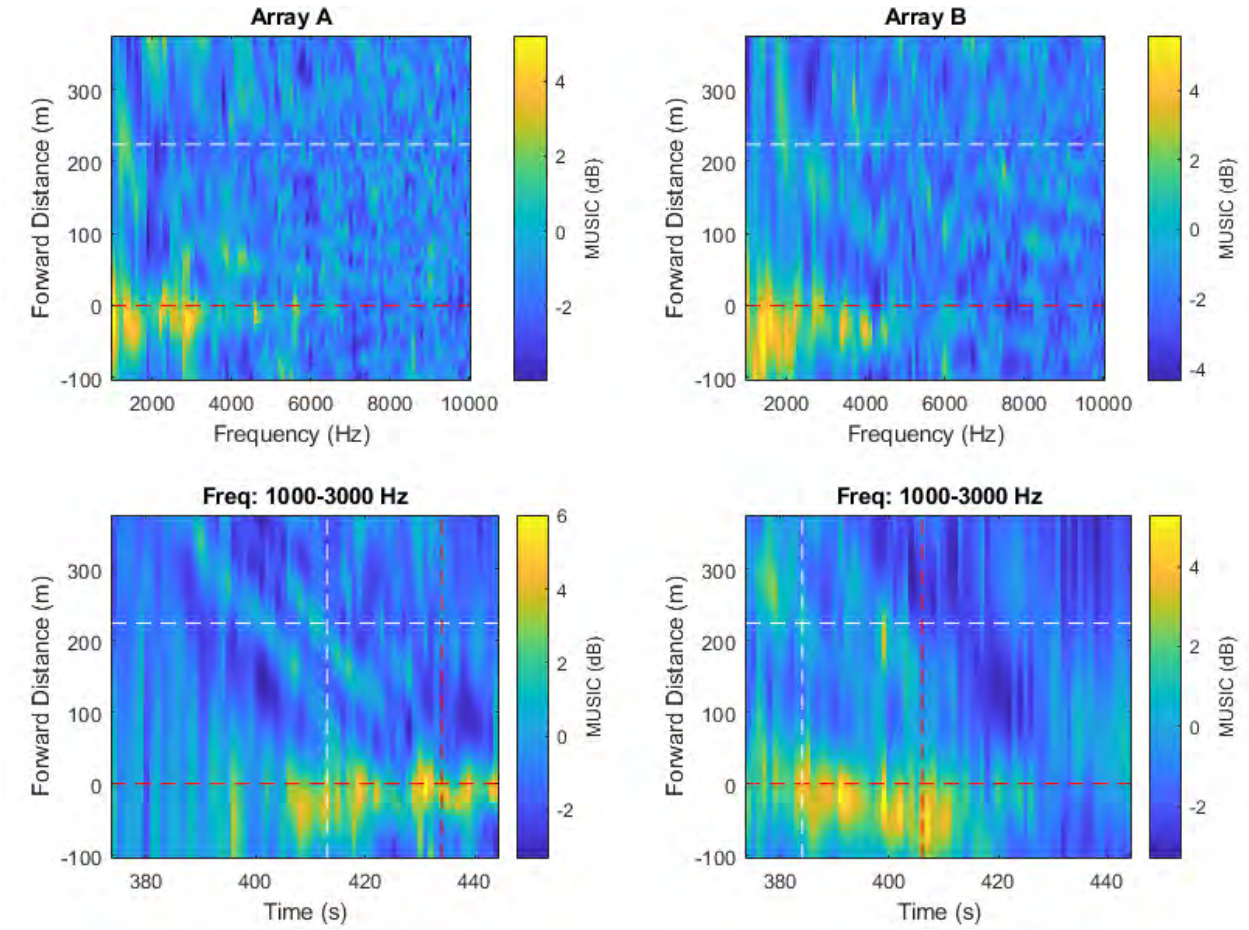

Figure 185 High-frequency noise maps obtained using the spatial spectra provided by the MUSIC algorithm implemented using individual arrays.

A.29. Pass #29 (Type: Bulker. Length: 199 m. Speed: 13.7 kn)

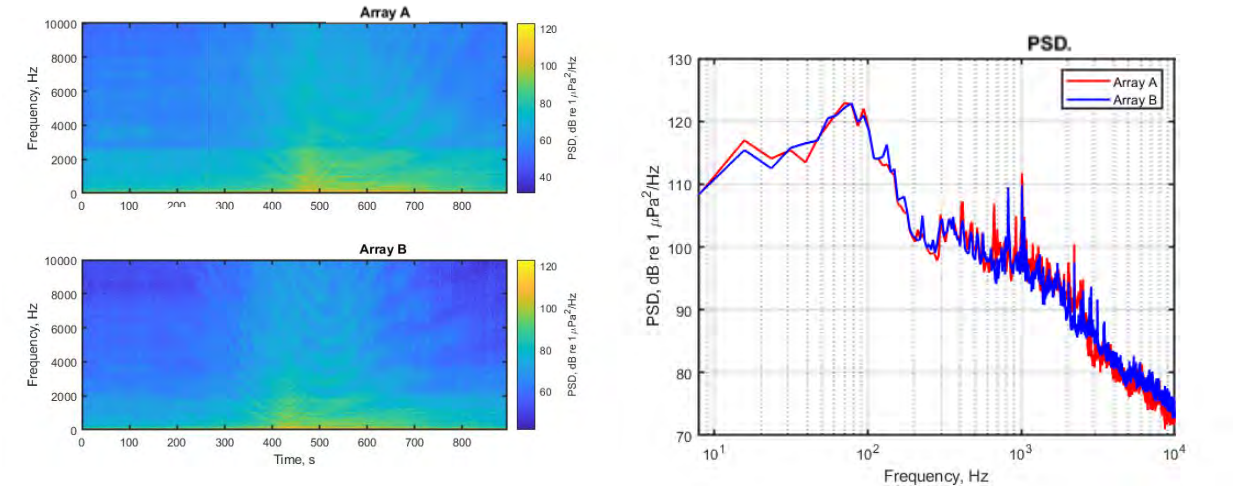

Figure 186 Spectrograms (left) and PSD (right) of ship noise observed on outputs of Arrays A and B.

A.29.1. Low- and mid-frequency noise maps

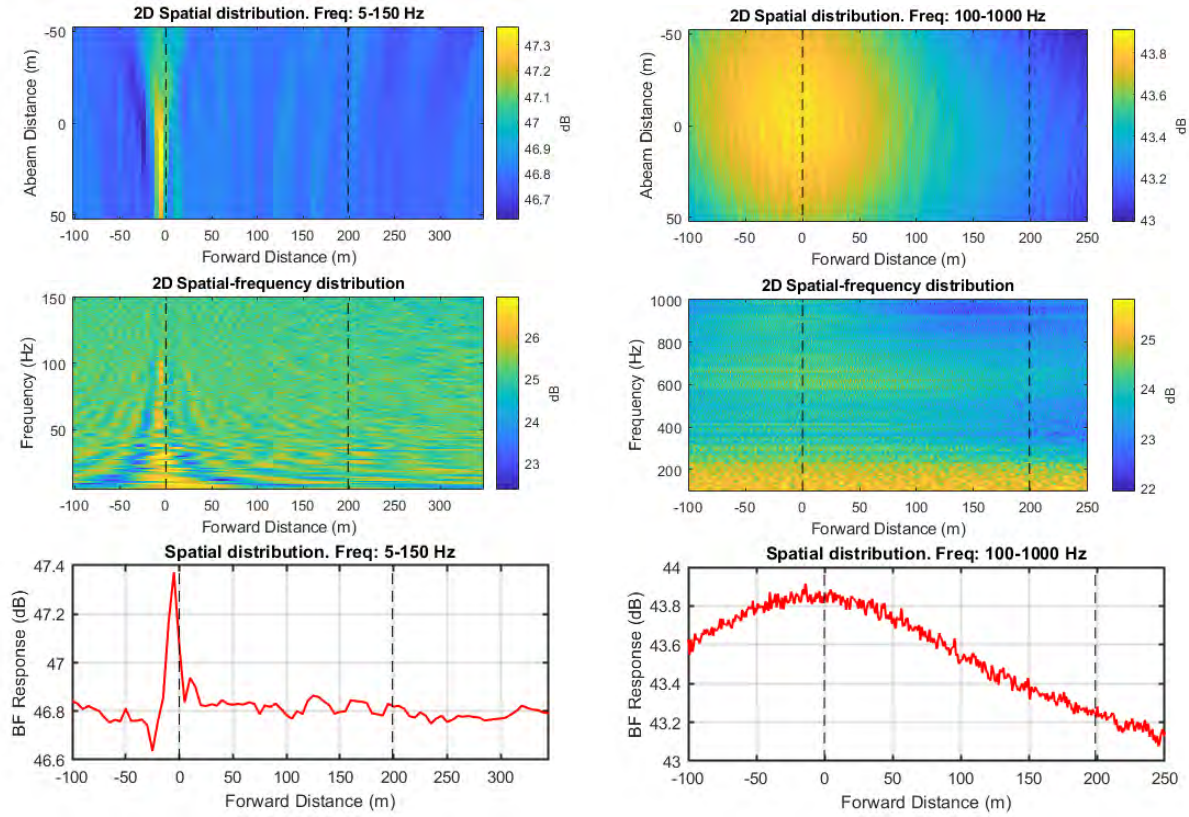

Figure 187 Noise maps from standard beamforming using combined array for Vessel Pass #29: 2D maps in spatial domain for two frequency ranges (top); 2D maps in vessel forward distance and frequency domain for two frequency ranges (middle); and graph of BF response versus forward distance for two frequency ranges (bottom). Frequency ranges are 5 to150 Hz (left) and 100 to1000 Hz (right).

A.29.2. High-frequency noise maps

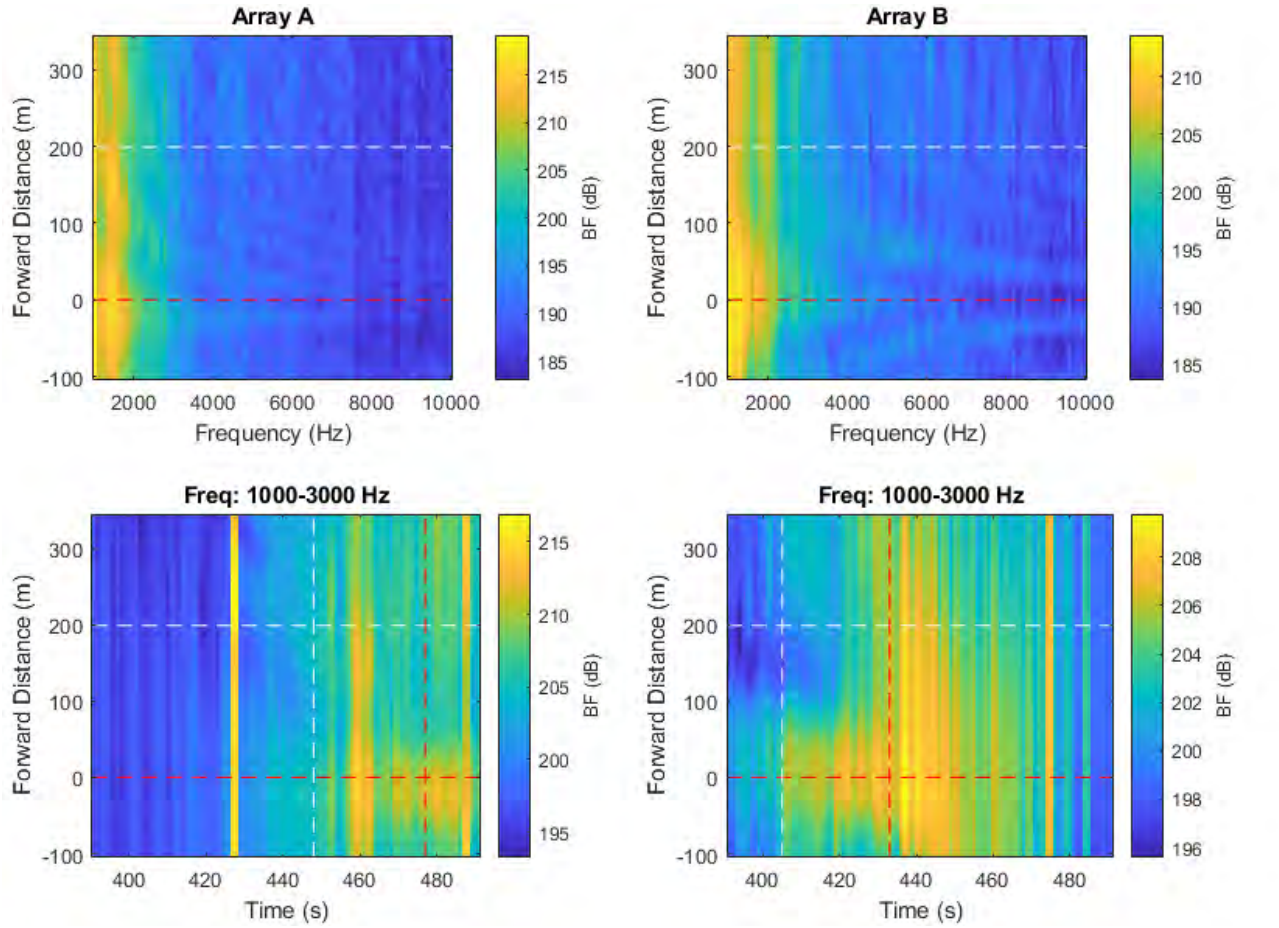

Figure 188 High-frequency noise maps from beamforming with individual arrays. Top maps show the BF response versus forward distance along vessel, measured approximately from the stern, versus frequency. Bottom maps show BF response versus forward distance and snapshot time. Horizontal dashed lines indicate the stern and bow positions of the vessel. Vertical dashed lines represent the CPA times of the bow and stern at each array.

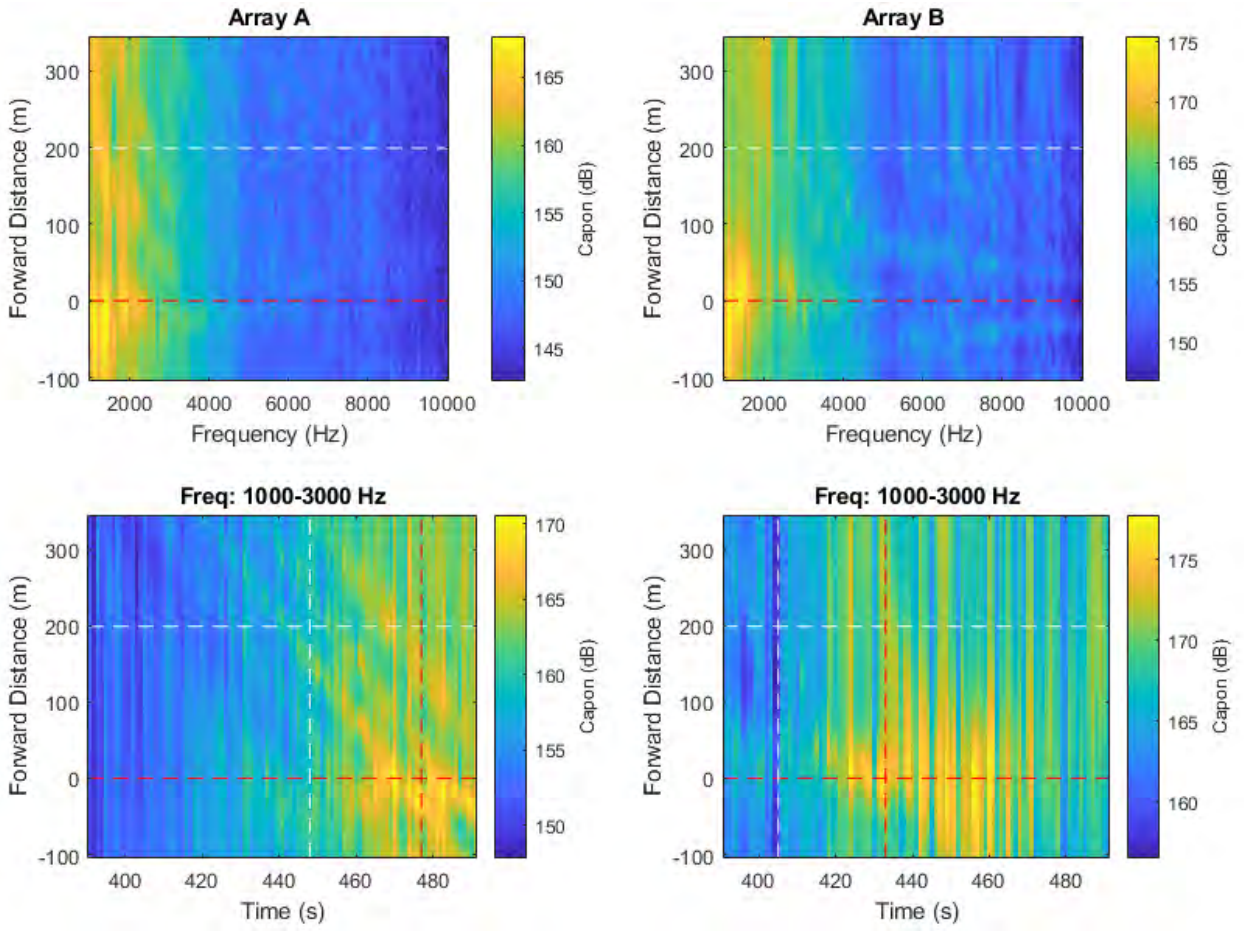

Figure 189 High-frequency noise maps obtained using the spatial spectra provided by the Capon algorithm implemented using individual arrays.

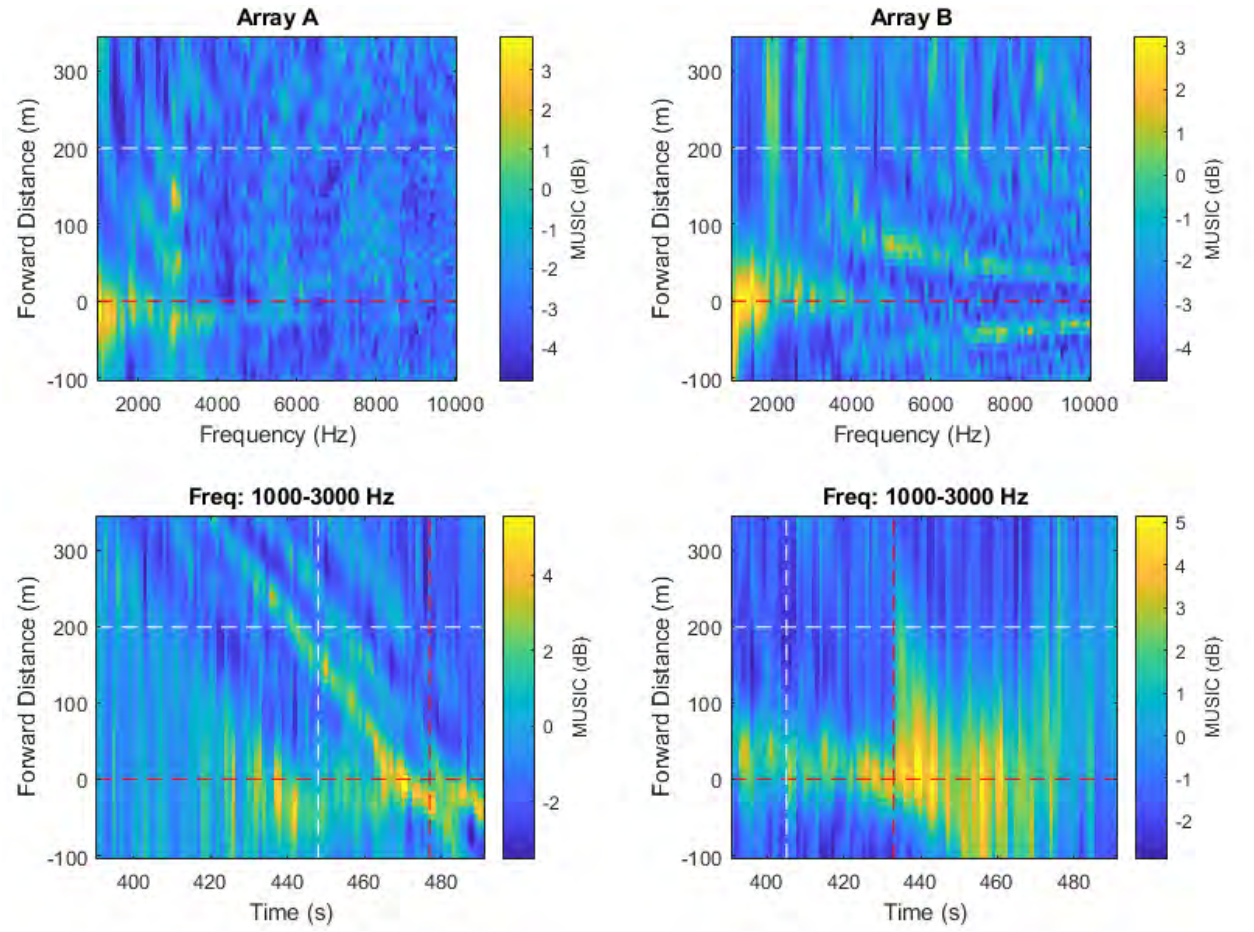

Figure 190 High-frequency noise maps obtained using the spatial spectra provided by the MUSIC algorithm implemented using individual arrays.

A.30. Pass #30 (Type: Container. Length: 304 m. Speed: 19.1 kn)

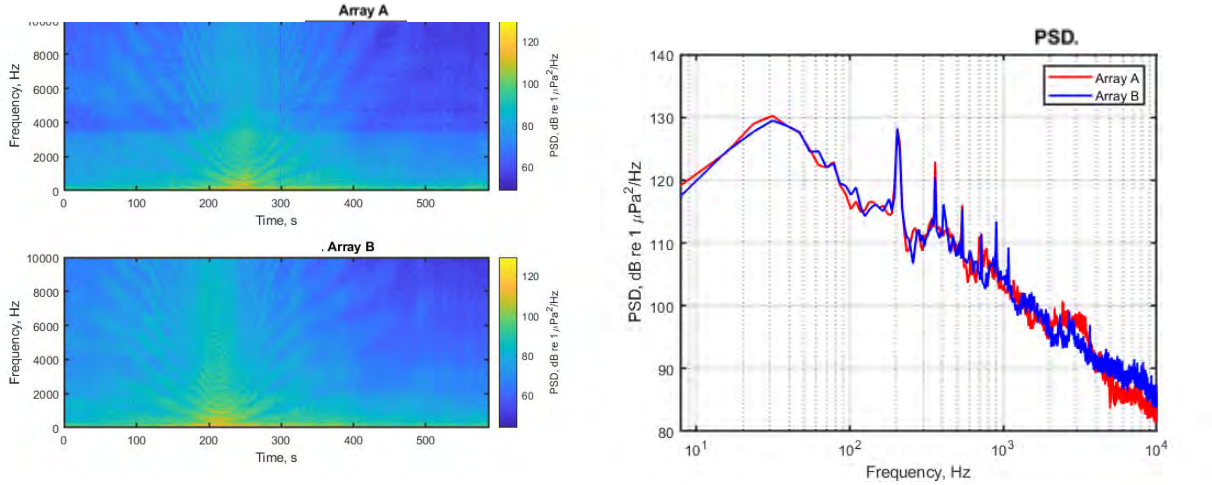

Figure 191 Spectrograms (left) and PSD (right) of ship noise observed on outputs of Arrays A and B.

A.30.1. Low- and mid-frequency noise maps

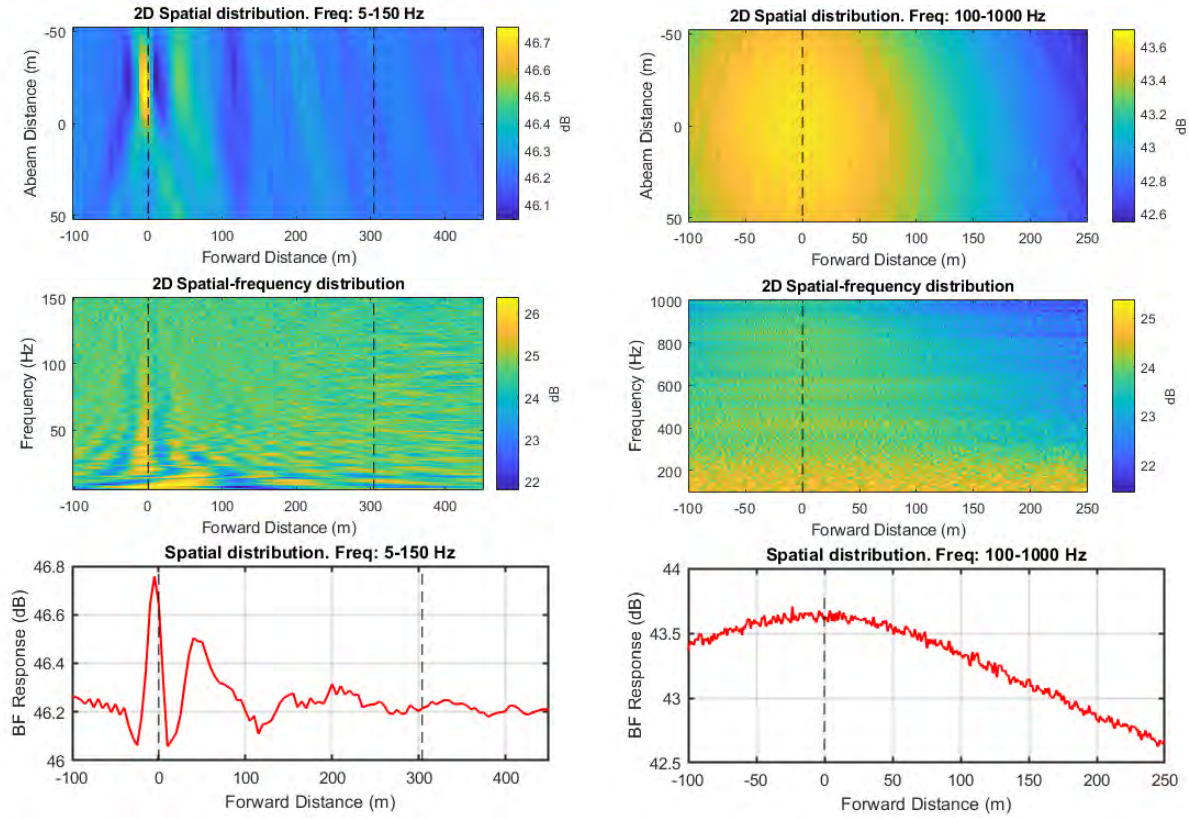

Figure 192 Noise maps from standard beamforming using combined array for Vessel Pass #30: 2D maps in spatial domain for two frequency ranges (top); 2D maps in vessel forward distance and frequency domain for two frequency ranges (middle); and graph of BF response versus forward distance for two frequency ranges (bottom). Frequency ranges are 5 to150 Hz (left) and 100 to1000 Hz (right).

A.30.2. High-frequency noise maps

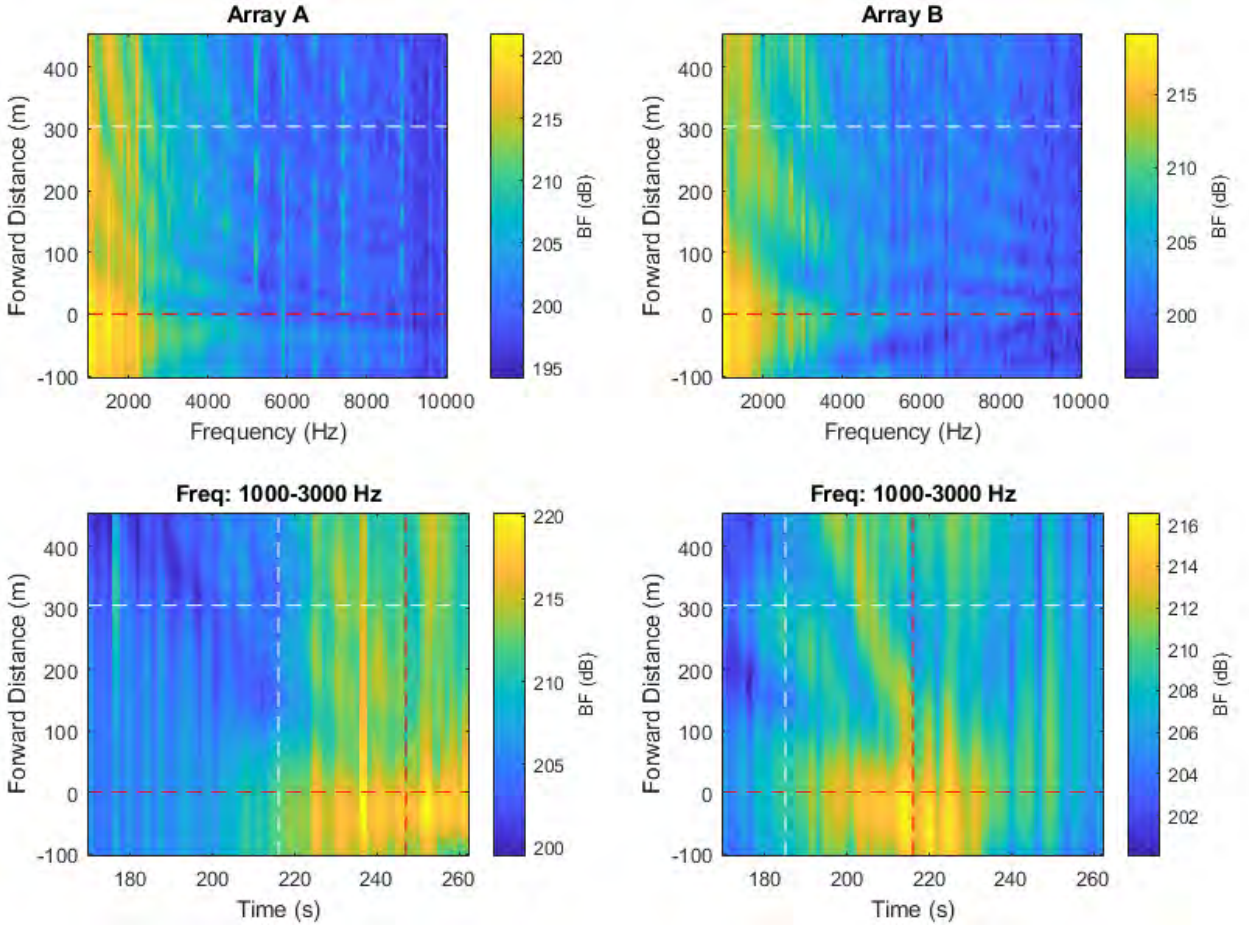

Figure 193 High-frequency noise maps from beamforming with individual arrays. Top maps show the BF response versus forward distance along vessel, measured approximately from the stern, versus frequency. Bottom maps show BF response versus forward distance and snapshot time. Horizontal dashed lines indicate the stern and bow positions of the vessel. Vertical dashed lines represent the CPA times of the bow and stern at each array.

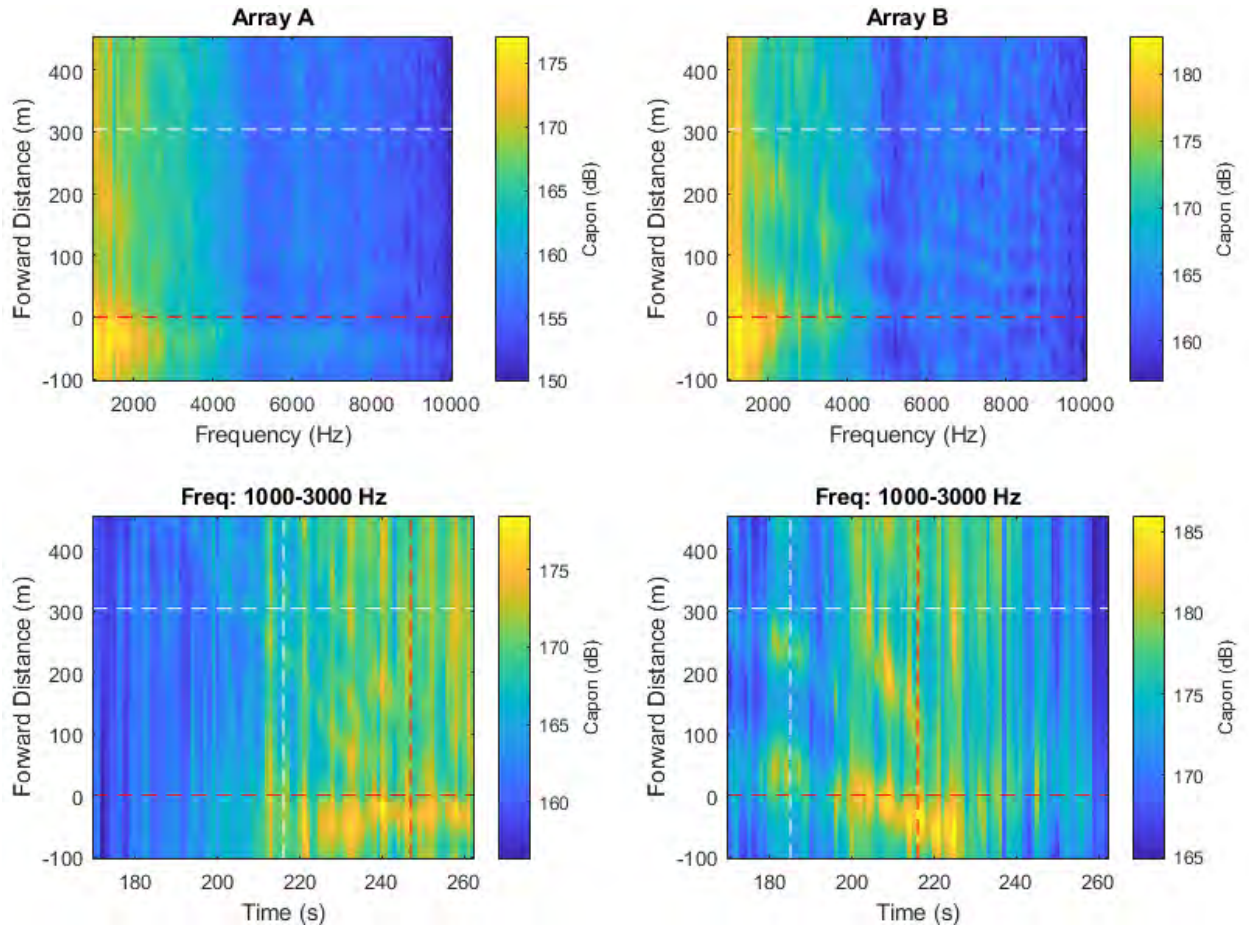

Figure 194 High-frequency noise maps obtained using the spatial spectra provided by the Capon algorithm implemented using individual arrays.

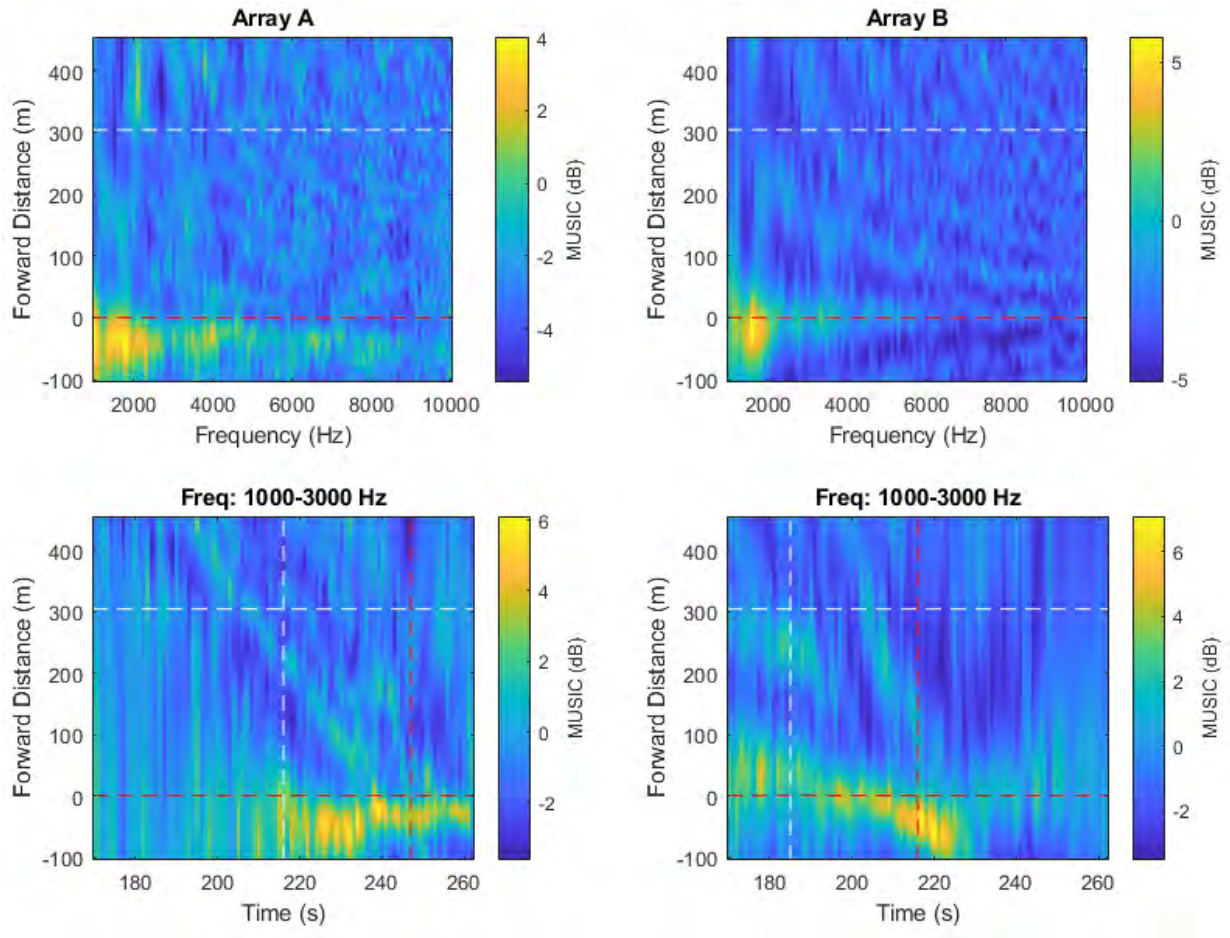

Figure 195 High-frequency noise maps obtained using the spatial spectra provided by the MUSIC algorithm implemented using individual arrays.

A.31. Pass #31 (Type: Bulker. Length: 229 m. Speed: 14.2 kn)

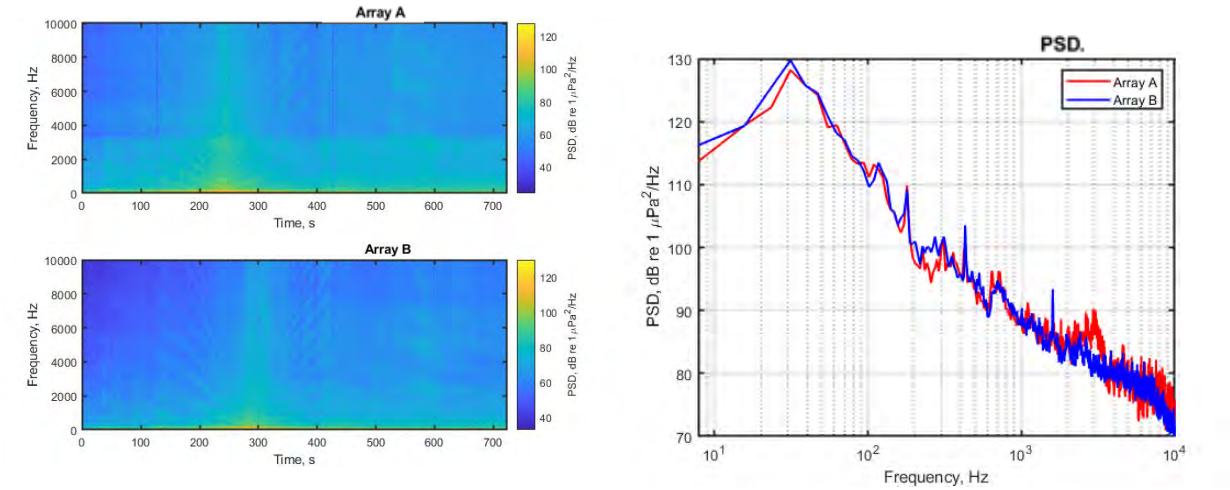

Figure 196 Spectrograms (left) and PSD (right) of ship noise observed on outputs of Arrays A and B.

A.31.1. Low- and mid-frequency noise maps

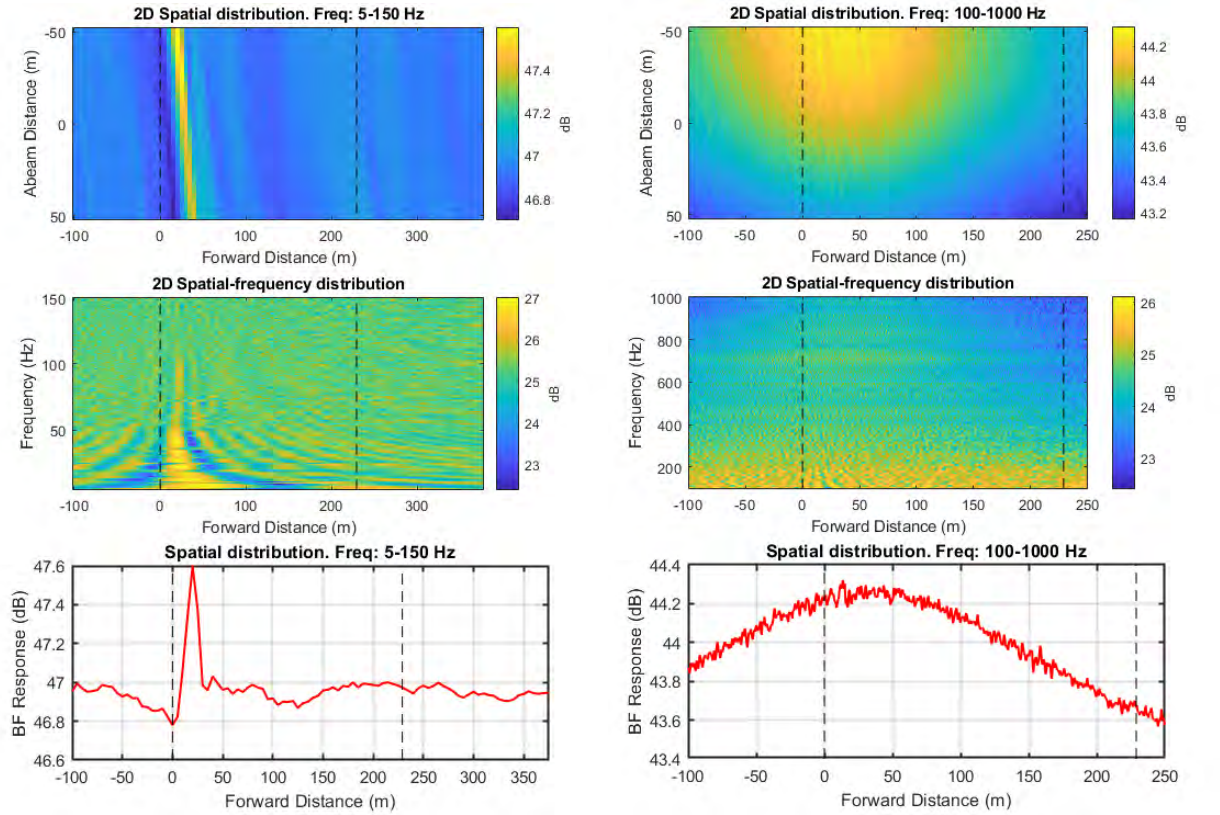

Figure 197 Noise maps from standard beamforming using combined array for Vessel Pass #31: 2D maps in spatial domain for two frequency ranges (top); 2D maps in vessel forward distance and frequency domain for two frequency ranges (middle); and graph of BF response versus forward distance for two frequency ranges (bottom). Frequency ranges are 5 to150 Hz (left) and 100 to1000 Hz (right).

A.31.2. High-frequency noise maps

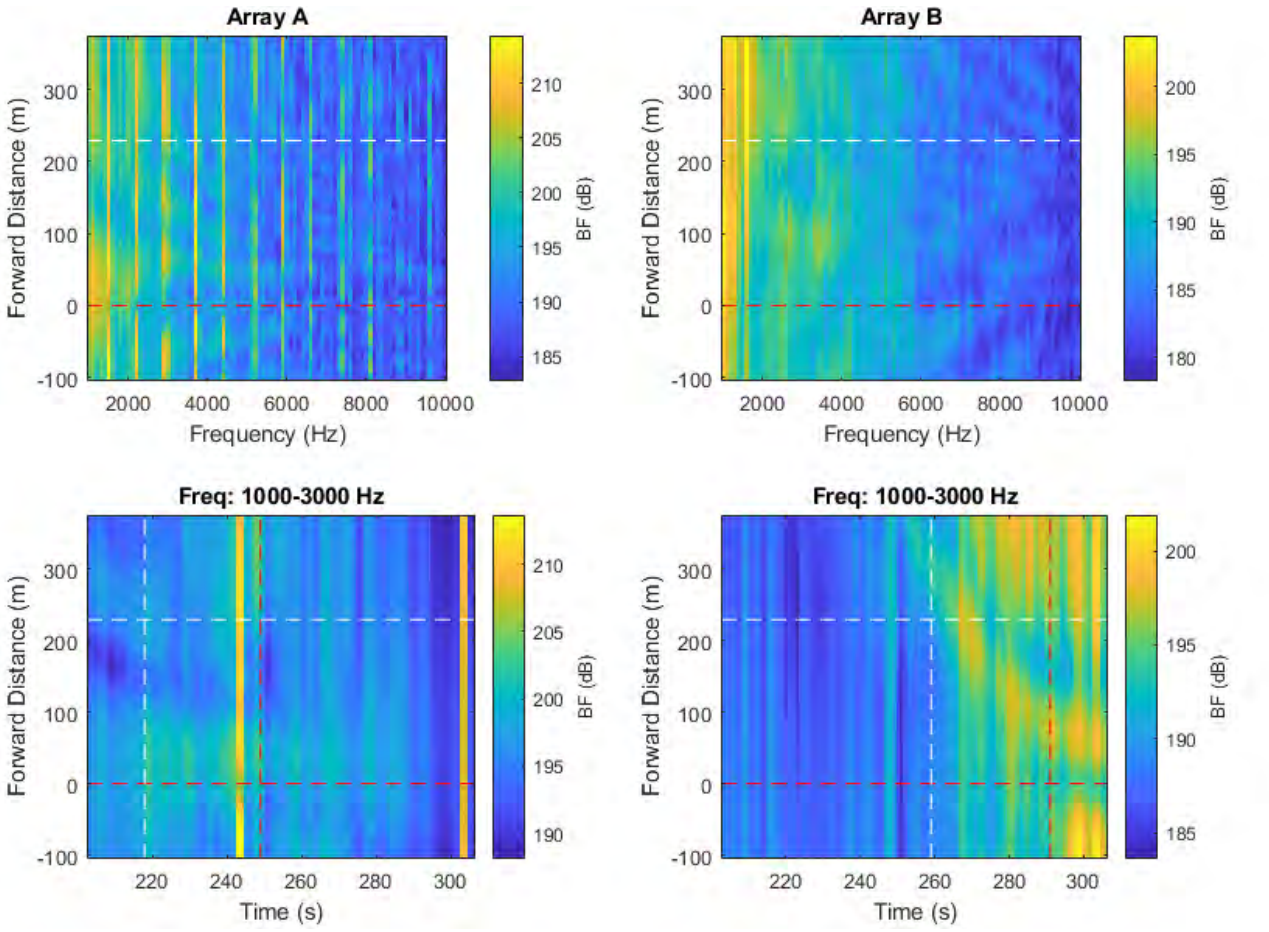

Figure 198 High-frequency noise maps from beamforming with individual arrays. Top maps show the BF response versus forward distance along vessel, measured approximately from the stern, versus frequency. Bottom maps show BF response versus forward distance and snapshot time. Horizontal dashed lines indicate the stern and bow positions of the vessel. Vertical dashed lines represent the CPA times of the bow and stern at each array.

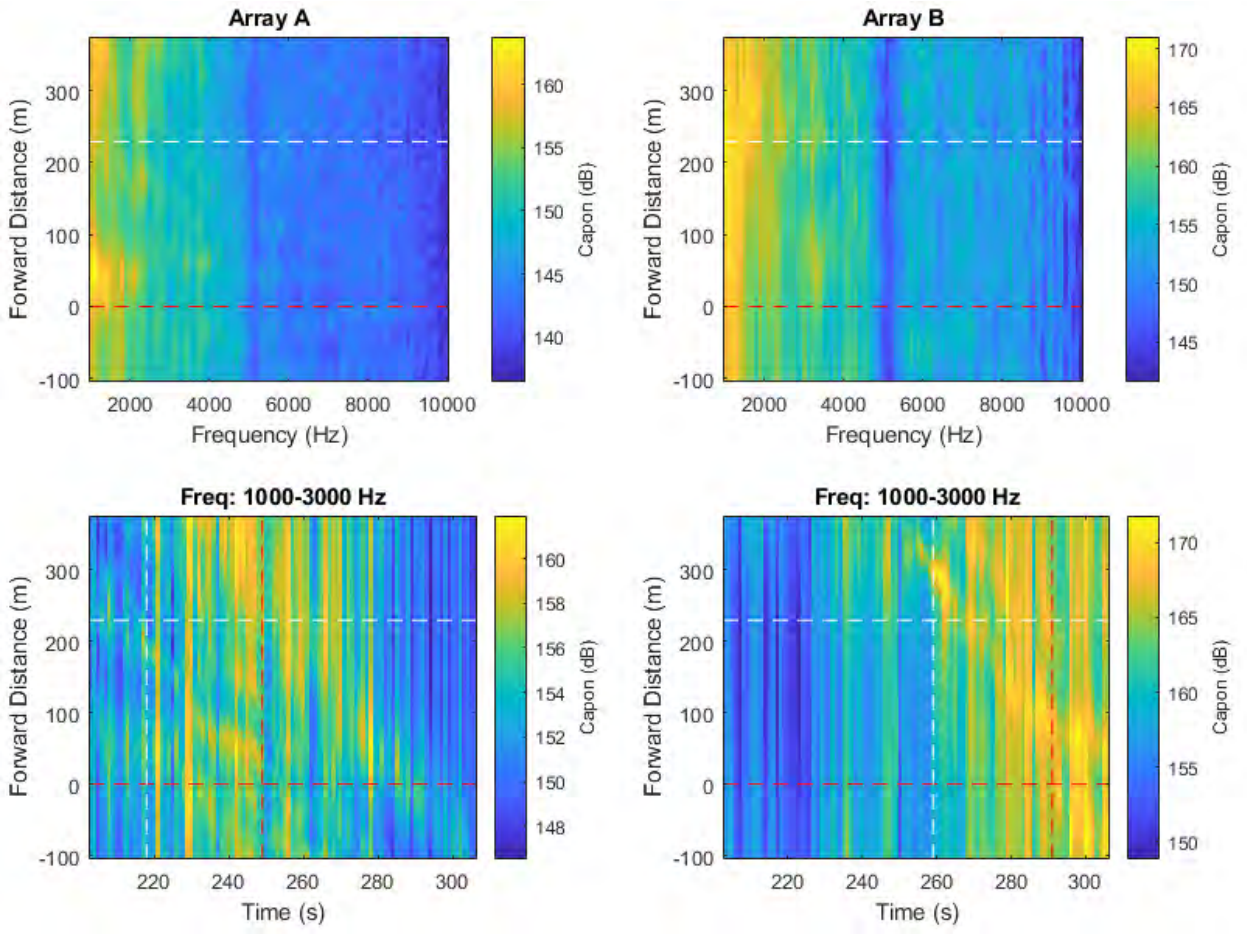

Figure 199 High-frequency noise maps obtained using the spatial spectra provided by the Capon algorithm implemented using individual arrays.

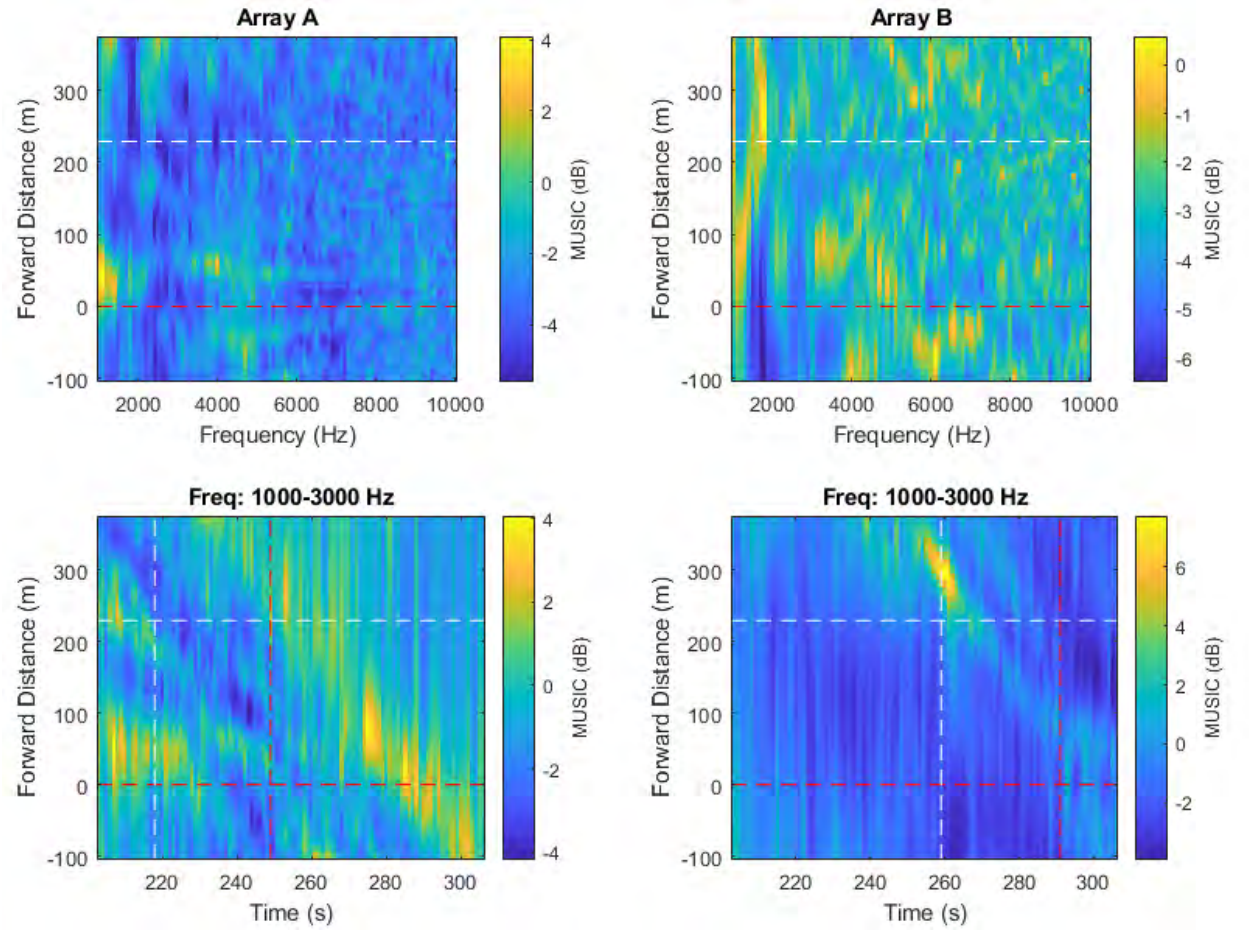

Figure 200 High-frequency noise maps obtained using the spatial spectra provided by the MUSIC algorithm implemented using individual arrays.

A.32. Pass #32 (Type: Bulker. Length: 229 m. Speed: 12.6 kn)

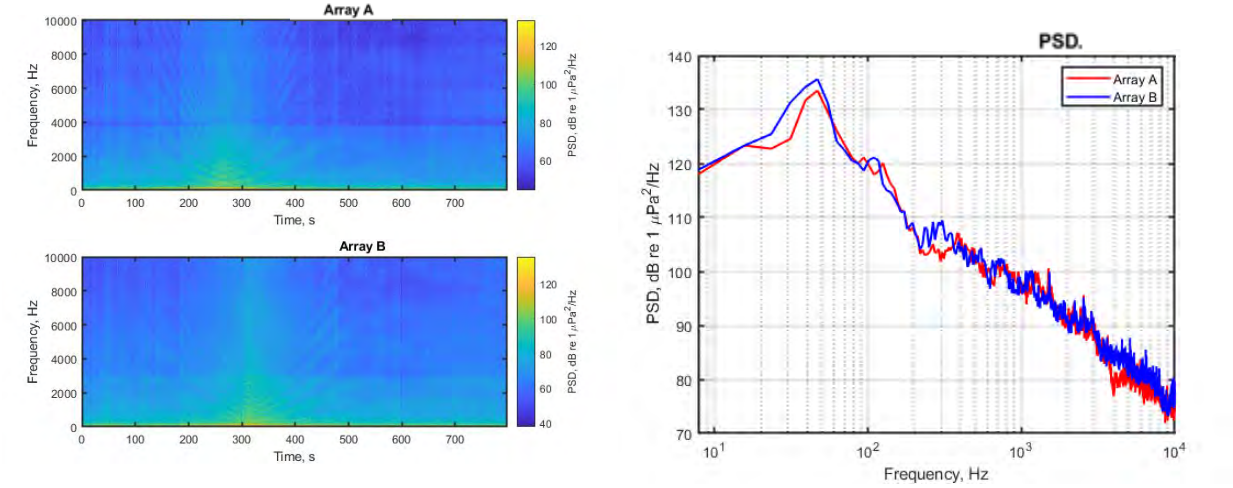

Figure 201 Spectrograms (left) and PSD (right) of ship noise observed on outputs of Arrays A and B.

A.32.1. Low- and mid-frequency noise maps

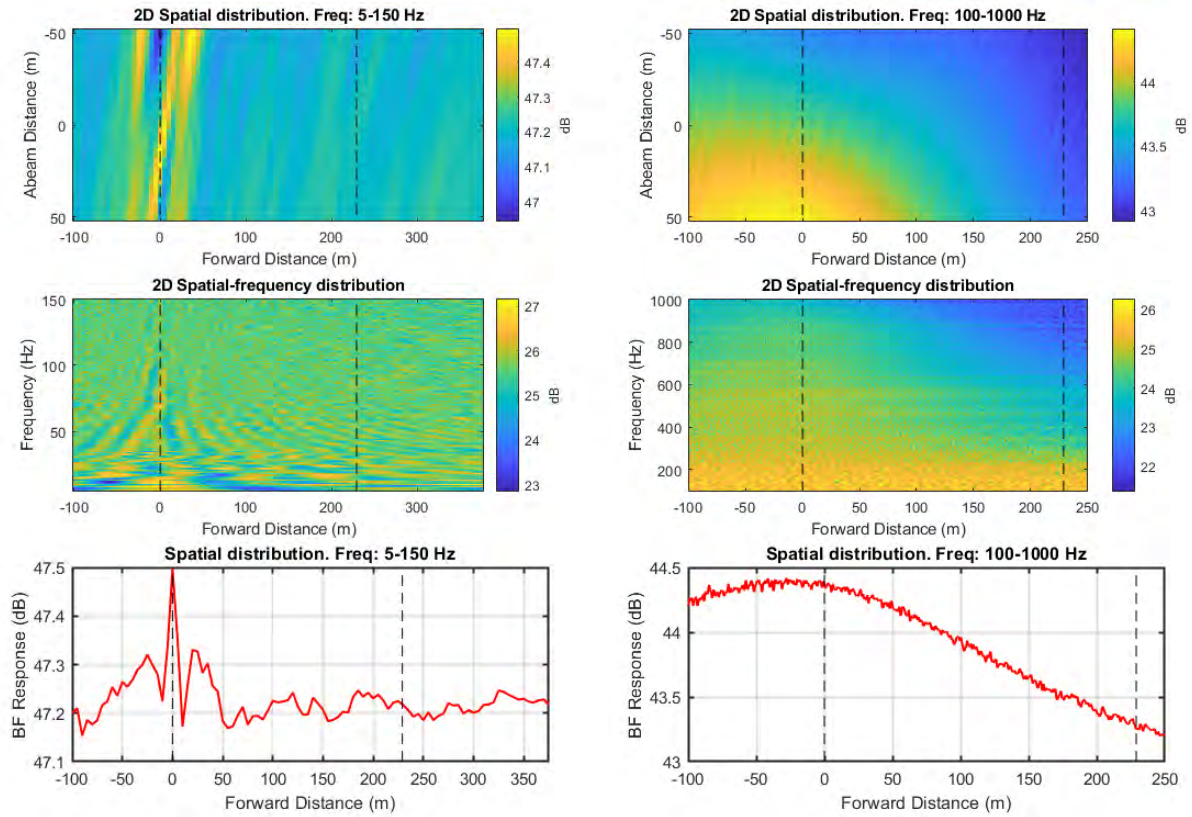

Figure 202 Noise maps from standard beamforming using combined array for Vessel Pass #32: 2D maps in spatial domain for two frequency ranges (top); 2D maps in vessel forward distance and frequency domain for two frequency ranges (middle); and graph of BF response versus forward distance for two frequency ranges (bottom). Frequency ranges are 5 to150 Hz (left) and 100 to1000 Hz (right).

A.32.2. High-frequency noise maps

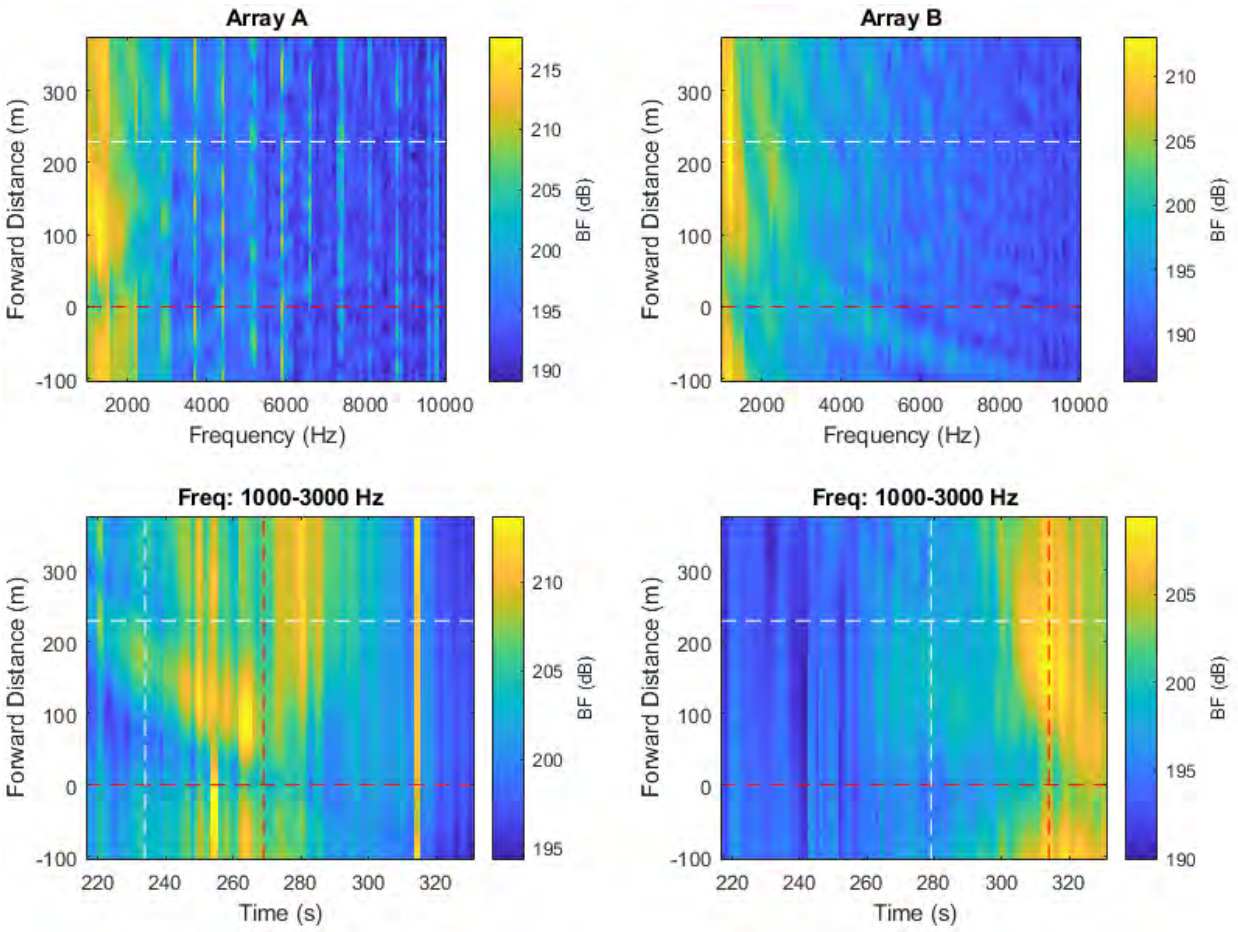

Figure 203 High-frequency noise maps from beamforming with individual arrays. Top maps show the BF response versus forward distance along vessel, measured approximately from the stern, versus frequency. Bottom maps show BF response versus forward distance and snapshot time. Horizontal dashed lines indicate the stern and bow positions of the vessel. Vertical dashed lines represent the CPA times of the bow and stern at each array.

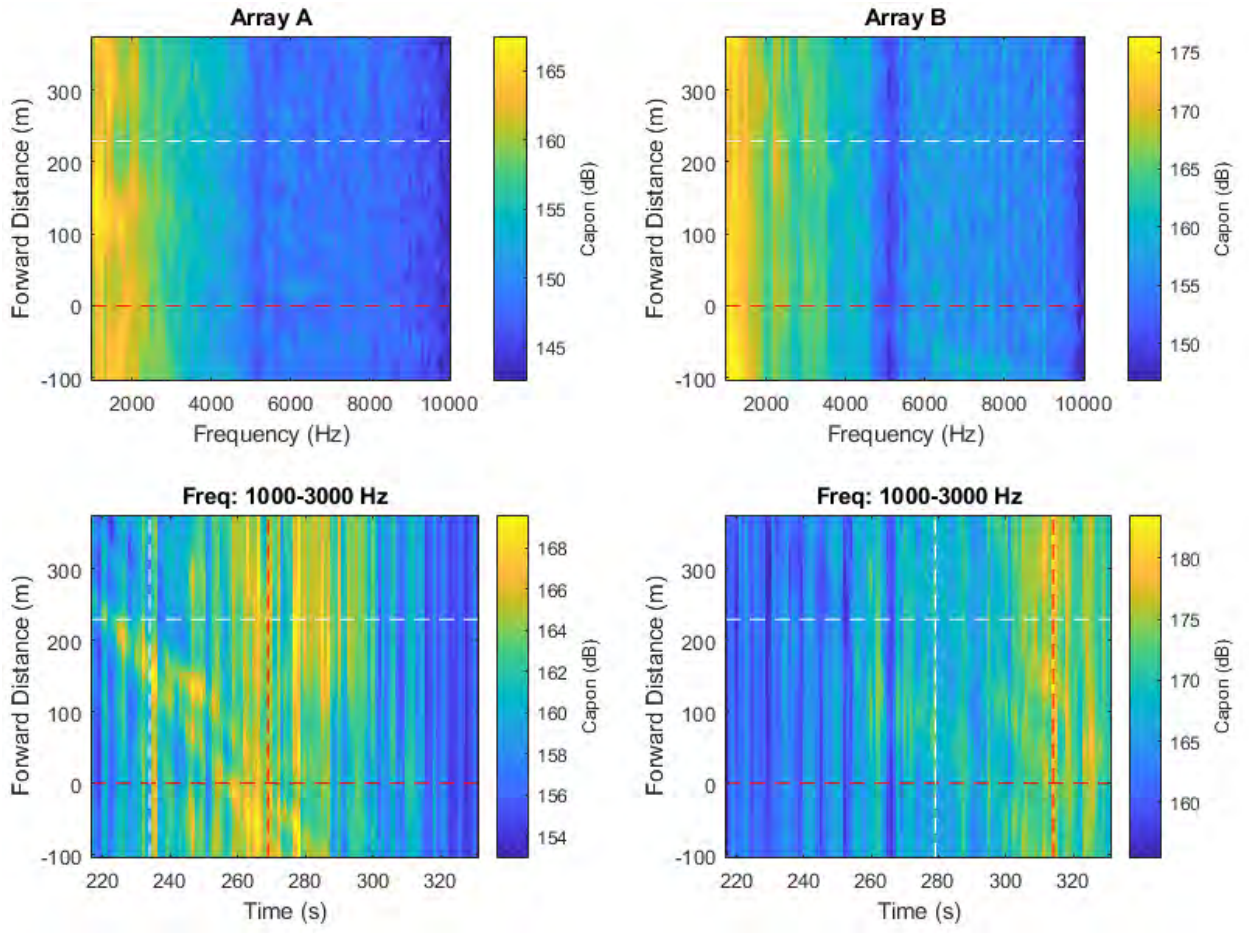

Figure 204 High-frequency noise maps obtained using the spatial spectra provided by the Capon algorithm implemented using individual arrays.

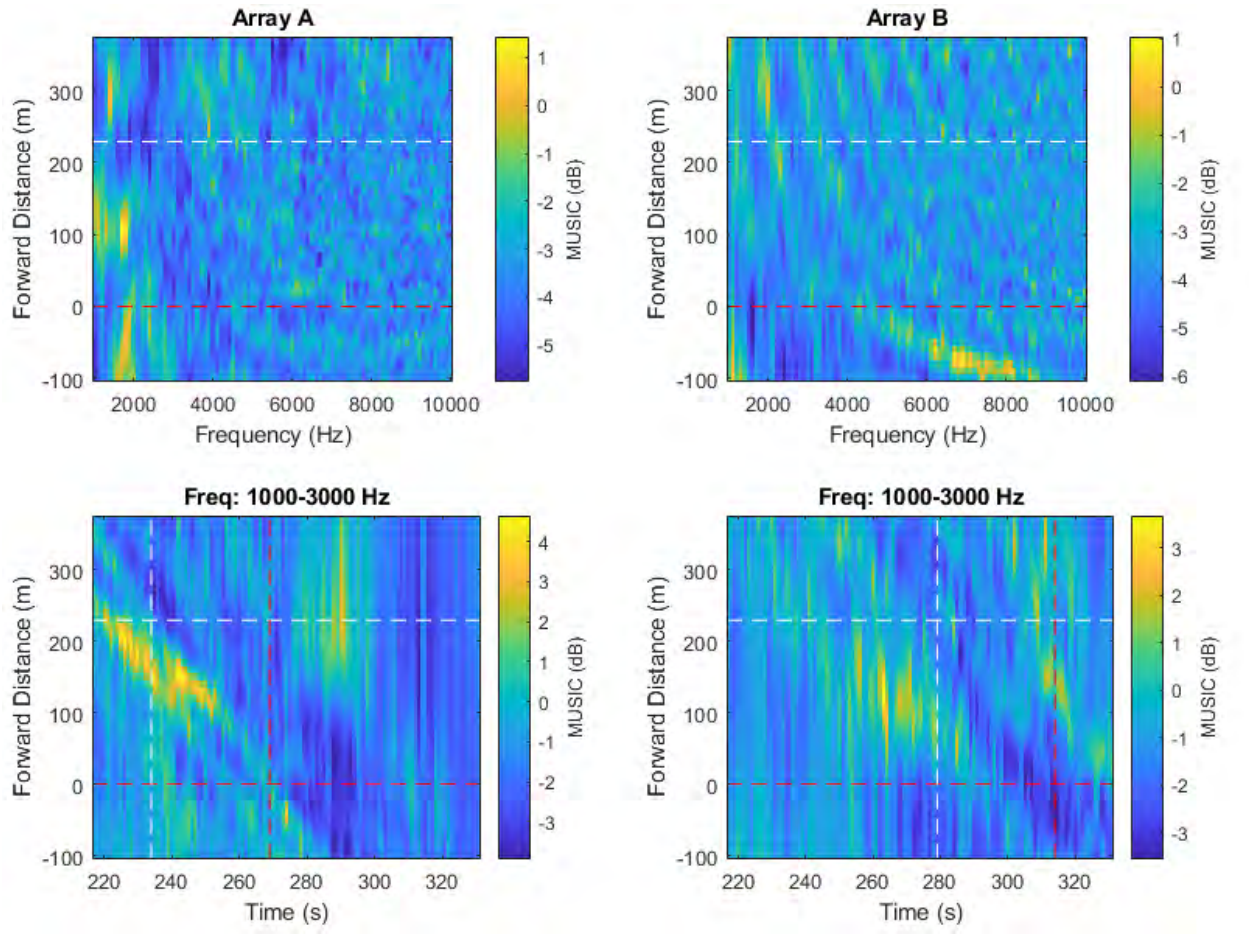

Figure 205 High-frequency noise maps obtained using the spatial spectra provided by the MUSIC algorithm implemented using individual arrays.

A.33. Pass #33 (Type: Vehicle Carrier. Length: 199 m. Speed: 17.2 kn)

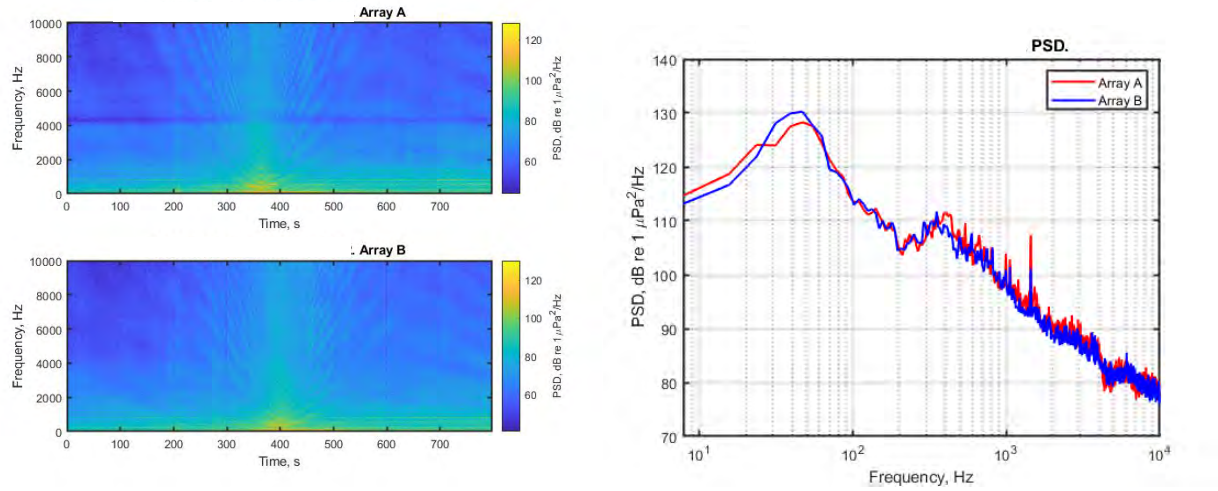

Figure 206 Spectrograms (left) and PSD (right) of ship noise observed on outputs of Arrays A and B.

A.33.1. Low- and mid-frequency noise maps

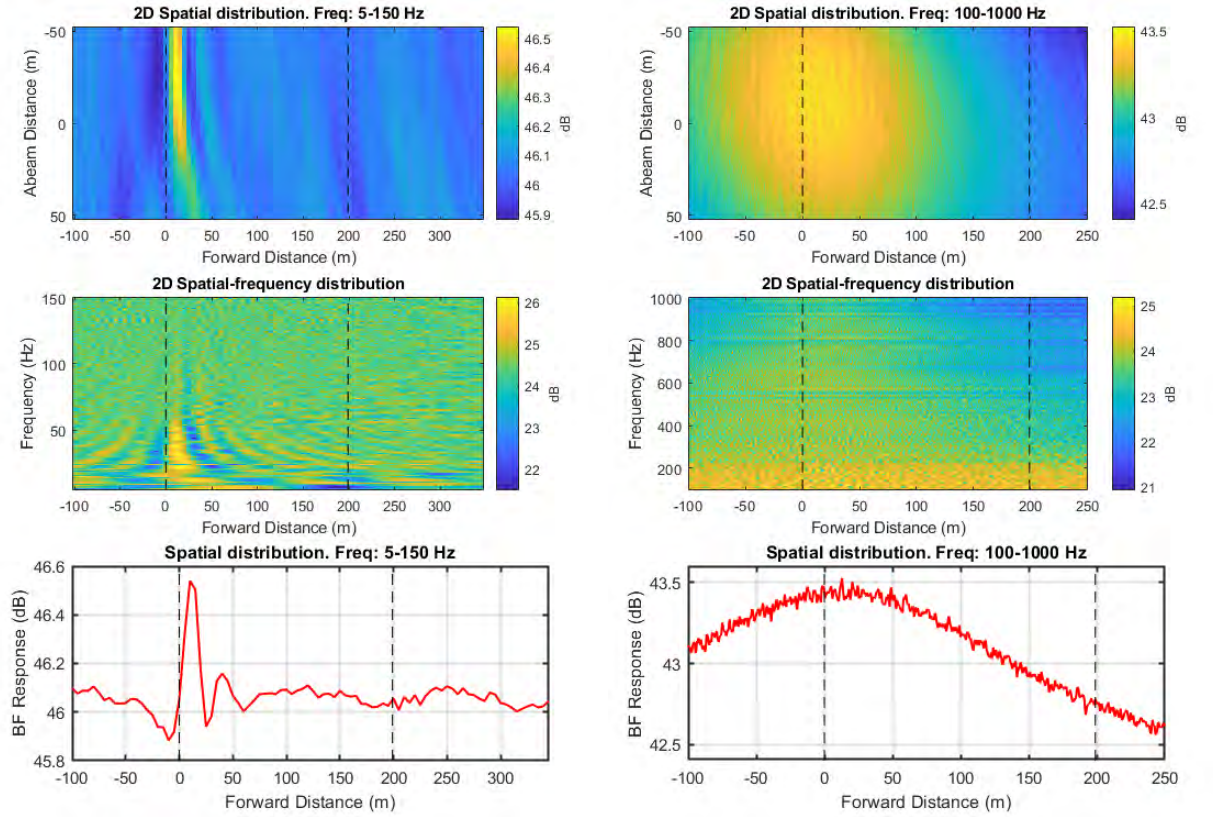

Figure 207 Noise maps from standard beamforming using combined array for Vessel Pass #34: 2D maps in spatial domain for two frequency ranges (top); 2D maps in vessel forward distance and frequency domain for two frequency ranges (middle); and graph of BF response versus forward distance for two frequency ranges (bottom). Frequency ranges are 5 to150 Hz (left) and 100 to1000 Hz (right).

A.33.2. High-frequency noise maps

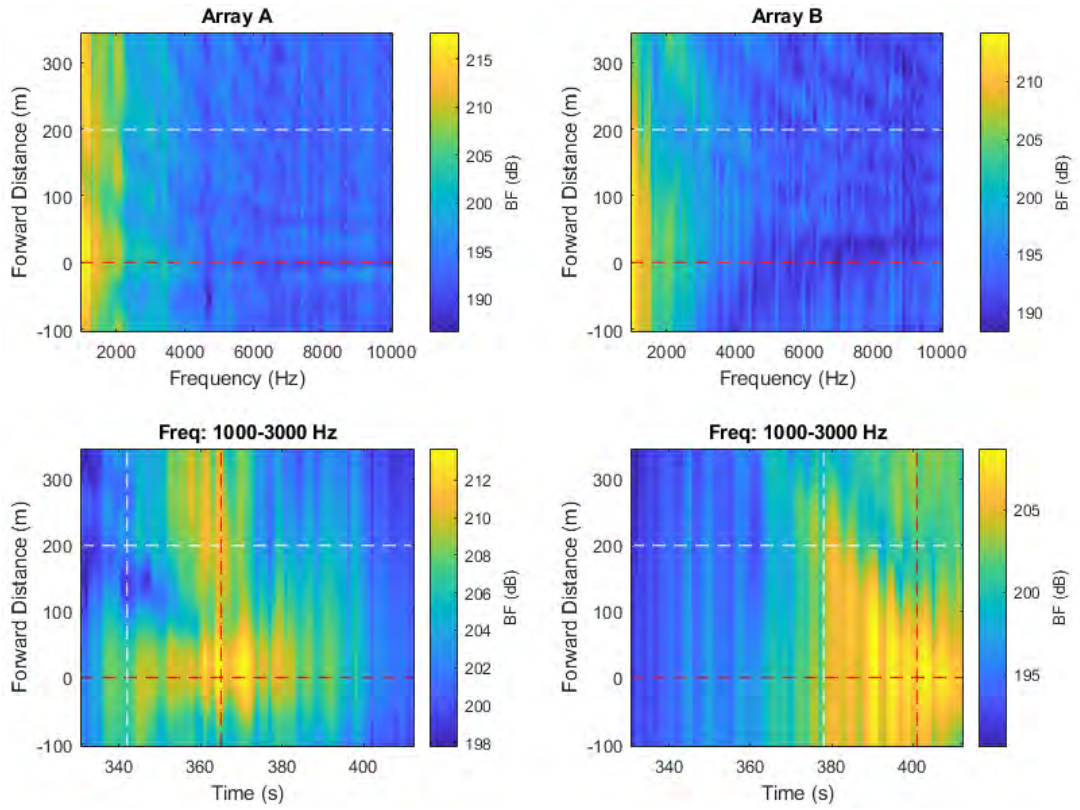

Figure 208 High-frequency noise maps from beamforming with individual arrays. Top maps show the BF response versus forward distance along vessel, measured approximately from the stern, versus frequency. Bottom maps show BF response versus forward distance and snapshot time. Horizontal dashed lines indicate the stern and bow positions of the vessel. Vertical dashed lines represent the CPA times of the bow and stern at each array.

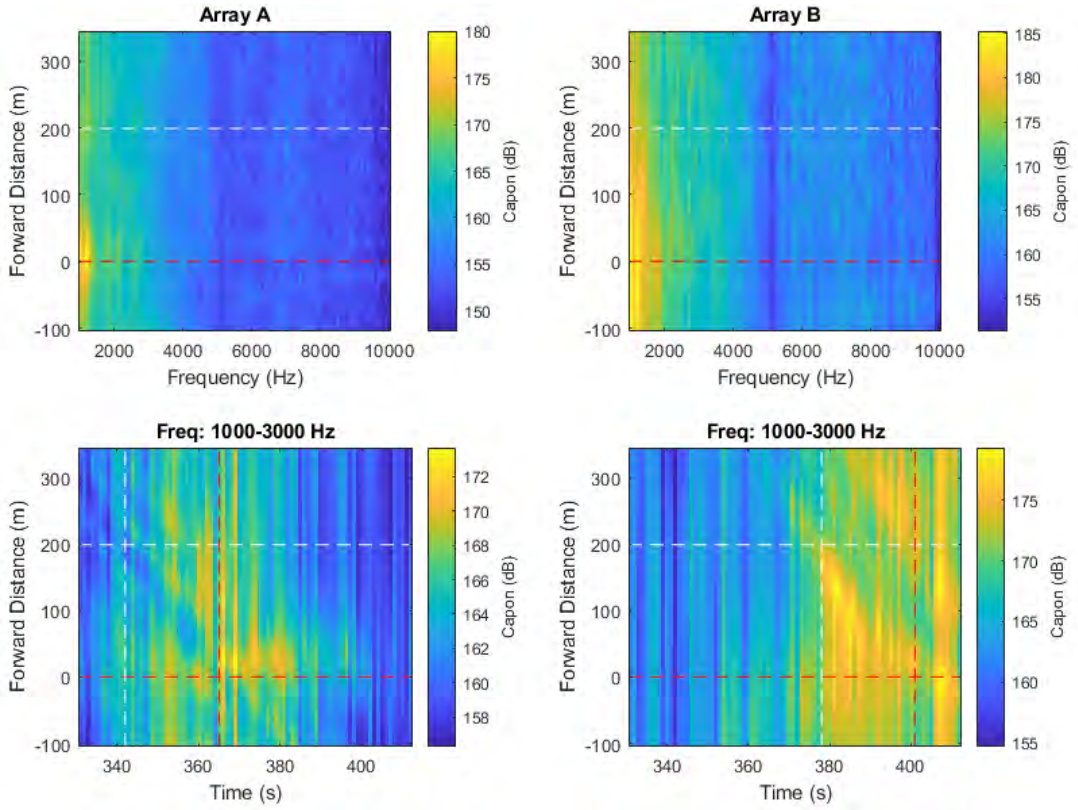

Figure 209 High-frequency noise maps obtained using the spatial spectra provided by the Capon algorithm implemented using individual arrays.

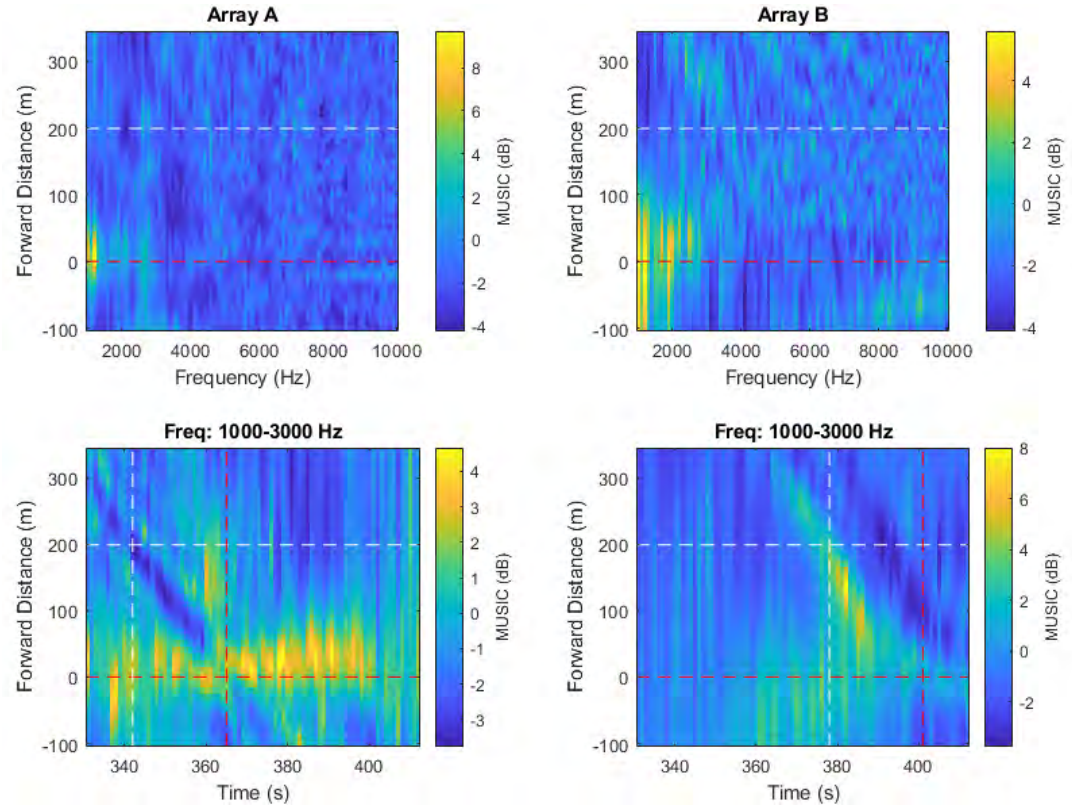

Figure 210 High-frequency noise maps obtained using the spatial spectra provided by the MUSIC algorithm implemented using individual arrays.

A.34. Pass #34 (Type: Bulker. Length: 225 m. Speed: 13.2 kn)

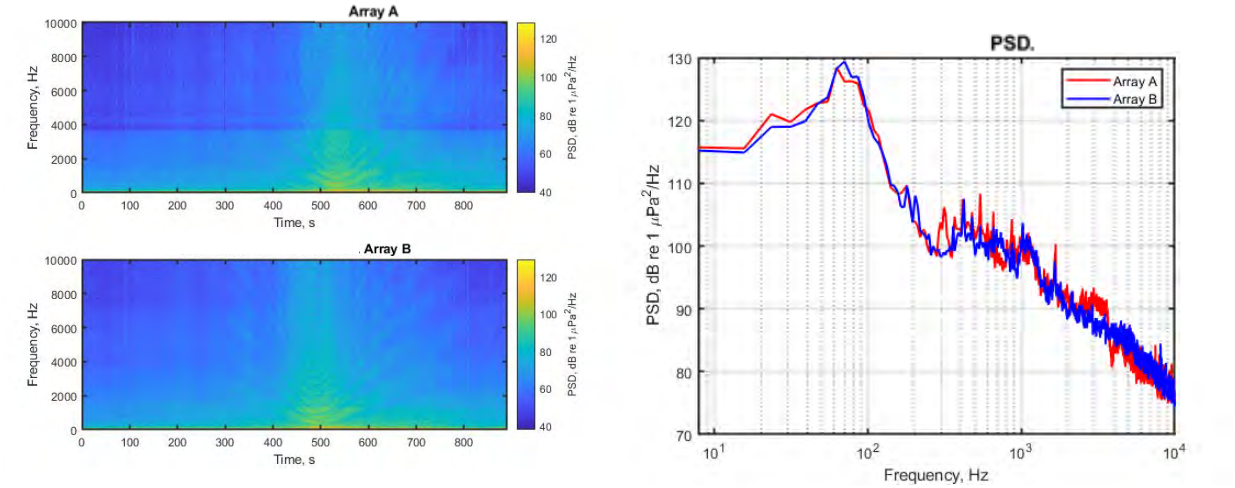

Figure 211 Spectrograms (left) and PSD (right) of ship noise observed on outputs of Arrays A and B.

A.34.1. Low- and mid-frequency noise maps

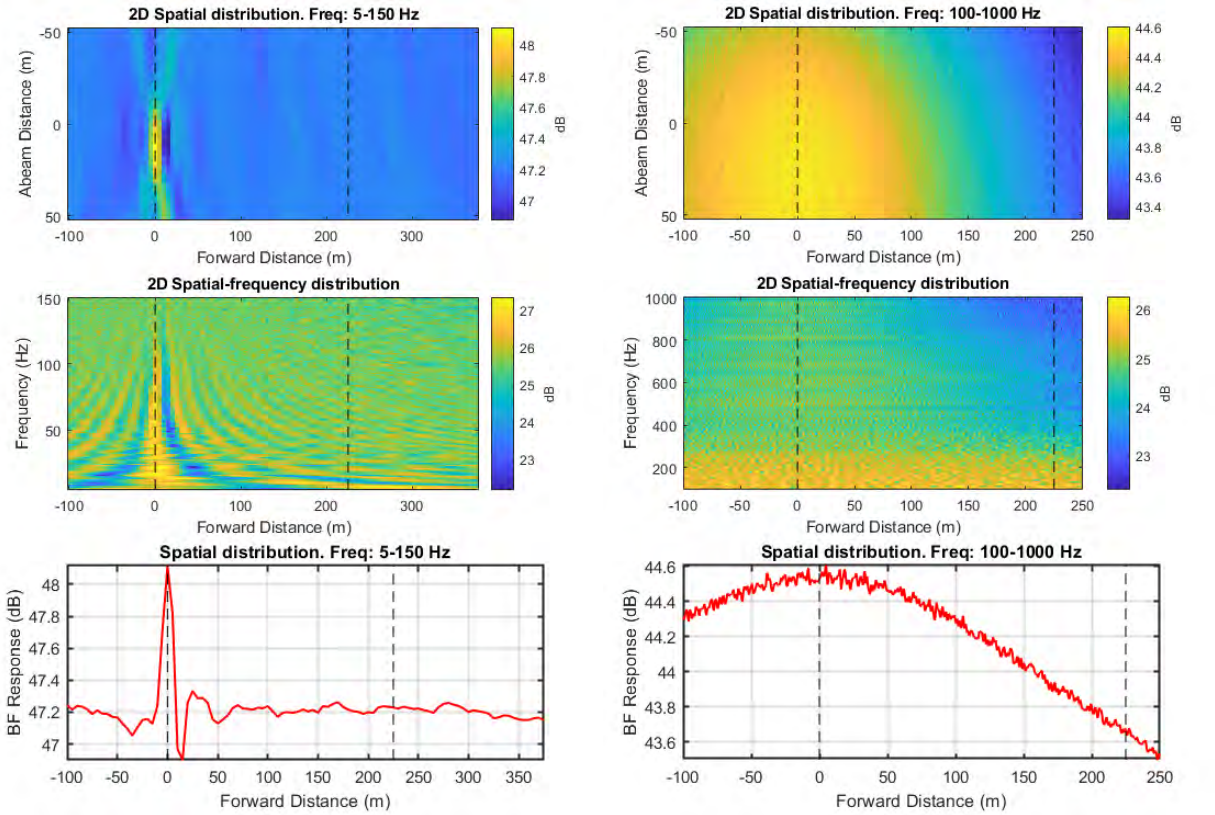

Figure 212 Noise maps from standard beamforming using combined array for Vessel Pass #34: 2D maps in spatial domain for two frequency ranges (top); 2D maps in vessel forward distance and frequency domain for two frequency ranges (middle); and graph of BF response versus forward distance for two frequency ranges (bottom). Frequency ranges are 5 to150 Hz (left) and 100 to1000 Hz (right).

A.34.2. High-frequency noise maps

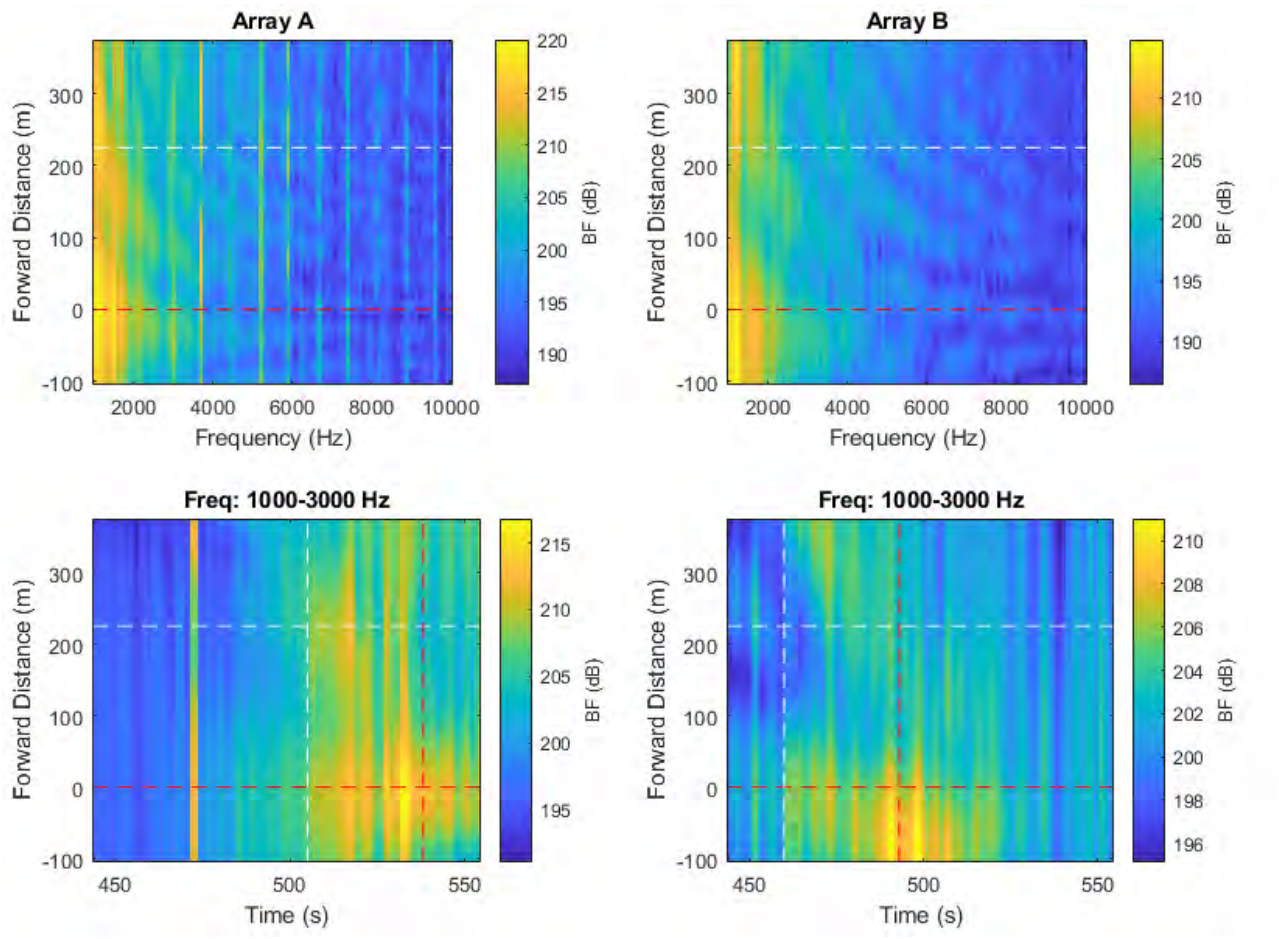

Figure 213 High-frequency noise maps from beamforming with individual arrays. Top maps show the BF response versus forward distance along vessel, measured approximately from the stern, versus frequency. Bottom maps show BF response versus forward distance and snapshot time. Horizontal dashed lines indicate the stern and bow positions of the vessel. Vertical dashed lines represent the CPA times of the bow and stern at each array.

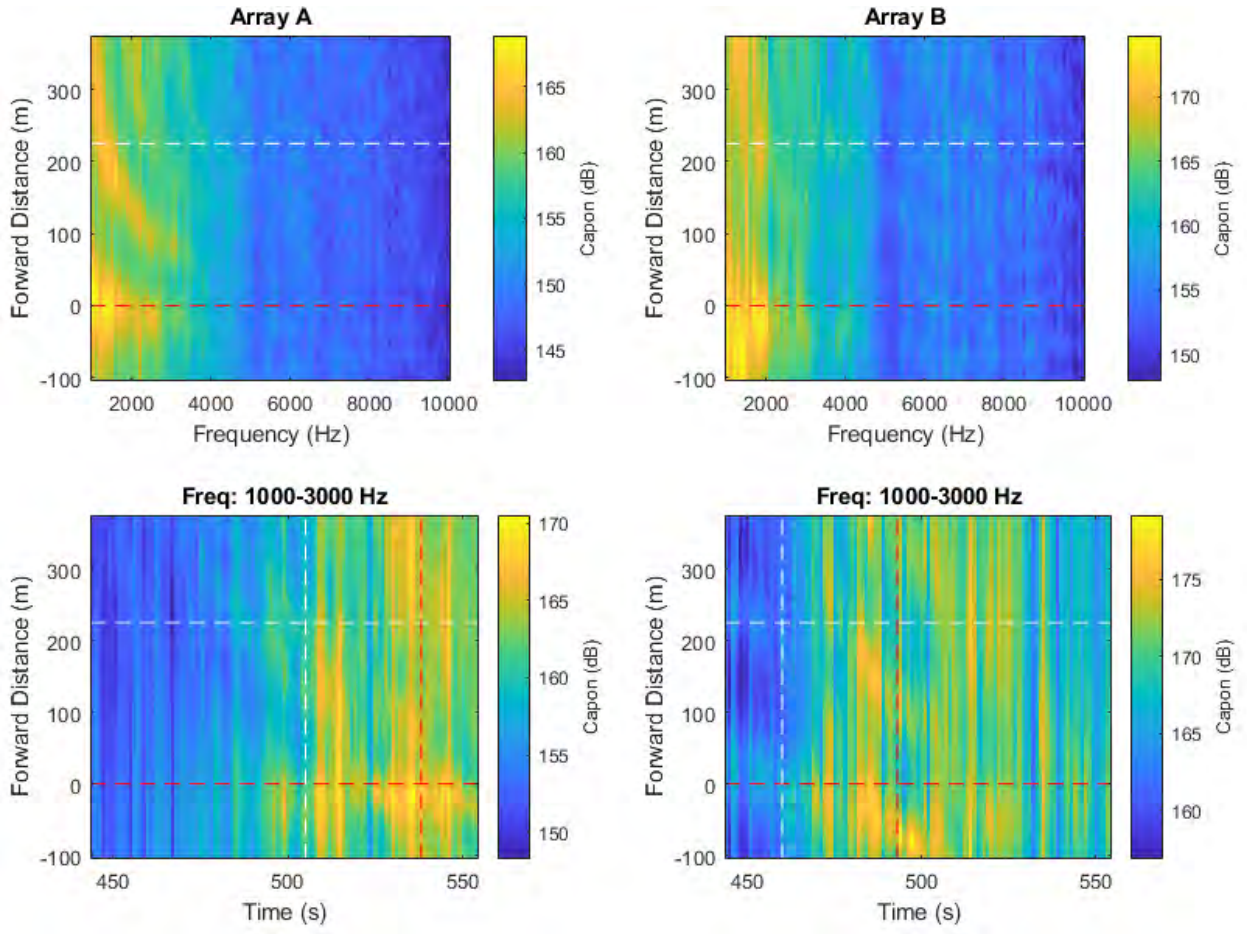

Figure 214 High-frequency noise maps obtained using the spatial spectra provided by the Capon algorithm implemented using individual arrays.

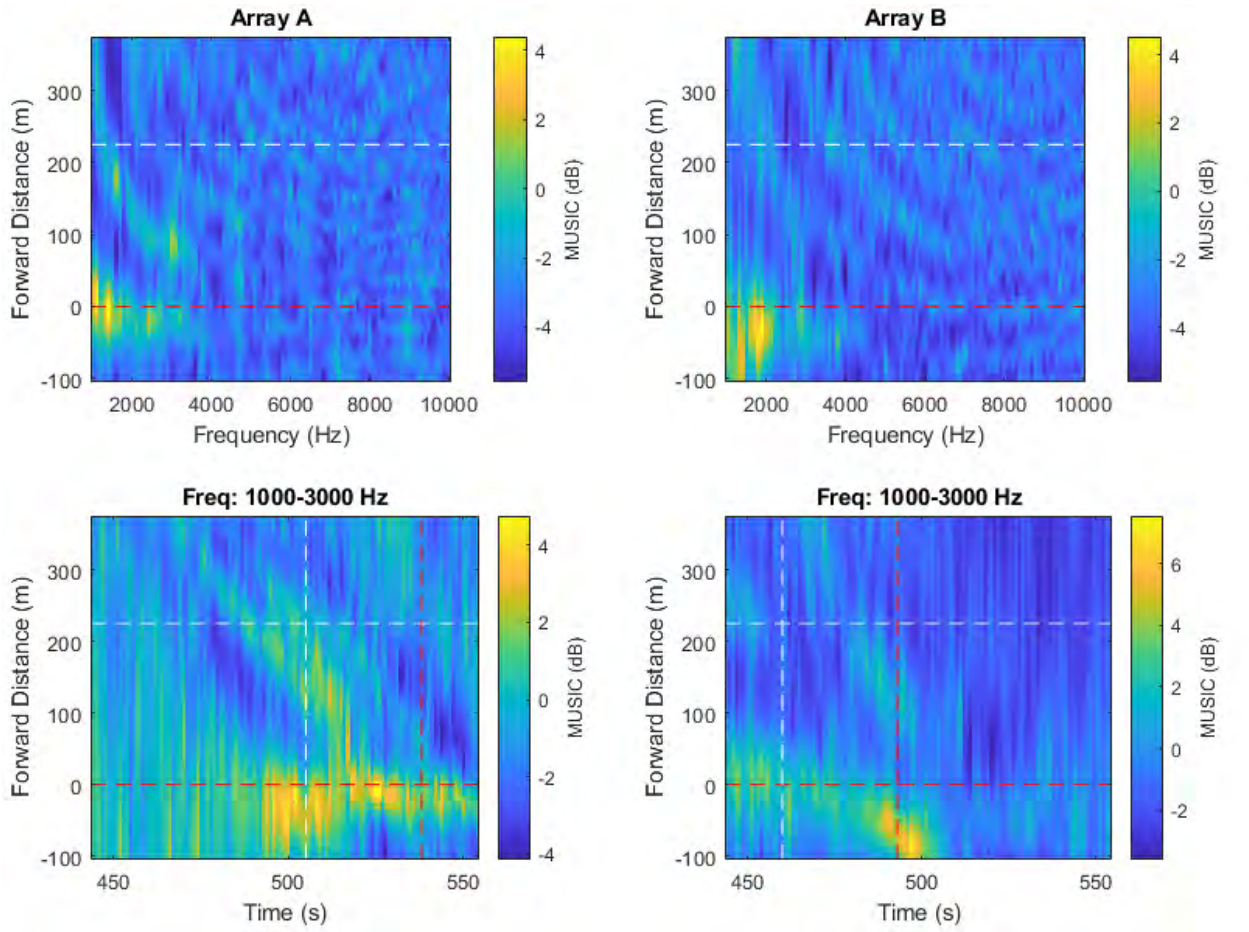

Figure 215 High-frequency noise maps obtained using the spatial spectra provided by the MUSIC algorithm implemented using individual arrays.

A.35. Pass #35 (Type: Container. Length: 277 m. Speed: 18.2 kn)

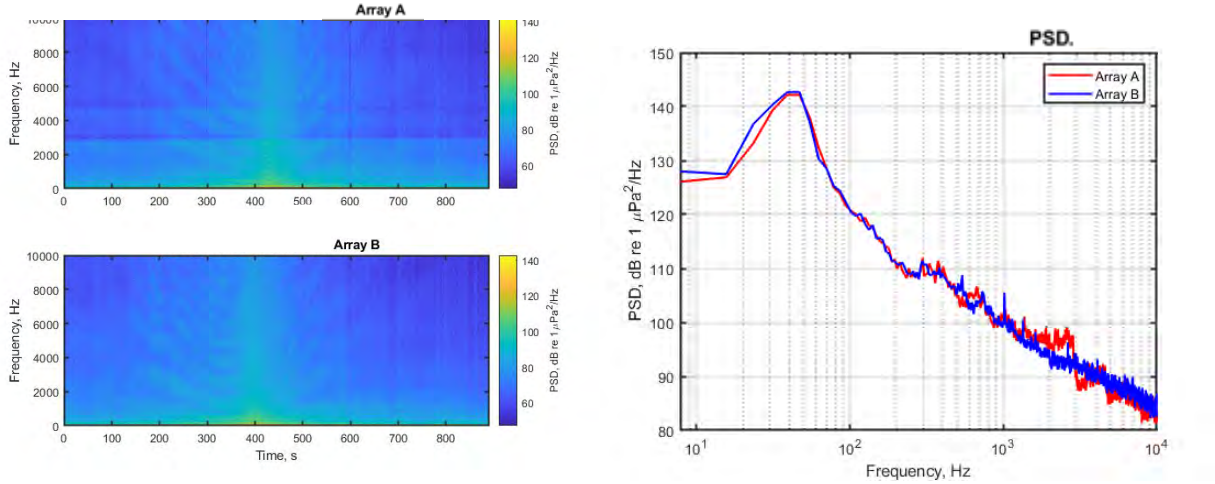

Figure 216 Spectrograms (left) and PSD (right) of ship noise observed on outputs of Arrays A and B.

A.35.1. Low- and mid-frequency noise maps

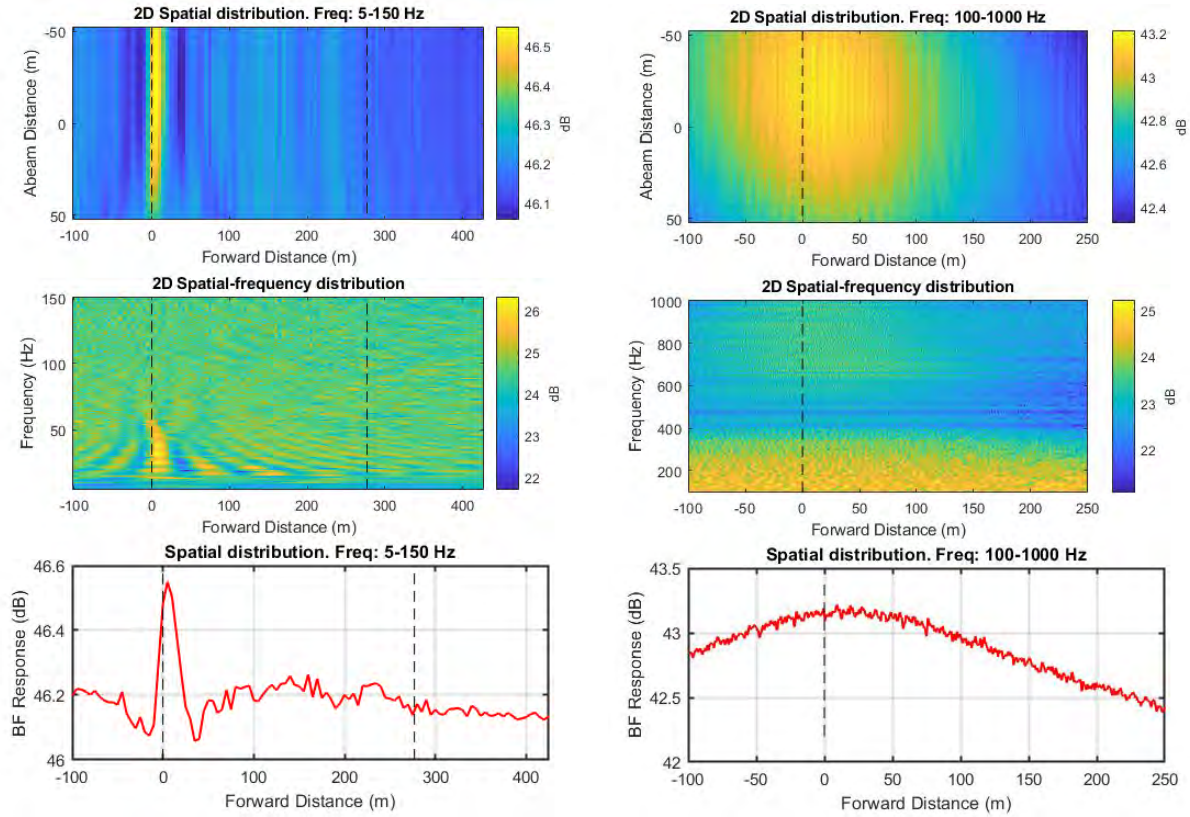

Figure 217 Noise maps from standard beamforming using combined array for Vessel Pass #35: 2D maps in spatial domain for two frequency ranges (top); 2D maps in vessel forward distance and frequency domain for two frequency ranges (middle); and graph of BF response versus forward distance for two frequency ranges (bottom). Frequency ranges are 5 to150 Hz (left) and 100 to1000 Hz (right).

A.35.2. High-frequency noise maps

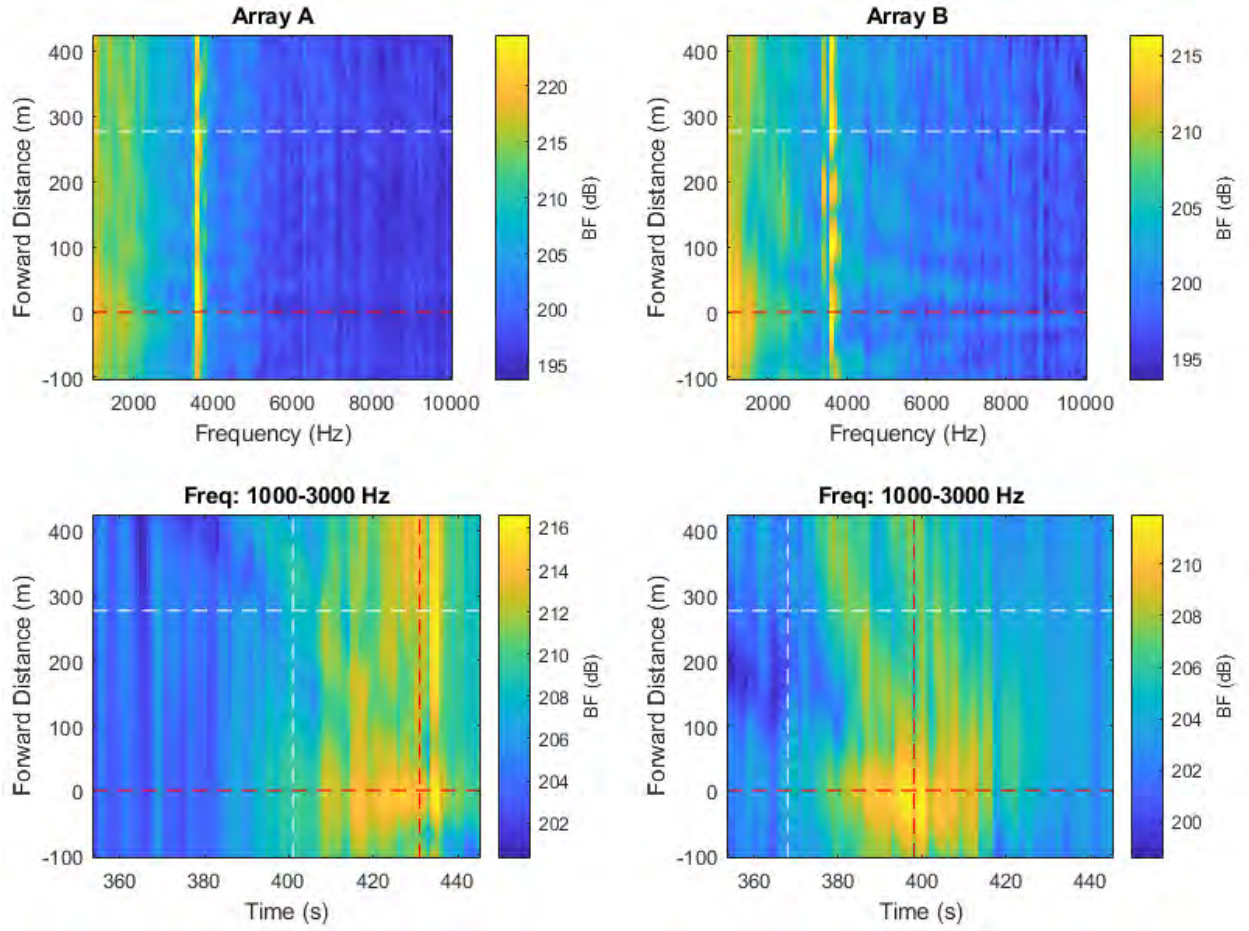

Figure 218 High-frequency noise maps from beamforming with individual arrays. Top maps show the BF response versus forward distance along vessel, measured approximately from the stern, versus frequency. Bottom maps show BF response versus forward distance and snapshot time. Horizontal dashed lines indicate the stern and bow positions of the vessel. Vertical dashed lines represent the CPA times of the bow and stern at each array.

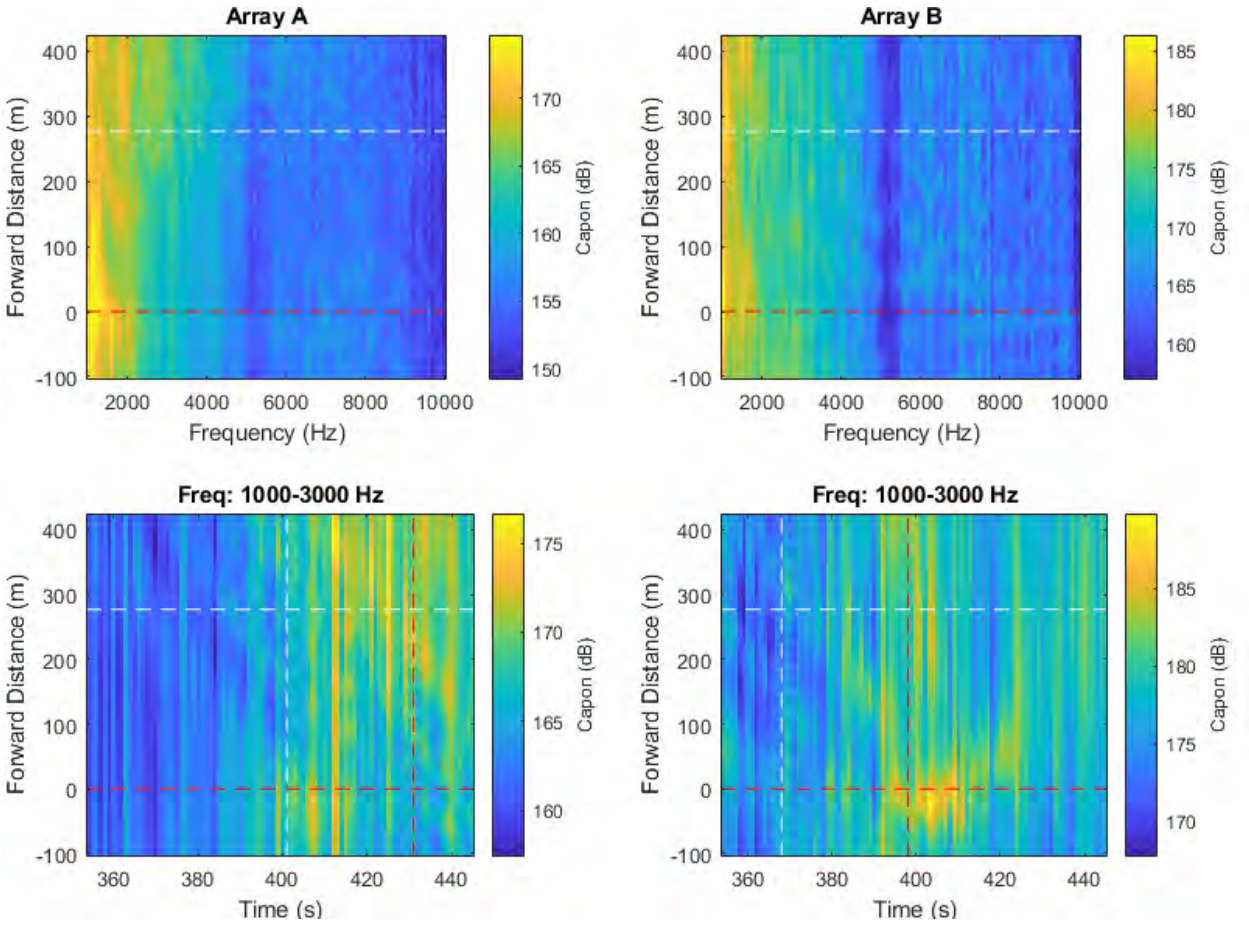

Figure 219 High-frequency noise maps obtained using the spatial spectra provided by the Capon algorithm implemented using individual arrays.

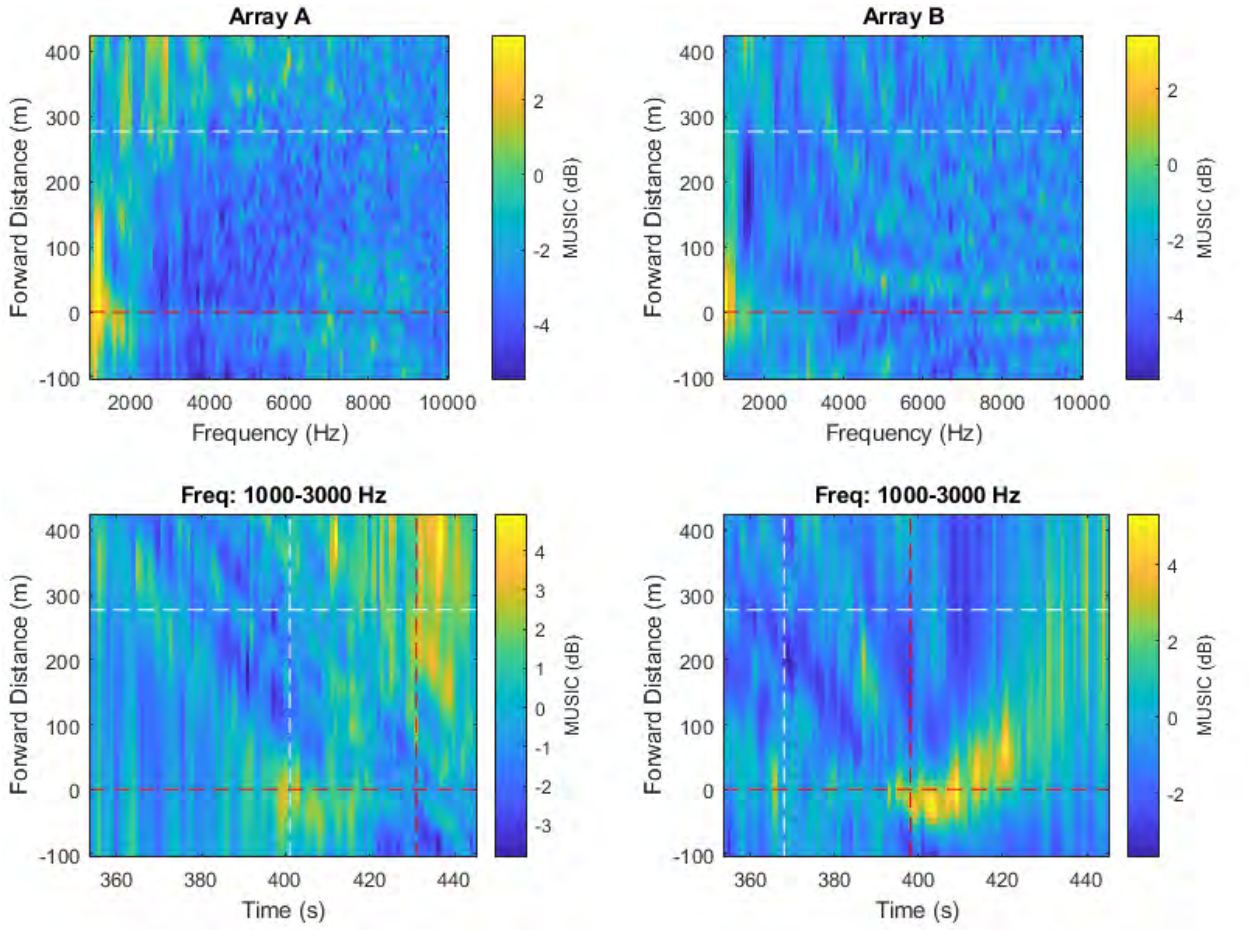

Figure 220 High-frequency noise maps obtained using the spatial spectra provided by the MUSIC algorithm implemented using individual arrays.

A.36. Pass #36 (Type: Tanker. Length: 277 m. Speed: 12.9 kn)

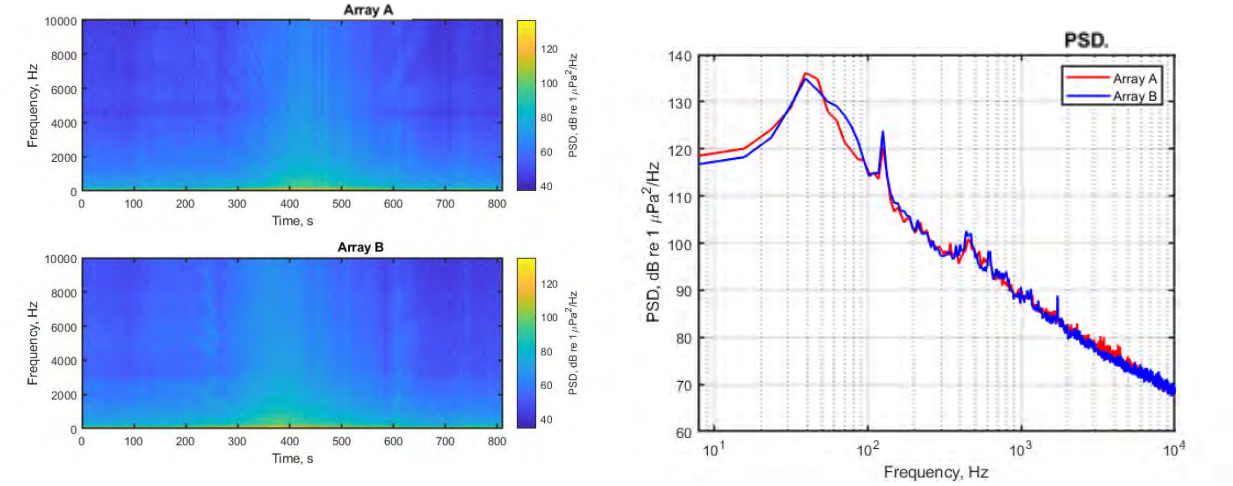

Figure 221 Spectrograms (left) and PSD (right) of ship noise observed on outputs of Arrays A and B.

A.36.1. Low- and mid-frequency noise maps

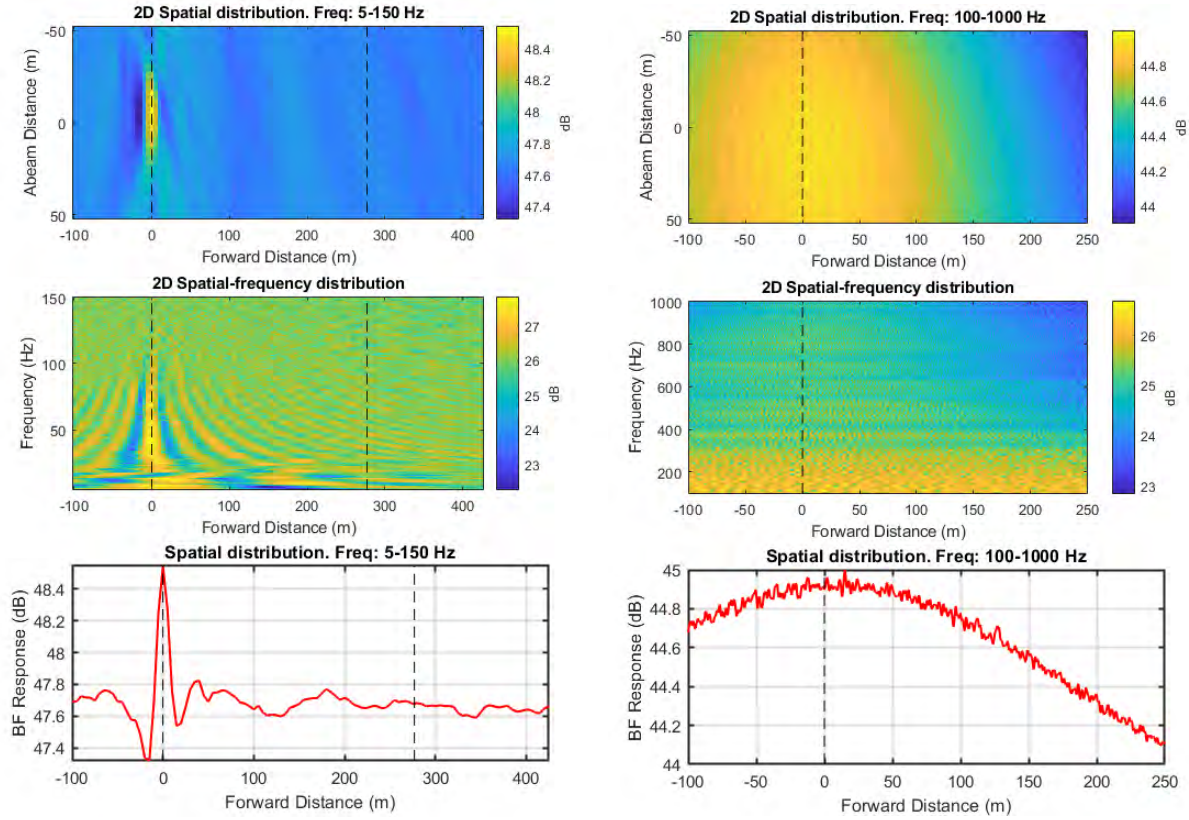

Figure 222 Noise maps from standard beamforming using combined array for Vessel Pass #37: 2D maps in spatial domain for two frequency ranges (top); 2D maps in vessel forward distance and frequency domain for two frequency ranges (middle); and graph of BF response versus forward distance for two frequency ranges (bottom). Frequency ranges are 5 to150 Hz (left) and 100 to1000 Hz (right).

A.36.2. High-frequency noise maps

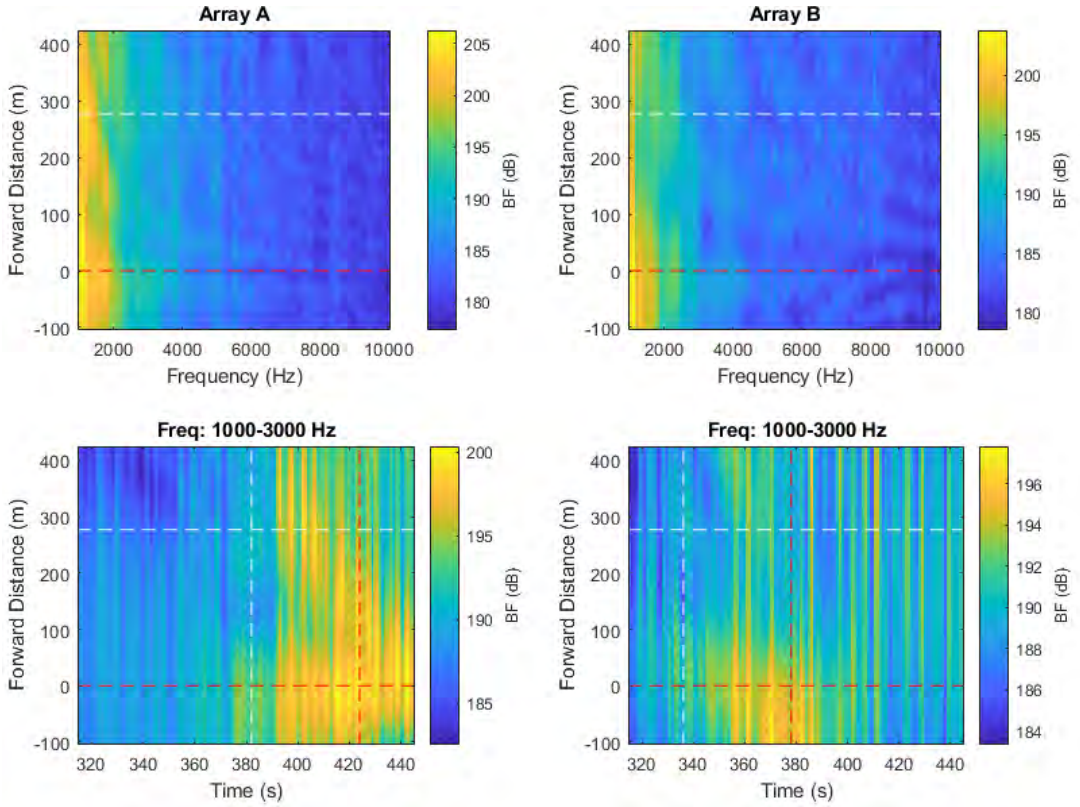

Figure 223 High-frequency noise maps from beamforming with individual arrays. Top maps show the BF response versus forward distance along vessel, measured approximately from the stern, versus frequency. Bottom maps show BF response versus forward distance and snapshot time. Horizontal dashed lines indicate the stern and bow positions of the vessel. Vertical dashed lines represent the CPA times of the bow and stern at each array.

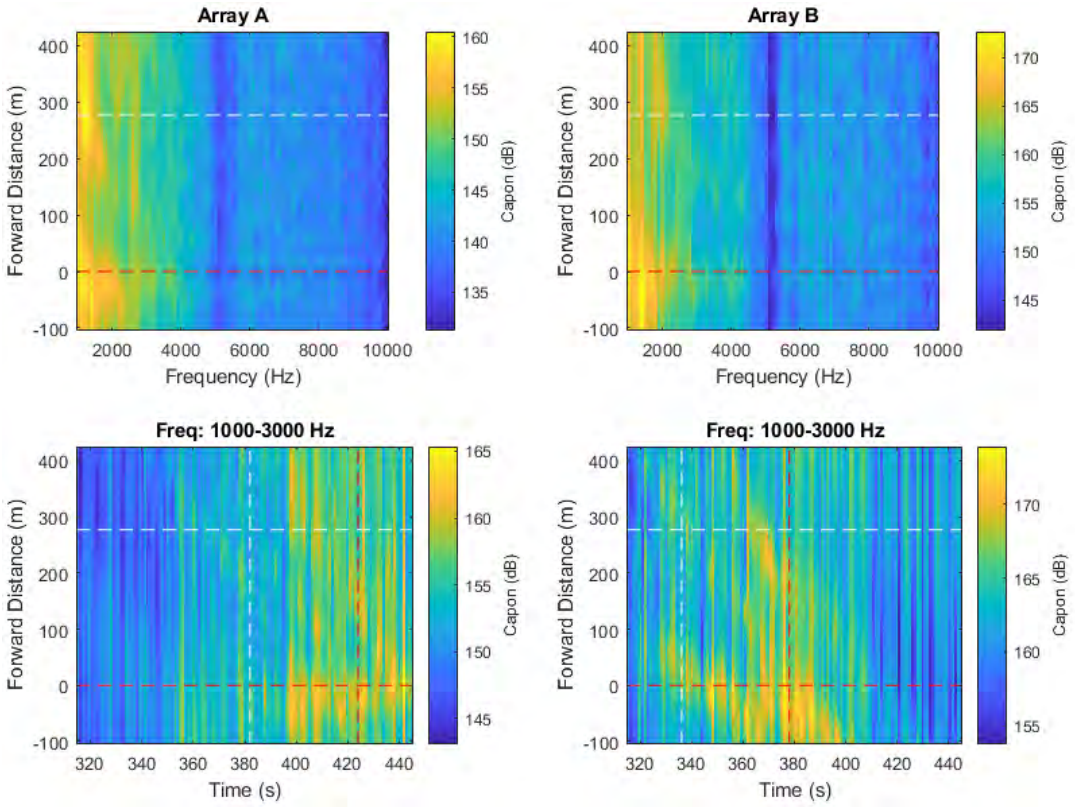

Figure 224 High-frequency noise maps obtained using the spatial spectra provided by the Capon algorithm implemented using individual arrays.

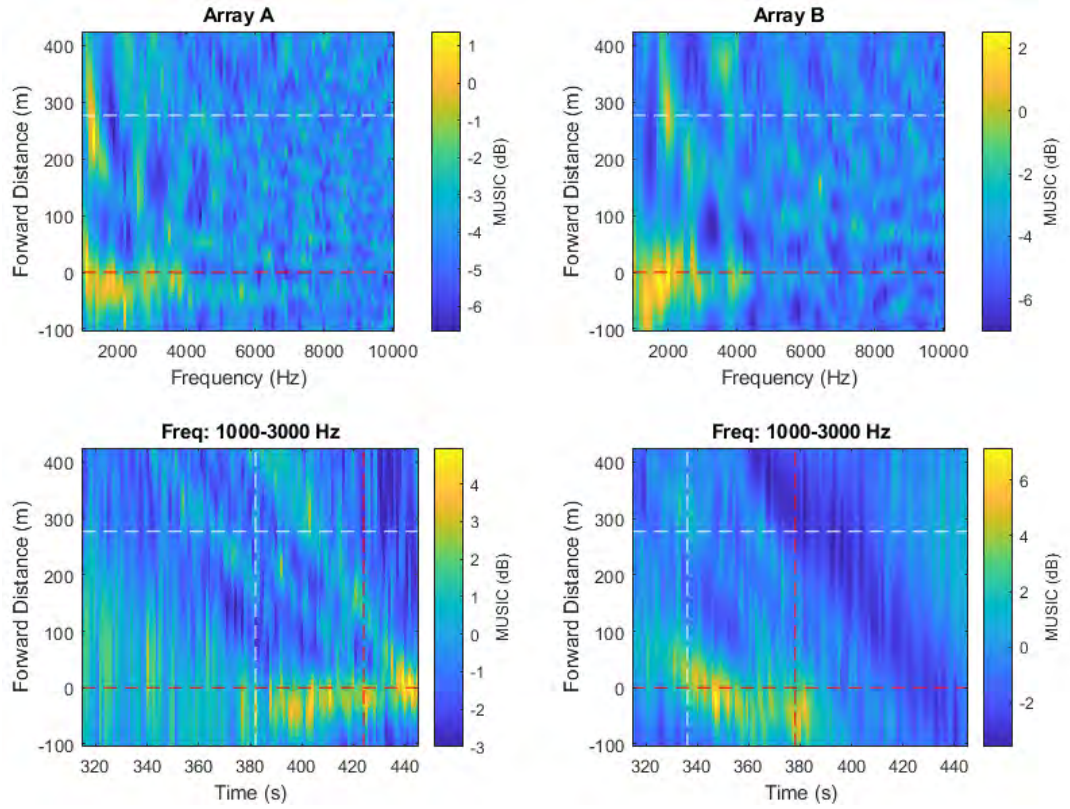

Figure 225 High-frequency noise maps obtained using the spatial spectra provided by the MUSIC algorithm implemented using individual arrays.

A.37. Pass #37 (Type: Bulker. Length: 182 m. Speed: 12.7 kn)

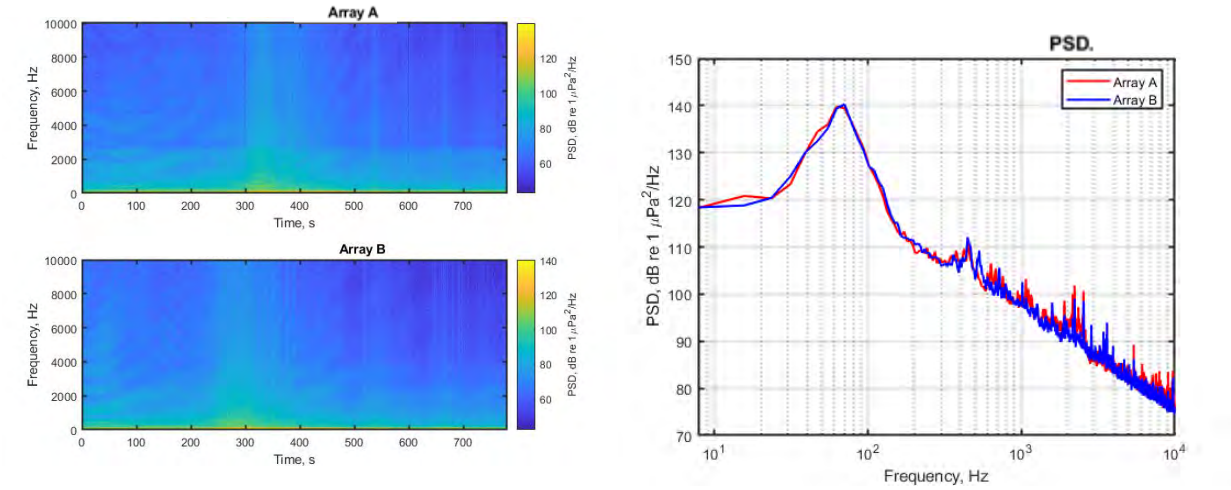

Figure 226 Spectrograms (left) and PSD (right) of ship noise observed on outputs of Arrays A and B.

A.37.1. Low- and mid-frequency noise maps

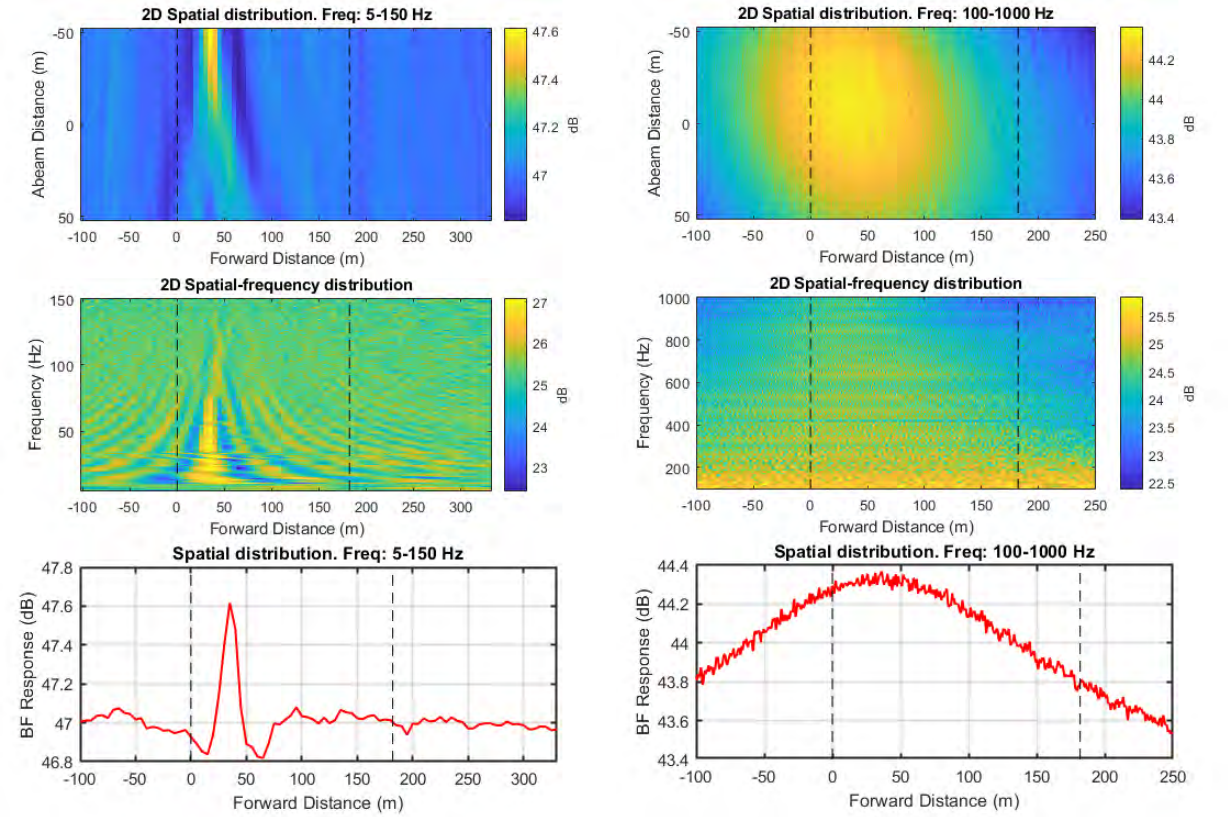

Figure 227 Noise maps from standard beamforming using combined array for Vessel Pass #37: 2D maps in spatial domain for two frequency ranges (top); 2D maps in vessel forward distance and frequency domain for two frequency ranges (middle); and graph of BF response versus forward distance for two frequency ranges (bottom). Frequency ranges are 5 to150 Hz (left) and 100 to1000 Hz (right).

A.37.2. High-frequency noise maps

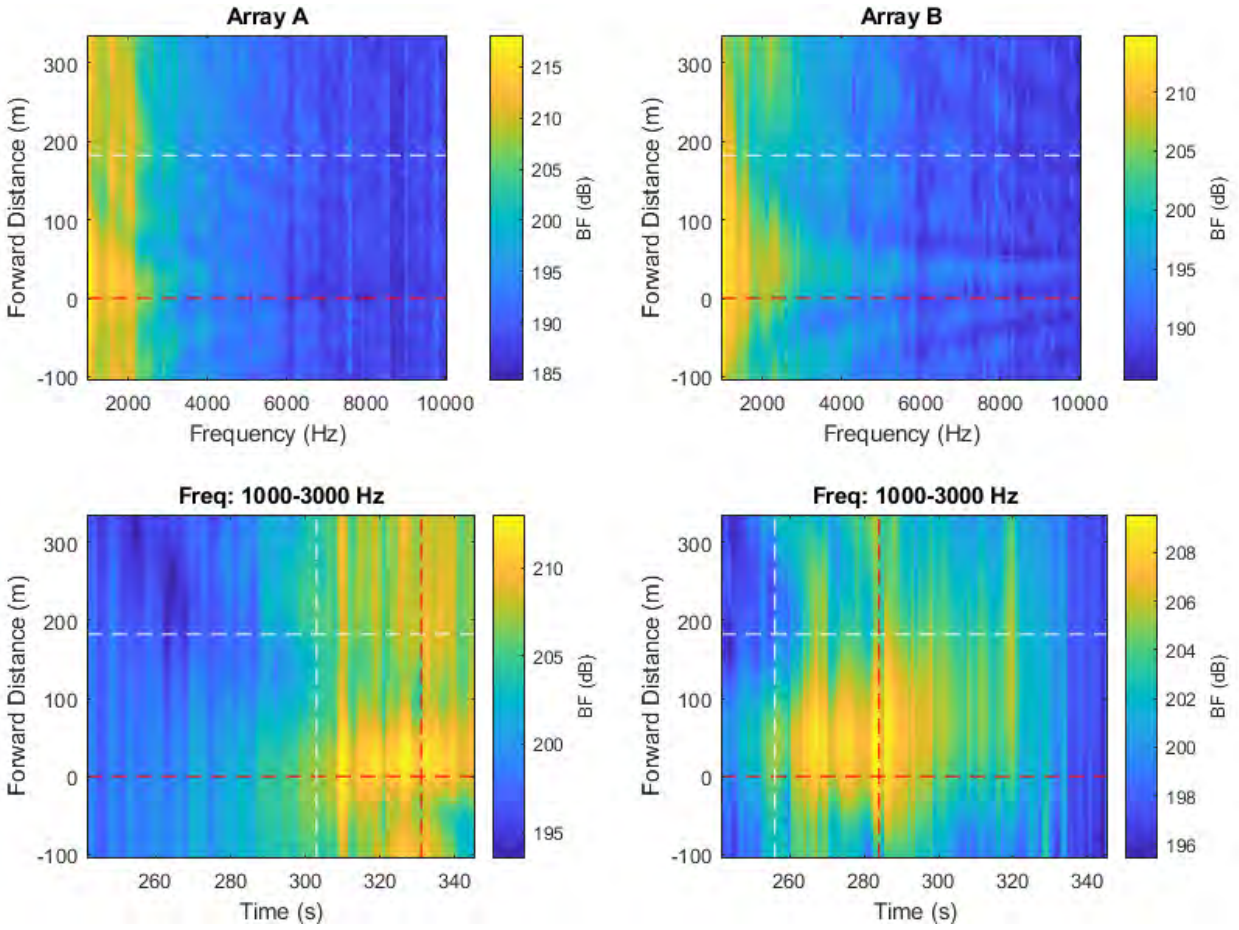

Figure 228 High-frequency noise maps from beamforming with individual arrays. Top maps show the BF response versus forward distance along vessel, measured approximately from the stern, versus frequency. Bottom maps show BF response versus forward distance and snapshot time. Horizontal dashed lines indicate the stern and bow positions of the vessel. Vertical dashed lines represent the CPA times of the bow and stern at each array.

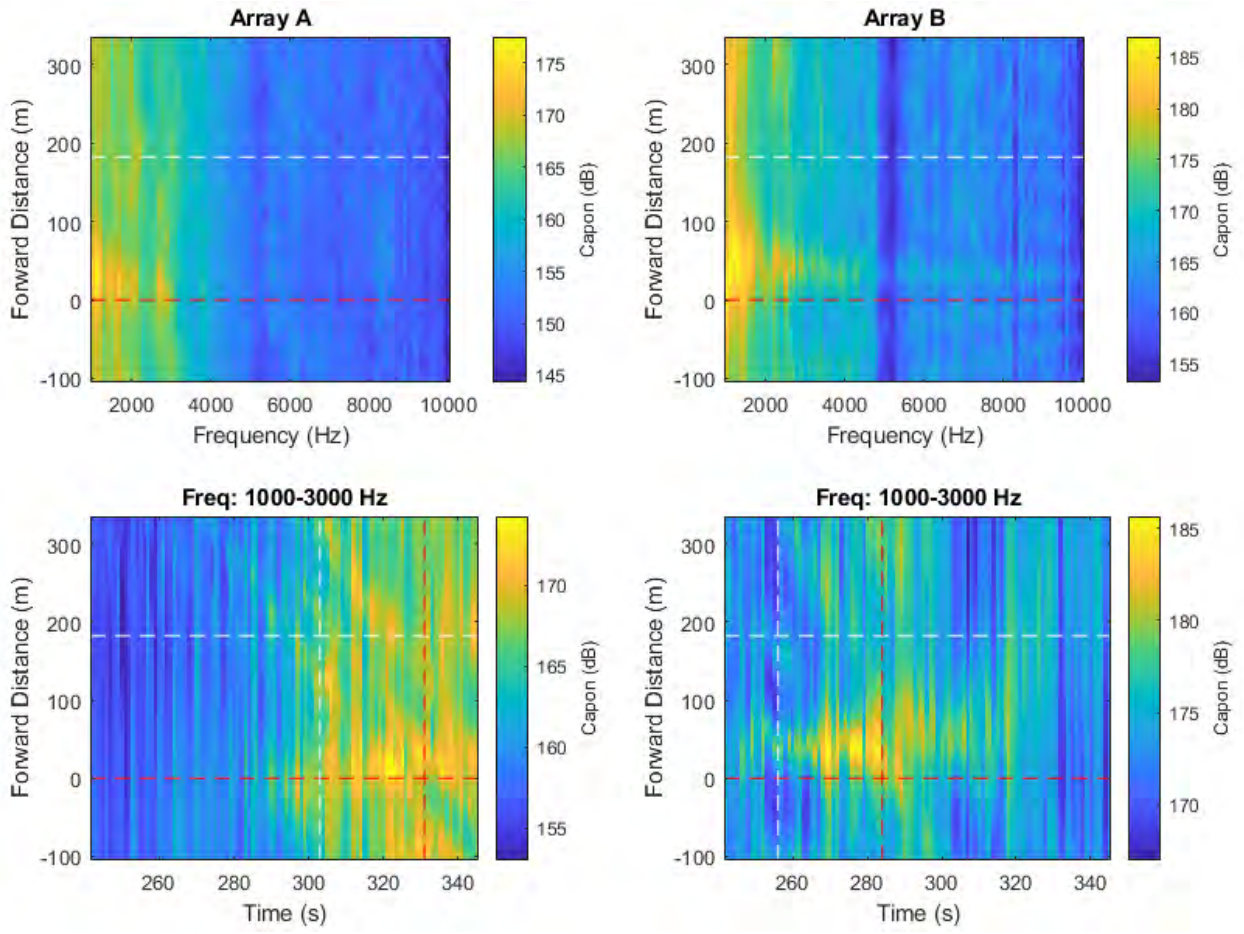

Figure 229 High-frequency noise maps obtained using the spatial spectra provided by the Capon algorithm implemented using individual arrays.

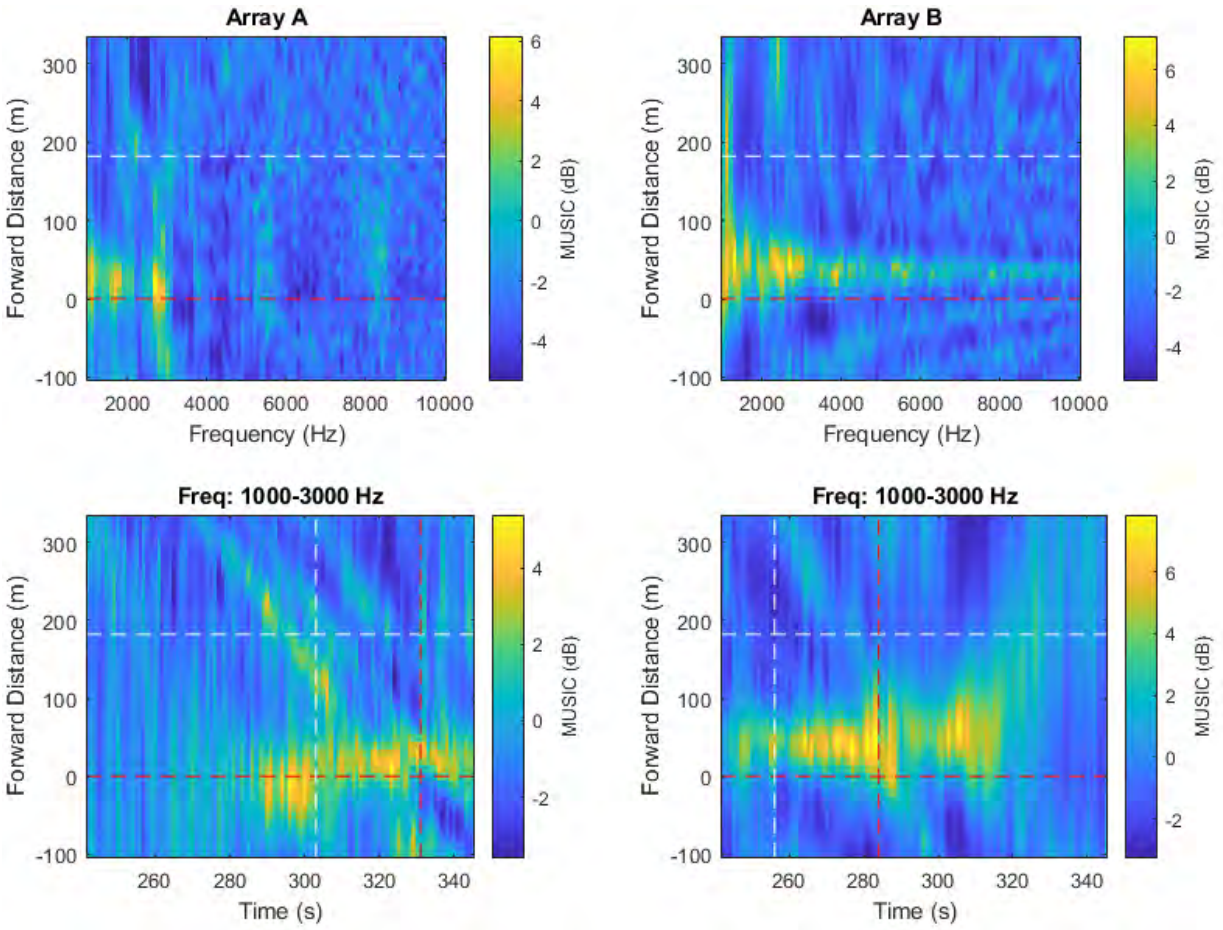

Figure 230 High-frequency noise maps obtained using the spatial spectra provided by the MUSIC algorithm implemented using individual arrays.

A.38. Pass #38 (Type: Bulker. Length: 180 m. Speed: 14.9 kn)

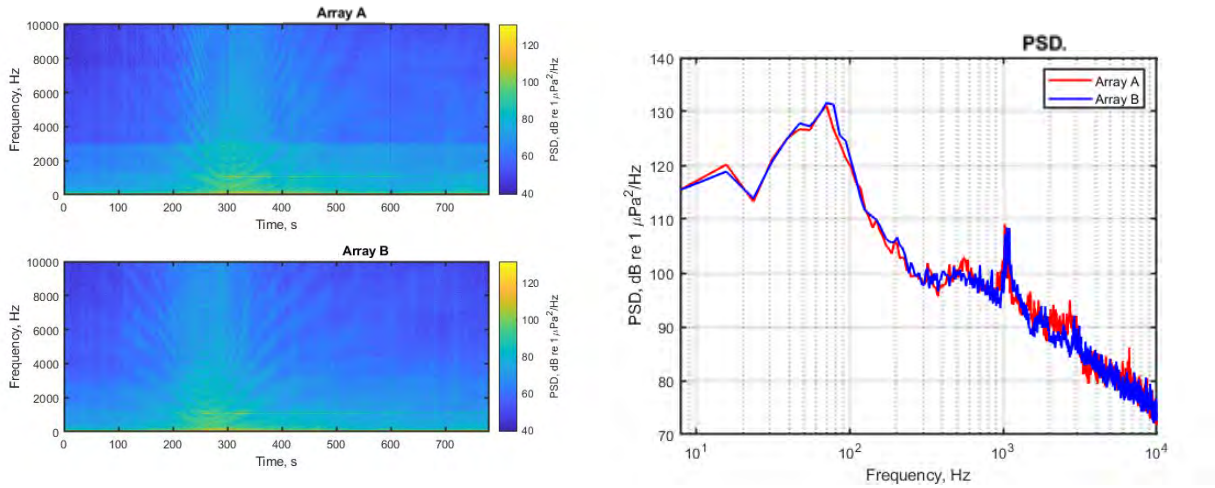

Figure 231 Spectrograms (left) and PSD (right) of ship noise observed on outputs of Arrays A and B.

A.38.1. Low- and mid-frequency noise maps

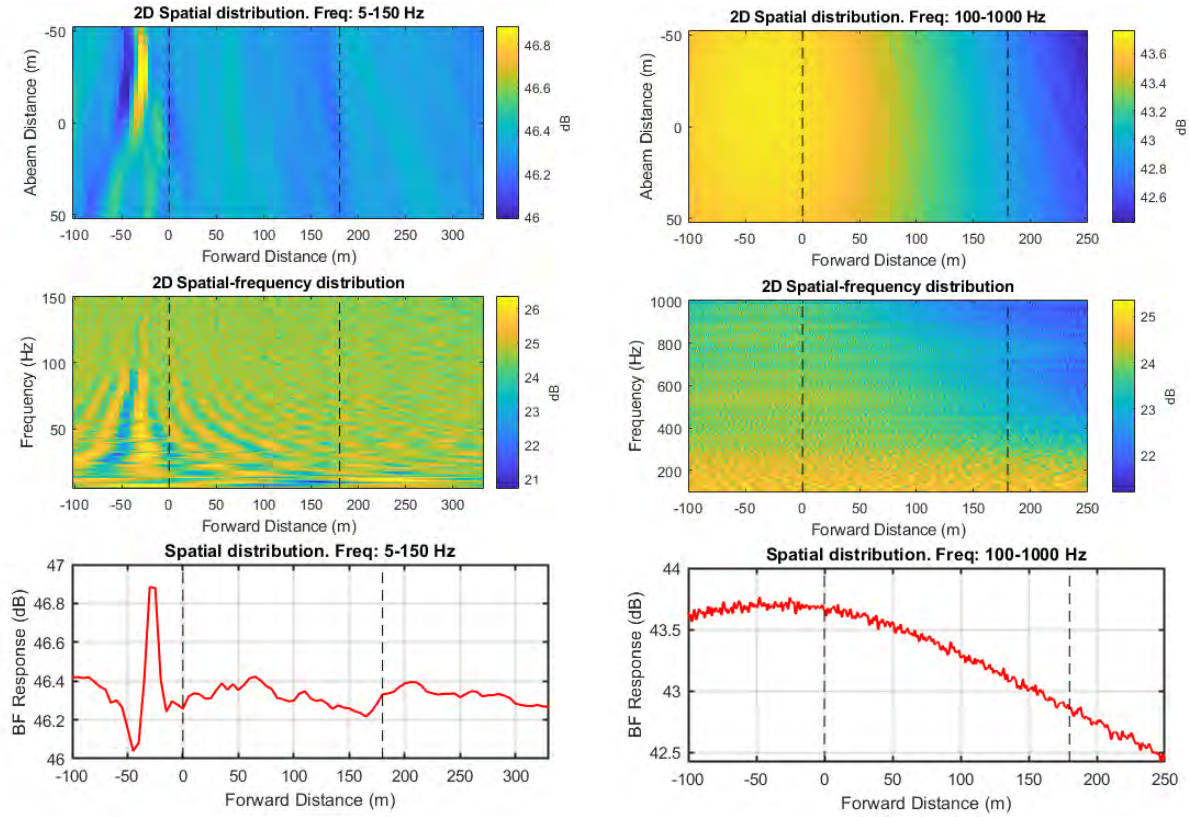

Figure 232 Noise maps from standard beamforming using combined array for Vessel Pass #38: 2D maps in spatial domain for two frequency ranges (top); 2D maps in vessel forward distance and frequency domain for two frequency ranges (middle); and graph of BF response versus forward distance for two frequency ranges (bottom). Frequency ranges are 5 to150 Hz (left) and 100 to1000 Hz (right).

A.38.2. High-frequency noise maps

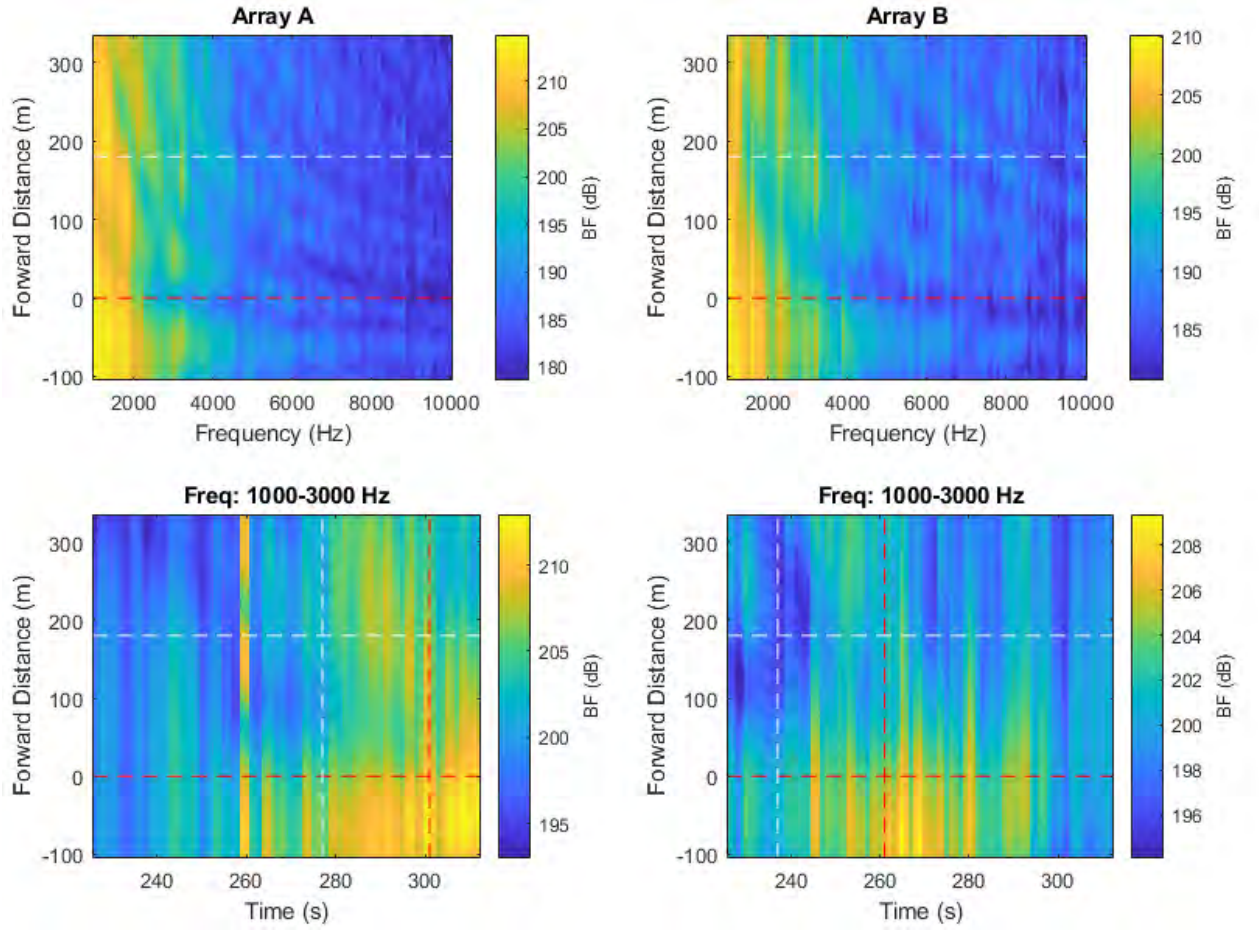

Figure 233 High-frequency noise maps from beamforming with individual arrays. Top maps show the BF response versus forward distance along vessel, measured approximately from the stern, versus frequency. Bottom maps show BF response versus forward distance and snapshot time. Horizontal dashed lines indicate the stern and bow positions of the vessel. Vertical dashed lines represent the CPA times of the bow and stern at each array.

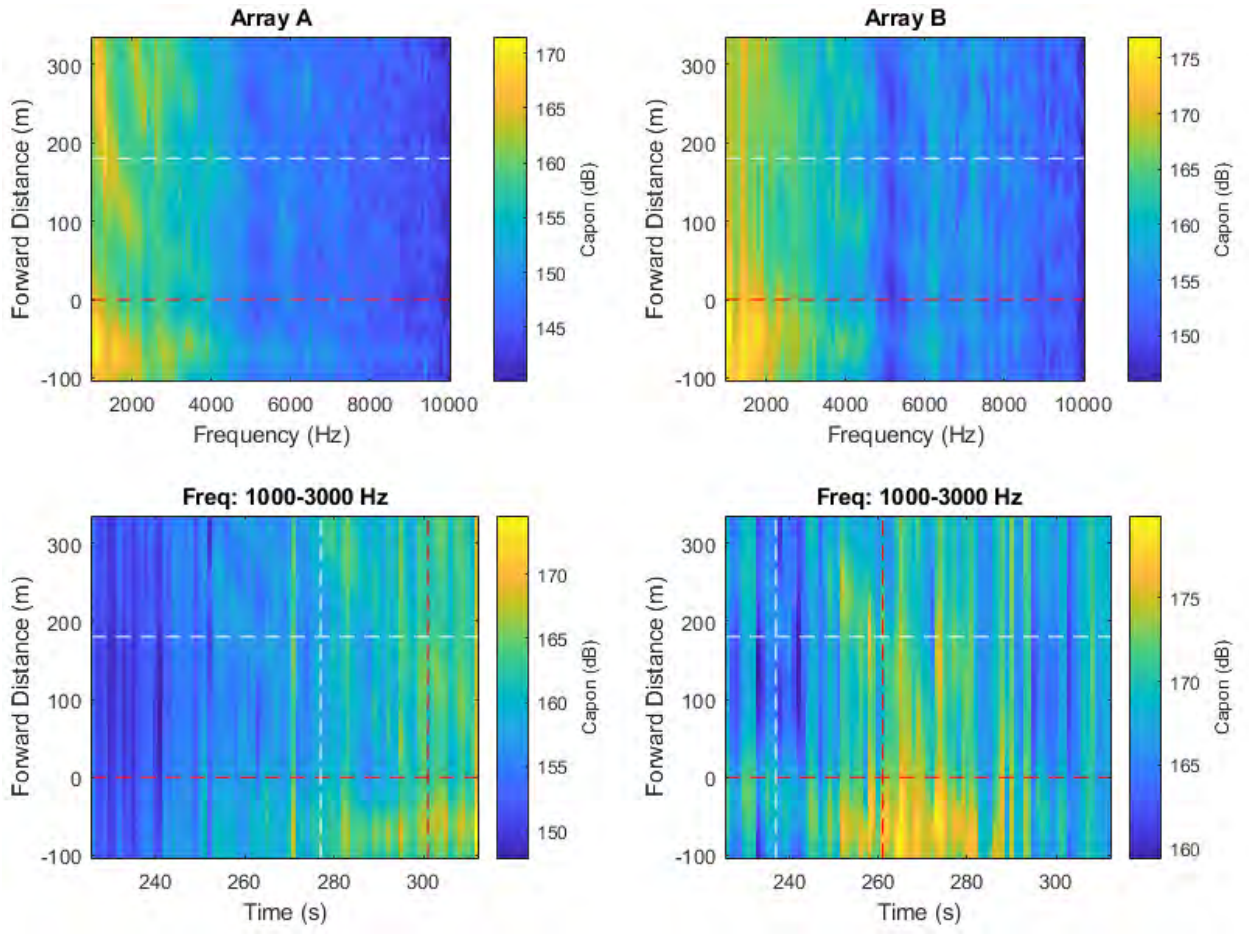

Figure 234 High-frequency noise maps obtained using the spatial spectra provided by the Capon algorithm implemented using individual arrays.

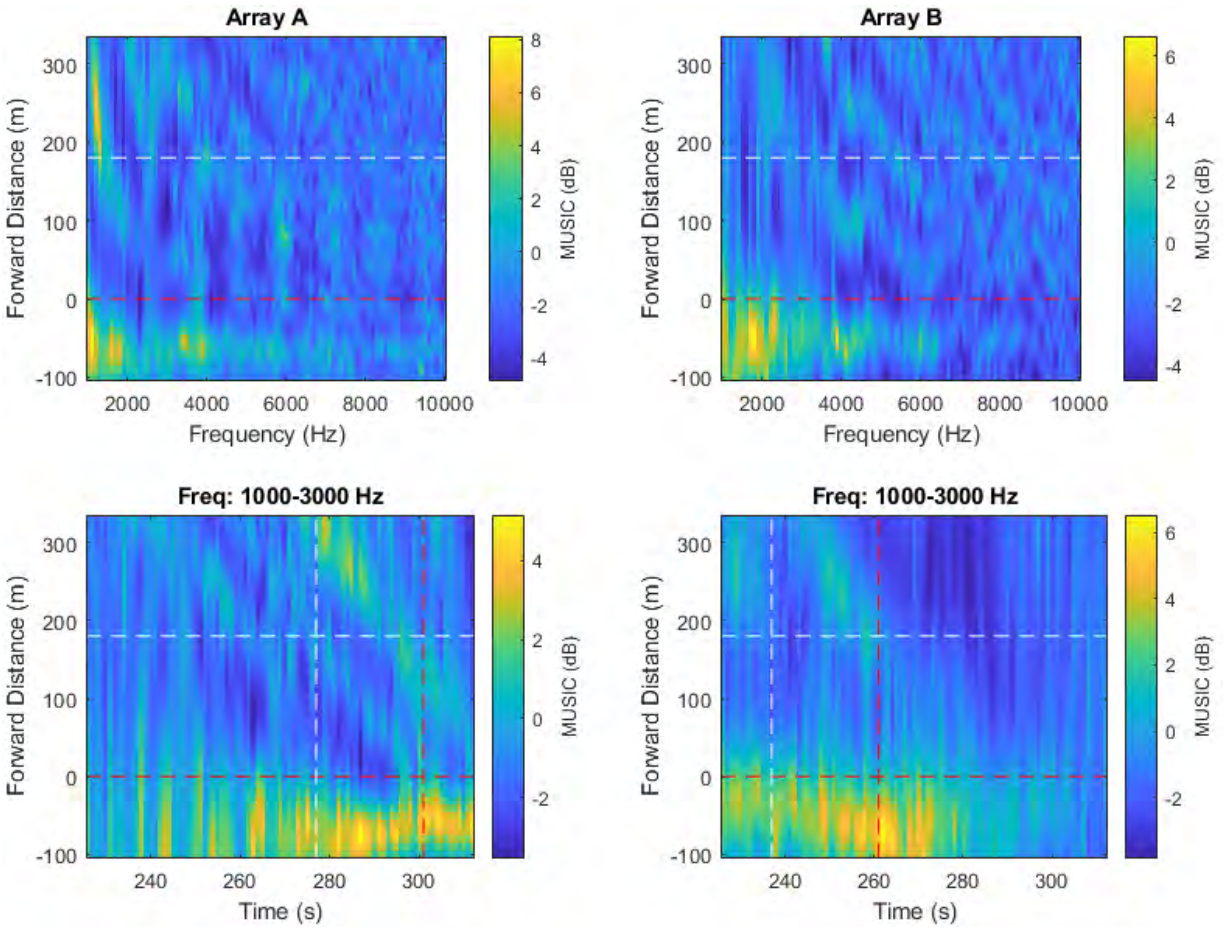

Figure 235 High-frequency noise maps obtained using the spatial spectra provided by the MUSIC algorithm implemented using individual arrays.

A.39. Pass #39 (Type: Bulker. Length: 180 m. Speed: 12.6 kn)

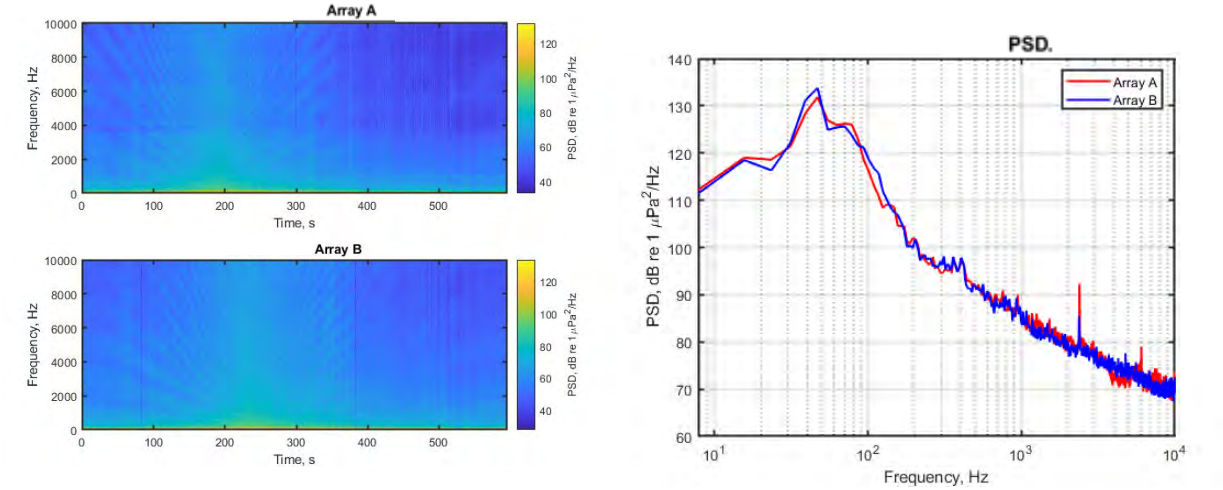

Figure 236 Spectrograms (left) and PSD (right) of ship noise observed on outputs of Arrays A and B.

A.39.1. Low- and mid-frequency noise maps

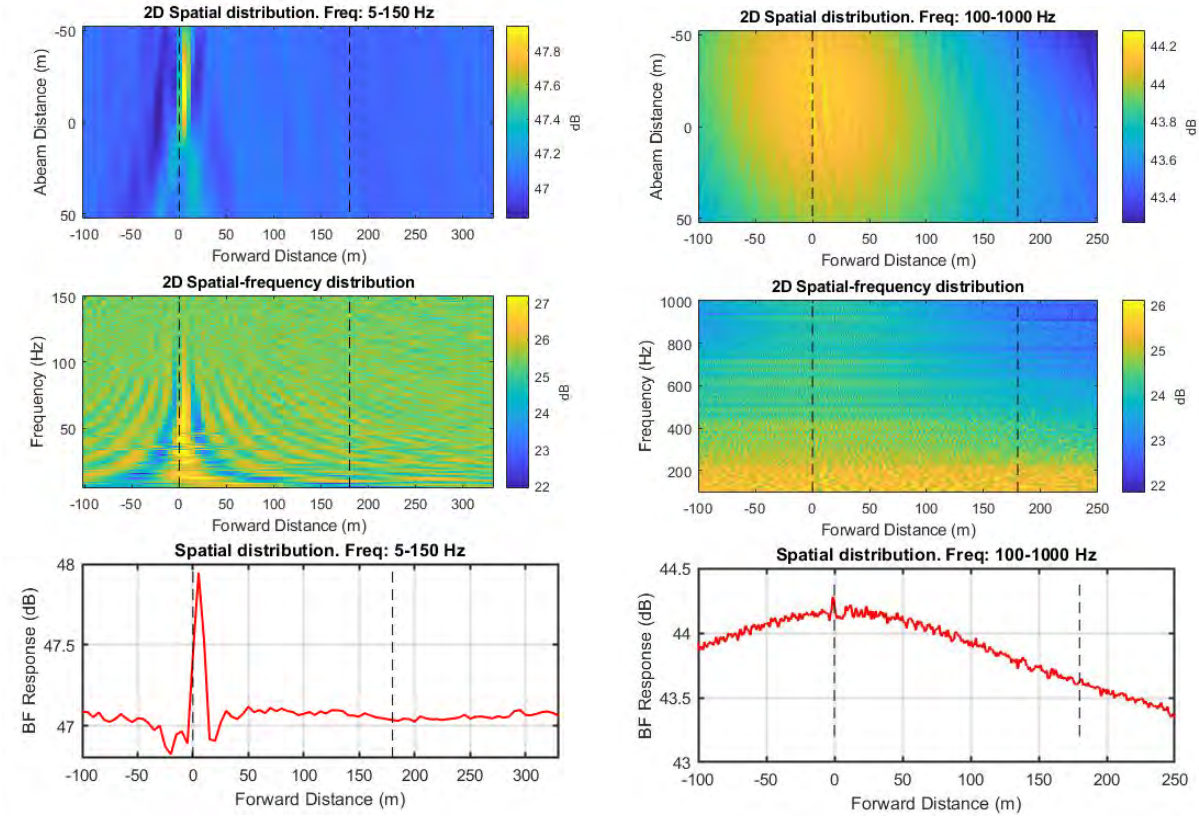

Figure 237 Noise maps from standard beamforming using combined array for Vessel Pass #39: 2D maps in spatial domain for two frequency ranges (top); 2D maps in vessel forward distance and frequency domain for two frequency ranges (middle); and graph of BF response versus forward distance for two frequency ranges (bottom). Frequency ranges are 5 to150 Hz (left) and 100 to1000 Hz (right).

A.39.2. High-frequency noise maps

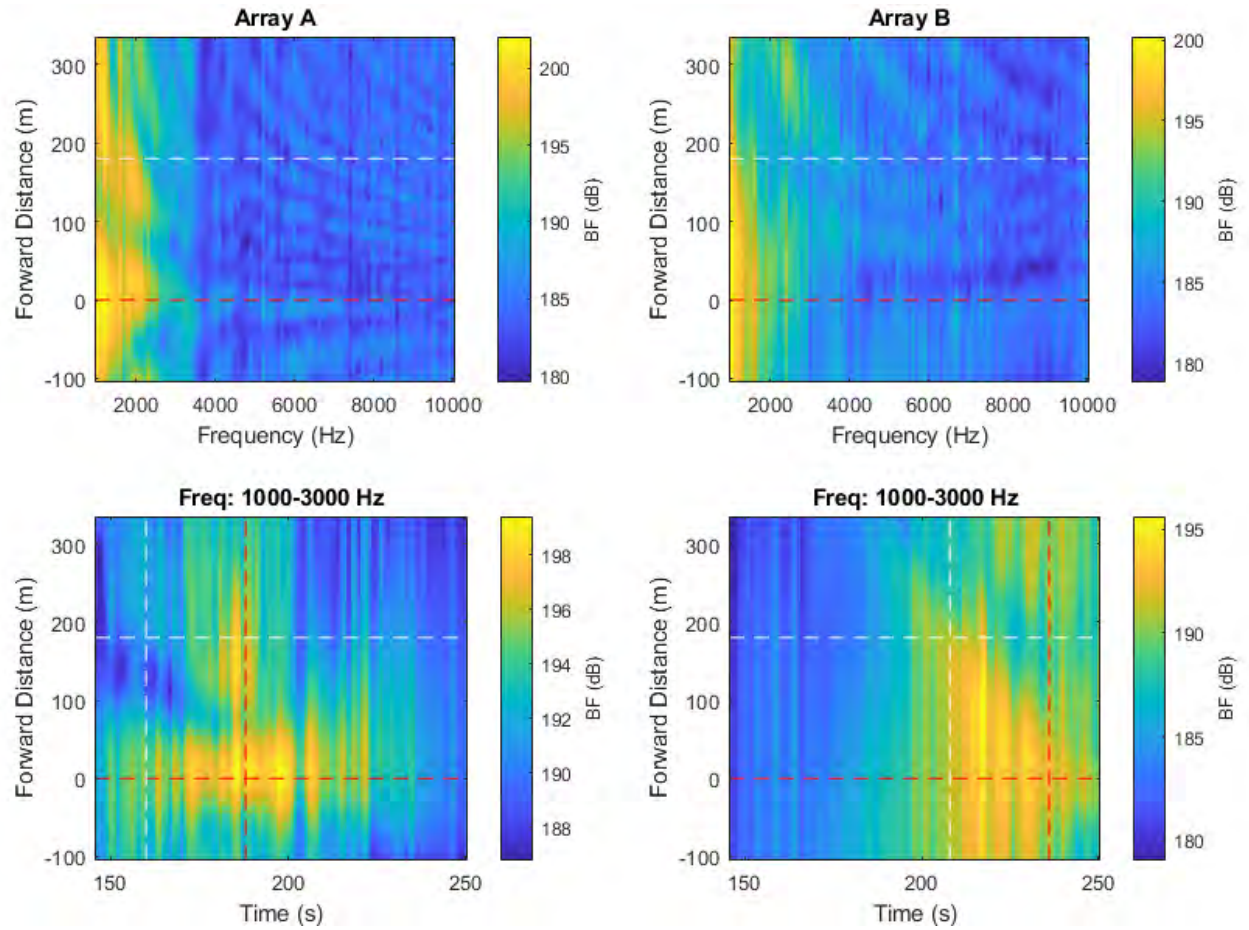

Figure 238 High-frequency noise maps from beamforming with individual arrays. Top maps show the BF response versus forward distance along vessel, measured approximately from the stern, versus frequency. Bottom maps show BF response versus forward distance and snapshot time. Horizontal dashed lines indicate the stern and bow positions of the vessel. Vertical dashed lines represent the CPA times of the bow and stern at each array.

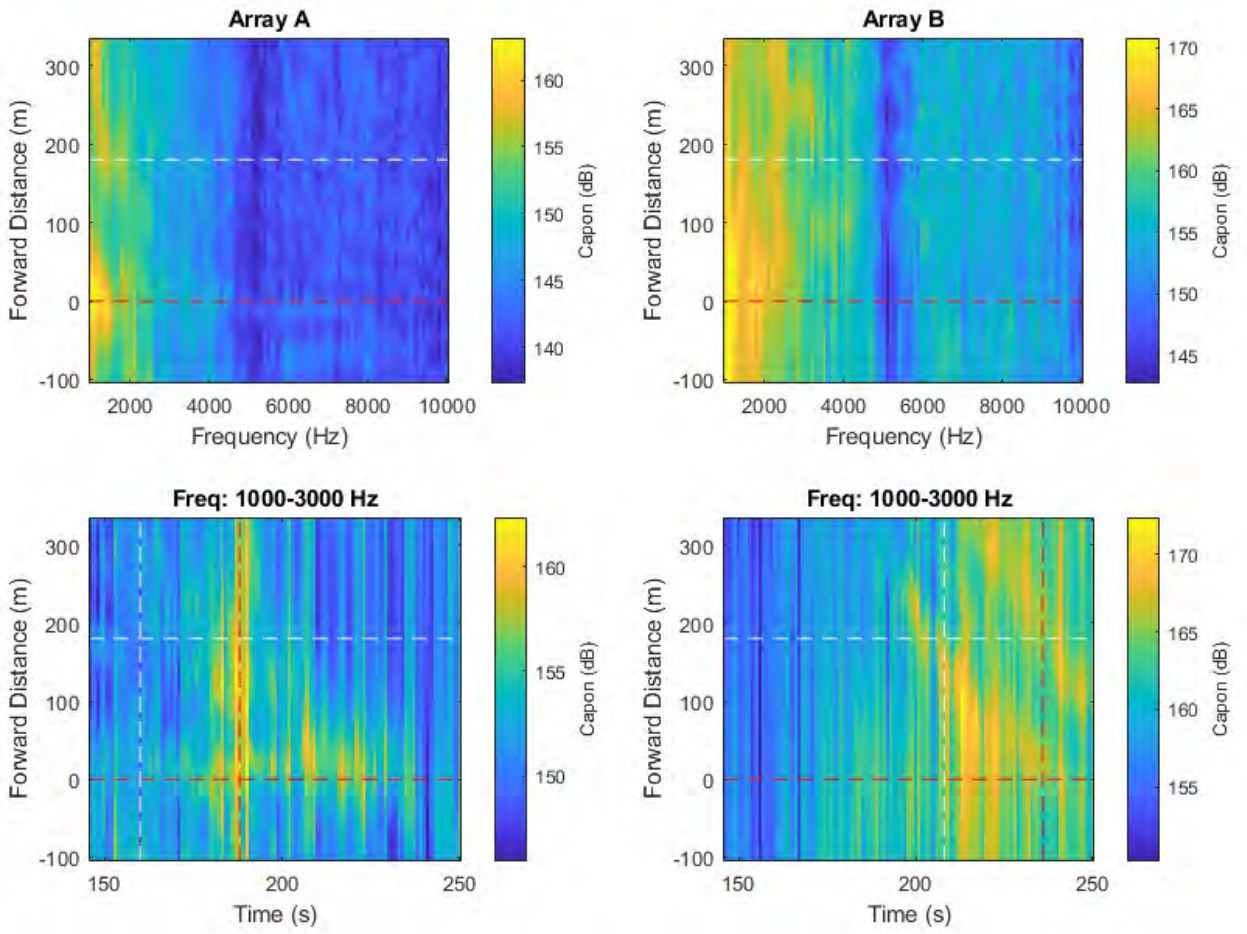

Figure 239 High-frequency noise maps obtained using the spatial spectra provided by the Capon algorithm implemented using individual arrays.

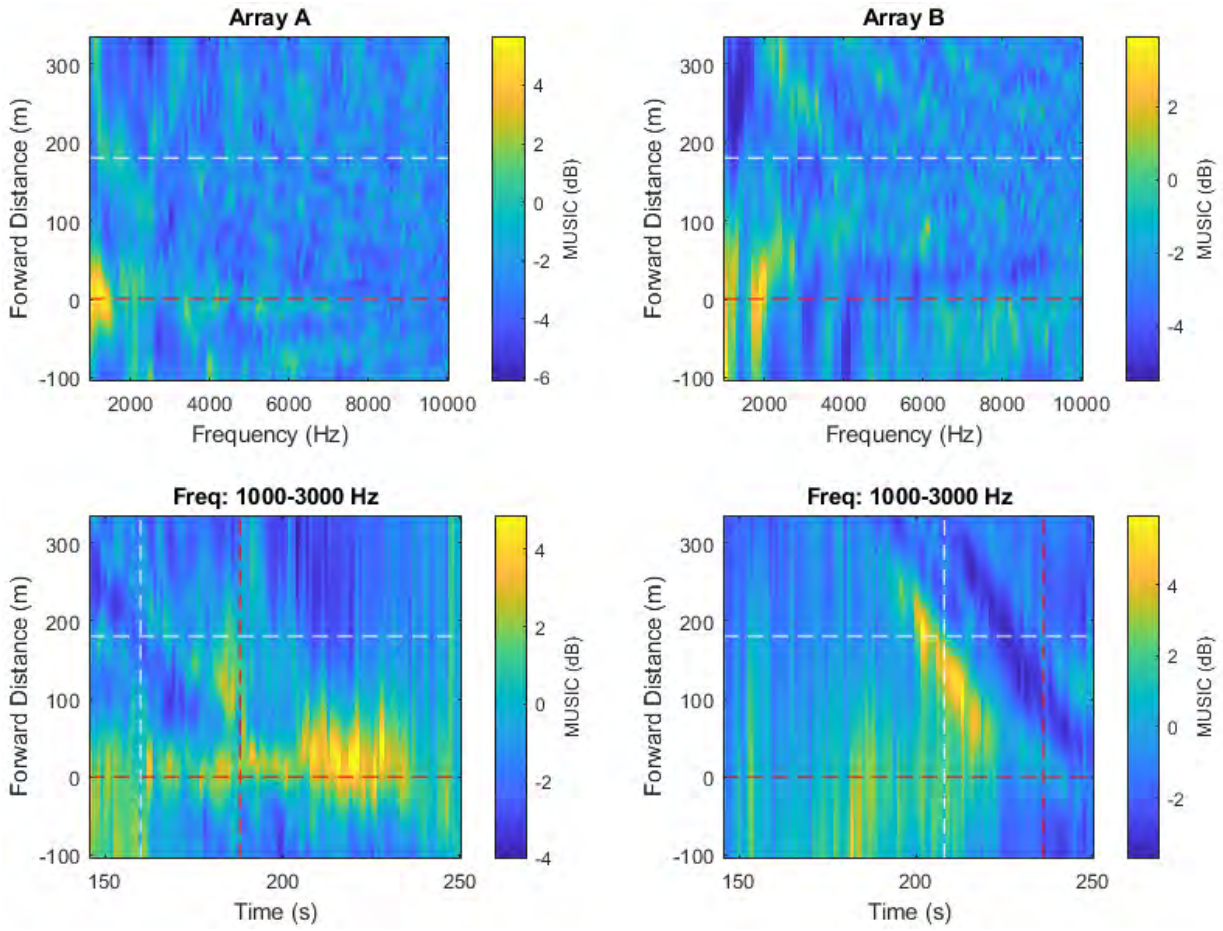

Figure 240 High-frequency noise maps obtained using the spatial spectra provided by the MUSIC algorithm implemented using individual arrays.

A.40. Pass #40 (Type: Cargo. Length: 171 m. Speed: 13.6 kn)

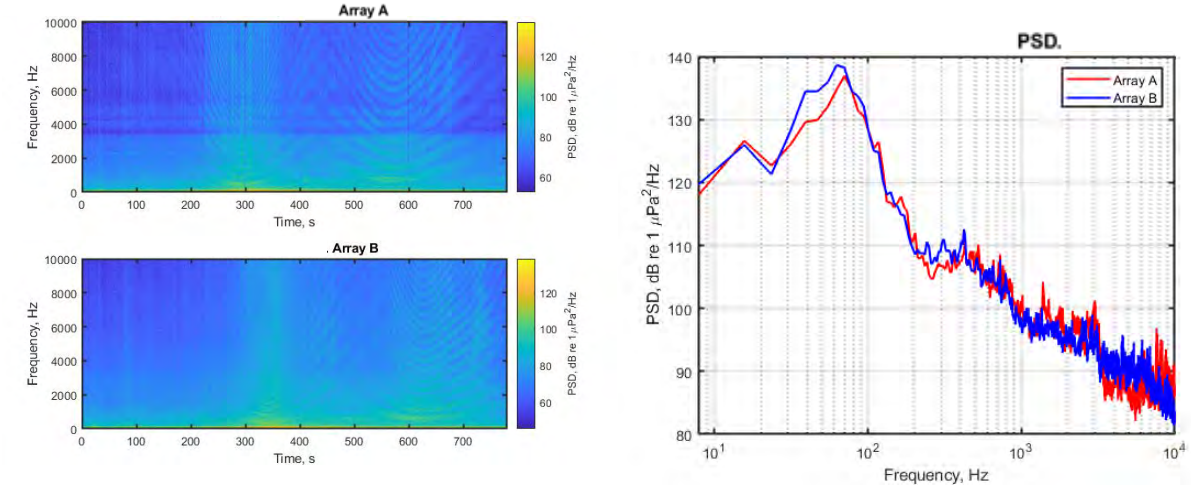

Figure 241 Spectrograms (left) and PSD (right) of ship noise observed on outputs of Arrays A and B.

A.40.1. Low- and mid-frequency noise maps

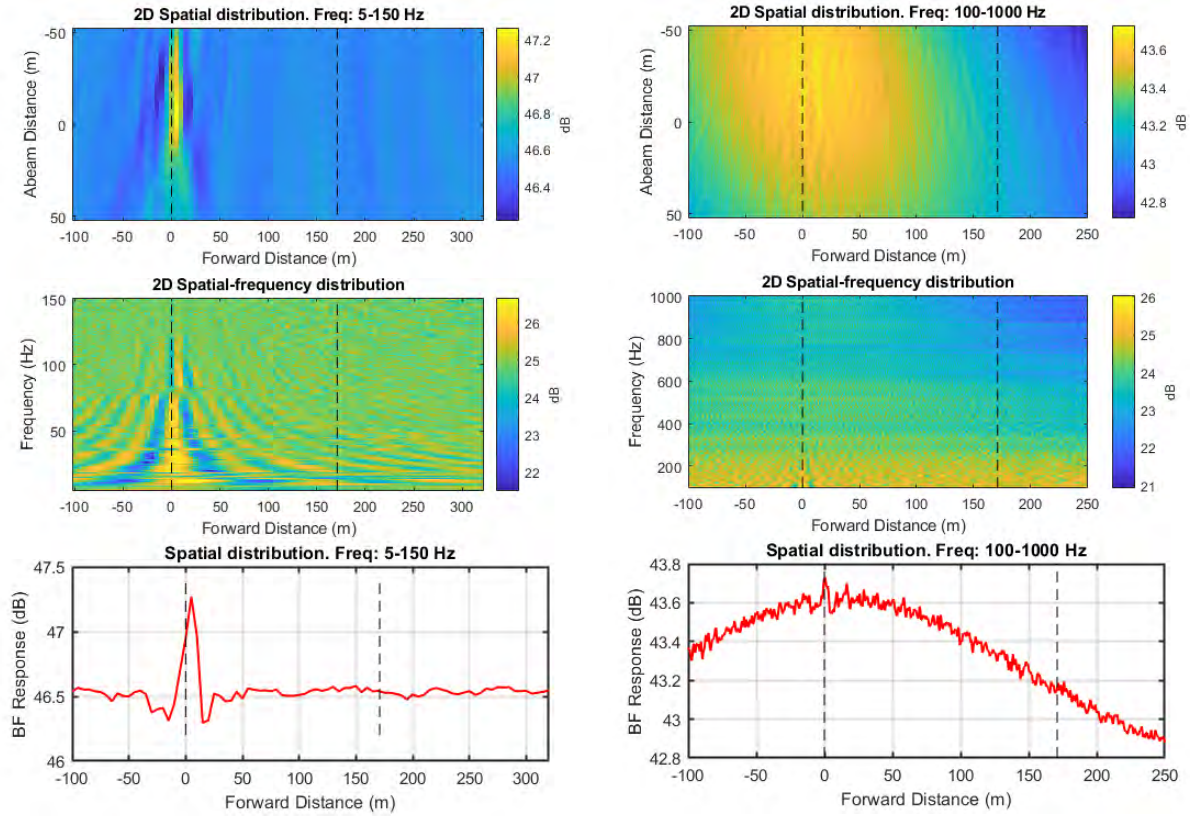

Figure 242 Noise maps from standard beamforming using combined array for Vessel Pass #40: 2D maps in spatial domain for two frequency ranges (top); 2D maps in vessel forward distance and frequency domain for two frequency ranges (middle); and graph of BF response versus forward distance for two frequency ranges (bottom). Frequency ranges are 5 to150 Hz (left) and 100 to1000 Hz (right).

A.40.2. High-frequency noise maps

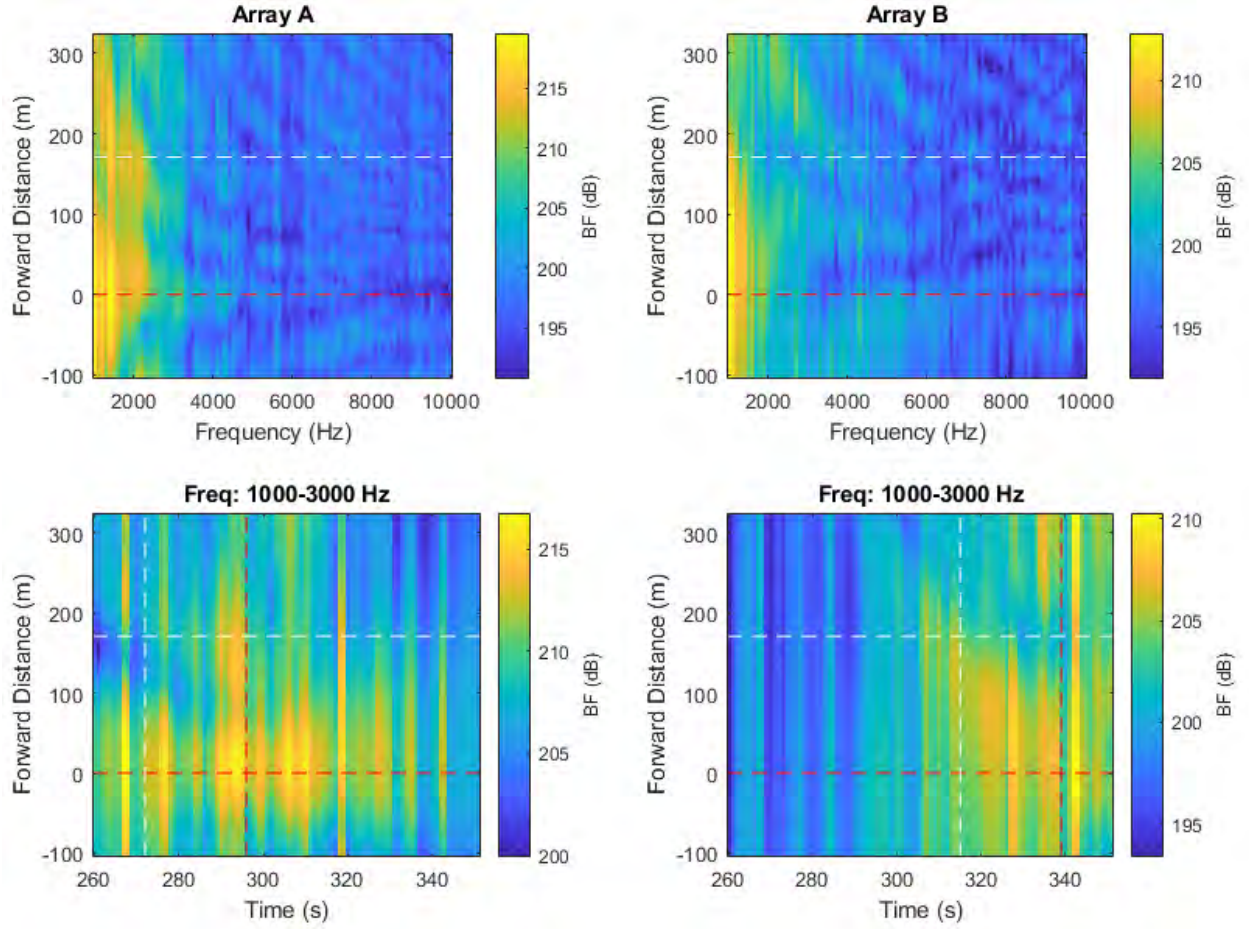

Figure 243 High-frequency noise maps from beamforming with individual arrays. Top maps show the BF response versus forward distance along vessel, measured approximately from the stern, versus frequency. Bottom maps show BF response versus forward distance and snapshot time. Horizontal dashed lines indicate the stern and bow positions of the vessel. Vertical dashed lines represent the CPA times of the bow and stern at each array.

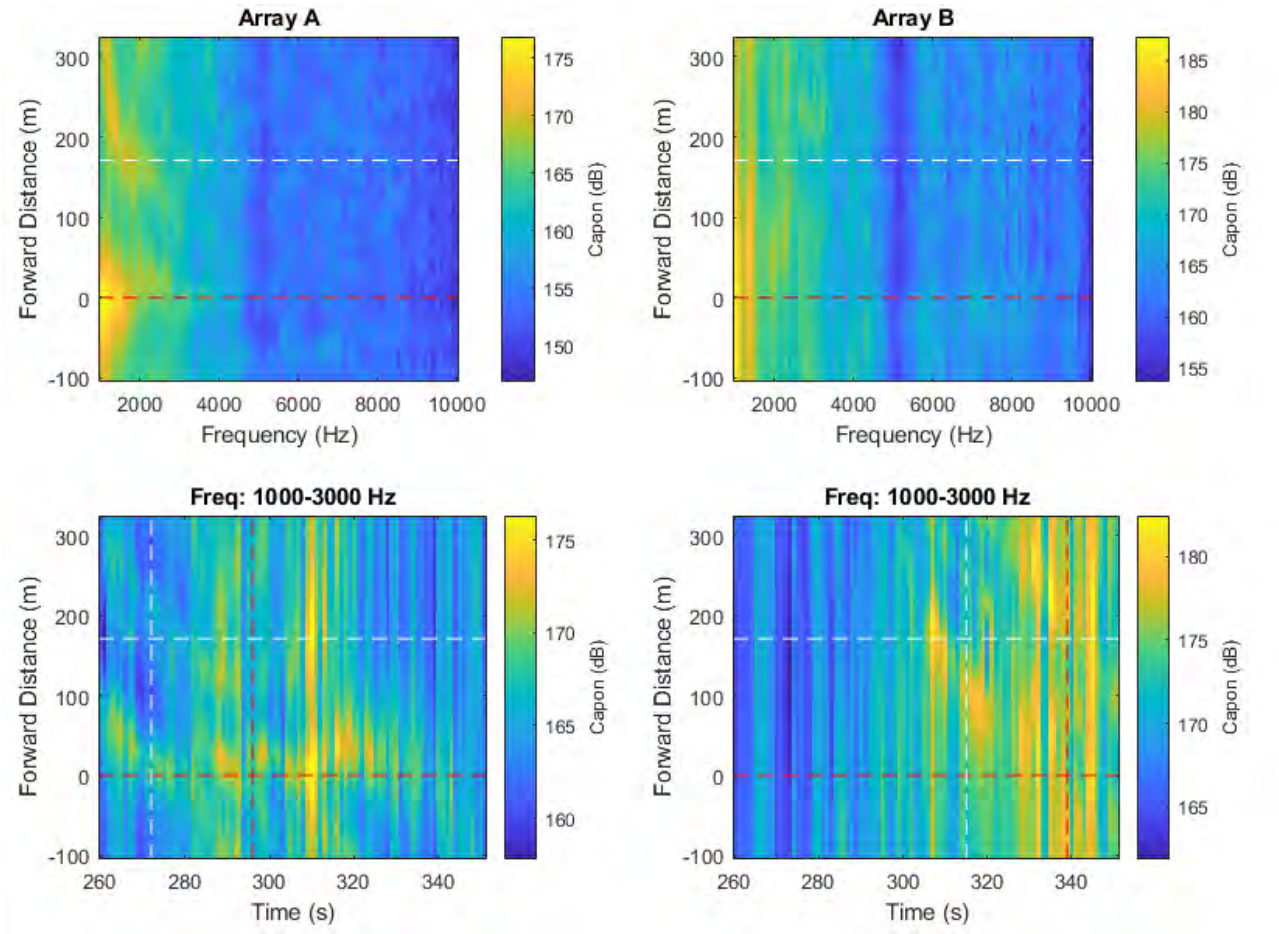

Figure 244 High-frequency noise maps obtained using the spatial spectra provided by the Capon algorithm implemented using individual arrays.

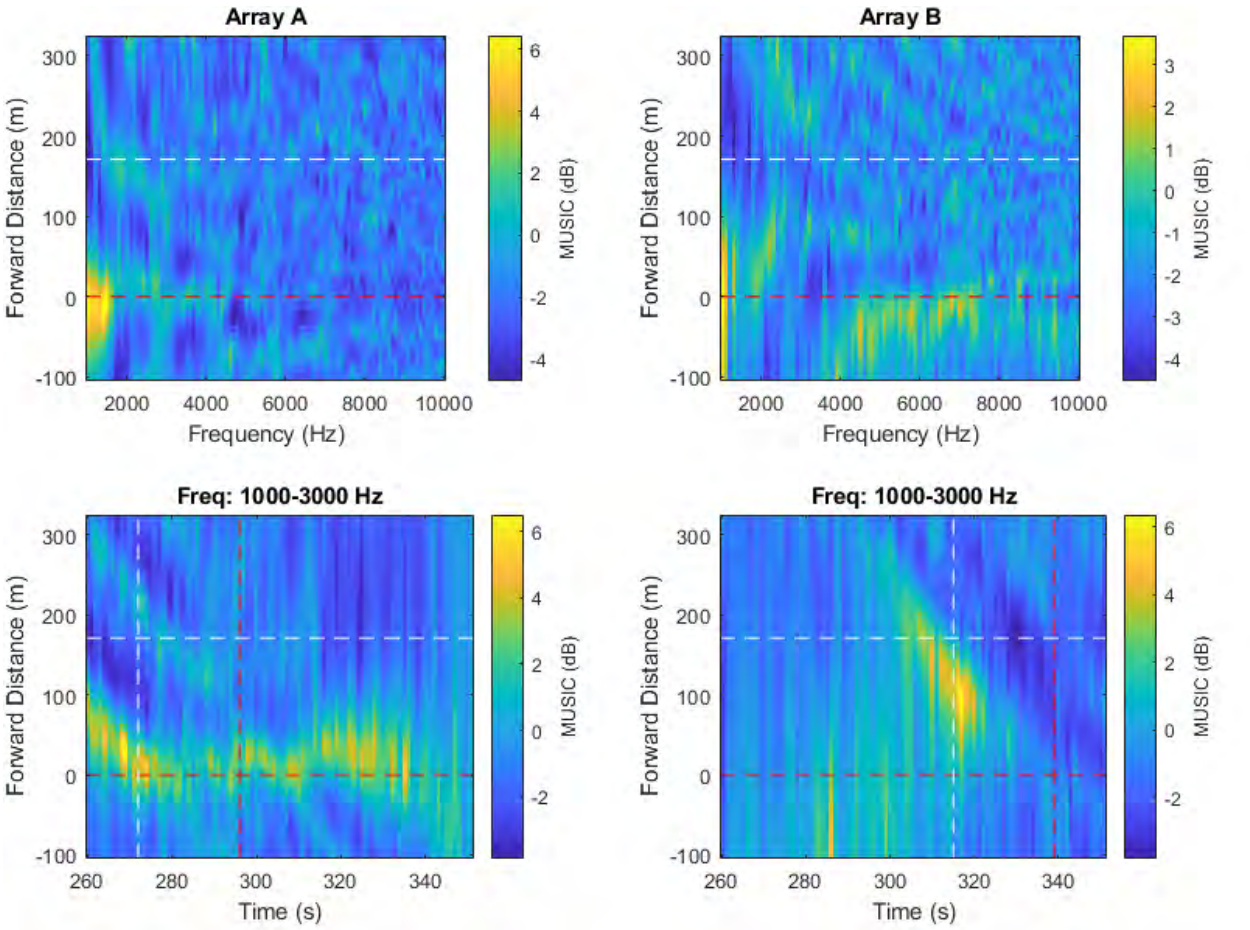

Figure 245 High-frequency noise maps obtained using the spatial spectra provided by the MUSIC algorithm implemented using individual arrays.

A.41. Pass #41 (Type: Cargo. Length: 185 m. Speed: 14.3 kn)

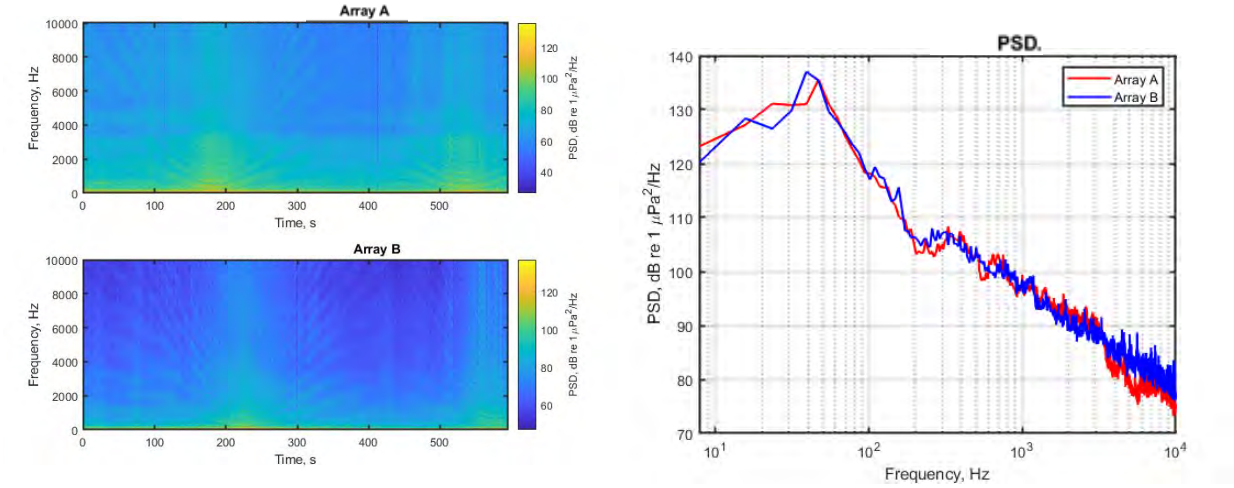

Figure 246 Spectrograms (left) and PSD (right) of ship noise observed on outputs of Arrays A and B.

A.41.1. Low- and mid-frequency noise maps

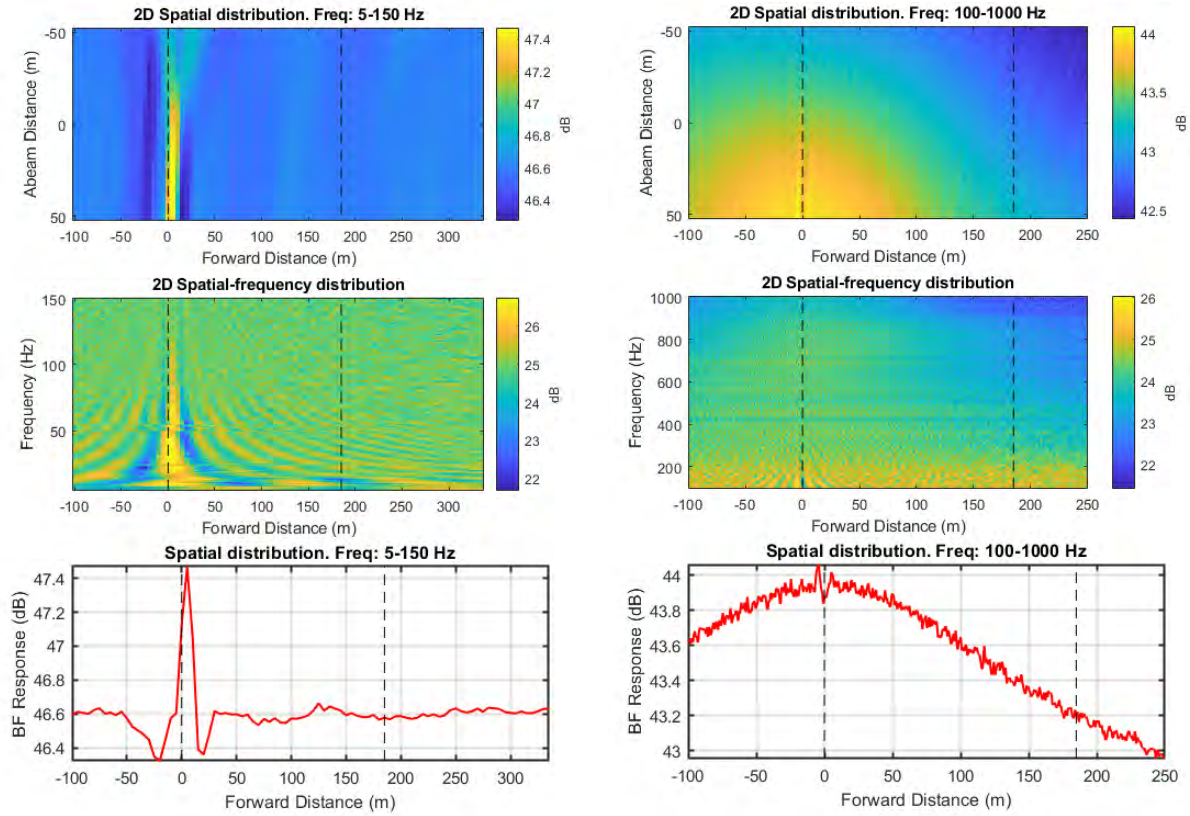

Figure 247 Noise maps from standard beamforming using combined array for Vessel Pass #41: 2D maps in spatial domain for two frequency ranges (top); 2D maps in vessel forward distance and frequency domain for two frequency ranges (middle); and graph of BF response versus forward distance for two frequency ranges (bottom). Frequency ranges are 5 to150 Hz (left) and 100 to1000 Hz (right).

A.41.2. High-frequency noise maps

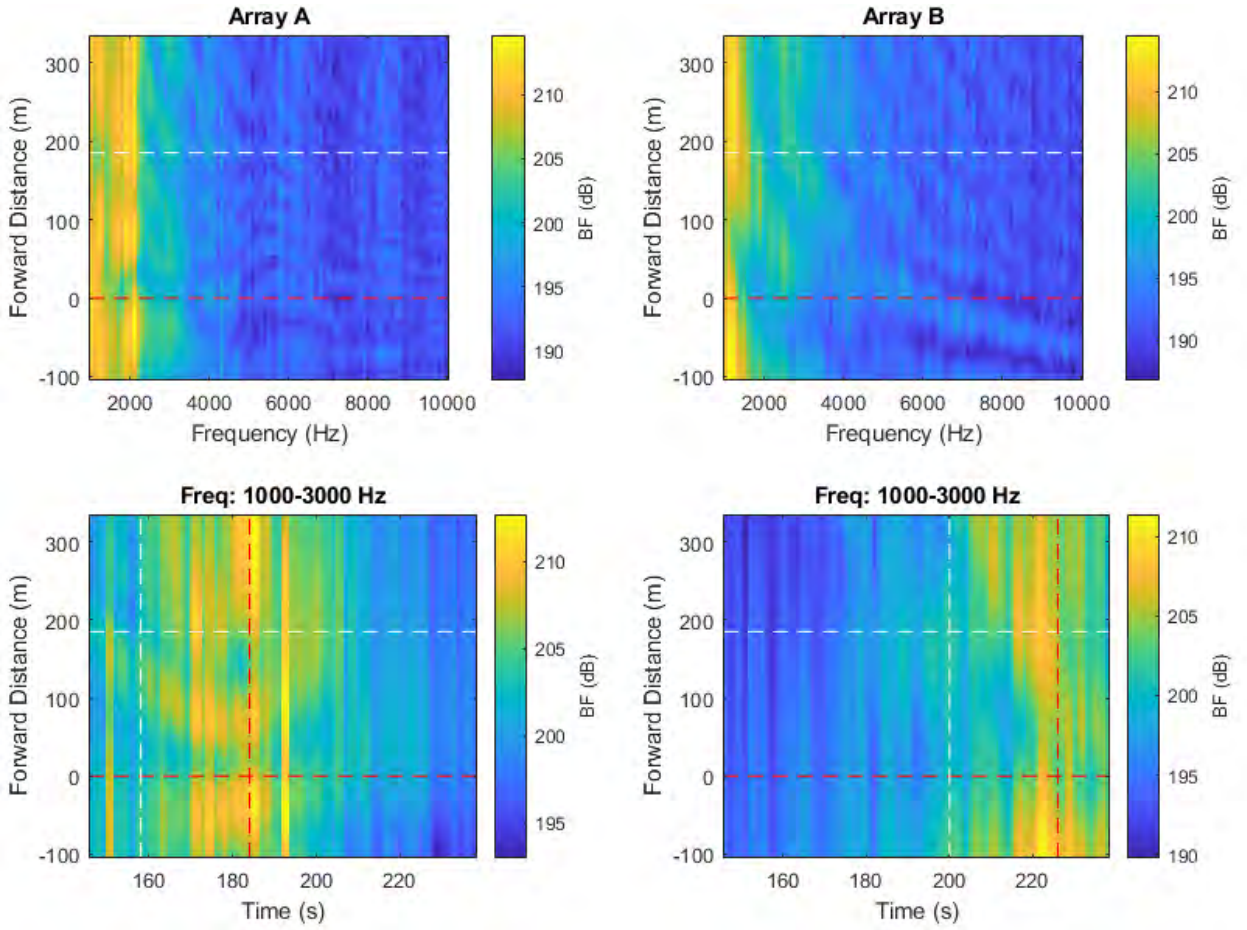

Figure 248 High-frequency noise maps from beamforming with individual arrays. Top maps show the BF response versus forward distance along vessel, measured approximately from the stern, versus frequency. Bottom maps show BF response versus forward distance and snapshot time. Horizontal dashed lines indicate the stern and bow positions of the vessel. Vertical dashed lines represent the CPA times of the bow and stern at each array.

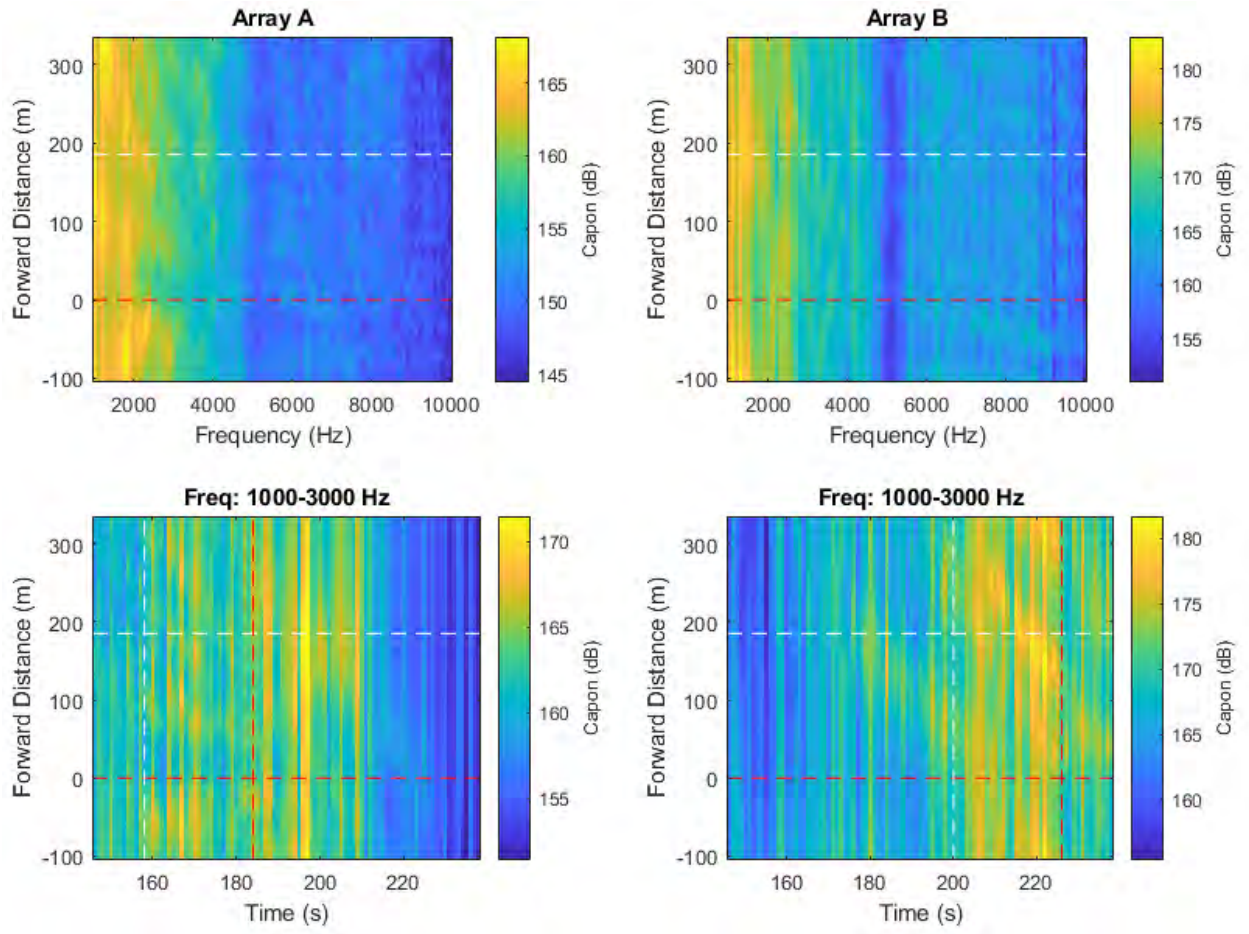

Figure 249 High-frequency noise maps obtained using the spatial spectra provided by the Capon algorithm implemented using individual arrays.

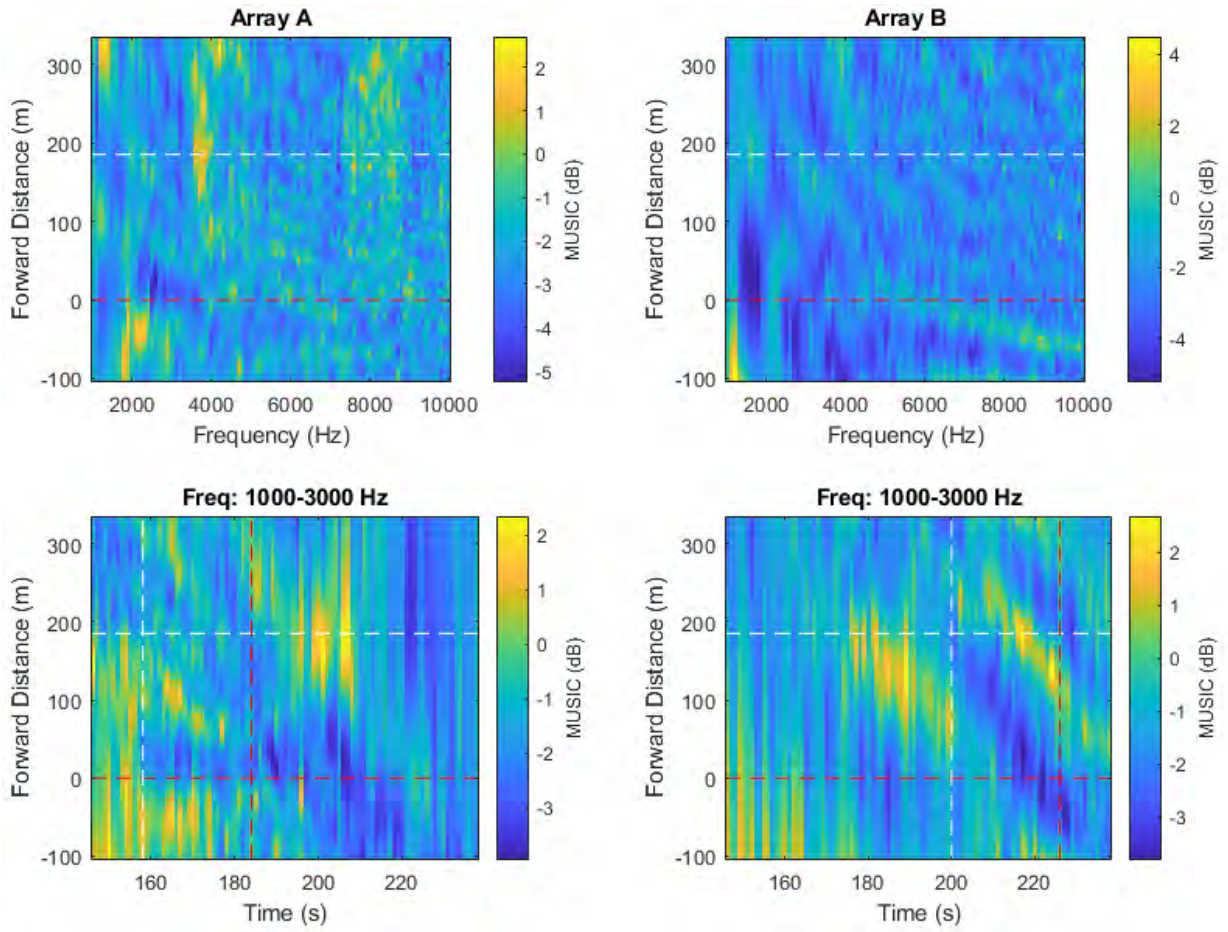

Figure 250 High-frequency noise maps obtained using the spatial spectra provided by the MUSIC algorithm implemented using individual arrays.

A.42. Pass #42 (Type: Bulker. Length: 292 m. Speed: 14.1 kn)

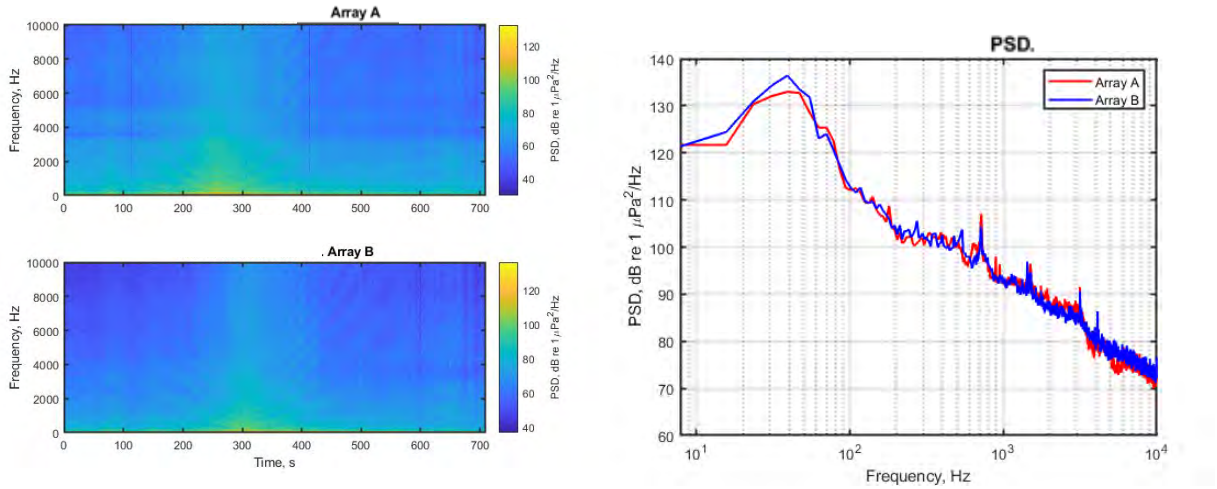

Figure 251 Spectrograms (left) and PSD (right) of ship noise observed on outputs of Arrays A and B.

A.42.1. Low- and mid-frequency noise maps

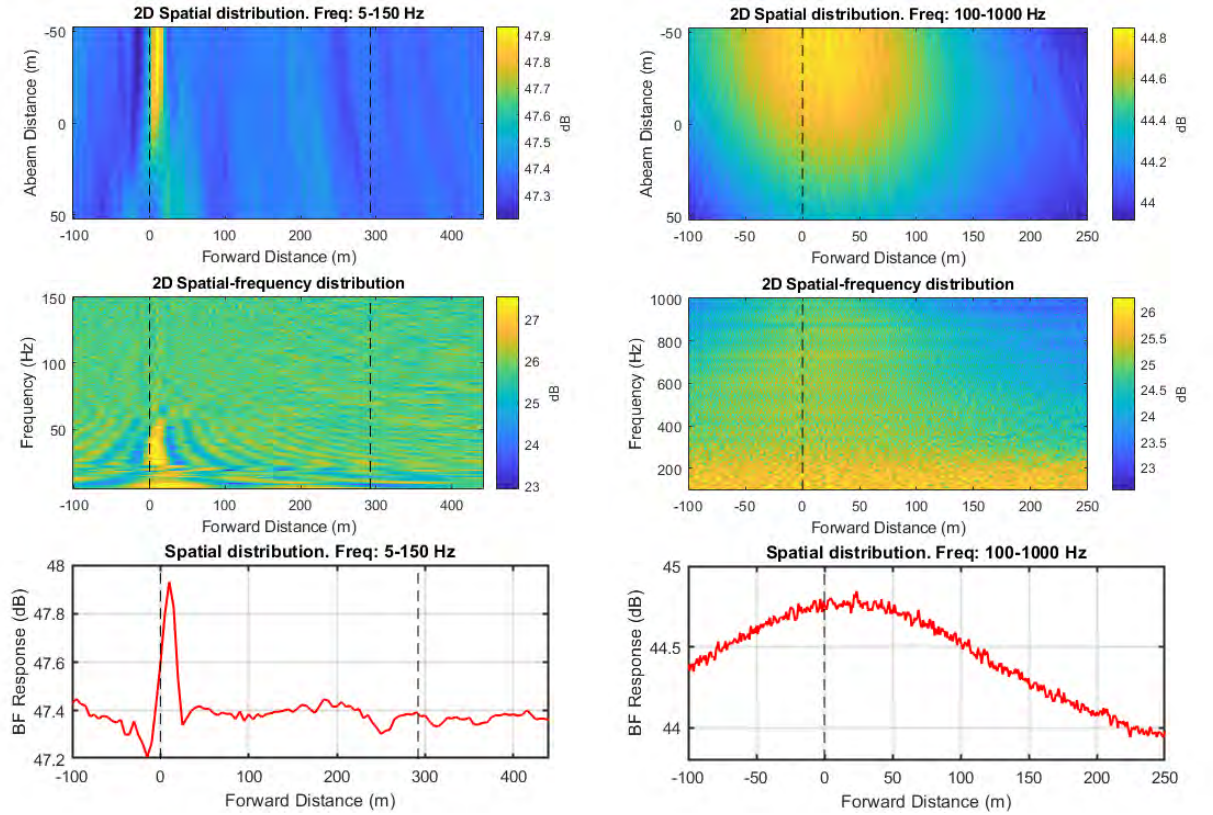

Figure 252 Noise maps from standard beamforming using combined array for Vessel Pass #42: 2D maps in spatial domain for two frequency ranges (top); 2D maps in vessel forward distance and frequency domain for two frequency ranges (middle); and graph of BF response versus forward distance for two frequency ranges (bottom). Frequency ranges are 5 to150 Hz (left) and 100 to1000 Hz (right).

A.42.2. High-frequency noise maps

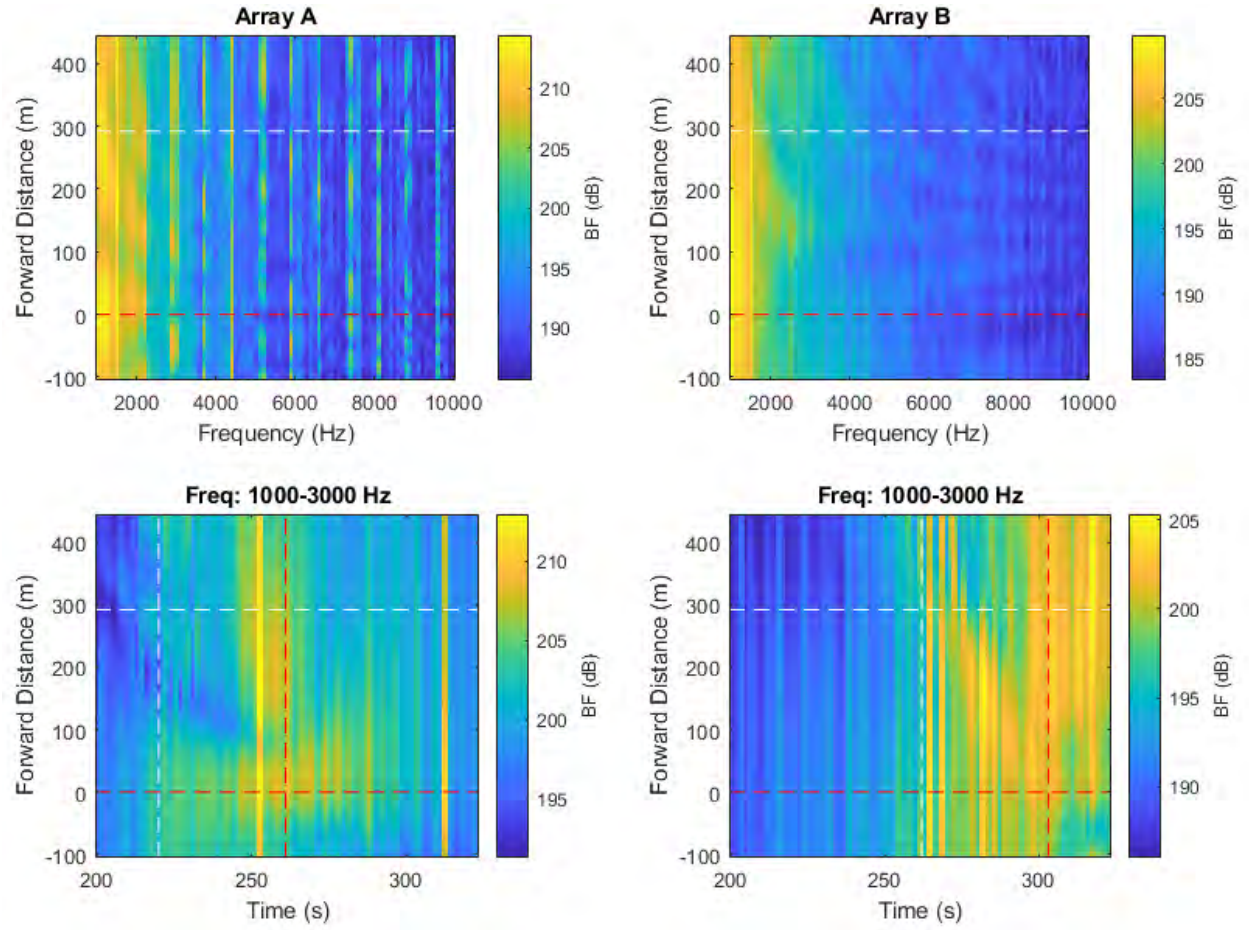

Figure 253 High-frequency noise maps from beamforming with individual arrays. Top maps show the BF response versus forward distance along vessel, measured approximately from the stern, versus frequency. Bottom maps show BF response versus forward distance and snapshot time. Horizontal dashed lines indicate the stern and bow positions of the vessel. Vertical dashed lines represent the CPA times of the bow and stern at each array.

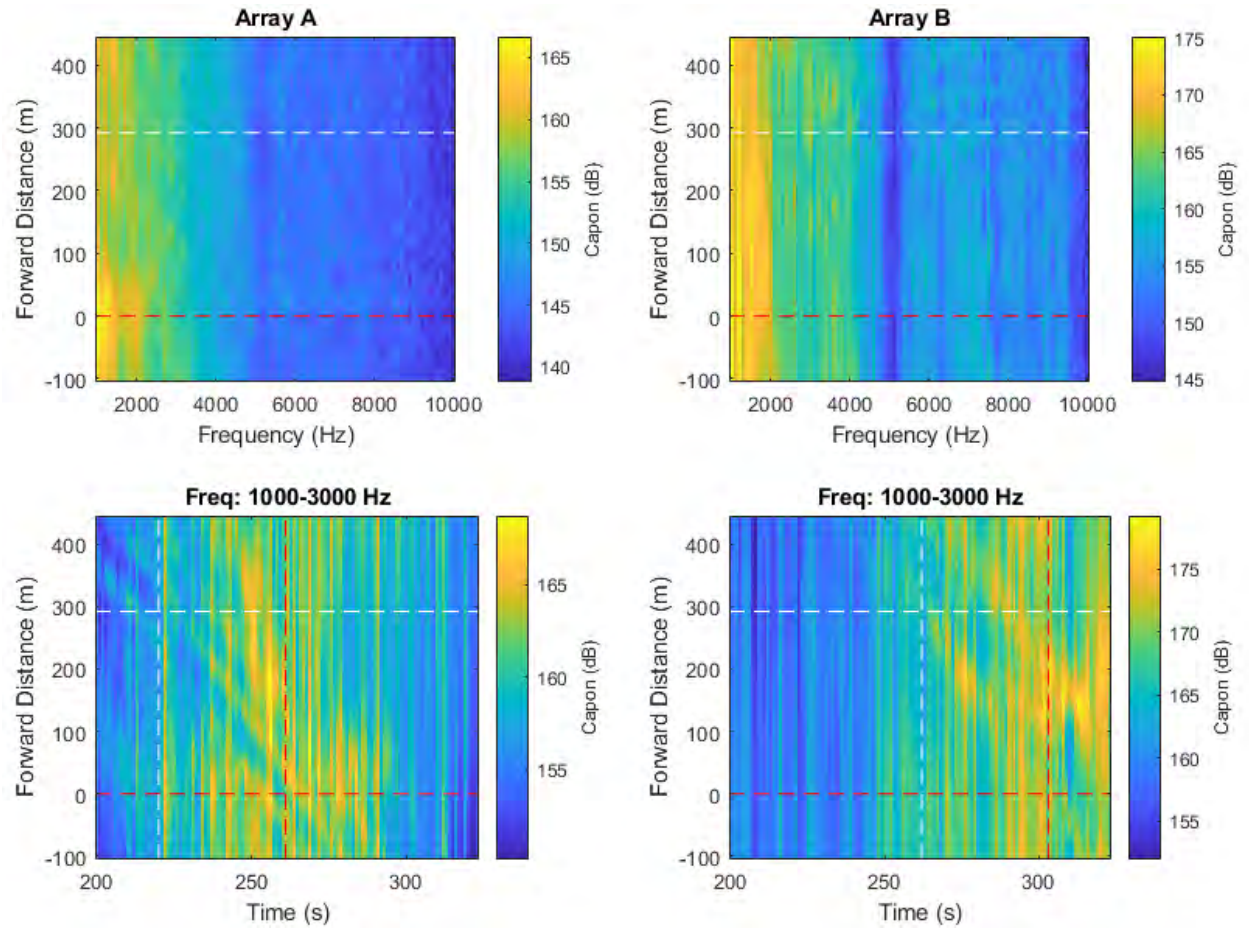

Figure 254 High-frequency noise maps obtained using the spatial spectra provided by the Capon algorithm implemented using individual arrays.

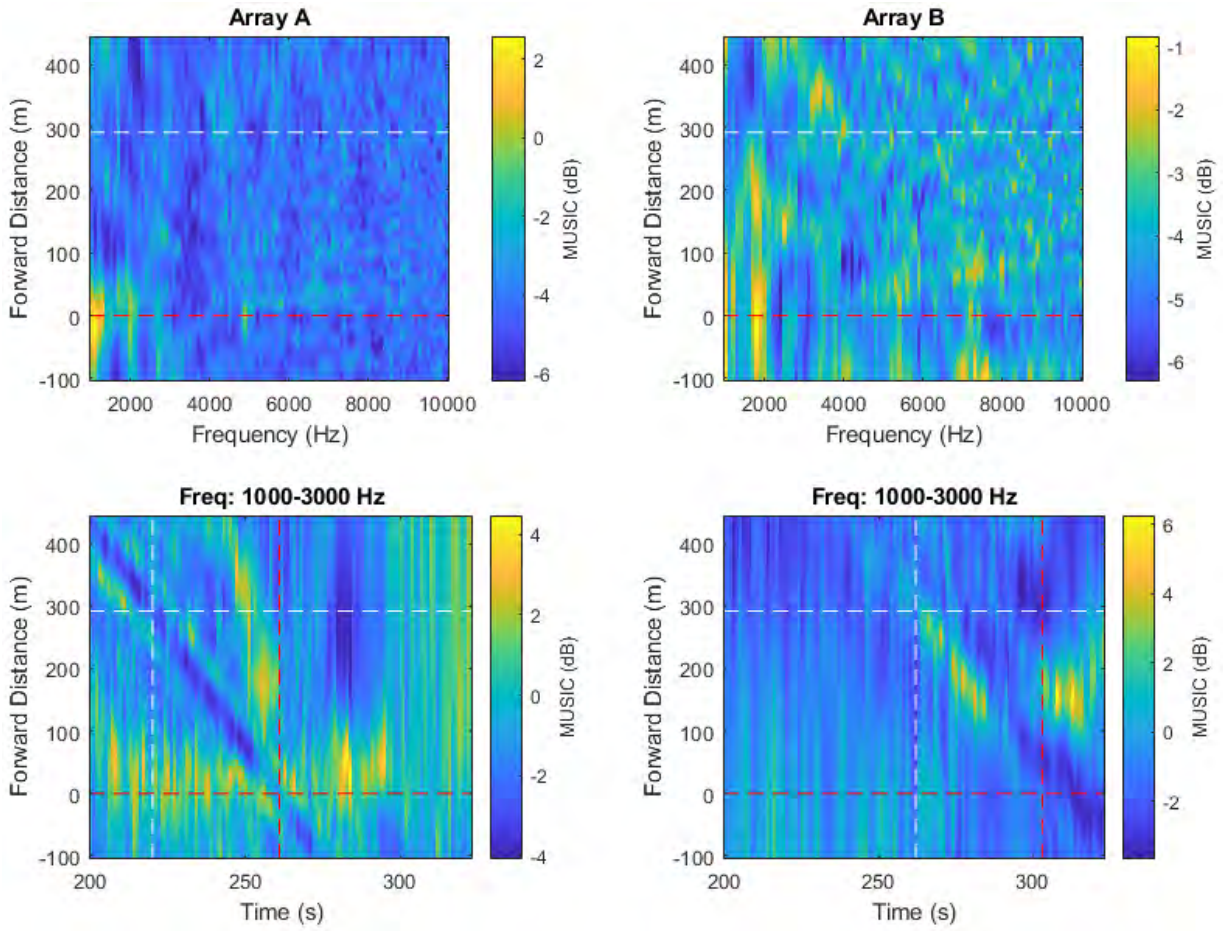

Figure 255 High-frequency noise maps obtained using the spatial spectra provided by the MUSIC algorithm implemented using individual arrays.

A.43. Pass #43 (Type: Container. Length: 347 m. Speed: 16.9 kn)

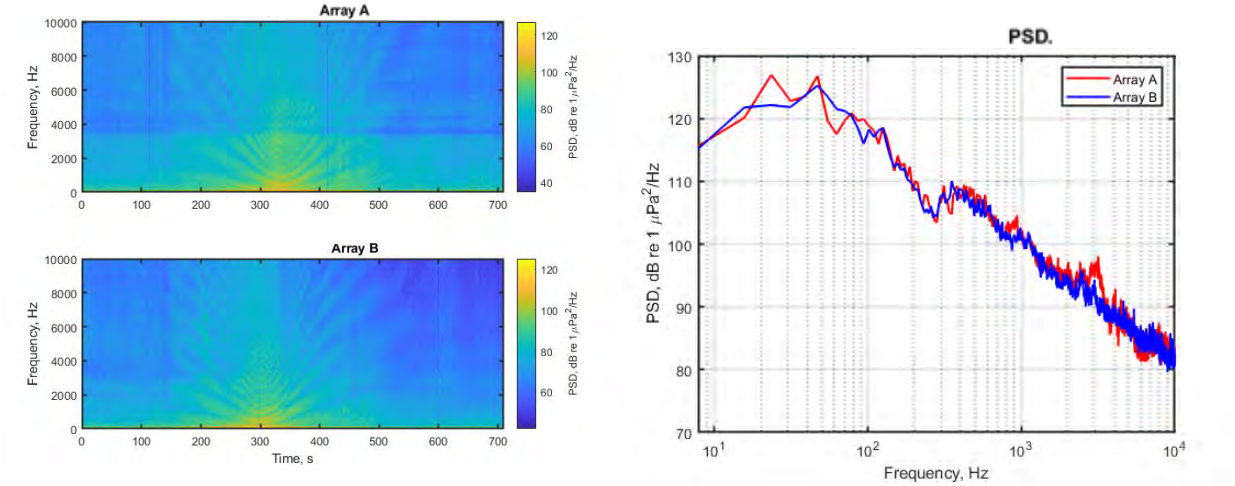

Figure 256 Spectrograms (left) and PSD (right) of ship noise observed on outputs of Arrays A and B.

A.43.1. Low- and mid-frequency noise maps

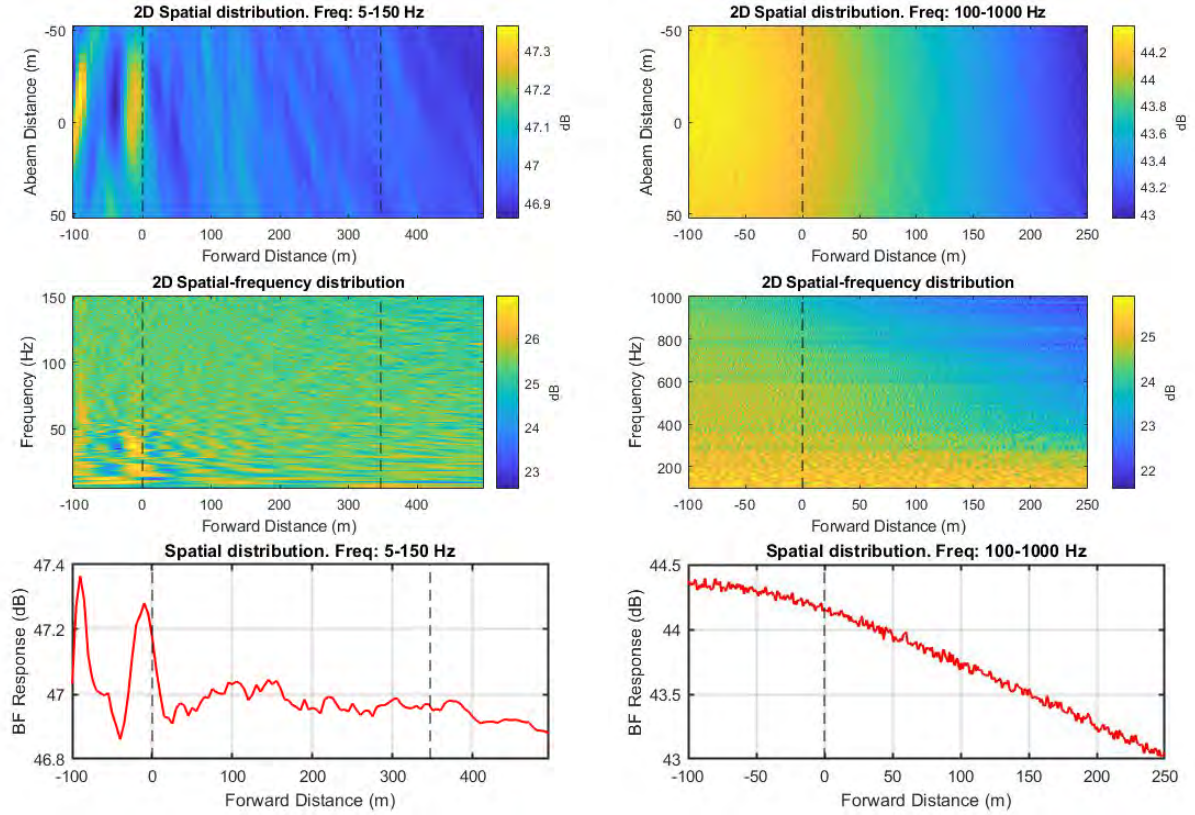

Figure 257 Noise maps from standard beamforming using combined array for Vessel Pass #43: 2D maps in spatial domain for two frequency ranges (top); 2D maps in vessel forward distance and frequency domain for two frequency ranges (middle); and graph of BF response versus forward distance for two frequency ranges (bottom). Frequency ranges are 5 to150 Hz (left) and 100 to1000 Hz (right).

A.43.2. High-frequency noise maps

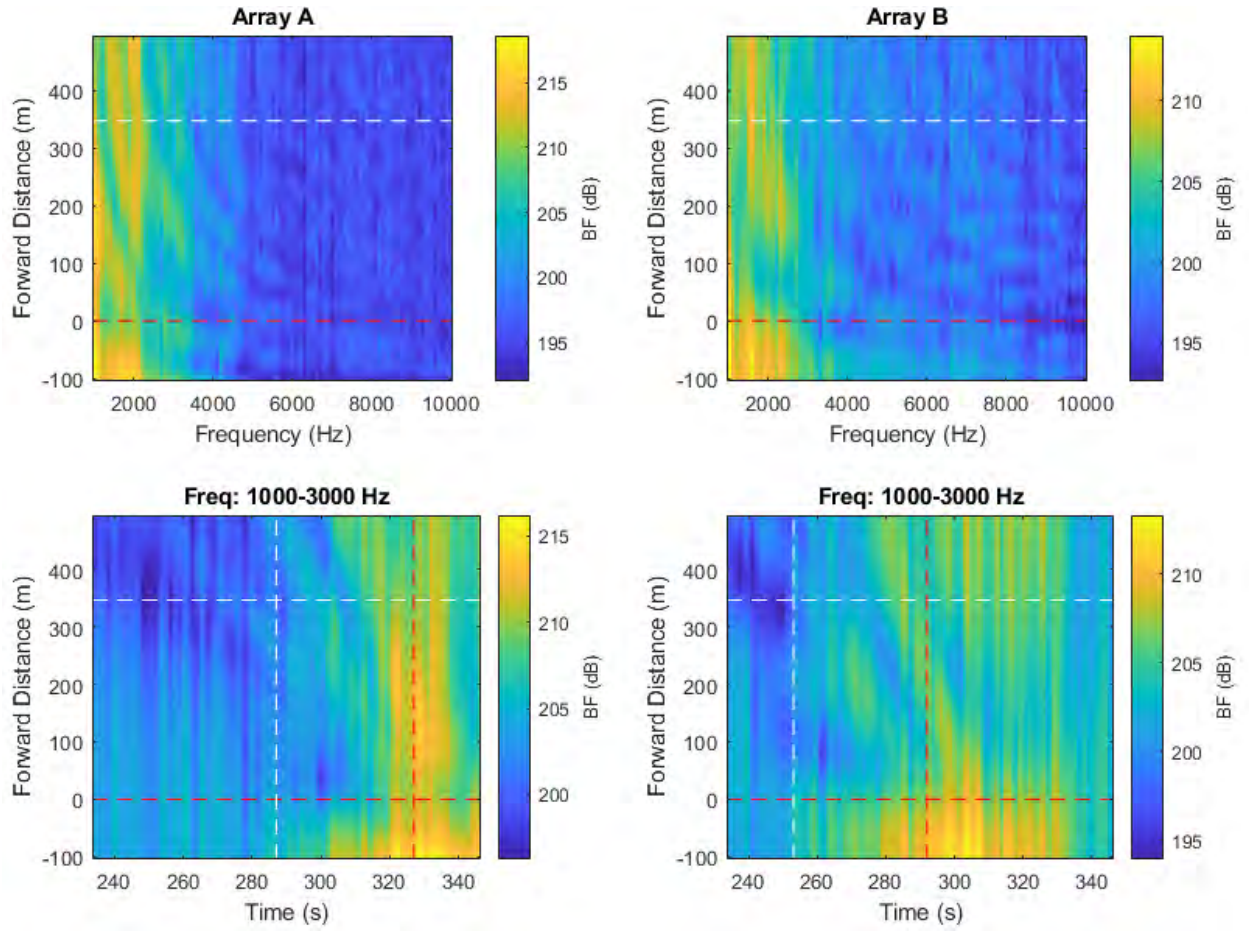

Figure 258 High-frequency noise maps from beamforming with individual arrays. Top maps show the BF response versus forward distance along vessel, measured approximately from the stern, versus frequency. Bottom maps show BF response versus forward distance and snapshot time. Horizontal dashed lines indicate the stern and bow positions of the vessel. Vertical dashed lines represent the CPA times of the bow and stern at each array.

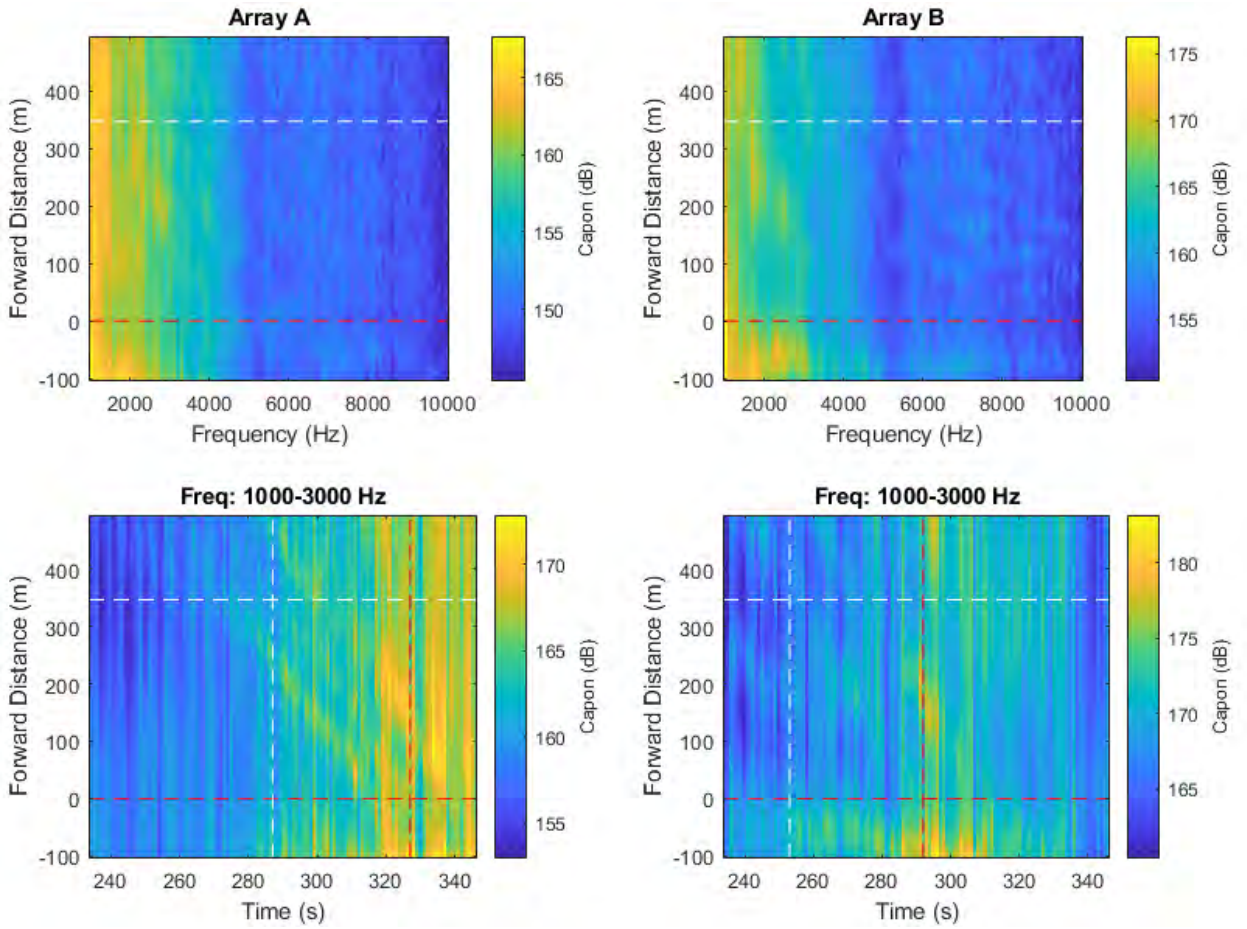

Figure 259 High-frequency noise maps obtained using the spatial spectra provided by the Capon algorithm implemented using individual arrays.

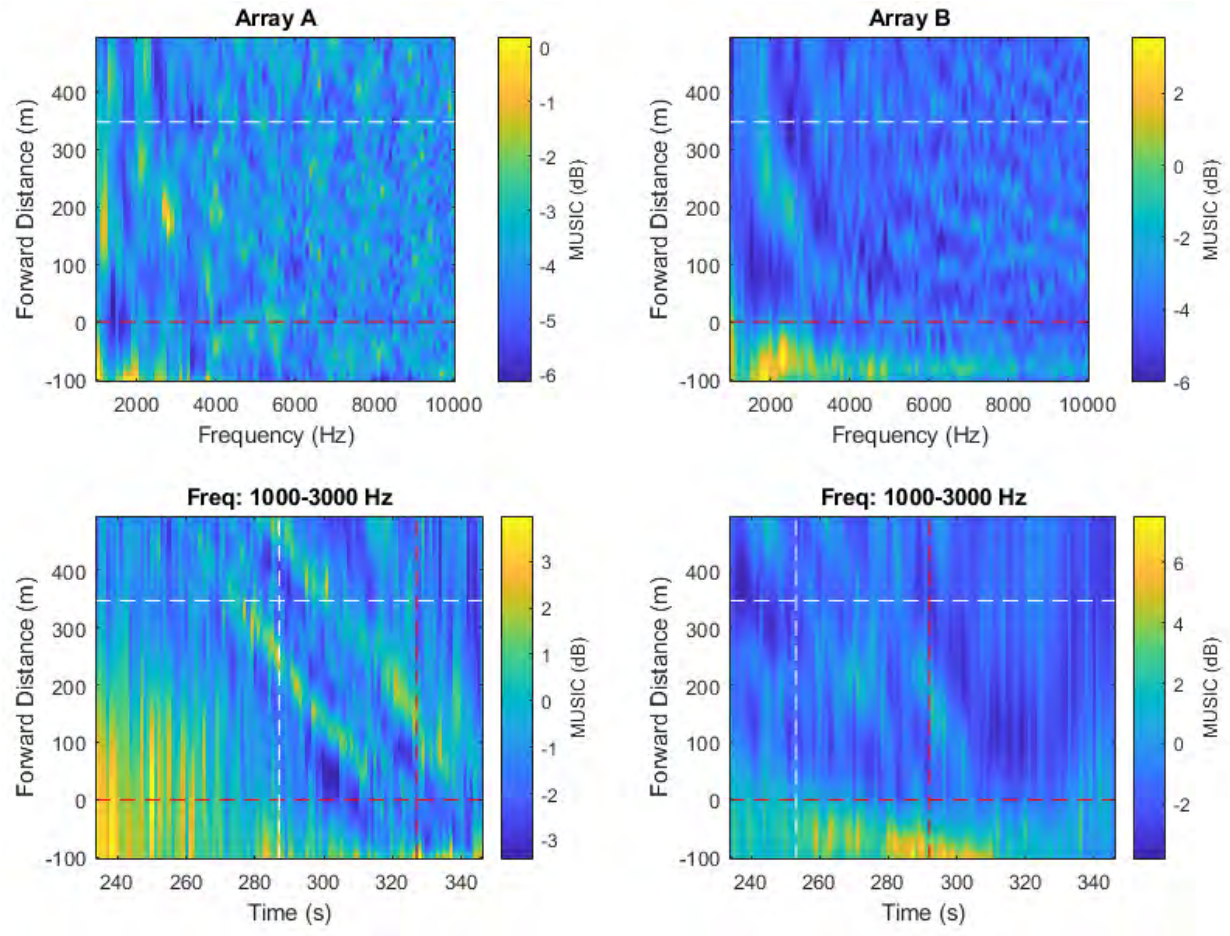

Figure 260 High-frequency noise maps obtained using the spatial spectra provided by the MUSIC algorithm implemented using individual arrays.

A.44. Pass #44 (Type: Bulker. Length: 225 m. Speed: 12.9 kn)

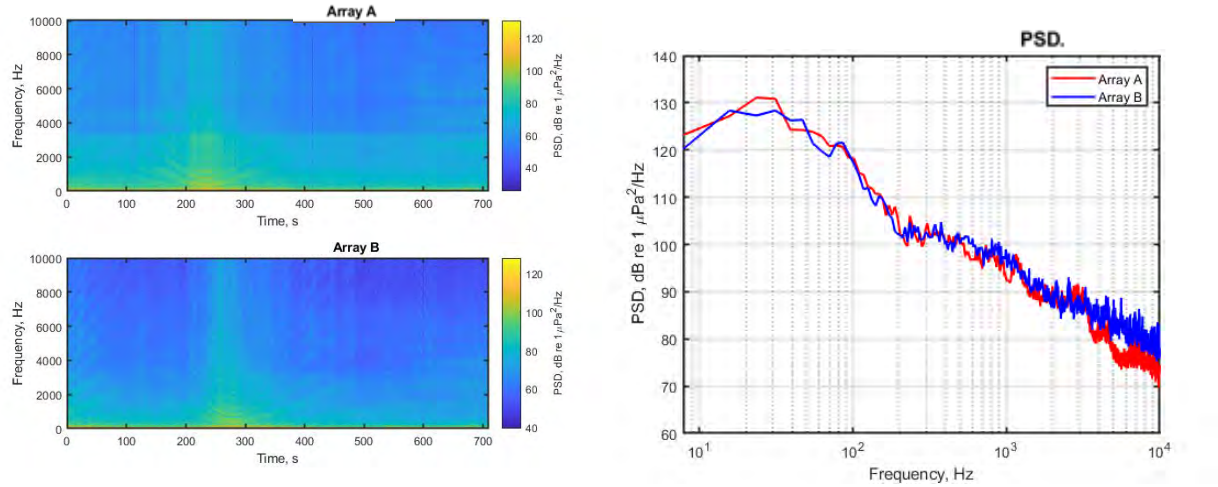

Figure 261 Spectrograms (left) and PSD (right) of ship noise observed on outputs of Arrays A and B.

A.44.1. Low- and mid-frequency noise maps

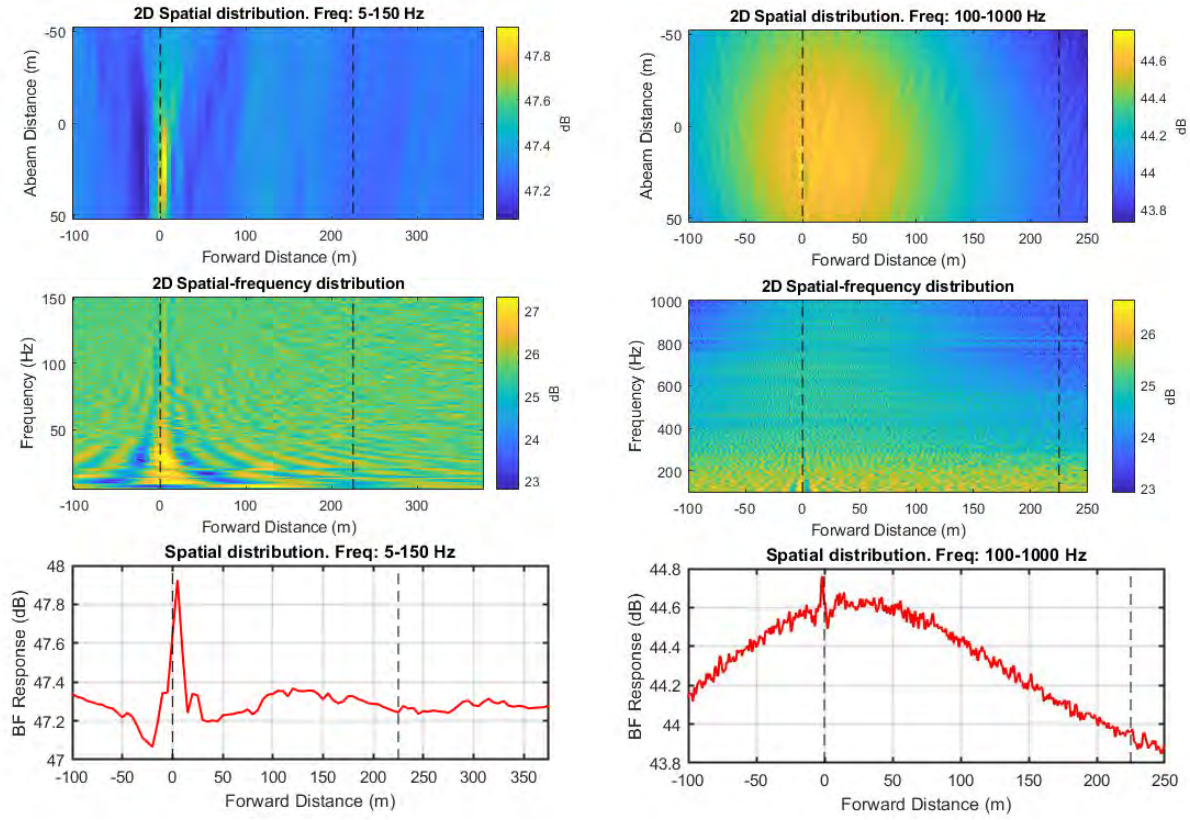

Figure 262 Noise maps from standard beamforming using combined array for Vessel Pass #44: 2D maps in spatial domain for two frequency ranges (top); 2D maps in vessel forward distance and frequency domain for two frequency ranges (middle); and graph of BF response versus forward distance for two frequency ranges (bottom). Frequency ranges are 5 to150 Hz (left) and 100 to1000 Hz (right).

A.44.2. High-frequency noise maps

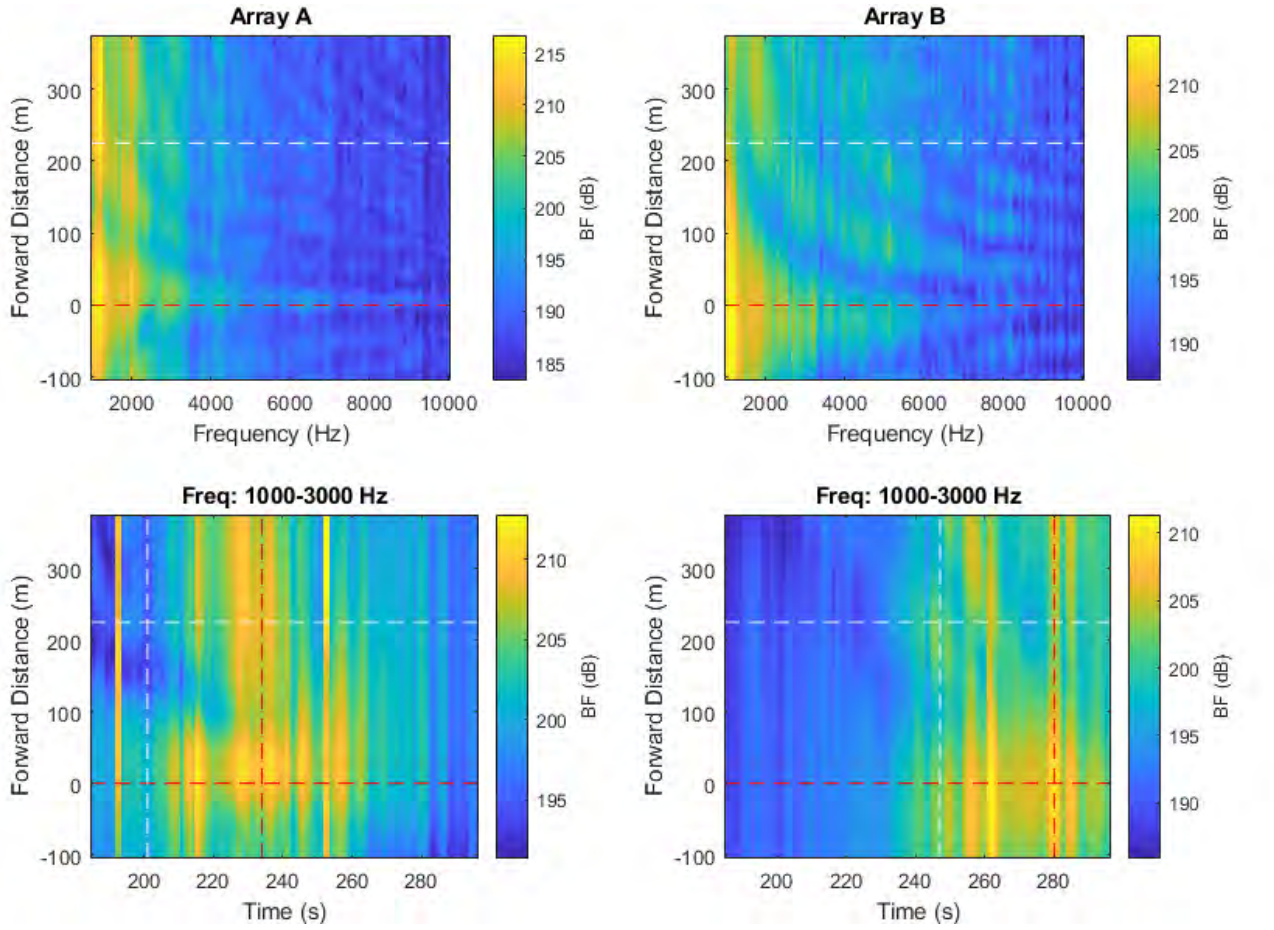

Figure 263 High-frequency noise maps from beamforming with individual arrays. Top maps show the BF response versus forward distance along vessel, measured approximately from the stern, versus frequency. Bottom maps show BF response versus forward distance and snapshot time. Horizontal dashed lines indicate the stern and bow positions of the vessel. Vertical dashed lines represent the CPA times of the bow and stern at each array.

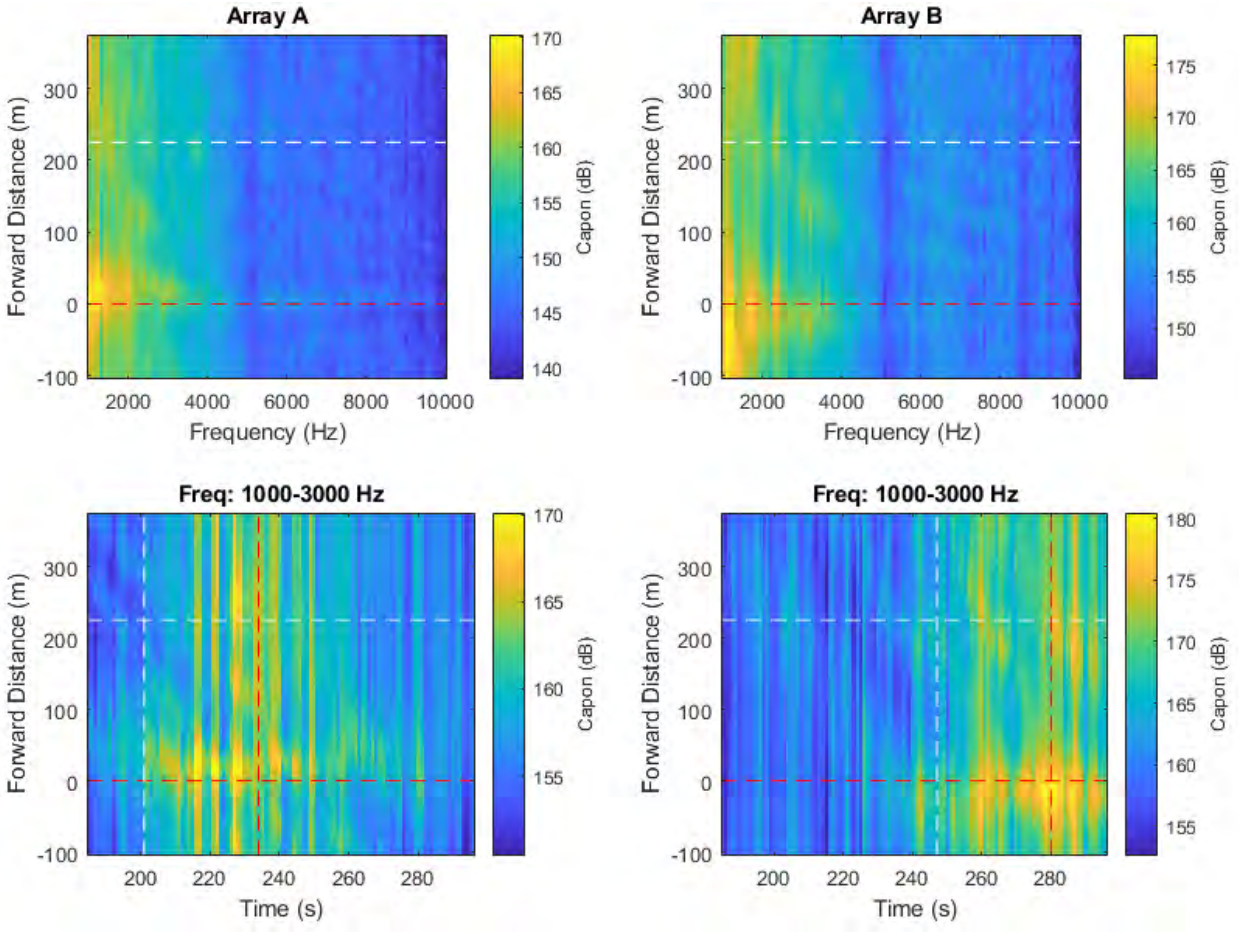

Figure 264 High-frequency noise maps obtained using the spatial spectra provided by the Capon algorithm implemented using individual arrays.

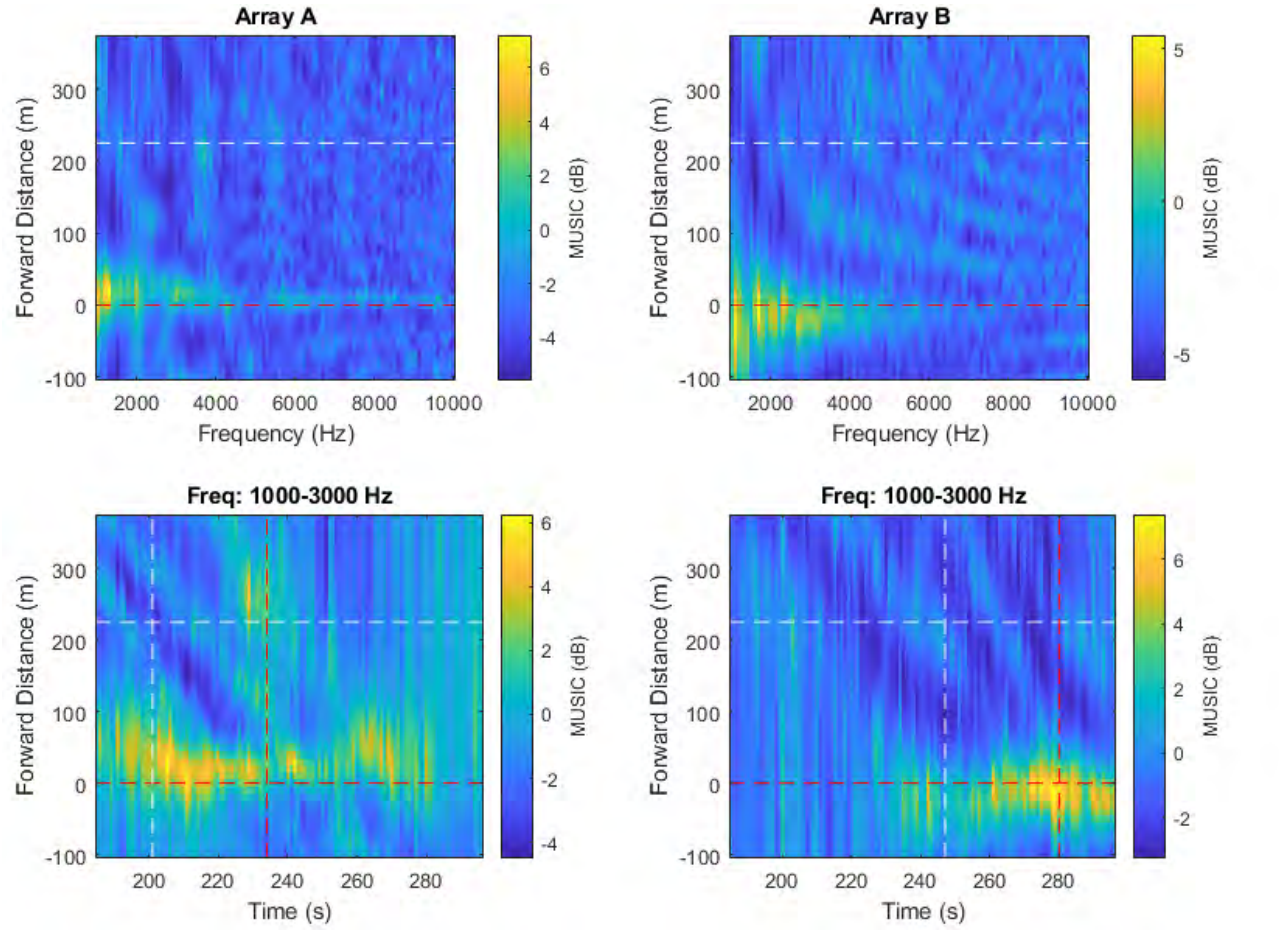

Figure 265 High-frequency noise maps obtained using the spatial spectra provided by the MUSIC algorithm implemented using individual arrays.